

**Multi-metallic complexes with N,O-donor reduced Schiff base
ligands: Synthesis, structure, self-assembly and catalytic
activity**

**Thesis submitted for the degree of
Doctor of Philosophy (Science)**

Of

Jadavpur University

2023

By

Saikat Mirdya



Department of Chemistry

Jadavpur University

Kolkata-700032

India

যাদবপুর বিশ্ববিদ্যালয়
কলকাতা-৭০০ ০৩২, ভারত



*JADAVPUR UNIVERSITY
KOLKATA-700032, INDIA

FACULTY OF SCIENCE : DEPARTMENT OF CHEMISTRY : INORGANIC CHEMISTRY SECTION

CERTIFICATE FROM THE SUPERVISOR

This is to certify that the thesis entitled “**Multi-metallic complexes with N,O-donor reduced Schiff baseligands: Synthesis, structure, self-assembly and catalytic activity**” submitted by Sri **Saikat Mirdya**, who got his name registered on 26th August, 2019 (Index Number No. 37/19/chem./26) for the award of Ph.D. (Science) degree of Jadavpur University, is absolutely based upon his own work under the supervision of Dr. Shouvik Chattopadhyay and that neither this thesis nor any part of it has been submitted for either any degree/diploma or any other academic award anywhere before.

Date: 13.06.2023

Shouvik Chattopadhyay

Dr. Shouvik Chattopadhyay
Professor
Department of Chemistry
Inorganic Section
Jadavpur University
Kolkata-700032

Dr. Shouvik Chattopadhyay
Professor
Department of Chemistry
Jadavpur University
Kolkata-700032

*Established on and from 24th December, 1955 vide Notification No. 10986-Edn/IU-42/55 dated 6th December, 1955 under Jadavpur University Act, 1955 (West Bengal Act XXXIII of 1955) followed by Jadavpur University Act, 1981 (West Bengal Act XXIV of 1981)

দ্রষ্টব্য : ২৪১৪-৬৬৬৬/৬১৯৪/৬৬৬৬/৬৬৬৬ প্রসারণ : ২৪৬৯
দ্রষ্টব্য : (৯১)-০৩৩-২৪১৪-৬৬৬৬/৬২১০/২৪১০-৭১২১

Website : www.jadavpur.edu
E-mail : registrar@admin.jdvu.ac.in

Phone : 2414-6666/6194/6643/6495/6443 Extn. 2469
Fax : (91)-033-2414-6414/6210/2413-7121



JADAVPUR UNIVERSITY
KOLKATA-700 032
MARK SHEET

NO.: CW/19052/ 0960

(For Ph.D/M. Phil. Course Work)

Results of the	PH.D. COURSE WORK EXAMINATION, 2022		
In	SCIENCE		
Name	SAIKAT MIRDYA	Class Roll No.	201920104016
Examination Roll No.	PHDCHEM22201		
held in	DECEMBER, 2022		

Subject Code / Name	Credit Hr.(c)	Marks
COMPULSORY UNITS:: CHEM/PHD/CPE-RPE/A/B RESEARCH & PUBLICATION ETHICS, RESEARCH METHODOLOGY & REVIEW WORK	8	62
ELECTIVE UNITS :: CHEM/PHD/I-1 :: APPLICATION OF SPECTROSCOPIC STUDIES IN CHEMICAL RESEARCH CHEM/PHD/I-2 :: MATERIALS, CATELYSES & ELECTROCHEMICAL STUDIES CHEM/PHD/I-3 :: METALS IN LIFE & REACTION DYNAMICS CHEM/PHD/I-4 :: SINGLE CRYSTAL X-RAY STR. SUPRAMOLECULAR CHEM.& DFT COMPUTN.	8	70

Total Marks : 132 (out of 200)

Remarks: p

Prepared by :

Checked by :

Date of issue : 28 / 04 / 2023

Controller of Examinations

DEDICATED TO

My Parents,

My Wife

&

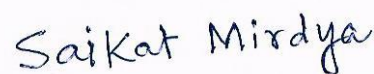
In-laws family

Preface

The whole work presented in this thesis deals with the synthesis and characterization of some di and polynuclear complexes with N,O-donor reduced Schiff base ligands. The thesis comprises six chapters of which Chapter **I** covers the literature survey on the coordination chemistry of multi-metallic complexes with reduced Schiff base ligands. The research works are presented in Chapters **II-V** of the thesis. The interesting observations are highlighted in Chapter **VI**.

The entire work was initiated in February, 2019. All information in this document have been obtained and presented in accordance with the academic rules and ethical conducts. I also declare that as required by these rules and conducts, I have cited and referenced all materials and results which are not original to this work. I take the responsibility of any unintentional oversight and errors, which might have crept in despite precautions.

Dated: 13.06.2023



Saikat Mirdya

Department of Chemistry

Inorganic Section

Jadavpur University

Kolkata – 700032

Acknowledgement

At the final step of my research work, I would like to acknowledge those people who have helped me in every way to pen this dissertation. First of all I would like to express my sincere gratitude to my guide, Dr. Shouvik Chattopadhyay, Professor, Department of Chemistry, Jadavpur University for giving me an opportunity to be a part of his research group. I am grateful to him for his continuous direction, assistance, inspiration and support throughout the research work. His dedication to research and responsibility for students is incredible. I would like to convey him for educating me in every step of my research work. This work could not have been possible without his tenacity and desire for research, two fundamental aspects to sustain in a scientific society.

I take this opportunity to sincerely acknowledge Prof. Subratanath Koner, Head of the Department of Chemistry, Jadavpur University and all other faculty members of the Department of Chemistry, Jadavpur University for assisting me whenever I need their help and support.

Most of the results described in this thesis would not have been obtained without a close collaboration with few laboratories. I owe a great deal of appreciation and gratitude to Dr. Antonio Bauza and Prof. Antonio Frontera, Department de Química, Universitat de les Illes Balers, Spain; Prof. Michael G. B. Drew, School of Chemistry, The University of Reading, United Kingdom; Dr. Snehasis Banerjee, Government College of Engineering and Leather Technology.

I would like to thank my M. Sc. project guide Dr. Rajaram Bal, Principal Scientists, CSIR-IIP, Dehradun, for the valuable advice and inspiration.

My dissertation would be incomplete without thanking my school and college teachers especially Mr. Anjan kumar Jana. Their support and encouragement have strengthened me in the path of my life. I am very much grateful to my lab-mates for providing me moral support and friendly atmosphere always during my research work. Special thanks to my lab-mates Mr. Susovan Bera, Mr. Rabi Sankar Sarkar, Mr. Sudip Bhunia, Mr. Mridul Karmakar, Mr. Wahedur Sk., Ms. Sovana Maity, Dr. Mainak Karmakar, Mr. Tamal Dutta and Mrs. Ipsita Mandal. My heartiest thank to my seniors Dr. Prasanta Kumar Bhaumik, Dr. Subrata Jana, Dr. Sumit Roy, Dr. Prasanta Bhowmik, Dr. Mithun Das, Dr. Anik Bhattacharyya, Dr. Nandita Sarkar, Dr. Samim Khan, Dr. Sourav Roy, Dr. Kousik Ghosh, Dr. Tanmoy Basak and Dr. Snehasish Thakur. I would like to mention few names, Dr. Jit Karmakar, Mr. Gurupada Bairy, Dr. Srikanta Jana, Mr. Avik Ghosh and Dr. Papu Dhibar, who have provided ample assistance whenever it is needed. Finally, I shall always be indebted to my parents, my wife, my family and my In-laws Family for being such a support throughout the ups and downs of my life. I cannot help thanking them enough for their sacrifices, care, support, motivation and unconditional love they have for me. My special regards to my brother, Shuvankar who always stands by me in all situations. In conclusion, I would like to pay high regards to all who have knowingly and unknowingly helped me in the successful completion of this dissertation.

Date: 13.06.2023

Kolkata, India



Saikat Mirdya

Department of Chemistry

Jadavpur University

Table of Content

Chapter Index	Description	Page
Chapter I	<i>General introduction, experimental section and summary of the thesis</i>	1-48
Section I.A	<i>A brief overview on the coordination chemistry of multi-metallic complexes with N,O-donor ligands</i>	3-33
Section I.B	<i>Materials and details of instrumentation</i>	35-44
Section I.C	<i>Summary of research work</i>	45-48
Chapter II	<i>A series of hydrogen bond mediated dinuclear nickel(II) complexes with reduced Schiff base ligands: An insight into the nature of hydrogen bonds in them</i>	49-139
Chapter III	<i>Dinuclear complexes with MO₂Pb cores (M=Cu/Ni)</i>	141-247
Section III.A	<i>An insight into the non-covalent Pb...S and S...S interactions in the solid-state structure of a hemidirected lead(II) complex</i>	143-179
Section III.B	<i>Formation of a tetranuclear supramolecule via non-covalent Pb...Cl tetrel bonding interaction in a hemidirected lead(II) complex with a nickel(II) containing metaloligand</i>	180-207
Chapter III.C	<i>Importance of π-Interactions Involving Chelate Rings in Addition to the Tetrel Bonds in a Series of Hemi-directed Nickel(II)/Lead(II) Complexes</i>	208-247
Chapter IV	<i>Two trinuclear complexes with Pb(O₂Ni)₂ cores</i>	248-271
Chapter V	<i>Tetranuclear complexes with CuO₂Cd cores: Exploratrion of their photocatalytic ability to degrade methylene blue</i>	272-309
Chapter VI	<i>Highlights of the thesis</i>	310-311
Appendix	<i>List of Publications</i>	

Chapter I

**General introduction, experimental
section and summary of the thesis**

Section IA

A brief overview on the coordination chemistry of multi-metallic complexes with N,O-donor reduced Schiff base ligands

The potential applications of multi-metallic complexes in information storage, magnetic arrays, porous hosts and light harvesting devices have attracted the attention of synthetic inorganic chemists and material scientists to synthesize different multi-metallic complexes with varieties of ligands [1-4]. The important and increasing roles of multi-metallic complexes in different industrial chemical catalysis is also noteworthy [5, 6]. Theoretical chemists are also interested to explore magnetic exchange coupling, potential energy surface treatments of thermal intra-molecular electron transfer, perturbation calculations for optically induced intra-system charge transfer including vibronic and superexchange coupling contributions etc. in these complexes [7-11].

The widely used symmetrical tetradentate N_2O_2 donor bis(salicylidene) Schiff base ligands (commonly known as H_2salen) have been synthesized by the 1:2 condensation of any primary diamine with any salicylaldehyde derivative [12-23]. Their enduring popularity may be related to the fact that they could be prepared very easily. The stability of the Schiff bases may also be another important reason. On the other hand, the most common geometry of a transition metal is octahedral and these tetra-dentate Schiff bases may occupy only four coordination sites of the metal ions leaving two sites free for coordination with other ligands

[24]. In most of the complexes, the N_2O_2 donor Schiff bases occupy the equatorial positions and axial positions are occupied by two mono-dentate ligands forming *trans* isomers as the main product [25, 26]. On the other hand, in some limited complexes, the N_2O_2 donor Schiff bases may occupy-three equatorial positions and one axial position, whereas two *cis* positions are occupied by two mono-dentate ligands or a chelating bi-dentate ligand forming the *cis* isomer [27, 28].

The di-negative anionic forms of these ligands have been widely used by synthetic inorganic chemists as tetradentate N_2O_2 -donor chelating ligands for the synthesis of mono-, di- and poly-nuclear complexes of several transition and non-transition metals. The bridging ability of the phenoxo oxygen atoms may also be utilised for the synthesis of poly-nuclear complexes [29-39]. Another common way to develop di- and poly-nuclear complexes with salen-type ligands is to use 3-alkoxysalicylaldehyde (instead of salicylaldehyde), so that compartmental $N_2O_2O_2'$ -donor Schiff bases, which may accommodate smaller metal ions in their inner N_2O_2 cavity and the relatively large cations in their outer O_4 cores, can be produced [40-44]. The salen-type Schiff bases can easily be reduced with a mild reducing agent to form the corresponding reduced Schiff base ligands, which are essentially secondary diamines and may be more beneficial due to their greater flexibility and stability over a wider range of solvents as well as in oxidizing and reducing conditions [45-49].

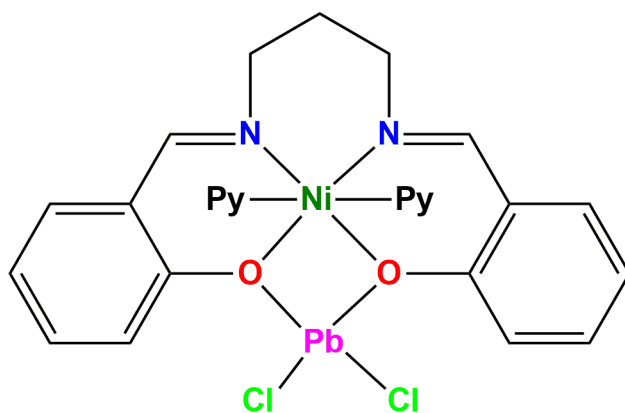
The entire work of this dissertation has essentially been designed with the synthesis and characterization of some multimetallic complexes with the reduced analogues of 'salen type' salicylaldimine Schiff base ligands. Several di and polynuclear complexes with salen type Schiff base ligands and their reduced analogues had been reported in literature before the

execution of present work. Following paragraphs present a brief literature survey of the synthesis and characterization of such complexes [50-90].

Complexes of H₂salen type tetradentate N₂O₂ donor ligands

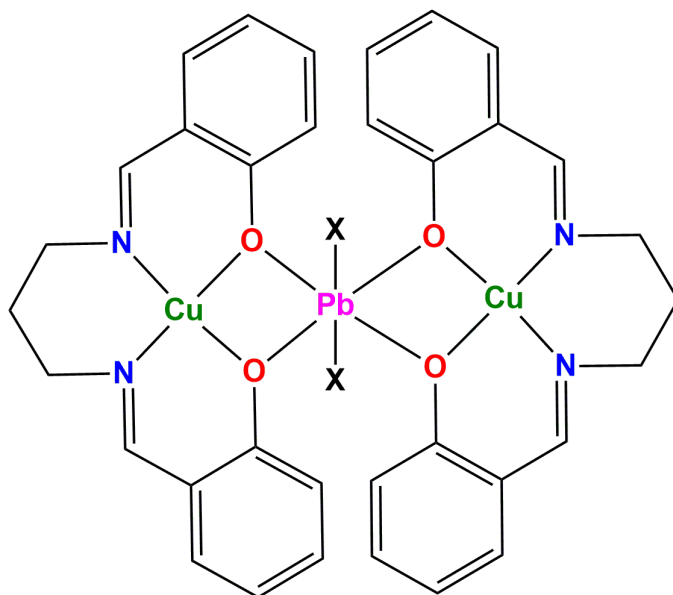
N,N'-bis(salicylidene)-1,3-propanediamine (H₂L¹) forms one dinuclear {[Py]₂Ni(μ-L¹)PbCl₂]·Py}, four trinuclear {[CuL¹]₂Pb(OCIO₃)₂}, {[CuL¹]₂Pb(NCS)₂}, {[CuL¹]₂PbCl₂}, {[CuL¹]₂PbI₂}} and one tetranuclear {[μ-DMF]₂[(H₂O)NiL¹Pb(SCN)]₂}} complexes. *N,N'*-bis(salicylidene)-2,2-dimethyl-1,3-propanediamine (H₂L²) forms only one trinuclear complex, {[CuL²]₂Pb(NCS)₂}. *N,N'*-bis(2'-hydroxy-1-phenylethanylidene)-1,3-propanediamine (H₂L³) forms one trinuclear complex, {[CuL³]₂Pb(NO₃)₂}, one tetranuclear complex, [(μ-adipato){Pb(L³Cu)L³Cu(OCIO₃)₂}]·2H₂O, and one polynuclear complex, {[CuL³]₂Pb(dca)₂]_n} having trinuclear asymmetric unit.

In complex {[Py]₂Ni(μ-L¹)PbCl₂]·Py}, the imine nitrogen atoms and phenoxo oxygen atoms of the dianion generated from *N,N'*-bis(salicylidene)-1,3-propanediamine equatorially coordinates nickel(II). The axial positions of nickel(II) is coordinated by two nitrogen atoms from two pyridine molecules. This [(py)₂NiL¹] moiety acts as a metalloligand to coordinate a lead(II) via two phenoxo oxygen atoms. Thus the phenoxo oxygen atoms of the salen ligand bridges nickel(II) and lead (II). Lead(II) is additionally coordinated by two chlorides to complete its coordination sphere, but all the coordinating atoms resides in one hemisphere only leading to hemidirected geometry of lead(II). The schematic representation of complex {[Py]₂Ni(μ-L¹)PbCl₂]·Py} is shown in Scheme 1.

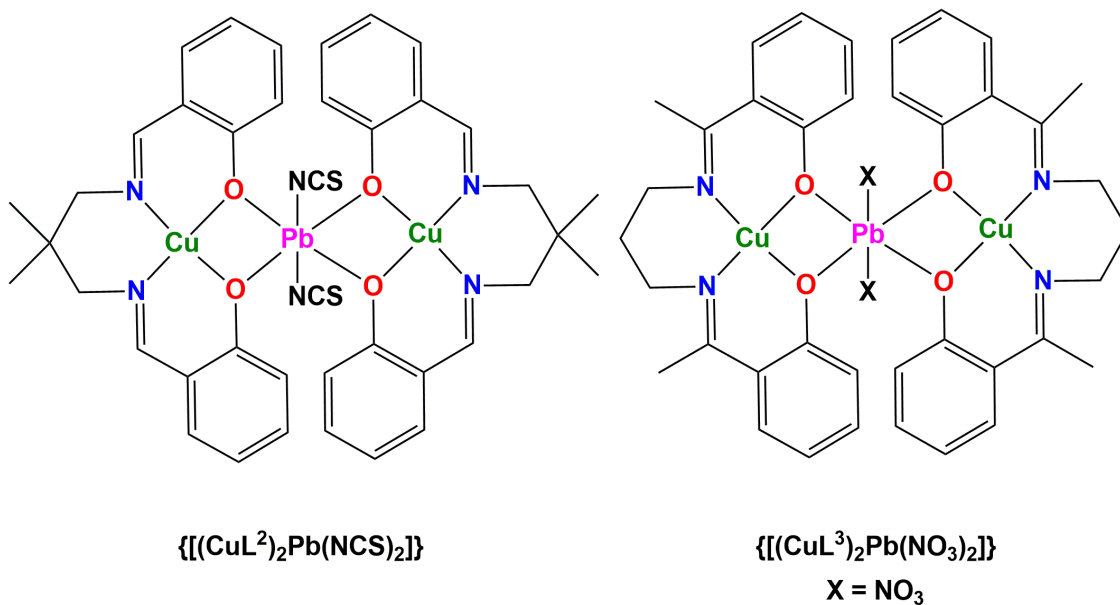


Scheme 1. Schematic representation of $\{[(\text{Py})_2\text{Ni}(\mu\text{-L}^1)\text{PbCl}_2]\cdot\text{Py}$. CCDC number is 182537.

The trinuclear complexes $\{[(\text{CuL}^1)_2\text{Pb}(\text{OCIO}_3)_2]\}$, $\{[(\text{CuL}^1)_2\text{Pb}(\text{NCS})_2]\}$, $\{[(\text{CuL}^1)_2\text{PbCl}_2]\}$, $\{[(\text{CuL}^1)_2\text{PbI}_2]\}$, $\{[(\text{CuL}^2)_2\text{Pb}(\text{NCS})_2]\}$ and $\{[(\text{CuL}^3)_2\text{Pb}(\text{NO}_3)_2]\}$ have very similar structures. In each case, two imine nitrogen and two phenoxo oxygen atoms of the dianion, $(\text{L}^3)^{2-}$, of the corresponding H_2salen type Schiff base N,N' -bis(2'-hydroxy-1-phenylethanylidene)-1,3-propanediamine coordinates the copper(II) to form a metalloligand (CuL^3) . Two units of this CuL^3 fragment, in turn, coordinate lead(II) via phenoxo oxygen atoms. Lead(II) is additionally coordinated by two co-ligands (e.g., perchlorate in $\{[(\text{CuL}^1)_2\text{Pb}(\text{OCIO}_3)_2]\}$, thiocyanate in $\{[(\text{CuL}^1)_2\text{Pb}(\text{NCS})_2]\}$ and $\{[(\text{CuL}^2)_2\text{Pb}(\text{NCS})_2]\}$, chloride in $\{[(\text{CuL}^1)_2\text{PbCl}_2]\}$, and iodide in $\{[(\text{CuL}^1)_2\text{PbI}_2]\}$) to complete its coordination sphere. The schematic representation of complexes $\{[(\text{CuL}^1)_2\text{Pb}(\text{OCIO}_3)_2]\}$, $\{[(\text{CuL}^1)_2\text{Pb}(\text{NCS})_2]\}$, $\{[(\text{CuL}^1)_2\text{PbCl}_2]\}$, $\{[(\text{CuL}^1)_2\text{PbI}_2]\}$, $\{[(\text{CuL}^2)_2\text{Pb}(\text{NCS})_2]\}$ and $\{[(\text{CuL}^3)_2\text{Pb}(\text{NO}_3)_2]\}$ are shown in Schemes 2 and 3. In all of these complexes, lead(II) centers are hexa-coordinated and are showing distorted octahedral geometry.



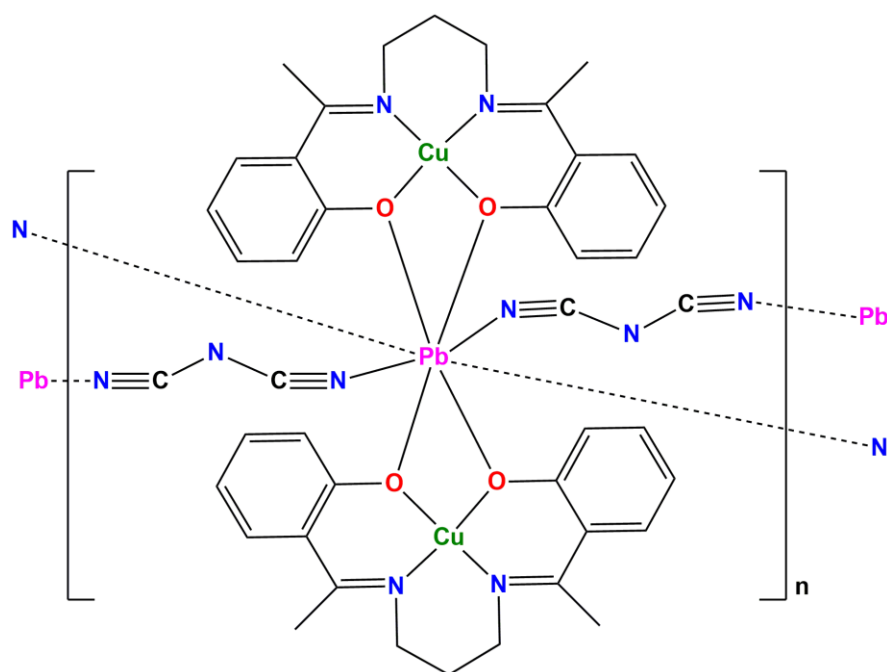
Scheme 2. Schematic representation of the complexes $\{[(\text{CuL}^1)_2\text{Pb}(\text{OCIO}_3)_2]\}$, $\{[(\text{CuL}^1)_2\text{Pb}(\text{NCS})_2]\}$, $\{[(\text{CuL}^1)_2\text{PbCl}_2]\}$ and $\{[(\text{CuL}^1)_2\text{PbI}_2]\}$. X = ClO_4 (in $\{[(\text{CuL}^1)_2\text{Pb}(\text{OCIO}_3)_2]\}$), NCS (in $\{[(\text{CuL}^1)_2\text{Pb}(\text{NCS})_2]\}$), Cl (in $\{[(\text{CuL}^1)_2\text{PbCl}_2]\}$ and I (in $\{[(\text{CuL}^1)_2\text{PbI}_2]\}$). CCDC no. are 1490211, 824246, 1225881 and 165,633 respectively.



Scheme 3. Schematic representation of the complexes. CCDC numbers are 824247 and 1490212 respectively.

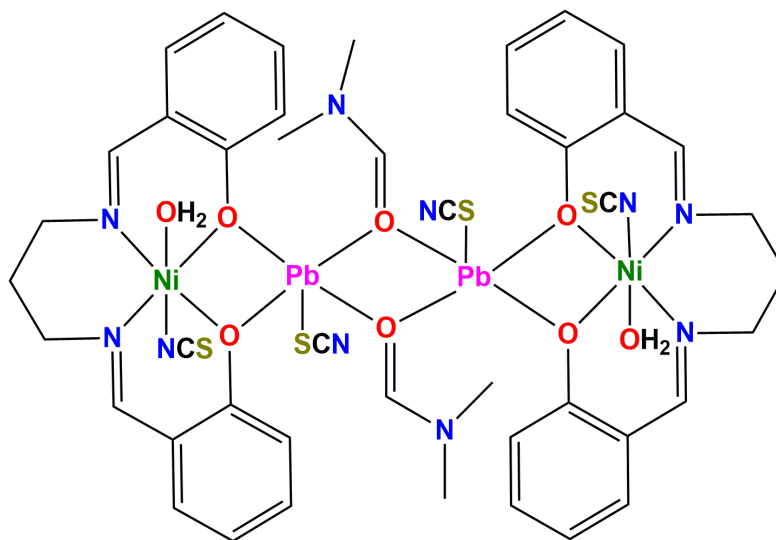
The structure of $\{[(\text{CuL}^3)_2\text{Pb}(\text{NO}_3)_2]\}$ is however, interesting as it apparently contains a octa-coordinated lead(II), where two oxygen atoms of each nitrate coordinates lead(II). Of these two oxygen atoms of a nitrate, one is also coordinated to a terminal copper(II) thus producing square pyramidal copper(II) in $\{[(\text{CuL}^3)_2\text{Pb}(\text{NO}_3)_2]\}$ (contrary to square planar copper(II) as was observed in other complexes, $\{[(\text{CuL}^1)_2\text{Pb}(\text{OCIO}_3)_2]\}$, $\{[(\text{CuL}^1)_2\text{Pb}(\text{NCS})_2]\}$, $\{[(\text{CuL}^1)_2\text{PbCl}_2]\}$, $\{[(\text{CuL}^1)_2\text{PbI}_2]\}$ and $\{[(\text{CuL}^2)_2\text{Pb}(\text{NCS})_2]\}$). The schematic representation of complex $\{[(\text{CuL}^3)_2\text{Pb}(\text{NO}_3)_2]\}$ is shown in Scheme 3. It is important to note that both the oxygen atoms of each nitrate may be considered to be occupying only one axial site of lead(II), as the O-Pb-O angle is very small ($\sim 46.230^\circ$). In that case, the geometry of lead(II) center may be considered as distorted octahedral.

The asymmetric unit $[(\text{CuL}^3)_2\text{Pb}(\text{dca})_2]$ of the poly-nuclear complex, $[(\text{CuL}^3)_2\text{Pb}(\text{dca})_2]_n$, is very close to the structures complexes $\{[(\text{CuL}^1)_2\text{Pb}(\text{OCIO}_3)_2]\}$, $\{[(\text{CuL}^1)_2\text{Pb}(\text{NCS})_2]\}$, $\{[(\text{CuL}^1)_2\text{PbCl}_2]\}$, $\{[(\text{CuL}^1)_2\text{PbI}_2]\}$ and $\{[(\text{CuL}^2)_2\text{Pb}(\text{NCS})_2]\}$, except that here the dicyanamide co-ligands coordinate symmetry-related neighbouring lead(II) centers in 1,5-bridging mode to generate its 1D chain structure. The schematic representation of $[(\text{CuL}^3)_2\text{Pb}(\text{dca})_2]_n$ is shown in Scheme 4.



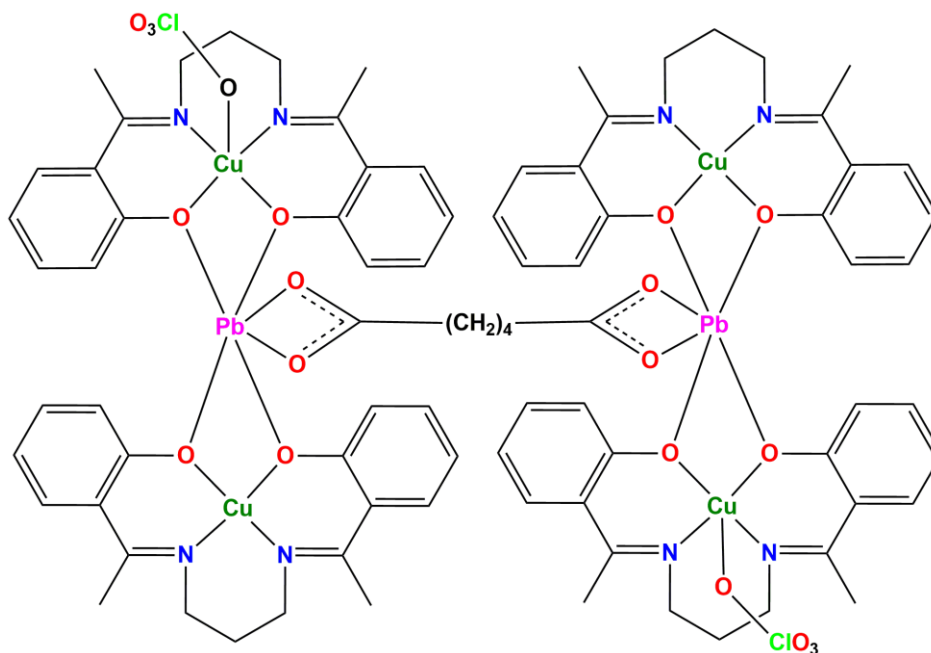
Scheme 4. Schematic representation of $[(\text{CuL}^3)_2\text{Pb}(\text{dca})_2]_n$. CCDC number is 1490214.

The tetranuclear complexes, $\{[(\mu\text{-DMF})_2\{(\text{H}_2\text{O})\text{NiL}^1\text{Pb}(\text{SCN})\}_2]\}$ and $\{[(\mu\text{-adipato})\{\text{Pb}(\text{L}^3\text{Cu})\text{L}^3\text{Cu}(\text{OCIO}_3)\}_2]\cdot 2\text{H}_2\text{O}\}$ are again constructed from dinuclear fragments by adipato bridges (in $\{[(\mu\text{-adipato})\{\text{Pb}(\text{L}^3\text{Cu})\text{L}^3\text{Cu}(\text{OCIO}_3)\}_2]\cdot 2\text{H}_2\text{O}\}$) or DMF bridges (in $\{[(\mu\text{-DMF})_2\{(\text{H}_2\text{O})\text{NiL}^1\text{Pb}(\text{SCN})\}_2]\}$). The nickel(II) center in dinuclear fragment of complex $\{[(\mu\text{-DMF})_2\{(\text{H}_2\text{O})\text{NiL}^1\text{Pb}(\text{SCN})\}_2]\}$ is octahedral and is equatorially coordinated by two imine nitrogen and two phenoxo oxygen atoms of $(\text{L}^1)^{2-}$ and is axially coordinated by an water and a thiocyanate. Each lead(II) is coordinated by four phenoxo oxygen atoms from two $[\text{NiL}^1(\text{H}_2\text{O})(\text{NCS})]$ fragments and a sulfur atom from a thiocyanate to form the dinuclear $[(\text{H}_2\text{O})(\text{NCS})\text{NiL}^1\text{Pb}(\text{NCS})]$ fragment. Two such fragments are bridged by two DMF molecules to form the tetranuclear moiety of complex $\{[(\mu\text{-DMF})_2\{(\text{H}_2\text{O})(\text{NCS})\text{NiL}^1\text{Pb}(\text{SCN})\}_2]\}$, as shown in Scheme 5.



Scheme 5. Schematic representation of $\{[(\mu\text{-DMF})_2\{(\text{H}_2\text{O})(\text{NCS})\text{NiL}^1\text{Pb}(\text{SCN})\}_2]\}$. CCDC number is 267588.

In case of complex $\{[(\mu\text{-adipato})\{\text{Pb}(\text{L}^3\text{Cu})\text{L}^3\text{Cu}(\text{OCIO}_3)\}_2]\cdot 2\text{H}_2\text{O}\}$, the dinuclear fragment is bridged by an adipate anion, $[\text{OOC}(\text{CH}_2)_4\text{COO}]^{2-}$. In each of the dinuclear fragment, lead(II) is coordinated by two metalloligands, $[\text{CuL}^3]$ and $[\text{CuL}^3(\text{OCIO}_3)]$ via two phenoxo oxygen atoms. The copper(II) center in CuL^3 is square planar, and that in $[\text{CuL}^3(\text{OCIO}_3)]$ is square pyramidal. The coordination geometry of lead(II) may be apparently considered as octahedral, but the O-Pb-O angle formed by the coordination of two oxygen atoms of the carboxylate group of adipate anion is very small ($\sim 520^\circ$) and therefore, both oxygen atoms may be considered to be occupying only one coordination site. The schematic representation of complex $\{[(\mu\text{-adipato})\{\text{Pb}(\text{L}^3\text{Cu})\text{L}^3\text{Cu}(\text{OCIO}_3)\}_2]\cdot 2\text{H}_2\text{O}\}$ is shown in Scheme 6.

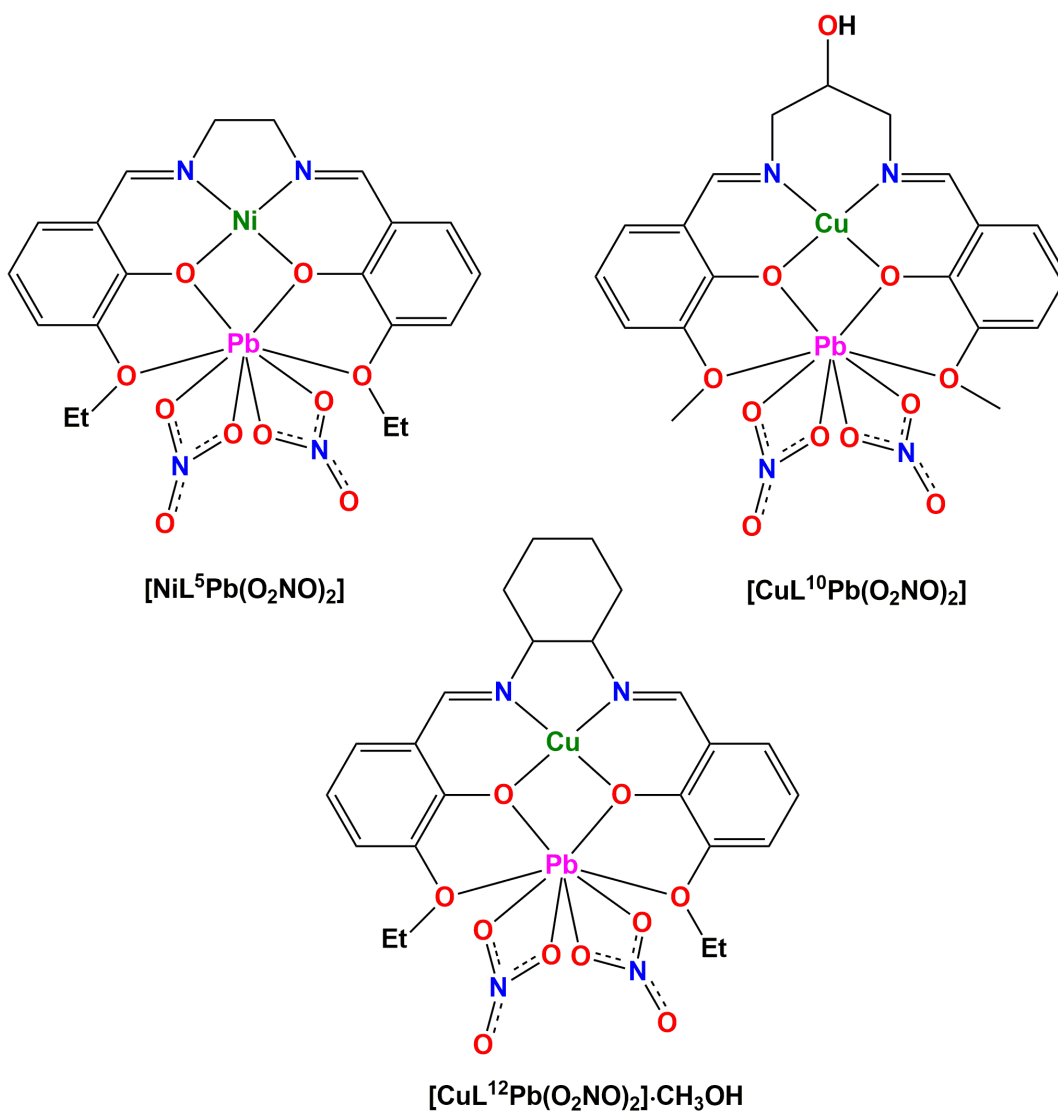


Scheme 6. Schematic representation of $\{[(\mu\text{-adipato})\{\text{Pb}(\text{L}^3\text{Cu})\text{L}^3\text{Cu}(\text{OCIO}_3)\}_2] \cdot 2\text{H}_2\text{O}\}$. Lattice water molecules are not shown for clarity. Lattice solvent molecules are not shown for clarity. CCDC number is 1490213.

Complexes of H_2salen type compartmental ligands

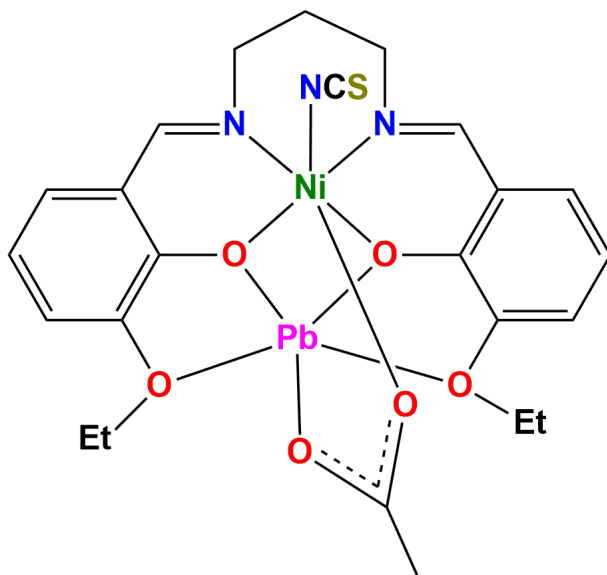
These compartmental ligands have one inner N_2O_2 donor compartment and another outer O_4 donor compartment. They usually act as hexadentate N_2O_4 donor ligands and form dinuclear complexes $\{[\text{NiL}^5\text{Pb}(\text{O}_2\text{NO})_2]\}$, $\{[(\text{H}_2\text{O})(\text{SCN})\text{NiL}^6\text{Pb}(\text{OAc})] \cdot \text{DMSO}\}$, $\{[(\text{SCN})\text{Ni}(\mu\text{-OAc})\text{L}^7\text{Pb}]\}$, $\{[(\text{H}_2\text{O})_2\text{NiL}^7\text{PbBr}_2]\}$, $\{[(\text{H}_2\text{O})_2\text{NiL}^7\text{Pb}(\text{O}_2\text{NO})_2]\}$, $\{[(\text{H}_2\text{O})_2\text{NiL}^7\text{PbCl}_2]\}$, $\{[(\text{H}_2\text{O})(\text{SCN})\text{NiL}^9\text{PbCl}]\}$, $\{[\text{CuL}^{10}\text{Pb}(\text{O}_2\text{NO})_2]\}$, $\{[(\text{H}_2\text{O})\text{CuL}^{11}\text{Pb}(\text{O}_2\text{NO})_2]\}$ and $[\text{CuL}^{12}\text{Pb}(\text{O}_2\text{NO})_2] \cdot \text{CH}_3\text{OH}$, in which the inner N_2O_2 cavity is occupied with copper(II) or nickel(II) and the outer O_4 cavity is occupied with lead(II) (vide infra). The copper(II) or nickel(II) center in the inner cavity is square planar in $\{[\text{NiL}^5\text{Pb}(\text{O}_2\text{NO})_2]\}$, $\{[\text{CuL}^{10}\text{Pb}(\text{O}_2\text{NO})_2]\}$ and

$\{[\text{CuL}^{12}\text{Pb}(\text{O}_2\text{NO})_2] \cdot \text{CH}_3\text{OH}\}$. The perspective views of complexes $\{[\text{NiL}^5\text{Pb}(\text{O}_2\text{NO})_2]\}$, $\{[\text{CuL}^{10}\text{Pb}(\text{O}_2\text{NO})_2]\}$ and $\{[\text{CuL}^{12}\text{Pb}(\text{O}_2\text{NO})_2] \cdot \text{CH}_3\text{OH}\}$ are shown in Scheme 7. In each of these complexes, lead(II) center is coordinated by two nitrate ions. The O-Pb-O angle is ~ 500 and this may indicate that both oxygen atoms are occupying a single coordination site of lead(II) in all three complexes. However, two Pb-O bonds are similar and therefore it is better to consider the nitrate as bidentate.



Scheme 7. Schematic representation of the complexes. Lattice solvent molecules are not shown for clarity. CCDC numbers are 813964, 887314 and 822178.

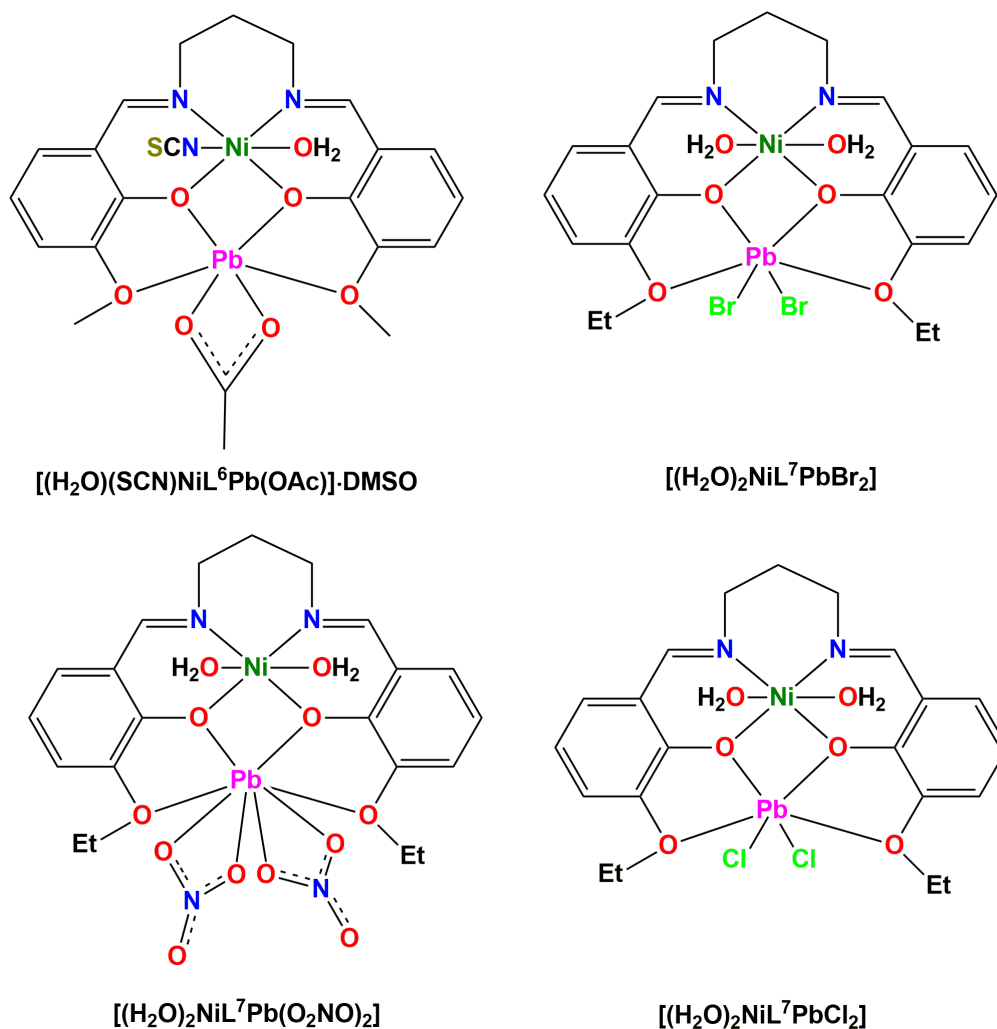
The copper(II) is square pyramidal in $\{[(\text{H}_2\text{O})\text{CuL}^{11}\text{Pb}(\text{O}_2\text{NO})_2]\}$, where the apical position is occupied by monodentate ligand, H_2O . The structure of complex $\{[(\text{SCN})\text{Ni}(\mu\text{-OAc})\text{L}^7\text{Pb}]\}$ is interesting, as here nickel(II) and lead(II) are bridged by an μ -1,3-acetate. The schematic representation of complex $[(\text{SCN})\text{Ni}(\mu\text{-OAc})\text{L}^7\text{Pb}]$ is shown in Scheme 8.



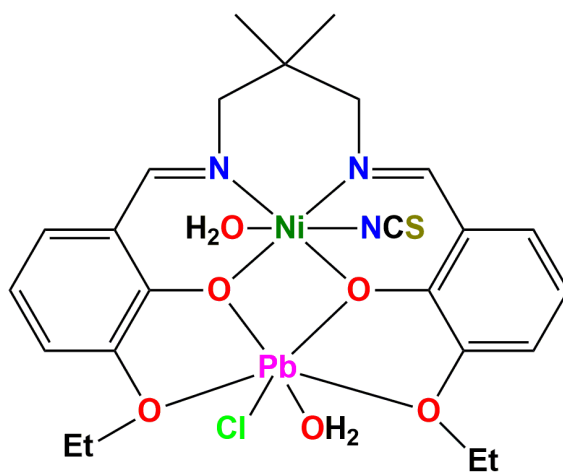
Scheme 8. Schematic representation of $[(\text{SCN})\text{Ni}(\mu\text{-OAc})\text{L}^7\text{Pb}]$. CCDC number is 768722.

The nickel(II) is showing octahedral coordination in each of complexes $\{[(\text{H}_2\text{O})(\text{SCN})\text{NiL}^6\text{Pb}(\text{OAc})]\cdot\text{DMSO}\}$, $\{[(\text{SCN})\text{Ni}(\mu\text{-OAc})\text{L}^7\text{Pb}]\}$, $\{[(\text{H}_2\text{O})_2\text{NiL}^7\text{PbBr}_2]\}$, $\{[(\text{H}_2\text{O})_2\text{NiL}^7\text{Pb}(\text{O}_2\text{NO})_2]\}$, $\{[(\text{H}_2\text{O})_2\text{NiL}^7\text{PbCl}_2]\}$ and $\{[(\text{H}_2\text{O})(\text{SCN})\text{NiL}^9\text{PbCl}]\}$, where the axial positions of nickel(II) may be occupied by some monodentate neutral/anionic co-ligands. Lead(II) is coordinated by appropriate number of anionic co-ligands in each complexes to satisfy the charge balance condition. The schematic representation of complexes

$\{[(\text{H}_2\text{O})(\text{SCN})\text{NiL}^6\text{Pb}(\text{OAc})]\cdot\text{DMSO}\}$, $\{[(\text{H}_2\text{O})_2\text{NiL}^7\text{PbBr}_2]\}$, $\{[(\text{H}_2\text{O})_2\text{NiL}^7\text{Pb}(\text{O}_2\text{NO})_2]\}$,
 $\{[(\text{H}_2\text{O})_2\text{NiL}^7\text{PbCl}_2]\}$ and $\{[(\text{H}_2\text{O})(\text{SCN})\text{NiL}^9\text{PbCl}]\}$ are shown in Scheme 9 and 10.

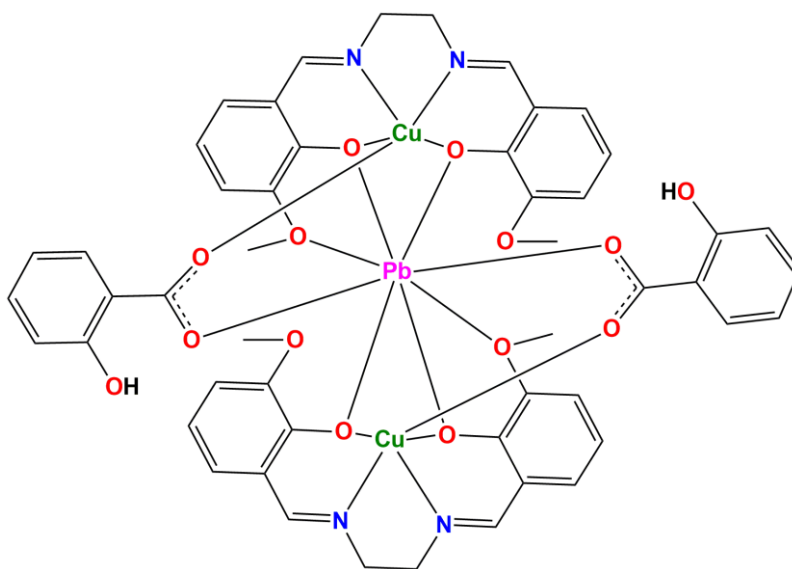


Scheme 9. Schematic representation of the complexes. Lattice solvent molecules are not shown for clarity. CCDC numbers are 1580464, 1038830, 1038831 and 1580465 respectively.



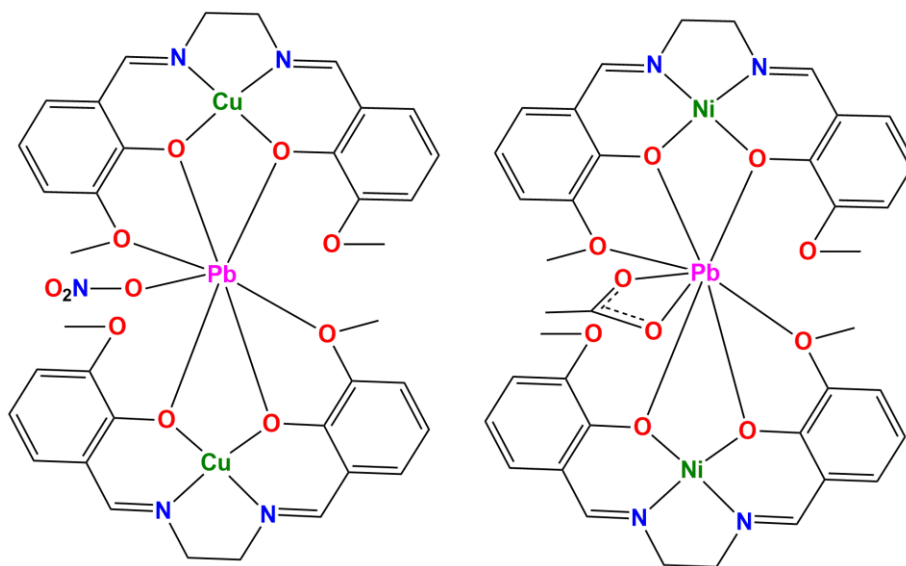
Scheme 10. Schematic representation of $\{[(\text{H}_2\text{O})(\text{SCN})\text{NiL}^9\text{PbCl}]\}$. CCDC no. is 1580467.

N,N'-bis(3-methoxysalicylidene)-1,2-diaminoethane (H_2L^4) forms three trinuclear complexes ($\{[(\mu\text{-Hsal})_2(\text{CuL}^4)_2\text{Pb}]\}$, $\{[(\text{CuL}^4)_2\text{Pb}(\text{ONO}_2)]\text{NO}_3\cdot\text{H}_2\text{O}\}$ and $\{[(\text{NiL}^4)_2\text{Pb}(\text{OAc})]\text{OAc}\cdot\text{H}_2\text{O}\}$) having interesting structures. In complex ($\{[(\mu\text{-Hsal})_2(\text{CuL}^4)_2\text{Pb}]\}$), the potential hexadentate *N,N'*-bis(3-methoxysalicylidene)-1,2-diaminoethane behaves as tetradentate N_2O_2 donor ligand keeping its methoxy part pendant. The central lead(II) is coordinated by the phenoxo groups of two terminal $[\text{CuL}^4]$ units. The schematic representation of central lead(II) and terminal copper(II) ions are additionally bridged by salicylate anion, as shown in Scheme 11.



Scheme 11. Schematic representation of $\{[(\mu\text{-Hsal})_2(\text{CuL}^4)_2\text{Pb}]\}$. CCDC number is 240554.

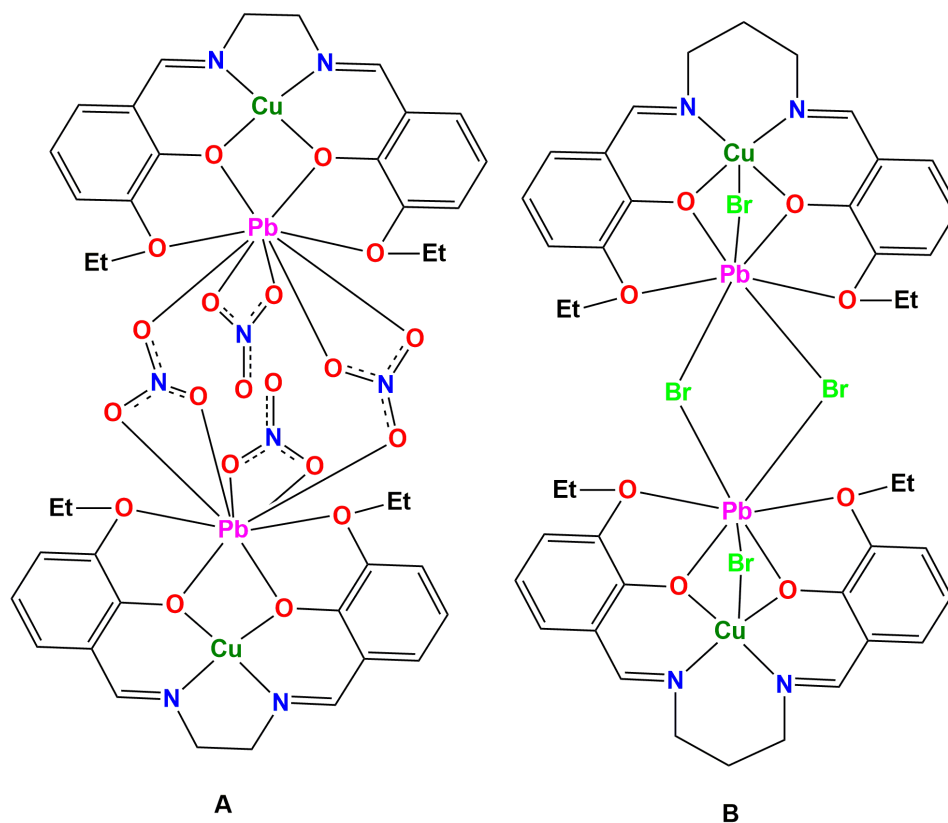
Complexes $\{[(\text{CuL}^4)_2\text{Pb}(\text{ONO}_2)]\text{NO}_3\cdot\text{H}_2\text{O}\}$ and $\{[(\text{NiL}^4)_2\text{Pb}(\text{OAc})]\text{OAc}\cdot\text{H}_2\text{O}\}$ have similar trinuclear skeletons, where the central lead(II) is coordinated by phenoxo and (some) methoxy groups of two ML^4 units $\{\text{M} = \text{copper(II)}$ in $\{[(\text{CuL}^4)_2\text{Pb}(\text{ONO}_2)]\text{NO}_3\cdot\text{H}_2\text{O}\}$ and nickel(II) in $\{[(\text{NiL}^4)_2\text{Pb}(\text{OAc})]\text{OAc}\cdot\text{H}_2\text{O}\}\}$. Central lead(II) is additionally coordinated by a monodentate nitrate in $\{[(\text{CuL}^4)_2\text{Pb}(\text{ONO}_2)]\text{NO}_3\cdot\text{H}_2\text{O}\}$ and an acetate in $\{[(\text{NiL}^4)_2\text{Pb}(\text{OAc})]\text{OAc}\cdot\text{H}_2\text{O}\}$. Again the O-Pb(II)-O formed by the two coordinating oxygen atoms of acetate group and lead(II) is very small ($\sim 470^\circ$). The schematic representation of complexes $\{[(\text{CuL}^4)_2\text{Pb}(\text{ONO}_2)]\text{NO}_3\cdot\text{H}_2\text{O}\}$ and $\{[(\text{NiL}^4)_2\text{Pb}(\text{OAc})]\text{OAc}\cdot\text{H}_2\text{O}\}$ are shown in Scheme 12.



Scheme 12. Schematic representation of $[(\text{CuL}^4)_2\text{Pb}(\text{ONO}_2)]\text{NO}_3\cdot\text{H}_2\text{O}$ (left) and $[(\text{NiL}^4)_2\text{Pb}(\text{OAc})]\text{OAc}\cdot\text{H}_2\text{O}$ (right). Lattice solvent molecules and counter anions are not shown for clarity. CCDC numbers are 240555 and 240557 respectively.

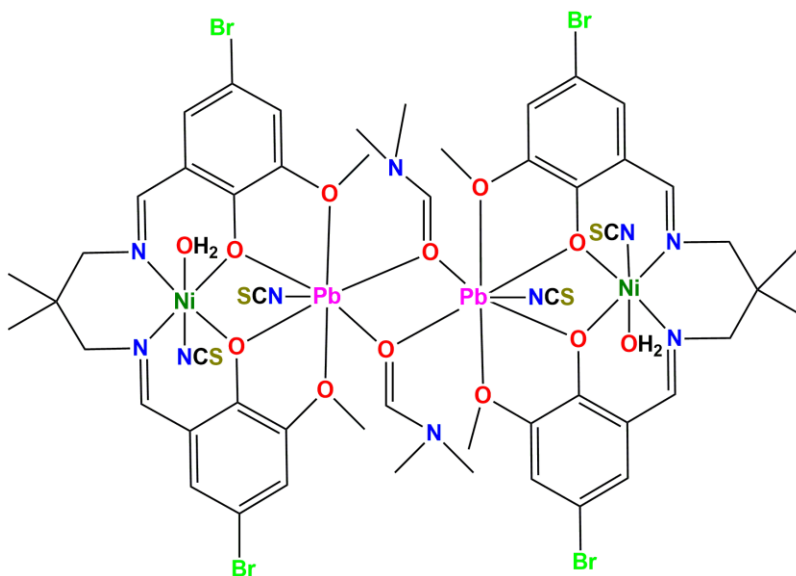
The structure of complex $[(\mu\text{-NO}_3)_2\{(\text{ONO}_2)\text{Pb}(\text{CuL}^5)\}_2]$ is interesting. It is a tetranuclear lead (II)/copper(II) complex and is formed by the joining of two dinuclear $[\text{CuL}^5\text{Pb}(\text{O}_2\text{NO})]$

(Scheme 13A) moieties with nitrate bridges. Complex $[(\mu\text{-Br})_2\{\text{PbL}^7(\mu\text{-Br})\text{Cu}\}_2]$ is a linear tetranuclear complex and is formed by joining two $[\text{CuL}^7\text{Pb}(\text{Br})]$ (Scheme 13B) moieties with bromide bridges.



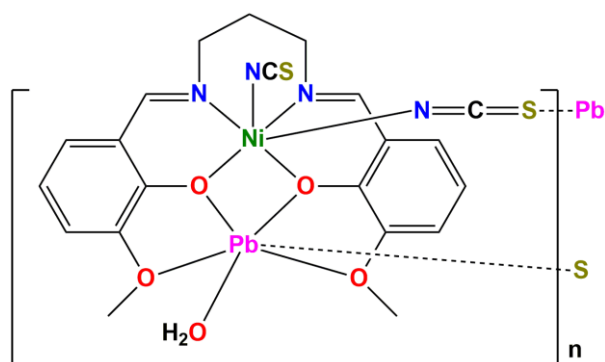
Scheme 13. Schematic representation of $[(\mu\text{-NO}_3)_2\{(\text{ONO}_2)\text{Pb}(\text{CuL}^5)\}_2]$ (A) and $[(\mu\text{-Br})_2\{\text{PbL}^7(\mu\text{-Br})\text{Cu}\}_2]$ (B). CCDC numbers are 735470 and 1038832 respectively.

Complex $\{[(\mu\text{-DMF})_2\{(\text{SCN})\text{PbL}^8\text{Ni}(\text{NCS})(\text{H}_2\text{O})\}_2]\}$ is a linear tetranuclear complex and is formed by joining two $[(\text{SCN})(\text{H}_2\text{O})\text{NiL}^8\text{Pb}]$ moieties with DMF bridges (Scheme 14). Thus the structure of complex $\{[(\mu\text{-DMF})_2\{(\text{SCN})\text{PbL}^8\text{Ni}(\text{NCS})(\text{H}_2\text{O})\}_2]\}$ is very similar to that of complex $[(\mu\text{-DMF})_2\{(\text{H}_2\text{O})\text{NiL}^1\text{Pb}(\text{SCN})\}_2]$, where also a DMF is used to bridge two dinuclear moieties to form a linear tetranuclear structure.



Scheme 14. Schematic representation of $\{[(\mu\text{-DMF})_2\{(\text{SCN})\text{PbL}^8\text{Ni}(\text{NCS})(\text{H}_2\text{O})\}_2]\}$. CCDC number is 1828388.

Complex $[(\text{SCN})\text{NiL}^6\text{Pb}(\mu\text{-SCN})(\text{OH}_2)]_n$ is an 1,3-thiocyanate bridged polymer and is formed from the dinuclear asymmetric unit, $[(\text{NCS})_2\text{NiL}^6\text{Pb}(\text{OH}_2)]$. The schematic representation of $[(\text{SCN})\text{NiL}^6\text{Pb}(\mu\text{-SCN})(\text{OH}_2)]_n$ is shown in Scheme 15.

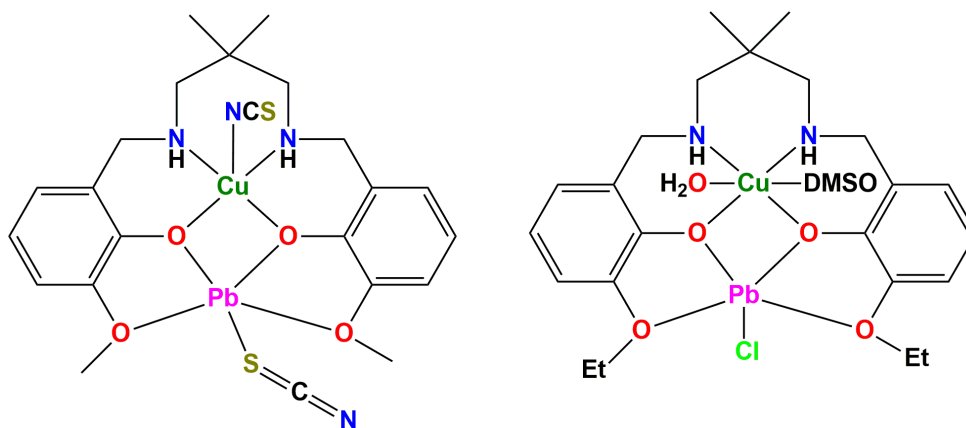


Scheme 15. Schematic representation of $[(\text{SCN})\text{NiL}^6\text{Pb}(\mu\text{-SCN})(\text{OH}_2)]_n$. CCDC number is 1832205.

Complexes with reduced forms of salen type ligands

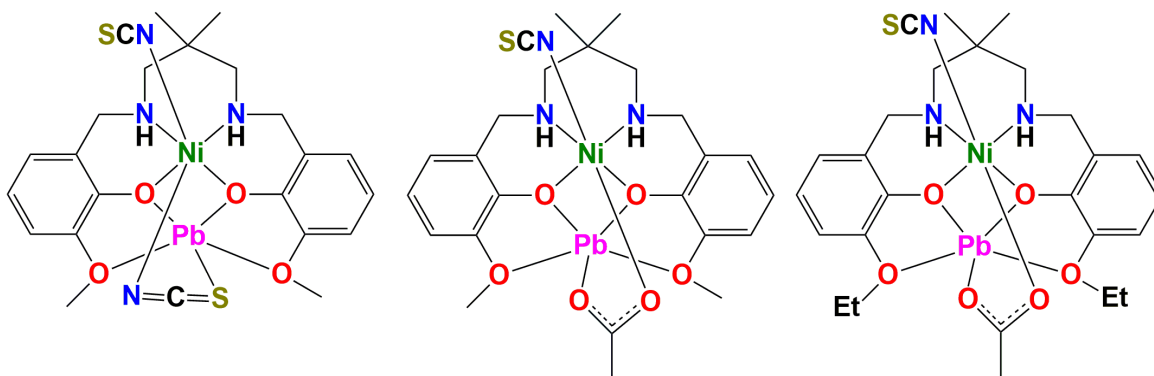
Ligands (2,2-dimethyl-1,3-propanediyl)bis(iminomethylene)bis(6-methoxyphenol) and (2,2-dimethyl-1,3-propanediyl)bis(iminomethylene)bis(6-ethoxyphenol) are compartmental N_2O_4 donor ligands having inner N_2O_2 cavity and outer O_4 cavity; and essentially forms dinuclear $\{[(SCN)CuL^{13}Pb(SCN)]\}$, $\{[(SCN)NiL^{13}(\mu-NCS)Pb]\}$, $\{[(SCN)NiL^{13}(\mu-OAC)Pb]\}$, $\{[(DMSO)(H_2O)NiL^{14}PbCl]NCS\}$ and $\{[(SCN)NiL^{14}(\mu-OAC)Pb]\}$ and trinuclear complexes $\{[(DMSO)NiL^{13}(OH_2)_2Pb](ClO_4)_2\}$ and $\{[(DMSO)NiL^{14}(OH_2)_2Pb](ClO_4)_2 \cdot 4DMSO\}$, all of which are essentially similar in structures with those of the di and trinuclear complexes of N,N' -bis(3-methoxysalicylidene)-1,2-diaminoethane (H_2L^4), N,N' -bis(3-ethoxysalicylidene)-1,2-diaminoethane (H_2L^5), N,N' -bis(3-methoxysalicylidene)-1,3-diaminopropane (H_2L^6), N,N' -bis(3-ethoxysalicylidene)-1,3-diaminopropane (H_2L^7), N,N' -bis(3-methoxysalicylidene)-2,2-dimethyl-1,3-diaminopropane (H_2L^8), N,N' -bis(3-ethoxysalicylidene)-2,2-dimethyl-1,3-diaminopropane (H_2L^9), N,N' -bis(3-methoxysalicylidene)-2-hydroxy-1,3-diaminopropane (H_2L^{10}), N,N' -bis(3-methoxysalicylidene)-1,2-cyclohexanediamine (H_2L^{11}), N,N' -bis(3-methoxysalicylidene)-1,2-phenylenediamine (H_2L^{12}).

Both complexes $\{[(SCN)CuL^{13}Pb(SCN)]\}$ and $\{[(DMSO)(H_2O)NiL^{14}PbCl]NCS\}$ are dinuclear and they are very similar in structure. The metal ion (copper/nickel) is present in the inner N_2O_2 donor compartment of the reduced Schiff bases in both of the complexes and lead(II) is present in the outer O_4 compartment. Lead(II) and copper (II)/nickel(II) are bridged by phenoxo oxygen atoms of the reduced Schiff bases. Additional monodentate ligands coordinate to both lead (II) and copper(II)/nickel(II) to complete their distorted octahedral geometry. The schematic representation of complexes $\{[(SCN)CuL^{13}Pb(SCN)]\}$ and $\{[(DMSO)(H_2O)NiL^{14}PbCl]NCS\}$ are shown in Scheme 16.



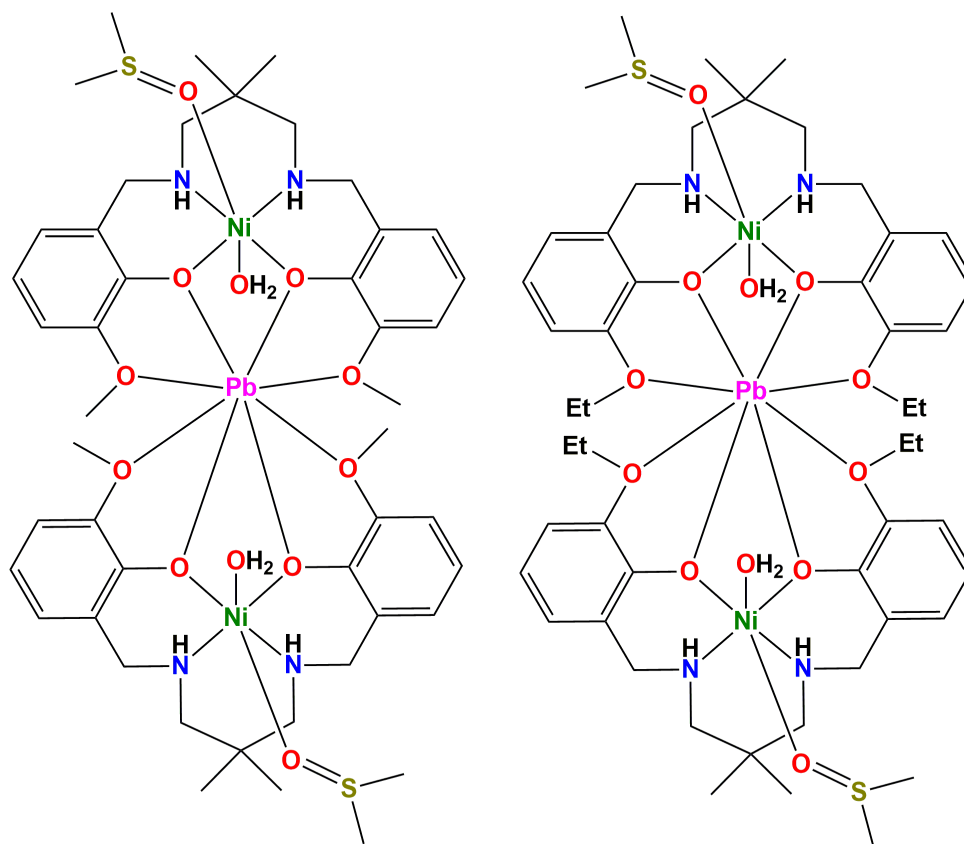
Scheme 16. Schematic representation of $\{[(\text{SCN})\text{CuL}^{13}\text{Pb}(\text{SCN})]\}$ (left) and $\{[(\text{DMSO})(\text{H}_2\text{O})\text{NiL}^{14}\text{PbCl}]\text{NCS}\}$ (right). Counter anion is not shown for clarity. CCDC numbers are 1953301 and 1946110 respectively.

Dinuclear complexes $\{[(\text{SCN})\text{NiL}^{13}(\mu\text{-NCS})\text{Pb}]\}$, $\{[(\text{SCN})\text{NiL}^{13}(\mu\text{-OAC})\text{Pb}]\}$ and $\{[(\text{SCN})\text{NiL}^{14}(\mu\text{-OAC})\text{Pb}]\}$ are more or less similar in structure. In each of these complexes, apart from phenoxo bridging, additional bridging (e.g. thiocynatae in $\{[(\text{SCN})\text{NiL}^{13}(\mu\text{-NCS})\text{Pb}]\}$, acetate in $\{[(\text{SCN})\text{NiL}^{13}(\mu\text{-OAC})\text{Pb}]\}$ and $\{[(\text{SCN})\text{NiL}^{14}(\mu\text{-OAC})\text{Pb}]\}$) is present between lead(II) and copper(II)/nickel(II). The schematic representation of the complexes $\{[(\text{SCN})\text{NiL}^{13}(\mu\text{-NCS})\text{Pb}]\}$, $\{[(\text{SCN})\text{NiL}^{13}(\mu\text{-OAC})\text{Pb}]\}$ and $\{[(\text{SCN})\text{NiL}^{14}(\mu\text{-OAC})\text{Pb}]\}$ are shown in Scheme 17.



Scheme 17. Schematic representation of $[(\text{SCN})\text{NiL}^{13}(\mu\text{-NCS})\text{Pb}]$ (left), $\{[(\text{SCN})\text{NiL}^{13}(\mu\text{-OAC})\text{Pb}]\}$ (middle) and $[(\text{SCN})\text{NiL}^{14}(\mu\text{-OAC})\text{Pb}]$ (right), CCDC numbers are 1938676, 1938677 and 1938678 respectively.

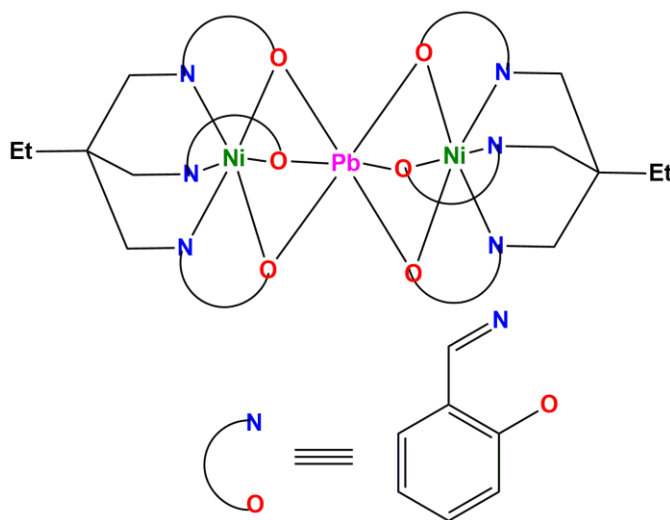
Complexes $\{[(\text{DMSO})\text{NiL}^{13}(\text{OH}_2)_2\text{Pb}](\text{ClO}_4)_2\}$ and $\{[(\text{DMSO})\text{NiL}^{14}(\text{OH}_2)_2\text{Pb}](\text{ClO}_4)_2 \cdot 4\text{DMSO}\}$ are trinuclear complexes (Scheme 18). In both complexes, the central lead(II) is octa-coordinated by four phenoxo and four methoxy oxygen atoms from two $[(\text{DMSO})(\text{H}_2\text{O})\text{NiL}]$ units $\{L = L^{13}$ in $\{[(\text{DMSO})\text{NiL}^{13}(\text{OH}_2)_2\text{Pb}](\text{ClO}_4)_2\}$ and $L = L^{14}$ in $\{[(\text{DMSO})\text{NiL}^{14}(\text{OH}_2)_2\text{Pb}](\text{ClO}_4)_2 \cdot 4\text{DMSO}\}$.



Scheme 18. Schematic representation of $\{[(\text{DMSO})\text{NiL}^{13}(\text{OH}_2)_2\text{Pb}](\text{ClO}_4)_2\}$ (left) and $\{[(\text{DMSO})\text{NiL}^{14}(\text{OH}_2)_2\text{Pb}](\text{ClO}_4)_2 \cdot 4\text{DMSO}\}$ (right). Lattice solvent molecules and counter anions are not shown for clarity. CCDC numbers are 1938679 and 1938680 respectively.

Complexes with tripodal ligands

Complexes $[(\mu\text{-Cl})_2\{(\text{Py})\text{NiL}^{15}\}_2\text{Pb}]$ and $[(\text{NiL}^{16})\text{Pb}]\cdot\text{Py}\cdot\text{H}_2\text{O}$ are formed with the tripodal hexadentate ligands, Tris-((2-hydroxybenzylidene)aminoethyl)amine and 1,1,1-tris-((2-hydroxybenzylidene)-aminomethyl)propane respectively. Complex $\{[(\text{NiL}^{16})_2\text{Pb}]\cdot\text{Py}\cdot\text{H}_2\text{O}\}$ is trinuclear and the central lead(II) is octahedrally coordinated by six phenoxo groups from two molecules of the tripodal ligands, 1,1,1-tris-((2-hydroxybenzylidene)-aminomethyl)propane. The nickel(II) centers are also octahedral and is coordinated by three imine nitrogen atoms and three phenoxo oxygen atoms of the tripodal ligands, 1,1,1-tris-((2-hydroxybenzylidene)-aminomethyl)propane. The schematic representation of complex $\{[(\text{NiL}^{16})\text{Pb}]\cdot\text{Py}\cdot\text{H}_2\text{O}\}$ is shown in Scheme 19. Complex $[(\mu\text{-Cl})_2\{(\text{Py})\text{NiL}^{15}\}_2\text{Pb}]$ is apparently dinuclear, where the nickel(II) center is octahedrally coordinated by three imine nitrogen atoms and three phenoxo oxygen atoms of the tripodal ligands, Tris-((2-hydroxybenzylidene)aminoethyl)amine. However, the chloride attached to lead(II) is interacting with a neighbouring symmetry related lead(II) to form a teranuclear supramolecule. This interaction could best be described as tetrel bonding (vide infra).



Scheme 19. Schematic representation of $[(\text{NiL}^{16})\text{Pb}]\cdot\text{Py}\cdot\text{H}_2\text{O}$. Lattice solvent molecules are not shown for clarity. CCDC number is 661266.

The coordination no of lead(II) in these complexes vary from $[(\text{SCN})\text{Ni}(\mu\text{-OAc})\text{L}^7\text{Pb}]$, $[(\text{H}_2\text{O})_2\text{NiL}^7\text{PbBr}_2]$ and $[(\text{H}_2\text{O})_2\text{NiL}^7\text{Pb}(\text{O}_2\text{NO})_2]$. The geometry of lead(II) center is also different in different complexes. Before discussing the geometry of lead(II) centers in the complexes, we have to decide the role of acetate and nitrate in the complexes. The acetate and nitrate in complexes $\{[\text{NiL}^5\text{Pb}(\text{O}_2\text{NO})_2]\}$, $\{[(\text{H}_2\text{O})(\text{SCN})\text{NiL}^6\text{Pb}(\text{OAc})]\cdot\text{DMSO}\}$, $[(\text{H}_2\text{O})_2\text{NiL}^7\text{Pb}(\text{O}_2\text{NO})_2]$, $[\text{CuL}^{10}\text{Pb}(\text{O}_2\text{NO})_2]$, $[(\text{H}_2\text{O})\text{CuL}^{11}\text{Pb}(\text{O}_2\text{NO})_2]$, $\{[\text{CuL}^{12}\text{Pb}(\text{O}_2\text{NO})_2]\cdot\text{CH}_3\text{OH}\}$, $\{[(\text{CuL}^3)_2\text{Pb}(\text{NO}_3)_2]\}$, $\{[(\text{NiL}^4)_2\text{Pb}(\text{OAc})]\text{OAc}\cdot\text{H}_2\text{O}\}$ and $\{[(\mu\text{-NO}_3)_2\{(\text{ONO}_2)\text{Pb}(\text{CuL}^5)_2\}]\}$ may apparently be considered as a chelating bidentate ligand. However, the value of the bite angle, O–Pb–O created by the two oxygen atoms, is small ($\sim 50^\circ$), we therefore consider that the two oxygen atoms share one axial site, as already discussed before. In other words, it may be considered that the acetate/nitrate group is occupying just one stereochemical site in the coordination sphere of lead(II). The geometry and coordination number of lead(II) in these complexes were therefore calculated assuming acetate/nitrate as a single entity occupying one stereochemical site. Another important is that when the coordination number of lead(II) is 5, the coordination sphere around lead(II) cannot be described as square pyramidal because of the vacancies in the equatorial plane, rather it may better be described as a pentagonal bipyramid with an axial site and an equatorial site unoccupied (e.g. $\{[(\text{H}_2\text{O})(\text{SCN})\text{NiL}^6\text{Pb}(\text{OAc})]\cdot\text{DMSO}\}$, $\{[(\text{SCN})\text{Ni}(\mu\text{-OAc})\text{L}^7\text{Pb}]\}$, $\{[(\text{H}_2\text{O})(\text{SCN})\text{NiL}^9\text{PbCl}]\}$, $\{[(\text{SCN})\text{CuL}^{13}\text{Pb}(\text{SCN})]\}$, $\{[(\text{SCN})\text{NiL}^{13}(\mu\text{-NCS})\text{Pb}]\}$, $\{[(\text{SCN})\text{NiL}^{13}(\mu\text{-OAc})\text{Pb}]\}$, $\{[(\text{DMSO})(\text{H}_2\text{O})\text{NiL}^{14}\text{PbCl}]\text{NCS}\}$, $\{[(\text{SCN})\text{NiL}^{14}(\mu\text{-OAc})\text{Pb}]\}$ etc). Similarly, when the coordination number of lead(II) is six, the geometry is best described as pentagonal bipyramid

with one equatorial site unoccupied in most of the cases (e.g. $\{[\text{NiL}^5\text{Pb}(\text{O}_2\text{NO})_2]\}$, $\{[(\text{H}_2\text{O})_2\text{NiL}^7\text{PbBr}_2]\}$, $\{[(\text{H}_2\text{O})_2\text{NiL}^7\text{Pb}(\text{O}_2\text{NO})_2]_6\}$, $\{[(\text{H}_2\text{O})_2\text{NiL}^7\text{PbCl}_2]\}$, $\{[\text{CuL}^{10}\text{Pb}(\text{O}_2\text{NO})_2]\}$, $\{[(\text{H}_2\text{O})\text{CuL}^{11}\text{Pb}(\text{O}_2\text{NO})_2]\}$, $\{[\text{CuL}^{12}\text{Pb}(\text{O}_2\text{NO})_2]\cdot\text{CH}_3\text{OH}\}$ etc) in complexes. In some cases, e.g. in complexes $\{[(\text{CuL}^1)_2\text{Pb}(\text{OCIO}_3)_2]\}$, $\{[(\text{CuL}^1)_2\text{Pb}(\text{NCS})_2]\}$, $\{[(\text{CuL}^1)_2\text{PbCl}_2]\}$, $\{[(\text{CuL}^1)_2\text{PbI}_2]\}$, $\{[(\text{CuL}^2)_2\text{Pb}(\text{NCS})_2]\}$, the coordination number of lead(II) is 6 and their geometry is best described as distorted octahedral. The coordination number of lead(II) is 4 with tetrahedral geometry in complex $\{[(\text{Py})_2\text{Ni}(\mu\text{-L}^1)\text{PbCl}_2]\cdot\text{Py}\}$.

References

- 1 (a) J. Li, D. Gryko, R. B. Dabke, J. R. Diers, D. F. Bocian, W. G. Kuhr and J. S. Lindsey, *J. Org. Chem.*, 2000, **65**, 7379; (b) T. Gross, F. Chevalier and J. S. Lindsey, *Inorg. Chem.*, 2001, **40**, 4762; (c) M. S. Fataftah, S. C. Coste, B. Vlasisavljevich, J. M. Zadrozny and D. E. Freedman, *Chem. Sci.*, 2016, **7**, 6160; (d) O. Sato, *Acc. Chem. Res.*, 2003, **36**, 692.
- 2 (a) L. Ouahab, *Coord. Chem. Rev.*, 1998, **178-180**, 1501; (b) H. Tamaki, Z. J. Zhong, N. Matsumoto, S. Kida, M. Koikawa, N. Achiwa, Y. Hashimoto and H. Okawa, *J. Am. Chem. Soc.*, 1992, **114** (**18**), 6974; (c) M. Kato and Y. Muto, *Coord. Chem. Rev.*, 1988, **92**, 45; (d) D. MasPOCH, D. Ruiz-Molina, K. WurSt, N. Domingo, M. Cavallini, F. Biscarini, J. Tejada, C. ovira and J. Veciana, *Nat. Mater.*, 2003, **2**, 190; (e) K. Fegy, D. Luneau, T. Ohm, C. Paulsen and P. Rey, *Angew. Chem. Int. Ed.*, 1998, **37**, 1270.
- 3 (a) L. L. Welbes and A. S. Borovik, *Acc. Chem. Res.*, 2005, **38**, 765; (b) S.-I. Noro, K. Fukuhara, K. Sugimoto, Y. Hijikata, K. Kuboa and T. Nakamura, *Dalton Trans.*, 2013, **42**, 11100; (c) S. Stepanow, M. Lingenfelder, A. Dmitriev, H. Spillmann, E. Delvigne, N. Lin, X. Deng, C. Cai, J. V. Barth and K. Kern, *Nat. Mater.*, 2004, **3**, 229; (d) A. M. Beatty, *Coord. Chem. Rev.*, 2003, **246**, 131; (e) S. Kitagawa, R. Kitaura and S.-I. Noro, *Angew. Chem. Int. Ed.*, 2004, **43**, 2334.
- 4 (a) V. Balzani, S. Campagna, G. Denti, A. Juris, S. Serroni and M. Venturi, *Acc. Chem. Res.*, 1998, **31**, 26; (b) R. C. Evans, P. Douglas and C. J. Winscom, *Coord. Chem. Rev.*, 2006, **250**, 2093; (c) C.-Y. Chen, M. Wang, J.-Y. Li, N. Pootrakulchote, L. Alibabaei, C.-H Ngocle, J.-D. Decoppet, J.-H. Tsai, C. Gratzel, C.-G. Wu, S. M. Zakeeruddin and M. Gratzel, *ACS Nano*, 2009, **3**, 3103; (d) Y. Kobuke, *Eur. J. Inorg. Chem.*, 2006, 2333; (e) T. Miyatake, H. Tamiaki, A. R. Holzwarth and K. Schaffner, *Helv. Chim. Acta*, 1999, **82**, 797.

5 (a) A. Toscani, K. A. Jantan, J. B. Hena, J. A. Robson, E. J. Parmenter, V. Fiorini, A. J. P. White, S. Stagni and J. D. E. T. Wilton-Ely, *Dalton Trans.*, 2017, **46**, 5558; (b) C. T. L. Ma and M. J. MacLachlan, *Angew. Chem. Int. Ed.*, 2005, **44**, 4178; (c) S. Mitzinger, L. Broeckeaert, W. Massa, F. Weigend and S. Dehnen, *Nat. Commun.*, 2016, **7**, 10480; (d) R. Sherwood, F. G. de Rivera, J. H. Wan, Q. Zhang and A. J. P. White, *Inorg. Chem.*, 2015, **54**, 4222; (e) K. Oliver, A. J. P. White, G. Hogarth and J. D. E. T. Wilton-Ely, *Dalton Trans.*, 2011, **40**, 5852; (f) J. F. Berry and C. M. Thomas, *Dalton Trans.*, 2017, **46**, 5472; (g) P. Buchwalter, J. Rosé and P. Braunstein, *Chem. Rev.*, 2015, **115**, 28; (h) S. Sung, H. Holmes, L. Wainwright, A. Toscani, G. J. Stasiuk, A. J. P. White, J. D. Bell and J. D. E. T. Wilton-Ely, *Inorg. Chem.*, 2014, **53**, 1989; (i) V. Ramamurthy and K. S. Schanze, *Multimetallic and Macromolecular Inorganic Photochemistry*, Marcel Dekker Inc. New York, 1997; (j) R. Sherwood, F. G. de Rivera, J. H. Wan, Q. Zhang, A. J. P. White, O. Rossell, G. Hogarth and J. D. E. T. Wilton-Ely, *Inorg. Chem.*, 2015, **54**, 4222; (k) R. C. Cammarota, M. V. Vollmer, J. Xie, J. Ye, J. C. Linehan, S. A. Burgess, A. M. Appel, L. Gagliardi and C. C. Lu, *J. Am. Chem. Soc.*, 2017, **139**, 14244; (l) G. Wang, Y. S. Ceylan, T. R. Cundari and H. V. R. Dias, *J. Am. Chem. Soc.*, 2017, **139**, 14292; (m) P. J. Connors, D. Tzalis, A. L. Dunnick, and Y. Tor, *Inorg. Chem.*, 1998, **37**, 1121.

6 (a) D. W. Christianson and C. A. Fierke, *Acc. Chem. Res.*, 1996, **29**, 331; (b) R. L. D'Ordine, R. S. Linger, C. J. Thai and V. J. Davisson, *Biochemistry*, 2012, **51**, 5791; (c) A. Majumdar, *Dalton Trans.*, 2014, **43**, 12135; (d) M. Balamurugan, E. Suresh and M. Palaniandavar, *Dalton Trans.*, 2016, **45**, 11422; (e) M. Costas, M. P. Mehn, M. P. Jensen and L. Que, Jr, *Chem. Rev.*, 2004, **104**, 939; (f) X. Engelmann, I. Monte-Perez and K. Ray, *Angew. Chem. Int. Ed.*, 2016, **55**, 7632; (g) M.

L. Zastrow and V. L. Pecoraro, *J. Am. Chem. Soc.*, 2013, **135**, 5895; (h) B. Hinnemann, P. G. Moses, J. Bonde, K. P. Jørgensen, J. H. Nielsen, S. Horch, I. Chorkendorff and J. K. Nørskov, *J. Am. Chem. Soc.*, 2005, **127**, 5308; (i) Y. lu, *Angew. Chem. Int. Ed.*, 2006, **45**, 5588; (j) L. Que Jr and W. B. Tolman, *Nature*, 2008, **455**, 333.

7 (a) J. He, P. Zhou, N. Jiao, S. Y. Ma, K. W. Zhang, R. Z. Wang and L. Z. Sun, *Sci. Rep.*, 2014, **4**, 1; (b) P. G. Bomben, K. C. D. Robson, P. A. Sedach and C. P. Berlinguette, *Inorg. Chem.*, 2009, **48**, 9631; (d) X. Zhang, Z.-K. Chen and K. P. Loh, *J. Am. Chem. Soc.*, 2009, **131**, 7210; (e) P. D. Frischmann, K. Mahata and F. Wurthner, *Chem. Soc. Rev.*, 2013, **42**, 1847.

8 (a) G. J. Meyer, *Inorg. Chem.*, **2005**, **44**, 6852; (b) K. S. Schanze and K. A. Walters, *Photoinduced Electron Transfer in Metal-Organic Dyads. In Molecular and Supramolecular Photochemistry*, V. Ramamurthy, K. S. Schanze, Eds.; Marcel Dekker: New York, 1999; Vol. **8**, Chapter 3, pp 75-126; (c) T. Tezgerevska, K. G. Alley and C. Boskovic, *Coord. Chem. Rev.*, 2014, **268**, 23; (d) R. R. Gagne, C. A. Koval, T. J. Smith and M. C. Cimolino, *J. Am. Chem. Soc.*, 1979, **131**, 4571.

9 (a) V. Balzani, *Electron Transfer in Chemistry* (Wiley-VCH, 2001); (b) S. Cho, M. W. Mara, X. Wang, J. V. Lockard, A. A. Rachford, F. N. Castellano and L. X. Chen, *J. Phys. Chem. A*, 2011, **115**, 3990; (c) N. S. Hush, *Prog. Inorg. Chem.*, 1967, **8**, 391.

10 (a) S. Santi, A. Bisello, R. Cardena and A. Donoli, *Dalton Trans.*, 2015, **44**, 5234; (b) M. Krockel, A. X. Trautwein, H. Winkler, D. Coucouvanis, A. Kostikas and V. Papaefthymiou, *Inorg. Chim. Acta*, 1998, **283**, 111; (c) S. V. Kruppa, F. Bappler, C. Holzer, W. Kloppe, R. Diller and C. Riehn, *J. Phys. Chem. Lett.*, 2018, **9**, 804; (d) A. Bencini, I. Ciofini, C. A. Daul and A. Ferretti, *J. Am. Chem. Soc.*, 1999, **121**, 11418.

- 11 (a) J. F. Endicott and Y.-J. Chen, *Coord. Chem. Rev.*, 2013, **257**, 1676; (b) P. J. Hay, J. C. Thibeault and R. Hoffmann, *J. Am. Chem. Soc.*, 1975, **131**, 4884; (c) A. Bencini, F. Totti, C. A. Daul, K. Doclo, P. Fantucci and V. Barone, *Inorg. Chem.*, 1997, **36**, 5022; (d) K. Fink, C. Wang and V. Staemmler, *Inorg. Chem.*, 1999, **38**, 3847.
- 12 I. Mondal, S. Chattopadhyay, *J. Coord. Chem.* 72 (2019) 3183–3209.
- 13 S. Banerjee, P. Ghorai, P. Sarkar, A. Panja, A. Saha, *Inorg. Chim. Acta* 499 (2020), 119176.
- 14 P. Bhowmik, H.P. Nayek, M. Corbella, N. Aliaga-Alcalde, S. Chattopadhyay, *Dalton Trans.* 40 (2011) 7916–7926.
- 15 K. Ghosh, K. Harms, A. Bauzá, A. Frontera, S. Chattopadhyay, *Dalton Trans.* 47 (2018) 331–347.
- 16 P. Mukherjee, C. Biswas, M.G.B. Drew, A. Ghosh, *Polyhedron* 26 (2007) 3121–3128.
- 17 S. Ghosh, S. Biswas, A. Bauza, M. Barceló-Oliver, A. Frontera, A. Ghosh, *Inorg. Chem.* 52 (2013) 7508–7523.
- 18 P. Mahapatra, S. Ghosh, S. Giri, V. Rane, R. Kadam, M.G.B. Drew, A. Ghosh, *Inorg. Chem.* 56 (2017) 5105–5121.
- 19 A. Panja, N. Shaikh, P. Vojtišek, S. Gao, P. Banerjee, *N. J. Chem.* 26 (2002) 1025–1028.
- 20 A. Panja, N. Shaikh, M. Ali, P. Vojtišek, P. Banerjee, *Polyhedron* 22 (2003) 1191–1198.
- 21 R. Karmakar, C.R. Choudhury, G. Bravic, J.P. Sutter, S. Mitra, *Polyhedron* 23 (2004) 949–954.
- 22 S. Saha, A. Sasmal, C.R. Choudhury, C.J. Gómez-García, E. Garribba, S. Mitra, *Polyhedron* 69 (2014) 262–269.
- 23 T.K. Ghosh, P. Mahapatra, S. Jana, A. Ghosh, *Cryst. Eng. Comm.* 21 (2019) 4620–4631.
- 24 M. Karmakar, S. Chattopadhyay, *J. Mol. Struct.* 1186 (2019) 155–186.

- 25 N. Sarkar, M.G.B. Drew, K. Harms, A. Batuza, A. Frontera, S. Chattopadhyay, *Cryst. Eng. Comm.* 20 (2018) 1077–1086.
- 26 T. Basak, K. Ghosh, C.J. Gomez-Garcia, S. Chattopadhyay, *Polyhedron* 146 (2018) 42–54.
- 27 S. Chattopadhyay, M.G.B. Drew, A. Ghosh, *Eur. J. Inorg. Chem.* (2008) 1693–1701.
- 28 K. Ghosh, S. Banerjee, S. Chattopadhyay, *Cryst. Eng. Comm.* 21 (2019) 6026–6037.
- 29 S. Chattopadhyay, G. Bocelli, A. Musatti, A. Ghosh, *Inorg, Chem. Comm.* 9 (2006) 1053–1057.
- 30 S. Roy, M.G.B. Drew, A. Bauza, A. Frontera, S. Chattopadhyay, *N. J. Chem.* 42 (2018) 6062–6076.
- 31 S. Biswas, R. Saha, A. Ghosh, *Organometallics* 31 (10) (2012) 3844–3850.
- 32 D. Majumdar, T.K. Pal, S.A. Sakib, S. Das, K. Bankura, D. Mishra, *Inorg, Chem. Comm.* 128 (2021), 108609.
- 33 M. Nayak, S. Sarkar, S. Hazra, H.A. Sparkes, J.A.K. Howard, S. Mohanta, *Cryst. Eng. Comm.* 13 (2011) 124–132.
- 34 S. Sarkar, S. Mohanta, *RSC Adv.* 1 (2011) 640–650.
- 35 S. Roy, A. Bhattacharyya, S. Purkait, A. Bouza, A. Frontera, S. Chattopadhyay, *Dalton Trans.* 45 (2016) 15048–15059.
- 36 T. Ghosh Dastidar, K. Ghosh, M.G.B. Drew, R.M. Gomila, A. Frontera, S. Chattopadhyay, *Polyhedron* 222 (2022), 115862.
- 37 A. Hazari, A. Ghosh, *J. Ind. Chem. Soc.* 95 (2018) 1597–1606.
- 38 K. Ghosh, K. Harms, S. Chattopadhyay, *Polyhedron* 123 (2017) 162–175.
- 39 S. Ghosh, A. Ghosh, *Inorg. Chim. Acta* 442 (2016) 64–69.

- 40 K. Ghosh, K. Harms, A. Bauzá, A. Frontera and S. Chattopadhyay, *Dalton Trans.*, 2018, 47, 331–347.
- 41 P. Bhowmik, K. Harms and S. Chattopadhyay, *Polyhedron*, 2013, 49, 113–120.
- 42 S. Roy, M. G. B. Drew, A. Bauza, A. Frontera and S. Chattopadhyay, *New J. Chem.*, 2018, 42, 6062–6076.
- 43 H. Wang, D. Zhang, Z. H. Ni, X. Li, L. Tian and J. Jiang, *Inorg. Chem.*, 2009, 48, 5946–5956.
- 44 S. Roy, I. Mondal, K. Harms and S. Chattopadhyay, *Polyhedron*, 2019, 159, 265–274.
- 45 A. Biswas, L. K. Das, M. G. B. Drew, G. Aromí, P. Gamez and A. Ghosh, *Inorg. Chem.*, 2012, 51, 7993–8001.
- 46 A. Hazari, S. Giri, C. Diaz and A. Ghosh, *Polyhedron*, 2016, 118, 70–80.
- 47 A. Hazari, C. J. Gómez-García, M. G. B. Drew and A. Ghosh, *Polyhedron*, 2017, 138, 145–153.
- 48 S. Roy, A. Dey, M. G. B. Drew, P. P. Ray and S. Chattopadhyay, *New J. Chem.*, 2019, 43, 5020–5031.
- 49 A. Hazari, C. Diaz and A. Ghosh, *Polyhedron*, 2018, 142, 16–24.
- 50 J. Reglinski, S. Morris, D.E. Stevenson, *Polyhedron* 21 (2002) 2167–2174.
51. S. Sarkar, S. Mohanta, *RSC Advances* 1 (2011) 640–650.
52. S. Roy, M.G.B. Drew, A. Bauza, A. Frontera, S. Chattopadhyay, *New J. Chem.* 42 (2018) 6062–6076.
53. S. Bhattacharya, S. Mohanta, *Inorg. Chim. Acta* 432 (2015) 169–175.
54. M. Dolai, T. Mistri, A. Panja, M. Ali, *Inorg. Chim. Acta* 399 (2013) 95–104.
55. E.C. Constable, G. Zhang, C.E. Housecroft, M. Neuburger, J.A. Zampese, *Inorg. Chim. Acta* 363 (2010) 4207–4213.

56. S. Mondal, S. Hazra, S. Sarkar, S. Sasmal, S. Mohanta, *J. Mol. Struct.* 1004 (2011) 204–214.
57. S. Mirdya, S. Banerjee, S. Chattopadhyay, *CrystEngComm* 22 (2020) 237–247.
58. S. Mirdya, S. Roy, S. Chatterjee, A. Bauza, A. Frontera, S. Chattopadhyay, *Cryst. Growth Des.* 19 (2019) 5869–5881.
59. S. Mirdya, A. Frontera, S. Chattopadhyay, *CrystEngComm* 21 (2019) 6859–6868.
60. P. Chakraborty, S. Mohanta, *Inorg. Chim. Acta* 455 (2017) 70–80.
61. S. Biswas, A. Ghosh, *I.J. Chem, Sect. A: Inorg., Bio-inorg., Phys., Theor. Anal. Chem.* 50 (2011) 1356–1362.
62. O. Atakol, S. Durmus, Z. Durmus, C. Arici, B. Cicek, *Synth. React. Inorg. Met. -Org. Chem.* 31 (2001) 1689–1704.
63. M. Sari, S. Durmus, O. Atakol, I. Svoboda, H. Fuess, *Acta Cryst.* 57E (2001) m201–m203.
64. J.H. Thurston, C.-G.-Z. Tang, D.W. Trahan, K.H. Whitmire, *Inorg. Chem.* 43 (2004) 2708–2713.
65. R. Kurtaran, L.T. Yildirim, A.D. Azaz, H. Namli, O. Atakol, *J. Inorg. Biochem.* 99 (2005) 1937–1944.
66. S. Hazra, S. Sasmal, M. Nayak, H.A. Sparkes, J.A.K. Howard, S. Mohanta, *CrystEngComm* 12 (2010) 470–477.
67. S. Roy, A. Dey, M.G.B. Drew, P.P. Ray, S. Chattopadhyay, *New J. Chem.* 43 (2019) 5020–5031.
68. A. Mustapha, K. Busch, M. Patykiewicz, A. Apedaile, J. Reglinski, A.R. Kennedy, T. J. Prior, *Polyhedron* 27 (2008) 868–878.
69. S. Roy, S. Halder, M.G.B. Drew, P.P. Ray, S. Chattopadhyay, *ACS Omega* 3 (2018) 12788–12796.

70. D. Visinescu, J.-P. Sutter, C.R. Perez, M. Andruh, *Inorg. Chim. Acta* 359 (2006) 433–440.
71. H.L. Wang, K. Wang, W. Cao, M. Bai, Y.Z. Bian, J.Z. Jiang, *Sci. China. Chem.* 55 (2012) 978–986.
72. M. Tadokoro, H. Sakiyama, N. Matsumoto, M. Kodera, H. Okawa, S. Kida, *J. Chem. Soc., Dalton Trans* (1992) 313–317.
73. M. Yonemura, Y. Matsumura, H. Furutachi, M. Ohba, H. Okawa, D.E. Fenton, *Inorg. Chem.* 36 (1997) 2711–2717.
74. M. Tadokoro, H. Okawa, N. Matsumoto, M. Koikawa, S. Kida, *J. Chem. Soc., Dalton Trans* (1991) 1657–1663.
75. H. Okawa, J. Nishio, M. Ohba, M. Tadokoro, N. Matsumoto, M. Koikawa, S. Kida, D.E. Fenton, *Inorg. Chem.* 32 (1993) 2949–2957.
76. K. Inoue, M. Ohba, H. Okawa, *Bull. Chem. Soc. Jpn.* 75 (2002) 99–107.
77. T. Shiga, T. Nakanishi, M. Ohba, H. Okawa, *Polyhedron* 24 (2005) 2732–2736.
78. V. Krisyuk, S.U. kyzy, T.V. Rybalova, I. Baidina, I. Korolkov, D. Chizhov, D. Bazhin, Y. Kudyakova, *J. Coord. Chem.* 71 (2018) 2194–2208.
79. I.A. Baidina, V.V. Krisyuyk, I.V. Korol'kov, P.A. Stabnikov, *Zh. Strukt. Khim. (Russ.) (J. Struct. Chem.)* 52 (2011) 1008–1011.
80. M. Shahid, M. Hamid, M. Mazhar, J. Akhtar, M. Zeller, A.D. Hunter, *Inorg. Chem. Commun.* 14 (2011) 288–291.
81. O.Y. Vassilyeva, L.A. Kovbasyuk, V.N. Kokozay, B.W. Skelton, W. Linert, *Polyhedron* 17 (1998) 85–91.
82. V.V. Krisyuk, S.V. Tkachev, I.A. Baidina, I.V. Korolkov, A.E. Turgambaeva, I. K. Igumenov, *J. Coord. Chem.* 68 (2015) 1890–1902.

83. L.A. Kovbasyuk, O.Y. Vassilyeva, V.N. Kokozay, W. Linert, J. Reedijk, B.W. Skelton, A.G. Oliver, J. Chem. Soc., Dalton Trans (1998) 2735–2738.
84. L.A. Kovbasyuk, O.Y. Vassilyeva, V.N. Kokozay, W. Linert, P.R. Raithby, J. Chem. Res (1999) 670–671.
85. O.Y. Vassilyeva, V.N. Kokozay, N.A. Zhukova, L.A. Kovbasyuk, Polyhedron 16 (1997) 263–266.
86. L.A. Kovbasyuk, O.Y. Vassilyeva, V.N. Kokozay, W. Linert, Z. Naturforsch B, Chem. Sci. 52 (1997) 337–339.
87. I.A. Baidina, V.V. Krysyuk, E.V. Peresyphkina, P.A. Stabnikov, Zh Strukt. Khim. (Russ.) (J. Struct. Chem.) 49 (2008) 489–493.
88. A.S. Berezin, V.V. Krisyuk, V.A. Nadolinny, I.A. Baidina, G.V. Romanenko, E. V. Korotaev, J. Coord. Chem. 70 (2017) 3434–3448.
89. X. Li, R. Cao, Z. Guo, J. Lu, Chem. Commun. (2006) 1938–1940.
90. A. Navulla, A.A. Tsirlin, A.M. Abakumov, R.V. Shpanchenko, H. Zhang, E. V. Dikarev, J. Am. Chem. Soc. 133 (2011) 692–694.

Section IB

Materials and details of instrumentation

I.B.1. Materials

All the starting materials and solvents used were purchased from Sigma-Aldrich, India (Presently Merck, India) and were of reagent grade. They were used as received, without any further purification. All syntheses and manipulations were carried out under aerobic conditions.

Caution!!!

Metal complexes containing azide or perchlorate are potentially explosive, particularly in presence of organic ligands. To avoid any troubles during the experimental work with such complexes, only a small amount of such material should be prepared, and it should be handled with great care.

I.B.2. Details of instrumentation

I.B.2.1. Physical Measurements

Elemental analyses (carbon, hydrogen and nitrogen) were performed using a PerkinElmer 240C elemental analyzer. Solid state infrared spectra in KBr pellets (4500-500 cm⁻¹) were recorded with a Perkin Elmer Spectrum Two spectrophotometer. The concentration of samples in KBr was kept in the range of 0.2% to 1% (Too much high concentration usually causes difficulties obtaining clear pellets). Electronic spectra (900-200nm) for the synthesized complexes were recorded on a Perkin Elmer Lambda 35 UV-visible spectrophotometer in

acetonitrile medium. The X-ray powder diffractograms were collected for polycrystalline samples of the complexes using a 0.7 mm glass capillary that were mounted and aligned on an Empyrean PANalytical powder diffractometer, using Cu-K α radiation ($\lambda = 1.54177 \text{ \AA}$). A total of 3 scans were collected at room temperature in the 2θ range of 5-40°. The experimental PXRD patterns of the bulk products were in good agreement with the simulated XRD patterns from single crystal X-ray diffraction results, indicating consistency of the bulk samples. The simulated patterns of the complexes were calculated from the single crystal structural data (cifs) using the CCDC Mercury software.

1.B.2.2. Hirshfeld Surface analyses

Hirshfeld surfaces [1-2] and the associated two-dimensional (2D) fingerprint [3-5] plots were calculated using Crystal Explorer,⁶ with bond lengths to hydrogen atoms set to standard values. [7] For a given crystal structure and set of spherical atomic electron densities, the Hirshfeld surface is unique [8] and thus it suggests the possibility of gaining additional insight into the intermolecular interaction of molecular crystals.

1.B.2.3. X-ray crystallography

Suitable single crystals of the complexes were used for data collection using a 'Bruker D8 QUEST area detector' diffractometer equipped with graphite-monochromated Mo K α radiation ($\lambda = 0.71073 \text{ \AA}$). The molecular structures were solved by direct method and specially the data of complex **12** was further improved using OLEX2. [9] Refinement was done by full-matrix least squares on F² using different SHELX packages [10]. Non-hydrogen atoms were refined with anisotropic thermal parameters. Hydrogen atoms attached to nitrogen atoms were located by difference Fourier maps and were kept at fixed positions. All other hydrogen atoms

were placed in their geometrically idealized positions and constrained to ride on their parent atoms. Multi-scan empirical absorption corrections were applied to the data using the program SADABS [11].

1.B.2.4. Figures and graphics

All the figures were plotted using DIAMOND [12], ORTEP-3 [13], POV-Ray [14] and structures were analyzed with Mercury v 2.3 [15].

1.B.2.5. Computational details

The energies of the complexes **1-4** were computed at the B3LYP-D/def2-SVP level of theory using the crystallographic coordinates by means of the Gaussian-09 program [16]. The Grimme's dispersion [17] correction has also been used since it is adequate for the evaluation of non-covalent interactions. The basis set superposition error for the calculation of interaction energies has been corrected using the counterpoise method [18]. The NCI index and NCI plot [19] isosurfaces have been used to characterize the non-covalent interactions. They correspond to both favorable and unfavorable interactions, as differentiated by the sign of the second density Hessian eigen value and defined by the isosurface color. The color scheme is a red-yellow-green-blue scale with red for q_{+cut} (repulsive) and blue for q_{-cut} (attractive), whereas yellow and green isosurfaces correspond to weak repulsive and weak attractive interactions, respectively [20].

All geometry optimizations of complex **5** are carried out using the density functional theory method at the B3LYP level with the Gaussian 09 program package. The Los Alamos effective core potential lanL2-DZ basis set was employed for the Pb and Cu atoms. On the other hand, the split-valence 6-31G(d) basis set was applied for the other atoms. The starting

structure of the investigated complex was derived from its X-ray crystallographic data. The geometry optimization is performed without any constraints, and the nature of stationary points was confirmed by normalmode analysis. The topological features derived from Bader's theory of atoms in molecules (AIM) approach was applied to understand the electron-density features like charge density (ρ) and Laplacian of charge density ($\nabla^2\rho$) using ADF2014.10. The recently developed reduced density gradient (RDG) based NCI (non-covalent interactions) index calculations were applied for real-space visualization of both attractive (van der Waals and hydrogen bonding) and repulsive (steric) interactions based on the properties of the electron density. Herein, the single-point calculations were based on the structure obtained from the X-ray studies and in these structures, the hydrogen atom positions were normalized before computation. This is already discussed in the Theoretical work section. Natural bond orbital (NBO) analysis was applied to investigate the stability of the molecule arising from charge delocalization. The interaction energies of dimers were calculated using basis set superposition error (BSSE) corrections by the following method:

$$\Delta E(AB) = E(AB) - E(A) - E(B) + (\text{BSSE value of dimer})$$

The energetic features of complex **6** are calculated at the B3LYP-D/def2-SVP level of theory using the crystallographic coordinates. For the calculations, the GAUSSIAN-09 program has been used [21]. Grimme's dispersion correction [22] has also been used as implemented in the GAUSSIAN-09 program since it is adequate for the evaluation of non-covalent interactions where dispersion effects are relevant. The basis set superposition error for the calculation of interaction energies has been corrected using the counterpoise method [23]. Molecular electrostatic potential (MEP) surfaces have been computed at the same level of theory and

represented using the 0.001 a.u. isosurface. Bader's quantum theory of "atoms in molecules" (QTAIM) has been used to characterize the noncovalent interactions using the AIMall program [24].

The geometries of the complexes **7-11** included in this study were computed at the PBE0-D3/def2-TZVP level of theory using the crystallographic coordinates. For the calculations TURBOMOLE 7.0 program [25] has been used. The Grimme's dispersion [26] correction has also been used since it is adequate for the evaluation of non-covalent interactions. The basis set superposition error for the calculation of interaction energies has been corrected using the counterpoise method [27]. The NCI plot [28] iso-surfaces have been used to characterize non-covalent interactions. They correspond to both favourable and unfavourable interactions, as differentiated by the sign of the second density Hessian eigenvalue and defined by the isosurface colour. The colour scheme is a red-yellow-green-blue scale with red for ρ +cut (repulsive) and blue for ρ -cut (attractive). Yellow and green isosurfaces correspond to weak repulsive and weak attractive interactions, respectively [29]. The Gaussian-0911 PBE-D/def2-TZVP level of theory wave function has been used to generate the NCI plot. The molecular electrostatic potential (MEP) surfaces have been computed using the Gaussian-09 program at the same level and using the 0.001 a.u. isosurface as a good estimation of the van der Waals surface and the surfaces have been visualized using the GaussView program [30].

1.B.2.5. Photocatalytic measurement

The photocatalytic experiment in aqueous solution has been carried out in usual process [31]. The catalytic degradation has been carried out separately with 100 mL of Methylene Blue (MB) solution (20 mg L^{-1}) with complexes (**12-13**) using as catalyst. The mixture has been stirred

for 10 min in a dark environment to get a balance between adsorption and desorption. The solution has been then stirred constantly. A 3 mL sample has been taken from the reaction system in an interval of 3 min and the supernatant liquid obtained by centrifugation has been used for collecting the UV–Vis spectrum. The characteristic peak for methylene blue (600 nm) has been employed to monitor the photocatalytic degradation.

References

- 1 M. A. Spackman and D. Jayatilaka, *CrystEngComm*, 2009, **11**, 19-32.
- 2 F. L. Hirshfeld, *Theor. Chim. Acta*, 1977, **44**, 129-138.
- 3 A. L. Rohl, M. Moret, W. Kaminsky, K. Claborn, J. J. McKinnon and B. Kahr, *Cryst. Growth Des.*, 2008, **8**, 4517-4525.
- 4 A. Parkin, G. Barr, W. Dong, C. J. Gilmore, D. Jayatilaka, J. J. McKinnon, M. A. Spackman and C. Wilson, *CrystEngComm*, 2007, **9**, 648-652.
- 5 M. A. Spackman and J. J. McKinnon, *CrystEngComm*, 2002, **4**, 378-392. 6 S. K. Wolff, D. J. Grimwood, J. J. McKinnon, D. Jayatilaka, M. A. Spackman, Crystal Explorer 2.0; University of Western Australia: Perth, Australia, 2007. <http://hirshfeldsurfacenet.blogspot.com/>.
- 7 F. H. Allen, O. Kennard, D. G. Watson, L. Brammer, A. G. Orpen and R. J. Taylor, *J. Chem. Soc. Perkin Trans.2*, **1987**, S1-S19.
- 8 J. J. Kinnon, M. A. Spackman, A. S. Mitchell, *Acta Cryst.*, 2004, **B60**, 627-668.
- 9 O. V. Dolomanov, L. J. Bourhis, R. J. Gildea, J. A. K. Howard and H. Puschmann, *J. Appl. Crystallogr.*, 2009, **42**, 339-341; (b) G. M. Sheldrick, *Acta Cryst.*, 2008, **A64**, 112-122.
- 10 G. M. Sheldrick, *Acta Cryst.*, 2015, **C71**, 3-8.
- 11 G. M. Sheldrick, SADABS, V2014/5, Software for Empirical Absorption Correction, University of Göttingen, Institute für Anorganische Chemie der Universität, Göttingen, Germany, 1999-2003.
- 37 M. N. Burnett and C. K. Johnson, ORTEP-3: Oak Ridge Thermal Ellipsoid Plot Program for
12. K. Diamond, Crystal Impact GbR, Germany, Bonn, 2007.
13. Crystal Structure Illustrations, Report ORNL-6895, Oak Ridge National Laboratory, Oak

Ridge, TN, USA, 1996.

14. *Persistence of Vision (TM) Raytracer*, Persistence of Vision Pty. Ltd., Williamstown, Victoria, Australia, 2004.

15. C. F. Macrae, I. J. Bruno, J. A. Chisholm, P. R. Edgington, P. McCabe, E. Pidcock, L. Rodriguez-Monge, R. Taylor, J. van de Streek and P. A. Wood, *J. Appl. Cryst.*, 2008, **41**, 466.

16. M.J. Frisch, G.W. Trucks, H.B. Schlegel, G.E. Scuseria, M.A. Robb, J.R. Cheeseman, G. Scalmani, V. Barone, B. Mennucci, G.A. Petersson, H. Nakatsuji, M. Caricato, X. Li, H.P. Hratchian, A.F. Izmaylov, J. Bloino, G. Zheng, J.L. Sonnenberg, M. Hada, M. Ehara, K. Toyota, R. Fukuda, J. Hasegawa, M. Ishida, T. Nakajima, Y. Honda, O. Kitao, H. Nakai, T. Vreven, J.A. Montgomery Jr., J.E. Peralta, F. Ogliaro, M. Bearpark, J.J. Heyd, E. Brothers, K.N. Kudin, V.N. Staroverov, R. Kobayashi, J. Normand, K. Raghavachari, A. Rendell, J.C. Burant, S.S. Iyengar, J. Tomasi, M. Cossi, N. Rega, J.M. Millam, M. Klene, J.E. Knox, J.B. Cross, V. Bakken, C. Adamo, J. Jaramillo, R. Gomperts, R.E. Stratmann, O. Yazyev, A.J. Austin, R. Cammi, C. Pomelli, J.W. Ochterski, R.L. Martin, K. Morokuma, V.G. Zakrzewski, G.A. Voth, P. Salvador, J.J. Dannenberg, S. Dapprich, A.D. Daniels, Ö. Farkas, J.B. Foresman, J.V. Ortiz, J. Cioslowski, D.J. Fox, Gaussian 09, Gaussian Inc, Wallingford CT, 2009.

17. S. Grimme, J. Antony, S. Ehrlich, H. Krieg, *J. Chem. Phys.* 132 (2010) 154104– 154117.

18. S.F. Boys, F. Bernardi, *Mol. Phys.* 19 (1970) 553–566.

19. J. Contreras-García, E.R. Johnson, S. Keinan, R. Chaudret, J.-P. Piquemal, D.N. Beratan, W. Yang, *J. Chem. Theory Comput.* 7 (2011) 625–632.

20. E.R. Johnson, S. Keinan, P. Mori-Sánchez, J. Contreras-García, A.J. Cohen, W. Yang, *J. Am. Chem. Soc.* 132 (2010) 6498–6506.

21. M. J. Frisch, G. W. Trucks, H. B. Schlegel, G. E. Scuseria, M. A. Robb, J. R. Cheeseman, G. Scalmani, V. Barone, B. Mennucci, G. A. Petersson, H. Nakatsuji, M. Caricato, X. Li, H. P. Hratchian, A. F. Izmaylov, J. Bloino, G. Zheng, J. L. Sonnenberg, M. Hada, M. Ehara, K. Toyota, R. Fukuda, J. Hasegawa, M. Ishida, T. Nakajima, Y. Honda, O. Kitao, H. Nakai, T. Vreven, J. A. Montgomery, Jr., J. E. Peralta, F. Ogliaro, M. Bearpark, J. J. Heyd, E. Brothers, K. N. Kudin, V. N. Staroverov, R. Kobayashi, J. Normand, K. Raghavachari, A. Rendell, J. C. Burant, S. S. Iyengar, J. Tomasi, M. Cossi, N. Rega, J. M. Millam, M. Klene, J. E. Knox, J. B. Cross, V. Bakken, C. Adamo, J. Jaramillo, R. Gomperts, R. E. Stratmann, O. Yazyev, A. J. Austin, R. Cammi, C. Pomelli, J. W. Ochterski, R. L. Martin, K. Morokuma, V. G. Zakrzewski, G. A. Voth, P. Salvador, J. J. Dannenberg, S. Dapprich, A. D. Daniels, Ö. Farkas, J. B. Foresman, J. V. Ortiz, J. Cioslowski and D. J. Fox, Gaussian 09, Gaussian, Inc., Wallingford CT, 2009.
22. S. Grimme, J. Antony, S. Ehrlich and H. Krieg, J. Chem. Phys., 2010, 132, 154104.
23. S. F. Boys and F. Bernardi, Mol. Phys., 1970, 19, 553–566.
24. T. A. Keith, AIMAll (Version 13.05.06), TK Gristmill Software, Overland Park, KS, 2013.
25. TURBOMOLE V7.0 2015, a development of University of Karlsruhe and Forschungszentrum Karlsruhe GmbH, 1989-2007, TURBOMOLE GmbH
26. Grimme, S.; Antony, J.; Ehrlich, S.; Krieg, H. A consistent and accurate ab initio parametrization of density functional dispersion correction (DFT-D) for the 94 elements H-Pu. J. Chem. Phys. 2010, 132, 154104–154109.
27. Boys, S. F.; Bernardi, F.; The calculation of small molecular interactions by the differences of separate total energies. Some procedures with reduced errors. Mol. Phys. 1970, 19, 553–566.
28. Contreras-García, J.; Johnson, E. R.; Keinan, S.; Chaudret, R.; Piquemal, J.-P.; Beratan, D. N.;

Yang, W. NCIPLOT: A Program for Plotting Noncovalent Interaction Regions. *J. Chem. Theory Comput.* 2011, 7, 625–632.

29. Johnson, E. R.; Keinan, S.; Mori-Sanchez, P.; Contreras-Garcia, J.; Cohen, A. J.; Yang, W. Revealing Noncovalent Interactions. *J. Am. Chem. Soc.* 2010, 132, 6498–6506.

30. Gaussian 09, Revision C.02, M. J. Frisch, G. W. Trucks, H. B. Schlegel, G. E. Scuseria, M. A. Robb, J. R. Cheeseman, G. Scalmani, V. Barone, G. A. Petersson, H. Nakatsuji, X. Li, M. Caricato, A. Marenich, J. Bloino, B. G. Janesko, R. Gomperts, B. Mennucci, H. P. Hratchian, J. V. Ortiz, A. F. Izmaylov, J. L. Sonnenberg, D. Williams-Young, F. Ding, F. Lipparini, F. Egidi, J. Goings, B. Peng, A. Petrone, T. Henderson, D. Ranasinghe, V. G. Zakrzewski, J. Gao, N. Rega, G. Zheng, W. Liang, M. Hada, M. Ehara, K. Toyota, R. Fukuda, J. Hasegawa, M. Ishida, T. Nakajima, Y. Honda, O. Kitao, H. Nakai, T. Vreven, K. Throssell, J. A. Montgomery, Jr., J. E. Peralta, F. Ogliaro, M. Bearpark, J. J. Heyd, E. Brothers, K. N. Kudin, V. N. Staroverov, T. Keith, R. Kobayashi, J. Normand, K. Raghavachari, A. Rendell, J. C. Burant, S. S. Iyengar, J. Tomasi, M. Cossi, J.M. Millam, M. Klene, C. Adamo, R. Cammi, J. W. Ochterski, R. L. Martin, K. Morokuma, O. Farkas, J. B. Foresman, D.J. Fox, Gaussian, Inc., Wallingford CT, 2016.

[31] T. Basak, A. Bhattacharyya, K. Harms, S. Chattopadhyay, *Polyhedron* 157 (2019) 449.

Section IC

Summary of research work

The thesis consists of six chapters, among them Chapter I deals with the overview of the coordination chemistry of different heteronuclear complexes with different Schiff base and reduced Schiff base ligands. The whole research work has been distributed into four Chapters from II to V and lastly significant observations have been highlighted in Chapter VI. Summary of the whole research work is discussed under this section.

Chapter II

A series of isostructural centrosymmetric hydrogen bonded dimeric nickel(II) complexes (**1-4**) of general formula, $[\text{Ni}_2(\text{HL})_2(\text{DMSO})_2(\text{H}_2\text{O})_2]\text{X}$ {where $\text{H}_2\text{L} = \text{N}_2\text{O}_4$ donor reduced Schiff base ligand, $[\text{H}_2\text{L}^1 = (2,2\text{-dimethyl-1,3-propanediyl})\text{bis(iminomethylene)bis(6-methoxyphenol)}$ and $\text{H}_2\text{L}^2 = (2,2\text{-dimethyl-1,3-propanediyl})\text{bis(iminomethylene)bis(6-ethoxyphenol)}$] and $\text{X} =$ counter anion}, are synthesized and characterized by elemental analysis, infrared and electronic spectra. The structures of all complexes have been confirmed by single crystal X-ray diffraction analysis. Each complex forms $\text{O}\cdots\text{H}\cdots\text{O}$ hydrogen bonded dimer in the solid state, where the $\text{O}\cdots\text{O}$ distance is very short, ranging from 2.424(3) to 2.437(3) Å. The hydrogen bonds are very strong as can be seen from the DFT estimated energy of these hydrogen bonds. Non-covalent interaction plot (NCI plot) index has been used to characterize them.

Chapter IIIA

A heterodinuclear copper(II)/lead(II) complex (**5**) with a compartmental 'reduced Schiff base' ligand (having inner N_2O_2 and outer $O_2O'_2$ compartments) has been synthesized and characterized. Single-crystal X-ray diffraction analysis confirmed its structure. The X-ray data indicate that the inner N_2O_2 compartment of the compartmental reduced Schiff base is occupied by copper(II) while the outer $O_2O'_2$ compartment is occupied by lead(II). A thiocyanate anion is coordinated to the copper(II) center via its N-end, whereas, another thiocyanate ion is linked to the lead(II) center via its S-end and is semi-coordinated to the copper(II) center through its N-end. A hemidirectionally coordinated lead(II) center is well suited for establishing tetrel bonding interactions. We estimated the BSSE (basis set superposition error) corrected energies of non-covalent $S\cdots S$, $Pb\cdots\pi$, and $\pi\cdots\pi$ interactions and N–H hydrogen bonding along with tetrel bonding by DFT calculations. To obtain an insight into the physical nature of these bonds, we extensively used Bader's quantum theory of atoms-in-molecules (QTAIM). Additionally, the non-covalent interaction reduced density gradient (NCI-RDG) method established nicely the presence of such non-covalent intermolecular interactions. Here, we also used natural bond orbital (NBO) analysis to find out the origin of $S\cdots S$ and $Pb\cdots S$ bonding.

Chapter IIIB

A hetero-dinuclear nickel(II)/lead(II) complex (**6**) with a compartmental 'reduced Schiff base' ligand (having inner N_2O_2 and outer $O_2O'_2$ compartments) has been prepared and characterized by elemental and spectral analysis. Single crystal X-ray diffraction analysis confirms its structure. Nickel(II) is placed in the inner N_2O_2 compartment and lead(II) is placed in the outer $O_2O'_2$ compartment of the compartmental reduced Schiff base. The complex forms

a tetranuclear supramolecule via non-covalent Pb...Cl tetrel bonding interactions. The DFT study is devoted to analyze these tetrel bonding interactions that involve the σ -hole at the hemi-coordinated Pb(II) atom. The tetrel bonding interactions have been characterized using Bader's theory of atoms in molecules (AIM).

Chapter IIIC

Three heteronuclear nickel(II)/lead(II) complexes (**7**, **8** and **9**) with two compartmental reduced Schiff base ligands were prepared and characterized. Their structures were confirmed by single crystal X-ray diffraction analyses. In each complex, nickel(II) is placed in the inner N2O2 compartment and lead(II) in the outer O2O2' compartment of reduced Schiff base ligands. Interesting molecular architectures were formed via supramolecular interactions in the solid state of the complexes. A density functional theory study is devoted to analyze unconventional tetrel bonding interactions established between the σ -hole at the hemicoordinated lead(II) and either the electron-rich thiocyanate or the π -system of the aromatic ligand. In addition, π -stacking assemblies between both the aromatic rings and five membered Pb-chelate rings were described and studied both with regard to their energies and by using the noncovalent plot index.

Chapter IV

Two hetero-tetranuclear nickel(II)/lead(II) complexes (**10** and **11**) have been prepared with a compartmental reduced Schiff base ligand. Both complexes have been characterized elemental and spectral analyses. Structures of both complexes have been confirmed by single crystal X-ray diffraction technique. Supramolecular architectures formed in their solid state structures were also analyzed.

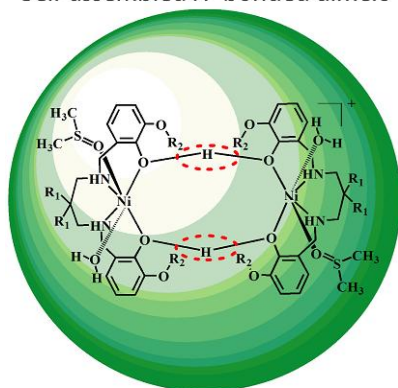
Chapter V

Two centrosymmetric hetero-tetranuclear copper(II)/cadmium(II) complexes (**12** and **13**) have been prepared with a compartmental reduced Schiff base ligand. Both complexes have been characterized elemental and spectral analyses. Structures of both complexes have been confirmed by single crystal X-ray diffraction technique. Both complexes contain CuO₂Cd cores. Here the bridging mode of azide and thiocyanate is quite different. Complex **12** contains μ -1,1-azide bridges between two cadmium(II) centres whereas in complex **13**, μ -1,1-thiocyanate bridges occur between copper(II) and cadmium(II) centres. The ability of both complexes to be used as photocatalyst in degrading methylene blue (MB) has been explored. The difference in photocatalytic performance may be correlated with their structures. Complex **12** shows better catalytic activity compared to complex **13**, and can degrade almost 62% MB in 18 min. Comparative IR studies (before and after the photocatalytic degradation process) confirmed the stability of both catalysts.

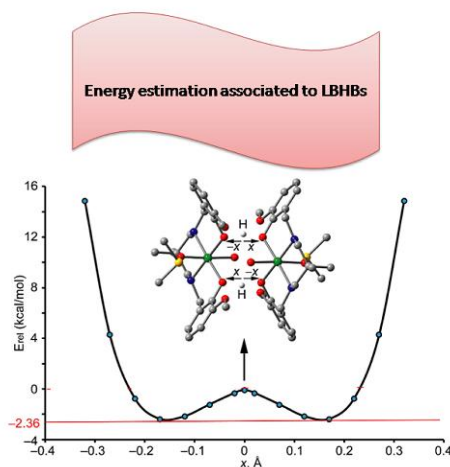
Chapter II

A series of hydrogen bond mediated dinuclear nickel(II) complexes with reduced Schiff base ligands: An insight into the nature of hydrogen bonds in them

Self-assembled H- bonded dimers



DFT Study



II.1. Introduction

The interaction energy of conventional hydrogen bonds basically depends on their geometric features like length and linearity. However, the difference in the pK_a values of the heavy atoms sharing the proton is also important.¹ The ΔH of formation of the water dimer is $\sim 5 \text{ kcal/mol}^1$ in the gas phase. However, the $\text{HO}-\text{H}\cdots\text{OH}_2$ hydrogen bond in water is weaker due to the large difference between the pK_a s of the donor group and the conjugate acid of the acceptor group (15.7 for H_2O and -1.7 for H_3O^+).² In the gas and solid state phases, hydrogen bonds between hetero atoms with similar pK_a s can be very short and strong (up to 30 kcal mol^{-1}).³⁻⁶ When groups of equal pK_a establish an hydrogen bond, three different situations may occur (see Figure II.1). The classical hydrogen bond where the hydrogen atom is covalently bonded to one of both oxygen atoms (dipole \cdots dipole interaction, see Figure II.1a). As the $\text{O}\cdots\text{O}$ distance is progressively shortened, the energy barrier lowers until it reaches the lower vibrational energy levels, thus leading to a low barrier hydrogen bond (LBHB, see Figure II.1b). In this case, the hydrogen atom can move freely between the two oxygen atoms with its average position is the center (high covalent character).^{7,8} Further shortening leads to a single-well hydrogen bond with the highest covalent character and interaction energy of the three situations.

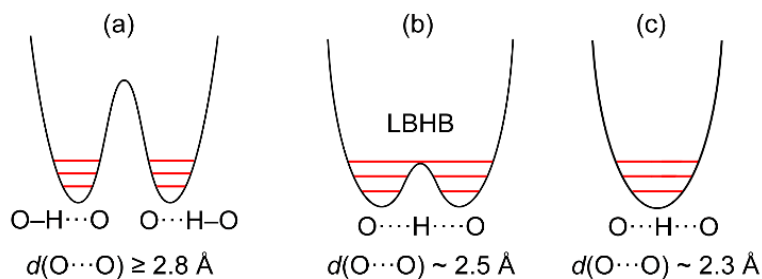


Fig. II.1: Energy diagrams for OH...H hydrogen bonds between groups of identical pKa. (a) Standard hydrogen bond with O...O distance $d(\text{O}\cdots\text{O}) \geq 2.8 \text{ \AA}$. (b) Low barrier hydrogen bond of $d(\text{O}\cdots\text{O}) \sim 2.55 \text{ \AA}$ (average position in the center). (c) Single-well hydrogen bond with $d(\text{O}\cdots\text{O}) \sim 2.3 \text{ \AA}$.

In this manuscript, we report the synthesis and X-ray characterization of a series of mononuclear nickel(II) complexes that form O...H...O hydrogen bonded dimers in the solid state where the O...O distance is very short, ranging from 2.35 to 2.45 Å. We have analyzed the hydrogen bonds using DFT calculations and the non covalent interaction plot (NCI plot) index to distinguish between the three possible situations represented in Figure II.1.

II.2. Experimental Section

II.2.1. Synthesis

II.2.1.1. Synthesis of Schiff base ligands

II.2.1.1.1. Synthesis of H_2L^a [N,N'-bis(3-methoxysalicylidene)-2,2-dimethyl-1,3-propanediamine], H_2L^b [N,N'-bis(3-ethoxysalicylidene)-2,2-dimethyl-1,3-propanediamine],

H_2L^c [*N,N'*-bis(3-methoxysalicylidene)-1,3-propanediamine] and H_2L^d [*N,N'*-bis(3-ethoxysalicylidene)-1,3-propanediamine]

A methanol solution (10 mL) of 2,2-dimethyl-1,3-propanediamine (1 mmol, 0.12 mL) was mixed separately with of 3-methoxysalicylaldehyde (2 mmol, 304 mg) and 3-ethoxysalicylaldehyde, (2 mmol, 332 mg) and the resulting solutions were allowed to reflux for ca. 2 h to synthesize two hexadentate N_2O_4 donor Schiff base ligands, H_2L^a [*N,N'*-bis(3-ethoxysalicylidene)2,2-dimethyl-1,3-propanediamine] and H_2L^b [*N,N'*-bis(3-methoxysalicylidene)-2,2-dimethyl-1,3-propanediamine] respectively. Other two hexadentate Schiff bases, H_2L^c [*N,N'*-bis(3-methoxysalicylidene)-1,3-propanediamine] and H_2L^d [*N,N'*-bis(3-ethoxysalicylidene)-1,3-propanediamine] were synthesized following the similar procedure as mentioned above except 1,3-propanediamine (1 mmol, 0.11 mL) was used as the diamine instead of 2,2-dimethyl-1,3-propanediamine.

II.2.1.2. Synthesis of the reduced Schiff base ligands

II.2.1.2.1. Synthesis of H_2L^1 [(2,2-dimethyl-1,3-propanediyl)bis(iminomethylene)bis(6-methoxyphenol)], H_2L^2 [(2,2-dimethyl-1,3-propanediyl)bis(iminomethylene)bis(6-ethoxyphenol)], H_2L^3 [(1,3-propanediyl)bis(iminomethylene)bis(6-methoxyphenol)] and H_2L^4 [(1,3-propanediyl)bis(iminomethylene)bis(6-ethoxyphenol)].

The prepared Schiff base solutions, H_2L^a , H_2L^b , H_2L^c , H_2L^d were cooled to 0°C, and solid sodium borohydride (4 mmol, 150 mg) was then added gently to these solution with constant

stirring. The solutions were further acidified with glacial acetic acid (10 mL) and placed under reduced pressure in a rotary evaporator ($\sim 60^{\circ}\text{C}$). The residue was dissolved in water (15 mL) and extracted with dichloromethane (15 mL) using a separating funnel. Finally, the dichloromethane part was dried using anhydrous sodium acetate to get the desired hexadentate N_2O_4 donor reduced Schiff base ligand, H_2L^1 , H_2L^2 , H_2L^3 and H_2L^4 respectively. The ligands were not purified and used directly for the synthesis of complexes 1, 2, 3 and 4 respectively.

II.2.1.3. Synthesis of complexes

II.2.1.3.1. Synthesis of $[\text{Ni}_2(\text{HL}^1)_2(\text{DMSO})_2(\text{H}_2\text{O})_2]\text{ClO}_4\cdot\text{H}_2\text{O}$ (1)

A methanol solution of nickel(II) perchlorate hexahydrate, (0.99 mmol, 257 mg), was added into the methanol solution of a reduced Schiff base ligand, H_2L^1 , with constant stirring and colour of the solution turned into dark green. Few drops of DMSO were added and the resulting solution was kept for crystallization. Dark green single crystals, suitable for X-ray diffraction, were obtained after 3-4 days on slow evaporation of the solution in open atmosphere.

Yield: 350 mg, ($\sim 54\%$, based on Ni). Anal. Calc. for $\text{C}_{46}\text{H}_{74}\text{N}_4\text{Ni}_2\text{O}_{22}\text{S}_2\text{Cl}_2$ (FW = 1287.49): C, 42.87; H, 5.74; N, 4.35%. Found: C, 42.8; H, 5.8; N, 4.3%. FT-IR (KBr, cm^{-1}): 3400 ($\nu_{\text{O-H}}$), 3270 ($\nu_{\text{N-H}}$), 2990-2850 ($\nu_{\text{C-H}}$). UV-Vis, λ_{max} (nm), [ϵ_{max} ($\text{dm}^3 \text{ mol}^{-1} \text{ cm}^{-1}$)] (DMSO), 730 (1.01×10^2), 625 (2.00×10^2), 355 (2.65×10^3), 280 (5.6×10^3).

II.2.1.3.2. Synthesis of $[\text{Ni}_2(\text{HL}^2)_2(\text{DMSO})_2(\text{H}_2\text{O})_2]\text{ClO}_4$ (2)

Complex **2** was synthesized following the similar procedure as that for complex **1** except that the reduced Schiff base ligand, H_2L^2 , was used instead of H_2L^1 . Dark green coloured crystalline complex suitable for X-ray diffraction, started to separate from the solution after 3-4 days on standing at room temperature and was collected by filtration.

Yield: 343 mg, (~ 53%, based on Ni). Anal. Calc. for $C_{100}H_{152}Cl_4N_8Ni_4O_{40}$ (FW = 2612.52): C, 53.5; H, 5.8; N, 4.2%. Found: C, 53.4; H, 5.7; N, 4.3%. FT-IR (KBr, cm^{-1}): 3395 (ν_{O-H}), 3280 (ν_{N-H}), 2990-2865 (ν_{C-H}). UV-Vis, λ_{max} (nm), [ϵ_{max} ($dm^3 mol^{-1} cm^{-1}$)] (DMSO), 720 (0.89×10^2), 620 (1.80×10^2), 355 (4.84×10^3), 274 (9.38×10^4).

II.2.1.3.3. Synthesis of $[Ni_2(HL^3)_2(DMSO)_2(H_2O)_2]NCS$ (3)

A methanol solution of nickel(II) thiocyanate tetrahydrate (1.01 mmol, 250 mg) was added into the methanol solution of a reduced Schiff base ligand, H_2L^3 , with constant stirring and colour of the solution turned into dark green. Few drops of DMSO were added and the resulting solution was kept for crystallization. Dark green single crystals, suitable for X-ray diffraction, were obtained after 2-3 days on slow evaporation of the solution in open atmosphere.

Yield: 354 mg, (~ 63%, based on Ni). Anal. Calc. for $C_{44}H_{66}N_6Ni_2O_{12}S_4$ (FW = 1116.65): C, 47.2; H, 5.9; N, 7.5%. Found: C, 47.2; H, 5.8; N, 7.6%. FT-IR (KBr, cm^{-1}): 3390 (ν_{O-H}), 3260 (ν_{N-H}), 3012-2840 (ν_{C-H}), 2045 (ν_{NCS}). UV-Vis, λ_{max} (nm), [ϵ_{max} ($dm^3 mol^{-1} cm^{-1}$)] (DMSO), 718 (1.40×10^2), 622 (2.78×10^3), 355 (4.34×10^2), 280 (9.49×10^4).

II.2.1.3.4. Synthesis of $[Ni_2(HL^4)_2(DMSO)_2(H_2O)_2]ClO_4$ (4)

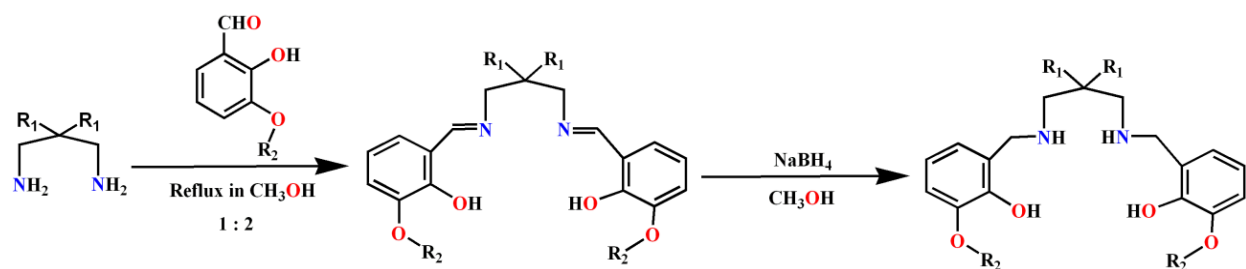
Complex **4** was synthesized following the similar procedure as that for complex **3** except that the reduced Schiff base ligand, H_2L^4 , was used instead of H_2L^3 . Dark green coloured crystalline complex suitable for X-ray diffraction, started to separate from the solution after 2-3 days on standing at room temperature and was collected by filtration.

Yield: 344 mg, (~54%, based on Ni). Anal. Calc. for $C_{46}H_{74}N_4Ni_2O_{20}S_2Cl_2$ (FW = 1255.49): C, 43.9; H, 5.9; N, 4.4%. Found: C, 43.8; H, 5.8; N, 4.5%. FT-IR (KBr, cm^{-1}): 3420 (ν_{O-H}), 3265 (ν_{N-H}), 2995-2870 (ν_{C-H}). UV-Vis, λ_{max} (nm), [ϵ_{max} ($dm^3 mol^{-1} cm^{-1}$)] (DMSO), 755 (0.58×10^2), 635 (0.93×10^2), 360 (3.8×10^3), 271 (8.86×10^3).

II.3. Results and discussion

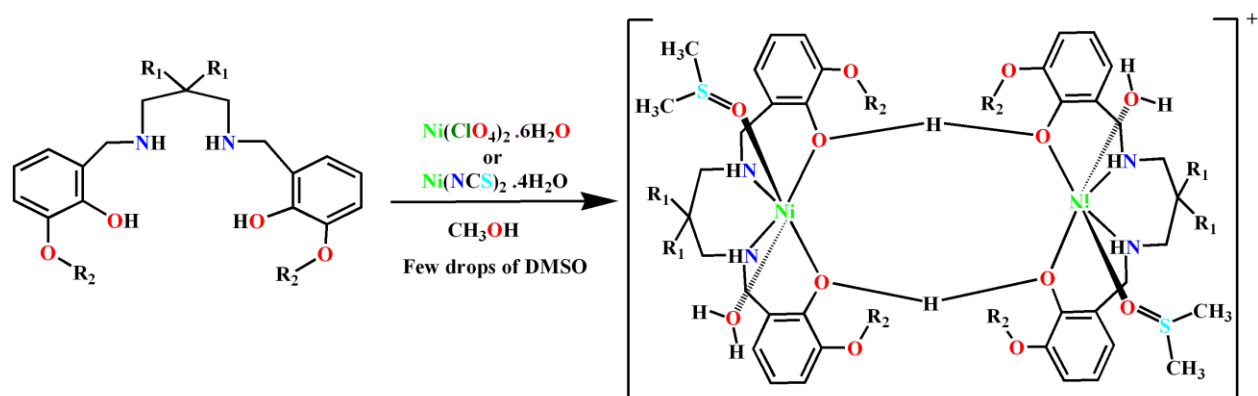
II.3.1. Synthesis

Two moles of 3-alkoxysalicylaldehydes (3-methoxy and 3-ethoxy) have been used to condense separately with 2,2-dimethyldiaminopropane and 1,3-diaminopropane in methanol medium to prepare four Schiff bases, H_2L^a , H_2L^b , H_2L^c and H_2L^d . These Schiff bases were then reduced with $NaBH_4$ in methanol under constant stirring at $0^\circ C$ to prepare four respective reduced Schiff bases, H_2L^1 , H_2L^2 , H_2L^3 and H_2L^4 respectively following the literature method.¹⁷



Scheme II.1: Synthetic route to 'reduced Schiff base' ligands.

These reduced Schiff bases on then reaction with nickel(II) perchlorate hexahydrate or nickel(II) thiocyanate in methanol and on adding few drops of DMSO to the individual reaction mixture gave rise to complexes **1-4**.



Scheme II.2: Synthetic route to complexes **1** ($R_1=Me$, $R_2=Me$), **2** ($R_1=Me$, $R_2=Et$), **3** ($R_1=H$, $R_2=Me$) and **4** ($R_1=H$, $R_2=Et$). Non coordinated counter anions have not been shown here.

Use of reduced Schiff base ligands seems to be crucial in forming these types of hydrogen bonded dimeric complexes, as the non-reduced Schiff bases were unable to produce such complexes. Many synthetic inorganic chemistry groups were prepared many homo and heteronuclear complexes with the corresponding non-reduced Schiff base ligands, but did not

get complexes similar to complexes **1-4**. More flexibility of the reduced Schiff bases compared to their non-reduced precursors may be reason of this observation.

II.3.2. Structure description

II.3.2.1. Description of structures $[Ni_2(HL^1)_2(DMSO)_2(H_2O)_2]ClO_4 \cdot H_2O$ (**1**), $[Ni_2(HL^2)_2(DMSO)_2(H_2O)_2]ClO_4$ (**2**) and $[Ni_2(HL^3)_2(DMSO)_2(H_2O)_2]NCS$ (**3**)

X-ray crystal structure determination reveals that each of complexes **1-3** crystallize in triclinic space group, *P*. Crystallographic data and refinement details have been summarized in Table II.1. Potential N₂O₄ donor hexadentate reduced Schiff bases, H_2L^1 , H_2L^2 , and H_2L^3 , have been used to prepare these complexes respectively. Selected bond lengths and bond angles have been listed in Tables II.2 and II.3 respectively. Each complex actually possesses a dinuclear moiety formed via strong hydrogen bonds. Each complex consists of two independent centrosymmetric dimers (A and B) with equivalent geometry. A view of the dimer A of complex **1** is given in Figure II.2. A view of the dimers (A) of complexes **2** and **3** are given in Figure II.3 and Figure II.4 respectively. The structure of dimer B of each complex is very similar to the structure of dimer A in respective complex (Figure II.5-II.7).

In each dimeric unit, nickel(II) centers are hexa-coordinated and adopt distorted octahedral geometry. Each nickel(II) center, {Ni(1) of A and Ni(2) of B} is equatorially coordinated by two amine nitrogen atoms, {N(1) and N(2) for Ni(1) and N(3) and N(4) for Ni(2)}, two phenoxo oxygen atoms, {O(1) and O(2) for Ni(1) and O(7) and O(8) for Ni(2)}, of the reduced

Schiff base units. The axial sites are coordinated by two oxygen atoms, {O(3) and O(4) for Ni(1) and O(9) and O(10) for Ni(2)} of coordinated water and DMSO molecule. Each of the reduced Schiff bases are dibasic in character, but loses only one proton to form mononegative anion, which, in turn, connects with another such moiety via strong hydrogen bonding to form the symmetric dimeric structure. The deprotonations of the hydroxyl group are well reflected in the nickel(II)-oxygen bond lengths (Table II.2). The deprotonated hydroxyl groups are bound strongly (shorter bond length) with nickel(II) centers compared with the non-deprotonated hydroxyl groups.¹⁸ The saturated six membered chelate rings, Ni(1)-N(1)-C(9)-C(10)-C(13)-N(2), Ni(1)-N(1)-C(10)-C(11)-C(14)-N(2) and Ni(1)-N(1)-C(9)-C(10)-C(11)-N(2), in dimer A of complexes **1**, **2** and **3** respectively represent individual chair conformations with puckering parameters,¹⁹ $q(2) = 0.583(4) \text{ \AA}$, $\phi = 168(2)^\circ$, $q(2) = 0.589(8) \text{ \AA}$, $\phi = 199(7)^\circ$ and $q(2) = 0.610(6) \text{ \AA}$, $\phi = 3(9)^\circ$ respectively. Similarly the saturated six membered chelate rings, Ni(2)-N(3)-C(32)-C(33)-C(36)-N(4), Ni(2)-N(3)-C(35)-C(36)-C(39)-N(4) and Ni(2)-N(3)-C(30)-C(31)-C(32)-N(4), in dimer B of complexes **1**, **2** and **3** respectively also represent individual chair conformations with puckering parameters, $q(2) = 0.563(7) \text{ \AA}$, $\phi = 180(3)^\circ$, $q(2) = 0.563(7) \text{ \AA}$, $\phi = 180(3)^\circ$ and $q(2) = 0.610(6) \text{ \AA}$, $\phi = 184(8)^\circ$ respectively.

II.3.2.2. $[Ni_2(HL^4)_2(DMSO)_2(H_2O)_2]ClO_4$ (**4**)

X-ray crystal structure determination reveals that complex **4** crystallizes in monoclinic space group, $C2/c$. A potential N_2O_4 donor hexadentate reduced Schiff base, H_2L^4 , have been used to prepare this complex. It contains a dinuclear moiety formed via strong hydrogen bonds. The structure of complex **4** has been shown in Figure II.8. The geometry around each nickel(II) centers are quite similar to that described for complexes **1-3** but it exists as only one dimeric

unit. Both the nickel(II) centers are hexa-coordinated and adopt distorted octahedral geometry. Each nickel(II) center, is equatorially coordinated by two amine nitrogen atoms, {N(1) and N(2)} and two phenoxo oxygen atoms, {O(1) and O(2)}, of the reduced Schiff base unit. The axial sites are coordinated by two oxygen atoms, {O(3) and O(4)}, of coordinated water and DMSO molecule. The saturated six membered chelate rings, Ni(1)-N(1)-C(10)-C(11)-C(12)-N(2), in of complex **4** represent chair conformations with puckering parameters , $q(2) = 0.589(5) \text{ \AA}$, $\phi = 182(2)^\circ$.

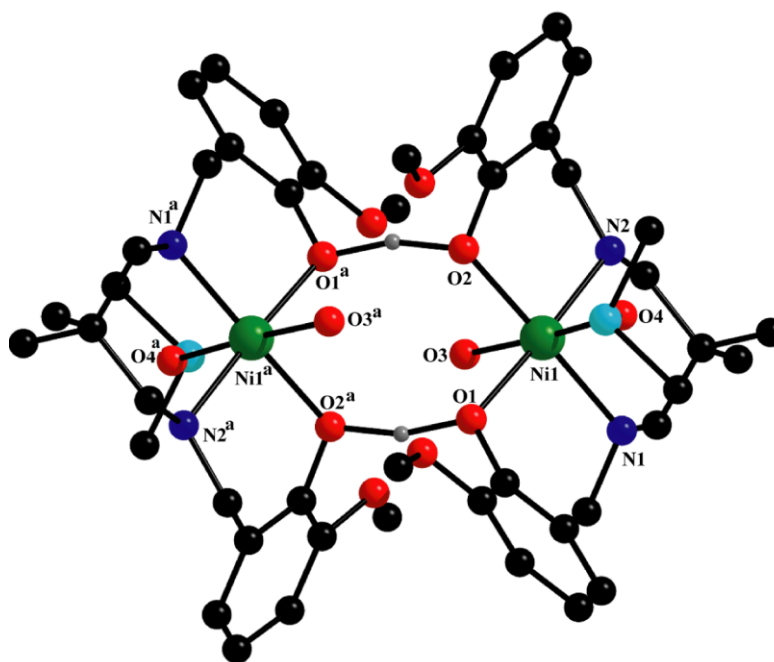
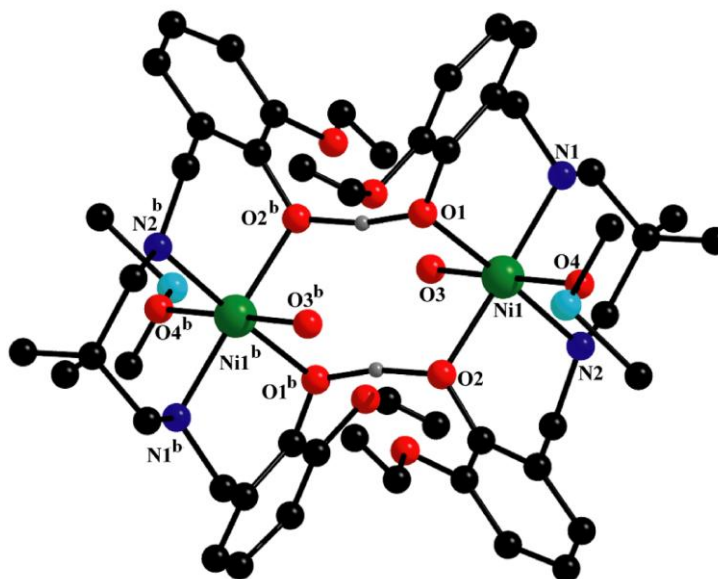
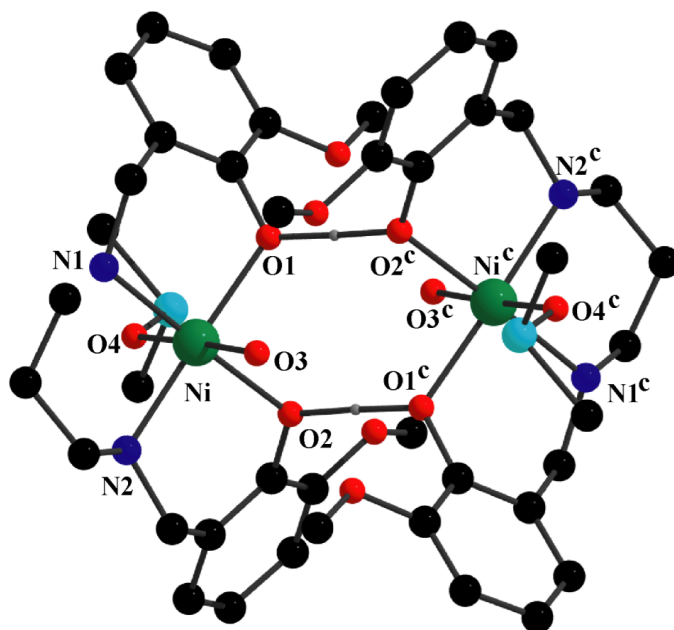


Fig. II.2: Perspective view of dimer A of complex **1** with selective atom-numbering scheme. Non co-ordinated perchlorate ion and hydrogen atoms have been omitted for clarity apart from those between the phenolic oxygen atoms.



Complex 2

Fig. II.3: Perspective view of dimer A of complex **2** with selective atom-numbering scheme. Non co-ordinated counter anions and hydrogen atoms have been omitted for clarity apart from those between the phenolic oxygen atoms.



Complex 3

Fig. II.4: Perspective view of dimer A of complex **3** with selective atom-numbering scheme. Non co-ordinated counter anions and hydrogen atoms have been omitted for clarity apart from those between the phenolic oxygen atoms.

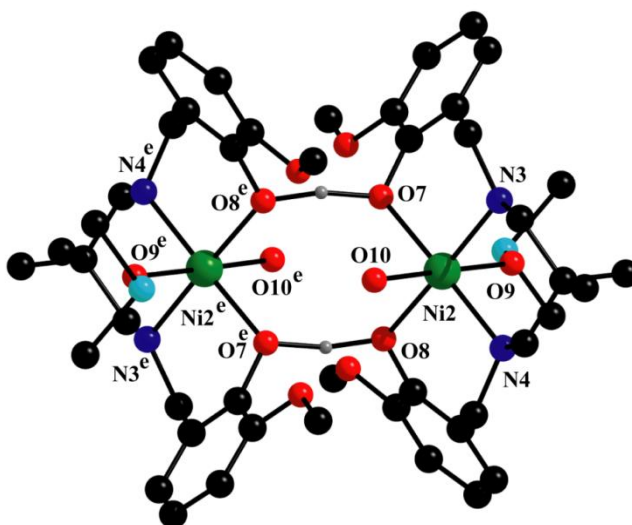


Fig. II.5: Perspective view of dimer B of complex **1** with selective atom-numbering scheme. Non co-ordinated perchlorate ion and hydrogen atoms have been omitted for clarity apart from those between the phenolic oxygen atoms. Symmetry transformation: $^e = 1-x, 2-y, 2-z$.

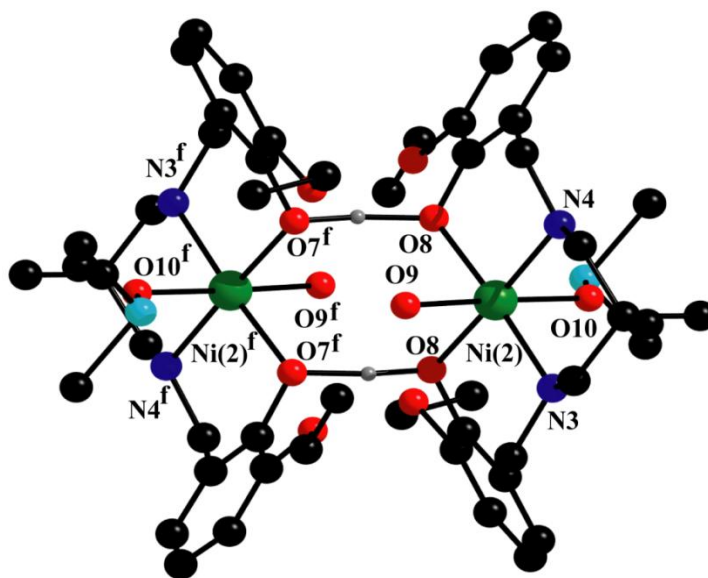


Fig. II.6: Perspective view of dimer B of complex **2** with selective atom-numbering scheme. Non co-ordinated perchlorate ion and hydrogen atoms have been omitted for clarity apart from those between the phenolic oxygen atoms. Symmetry transformation: $^f = -x, 1-y, 2-z$.

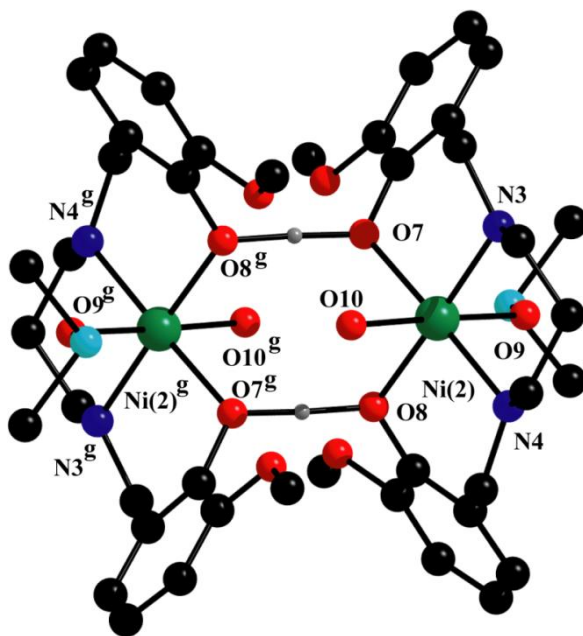


Fig. II.7: Perspective view of dimer B of complex **3** with selective atom-numbering scheme. Non co-ordinated thiocyanate ion and hydrogen atoms have been omitted for clarity apart from those between the phenolic oxygen atoms. Symmetry transformation: $^g = 1-x, -y, 2-z$.

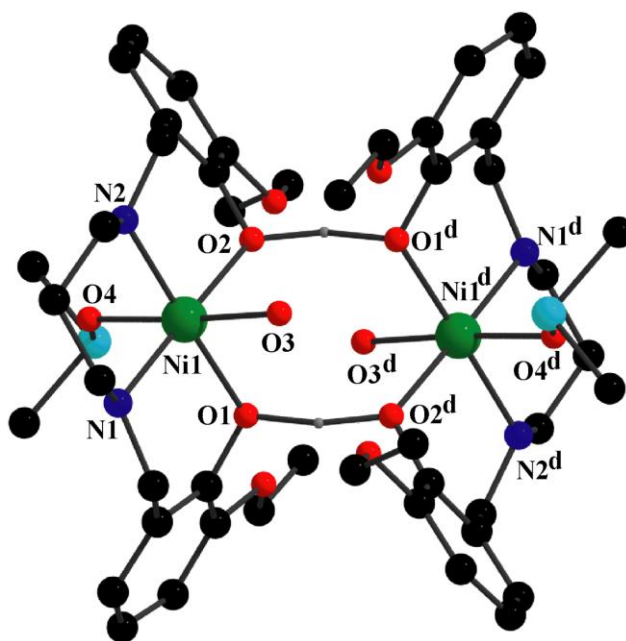


Fig. II.8: Perspective view of complex **4** with selective atom-numbering scheme. Non coordinated perchlorate ions and hydrogen atoms have been omitted for clarity apart from those between the phenolic oxygen atoms.

Table II.1. Crystal data and refinement details of complexes **1-4**.

Complex	1	2	3	4
Formula	$\text{C}_{46}\text{H}_{74}\text{N}_4\text{Ni}_2\text{O}_{22}\text{S}_2\text{Cl}_2$	$\text{C}_{100}\text{H}_{152}\text{Cl}_4\text{N}_8\text{Ni}_4\text{O}_{40}$	$\text{C}_{44}\text{H}_{66}\text{N}_6\text{Ni}_2\text{O}_{12}\text{S}_4$	$\text{C}_{46}\text{H}_{74}\text{N}_4\text{Ni}_2\text{O}_{20}\text{S}_2\text{Cl}_2$
Formula Weight	1287.49	2611.10	1116.65	1255.49
Crystal System	Triclinic	Triclinic	Triclinic	Monoclinic
Space group	<i>P</i>	<i>P</i>	<i>P</i>	<i>C2/c</i>

a(Å)	13.044(11)	12.344(3)	13.422(1)	22.317(2)
b(Å)	14.575(13)	14.130(3)	13.651(2)	15.316(11)
c(Å)	17.002(15)	20.995(4)	15.229(4)	16.547(13)
$\alpha(^{\circ})$	83.19(2)	80.25(5)	90.03(4)	-
$\beta(^{\circ})$	68.10(4)	78.99(5)	90.08(3)	91.15(3)
$\gamma(^{\circ})$	88.22(15)	65.07(5)	106.16(3)	-
$V(\text{\AA}^3)$	2978(5)	3243.6(12)	2680.4(6)	5655.0(7)
Z	2	1	2	4
$d(\text{calc}) [\text{gcm}^{-3}]$	1.436	1.337	1.384	1.475
$\mu [\text{mm}^{-1}]$	0.868	0.796	0.919	0.910
F(000)	1352	1372	1176	2640
Total Reflections	81266	75605	29359	34336
Unique Reflections	9526	11546	9559	5009
Observed data	8267	7735	6735	4135

[I > 2 σ(I)]				
R(int)	0.032	0.070	0.056	0.042
*R1, wR2 (all data)	0.0540, 0.1461	0.1218, 0.2633	0.0978, 0.2227	0.0717, 0.1820
R1, wR2 ([I > 2 σ(I)])	0.0445, 0.1322	0.0809, 0.2162	0.0690, 0.1879	0.0600, 0.1700
Residual Electron Density (eÅ ⁻³)	1.222, -1.014	0.959, -0.711	1.265, -0.844	1.493, -0.713
CCDC	1948661	1948662	1948663	1948664

$$*R1 = \Sigma ||F_o| - |F_c|| / \Sigma |F_o| \text{ and } wR2 = \Sigma w(|F_o|^2 - |F_c|^2)^2 / \Sigma w|F_o|^2)^{1/2}$$

Table II.2. Selected bond lengths (Å) of dimer A of complexes **1-3** and complex **4**.

Complex	1	2	3	4
Ni(1)-O(1)	2.080(3)	2.085(4)	2.076(3)	2.096(3)
Ni(1)-O(2)	2.072(3)	2.085(6)	2.095(3)	2.101(3)
Ni(1)-O(3)	2.102(3)	2.082(5)	2.086(4)	2.085(3)

Ni(1)-O(4)	2.082(3)	2.071(5)	2.082(4)	2.086(3)
Ni(1)-N(1)	2.100(3)	2.097(7)	2.095(5)	2.103(3)
Ni(1)-N(2)	2.102(3)	2.096(6)	2.085(5)	2.094(3)

Table II.3. Selected bond lengths (Å) of dimer B of complexes **1-3**.

Complex	1	2	3
Ni(2)-O(8)	2.080(3)	2.076(4)	2.087(3)
Ni(2)-O(9)	2.077(3)	2.089(5)	2.076(3)
Ni(2)-O(10)	2.099(4)	2.077(4)	2.091(4)
Ni(2)-N(3)	2.095(4)	2.084(5)	2.089(3)
Ni(2)-N(4)	2.093(3)	2.094(4)	2.084(5)
Ni(2)-O(7)	2.077(3)	2.080(4)	2.090(5)

Table II.4. Selected bond angles (°) of complexes **1-4**.

Complex	1	2	3	4
O(1)-Ni(1)-O(2)	87.19(10)	86.38(4)	88.20(13)	87.97(10)

O(1)-Ni(1)-O(3)	87.63(11)	88.70(2)	87.46(13)	86.96(11)
O(1)-Ni(1)-O(4)	91.49(10)	93.68(16)	92.09(13)	91.21(12)
O(1)-Ni(1)-N(1)	89.72(11)	90.70(2)	89.83(1)	89.49(15)
O(1)-Ni(1)-N(2)	176.38(11)	177.00(2)	178.01(3)	177.89(12)
O(2)-Ni(1)-O(3)	87.57(11)	88.7(2)	87.81(14)	88.05(11)
O(2)-Ni(1)-O(4)	95.70(10)	93.30(2)	94.10(14)	94.22(11)
O(2)-Ni(1)-N(1)	176.90(11)	177.00(2)	177.93(15)	177.33(14)
O(2)-Ni(1)-N(2)	90.11(12)	90.60(2)	89.81(17)	90.06(12)
O(3)-Ni(1)-O(4)	176.57(11)	177.00(2)	178.02(16)	177.04(12)
O(3)-Ni(1)-N(1)	92.13(11)	92.40(3)	92.72(2)	92.65(14)
O(3)-Ni(1)-N(2)	94.66(13)	91.50(2)	92.51(17)	93.75(14)
O(4)-Ni(1)-N(1)	84.54(11)	85.80(3)	85.35(17)	85.00(15)
O(4)-Ni(1)-N(2)	86.38(13)	86.30(4)	88.01(2)	88.16(15)
N(1)-Ni(1)-N(2)	92.99(13)	92.30(3)	92.17(4)	92.47(15)
O(10)-Ni(2)-N(4)	93.55(12)	86.25(4)	92.76(2)	-
N(3)-Ni(2)-N(4)	91.36(12)	94.18(3)	92.6(2)	-

O(7)-Ni(2)-O(8)	87.74(9)	86.10(15)	88.22(13)	-
O(7)-Ni(2)-O(9)	94.69(10)	89.17(4)	94.25(14)	-
O(7)-Ni(2)-O(10)	86.94(10)	91.86(1)	87.45(11)	-
O(7)-Ni(2)-N(3)	90.46(10)	89.49(1)	89.56(2)	-
O(7)-Ni(2)-N(4)	178.10(11)	175.76(2)	177.83(15)	-
O(8)-Ni(2)-O(9)	93.81(10)	88.50(3)	92.18(13)	-
O(8)-Ni(2)-O(10)	87.22(10)	94.35(1)	87.36(13)	-
O(8)-Ni(2)-N(3)	178.19(11)	175.56(1)	177.76(3)	-
O(8)-Ni(2)-N(4)	90.45(10)	90.26(3)	89.64(1)	-
O(9)-Ni(2)-O(10)	178.11(11)	177.05(2)	178.23(14)	-
O(9)-Ni(2)-N(3)	86.25(11)	91.38(2)	87.74(2)	-
O(9)-Ni(2)-N(4)	84.86(11)	92.90(2)	85.52(4)	-
O(10)-Ni(2)-N(3)	92.77(12)	86.25(4)	92.78(2)	-

II.3.3. Supramolecular interactions in solid state

The details of hydrogen bonding interactions in complexes **1-4** have been given in Table

II.5. Complexes **1-3** show similar kind hydrogen bonding interactions. Three hydrogen atoms,

H(1), H(3A) and H(3B), available in the ligand part in each complex are efficient for effective hydrogen bonding. A hydrogen atom, H(1), attached to a phenoxy oxygen atom, O(1), is involved in strong intermolecular hydrogen bonding interaction with a symmetry related $\{^a = 1-x, 1-y, 1-z$, in complex **1**, $^b = 1-x, -y, 1-z$, in complex **2** and $^c = -x, 1-y, 1-z$, in complex **3**} phenoxy oxygen atom, O(2), which leads to the formation of a dimeric unit **{Ni1}₂**.

Two remaining hydrogen atoms, H(3A) and H(3B), attached to a oxygen atom, O(3), are involved in intermolecular hydrogen bonding interactions with symmetry related $\{^a = 1-x, -y, 1-z$, in complex **1** and $^b = 1-x, -y, 1-z$, in complex **2** and $^c = -x, 1-y, 1-z$, in complex **3**} alkoxy oxygen atoms, O(5) and O(6), respectively. Similar kind of hydrogen bonding interactions are also been observed in dimer B unit in each complex (Table II.5). Pictorial representation of hydrogen bond interactions in dimer A of complexes **1**, **2** and **3** have been shown in Figures II.9, II.10 and II.11 respectively. In complex **4**, a hydrogen atom, H(1) attached to a phenoxy oxygen atom, O(1), is hydrogen bonded with its adjacent symmetry related phenoxy oxygen atom, O(2)^d {symmetry transformation, $^d = 3/2-x, 3/2-y, 1-z$ } to form a dimeric unit. The hydrogen bonding interactions in complex **4** has been already shown in Figures II.8 (see above).

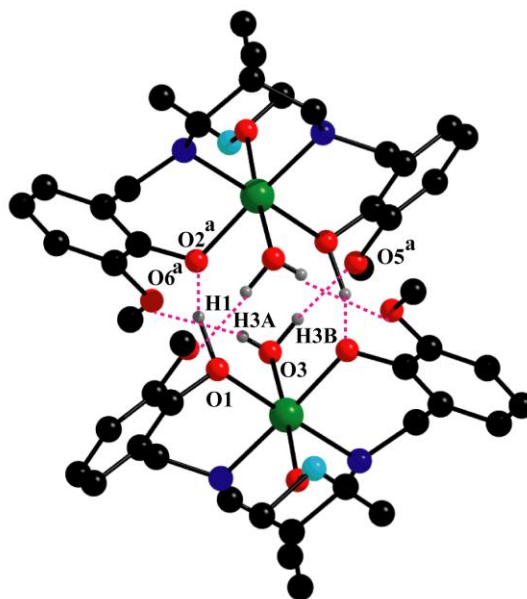


Fig. II.9: Perspective view of intermolecular hydrogen bonding interaction in dimer A of complex

1. Only the relevant hydrogen atoms have been shown for clarity. Symmetry transformation: ^a

=1-x, 1-y, 1-z.

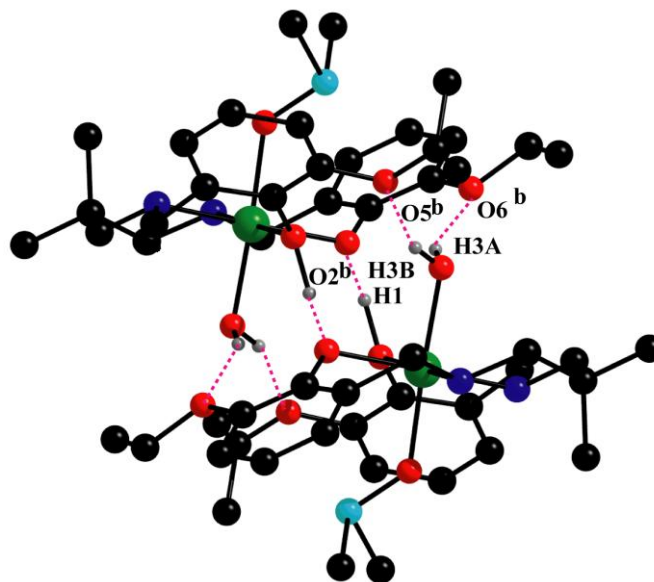


Fig. II.10: Perspective view of intermolecular hydrogen bonding interaction in dimer A of complex **2**. Only the relevant hydrogen atoms have been shown for clarity. Symmetry transformation: ^b = 1-x, -y, 1-z.

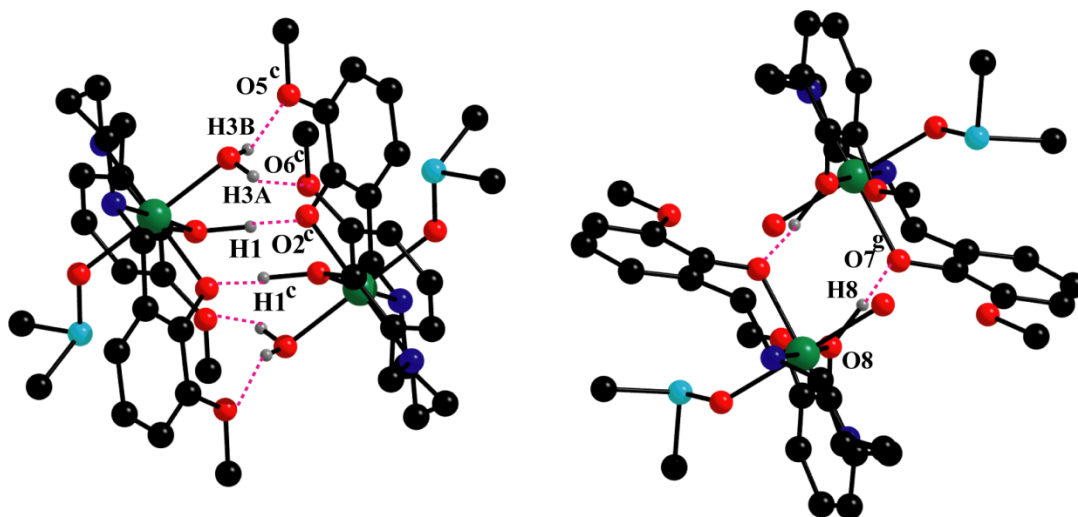


Fig. II.11: Perspective view of significant hydrogen bonding interaction in dimer A and B of complex **3**. Only the relevant hydrogen atoms have been shown for clarity. Symmetry transformation: ^c = -x, 1-y, 1-z.

Table II.5. Hydrogen bond distances (Å) and angles (°) for the complex **1-4**.

Complex	D-H...A	D-H	H...A	D...A	∠D-H...A
1	O(1)-H(1)...O(2) ^a	1.23(8)	1.23(8)	2.427(4)	163(6)
	O(3)-H(3A)...O(6) ^a	0.69(5)	2.15(5)	2.812(5)	162(5)
	O(3)-H(3B)...O(5) ^a	0.93(7)	1.87(6)	2.772(5)	163(5)

	O(8)-H(8)···O(7) ^e	1.19(5)	1.26(5)	2.426(4)	165(4)
	O(10)-H(10A)···O(12) ^e	0.69(4)	2.10(4)	2.772(5)	165(5)
	O(10)-H(10A)···O(11) ^e	0.74(5)	2.04(5)	2.762(5)	164(6)
2	O(1)-H(1)···O(2) ^b	1.20(9)	1.24(10)	2.426(6)	169(11)
	O(3)-H(3A)···O(6) ^b	0.79(8)	2.11(8)	2.823(9)	151(9)
	O(3)-H(3B)···O(5) ^b	0.79(8)	2.10(7)	2.843(8)	158(7)
	O(8)-H(8)···O(7) ^f	1.35(9)	1.09(9)	2.430(6)	170(6)
	O(9)-H(19A)···O(12) ^f	0.84(6)	2.02(6)	2.832(7)	162(6)
	O(9)-H(19B)···O(11) ^f	0.77(9)	2.04(9)	2.793(8)	160(12)
3	O(1)-H(1)···O(2) ^c	1.19(5)	1.24(5)	2.430(4)	175(6)
	O(3)-H(3A)···O(6) ^c	0.820(5)	2.000(5)	2.763(5)	155.00
	O(3)-H(3B)···O(5) ^c	0.71(5)	2.08(5)	2.761(6)	160(7)
	O(8)-H(8)···O(7) ^g	1.19(5)	1.25(5)	2.433(4)	174(5)
4	O(1)-H(1)···O(2) ^d	1.20(7)	1.29(7)	2.437(4)	155(5)

D = donor; H = hydrogen; A = acceptor, Symmetry transformation: ^a = 1-x, 1-y, 1-z, ^b = 1-x, -y, 1-z,

^c = -x, 1-y, 1-z, ^d = 3/2-x, 3/2-y, 1-z, ^e = 1-x, 2-y, 2-z, ^f = -x, 1-y, 2-z, ^g = 1-x, -y, 2-z.

These hydrogen bonded dimeric unit is further stabilized by strong C-H... π interactions. The details of C-H... π interactions have been listed in Table II.6. However no significant π ... π interactions have been found in each complex. Complex **1** shows significant C-H... π interactions involving the hydrogen atom, H(1B), attached to a carbon atom, C(1), with a symmetry related ($^h = x, y, -1+z$) phenyl ring, C(38)-C(39)-C(40)-C(41)-C(42)-C(43). Again two hydrogen atoms, H(22B) and H(23C) attached to two different methyl carbon atoms, C(22) and C(23), respectively are involved in intramolecular C-H... π interactions with two separate phenyl rings, C(2)-C(3)-C(4)-C(5)-C(6)-C(7) and C(15)-C(16)-C(17)-C(18)-C(19)-C(20), respectively.

Moreover two similar hydrogen atoms, H(45B) and H(46B), attached to two different methyl carbon atoms, C(45) and C(46), respectively of another subunit show similar type of intramolecular C-H... π interactions with two separate phenyl rings, C(25)-C(26)-C(27)-C(28)-C(29)-C(30) and C(38)-C(39)-C(40)-C(41)-C(42)-C(43), respectively. The hydrogen bonding interactions in complex **1** has been shown in Figure II.12.

In complex **2**, two hydrogen atoms, H(24B) and H(25C), attached to the carbon atoms, C(24) and C(25) respectively participates in intermolecular C-H... π interaction with the phenyl rings, C(2)-C(3)-C(4)-C(5)-C(6)-C(7) and C(15)-C(16)-C(17)-C(18)-C(19)-C(20), respectively (Figure II.13).

In complex **3**, two hydrogen atoms, H(10C) and H(10D), attached to the methyl carbon atom, C(24) and C(25), participates in intermolecular C-H... π interaction with the symmetry related ($i = -x, -y, 2-z$) phenyl rings, C(23)-C(24)-C(25)-C(26)-C(27)-C(28) and C(34)-C(35)-C(36)-C(37)-C(38)-C(39), respectively (Figure II.13). In addition two other hydrogen atoms, H(20B) and H(21C), attached to two separate methyl carbon atoms, C(20) and C(21), respectively participates in intramolecular C-H... π interaction with the phenyl rings, C(13)-C(14)-C(15)-C(16)-C(17)-C(18) and C(2)-C(3)-C(4)-C(5)-C(6)-C(7), respectively (Figure II.14).

In complex **4**, H(22C) and H(23B), attached to the methyl carbon atom, C(22) and C(23), respectively, participate in intramolecular C-H... π interactions with two separate phenyl rings, C(14)-C(15)-C(16)-C(17)-C(18)-C(19) and C(3)-C(4)-C(5)-C(6)-C(7)-C(8), respectively while another hydrogen atom, H(11A), attached to a carbon atom, C(11), is involved in intermolecular C-H... π interaction with a symmetry related ($m = 3/2-x, -1/2-y, 1/2-z$) phenyl ring, C(3)-C(4)-C(5)-C(6)-C(7)-C(8) to form a supramolecular chain (Figure II.15).

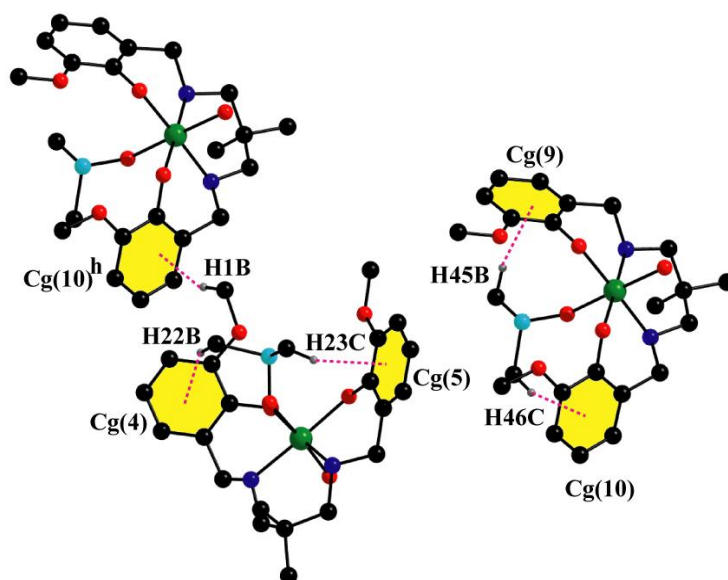


Fig. II.12: Perspective view of significant C-H \cdots π interactions in complex **1** with selective atom numbering scheme. Only relevant atoms have been shown in the figure for clarity. Symmetry transformation: ^h = x, y, -1+z.

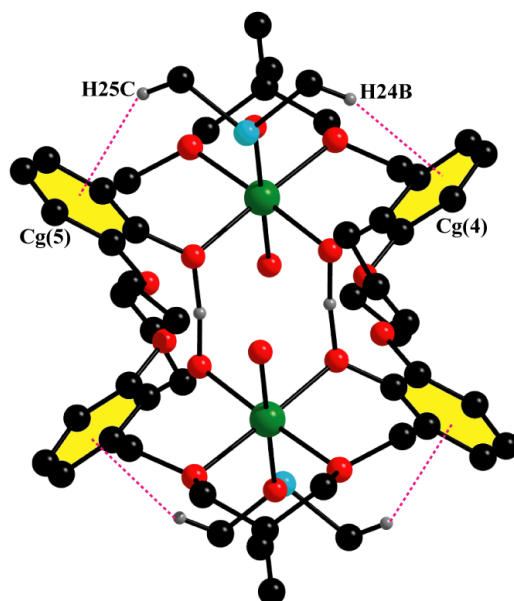


Fig. II.13: Perspective view of intramolecular C-H \cdots π stacking interactions in complex **2**. Only relevant hydrogen atoms have been shown in the figure for clarity.

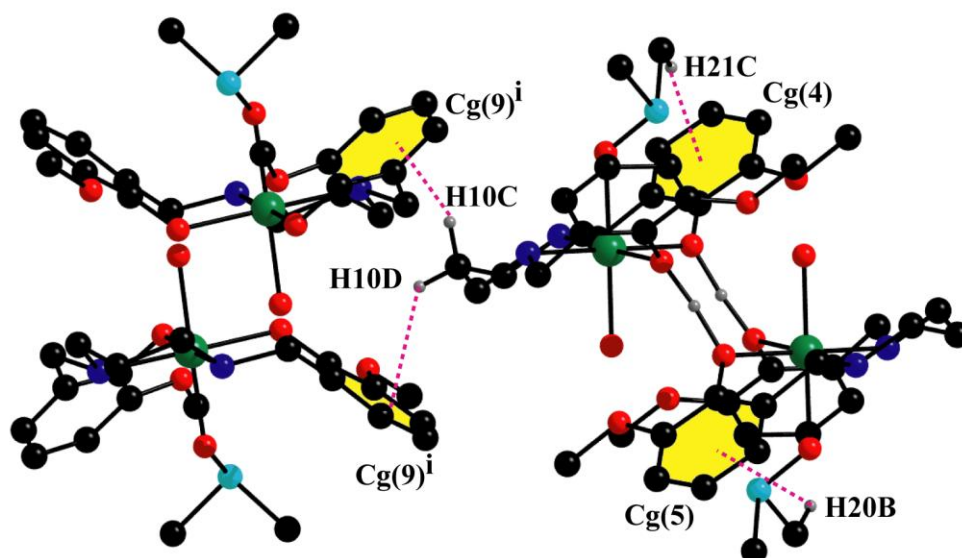


Fig. II.14: Perspective view of significant C-H \cdots π interactions in complex **3** with selective atom numbering scheme. Only relevant hydrogen atoms have been shown in the figure for clarity. Symmetry transformation: ⁱ = -x, -y, 2-z.

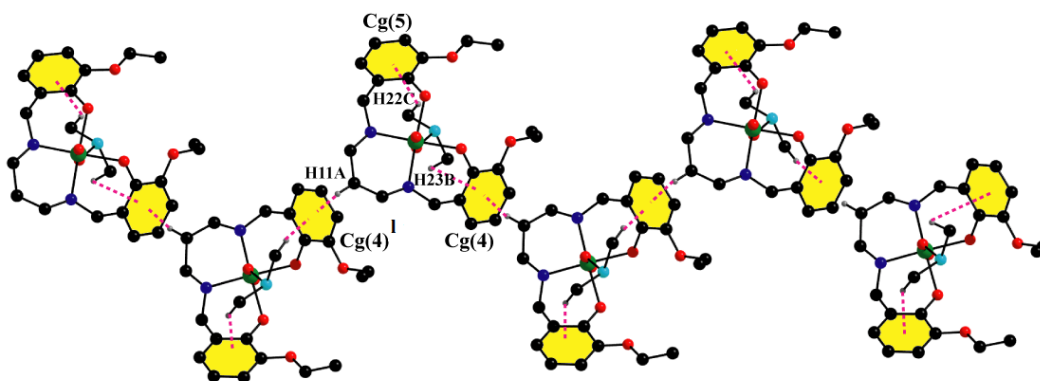


Fig. II.15: Perspective view of a supramolecular chain through intermolecular C-H $\cdots\pi$ stacking interactions in complex **4**. Only relevant atoms have been shown in the figure for clarity.

Symmetry transformation: $^l = 3/2-x, -1/2-y, 1/2-z$.

Table II.6. Geometric features (distances in Å and angles in °) of the C-H $\cdots\pi$ interactions obtained for complexes **1-4**.

Complexes	C-H \cdots Cg(ring)	H \cdots Cg(Å)	C-H \cdots Cg	C \cdots Cg (Å)
1	C(1)-H(1B) \cdots Cg(10) ^h	2.65	166	3.585(6)
	C(22)-H(22B) \cdots Cg(4)	2.92	155	3.810(8)
	C(23)-H(23C) \cdots Cg(5)	2.87	140	3.662(9)
	C(45)-H(45B) \cdots Cg(9)	2.81	144	3.629(7)
	C(46)-H(46B) \cdots Cg(10)	2.75	157	3.648(6)
2	C(24)-H(24B) \cdots Cg(4)	2.75	156	3.652(13)
	C(25)-H(25C) \cdots Cg(5)	2.82	144	3.646(15)
3	C(10)-H(10C) \cdots Cg(9) ⁱ	2.76	129	3.453(7)
	C(10)-H(10D) \cdots Cg(10) ⁱ	2.70	139	3.498(7)
	C(20)-H(20B) \cdots Cg(5)	2.67	146	3.504(8)
	C(21)-H(21C) \cdots Cg(4)	2.70	155	3.595(9)
	C(31)-H(31A) \cdots Cg(5) ^j	2.75	129	3.449(7)
	C(31)-H(31B) \cdots Cg(4) ^k	2.71	138	3.499(7)
	C(41)-H(41C) \cdots Cg(10)	2.71	154	3.605(9)

	C(42)-H(42B)⋯Cg(9)	2.66	146	3.499(8)
4	C(11)-H(11A)⋯Cg(4) ⁱ	2.61	146	3.459(3)
	C(22)-H(22C)⋯Cg(5)	2.68	146	3.523(7)
	C(22)-H(23B)⋯Cg(4)	2.91	152	3.787(8)

Symmetry transformation: ^h = x, y, -1+z, ⁱ = -x, -y, 2-z, ^j = 1-x, 1-y, 2-z, ^k = 1+x, y, 1+z, ^l = 3/2-x, -1/2-y, 1/2-z.

For complex **1**: Cg(4) = Centre of gravity of the ring [C(2)- C(3)-C(4)-C(5)-C(6)-C(7)]

Cg(5) = Centre of gravity of the ring [C(15)- C(16)-C(17)-C(18)-C(19)-C(20)]

Cg(9) = Centre of gravity of the ring [C(25)- C(26)-C(27)-C(28)-C(29)-C(30)]

Cg(10) = Centre of gravity of the ring [C(38)- C(39)-C(40)-C(41)-C(42)-C(43)]

For complex **2**: Cg(4) = Centre of gravity of the ring [C(3)- C(4)-C(5)-C(6)-C(7)-C(8)]

Cg(5) = Centre of gravity of the ring [C(16)- C(17)-C(18)-C(19)-C(20)-C(21)]

For complex **3**: Cg(4) = Centre of gravity of the ring [C(2)- C(3)-C(4)-C(5)-C(6)-C(7)]

Cg(5) = Centre of gravity of the ring [C(13)- C(14)-C(15)-C(16)-C(17)-C(18)]

Cg(9) = Centre of gravity of the ring [C(23)- C(24)-C(25)-C(26)-C(27)-C(28)]

Cg(10) = Centre of gravity of the ring [C(34)- C(35)-C(36)-C(37)-C(38)-C(39)]

For complex **4**: Cg(4) = Centre of gravity of the ring [C(3)- C(4)-C(5)-C(6)-C(7)-C(8)]

Cg(5) = Centre of gravity of the ring [C(14)- C(15)-C(16)-C(17)-C(18)-C(19)]

II. 3.4. Hirshfeld surfaces analysis

The Hirshfeld surface emerged from an attempt to delineate the space covered by a molecule in a crystal for the purpose of dividing the crystal electron density into molecular fragments.²⁰ The Hirshfeld surfaces of four complexes are mapped over d_{norm} (range -0.1 Å to 1.5 Å), shape index and curvedness (Figure II.16). Red spots appear on the Hirshfeld surfaces mapped with d_{norm} represent the dominant interactions within the complex in solid state. Various intermolecular interactions are summed up effectively in the spots with the large circular depressions (deep red) noticeable on the d_{norm} surfaces indicates the dominance of hydrogen bonding interactions and other weak interactions. The 2D fingerprint plot of Hirshfeld surfaces for all complexes and the comparative contributions of different interactions overlapping in full fingerprint plots have been provided in Figure S5. In the 2D fingerprint plot intermolecular interactions appear as distinct spikes. Complementary regions are observable in the 2D fingerprint plots where one molecule act as donor ($d_e > d_i$) and the other as an acceptor ($d_e < d_i$). The relative percentages of intermolecular interactions of four complexes have been shown in Figure II.17.

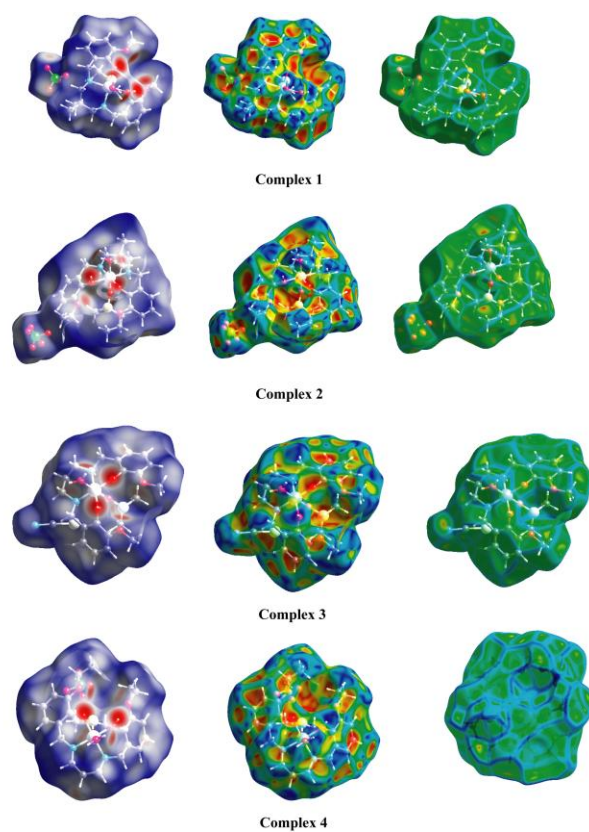


Fig. II.16: Hirshfeld surfaces mapped with d_{norm} (left column), shape index (middle) and curvedness (right column) of complexes **1-4**.

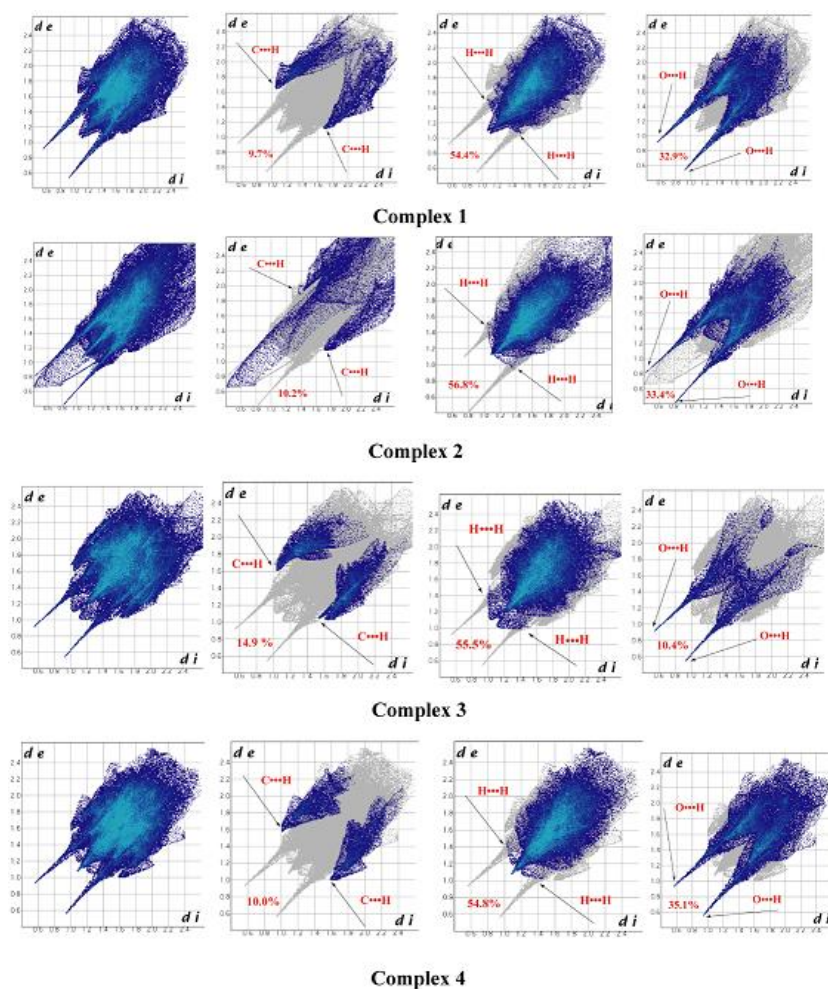


Fig. II.17: Fingerprint plot: Full (extreme left), resolved into H...C/C...H (second from the left), H...N/N...H (second from the right) and H...O/O...H (extreme right) contacts contributed to the total Hirshfeld Surface area of complexes **1-4**

II. 3.5. DFT results

The X-ray structures of complexes **1-4** reveal that they crystallize forming di-cationic dimers where two strong hydrogen bonds are formed between the phenoxy oxygen atoms of the ligands (Figures II.8-II.10). The O...O distance is shorter than 2.5 Å and both O atoms are of

identical pK_a . Therefore, these hydrogen bonds have strong covalent character and we wonder if they belong to LBHBs or single-well hydrogen bonds. It has been analyzed using B3LYP-D/def2-SVP calculations the nature of the hydrogen bonds. The energy profile of complex **1** has been computed as a representative model. The plot of the energy profile has been shown in Figure II.18 and it shows that the hydrogen bonds correspond to LBHBs with a barrier of 2.36 kcal/mol for the synchronous movement of both Hs in opposite directions (maintaining the inversion center since the X-ray geometry corresponds to the P-1 symmetry point group). Therefore the barrier for each hydrogen bond is only 1.18 kcal/mol, in agreement with the short O...O distance (2.426 Å in the model used for the calculations). These results suggest that in complexes **1–4** the hydrogen atoms can move freely between the two oxygen atoms and their average position in the O...O center.

The energetic features of the LBHBs also additional hydrogen bonds that are established between the coordinated water molecules and the methoxy groups of the ligand (see blue dashed lines in Figure II.19) has also been analyzed. The dimerization energy is very large ($\Delta E_1 = -107.7$ kcal/mol) due to the contribution of the strong LBHBs and the conventional O–H...O bonds that are expected to be also strong due to the enhanced acidity of these protons due to the coordination of the water molecule to the nickel(II) metal center. In an effort to estimate the contribution of the LBHBs, a theoretical model have been used where the water molecules are eliminated (Figure II.19b). As a result, the conventional hydrogen bonds are not established and the interaction energy drops to $\Delta E_2 = -73.3$ kcal/mol, that corresponds to the contribution of both LBHBs and also some additional van der Waals interactions established between the bulk of both molecules. This large interaction energy confirms the strong covalent nature of

these hydrogen bonds. This result is agreement with previous investigations in hydrogen bonds between hetero atoms with identical pK_a s where the ΔH of formation can approach 30 kcal/mol.⁴ Furthermore, the difference between ΔE_1 and ΔE_2 is a rough estimation of the four O–H...O bonds established by the coordinated water molecules and methoxy groups (–8.6 kcal/mol per hydrogen bond).

Finally, non covalent interaction plot (NCI plot) index has been made to further characterize the hydrogen bonds. It allows a direct assessment of host-guest complementarity and the extent to which non-covalent interactions stabilize a complex. Figure II.20 shows the NCI plot obtained for the self-assembled dimer extracted from the solid state of complex **1**. The NCI index indicates that the LBHBs are covalent bonds, since no isosurface is found between the H and O atoms. The O–H...O hydrogen bonds involving the coordinated water molecules are characterized by small and intense blue isosurfaces, thus supporting the strong nature of the interactions. Several green isosurfaces are also present between both monomeric units, thus revealing the existence of additional weak interactions that also stabilize the assembly.

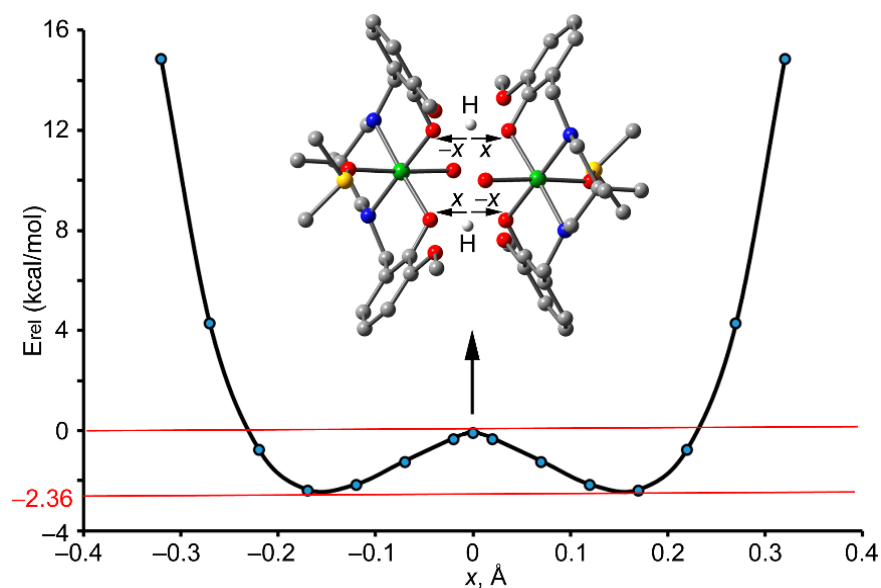


Fig. II.18: Energy diagram obtained for complex **1** at the B3LYP-D/def2-SVP level of theory. The energies are relative to the maximum. The hydrogen atoms were moved toward opposite directions of maintain the inversion center of symmetry.

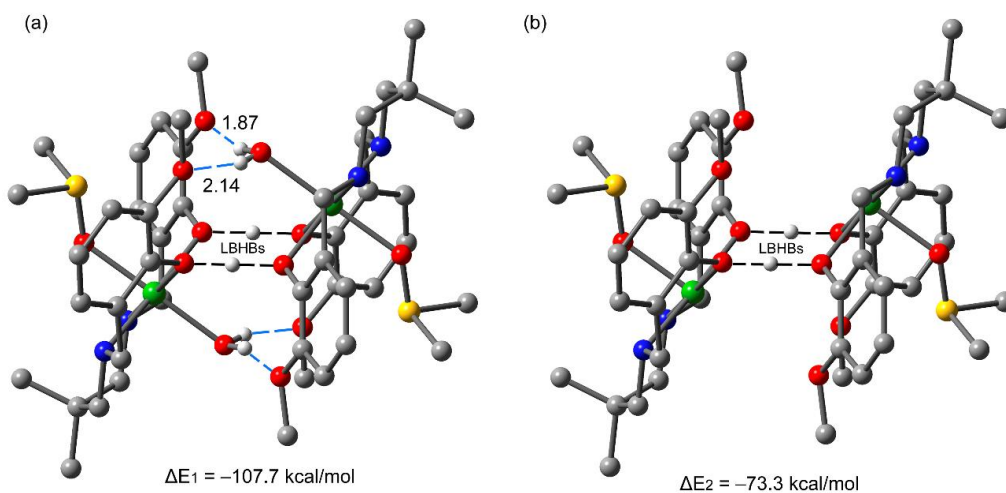


Fig. II.19: Theoretical models used to evaluate the LBHBs in complex **1** (a) and a mutated complex where two water molecules have been eliminated (b). Distances in Å.

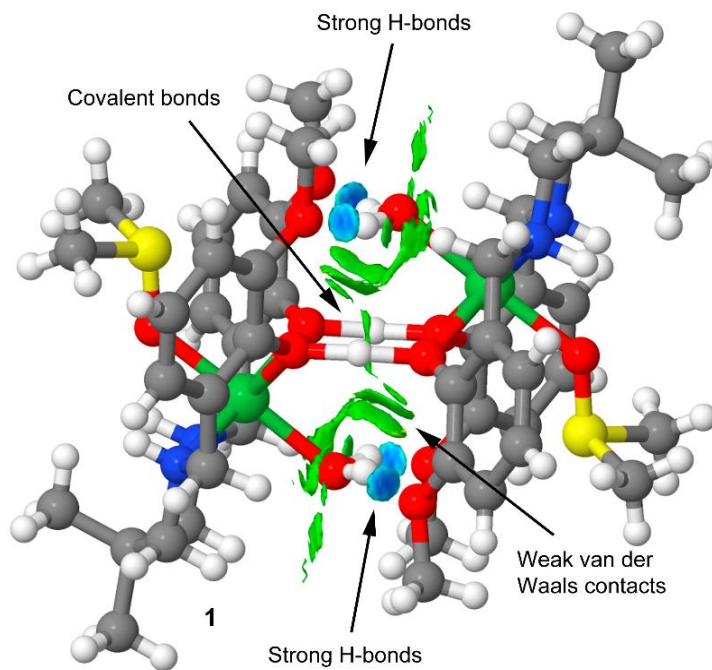


Fig. II.20: NCI plot of the self-assembled dimer of complex **1**. The gradient cut-off is $s = 0.35$ au, and the color scale is $-0.04 < \rho < 0.04$ au.

II. 3.5. IR and electronic spectra

A moderately sharp band in the range of $3280\text{--}3225\text{ cm}^{-1}$ has been noticed in the IR spectrum of each complex which may be assigned as the N–H stretching vibration of the reduced Schiff base ligand.²¹ Broad bands in the range of $3010\text{--}2865\text{ cm}^{-1}$ due to alkyl C–H stretching vibrations are routinely noticed in IR spectra of all complexes.²² Appearance of a broad band in each complex around 3400 cm^{-1} indicates the presence of O–H stretching vibrations of water molecules. A very strong band is obtained around 2045 cm^{-1} only in complex

3 due to the presence of non-coordinated thiocyanate ions.²³ IR spectra of all complexes have been given in Figures II.21-II.24.

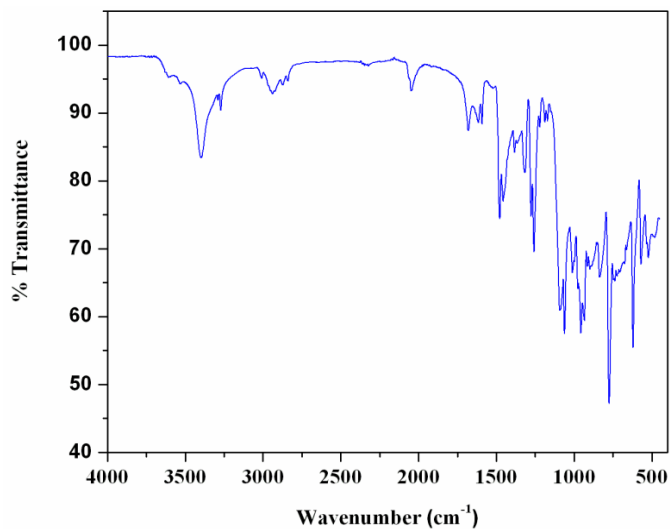


Fig. II.21: IR spectrum of complex 1

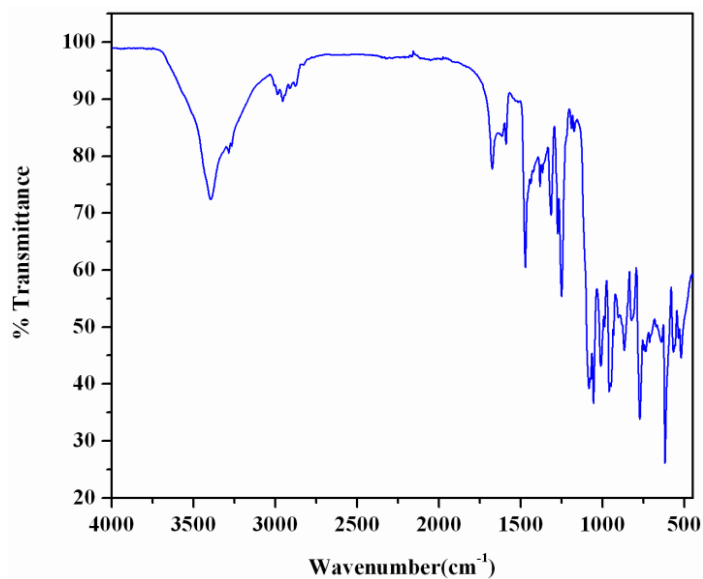


Fig. II.22: IR spectrum of complex 2

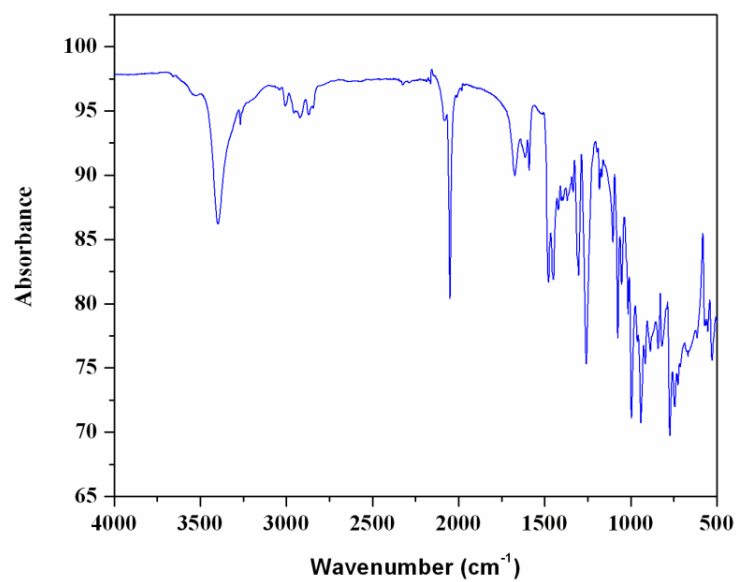


Fig. II.23: IR spectrum of complex 3

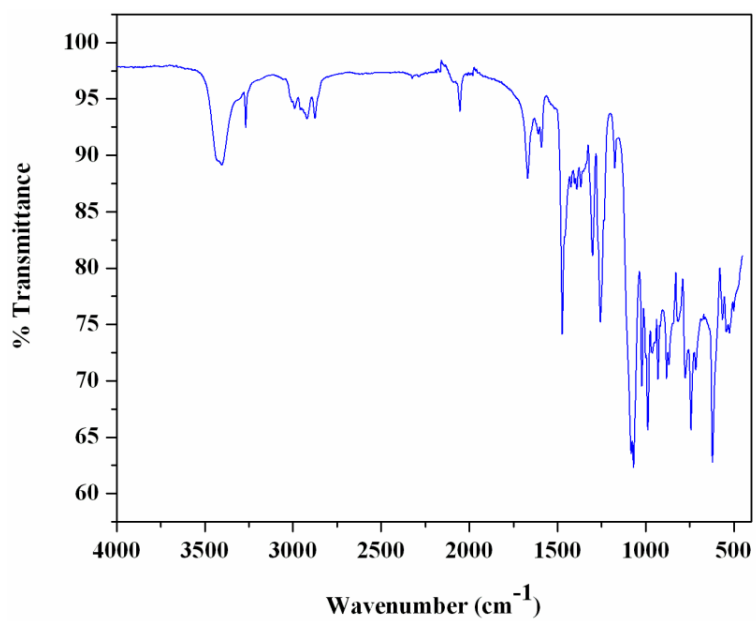


Fig. II.24: IR spectrum of complex 4

Electronic spectra of all four complexes in DMSO show two distinguished bands in the visible range around 625 nm and 735 nm. These bands may be assigned as ${}^3T_{1g}(F) \leftarrow {}^3A_{2g}(F)$ and ${}^3T_{2g}(F) \leftarrow {}^3A_{2g}(F)$, respectively.²⁴ The intense absorption bands at ~ 355 nm may be assigned as ligand to metal charge transfer (LMCT) bands, which obscure the 3rd d–d band, ${}^3T_{1g}(P) \leftarrow {}^3A_{2g}(F)$, expected for any octahedral nickel(II).²⁵ In addition, high energy absorption bands around 275 nm have been assigned to intra-ligand $\pi \rightarrow \pi^*$ transitions.²⁶ Electronic spectra of all complexes have been given in Figure II.25-II.28.

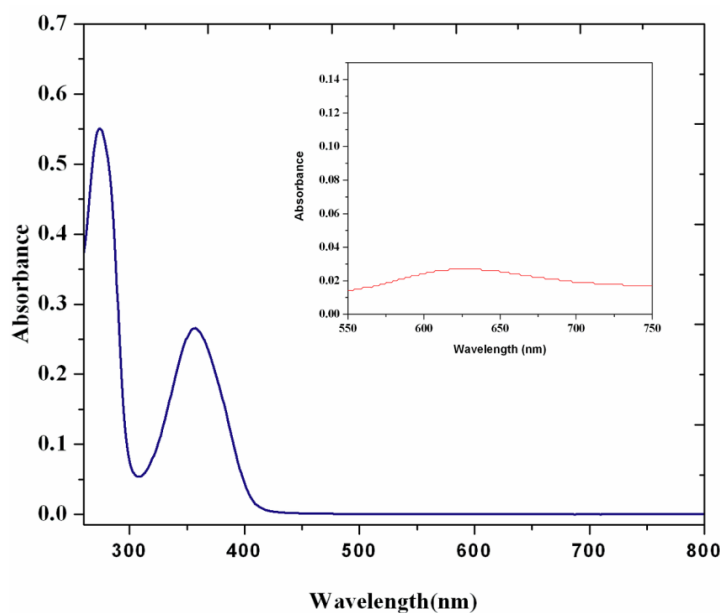


Fig. II.25: Electronic spectrum of complex **1**. Inset shows the selected small range (550-750 nm) electronic spectrum of the complex.

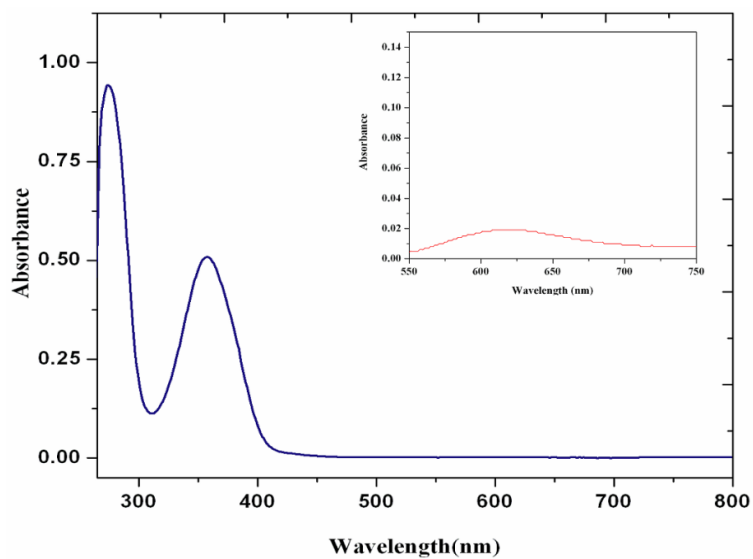


Fig. II.26: Electronic spectrum of complex **2**. Inset shows the selected small range (550-750 nm) electronic spectrum of the complex.

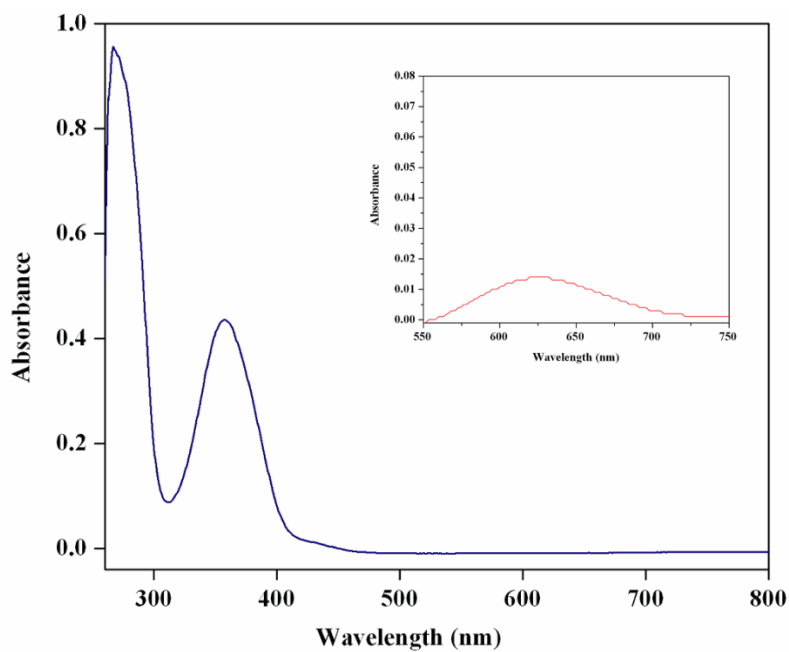


Fig. II.27: Electronic spectrum of complex **3**. Inset shows the selected small range (550-750 nm) electronic spectrum of the complex.

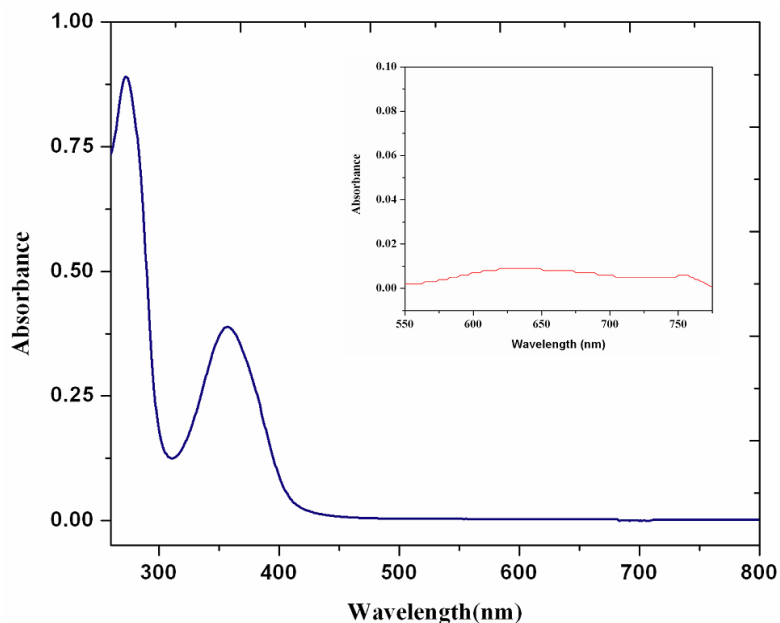


Fig. II.28: Electronic spectrum of complex **4**. Inset shows the selected small range (550-760 nm) electronic spectrum of the complex.

II. 4. Conclusion

In summary, we have synthesized and characterized four nickel(II) complexes (**1-4**) that form self-assembled dimers in the solid state where low barrier hydrogen bonds appear to play a prominent role. Structures of all complexes were confirmed by single crystal X-ray diffraction study. Each complex may be represented by a general formula $[Ni_2(HL)_2(DMSO)_2(H_2O)_2]X$ [$H_2L = N_2O_4$ donor reduced Schiff base ligand, X =counter anion]; X is perchlorate in **1**, **2** and **4** and X =thiocyanate in **3**. Use of reduced Schiff bases seems to be essential to form this type of hydrogen bonded dimeric species, as the non-reduced analogues of these Schiff bases fails to

prepare such complexes. More flexibility of the reduced Schiff bases compared to their Schiff base precursor may be the driving force in forming these complexes. The hydrogen bonds have been evaluated energetically and using the non covalent interaction plot. We conclude that the barrier is very low and, consequently, the hydrogen atoms can move freely with their average position between both oxygen atoms. The energy associated to the low barrier hydrogen bonds is very large due to the strong covalent character of the interaction.

References

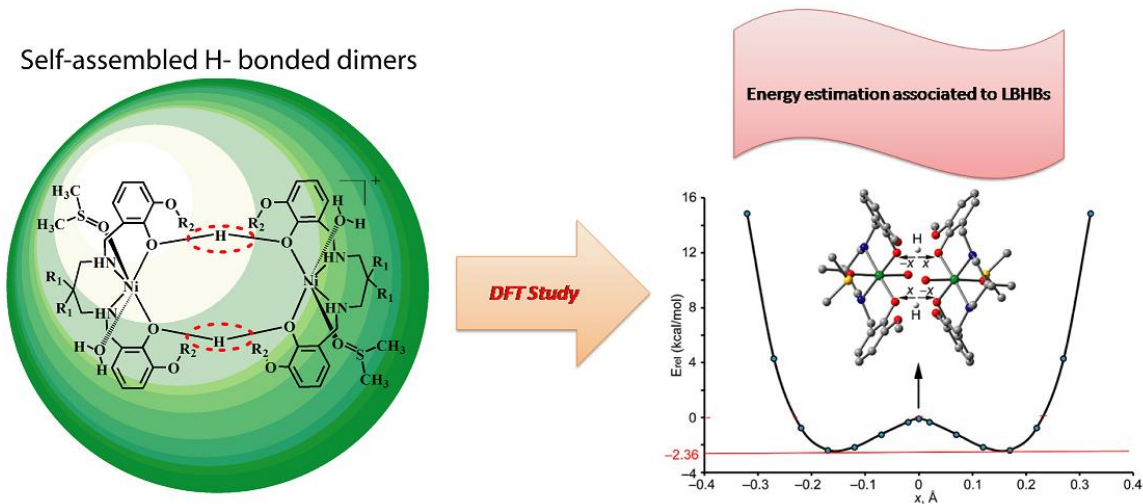
- 1 W. W. Cleland, P. A. Frey and J. A. Gerlt, *J. Bio. Chem.*, 1998, **273**, 25529-25532.
- 2 G. A. Jeffrey, *Introduction to Hydrogen Bonding*, Oxford University Press, New York, 1997.
- 3 M. Garcia-Viloca, A. Gonzalez-Lafont and J. M. Lluch, *J. Am. Chem. Soc.*, 1997, **119**, 1081–1086.
- 4 M. A. McAllister, *Can. J. Chem.*, 1997, **75**, 1195–1202.
- 5 K. Abu-Dari, K. N. Raymond and D. P. Freyberg, *J. Am. Chem. Soc.*, 1979, **101**, 3688–3689.
- 6 K. Abu-Dari, D. P. Freyberg and K. N. Raymond, *Inorg. Chem.*, 1979, **18**, 2427–2433.
- 7 T. Steiner and W. Saenger, *Acta Crystallogr. Sect. B Struct. Sci.*, 1994, **50**, 348–357.
- 8 P. Gilli, V. Bertolase, V. Ferretti and G. Gilli, *J. Am. Chem. Soc.*, 1994, **116**, 909–915.
- 9 K. P. Sarma and R. K. Poddar, *Transition Met. Chem.*, 1984, **9**, 135-138.
- 10 G.M. Sheldrick, *Acta Crystallogr., Sect.*, 2015, **C 71**, 3–8.
- 11 G. M. Sheldrick, SADABS, **V2014/5**, Software for Empirical Absorption Correction, University of Göttingen, Institute für Anorganische Chemie der Universität, Göttingen, Germany, 1999–2003.

- 12 M. J. Frisch, G. W. Trucks, H. B. Schlegel, G. E. Scuseria, M. A. Robb, J. R. Cheeseman, G. Scalmani, V. Barone, B. Mennucci, G. A. Petersson, H. Nakatsuji, M. Caricato, X. Li, H. P. Hratchian, A. F. Izmaylov, J. Bloino, G. Zheng, J. L. Sonnenberg, M. Hada, M. Ehara, K. Toyota, R. Fukuda, J. Hasegawa, M. Ishida, T. Nakajima, Y. Honda, O. Kitao, H. Nakai, T. Vreven, J. A. Montgomery, Jr., J. E. Peralta, F. Ogliaro, M. Bearpark, J. J. Heyd, E. Brothers, K. N. Kudin, V. N. Staroverov, R. Kobayashi, J. Normand, K. Raghavachari, A. Rendell, J. C. Burant, S. S. Iyengar, J. Tomasi, M. Cossi, N. Rega, J. M. Millam, M. Klene, J. E. Knox, J. B. Cross, V. Bakken, C. Adamo, J. Jaramillo, R. Gomperts, R. E. Stratmann, O. Yazyev, A. J. Austin, R. Cammi, C. Pomelli, J. W. Ochterski, R. L. Martin, K. Morokuma, V. G. Zakrzewski, G. A. Voth, P. Salvador, J. J. Dannenberg, S. Dapprich, A. D. Daniels, Ö. Farkas, J. B. Foresman, J. V. Ortiz, J. Cioslowski and D. J. Fox, Gaussian 09 (Gaussian, Inc., Wallingford CT, 2009).
- 13 S. Grimme, J. Antony, S. Ehrlich and H. Krieg, *J. Chem. Phys.*, 2010, **132**, 154104-154117.
- 14 S. F. Boys and F. Bernardi, *Mol. Phys.*, 1970, **19**, 553-566.
- 15 J. Contreras-García, E. R. Johnson, S. Keinan, R. Chaudret, J.-P. Piquemal, D. N. Beratan and W. Yang, *J. Chem. Theory Comput.*, 2011, **7**, 625–632.
- 16 Johnson, E. R.; Keinan, S.; Mori-Sánchez, P.; Contreras-García, J.; Cohen, A. J.; Yang, W. Revealing noncovalent interactions. *J. Am. Chem. Soc.* **2010**, *132*, 6498–6506.
- 17 A. Banerjee, A. Frontera and S. Chattopadhyay, *Dalton Trans.*, 2019, **48**, 11433-11447.

- 18 D. Matoga, J. Szklarzewicz, K. Stadnicka and M. S. Shongwe, *Inorg.Chem.*, 2007, **46**, 9042-9044.
- 19 Cremer, D.; Pople, J. A. A General Definition of Ring Puckering Coordinates. *J. Am. Chem. Soc.* 1975, **97**, 1354-1358.
- 20 F. L. Hirshfeld, *Theor. Chim. Acta.*, 1977, **44**, 129–138.
- 21 (a) A. Hazari, A. Das, P. Mahapatra and A. Ghosh, *Polyhedron*, 2017, **134**, 99-106; (b) S. Mirdya, A. Frontera and S. Chattopadhyay, *CrystEngComm*, 2019, DOI: 10.1039/C9CE01283D.
- 22 (a) S. Roy, T. Basak, S. Khan, M. G. B. Drew, A. Bauzá, A. Frontera and S. Chattopadhyay, *ChemistrySelect*, 2017, **2**, 9336-9343; (b) S. Mirdya, T. Basak and S. Chattopadhyay, *Polyhedron*, 2019, **170**, 253–263.
- 23 (a) S. Mirdya, S. Roy, S. Chatterjee, A. Bauzá, A. Frontera and S. Chattopadhyay, *Cryst. Growth Des.*, 2019, DOI: 10.1021/acs.cgd.9b00881; (b) K. Ghosh, K. Harms, A. Bauzá, A. Frontera and S. Chattopadhyay, *Dalton Trans.*, 2018, **47**, 331-347.
- 24 A. Bhattacharyya, P. K. Bhaumik, M. Das, A. Bauzá, P. P. Jana, K. Harms, A. Frontera and S. Chattopadhyay, *Polyhedron*, **2015**, *101*, 257–269.
- 25 S. Chattopadhyay, M. G. B. Drew and A. Ghosh, *Polyhedron*, 2007, **26**, 3513–3522.
- 26 A. Bhattacharyya, P. K. Bhaumik, P. P. Jana and S. Chattopadhyay, *Polyhedron* **2014**, *78*, 40–45.

Chapter II

A series of hydrogen bond mediated dinuclear nickel(II) complexes with reduced Schiff base ligands: An insight into the nature of hydrogen bonds in them



II.1. Introduction

The interaction energy of conventional hydrogen bonds basically depends on their geometric features like length and linearity. However, the difference in the pK_a values of the heavy atoms sharing the proton is also important.¹ The ΔH of formation of the water dimer is $\sim 5 \text{ kcal/mol}^1$ in the gas phase. However, the $\text{HO}-\text{H}\cdots\text{OH}_2$ hydrogen bond in water is weaker due to the large difference between the pK_a s of the donor group and the conjugate acid of the acceptor group (15.7 for H_2O and -1.7 for H_3O^+).² In the gas and solid state phases, hydrogen bonds between hetero atoms with similar pK_a s can be very short and strong (up to 30 kcal mol^{-1}).³⁻⁶ When groups of equal pK_a establish an hydrogen bond, three different situations may occur (see Figure II.1). The classical hydrogen bond where the hydrogen atom is covalently bonded to one of both oxygen atoms (dipole \cdots dipole interaction, see Figure II.1a). As the $\text{O}\cdots\text{O}$ distance is progressively shortened, the energy barrier lowers until it reaches the lower vibrational energy levels, thus leading to a low barrier hydrogen bond (LBHB, see Figure II.1b). In this case, the hydrogen atom can move freely between the two oxygen atoms with its average position is the center (high covalent character).^{7,8} Further shortening leads to a single-well hydrogen bond with the highest covalent character and interaction energy of the three situations.

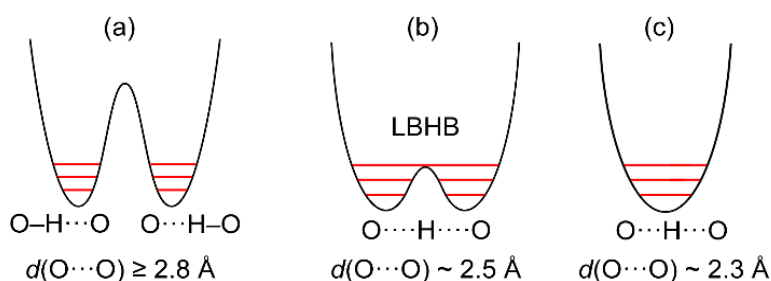


Fig. II.1: Energy diagrams for OH...H hydrogen bonds between groups of identical pKa. (a) Standard hydrogen bond with O...O distance $d(\text{O}\cdots\text{O}) \geq 2.8 \text{ \AA}$. (b) Low barrier hydrogen bond of $d(\text{O}\cdots\text{O}) \sim 2.55 \text{ \AA}$ (average position in the center). (c) Single-well hydrogen bond with $d(\text{O}\cdots\text{O}) \sim 2.3 \text{ \AA}$.

In this manuscript, we report the synthesis and X-ray characterization of a series of mononuclear nickel(II) complexes that form O...H...O hydrogen bonded dimers in the solid state where the O...O distance is very short, ranging from 2.35 to 2.45 Å. We have analyzed the hydrogen bonds using DFT calculations and the non covalent interaction plot (NCI plot) index to distinguish between the three possible situations represented in Figure II.1.

II.2. Experimental Section

II.2.1. Synthesis

II.2.1.1. Synthesis of Schiff base ligands

II.2.1.1.1. Synthesis of H_2L^a [N,N'-bis(3-methoxysalicylidene)-2,2-dimethyl-1,3-propanediamine], H_2L^b [N,N'-bis(3-ethoxysalicylidene)-2,2-dimethyl-1,3-propanediamine], H_2L^c [N,N'-bis(3-methoxysalicylidene)-1,3-propanediamine] and H_2L^d [N,N'-bis(3-ethoxysalicylidene)-1,3-propanediamine]

A methanol solution (10 mL) of 2,2-dimethyl-1,3-propanediamine (1 mmol, 0.12 mL) was mixed separately with of 3-methoxysalicylaldehyde (2 mmol, 304 mg) and 3-ethoxysalicylaldehyde, (2 mmol, 332 mg) and the resulting solutions were allowed to reflux for

ca. 2 h to synthesize two hexadentate N_2O_4 donor Schiff base ligands, H_2L^a [*N,N'*-bis(3-ethoxysalicylidene)2,2-dimethyl-1,3-propanediamine] and H_2L^b [*N,N'*-bis(3-ethoxysalicylidene)-2,2-dimethyl-1,3-propanediamine] respectively. Other two hexadentate Schiff bases, H_2L^c [*N,N'*-bis(3-methoxysalicylidene)-1,3-propanediamine] and H_2L^d [*N,N'*-bis(3-ethoxysalicylidene)-1,3-propanediamine] were synthesized following the similar procedure as mentioned above except 1,3-propanediamine (1 mmol, 0.11 mL) was used as the diamine instead of 2,2-dimethyl-1,3-propanediamine.

II.2.1.2. Synthesis of the reduced Schiff base ligands

II.2.1.2.1. Synthesis of H_2L^1 [(2,2-dimethyl-1,3-propanediyl)bis(iminomethylene)bis(6-methoxyphenol)]

The prepared Schiff base solution, H_2L^a was cooled to 0°C, and solid sodium borohydride (4 mmol, 150 mg) was then added gently to this solution with constant stirring. The solution was further acidified with glacial acetic acid (10 mL) and placed under reduced pressure in a rotary evaporator (~60°C). The residue was dissolved in water (15 mL) and extracted with dichloromethane (15 mL) using a separating funnel. Finally the dichloromethane part was dried using anhydrous sodium acetate to get the desired hexadentate N_2O_4 donor reduced Schiff base ligand, H_2L^1 . The ligand was not purified and used directly for the synthesis of complex **1**.

II.2.1.2.2. Synthesis of H_2L^2 [(2,2-dimethyl-1,3-propanediyl)bis(iminomethylene)bis(6-ethoxyphenol)]

A potential hexadentate N_2O_4 donor reduced Schiff base was synthesized following the similar procedure as used for Schiff base, H_2L^1 , except H_2L^b was used as the Schiff base derivative. It was not purified and was used directly for the synthesis of complex **2**.

II.2.1.2.3. Synthesis of H_2L^3 [(1,3-propanediyl)bis(iminomethylene)bis(6-methoxyphenol)]

A potential hexadentate N_2O_4 donor reduced Schiff base was synthesized following the same procedure as described above, except H_2L^c was used as the Schiff base derivative. It was not purified and was used directly for the synthesis of complex **3**.

II.2.1.2.4. Synthesis of H_2L^4 [(1,3-propanediyl)bis(iminomethylene)bis(6-ethoxyphenol)]

A potential hexadentate N_2O_4 donor reduced Schiff base was synthesized following the same procedure as described above, except H_2L^d was used as the Schiff base derivative. It was not purified and was used directly for the synthesis of complex **4**.

II.2.1.3. Synthesis of complexes

II.2.1.3.1. Synthesis of $[Ni_2(HL^1)_2(DMSO)_2(H_2O)_2]ClO_4 \cdot H_2O$ (1)

A methanol solution of nickel(II) perchlorate hexahydrate, (0.99 mmol, 257 mg), was added into the methanol solution of a reduced Schiff base ligand, H_2L^1 , with constant stirring and colour of the solution turned into dark green. Few drops of DMSO were added and the resulting solution was kept for crystallization. Dark green single crystals, suitable for X-ray diffraction, were obtained after 3-4 days on slow evaporation of the solution in open atmosphere.

Yield: 350 mg, (~54%, based on Ni). Anal. Calc. for $C_{46}H_{74}N_4Ni_2O_{22}S_2Cl_2$ (FW = 1287.49): C, 42.87; H, 5.74; N, 4.35%. Found: C, 42.8; H, 5.8; N, 4.3%. FT-IR (KBr, cm^{-1}): 3400 (ν_{O-H}), 3270 (ν_{N-H}), 2990-2850 (ν_{C-H}). UV-Vis, λ_{max} (nm), [ϵ_{max} ($dm^3 mol^{-1} cm^{-1}$)] (DMSO), 730 (1.01×10^2), 625 (2.00×10^2), 355 (2.65×10^3), 280 (5.6×10^3).

II.2.1.3.2. Synthesis of $[Ni_2(HL^2)_2(DMSO)_2(H_2O)_2]ClO_4$ (2)

Complex **2** was synthesized following the similar procedure as that for complex **1** except that the reduced Schiff base ligand, H_2L^2 , was used instead of H_2L^1 . Dark green coloured crystalline complex suitable for X-ray diffraction, started to separate from the solution after 3-4 days on standing at room temperature and was collected by filtration.

Yield: 343 mg, (~ 53%, based on Ni). Anal. Calc. for $C_{100}H_{152}Cl_4N_8Ni_4O_{40}$ (FW = 2612.52): C, 53.5; H, 5.8; N, 4.2%. Found: C, 53.4; H, 5.7; N, 4.3%. FT-IR (KBr, cm^{-1}): 3395 (ν_{O-H}), 3280 (ν_{N-H}), 2990-2865 (ν_{C-H}). UV-Vis, λ_{max} (nm), [ϵ_{max} ($dm^3 mol^{-1} cm^{-1}$)] (DMSO), 720 (0.89×10^2), 620 (1.80×10^2), 355 (4.84×10^3), 274 (9.38×10^4).

II.2.1.3.3. Synthesis of $[Ni_2(HL^3)_2(DMSO)_2(H_2O)_2]NCS$ (3)

A methanol solution of nickel(II) thiocyanate tetrahydrate (1.01 mmol, 250 mg) was added into the methanol solution of a reduced Schiff base ligand, H_2L^3 , with constant stirring and colour of the solution turned into dark green. Few drops of DMSO were added and the resulting solution was kept for crystallization. Dark green single crystals, suitable for X-ray diffraction, were obtained after 2-3 days on slow evaporation of the solution in open atmosphere.

Yield: 354 mg, (~ 63%, based on Ni). Anal. Calc. for $C_{44}H_{66}N_6Ni_2O_{12}S_4$ (FW = 1116.65): C, 47.2; H, 5.9; N, 7.5%. Found: C, 47.2; H, 5.8; N, 7.6%. FT-IR (KBr, cm^{-1}): 3390 (ν_{O-H}), 3260 (ν_{N-H}), 3012-2840 (ν_{C-H}), 2045 (ν_{NCS}). UV-Vis, $\lambda_{max}(nm)$, [ϵ_{max} ($dm^3 mol^{-1} cm^{-1}$)] (DMSO), 718 (1.40×10^2), 622 (2.78×10^3), 355 (4.34×10^2), 280 (9.49×10^4).

II.2.1.3.4. Synthesis of $[Ni_2(HL^4)_2(DMSO)_2(H_2O)_2]ClO_4$ (4)

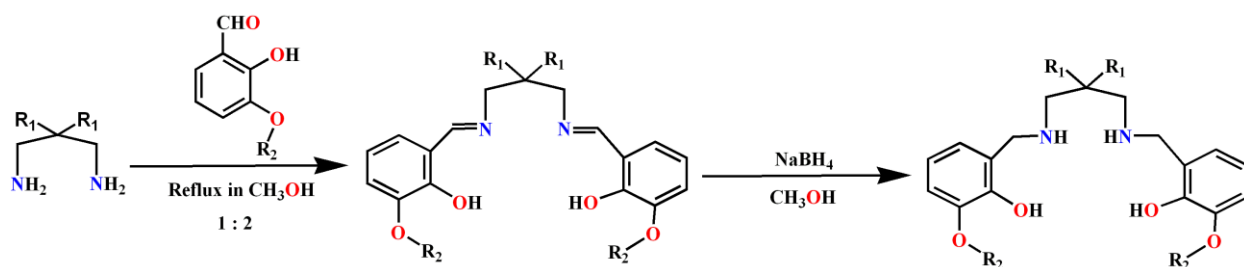
Complex **4** was synthesized following the similar procedure as that for complex **3** except that the reduced Schiff base ligand, H_2L^4 , was used instead of H_2L^3 . Dark green coloured crystalline complex suitable for X-ray diffraction, started to separate from the solution after 2-3 days on standing at room temperature and was collected by filtration.

Yield: 344 mg, (~54%, based on Ni). Anal. Calc. for $C_{46}H_{74}N_4Ni_2O_{20}S_2Cl_2$ (FW = 1255.49): C, 43.9; H, 5.9; N, 4.4%. Found: C, 43.8; H, 5.8; N, 4.5%. FT-IR (KBr, cm^{-1}): 3420 (ν_{O-H}), 3265 (ν_{N-H}), 2995-2870 (ν_{C-H}). UV-Vis, λ_{max} (nm), [ϵ_{max} ($dm^3 mol^{-1} cm^{-1}$)] (DMSO), 755 (0.58×10^2), 635 (0.93×10^2), 360 (3.8×10^3), 271 (8.86×10^3).

II.3. Results and discussion

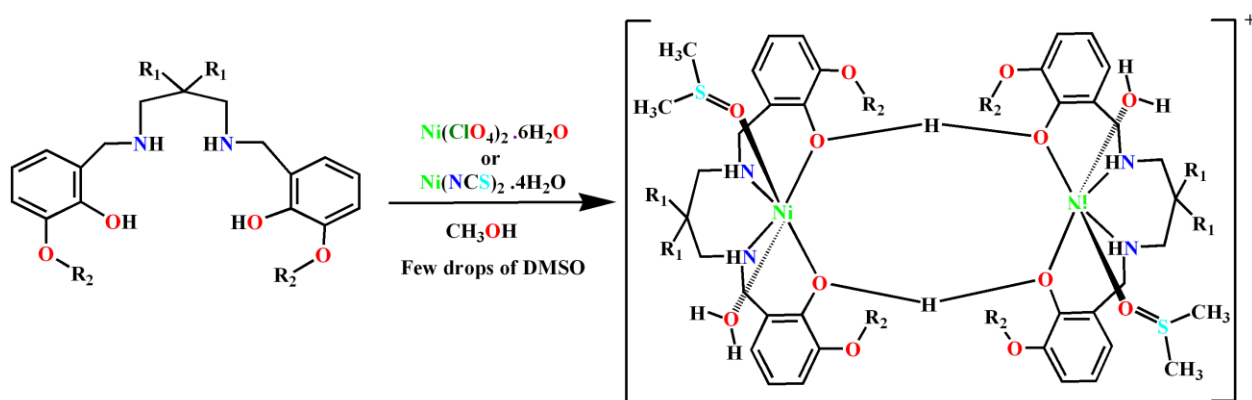
II.3.1. Synthesis

Two moles of 3-alkoxysalicylaldehydes (3-methoxy and 3-ethoxy) have been used to condense separately with 2,2-dimethyldiaminopropane and 1,3-diaminopropane in methanol medium to prepare four Schiff bases, H_2L^a , H_2L^b , H_2L^c and H_2L^d . These Schiff bases were then reduced with $NaBH_4$ in methanol under constant stirring at $0^\circ C$ to prepare four respective reduced Schiff bases, H_2L^1 , H_2L^2 , H_2L^3 and H_2L^4 respectively following the literature method.¹⁷



Scheme II.1: Synthetic route to 'reduced Schiff base' ligands.

These reduced Schiff bases on then reaction with nickel(II) perchlorate hexahydrate or nickel(II) thiocyanate in methanol and on adding few drops of DMSO to the individual reaction mixture gave rise to complexes **1-4**.



Scheme II.2: Synthetic route to complexes **1** ($R_1=Me$, $R_2=Me$), **2** ($R_1=Me$, $R_2=Et$), **3** ($R_1=H$, $R_2=Me$) and **4** ($R_1=H$, $R_2=Et$). Non coordinated counter anions have not been shown here.

Use of reduced Schiff base ligands seems to be crucial in forming these types of hydrogen bonded dimeric complexes, as the non-reduced Schiff bases were unable to produce such complexes. Many synthetic inorganic chemistry groups were prepared many homo and heteronuclear complexes with the corresponding non-reduced Schiff base ligands, but did not get complexes similar to complexes **1-4**. More flexibility of the reduced Schiff bases compared to their non-reduced precursors may be reason of this observation.

II.3.2. Structure description

II.3.2.1. Description of structures $[Ni_2(HL^1)_2(DMSO)_2(H_2O)_2]ClO_4 \cdot H_2O$ (**1**), $[Ni_2(HL^2)_2(DMSO)_2(H_2O)_2]ClO_4$ (**2**) and $[Ni_2(HL^3)_2(DMSO)_2(H_2O)_2]NCS$ (**3**)

X-ray crystal structure determination reveals that each of complexes **1-3** crystallize in triclinic space group, $P\bar{1}$. Crystallographic data and refinement details have been summarized in Table II.A.1. Potential N_2O_4 donor hexadentate reduced Schiff bases, H_2L^1 , H_2L^2 , and H_2L^3 , have been used to prepare these complexes respectively. Selected bond lengths and bond angles have been listed in Tables II.A.2 and II.A.3 respectively. Each complex actually possesses a dinuclear moiety formed via strong hydrogen bonds. Each complex consists of two independent centrosymmetric dimers (A and B) with equivalent geometry. A view of the dimer A of complex **1** is given in Figure II.2. A view of the dimers (A) of complexes **2** and **3** are given in Figure II.3. The structure of dimer B of each complex is very similar to the structure of dimer A in respective complex (Figure II.4-II.6).

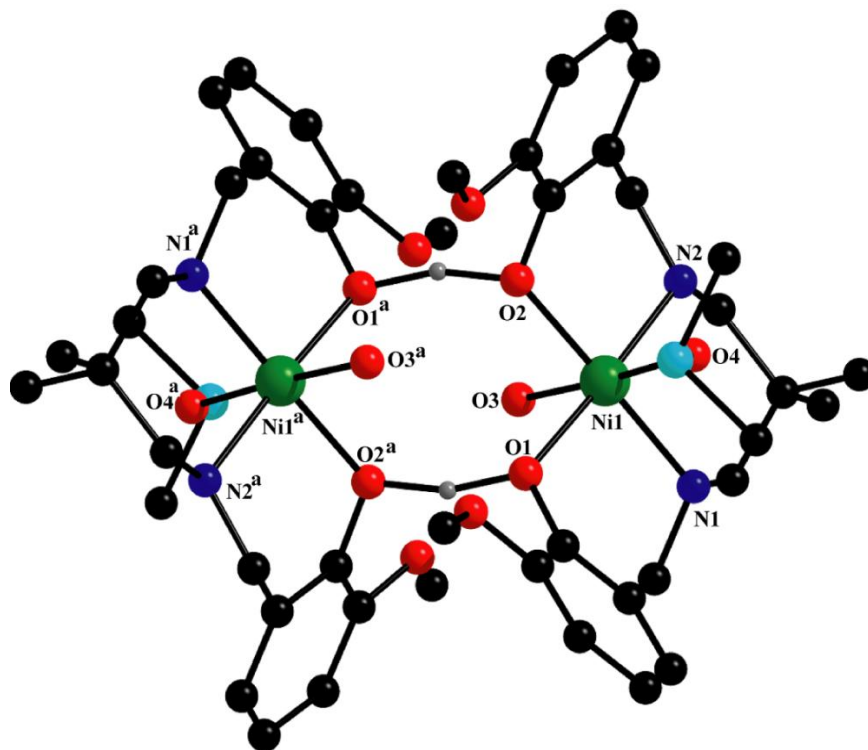
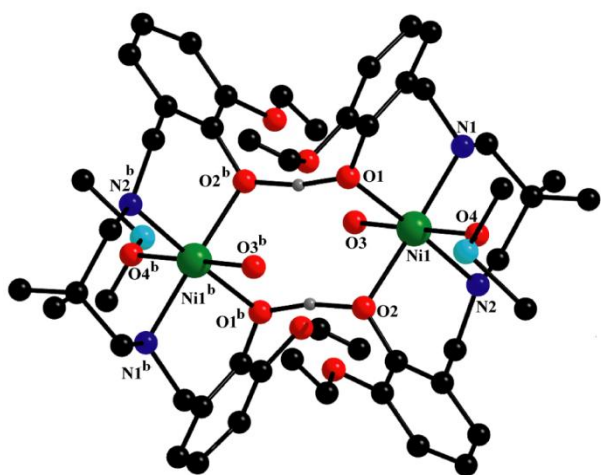


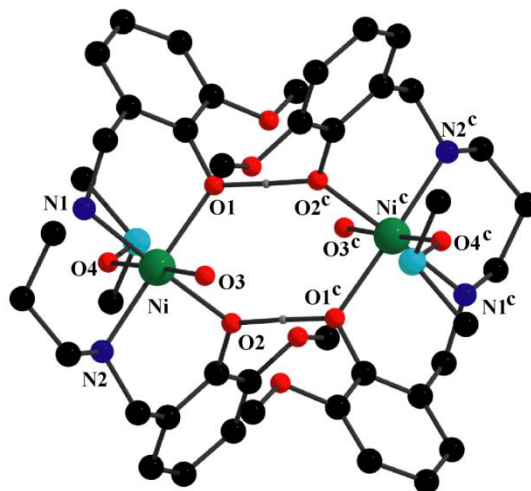
Fig. II.2: Perspective view of dimer A of complex **1** with selective atom-numbering scheme. Non co-ordinated perchlorate ion and hydrogen atoms have been omitted for clarity apart from those between the phenolic oxygen atoms.

In each dimeric unit, nickel(II) centers are hexa-coordinated and adopt distorted octahedral geometry. Each nickel(II) center, {Ni(1) of A and Ni(2) of B} is equatorially coordinated by two amine nitrogen atoms, {N(1) and N(2) for Ni(1) and N(3) and N(4) for Ni(2)}, two phenoxo oxygen atoms, {O(1) and O(2) for Ni(1) and O(7) and O(8) for Ni(2)}, of the reduced Schiff base units. The axial sites are coordinated by two oxygen atoms, {O(3) and O(4) for Ni(1) and O(9) and O(10) for Ni(2)} of coordinated water and DMSO molecule. Each of the reduced Schiff bases are dibasic in character, but loses only one proton to form mononegative anion, which, in turn, connects with another such moiety via strong hydrogen bonding to form the

symmetric dimeric structure. The deprotonations of the hydroxyl group are well reflected in the nickel(II)-oxygen bond lengths (Table 2). The deprotonated hydroxyl groups are bound strongly (shorter bond length) with nickel(II) centers compared with the non-deprotonated hydroxyl groups.¹⁸ The saturated six membered chelate rings, Ni(1)-N(1)-C(9)-C(10)-C(13)-N(2), Ni(1)-N(1)-C(10)-C(11)-C(14)-N(2) and Ni(1)-N(1)-C(9)-C(10)-C(11)-N(2), in dimer A of complexes **1**, **2** and **3** respectively represent individual chair conformations with puckering parameters,¹⁹ $q(2) = 0.583(4) \text{ \AA}$, $\phi = 168(2)^\circ$, $q(2) = 0.589(8) \text{ \AA}$, $\phi = 199(7)^\circ$ and $q(2) = 0.610(6) \text{ \AA}$, $\phi = 3(9)^\circ$ respectively. Similarly the saturated six membered chelate rings, Ni(2)-N(3)-C(32)-C(33)-C(36)-N(4), Ni(2)-N(3)-C(35)-C(36)-C(39)-N(4) and Ni(2)-N(3)-C(30)-C(31)-C(32)-N(4), in dimer B of complexes **1**, **2** and **3** respectively also represent individual chair conformations with puckering parameters, $q(2) = 0.563(7) \text{ \AA}$, $\phi = 180(3)^\circ$, $q(2) = 0.563(7) \text{ \AA}$, $\phi = 180(3)^\circ$ and $q(2) = 0.610(6) \text{ \AA}$, $\phi = 184(8)^\circ$ respectively.



Complex 2



Complex 3

Fig. II.3: Perspective view of dimer A of complexes **2** and **3** with selective atom-numbering scheme. Non co-ordinated counter anions and hydrogen atoms have been omitted for clarity apart from those between the phenolic oxygen atoms.

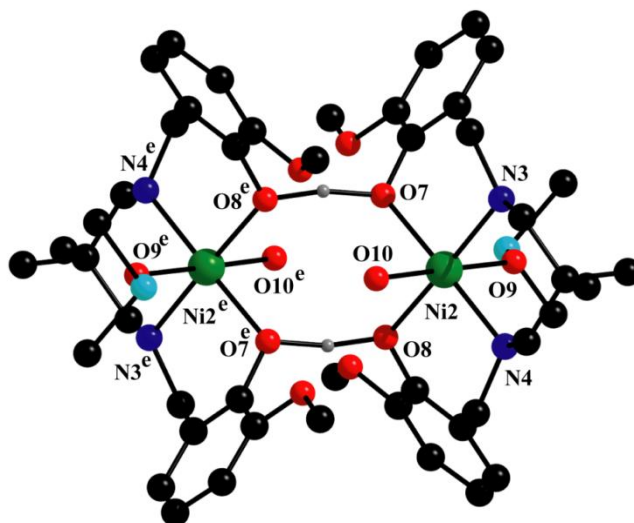


Fig. II.4: Perspective view of dimer B of complex **1** with selective atom-numbering scheme. Non co-ordinated perchlorate ion and hydrogen atoms have been omitted for clarity apart from those between the phenolic oxygen atoms. Symmetry transformation: $^e = 1-x, 2-y, 2-z$.

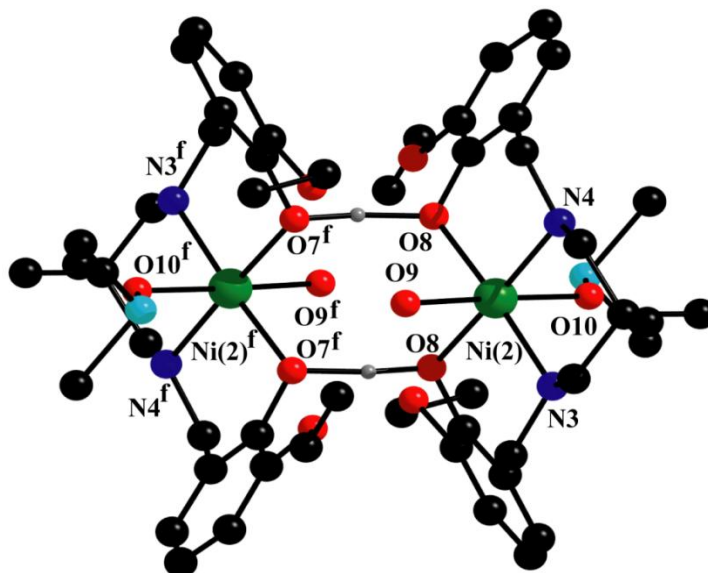


Fig. II.5: Perspective view of dimer B of complex **2** with selective atom-numbering scheme. Non co-ordinated perchlorate ion and hydrogen atoms have been omitted for clarity apart from those between the phenolic oxygen atoms. Symmetry transformation: $^f = -x, 1-y, 2-z$.

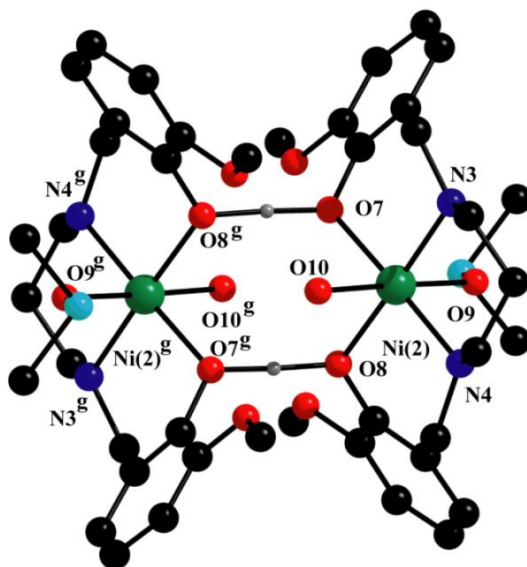


Fig. II.6: Perspective view of dimer B of complex **3** with selective atom-numbering scheme. Non co-ordinated thiocyanate ion and hydrogen atoms have been omitted for clarity apart from those between the phenolic oxygen atoms. Symmetry transformation: $^g = 1-x, -y, 2-z$.

II.3.2.2. $[Ni_2(HL^4)_2(DMSO)_2(H_2O)_2]ClO_4$ (**4**)

X-ray crystal structure determination reveals that complex **4** crystallizes in monoclinic space group, $C2/c$. A potential N_2O_4 donor hexadentate reduced Schiff base, H_2L^4 , have been used to prepare this complex. It contains a dinuclear moiety formed via strong hydrogen bonds. The structure of complex **4** has been shown in Figure II.7. The geometry around each nickel(II) centers are quite similar to that described for complexes **1-3** but it exists as only one dimeric unit. Both the nickel(II) centers are hexa-coordinated and adopt distorted octahedral geometry.

Each nickel(II) center, is equatorially coordinated by two amine nitrogen atoms, {N(1) and N(2)} and two phenoxo oxygen atoms, {O(1) and O(2)}, of the reduced Schiff base unit. The axial sites are coordinated by two oxygen atoms, {O(3) and O(4)}, of coordinated water and DMSO molecule. The saturated six membered chelate rings, Ni(1)-N(1)-C(10)-C(11)-C(12)-N(2), in of complex **4** represent chair conformations with puckering parameters , $q(2) = 0.589(5) \text{ \AA}$, $\phi = 182(2)^\circ$.

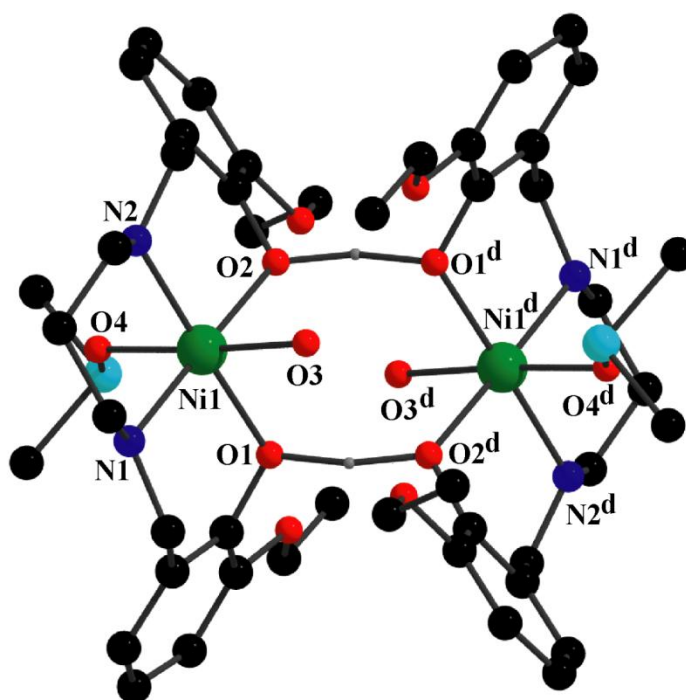


Fig. II.7: Perspective view of complex **4** with selective atom-numbering scheme. Non coordinated perchlorate ions and hydrogen atoms have been omitted for clarity apart from those between the phenolic oxygen atoms.

Table II.1. Crystal data and refinement details of complexes **1-4**.

Complex	1	2	3	4
Formula	C ₄₆ H ₇₄ N ₄ Ni ₂ O ₂₂ S ₂ Cl ₂	C ₁₀₀ H ₁₅₂ Cl ₄ N ₈ Ni ₄ O ₄₀	C ₄₄ H ₆₆ N ₆ Ni ₂ O ₁₂ S ₄	C ₄₆ H ₇₄ N ₄ Ni ₂ O ₂₀ S ₂ Cl ₂
Formula Weight	1287.49	2611.10	1116.65	1255.49
Crystal System	Triclinic	Triclinic	Triclinic	Monoclinic
Space group	$P\bar{1}$	$P\bar{1}$	$P\bar{1}$	$C2/c$
a(Å)	13.044(11)	12.344(3)	13.422(1)	22.317(2)
b(Å)	14.575(13)	14.130(3)	13.651(2)	15.316(11)
c(Å)	17.002(15)	20.995(4)	15.229(4)	16.547(13)
α(°)	83.19(2)	80.25(5)	90.03(4)	-
β(°)	68.10(4)	78.99(5)	90.08(3)	91.15(3)
γ(°)	88.22(15)	65.07(5)	106.16(3)	-
V(Å ³)	2978(5)	3243.6(12)	2680.4(6)	5655.0(7)
Z	2	1	2	4
d(calc) [gcm ⁻³]	1.436	1.337	1.384	1.475

μ [mm ⁻¹]	0.868	0.796	0.919	0.910
F(000)	1352	1372	1176	2640
Total Reflections	81266	75605	29359	34336
Unique Reflections	9526	11546	9559	5009
Observed data [I > 2 σ (I)]	8267	7735	6735	4135
R(int)	0.032	0.070	0.056	0.042
*R1, wR2 (all data)	0.0540, 0.1461	0.1218, 0.2633	0.0978, 0.2227	0.0717, 0.1820
R1, wR2 ([I > 2 σ (I)])	0.0445, 0.1322	0.0809, 0.2162	0.0690, 0.1879	0.0600, 0.1700
Residual Electron Density (eÅ ⁻³)	1.222, -1.014	0.959, -0.711	1.265, -0.844	1.493, -0.713

$$*R1 = \sum ||F_o| - |F_c|| / \sum |F_o| \text{ and } wR2 = \sum w(|F_o|^2 - |F_c|^2)^2 / \sum w|F_o|^2)^{1/2}$$

Table II.2. Selected bond lengths (Å) of dimer A of complexes **1-3** and complex **4**.

Complex	1	2	3	4
Ni(1)-O(1)	2.080(3)	2.085(4)	2.076(3)	2.096(3)
Ni(1)-O(2)	2.072(3)	2.085(6)	2.095(3)	2.101(3)
Ni(1)-O(3)	2.102(3)	2.082(5)	2.086(4)	2.085(3)
Ni(1)-O(4)	2.082(3)	2.071(5)	2.082(4)	2.086(3)
Ni(1)-N(1)	2.100(3)	2.097(7)	2.095(5)	2.103(3)
Ni(1)-N(2)	2.102(3)	2.096(6)	2.085(5)	2.094(3)

Table II.3. Selected bond lengths (Å) of dimer B of complexes **1-3**.

Complex	1	2	3
Ni(2)-O(8)	2.080(3)	2.076(4)	2.087(3)
Ni(2)-O(9)	2.077(3)	2.089(5)	2.076(3)
Ni(2)-O(10)	2.099(4)	2.077(4)	2.091(4)
Ni(2)-N(3)	2.095(4)	2.084(5)	2.089(3)
Ni(2)-N(4)	2.093(3)	2.094(4)	2.084(5)

Ni(2)-O(7)	2.077(3)	2.080(4)	2.090(5)
------------	----------	----------	----------

Table II.4. Selected bond angles (°) of complexes **1-4**.

Complex	1	2	3	4
O(1)-Ni(1)-O(2)	87.19(10)	86.38(4)	88.20(13)	87.97(10)
O(1)-Ni(1)-O(3)	87.63(11)	88.70(2)	87.46(13)	86.96(11)
O(1)-Ni(1)-O(4)	91.49(10)	93.68(16)	92.09(13)	91.21(12)
O(1)-Ni(1)-N(1)	89.72(11)	90.70(2)	89.83(1)	89.49(15)
O(1)-Ni(1)-N(2)	176.38(11)	177.00(2)	178.01(3)	177.89(12)
O(2)-Ni(1)-O(3)	87.57(11)	88.7(2)	87.81(14)	88.05(11)
O(2)-Ni(1)-O(4)	95.70(10)	93.30(2)	94.10(14)	94.22(11)
O(2)-Ni(1)-N(1)	176.90(11)	177.00(2)	177.93(15)	177.33(14)
O(2)-Ni(1)-N(2)	90.11(12)	90.60(2)	89.81(17)	90.06(12)
O(3)-Ni(1)-O(4)	176.57(11)	177.00(2)	178.02(16)	177.04(12)
O(3)-Ni(1)-N(1)	92.13(11)	92.40(3)	92.72(2)	92.65(14)
O(3)-Ni(1)-N(2)	94.66(13)	91.50(2)	92.51(17)	93.75(14)

O(4)-Ni(1)-N(1)	84.54(11)	85.80(3)	85.35(17)	85.00(15)
O(4)-Ni(1)-N(2)	86.38(13)	86.30(4)	88.01(2)	88.16(15)
N(1)-Ni(1)-N(2)	92.99(13)	92.30(3)	92.17(4)	92.47(15)
O(10)-Ni(2)-N(4)	93.55(12)	86.25(4)	92.76(2)	-
N(3)-Ni(2)-N(4)	91.36(12)	94.18(3)	92.6(2)	-
O(7)-Ni(2)-O(8)	87.74(9)	86.10(15)	88.22(13)	-
O(7)-Ni(2)-O(9)	94.69(10)	89.17(4)	94.25(14)	-
O(7)-Ni(2)-O(10)	86.94(10)	91.86(1)	87.45(11)	-
O(7)-Ni(2)-N(3)	90.46(10)	89.49(1)	89.56(2)	-
O(7)-Ni(2)-N(4)	178.10(11)	175.76(2)	177.83(15)	-
O(8)-Ni(2)-O(9)	93.81(10)	88.50(3)	92.18(13)	-
O(8)-Ni(2)-O(10)	87.22(10)	94.35(1)	87.36(13)	-
O(8)-Ni(2)-N(3)	178.19(11)	175.56(1)	177.76(3)	-
O(8)-Ni(2)-N(4)	90.45(10)	90.26(3)	89.64(1)	-
O(9)-Ni(2)-O(10)	178.11(11)	177.05(2)	178.23(14)	-
O(9)-Ni(2)-N(3)	86.25(11)	91.38(2)	87.74(2)	-

O(9)-Ni(2)-N(4)	84.86(11)	92.90(2)	85.52(4)	-
O(10)-Ni(2)-N(3)	92.77(12)	86.25(4)	92.78(2)	-

II.3.3. Supramolecular interactions in solid state

The details of hydrogen bonding interactions in complexes **1-4** have been given in Table II.4. Complexes **1-3** show similar kind hydrogen bonding interactions. Three hydrogen atoms, H(1), H(3A) and H(3B), available in the ligand part in each complex are efficient for effective hydrogen bonding. A hydrogen atom, H(1), attached to a phenoxy oxygen atom, O(1), is involved in strong intermolecular hydrogen bonding interaction with a symmetry related $\{^a = 1-x, 1-y, 1-z$, in complex **1**, $^b = 1-x, -y, 1-z$, in complex **2** and $^c = -x, 1-y, 1-z$, in complex **3**} phenoxy oxygen atom, O(2), which leads to the formation of a dimeric unit $\{\text{Ni1}\}_2$.

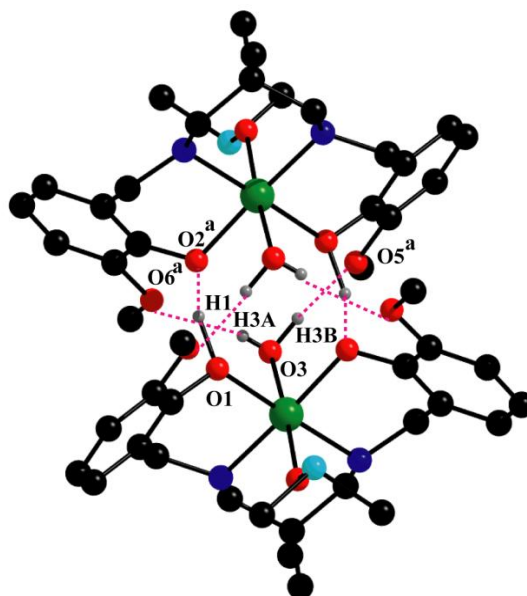


Fig. II.8: Perspective view of intermolecular hydrogen bonding interaction in dimer A of complex

1. Only the relevant hydrogen atoms have been shown for clarity. Symmetry transformation: ^a = 1-x, 1-y, 1-z.

Two remaining hydrogen atoms, H(3A) and H(3B), attached to a oxygen atom, O(3), are involved in intermolecular hydrogen bonding interactions with symmetry related {^a = 1-x, -y, 1-z, in complex **1** and ^b = 1-x, -y, 1-z, in complex **2** and ^c = -x,1-y,1-z, in complex **3**} alkoxy oxygen atoms, O(5) and O(6), respectively. Similar kind of hydrogen bonding interactions are also been observed in dimer B unit in each complex (Table 4). Pictorial representation of hydrogen bond interactions in dimer A of complexes **1**, **2** and **3** have been shown in Figures II.8, II.9 and II.10 respectively. In complex **4**, a hydrogen atom, H(1) attached to a phenoxy oxygen atom, O(1), is hydrogen bonded with its adjacent symmetry related phenoxy oxygen atom, O(2)^d {symmetry transformation, ^d = 3/2-x,3/2-y,1-z} to form a dimeric unit. The hydrogen bonding interactions in complex **4** has been already shown in Figure 3 (see above).

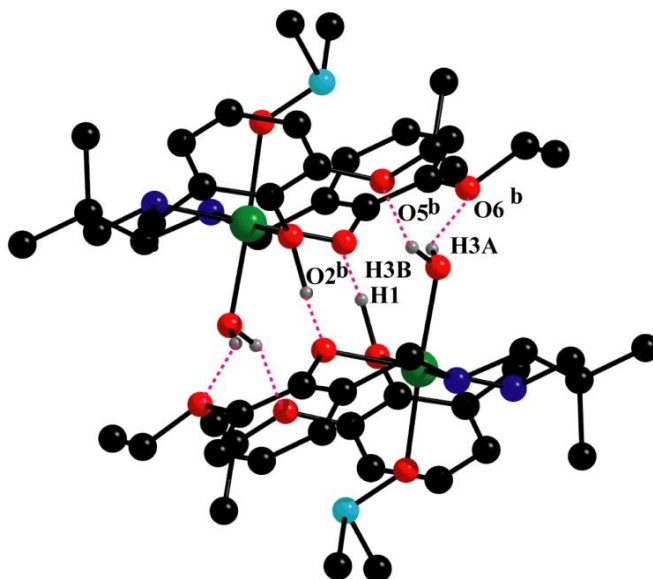


Fig. II.9: Perspective view of intermolecular hydrogen bonding interaction in dimer A of complex **2**. Only the relevant hydrogen atoms have been shown for clarity. Symmetry transformation: ^b = 1-x, -y, 1-z.

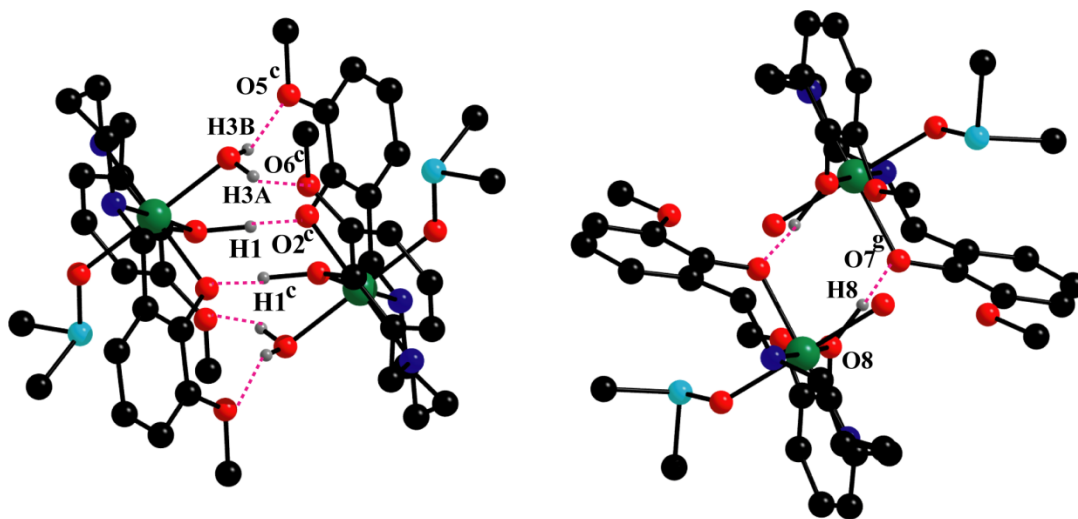


Fig. II.10: Perspective view of significant hydrogen bonding interaction in dimer A and B of complex **3**. Only the relevant hydrogen atoms have been shown for clarity. Symmetry transformation: ^c = -x, 1-y, 1-z.

Table II.5. Hydrogen bond distances (Å) and angles (°) for the complex **1-4**.

Complex	D—H···A	D-H	H···A	D···A	∠D-H···A
1	O(1)-H(1)···O(2) ^a	1.23(8)	1.23(8)	2.427(4)	163(6)
	O(3)-H(3A)···O(6) ^a	0.69(5)	2.15(5)	2.812(5)	162(5)
	O(3)-H(3B)···O(5) ^a	0.93(7)	1.87(6)	2.772(5)	163(5)

	O(8)-H(8)···O(7) ^e	1.19(5)	1.26(5)	2.426(4)	165(4)
	O(10)-H(10A)···O(12) ^e	0.69(4)	2.10(4)	2.772(5)	165(5)
	O(10)-H(10A)···O(11) ^e	0.74(5)	2.04(5)	2.762(5)	164(6)
2	O(1)-H(1)···O(2) ^b	1.20(9)	1.24(10)	2.426(6)	169(11)
	O(3)-H(3A)···O(6) ^b	0.79(8)	2.11(8)	2.823(9)	151(9)
	O(3)-H(3B)···O(5) ^b	0.79(8)	2.10(7)	2.843(8)	158(7)
	O(8)-H(8)···O(7) ^f	1.35(9)	1.09(9)	2.430(6)	170(6)
	O(9)-H(19A)···O(12) ^f	0.84(6)	2.02(6)	2.832(7)	162(6)
	O(9)-H(19B)···O(11) ^f	0.77(9)	2.04(9)	2.793(8)	160(12)
3	O(1)-H(1)···O(2) ^c	1.19(5)	1.24(5)	2.430(4)	175(6)
	O(3)-H(3A)···O(6) ^c	0.820(5)	2.000(5)	2.763(5)	155.00
	O(3)-H(3B)···O(5) ^c	0.71(5)	2.08(5)	2.761(6)	160(7)
	O(8)-H(8)···O(7) ^g	1.19(5)	1.25(5)	2.433(4)	174(5)
4	O(1)-H(1)···O(2) ^d	1.20(7)	1.29(7)	2.437(4)	155(5)

D = donor; H = hydrogen; A = acceptor, Symmetry transformation: ^a = 1-x, 1-y, 1-z, ^b = 1-x, -y, 1-z,

^c = -x, 1-y, 1-z, ^d = 3/2-x, 3/2-y, 1-z, ^e = 1-x, 2-y, 2-z, ^f = -x, 1-y, 2-z, ^g = 1-x, -y, 2-z.

These hydrogen bonded dimeric unit is further stabilized by strong C-H $\cdots\pi$ interactions. The details of C-H $\cdots\pi$ interactions have been listed in Table 5. However no significant $\pi\cdots\pi$ interactions have been found in each complex. Complex **1** shows significant C-H $\cdots\pi$ interactions involving the hydrogen atom, H(1B), attached to a carbon atom, C(1), with a symmetry related ($^h = x, y, -1+z$) phenyl ring, C(38)-C(39)-C(40)-C(41)-C(42)-C(43). Again two hydrogen atoms, H(22B) and H(23C) attached to two different methyl carbon atoms, C(22) and C(23), respectively are involved in intramolecular C-H $\cdots\pi$ interactions with two separate phenyl rings, C(2)-C(3)-C(4)-C(5)-C(6)-C(7) and C(15)-C(16)-C(17)-C(18)-C(19)-C(20), respectively.

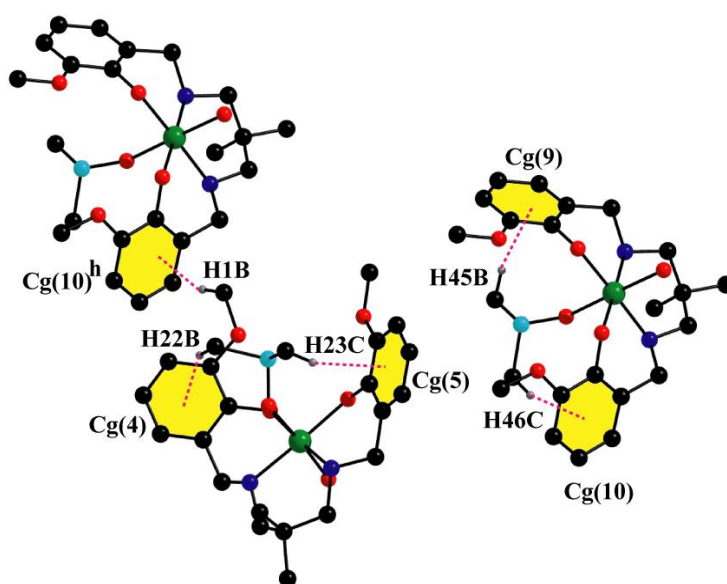


Fig. II.11: Perspective view of significant C-H $\cdots\pi$ interactions in complex **1** with selective atom numbering scheme. Only relevant atoms have been shown in the figure for clarity. Symmetry transformation: $^h = x, y, -1+z$.

Moreover two similar hydrogen atoms, H(45B) and H(46B), attached to two different methyl carbon atoms, C(45) and C(46), respectively of another subunit show similar type of

intramolecular C-H \cdots π interactions with two separate phenyl rings, C(25)-C(26)-C(27)-C(28)-C(29)-C(30) and C(38)-C(39)-C(40)-C(41)-C(42)-C(43), respectively. The hydrogen bonding interactions in complex **1** has been shown in Figure 7.

In complex **2**, two hydrogen atoms, H(24B) and H(25C), attached to the carbon atoms, C(24) and C(25) respectively participates in intermolecular C-H \cdots π interaction with the phenyl rings, C(2)-C(3)-C(4)-C(5)-C(6)-C(7) and C(15)-C(16)-C(17)-C(18)-C(19)-C(20), respectively (Figure 8).

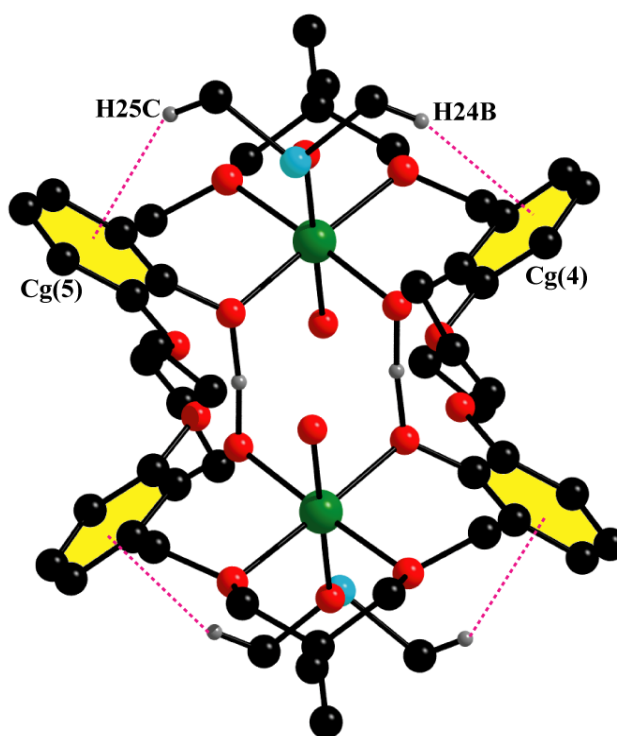


Fig. II.12: Perspective view of intramolecular C-H \cdots π stacking interactions in complex **2**. Only relevant hydrogen atoms have been shown in the figure for clarity.

In complex **3**, two hydrogen atoms, H(10C) and H(10D), attached to the methyl carbon atom, C(24) and C(25), participates in intermolecular C-H \cdots π interaction with the symmetry

related ($^i = -x, -y, 2-z$) phenyl rings, C(23)-C(24)-C(25)-C(26)-C(27)-C(28) and C(34)-C(35)-C(36)-C(37)-C(38)-C(39), respectively (Figure 9). In addition two other hydrogen atoms, H(20B) and H(21C), attached to two separate methyl carbon atoms, C(20) and C(21), respectively participates in intramolecular C-H $\cdots\pi$ interaction with the phenyl rings, C(13)-C(14)-C(15)-C(16)-C(17)-C(18) and C(2)-C(3)-C(4)-C(5)-C(6)-C(7), respectively (Figure 9).

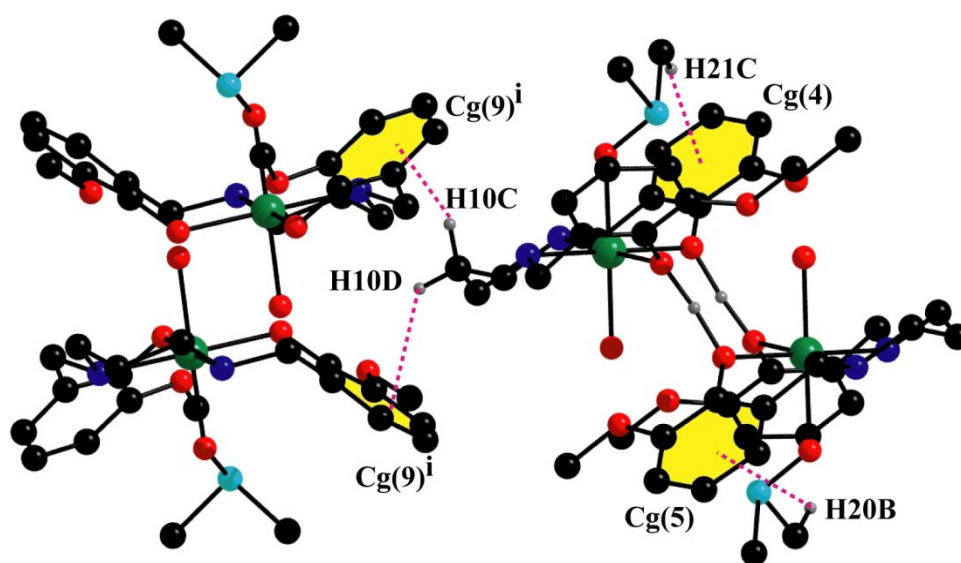


Fig. II.13: Perspective view of significant C-H $\cdots\pi$ interactions in complex **3** with selective atom numbering scheme. Only relevant hydrogen atoms have been shown in the figure for clarity. Symmetry transformation: $^i = -x, -y, 2-z$.

Table II.6. Geometric features (distances in Å and angles in °) of the C-H $\cdots\pi$ interactions obtained for complexes **1-4**.

Complexes	C-H \cdots Cg(ring)	H \cdots Cg(Å)	C-H \cdots Cg	C \cdots Cg (Å)
1	C(1)-H(1B) \cdots Cg(10) ^h	2.65	166	3.585(6)

	C(22)-H(22B)⋯Cg(4)	2.92	155	3.810(8)
	C(23)-H(23C)⋯Cg(5)	2.87	140	3.662(9)
	C(45)-H(45B)⋯Cg(9)	2.81	144	3.629(7)
	C(46)-H(46B)⋯Cg(10)	2.75	157	3.648(6)
2	C(24)-H(24B)⋯Cg(4)	2.75	156	3.652(13)
	C(25)-H(25C)⋯Cg(5)	2.82	144	3.646(15)
3	C(10)-H(10C)⋯Cg(9) ⁱ	2.76	129	3.453(7)
	C(10)-H(10D)⋯Cg(10) ⁱ	2.70	139	3.498(7)
	C(20)-H(20B)⋯Cg(5)	2.67	146	3.504(8)
	C(21)-H(21C)⋯Cg(4)	2.70	155	3.595(9)
	C(31)-H(31A)⋯Cg(5) ^j	2.75	129	3.449(7)
	C(31)-H(31B)⋯Cg(4) ^k	2.71	138	3.499(7)
	C(41)-H(41C)⋯Cg(10)	2.71	154	3.605(9)
	C(42)-H(42B)⋯Cg(9)	2.66	146	3.499(8)
4	C(11)-H(11A)⋯Cg(4) ^l	2.61	146	3.459(3)
	C(22)-H(22C)⋯Cg(5)	2.68	146	3.523(7)
	C(22)-H(23B)⋯Cg(4)	2.91	152	3.787(8)

Symmetry transformation: ^h = x, y, -1+z, ⁱ = -x, -y, 2-z, ^j = 1-x, 1-y, 2- z, ^k = 1+x, y, 1+ z, ^l = 3/2-x, -1/2-y, 1/2-z.

For complex **1**: Cg(4) = Centre of gravity of the ring [C(2)- C(3)-C(4)-C(5)-C(6)-C(7)]

Cg(5) = Centre of gravity of the ring [C(15)- C(16)-C(17)-C(18)-C(19)-C(20)]

Cg(9) = Centre of gravity of the ring [C(25)- C(26)-C(27)-C(28)-C(29)-C(30)]

Cg(10) = Centre of gravity of the ring [C(38)- C(39)-C(40)-C(41)-C(42)-C(43)]

For complex **2**: Cg(4) = Centre of gravity of the ring [C(3)- C(4)-C(5)-C(6)-C(7)-C(8)]

Cg(5) = Centre of gravity of the ring [C(16)- C(17)-C(18)-C(19)-C(20)-C(21)]

For complex **3**: Cg(4) = Centre of gravity of the ring [C(2)- C(3)-C(4)-C(5)-C(6)-C(7)]

Cg(5) = Centre of gravity of the ring [C(13)- C(14)-C(15)-C(16)-C(17)-C(18)]

Cg(9) = Centre of gravity of the ring [C(23)- C(24)-C(25)-C(26)-C(27)-C(28)]

Cg(10) = Centre of gravity of the ring [C(34)- C(35)-C(36)-C(37)-C(38)-C(39)]

For complex **4**: Cg(4) = Centre of gravity of the ring [C(3)- C(4)-C(5)-C(6)-C(7)-C(8)]

Cg(5) = Centre of gravity of the ring [C(14)- C(15)-C(16)-C(17)-C(18)-C(19)]

In complex **4**, H(22C) and H(23B), attached to the methyl carbon atom, C(22) and C(23), respectively, participate in intramolecular C-H... π interactions with two separate phenyl rings, C(14)-C(15)-C(16)-C(17)-C(18)-C(19) and C(3)-C(4)-C(5)-C(6)-C(7)-C(8), respectively while another hydrogen atom, H(11A), attached to a carbon atom, C(11), is involved in intermolecular C-H... π interaction with a symmetry related ($m = 3/2-x, -1/2-y, 1/2-z$) phenyl ring, C(3)-C(4)-C(5)-C(6)-C(7)-C(8) to form a supramolecular chain (Figure 10).

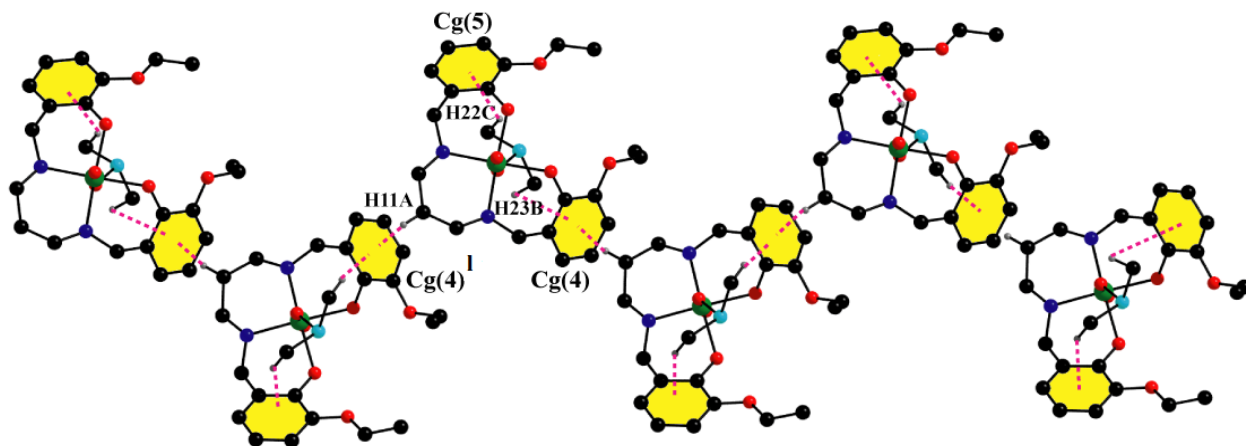


Fig. II.14: Perspective view of a supramolecular chain through intermolecular C-H... π stacking interactions in complex **4**. Only relevant atoms have been shown in the figure for clarity. Symmetry transformation: $I = 3/2-x, -1/2-y, 1/2-z$.

II. 3.4. Hirshfeld surfaces analysis

The Hirshfeld surface emerged from an attempt to delineate the space covered by a molecule in a crystal for the purpose of dividing the crystal electron density into molecular fragments.²⁰ The Hirshfeld surfaces of four complexes are mapped over d_{norm} (range -0.1 Å to 1.5 Å), shape index and curvedness (Figure 11). Red spots appear on the Hirshfeld surfaces mapped with d_{norm} represent the dominant interactions within the complex in solid state. Various intermolecular interactions are summed up effectively in the spots with the large circular depressions (deep red) noticeable on the d_{norm} surfaces indicates the dominance of hydrogen bonding interactions and other weak interactions. The 2D fingerprint plot of Hirshfeld surfaces for all complexes and the comparative contributions of different interactions overlapping in full fingerprint plots have been provided in Figure S5. In the 2D fingerprint plot

intermolecular interactions appear as distinct spikes. Complementary regions are observable in the 2D fingerprint plots where one molecule act as donor ($d_e > d_i$) and the other as an acceptor ($d_e < d_i$). The relative percentages of intermolecular interactions of four complexes have been shown in Figure S5 (see ESI).

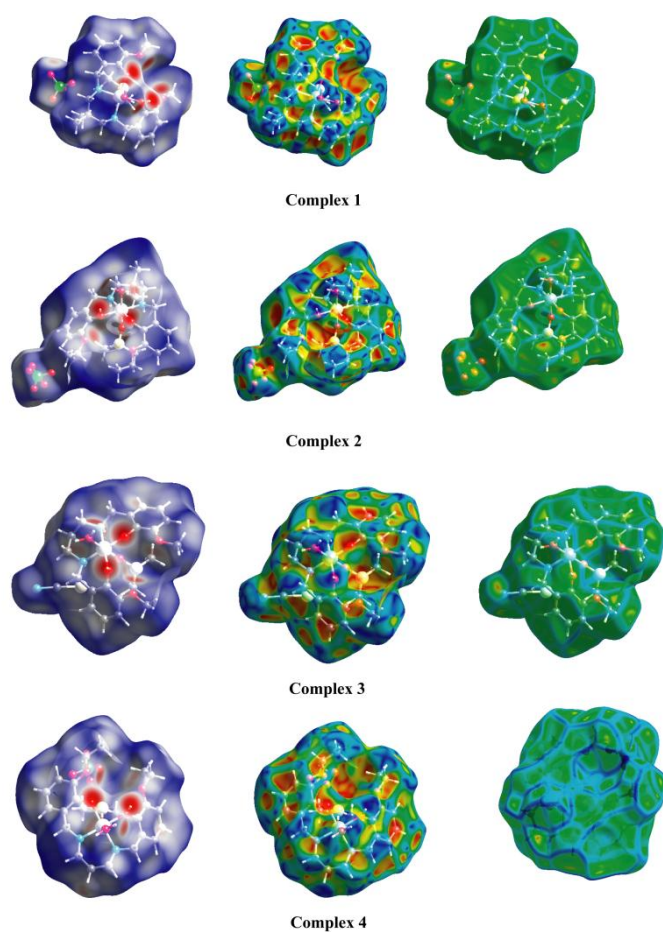


Fig. II.15: Hirshfeld surfaces mapped with d_{norm} (left column), shape index (middle) and curvedness (right column) of complexes **1-4**.

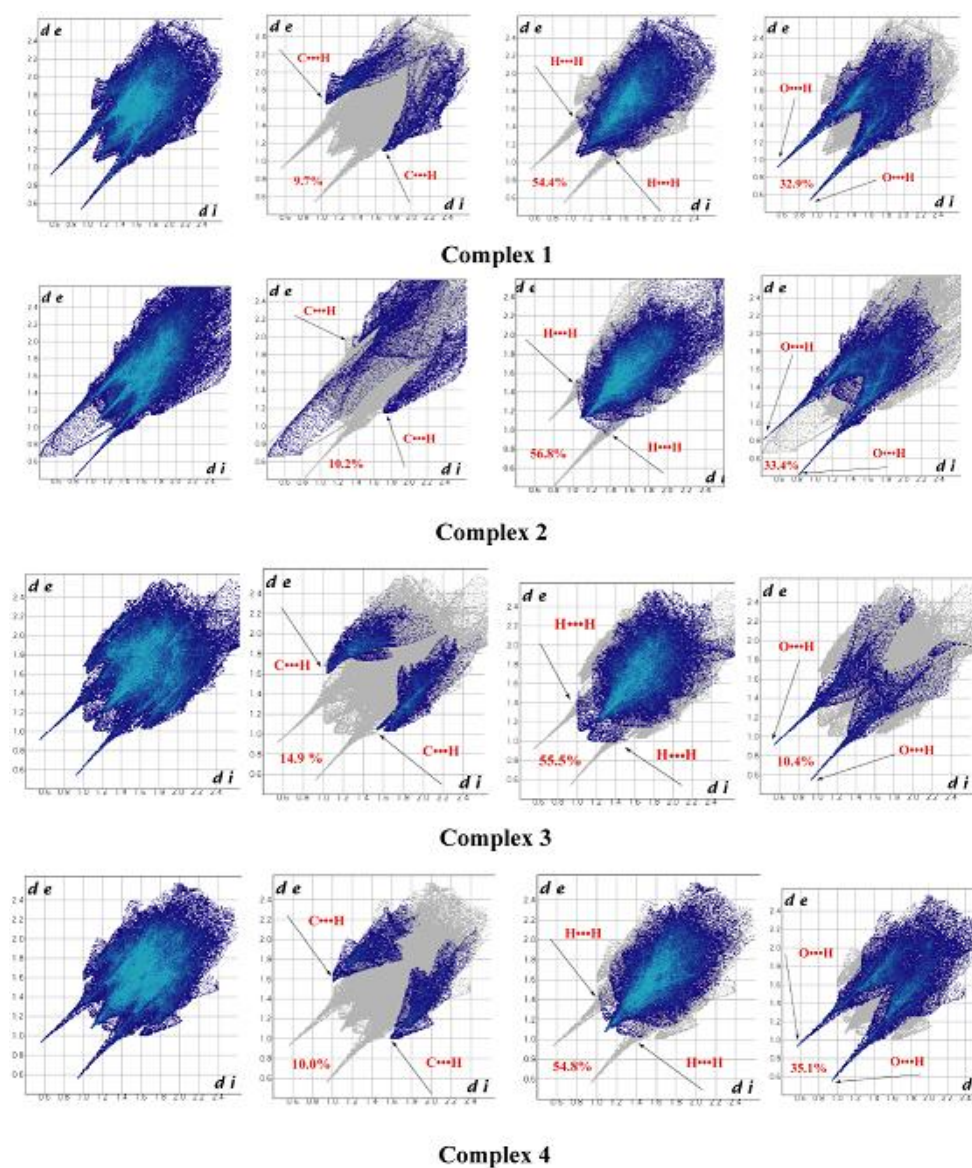


Fig. II.16: Fingerprint plot: Full (extreme left), resolved into $\text{H}\cdots\text{C}/\text{C}\cdots\text{H}$ (second from the left), $\text{H}\cdots\text{N}/\text{N}\cdots\text{H}$ (second from the right) and $\text{H}\cdots\text{O}/\text{O}\cdots\text{H}$ (extreme right) contacts contributed to the total Hirshfeld Surface area of complexes **1–4**

II. 3.5. DFT results

The X-ray structures of complexes **1–4** reveal that they crystallize forming dicationic dimers where two strong hydrogen bonds are formed between the phenoxy oxygen atoms of

the ligands (Figures 2-4). The O...O distance is shorter than 2.5 Å and both O atoms are of identical pK_a . Therefore, these hydrogen bonds have strong covalent character and we wonder if they belong to LBHBs or single-well hydrogen bonds. It has been analyzed using B3LYP-D/def2-SVP calculations the nature of the hydrogen bonds. The energy profile of complex **1** has been computed as a representative model. The plot of the energy profile has been shown in Figure 12 and it shows that the hydrogen bonds correspond to LBHBs with a barrier of 2.36 kcal/mol for the synchronous movement of both Hs in opposite directions (maintaining the inversion center since the X-ray geometry corresponds to the P-1 symmetry point group). Therefore the barrier for each hydrogen bond is only 1.18 kcal/mol, in agreement with the short O...O distance (2.426 Å in the model used for the calculations). These results suggest that in complexes **1–4** the hydrogen atoms can move freely between the two oxygen atoms and their average position in the O...O center.

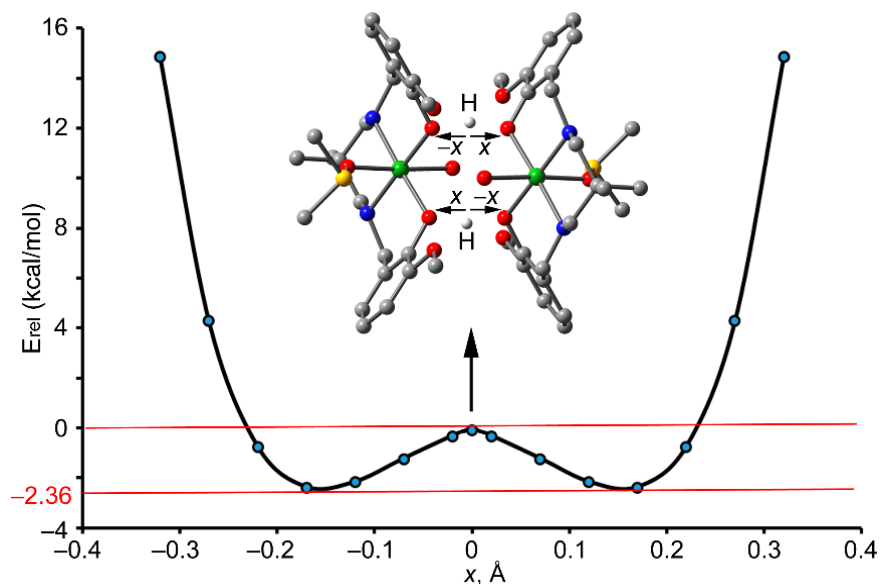


Fig. II.17: Energy diagram obtained for complex **1** at the B3LYP-D/def2-SVP level of theory. The energies are relative to the maximum. The hydrogen atoms were moved toward opposite directions of maintain the inversion center of symmetry.

The energetic features of the LBHBs also additional hydrogen bonds that are established between the coordinated water molecules and the methoxy groups of the ligand (see blue dashed lines in Figure 13) has also been analyzed. The dimerization energy is very large ($\Delta E_1 = -107.7$ kcal/mol) due to the contribution of the strong LBHBs and the conventional O–H...O bonds that are expected to be also strong due to the enhanced acidity of these protons due to the coordination of the water molecule to the nickel(II) metal center. In an effort to estimate the contribution of the LBHBs, a theoretical model have been used where the water molecules are eliminated (Figure 13b). As a result, the conventional hydrogen bonds are not established and the interaction energy drops to $\Delta E_2 = -73.3$ kcal/mol, that corresponds to the contribution of both LBHBs and also some additional van der Waals interactions established between the bulk of both molecules. This large interaction energy confirms the strong covalent nature of these hydrogen bonds. This result is agreement with previous investigations in hydrogen bonds between hetero atoms with identical pK_a s where the ΔH of formation can approach 30 kcal/mol.⁴ Furthermore, the difference between ΔE_1 and ΔE_2 is a rough estimation of the four O–H...O bonds established by the coordinated water molecules and methoxy groups (-8.6 kcal/mol per hydrogen bond).

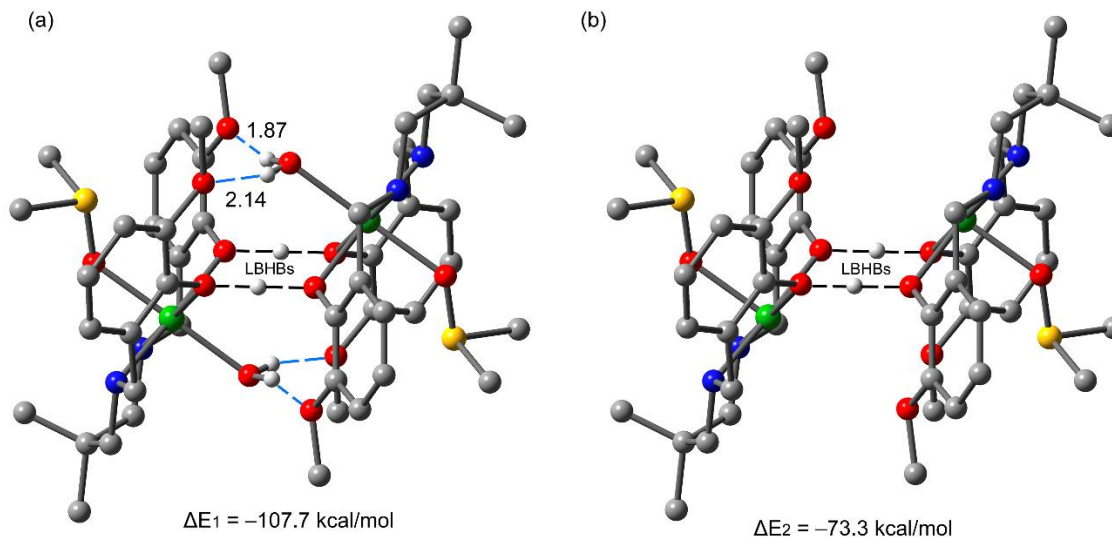


Fig. II.18: Theoretical models used to evaluate the LBHBs in complex **1** (a) and a mutated complex where two water molecules have been eliminated (b). Distances in Å.

Finally, non covalent interaction plot (NCI plot) index has been made to further characterize the hydrogen bonds. It allows a direct assessment of host-guest complementarity and the extent to which non-covalent interactions stabilize a complex. Figure 14 shows the NCI plot obtained for the self-assembled dimer extracted from the solid state of complex **1**. The NCI index indicates that the LBHBs are covalent bonds, since no isosurface is found between the H and O atoms. The O–H···O hydrogen bonds involving the coordinated water molecules are characterized by small and intense blue isosurfaces, thus supporting the strong nature of the interactions. Several green isosurfaces are also present between both monomeric units, thus revealing the existence of additional weak interactions that also stabilize the assembly.

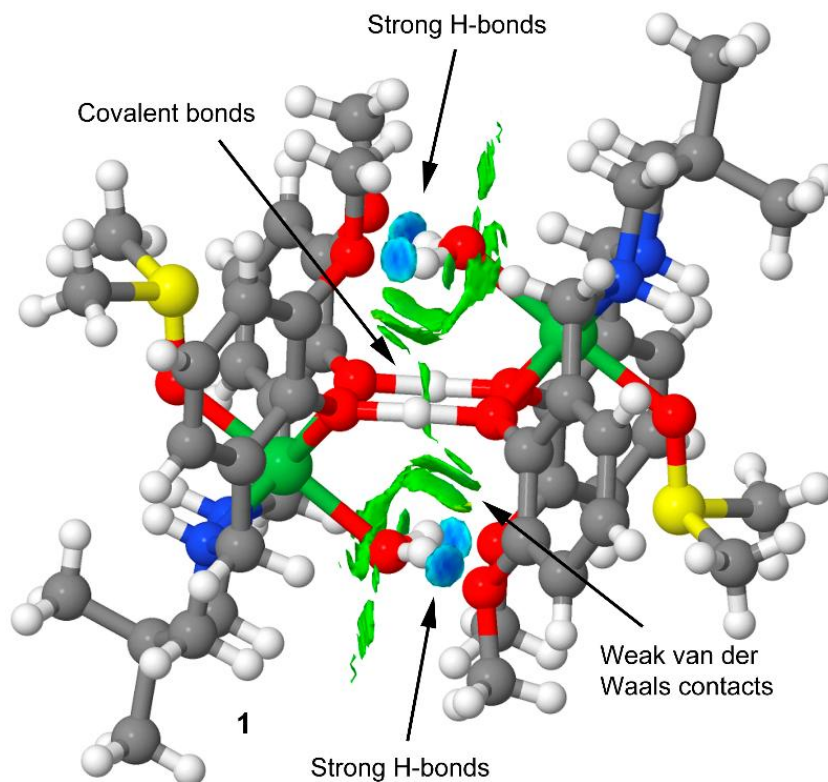


Fig. II.19: NCI plot of the self-assembled dimer of complex **1**. The gradient cut-off is $s = 0.35$ au, and the color scale is $-0.04 < \rho < 0.04$ au.

II. 3.5. IR and electronic spectra

A moderately sharp band in the range of $3280\text{--}3225\text{ cm}^{-1}$ has been noticed in the IR spectrum of each complex which may be assigned as the N–H stretching vibration of the reduced Schiff base ligand.²¹ Broad bands in the range of $3010\text{--}2865\text{ cm}^{-1}$ due to alkyl C–H stretching vibrations are routinely noticed in IR spectra of all complexes.²² Appearance of a broad band in each complex around 3400 cm^{-1} indicates the presence of O–H stretching vibrations of water molecules. A very strong band is obtained around 2045 cm^{-1} only in complex **3** due to the presence of non-coordinated thiocyanate ions.²³ IR spectra of all complexes have been given in Figures S6–S9 (ESI).

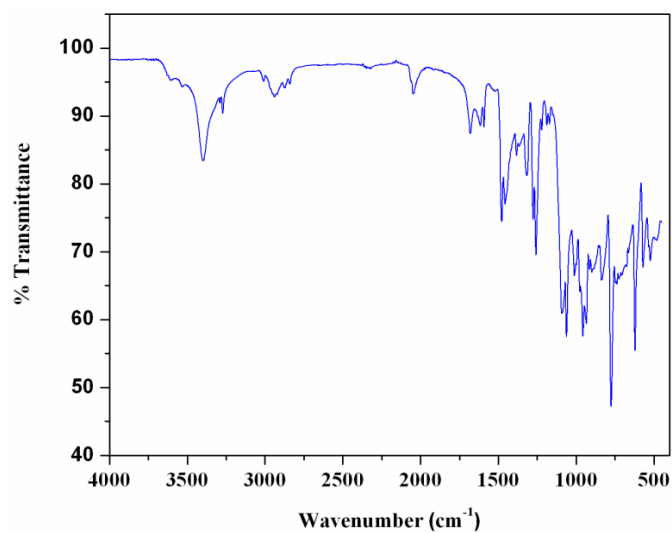


Fig. II.20: IR spectrum of complex 1

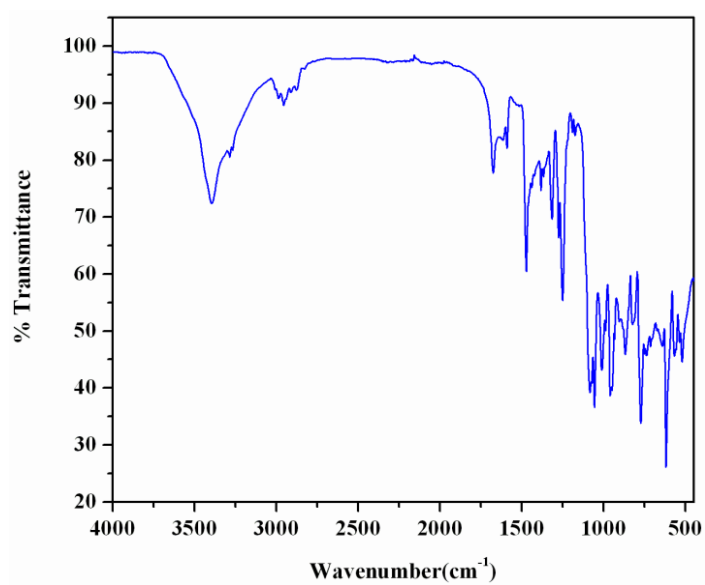


Fig. II.21: IR spectrum of complex 2

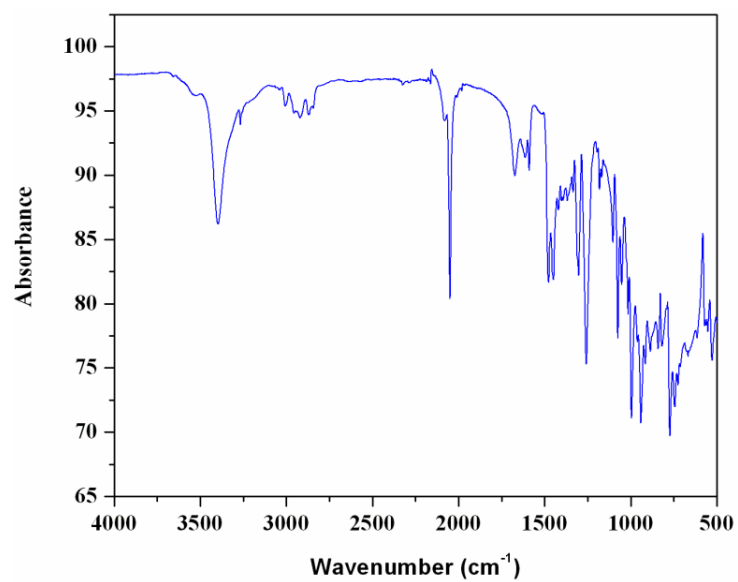


Fig. II.22: IR spectrum of complex 3

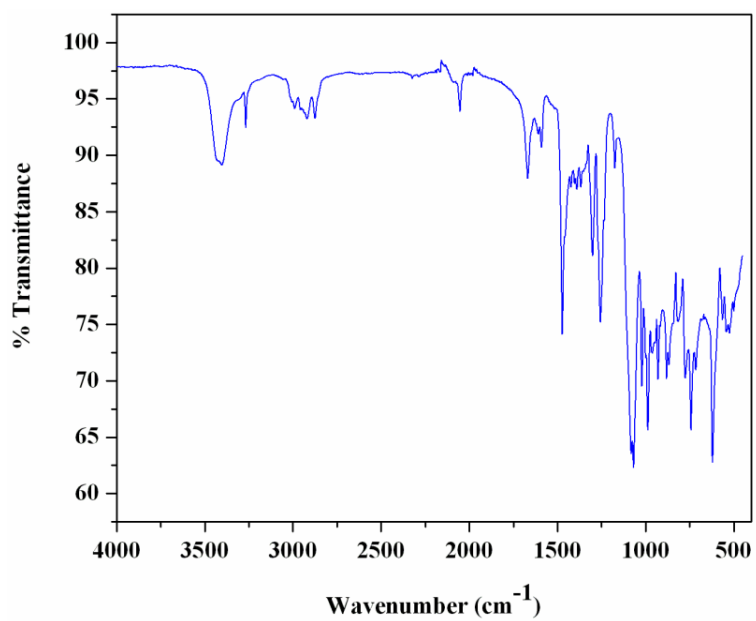


Fig. II.23: IR spectrum of complex 4

Electronic spectra of all four complexes in DMSO show two distinguished bands in the visible range around 625 nm and 735 nm. These bands may be assigned as ${}^3T_{1g}(F) \leftarrow {}^3A_{2g}(F)$ and ${}^3T_{2g}(F) \leftarrow {}^3A_{2g}(F)$, respectively.²⁴ The intense absorption bands at ~ 355 nm may be assigned as ligand to metal charge transfer (LMCT) bands, which obscure the 3rd d–d band, ${}^3T_{1g}(P) \leftarrow {}^3A_{2g}(F)$, expected for any octahedral nickel(II).²⁵ In addition, high energy absorption bands around 275 nm have been assigned to intra-ligand $\pi \rightarrow \pi^*$ transitions.²⁶ Electronic spectra of all complexes have been given in Figures S10-S13 (ESI).

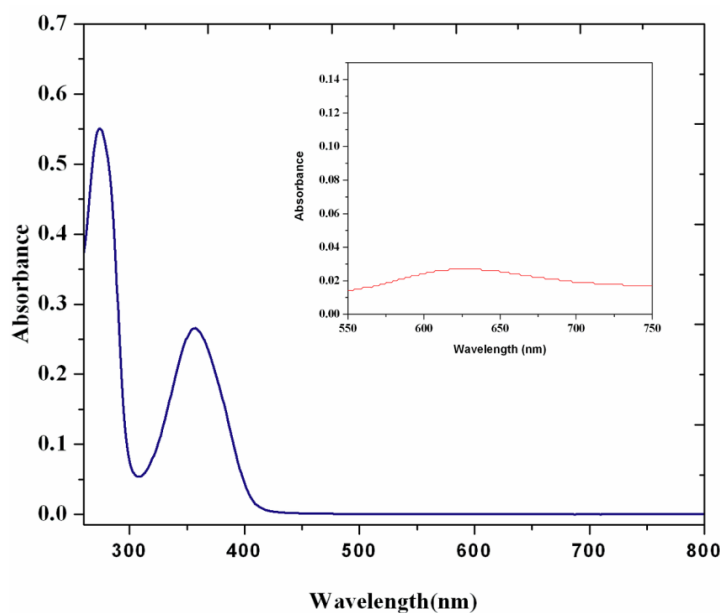


Fig. II.24: Electronic spectrum of complex **1**. Inset shows the selected small range (550-750 nm) electronic spectrum of the complex.

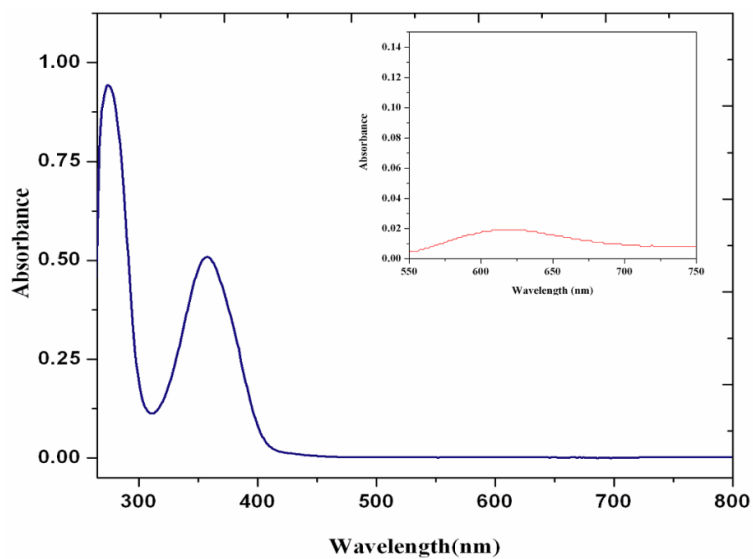


Fig. II.25: Electronic spectrum of complex **2**. Inset shows the selected small range (550-750 nm) electronic spectrum of the complex.

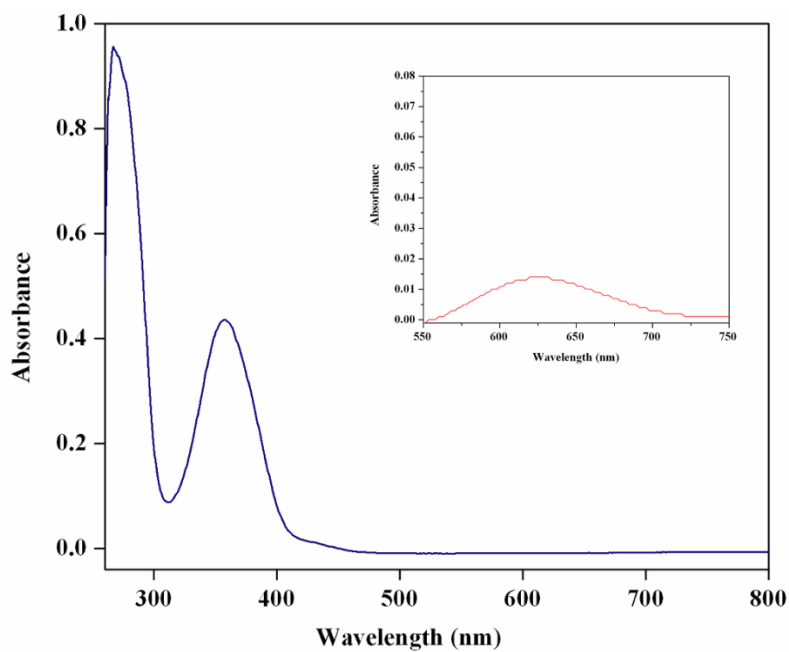


Fig. II.26: Electronic spectrum of complex **3**. Inset shows the selected small range (550-750 nm) electronic spectrum of the complex.

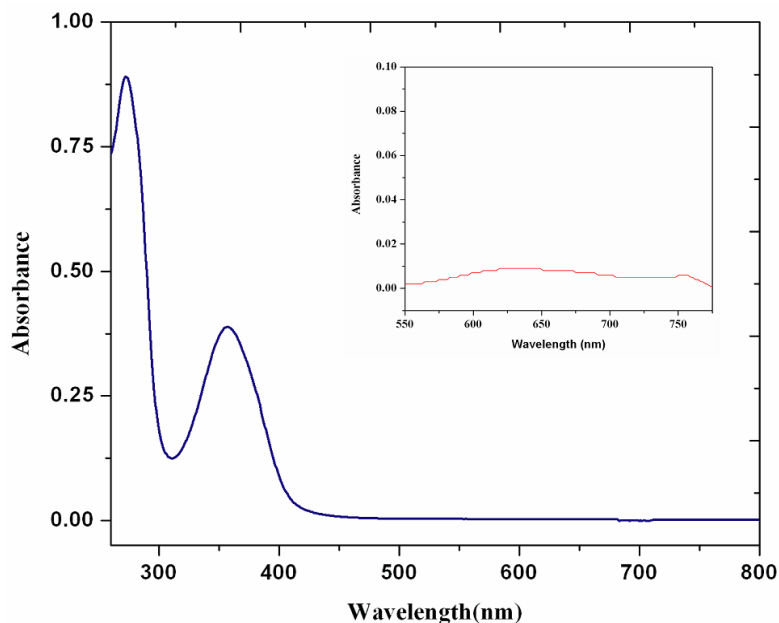


Fig. II.27: Electronic spectrum of complex **4**. Inset shows the selected small range (550-760 nm) electronic spectrum of the complex.

II. 3. Conclusion

In summary, we have synthesized and characterized four nickel(II) complexes (**1-4**) that form self-assembled dimers in the solid state where low barrier hydrogen bonds appear to play a prominent role. Structures of all complexes were confirmed by single crystal X-ray diffraction study. Each complex may be represented by a general formula $[Ni_2(HL)_2(DMSO)_2(H_2O)_2]X$ [$H_2L = N_2O_4$ donor reduced Schiff base ligand, X =counter anion]; X is perchlorate in **1**, **2** and **4** and X =thiocyanate in **3**. Use of reduced Schiff bases seems to be essential to form this type of hydrogen bonded dimeric species, as the non-reduced analogues of these Schiff bases fails to prepare such complexes. More flexibility of the reduced Schiff bases compared to their Schiff base precursor may be the driving force in forming these complexes. The hydrogen bonds have been evaluated energetically and using the non covalent interaction plot. We conclude that the

barrier is very low and, consequently, the hydrogen atoms can move freely with their average position between both oxygen atoms. The energy associated to the low barrier hydrogen bonds is very large due to the strong covalent character of the interaction.

References

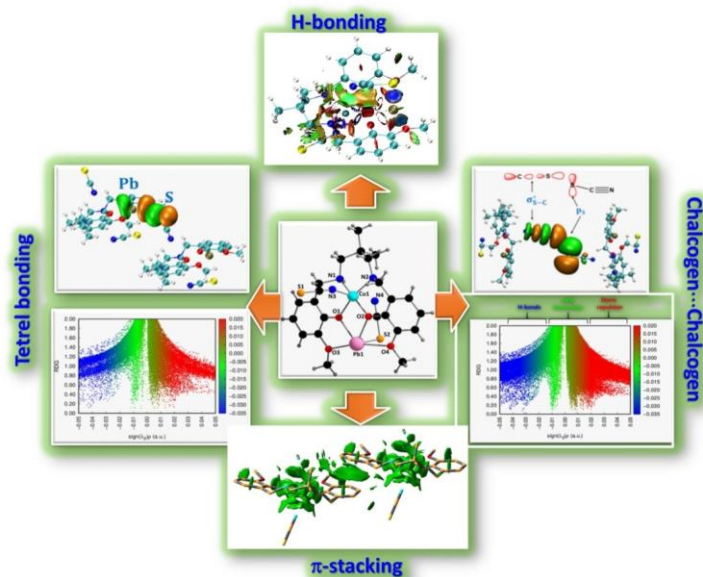
- 1 W. W. Cleland, P. A. Frey and J. A. Gerlt, *J. Bio. Chem.*, 1998, **273**, 25529-25532.
- 2 G. A. Jeffrey, *Introduction to Hydrogen Bonding*, Oxford University Press, New York, 1997.
- 3 M. Garcia-Viloca, A. Gonzalez-Lafont and J. M. Lluch, *J. Am. Chem. Soc.*, 1997, **119**, 1081–1086.
- 4 M. A. McAllister, *Can. J. Chem.*, 1997, **75**, 1195–1202.
- 5 K. Abu-Dari, K. N. Raymond and D. P. Freyberg, *J. Am. Chem. Soc.*, 1979, **101**, 3688–3689.
- 6 K. Abu-Dari, D. P. Freyberg and K. N. Raymond, *Inorg. Chem.*, 1979, **18**, 2427–2433.
- 7 T. Steiner and W. Saenger, *Acta Crystallogr. Sect. B Struct. Sci.*, 1994, **50**, 348–357.
- 8 P. Gilli, V. Bertolase, V. Ferretti and G. Gilli, *J. Am. Chem. Soc.*, 1994, **116**, 909–915.
- 9 K. P. Sarma and R. K. Poddar, *Transition Met. Chem.*, 1984, **9**, 135-138.
- 10 G.M. Sheldrick, *Acta Crystallogr., Sect.*, 2015, **C 71**, 3–8.
- 11 G. M. Sheldrick, SADABS, **V2014/5**, Software for Empirical Absorption Correction, University of Göttingen, Institute für Anorganische Chemie der Universität, Göttingen, Germany, 1999–2003.

- 12 M. J. Frisch, G. W. Trucks, H. B. Schlegel, G. E. Scuseria, M. A. Robb, J. R. Cheeseman, G. Scalmani, V. Barone, B. Mennucci, G. A. Petersson, H. Nakatsuji, M. Caricato, X. Li, H. P. Hratchian, A. F. Izmaylov, J. Bloino, G. Zheng, J. L. Sonnenberg, M. Hada, M. Ehara, K. Toyota, R. Fukuda, J. Hasegawa, M. Ishida, T. Nakajima, Y. Honda, O. Kitao, H. Nakai, T. Vreven, J. A. Montgomery, Jr., J. E. Peralta, F. Ogliaro, M. Bearpark, J. J. Heyd, E. Brothers, K. N. Kudin, V. N. Staroverov, R. Kobayashi, J. Normand, K. Raghavachari, A. Rendell, J. C. Burant, S. S. Iyengar, J. Tomasi, M. Cossi, N. Rega, J. M. Millam, M. Klene, J. E. Knox, J. B. Cross, V. Bakken, C. Adamo, J. Jaramillo, R. Gomperts, R. E. Stratmann, O. Yazyev, A. J. Austin, R. Cammi, C. Pomelli, J. W. Ochterski, R. L. Martin, K. Morokuma, V. G. Zakrzewski, G. A. Voth, P. Salvador, J. J. Dannenberg, S. Dapprich, A. D. Daniels, Ö. Farkas, J. B. Foresman, J. V. Ortiz, J. Cioslowski and D. J. Fox, Gaussian 09 (Gaussian, Inc., Wallingford CT, 2009).
- 13 S. Grimme, J. Antony, S. Ehrlich and H. Krieg, *J. Chem. Phys.*, 2010, **132**, 154104-154117.
- 14 S. F. Boys and F. Bernardi, *Mol. Phys.*, 1970, **19**, 553-566.
- 15 J. Contreras-García, E. R. Johnson, S. Keinan, R. Chaudret, J.-P. Piquemal, D. N. Beratan and W. Yang, *J. Chem. Theory Comput.*, 2011, **7**, 625–632.
- 16 Johnson, E. R.; Keinan, S.; Mori-Sánchez, P.; Contreras-García, J.; Cohen, A. J.; Yang, W. Revealing noncovalent interactions. *J. Am. Chem. Soc.* **2010**, *132*, 6498–6506.
- 17 A. Banerjee, A. Frontera and S. Chattopadhyay, *Dalton Trans.*, 2019, **48**, 11433-11447.

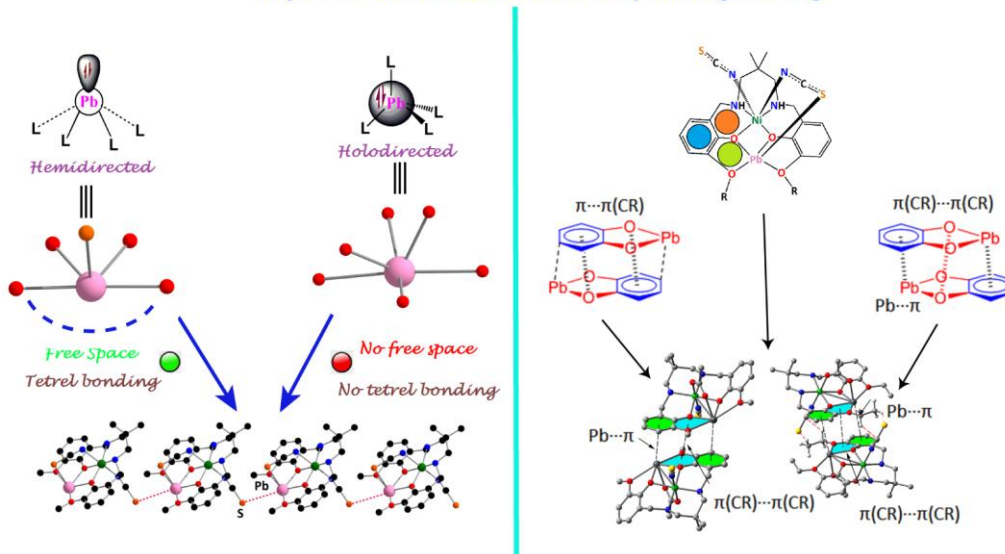
- 18 D. Matoga, J. Szklarzewicz, K. Stadnicka and M. S. Shongwe, *Inorg.Chem.*, 2007, **46**, 9042-9044.
- 19 Cremer, D.; Pople, J. A. A General Definition of Ring Puckering Coordinates. *J. Am. Chem. Soc.* 1975, **97**, 1354-1358.
- 20 F. L. Hirshfeld, *Theor. Chim. Acta.*, 1977, **44**, 129–138.
- 21 (a) A. Hazari, A. Das, P. Mahapatra and A. Ghosh, *Polyhedron*, 2017, **134**, 99-106; (b) S. Mirdya, A. Frontera and S. Chattopadhyay, *CrystEngComm*, 2019, DOI: 10.1039/C9CE01283D.
- 22 (a) S. Roy, T. Basak, S. Khan, M. G. B. Drew, A. Bauzá, A. Frontera and S. Chattopadhyay, *ChemistrySelect*, 2017, **2**, 9336-9343; (b) S. Mirdya, T. Basak and S. Chattopadhyay, *Polyhedron*, 2019, **170**, 253–263.
- 23 (a) S. Mirdya, S. Roy, S. Chatterjee, A. Bauzá, A. Frontera and S. Chattopadhyay, *Cryst. Growth Des.*, 2019, DOI: 10.1021/acs.cgd.9b00881; (b) K. Ghosh, K. Harms, A. Bauzá, A. Frontera and S. Chattopadhyay, *Dalton Trans.*, 2018, **47**, 331-347.
- 24 A. Bhattacharyya, P. K. Bhaumik, M. Das, A. Bauzá, P. P. Jana, K. Harms, A. Frontera and S. Chattopadhyay, *Polyhedron*, **2015**, *101*, 257–269.
- 25 S. Chattopadhyay, M. G. B. Drew and A. Ghosh, *Polyhedron*, 2007, **26**, 3513–3522.
- 26 A. Bhattacharyya, P. K. Bhaumik, P. P. Jana and S. Chattopadhyay, *Polyhedron* **2014**, *78*, 40–45.

Chapter III

Dinuclear complexes with MO_2Pb cores ($\text{M}=\text{Cu}/\text{Ni}$)



Supramolecular interactions in crystal engineering



Section IIIA

An insight into the non-covalent Pb \cdots S and S \cdots S interactions in the solid-state structure of a hemidirected lead(II) complex

III.A .1. Introduction

Lead is a heavy metal with an atomic number 82. Its large radius, ability to adopt different coordination numbers from 2 to 8 and ability to exist in variable valence states leading to versatile coordination chemistry attracted synthetic inorganic chemists to prepare new complexes of lead.¹⁻⁴ Lead containing materials are extensively used in semiconductors, batteries, ferroelectric materials and non-linear optical materials.⁵⁻⁹ On the other hand, lead is very toxic even in very low concentration and is a dangerous biological poison similar to mercury, if not more.¹⁰⁻¹⁶ Disodium calcium EDTA are used in chelation therapy to take away lead(II) from human body.¹⁷⁻²¹ Many bio-inorganic chemists are working to develop other chelating ligands for the treatment of lead intoxication.²²⁻²⁵

[Xe]4f¹⁴5d¹⁰6s²6p² is the electronic configuration of lead (Pb). Due to their very weak screening efficiency, fourteen electrons in 4f and ten electrons in 3d orbitals increase the effective nuclear charge of lead acting on outermost 6s² electrons and make the electron pair essentially inert. The penetrating property of the 6s orbital is also very high and has a pronounced effect on lowering the energy of these two electrons. Relativistic increase in the

mass of $6s^2$ electrons also stabilizes $6s^2$ electrons. Lead is, therefore, showing +2 oxidation state in most of its complexes and is containing a lone pair of electrons.²⁶⁻³¹ In some of these complexes, this lone pair is, however, stereochemically active leading to hemidirectional complexes^{32,33} and in the rest of the complexes, the lone pair is stereochemically inactive leading to holodirected complexes.^{34,35} Theoretical chemists are currently engaged in rationalizing the extent to which the lone pair is stereochemically active in lead(II) complexes.³⁶⁻

40

Supramolecular chemistry is a result of various noncovalent interactions⁴¹⁻⁴³, including a large range of attractive and repulsive forces^{42,43} such as ion-ion interactions, hydrogen bonding, $\pi \cdots \pi$ interactions, ion-dipole interactions, van der Waals forces and dipole-dipole interactions, etc.⁴⁴⁻⁴⁷ These are often jointly working in one supramolecular complex. These non-covalent forces are attributable to the self-assembly of large molecules, crystal packing, and biological pattern identification.⁴⁸⁻⁵¹ Other well known non-covalent interactions, such as short contact among halogen/chalcogen atoms⁵²⁻⁵⁶, may also promote the formation of interesting supramolecular assemblies.⁵⁷⁻⁶⁰ Another important non-covalent interaction is σ -hole interaction, which is less studied. Strong σ -hole interactions may occur in complexes of group IV elements and usually involves tetrel bonding interactions, especially in the cases of lead.⁶¹⁻⁷²

In one of our previous works, few 'nickel(II)-salen' type metalloligands with reduced Schiff base was used to prepare a few holodirected and hemidirected lead(II) complexes.^{73,74} In this work, we have reduced a compartmental 'salen type' Schiff base into a compartmental

‘reduced Schiff base’ (having N_2O_2 and $\text{O}_2\text{O}_2'$ pockets), which entraps copper(II) and lead(II) in inner N_2O_2 and outer $\text{O}_2\text{O}_2'$ compartments respectively to produce a hetero-dinuclear copper(II)/lead(II) complex, $[(\text{SCN})\text{CuL}^1\text{Pb}(\text{SCN})]$ (5). Lead(II) is showing hemi-directed geometry in the complex. Non-covalent interactions in the supramolecular assembly of the complex were studied energetically by means of theoretical DFT calculations. A most interesting observation is the existence of $\text{S}\cdots\text{S}$ and $\text{Pb}\cdots\text{S}$ interactions. These interactions have also been analyzed using several computational tools, including Bader's “atoms-in-molecules” (AIM) and MEP analyses.

III.A .2. Experimental section

III.A .2.1: *Synthesis*

III.A.2.1.1. Synthesis of Schiff base ligands

III.A.2.1.1.1: Preparation of the ligand, 2,2'-[(2,2-dimethyl-1,3-propanediyl)bis(iminomethylene)]bis[6-methoxy-phenol] (H_2L^1)

H_2L^1 ligand preparation has been given in II.2.1 (See Chapter 2).

III.A.2.1.1.2: Preparation of $[(\text{SCN})\text{CuL}^1\text{Pb}(\text{SCN})]$ (5)

A methanol solution (5 mL) of lead(II) nitrate (~340 mg, 1 mmol) was added to the methanol solution (20 mL) of H₂L 1 and the resulting solution was stirred for 15 min. A methanol (10 mL) solution of copper(II) acetate monohydrate (200 mg, 1 mmol) was then added to it. After 15 min of stirring, methanol (10 mL) solution of sodium thiocyanate (180 mg, 2 mmol) was added to it. The stirring was continued for 2h. The reaction mixture was left unperturbed for slow evaporation of the solvent at room temperature. Single crystals, suitable for X-ray diffraction, were obtained after 3–4 days upon slow evaporation of the solution in an open atmosphere. Yield: 530 mg (~70%) based on copper(II). Anal. Calc. for C₂₃H₂₆N₄CuO₄PbS₂ (FW: 759.36): C, 36.48; H, 3.46; N, 7.40; Found: C, 36.3; H, 3.2; N, 7.5%. FT-IR (KBr, cm⁻¹): 3248-3232 (νN–H); 2951-2838 (νC–H); 2091 (νNCS), 2068 (νSCN). λ_{max} (nm) [ε_{max}(lit mol⁻¹ cm⁻¹)] (DMF): 282 (5.27 X 10³); 340 (9.76 X 10²); 405 (9.46 X 10²); 618 (1.31 X 10³).

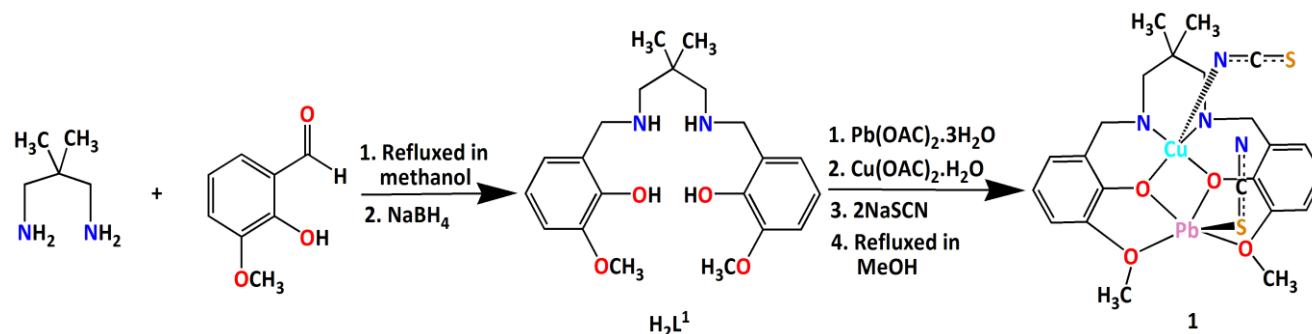
III.A .3. Results and discussion

III.A .3. 1. Synthesis

2,2-dimethyl-1,3-diaminopropane was refluxed with 3-methoxysalicylaldehyde in 1:2 ratio, followed by the addition of NaBH₄ to form N₂O₂O₂' donor compartmental reduced Schiff base ligand, H₂L¹, following the literature method.^{75,76} The ligand (H₂L¹) on reaction with copper(II) acetate monohydrate followed by lead(II) acetate trihydrate and sodium thiocyanate

in 1:1:2 ratio produced the hetero dinuclear complex. Formation of the complex is shown in

Scheme III.A.1.



Scheme III.A.1: Synthetic route to the complex.

III.A .3. 2 : *Description of [(SCN)CuL¹Pb(SCN)] (5)*

The X-ray crystal structure determination reveals that the complex crystallizes in triclinic space group, $P\bar{1}$. Molecular structure of the complex is built from isolated hetero-dinuclear molecule of [(SCN)CuL¹Pb(SCN)]. Molecular structure of the complex is shown in Figure III.A.1.

The N₂O₂O₂' donor compartmental reduced Schiff base ligand (H₂L¹) is used to prepare the complex in which copper(II) centre, Cu(1), is placed in the inner N₂O₂ cavity and lead(II) centre, Pb(1), is placed in the outer O₂O₂' cavity. Both the copper(II) and lead(II) centers are pentacoordinated. The copper(II) center, Cu(1), has square pyramidal geometry, where two amine nitrogen atoms, N(1) and N(2), and two phenoxo oxygen atoms, O(1) and O(2), of the deprotonated reduced Schiff base, constitute the equatorial plane. The axial position of the copper(II) centre is occupied by a nitrogen atom, N(3), from a terminal thiocyanate molecule. The geometry of any pentacoordinated metal centre may conveniently be measured by the

Addison parameter (τ)⁷⁷ [$\tau = (\Theta - \Phi) / 60$, where Θ and Φ are the two largest ligand-metal-ligand angles of the coordination sphere]. In the title complex, the geometry around the copper(II) centre, Cu(1), is square pyramidal with $\tau = 0.02$. On the other hand, phenoxo oxygen atoms, O(1) and O(2), of the deprotonated reduced Schiff base also coordinate to lead(II) centre, Pb(1). The potential donor methoxy oxygen atoms, O(3) and O(4), of the compartmental reduced Schiff base also coordinate to lead(II), but at much longer distances to form equatorial planes. The geometry around the lead(II) centre, Pb(1), is distorted square pyramidal (dsp) with $\tau = 0.493$. The sulphur atom, S(2), from terminal thiocyanate molecule coordinate to the lead(II) centre in axial position with Pb(1)–S(2)–C(23) angle $96.8(2)^\circ$ where the N-terminal of the same thiocyanate molecule is directed towards copper(II) center with Cu(1)⋯N(4)–S(2) angle $94.9(4)^\circ$. The N(4)⋯Cu(1) distance [$3.057(4) \text{ \AA}$], is larger than the distances of N(1)–Cu(1) [$2.019(4)$], N(2)–Cu(1) [$2.037(3)$] and also Pb(1)–S(2) [$2.7914(15) \text{ \AA}$], which indicates partial bridging interaction of thiocyanate between Cu(1) and Pb(1). The deviations of the four coordinating atoms, O(1), O(2), N(1) and N(2), in the basal plane from the mean plane passing through them and those of the copper(II) centre from the same planes are $-0.008(3)$, $-0.075(3)$, $-0.077(3)$, $-0.016(4) \text{ \AA}$ and $0.176(5)$ respectively for the complex. The saturated six-membered chelate ring [Cu(1)–N(1)–C(9)–C(10)–C(13)–N(2)] has envelope conformation with puckering parameters,^{78,79} $q = 0.531(5) \text{ \AA}$; $\theta = 25.2(4)^\circ$; $\phi = 185.1(12)^\circ$. The Cu(1)O(1)O(2)Pb(1) core is almost planar as the angle between Cu(1)O(1)O(2) and O(1)O(2)Pb(1) plane is $7.26(9)^\circ$, and the dihedral angle of O(1)Pb(1)O(2)Cu(1) is $5.85(11)^\circ$. The distance between the Cu(1) and Pb(1) is $3.504(5) \text{ \AA}$. The bridging angles Cu(1)–O(1)–Pb(1) and Cu(1)–O(2)–Pb(1) are $106.5(1)^\circ$ and $106.0(1)^\circ$, respectively.

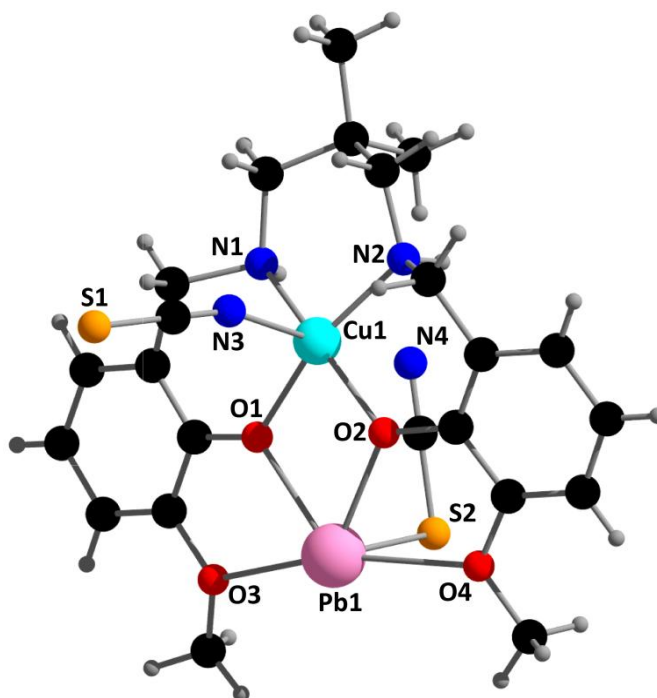


Fig. III.A.1: Perspective view of the complex with a selective atom numbering scheme.

III.A .3.3. Supramolecular interactions

The solid-state structure of the complex is well constructed through two types of non-covalent interactions such as $\pi\cdots\pi$ stacking interaction, cation $\cdots\pi$ interaction. The phenyl ring Cg(7) [C(2)–C(3)–C(4)–C(5)–C(6)–C(7)] undergoes a strong face-to-face $\pi\cdots\pi$ stacking interaction with the neighboring phenyl ring Cg(8) [C(15)–C(16)–C(17)–C(18)–C(19)–C(20)] of symmetry (^a = -1+x,y,z). A one-dimensional array is formed because of this type of $\pi\cdots\pi$ stacking interaction (Figure III.A.2).

A cation $\cdots\pi$ interaction is also observed in the complex. The lead(II) centre, Pb(1), is involved in cation $\cdots\pi$ interaction with a symmetry-related (1-x,1-y,-z) phenyl ring Cg(8), [C(15)–

C(16)–C(17)–C(18)–C(19)–C(20)], which leads to the formation of a dimer structure (Figure III.A. 3).

Relying on the structural discussion by Shimoni-Livny et al.,⁸⁰ the hemidirectionally coordinated lead(II) center has a significant void opposite to ligand (H_2L^1) and thiocyanate coligand, which is similar to other lead(II) complexes.⁸¹ All bonds around lead(II) atom are basically concentrated within less than one hemisphere of the coordination sphere, leaving a large gap on the lead(II) ion. This also allows close interaction with the sulfur atom, $(\text{S}1)^c$, of the thiocyanate from an adjacent molecule ($^c=x, -1+y, z$) at 3.517(2) Å which leads to the formation of a 1D polymeric chain, as shown in Figure III.A. 4. There is another captivating interaction between $\text{S}(1)$ and $\text{S}(1)^d$ [$^d=2-x, 2-y, -z$] at 3.593(2) Å which leads to the formation of supramolecular dimer structure, as shown in Figure III.A. 5. Both $\text{Pb}1\cdots\text{S}1^a$ and $\text{S}1\cdots\text{S}1^b$ interactions lead to the formation of a 2D polymeric network, as shown in Figure III.A. 6.

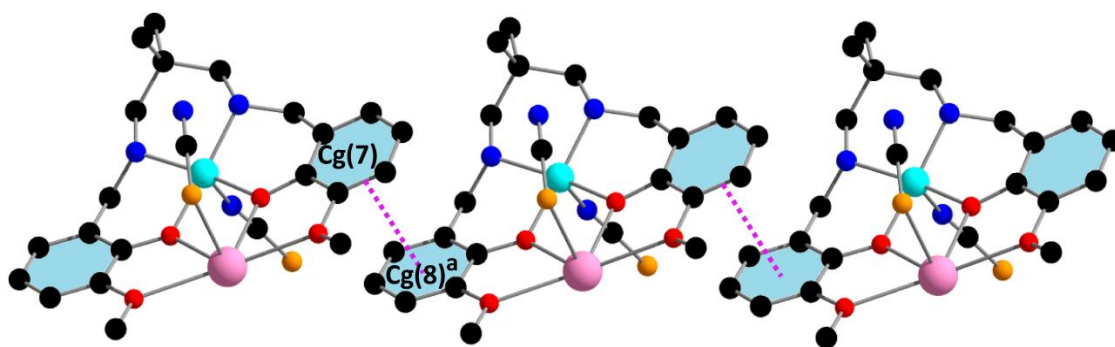


Fig. III.A.2: 1D chain of intermolecular $\pi\cdots\pi$ stacking interactions. All hydrogen atoms and uncoordinated perchlorate anions are omitted for clarity. Symmetry elements $^a=1+x,y,z$. Where, $\text{Cg}(7)\cdots\text{Cg}(8)^a = 3.771(3)$ Å, $\text{Cg}(I)\cdots\text{Prep} = 3.5646(18)$ Å, $\text{Cg}(J)\cdots\text{Prep} = -3.5399(19)$, $\alpha = 13.5(2)^\circ$.

α = dihedral angle between ring I and ring J, Cg(I)⋯Perp.=perpendicular distance of Cg(I) on ring J, Cg(J)⋯Perp.=perpendicular distance of Cg(J) on ring I. Cg(7)=centre of mass of the ring [C(2)–C(3)–C(4)–C(5)–C(6)–C(7)] and Cg(8)=centre of mass of the ring [C(15)–C(16)–C(17)–C(18)–C(19)–C(20)] for the complex.

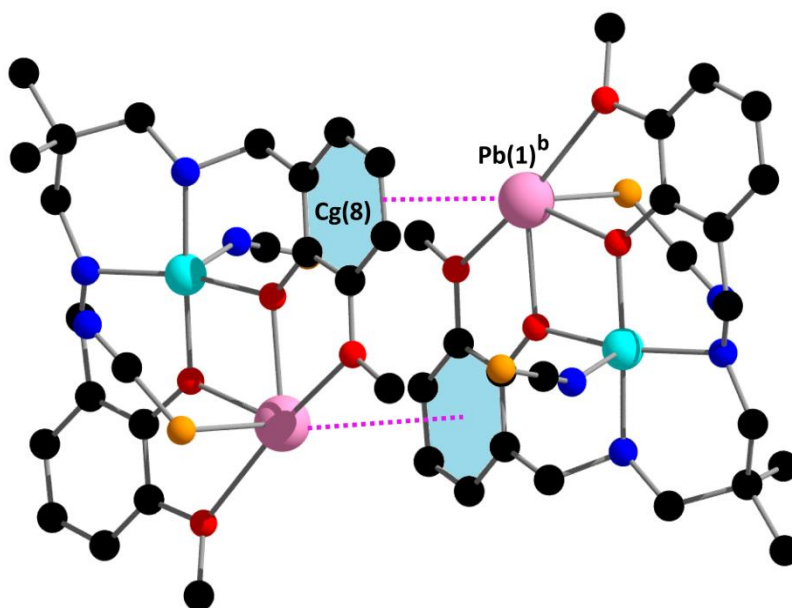


Fig. III.A.3: Supramolecular dimer of the complex, generated through cation⋯ π interactions. All hydrogen atoms and uncoordinated perchlorate anions are omitted for clarity. Symmetry elements $^b=1-x, 1-y, -z$. Where, Cg(8)⋯Pb(1) = 3.563 Å, Pb(1)⋯Perp = -3.359 Å, β = 19.43°.

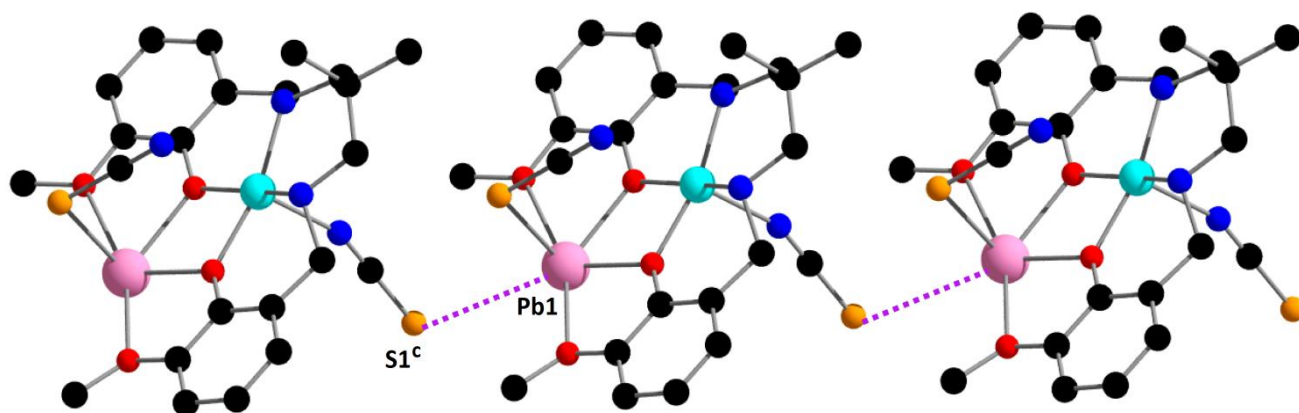


Fig. III.A.4: 1D coordination polymer of the complex considering an interaction between Pb(1) and S(1)^a at 3.517(2) Å. Symmetry transformation ^c=x,-1+y,z.

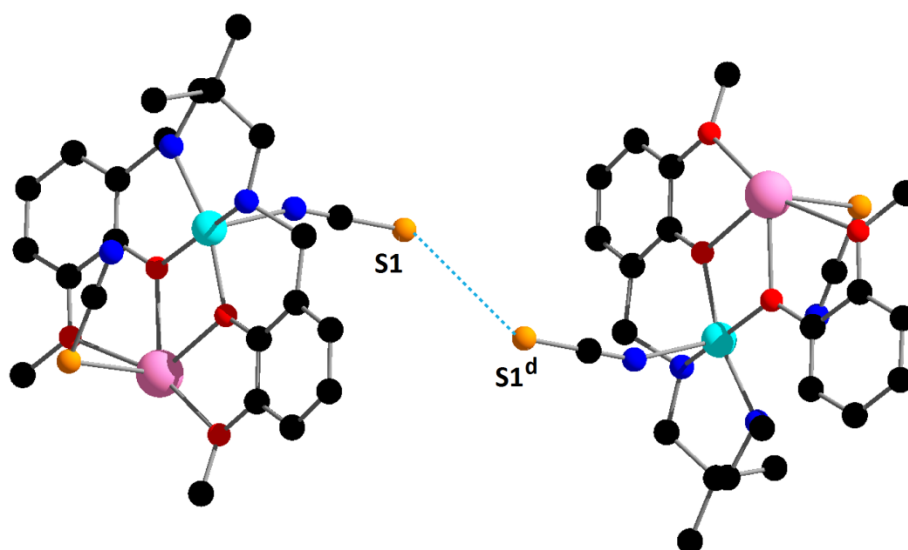


Fig. III.A.5: Dimer form of the complex considering an interaction between S(1) and S(1)^d at 3.593(2) Å. Symmetry transformation ^d=2-x,2-y,-z

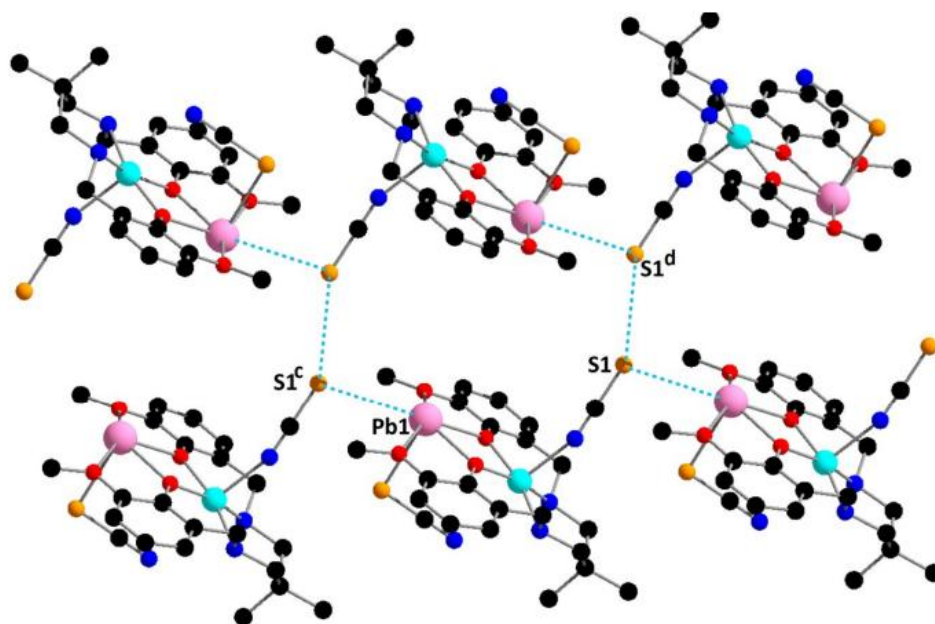


Fig. III.A.6: 2D polymeric network of the complex considering both interactions between Pb(1) and S(1)c at 3.517(2) Å ; between S(1) and S(1)d at 3.593(2) Å . Symmetry transformation c= x, -1+y,z and d= 2-x,2-y,-z.

Table. III.A.1: Crystal data and refinement details of the complex.

Formula	C ₂₃ H ₂₈ PbCuN ₄ O ₄ S ₂ (5)
Formula Weight	759.36
Temperature (K)	273
Crystal system	Triclinic
Space group	$P\bar{1}$
a(Å)	9.3667(7)
b(Å)	9.5064(7)
c(Å)	15.1076(11)
α	84.047(2)
β	75.365(2)
γ	79.476(2)
Z	2
d_{calc} (g cm ⁻³)	1.974
μ (mm ⁻¹)	7.615
$F(000)$	738
Total Reflections	38018
Unique Reflections	5231
Observed data [$I > 2 \sigma(I)$]	4885
No. of parameters	324
R(int)	0.054
R1,wR2(all data)	0.0287, 0.0653
R1,wR2 [$I > 2 \sigma(I)$]	0.0258, 0.0638
CCDC	1953301

Table. III.A.2: Selected bond lengths (Å) of the complex.

Pb(1)–O(1)	2.375(3)	Cu(1)–O(1)	1.988(3)
Pb(1)–O(2)	2.358(3)	Cu(1)–O(2)	2.021(3)
Pb(1)–O(3)	2.631(4)	Cu(1)–N(1)	2.019(3)
Pb(1)–O(4)	2.609(4)	Cu(1)–N(2)	2.037(4)
Pb(1)–S(2)	2.7914(15)	Cu(1)–N(3)	2.232(4)

Table. III.A.3: Selected bond angles (°) of the complex.

O(1)–Pb(1)–O(2)	66.34(10)	O(3)–Pb(1)–O(4)	159.82(9)
O(1)–Cu(1)–O(2)	80.47(12)	O(2)–Cu(1)–N(2)	89.23(14)
O(2)–Pb(1)–O(4)	64.57(10)	S(2)–Pb(1)–O(1)	88.94(7)
O(1)–Cu(1)–N(1)	91.74(14)	O(2)–Cu(1)–N(3)	101.38(14)
O(1)–Pb(1)–O(3)	64.01(10)	S(2)–Pb(1)–O(2)	90.88(8)
O(1)–Cu(1)–N(2)	165.98(14)	N(1)–Cu(1)–N(2)	95.89(16)
O(2)–Pb(1)–O(3)	130.24(10)	S(2)–Pb(1)–O(3)	85.19(9)
O(1)–Cu(1)–N(3)	98.16(14)	N(1)–Cu(1)–N(3)	93.17(15)
O(1)–Pb(1)–O(4)	129.47(10)	S(2)–Pb(1)–O(4)	80.59(8)
O(2)–Cu(1)–N(1)	164.29(13)	N(2)–Cu(1)–N(3)	93.15(16)

III.A .3. 4: IR and electronic spectra

The IR spectrum of the complex is in a good agreement with X-ray structural data. In the IR spectrum of the complex, there are two successive strong bands observed at 2091 and 2068 cm^{-1} , indicating the presence of terminal (N-bonded) and terminal (S-bonded) thiocyanate, respectively.⁸² A moderately strong band due to stretching vibration of N–H bond appears in the range of 3248–3232 cm^{-1} .^{83,84} Bands near the range of 2951–2838 cm^{-1} are due to alkyl C–H bond stretching vibrations, which are customarily noticed in the IR spectrum of the complex.⁸⁵ The IR spectrum of the complex is shown in Figure III.A. 7.

Electronic spectrum of the complex in DMF displays one absorption band in the visible region at 618 nm which may be considered as $^2T_{2g}(D) \leftarrow ^2E_g(D)$ transition for copper(II).^{86,87} A broad band of low intense features near 405 nm may be attributed to ligand-to-metal charge Transfer (LMCT) transition from the N donor centres of Schiff base to copper(II).^{88,89} Another very low intensity band at 335 nm may be attributed to $n \rightarrow \pi^*$ transition of the ligand.⁹⁰ The high intensity band occur at 282 nm is attributed to $\pi \rightarrow \pi^*$ transition of the ligand.⁹¹ The UV-vis spectrum of the complex is shown in Figure III.A. 8.

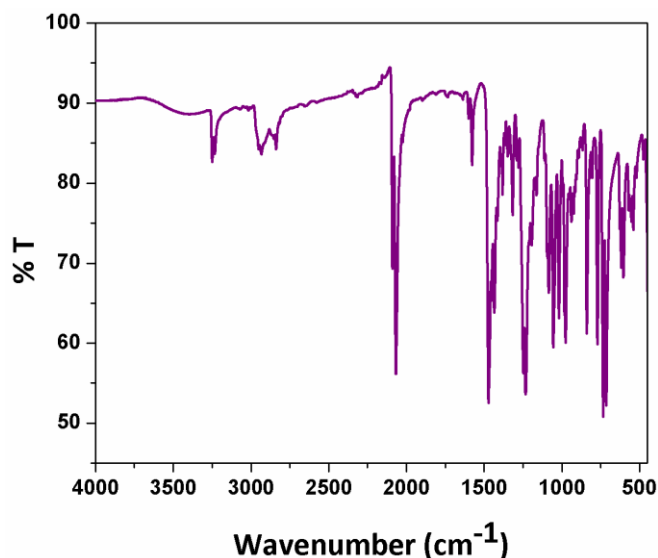


Fig. III.A. 7: IR-spectrum of the complex.

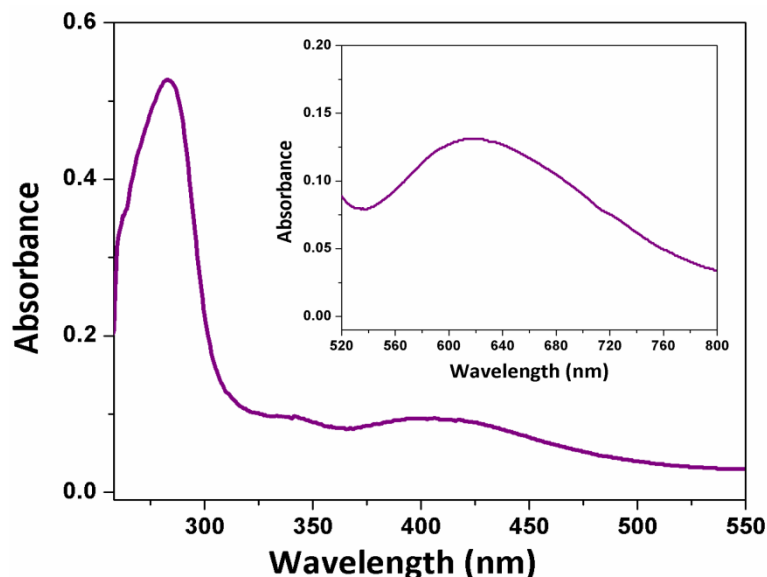


Fig. III.A. 8: UV-Vis spectrum of the complex. Inset shows spectrum in 520-800 nm range.

III.A .3.5: Theoretical study

The focus of the theoretical work is to evaluate the electronic and energetic features of Pb \cdots S tetrel bonding and some other weak non-covalent interactions, namely, S \cdots S and N \cdots H hydrogen bonding which are further characterized by the Hirshfeld analysis (Figure. III.A.6- Figure. III.A. 16) and also Pb \cdots π and $\pi\cdots\pi$, found in the solid-state of the investigated complex. As discussed in the experimental section, we used dimer of the title complex to explore such interactions.

III.A .3.5.1. S \cdots S interactions:

As observed in the crystal structure, the distance between two sulfur atoms (3.59 Å) is within the sum of their van der Waals radii (3.6 Å) indicating a significant chalcogen-chalcogen interactions as we have found in literature.^{92,93} These literature results suggest that in the chalcogen-chalcogen interaction, $p-\sigma^*$ plays an important role to stabilize such interaction as shown in Figure. III.A. 9. In our case, as shown in Figure. III.A. 9, the S...S interaction is stabilized by the overlap of filled $3p_S$ orbital at sulfur atom of one monomer and empty σ_{S-C}^* antibonding orbital at the sulfur atom of another monomer. Also, Figure. III.A. 9 shows the NBO calculated donor and acceptor orbitals. The estimated stabilization energy $E^{(2)}$ associated with $p_S \rightarrow \sigma_{S-C}^*$ charge transfer (delocalization) is 0.34 kcal/mol computed at B₃LYP/Lanl₂DZ/6-31G(d) level using NBO analysis.

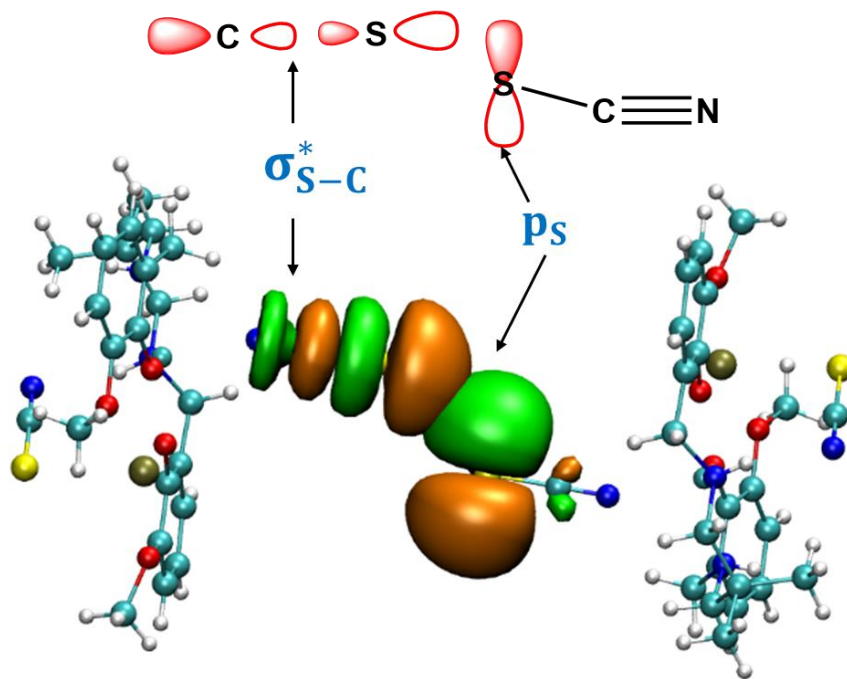


Fig. III.A. 9: Isosurfaces for a value of 0.03 a.u. showing the interaction of filled p orbital at center S of one monomer and empty σ^* orbital at center S of another monomer computed from NBO analyses.

Moreover, the S...S interaction is also supported from Bader's theory of atoms in molecules. As shown in Figure. III.A.11, we found a bond critical point, CP3 ($\rho \approx 0.0633$ a.u.) between two sulfur atoms at two different monomers. We also computed the Lagrangian kinetic energy and potential energy density at the BCP and the corresponding values are 0.1086 and -0.1001 a.u., respectively.

Furthermore, the reduced density gradient (RDG), s , was calculated to represent the deviation from a homogeneous electron distribution.⁹⁴ As presented in the following equ. (1), ∇ is the gradient operator and $|\nabla\rho|$ is the electronic density gradient mode. Now, it is a useful approach to explore and visualize different kinds of noncovalent interactions (NCIs) in real space such as both intra- and intermolecular weak interactions like hydrogen bonds and Van der Waals forces. Therefore, the NCI index is used to investigate NCIs in the investigated complex.

$$s = \frac{1}{2(3\pi^2)^{\frac{1}{3}}} \frac{|\nabla\rho|}{\rho^{\frac{4}{3}}} \quad (1)$$

The color mapped isosurfaces and corresponding scatter diagrams of RDG versus sign $(\lambda_2)\rho$ for the investigated complex in the monomer and dimers are shown in Figure. III.A. 13. As stated, the results are used to characterize the type of multiple weak interactions like S...S, Pb...S and H-bonds via colored isosurfaces according to the values of sign $(\lambda_2)\rho$. The sign of

λ_2 is used to distinguish bonded ($\lambda_2 < 0$) and nonbonded ($\lambda_2 > 0$) interactions, whereas the electron density is an indicator of the bonding strength. Large negative values of $\text{sign}(\lambda_2)\rho$ are indicative of attractive interactions (such as hydrogen bonding), whereas, if $\text{sign}(\lambda_2)\rho$ is large and positive, the interaction is nonbonding (usually steric effect). Values near zero indicate weak vdW interactions. The color of RDG (s) vs. $\text{sign}(\lambda_2)\rho$ and the isosurfaces have the same meaning; blue color represents hydrogen bonds; green, van der Waals forces; and red, steric hindrance. The darker the corresponding color, the stronger is the interaction.

The color mapped isosurfaces and corresponding scatter diagrams of RDG versus $\text{sign}(\lambda_2)\rho$ for the complex in dimeric form is shown in Figure. III.A. 13. The green region in Figure. III.A. 13a clearly characterizes the weak S...S interaction between two monomers in the solid-state. The BSSE corrected interaction energy for calculated from S...S interactions is -1.6 kcal/mol.

III.A .3.5.2. Pb...S tetrel bonding:

In the solid state structure of the investigated complex, an existence of intermolecular tetrel bonding interaction is characterized by a bond critical point (CP1) and a bond path interconnecting the S and Pb atoms in a dimeric unit ($\rho = 0.06936$ a.u.). The strengths is significantly strong which is evident from the MEP analysis. The MEP surface at the S and Pb atoms shows that a σ -hole of 22 kcal/mol is observed at the Pb center along with a strong nucleophilic center at S atom of -20 kcal/mol (Figure. III.A. 13a) As a result, BSSE corrected interaction energy computed for the tetrel bonding is -13.6 kcal/mol. The NBO analysis shows that the stabilization energy $E^{(2)}$ associated with charge transfer (delocalization) from S to Pb

center is 13.79 kcal/mol computed at B₃LYP/LanI₂DZ/6-31G(d) (Figure. III.A. 10). Additionally, we have characterized the existence of Pb...S tetrel bond by the RDG plots and NCI surfaces (Figure. III.A. 13d).

III.A .3.5.3. H-bonding:

We characterized two types of H-bondings in the investigated complex: intramolecular and intermolecular. In the monomer, intramolecular H-bonding is characterized by AIM analysis which gives an orange sphere as BCP (Figure. III.A. 11f) between N of SCN and amine hydrogen of Schiff base. The existence of such H-bonding is well supported by the RDG plots and NCI surfaces as shown in Figure. III.A. 13c.

In the dimer, we have found some additional intermolecular H-bonding as characterized very clearly from the NCI surfaces and AIM analysis. We identified a BCP ($\rho = 0.0149$ a.u.) between amine N of one monomer and H of another monomer. Additionally, the scatter RDG plot shows some additional blue dots at the left side to identify the intermolecular H-bonding (Figure. III.A. 13b). As a consequence, the BSSE corrected interaction energy of this complex is -7.1 kcal/mol.

III.A .3.5.4. Pb... π and π ... π interactions:

As stated in the experimental section, we have found π ... π interaction between two benzene rings on two monomers. In the investigated complex, we confirmed the existence of the π ... π interactions by using AIM analysis. In the dimer, the computed results show that two BCPs are found, one of which (CP2) is shown in Figure 10, between σ (C-H) framework of one ring and π -electrons on another ring. The attractive interaction is also evident from the MEP

surfaces (Figure. III.A. 12b). Further, we established the existence of the $\pi\cdots\pi$ stacking by utilizing RDG surfaces as shown in Figure. III.A. 13(e). A very clean image of green color between two rings strongly supports the statement. As a result of $\pi\cdots\pi$ interaction, we computed the BSSE interaction energy of -1.15 kcal/mol.

Interestingly, from the AIM analysis, we detected another weak interaction between the cation Pb(II) and π -electrons, referred to as $\text{Pb}\cdots\pi$ interaction. The properties of the BCP (CP4) shows that this interaction is stronger ($\rho = 0.2394$ a.u.) than the other CPs discussed previously. The MEP surface of $\text{Pb}\cdots\pi$ interaction (Figure. III.A. 12b) clearly indicates that this is electrostatically very favorable due to potential difference between a strong σ -hole at Pb center ($+18$ kcal/mol) and aromatic ring (-6.9 kcal/mol). The interaction is further characterized by NCI-RDG surface showing a green plate between Pb(II) center and aromatic ring as shown in Figure. III.A. 13f. As a consequence, the computed the BSSE corrected interaction energy of $\text{Pb}\cdots\pi$ interaction is -13.6 kcal/mol.

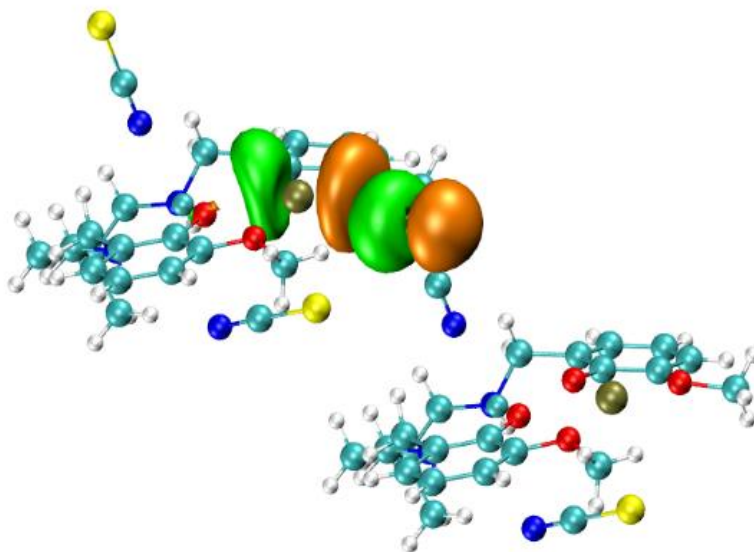


Fig. III.A. 10: Isosurfaces for a value of 0.03 a.u. showing the interaction between orbital at S of one monomer and orbital at Pb of another monomer indicating a tetrel bond computed from NBO analysis.

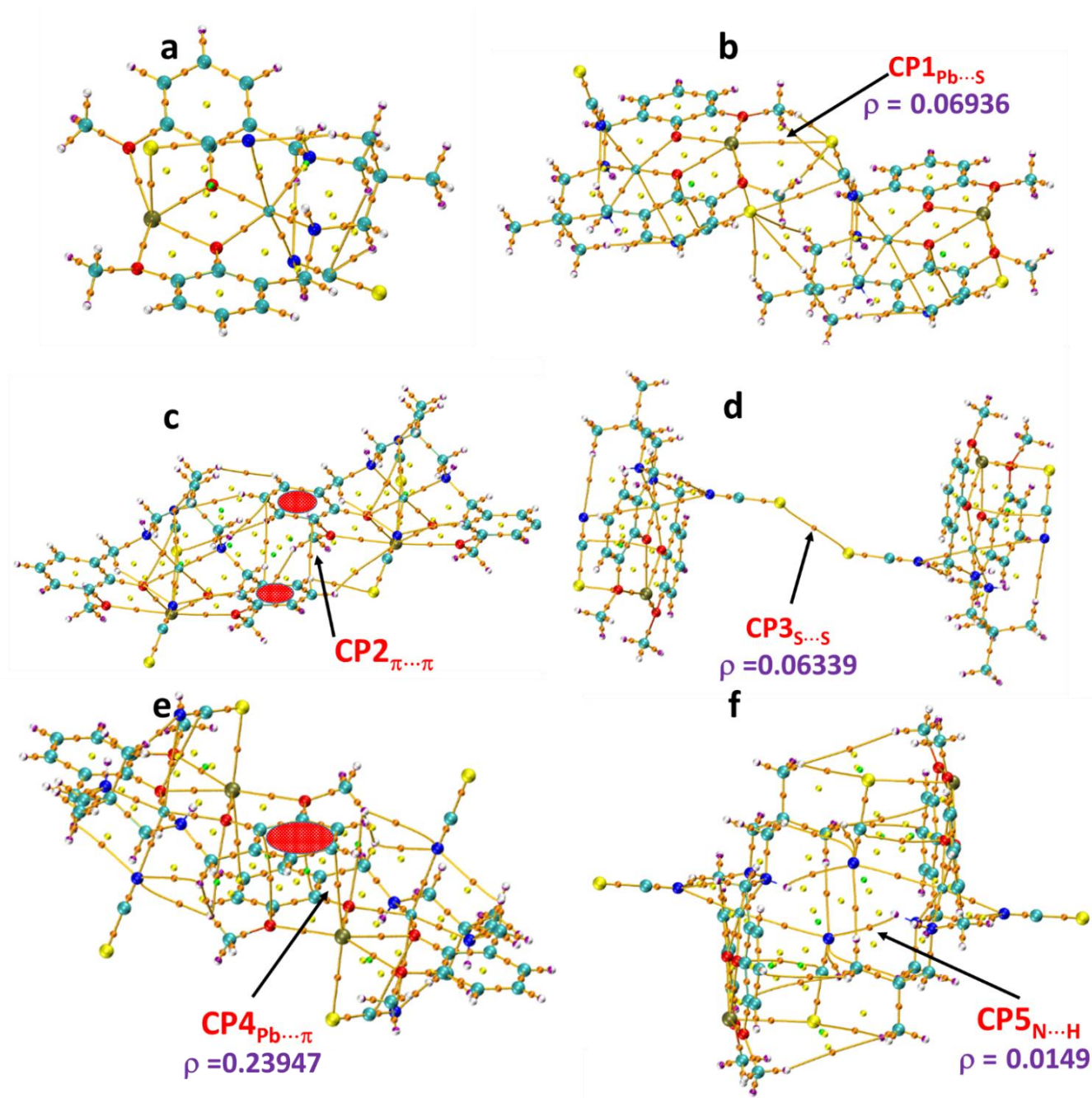


Fig. III.A. 11: AIM analyses of the monomer (a) and dimers of investigated complex showing (b) Pb...S (c) $\pi\cdots\pi$ (d) S...S (e) Pb... π (f) intermolecular hydrogen bonding, N...H-N. Bond, ring and cage critical points are represented by orange, yellow and green spheres, respectively.

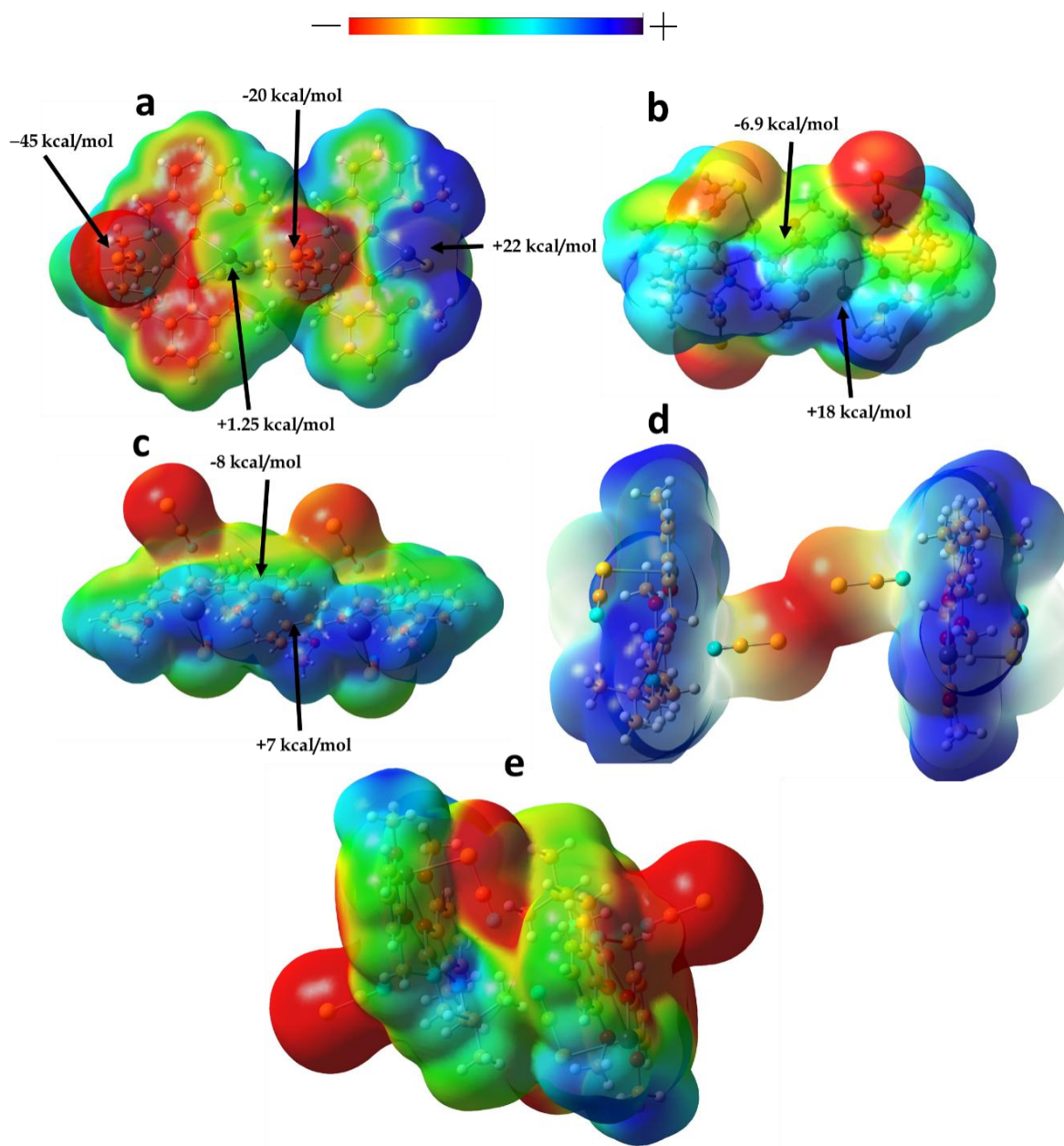


Fig. III.A. 12. MEP surface (isosurface = 0.001 a.u.) of the investigated complex. MEP values at selected points of the surface in the complex showing (a) Pb \cdots S (b) Pb \cdots π (c) $\pi\cdots\pi$ (d) S \cdots S (e) H-bonding interactions

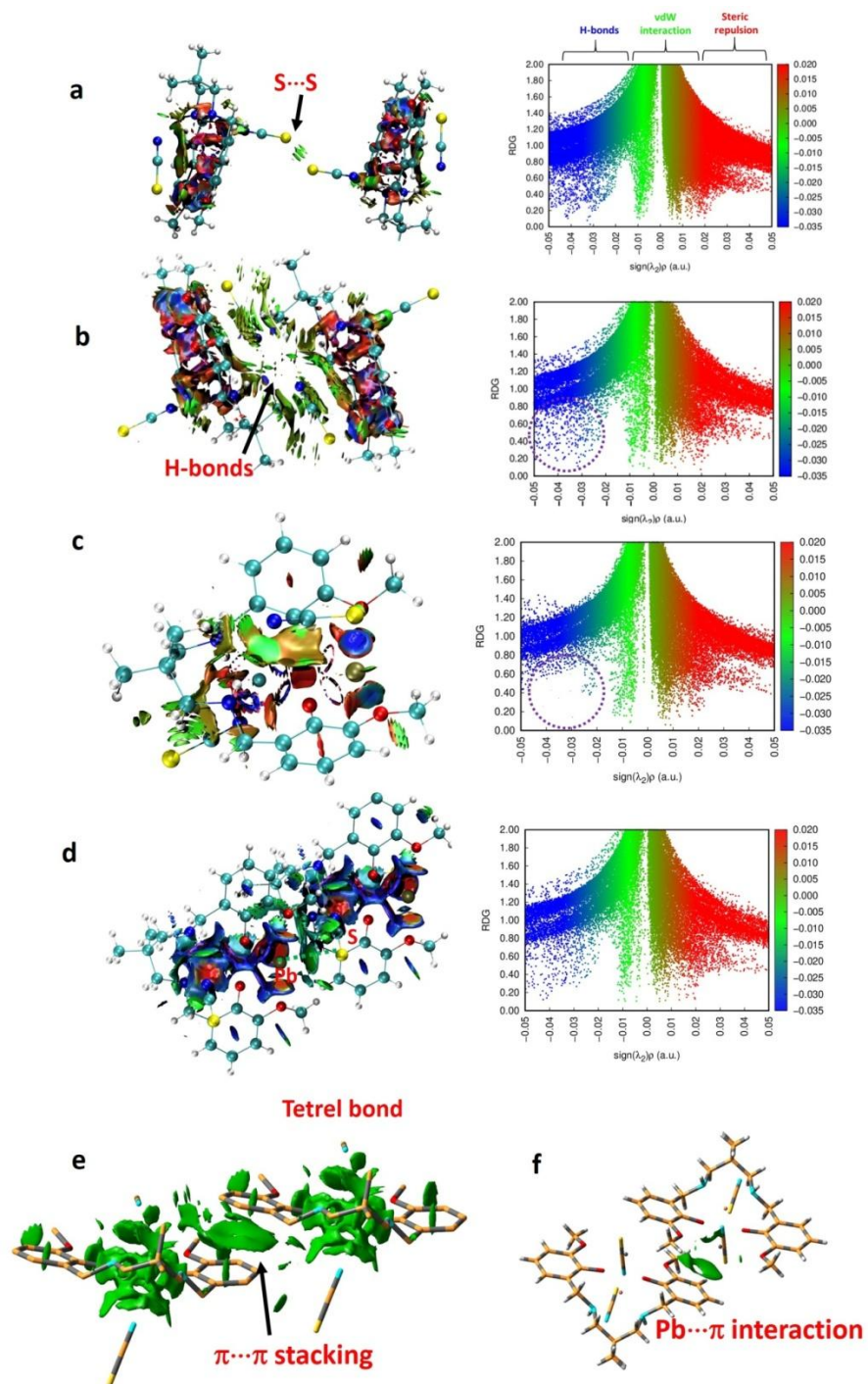


Fig. III.A.13: Noncovalent interaction (NCI) analysis of the investigated complex computed at B₃LYP/LanL₂DZ/6-31G(d) level showing (a) S···S interaction (b) intermolecular H-bonding (c) intramolecular H-bonding (d) Pb···S tetrel bonding (e) π ··· π interaction (f) Pb··· π interaction

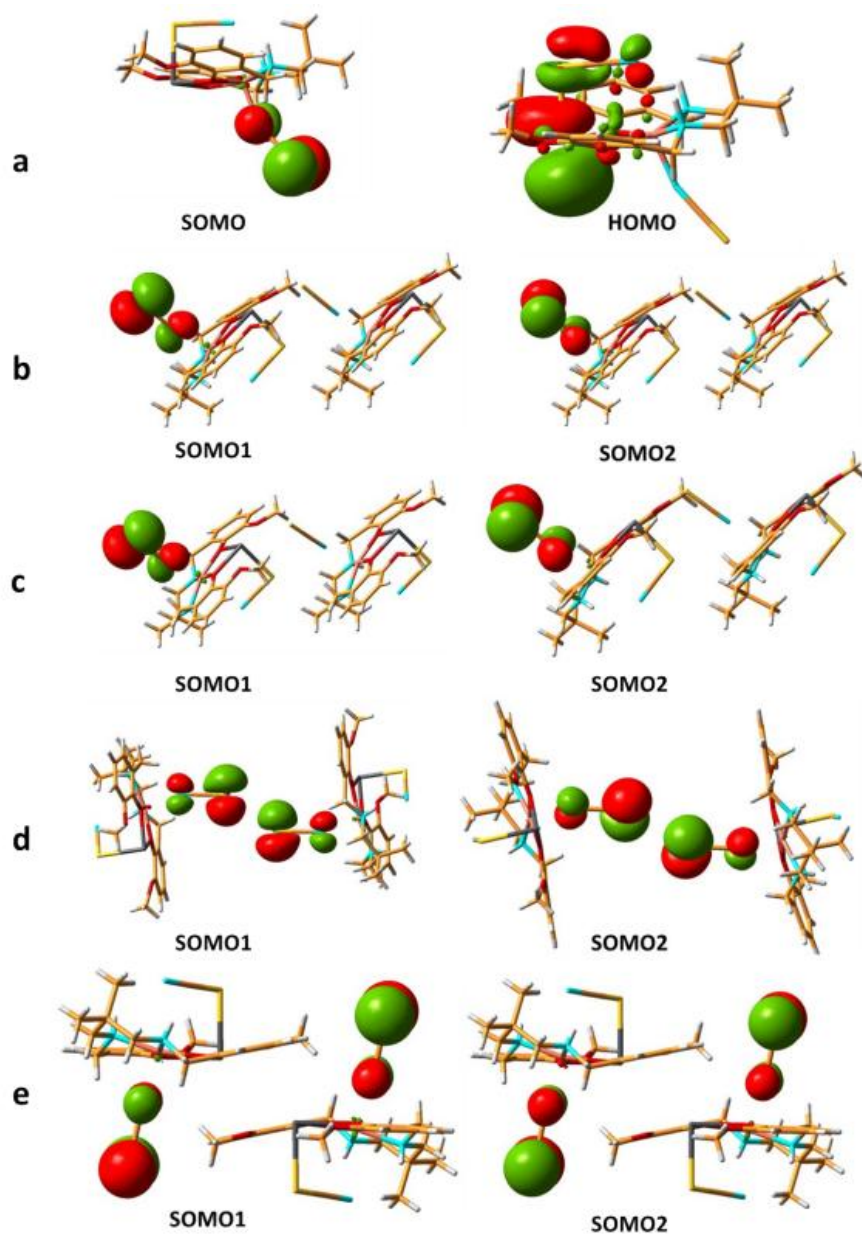


Fig. III.A.14: Frontier Molecular Orbital pictures of the investigated complex showing SOMO and HOMO (a); SOMO1 and SMO2 of the dimers (of the investigated complex) produced by Pb...S (b); $\pi\cdots\pi$ (c); S...S (d) and Pb... π (e) interactions.

III.A .3.6: Hirshfeld surfaces

The Hirshfeld surface arises from an endeavor to define the space occupied by a molecule in a crystal for the purpose of subdividing the crystal electron density into molecular fragments.⁹⁵ d_{norm} is a normalised contact distance⁹⁶, where Intermolecular contacts are decorated in the d_{norm} surface (when atoms make intermolecular contacts closer than the sum of their van der Waals radii, these contacts will be highlighted in red whereas longer contacts are blue, and contacts around the sum of van der Waals radii are white). Hirshfeld surfaces of the complex mapped over d_{norm} (range of -0.110 to 1.415 Å). Red spots on these surfaces indicate the dominant interactions [N...H/H...N, S...H/H...S and O...H/H...O] in the complex. As the Hirshfeld surface interpret the shape of the molecule in terms of its surrounding crystalline environment, the local shape of the surface may provide some chemical insight whereas shape index is a qualitative measure of shape and can be sensitive to very subtle changes in surface shape, particularly in regions where the total curvature (or the curvedness) is very low.⁹⁷ The 2D fingerprint plots,⁸ which are used to analyze the intermolecular contacts at the same time, revealed that the main intermolecular interactions in the complex are S...H/H...S, N...H/H...N or O...H/H...O. The Hirshfeld surfaces and the corresponding 2D fingerprint plots for complex is shown in Figure. III.A. 15. We are particularly

interested to investigate if the $\text{Pb}\cdots\text{S}$ and $\text{S}\cdots\text{S}$ non-covalent bonds can also be supported using Hirshfeld surface analysis. Gratifyingly, the non covalent bond was characterized by the spikes of the breakdown fingerprint plot. The complex exhibits $\text{Pb}\cdots\text{S}/\text{S}\cdots\text{Pb}$ non-covalent bond that contribute 1.0% of the total Hirshfeld surface area and is evident in the (d_i, d_e) region of (2.087 Å, 2.705 Å). A close inspection of the fingerprint plot revealed that the sharp spikes with the shortest $(d_e + d_i) = 3.096$ Å in the complex correspond to $\text{Pb}\cdots\text{S}/\text{S}\cdots\text{Pb}$ interaction.

(Figure. III.A. 16) $\text{Pb}\cdots\text{S}$ and $\text{S}\cdots\text{S}$ contacts are also observed in the complex. These contacts confirm the existence of the $\text{Pb}\cdots\text{S}$ tetrel bonding and $\text{S}\cdots\text{S}$ interaction in the complex (Fig. 7).

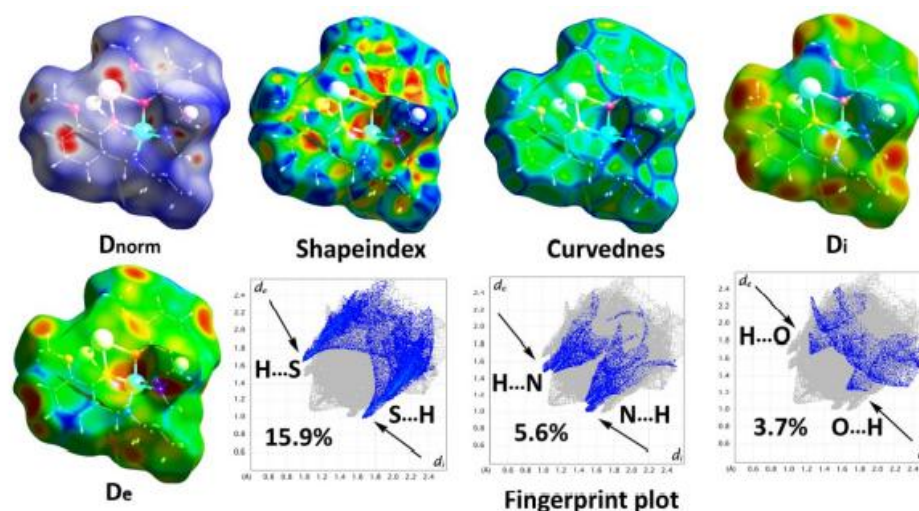


Fig. III.A. 15: Hirshfeld surfaces and fingerprint plots of the complex.

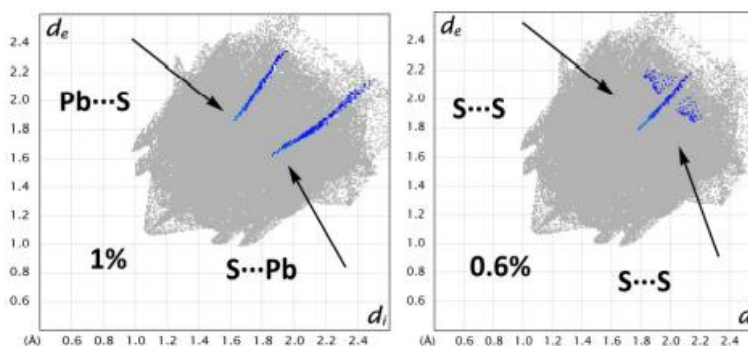


Fig. III.A. 16: Fingerprint plot resolved into Pb...S/S...S contact and S...S/S...S contact contributed to the total Hirshfeld Surface area of the complex

III.A. 4: Concluding remarks

In summary, we report the syntheses and structural characterization of a new heterodinuclear copper(II)/lead(II) complex with N₂O₄ donor compartmental reduced Schiff base ligand. In the solid-state, the complex exhibits relevant tetrel bonding and chalcogen-chalcogen interactions that generate interesting supramolecular assemblies. The complex contains hemidirectionally coordinated lead(II) center and organic aromatic molecule which be important to understand the X-ray structure of organic–inorganic material systems. In addition to the uses of NCI-RDG analysis, to support for the existence of tetrel bonding, NBO results show that the nature of the tetrel-bonding is formed between the donor atom S of SCN and acceptor atom Pb ($lp_S \rightarrow lp_{Pb}^*$) with a high second-order stabilization energy of $E^{(2)} \approx 13.8$ kcal/mol. Further, the S...S interaction, like general chalcogen-chalcogen bond, is an $p_S \rightarrow \sigma_{S-C}^*$ orbital delocalization with $E^{(2)} \approx 0.34$ kcal/mol. The other three interactions, namely, Pb... π , $\pi \cdots \pi$ and both intra- and intermolecular H-bonding are well supported qualitatively and quantitatively with the help of NCI-RDG, QTAIM, MEP surface, and NBO analyses. Among these interactions, we have found that Pb... π has the highest interaction energies of -13.6 kcal/mol.

III.A. 5: Computational Details

A DFT study is carried out to understand the electronic structure of the investigated complex. All geometry optimizations of the complex are carried out using the density functional theory method at the B₃LYP level with the Gaussian 09 program package. Los Alamos Effective Core Potentials lanL₂DZ basis set was employed for the Pb and Cu atoms. On the other hand, the split-valence 6-31G(d) basis set was applied for the other atoms. The starting structure of the investigated complex was used from its X-ray crystallographic data. The geometry optimization is performed without any constraint, and the nature of stationary points was confirmed by normal-mode analysis. The topological features derived from Bader's theory of atoms in molecules (AIM) approach was applied to understand the electron-density features like charge density (ρ) and Laplacian of charge density ($\nabla^2\rho$) using ADF2014.10. The recently developed Reduced Density Gradient (RDG) based NCI (noncovalent interactions) index calculations were applied for real-space visualization of both attractive (van der Waals and hydrogen-bonding) and repulsive (steric) interactions based on properties of the electron density. This is already discussed in the theoretical work section. Natural bond orbital (NBO) analysis was applied to investigate the stability of the molecule arising from charge delocalization. The interaction energies of dimers were calculated using *basis set* superposition error (BSSE) corrections by the following methods:

$$\Delta E(AB) = E(AB) - E(A) - E(B) + (\text{BSSE value of dimer})$$

References

- 1 D. L. Reger, T. D. Wright, C. A. Little, J. J. S. Lamba and M. D. Smith, *Inorg. Chem.*, 2001, **40**, 3810–3814.
- 2 H. Fleischer and D. Schollmeyer, *Inorg. Chem.*, 2004, **43**, 5529–5536.
- 3 A. Morsali and A. R. Mahjoub, *Helv. Chim. Acta.*, 2004, **87**, 2717–2722.
- 4 J. Parr, *Polyhedron*, 1997, **16**, 551–566.
- 5 A. Olvera, G.; Shi, H. Djieutedjeu, A. Page, C. Uher, E. Kioupakis and P. F. P. Poudeu, *Inorg. Chem.*, 2015, **54**, 746–755.
- 6 C. A. Randall, A. S. Bhalla, T. R. Shrout and L. E. Cross, *J. Mater. Res.*, 1990, **5**, 829–834.
- 7 F. Cheng, J. Liang, Z. Tao and J. Chen, *Adv. Mater.*, 2011, **23**, 1695–1715.
- 8 L. Zhang, Y.-Y. Qin, Z.-J. Li, Q.-P. Lin, J.-K. Cheng, J. Zhang and Y.-G. Yao, *Inorg. Chem.*, 2008, **47**, 8286–8293.
- 9 Y. Cheng, T. J. Emge and J. G. Brennan, *Inorg. Chem.*, 1996, **35**, 342–346.
- 10 J. J. Chisholm, *Sci. Am.*, 1971, **224**, 15–23.

- 11 B. P. Lanphear, D. A. Burgoon, S. W. Rust, S. Eberly and W. Galke, *Environ. Res.*, 1998, **76**, 120–130.
- 12 T. G. Spiro and W. M. Stigliani, *Chemistry of the Environment*, Prentice Hall, Upper Saddle River, NJ. 1996.
- 13 F. Cuenot, M. Meyer, A. Bucaille, R. A. Guillard, *J. Mol. Liq.*, 2005, **118**, 89–99.
- 14 R. M. Harrison and D. R. H. Laxen, *Lead Pollution*, Chapman & Hall, London. 1981.
- 15 J. M. Christensen and J. Kristiansen, in *Handbook of Metals in Clinical and Analytical Chemistry* ed. H. Seiler, G. A. Sigel, H. Sigel and M. Dekker, New York. 1994, 425–440.
- 16 R. A. Goyer, in *Handbook on Toxicity of Inorganic Compounds*, ed. H. G. Seiler, H. Sigel, A. Sigel and M. Dekker, New York. 1988.
- 17 D. A. Cory-Slechta, B. Weiss and C. Cox, *J. Pharmacol. Exp. Ther.*, 1987, **243**, 804–813.
- 18 D. E. Glotzer and K. A. Freedberg and H. Baucher, *Med. Decis. Making.*, 1995, **15**, 13–24.
- 19 D. E. Glotzer and H. Baucher, *J. Pediatrics.*, 1992, **89**, 614–618.
- 20 CDC (Centers for Disease Control), *Preventing Lead Poisoning in Young Children*. A statement by The Centers for Disease Control-October, 1991. U.S. Department of Health and Human Services/Public Health Service/Centers for Disease Control.
- 21 M. E. Markowitz and J. F. Rosen, *J. Pediatr.* 1991, **119**, 305–310.

- 22 R. Ferreirs-Martínez, D. Esteban-Gomez, E. Toth, A. de Blas, C. Platas-Iglesias, T. Rodríguez-Blas, *Inorg. Chem.*, 2011, **50**, 3772–3784.
- 23 J. M. Ratcliffe, *Lead in Man and Environment*, John Wiley & Sons, New York, 1981.
- 24 M. D. J. J. Chisolm Jr, *J. Pediatr.*, 1968, **73**, 1–38.
- 25 S.-R. Fan and L.-G. Zhu, *Inorg. Chem.*, 2007, **46**, 6785–6793.
- 26 P. Pyykkö and J.-P. Desclaux, *Acc. Chem. Res.*, 1979, **12**, 276–281.
- (27) N. V. Sidgwick and H. M. Powell, Bakerian Lecture: Stereochemical types and valency groups. *Proc. R. Soc. London, Ser. A.*, 1940, **176**, 153.
- 28 M. S. Banna, *J. Chem. Educ.*, 1985, **62**, 197–198.
- 29 K. S. Pitzer, *Acc. Chem. Res.*, 1979, **12**, 271–276.
- 30 P. Pyykkö, *Chem. Rev.*, 1988, **88**, 563–594.
- 31 D. R. McKeney, *J. Chem. Educ.*, 1983, **60**, 112–116.
- 32 J. R. Thompson, D. Snider, J. E. C. Wren, S. Kroeker, V. E. Williams and D. B. *Eur. J. Inorg. Chem.*, 2017, 88–98.
- 33 R. L. Davidovich, V. Stavila, D. V. Marinin, E. I. Voit and K. H. Whitmire, *Coord. Chem. Rev.*, 2009, **253**, 1316–1352.
- 34 R. J. Gillespie and R. S. Nyholm, *Inorganic Stereochemistry. Q. Rev. (London)*, 1957, **11**, 339–380.

- 35 D. L. Reger, M. F. Huff, A. L. Rheingold and B. S. Haggert, *J. Am. Chem. Soc.*, 1992, **114**, 579–584.
- 36 R. Luckay, I. Cukrowski, J. Mashishi, J. H. Reibenspies, A. H. Bond, R. D. Rogers and R. D. Hancock, *J. Chem. Soc., Dalton Trans.*, 1997, 901–908.
- 37 C. Platas-Iglesias, D. Esteban-Gomez, T. Enriquez-Perez, F. Avecilla, A. de Blas, T. Rodriguez-Blas, *Inorg. Chem.*, 2005, **44**, 2224–2233.
- 38 D. Esteban-Go´mez, C. Platas-Iglesias, T. Enriquez-Pe´rez, F. Avecilla, A. Blas, T. Rodriguez-Blas, *Inorg. Chem.*, 2006, **45**, 5407–5416.
- 39 A. Walsh and G. W. Watson, *J. Solid State Chem.*, 2005, **178**, 1422–1428.
- 40 R. D. Hancock, M. S. Shaikjee, S. M. Dobson and J. C. Boeyens, *Inorg. Chim. Acta.*, 1988, **154**, 229–238.
- 41 J.-M. Lehn, *Supramolecular Chemistry: Concepts and Perspectives*; VCH: Weinheim, 1995.
- 42 J. W. Steed and J. L. Atwood, *Supramolecular Chemistry*; John Wiley & Sons: Chichester, 2000.
- 43 H. J. Schneider and A. Yatsimirsky, *Principles and Methods in Supramolecular Chemistry*; John Wiley & Sons: Chichester, 2000.
- 44 Y. Shen, N. Ma, L. Wu and H.-H. Song, *Inorg. Chim. Acta*, 2015, **429**, 51–60.
- 45 Y.-S. Yang, Y.-P. Yang, M. Liu, Q.-M. Qiu, Q.-H. Jin, J.-J. Sun, H. Chen, Y.-C. Dai and Q.-X. Meng, *Polyhedron*, 2015, **85**, 912–917.

- 46 S. Carboni, C. Gennari, L. Pignataro and U. Piarulli, *Dalton Trans.*, 2011, **40**, 4355–4373.
- 47 A. Bhattacharyya, P. K. Bhaumik, P. P. Jana and S. Chattopadhyay, *Polyhedron*, 2014, **78**, 40–45.
- 48 J. Xiao, P. Broz, A. W. Puri, E. Deu, M. Morell, D. M. Monack and M. A. Bogoyo, *J. Am. Chem. Soc.*, 2013, **135**, 9130–9138.
- 49 S. Naskar, D. Mishra, R. J. Butcher and S. K. Chattopadhyay, *Polyhedron*, 2007, **26**, 3703–3714.
- 50 A. Bauzá, D. Quiñonero, P. M. Deyà and A. Frontera, *Chem.–Asian J.*, 2013, **8**, 2708–2713.
- 51 L. M. Salonen, M. Ellermann and F. Diederich, *Angew. Chem., Int. Ed.*, 2011, **50**, 4808–4842.
- 52 V. R. Pedireddi, D. S. Reddy, B. S. Goud, D. C. Craig, A. D. Rae and G. R. Desiraju, *J. Chem. Soc., Perkin Trans. 2*, 1994, 2353–2360.
- 53 R. E.; Rosenfield, R. Parthasarathy and J. D. Dunitz, *J. Am. Chem. Soc.*, 1977, **99**, 4860–4862.
- 54 J. P. Glusker, *Curr. Chem.*, 1998, **198**, 1–56.
- 55 T. N. Guru Row and R. Parthasarathy, *J. Am. Chem. Soc.*, 1981, **103**, 477–479.
- 56 N. Ramasubbu and R. Parthasarathy, *Phosphorus Sulfur*, 1987, **31**, 221–229.
- 57 J. M. Williams, J. R. Ferraro, R. J. Thorn, K. D. Carlson, U. Geiser, H. H. Wang, A. M. Kini, M.-H. Whangbo, *Organic Superconductors*; Prentice Hall: Englewood Cliffs, NJ, 1992.

- 58 D. Paolantoni, J. Rubio-Magnieto, S. Cantel, J. Martinez, P. Dumy, M. Surin and S. Ulrich, *Chem. Commun.*, 2014, **50**, 14257-14260.
- 59 C. Estarellas, A. Frontera, D. Qui  onero and P. M. Dey  , *Angew. Chem., Int. Ed.*, 2011, **50**, 415-418.
- 60 S. Jana, K. Harms and S. Chattopadhyay, *J. Coord. Chem.*, 2014, **67**, 2954–2966.
- 61 G. Mahmoudi, A. Bauz  , M. Amini, E. Molins, J. T. Maged and A. Frontera, *Dalton Trans.*, 2016, **45**, 10708–10716.
- 62 A. Bauz  , T. J. Mooibroek and A. Frontera, *Angew. Chem., Int. Ed.*, 2013, **52**, 12317–12321.
- 63 A. Bauz  , T. J. Mooibroek and A. Frontera, *Chem. – Eur. J.*, 2014, **20**, 10245–10248.
- 64 R. S. Ruoff, T. Emilsson, A. I. Jaman, T. C. Germann and H. S. Gutowsky, *J. Chem. Phys.*, 1992, **96**, 3441–3446.
- 65 S. J. Grabowski, *Phys. Chem. Chem. Phys.*, 2014, **16**, 1824–1834.
- 66 I. Alkorta, I. Rozas and J. Elguero, *J. Phys. Chem. A*, 2001, **105**, 743–749.
- 67 E. C. Escudero-Ad  n, A. Bauz  , A. Frontera and P. Ballester, *ChemPhysChem.*, 2015, **16**, 2530–2533.
- 68 A. Bauza  , T. J. Mooibroek and A. Frontera, *Phys. Chem. Chem. Phys.*, 2014, **16**, 19192–19197.
- 69 A. Bauza  , T. J. Mooibroek and A. Frontera, *Chem. Commun.*, 2014, **50**, 12626–12629.

- 70 A. Bundhun, P. Ramasami, J. S. Murray and P. Politzer, *J. Mol. Model.*, 2013, **19**, 2739–2746.
- 71 A. Bauza', T. J. Mooibroek and A. Frontera, *Chem. Rec.*, 2016, **16**, 473–487.
- 72 C. Gourlaouen, O. Parisel and H. Gerard, *Dalton Trans.*, 2011, **40**, 11282–11288.
- 73 S. Mirdya, S. Roy, S. Chatterjee, A. Bauza A. Frontera and S. Chattopadhyay, *Cryst. Growth Des.*, 2019, DOI: 10.1021/acs.cgd.9b00881.
- 74 S. Mirdya, A. Frontera and S. Chattopadhyay, *CrystEngComm*, 2019, DOI: 10.1039/C9CE01283D.
- 75 A. Hazari, L. K. Das, R. M. Kadam, A. Bauzá, A. Frontera and A. Ghosh, *Dalton Trans.*, 2015, **44**, 3862–3876.
- 76 S. Mirdya, T. Basak and S. Chattopadhyay, *Polyhedron*, 2019, **170**, 253–263.
- 77 A. W. Addison, T. N. Rao, J. Reedijk, J. V. Rijn and G. C. Verschoor, *J. Chem. Soc., Dalton Trans.*, 1984, 1349-1356.
- 78 D. Cremer and J. A. Pople, *J. Am. Chem. Soc.*, 1975, **97**, 1354-1358.
- 79 D. Cremer, *ActaCrystallogr., Sect. B: Struct. Sci.*, 1984, **40**, 498–500.
- 80 L. Shimon-Livny, J. P. Glusker and C. W. Bock, *Inorg. Chem.*, 1998, **37**, 1853–1867.
- 81 M.-L. Hu, A. Morsali and L. Aboutorabi, *Coord. Chem. Rev.*, 2011, **255**, 2821–2859.
- 82 F. Mautner, M. Scherzer, C. Berger, , R. C. Fischer R. Vicente and S. S. Massoud, *Polyhedron.*, 2015, **85**, 20–26.
- 83 M. Das, S. Chatterjee, K. Harms, T. K. Mondal and S. Chattopadhyay, *Dalton Trans.*, 2014, **43**, 2936–2947.

- 84 M. Karmakar, S. Roy and S. Chattopadhyay, *New J. Chem.*, 2019, **43**, 10093-10102.
- 85 M. Andruh, *Chem. Commun.*, 2011, **47**, 3025–3042.
- 86 S. Roy; A. Bhattacharyya, S. Herrero, R. González-Prieto, A. Frontera and S. Chattopadhyay, *ChemistrySelect.*, 2017, **2**, 6535 – 6543.
- 87 M. A. Khan, A. A. Alqadami, M. Otero, M. R. Siddiqui, Z. A. Alothman, I. Alsohaimi, M. Rafatullah, A. E. Hamedelniel, *Chemosphere*, 2019, **218**, 1089–1099.
- 88 A. Biswas, L. K. Das, M. G. B. Drew, C. Diaz and A. Ghosh, *Inorg. Chem.*, 2012, **51**, 10111–10121.
- 89 A. Golcu, , M. Tumer, H. Demirelli and R. A. Wheatley, *Inorg. Chim. Acta*, 2005, **358**, 1785–1797.
- 90 S. Roy; T. Basak, S. Khan, M. G. B. Drew, A. Bauzá, A. Frontera and S. Chattopadhyay, *ChemistrySelect.*, 2017, **2**, 9336–9343.
- 91 S. Roy, K. Harms, A. Bauzá, A. Frontera and S. Chattopadhyay, *Polyhedron*, 2017, **121**, 199–205.
- 92 Bleiholder, C.; Werz, D. B.; Köppel, H.; Gleiter, R. Theoretical Investigations on Chalcogen–Chalcogen Interactions: What Makes These Nonbonded Interactions Bonding? *J. Am. Chem. Soc.*, **2006**, *128*, 2666-2674.
- 93 R. Gleiter, G. Haberhauer, D. B. Werz, F. Rominger, C. Bleiholder, *Chem. Rev.*, 2018, **118**, 2010–2041.
- 94 J. Contreras-García, W. Yang and E. R. Johnson, *J. Phys. Chem. A*, 2011, **115**, 12983-12990.

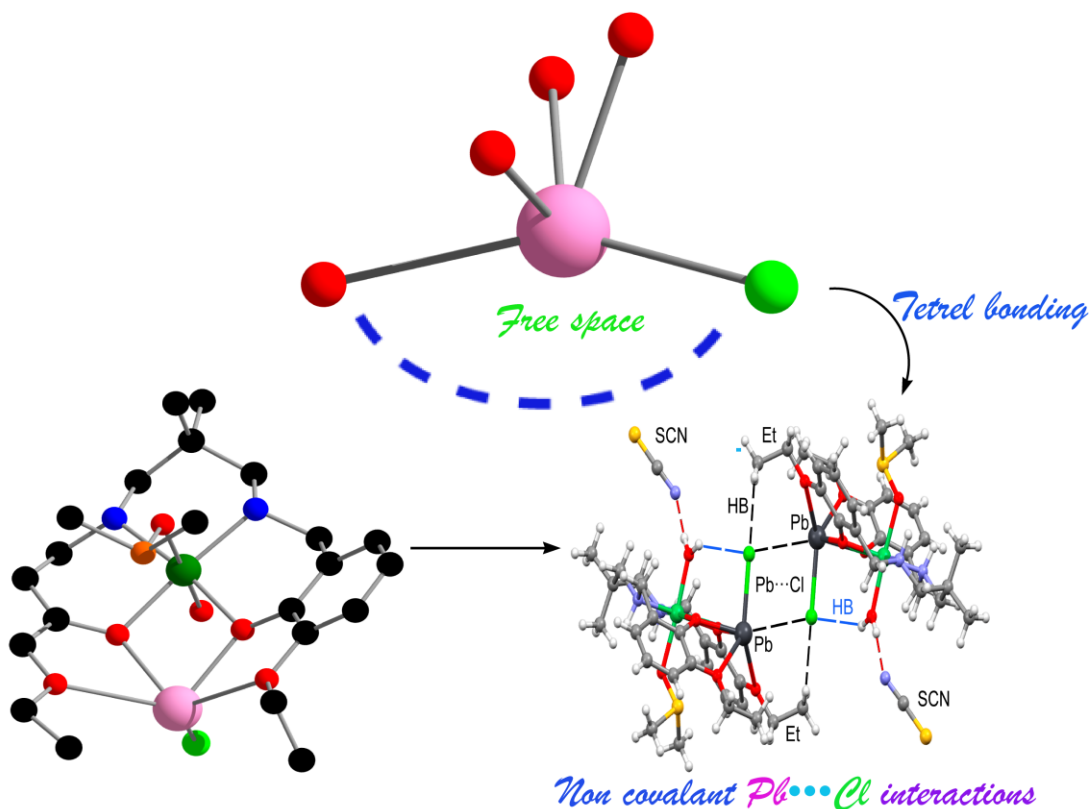
95. F. L. Hirshfeld, *Theor. Chim. Acta.*, 1977, 44, 129–138.

96 J. J. McKinnon, D. Jayatilaka and M. A. Spackman, *ChemCommun.*, 2007, 3814-3816.

97 J. J. McKinnon, M. A. Spackman and A. S. Mitchell, *ActaCryst. B.*, 2004, 60, 627-668.

Section IIIB

Formation of a tetranuclear supramolecule via non-covalent $\text{Pb}\cdots\text{Cl}$ tetrel bonding interaction in a hemidirected lead(II) complex with a nickel(II) containing metaloligand

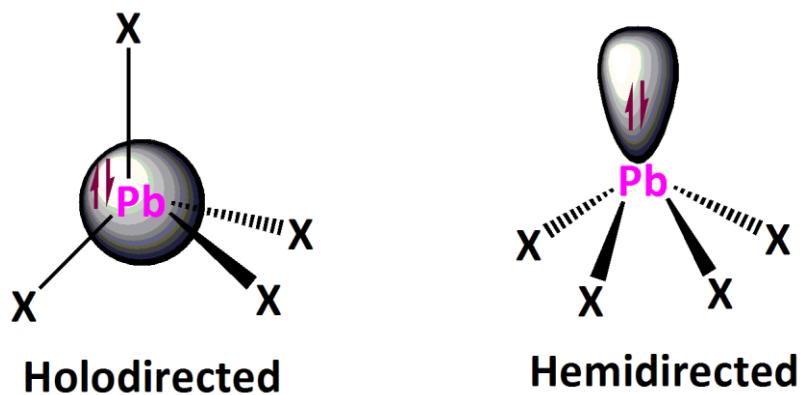


III.B .1. Introduction

A significant number of supramolecular coordination compounds have been synthesized in the recent years¹ and shown to have the potential to be used as probes, sensors and photonic devices². The most commonly used approach for engineering the crystal structure of such complexes employs non-covalent intermolecular forces, e.g. hydrogen bonding, π - π stacking, cation- π , C-H... π interactions etc.³ Other well recognized non-covalent interactions, such as halogen bonding and ion pairing have also been used to direct the formation of many supramolecular assemblies.⁴ They play a vital role in drug-receptor interactions, crystal engineering, enzyme inhibition, protein folding, etc.⁵ Structures of bio-molecules could also be controlled by these interactions.⁶ On the other hand, σ -hole interactions have been studied less. Strong σ -hole interactions may occur in complexes of group IV elements and usually involves tetrel bonding interactions, especially in the cases of lead.⁷ Tetrel bonds⁸ are generally characterized by two distinct classes of structural organizations, viz. Holodirected⁹ and hemidirected¹⁰ geometries (Scheme III.B. 1). In case of the former, the bonds of lead to donor atoms, are directed throughout the surface of an encompassing sphere, while in case of the later, the bonds of lead to ligand atoms are directed throughout a hemisphere, thereby exhibiting a clear void in the distribution of bonds to the ligands.¹¹

In the present work, one $N_2O_2O'_2$ donor compartmental reduced Schiff base, 2,2'-[(2,2-dimethyl-1,3-propanediyl)bis(iminomethylene)]bis[6-ethoxy-Phenol] (H_2L^1) has been used to prepare a hetero-dinuclear nickel(II)/lead(II) complex, $[(H_2O)(DMSO)NiLPbCl]SCN$ (6). The structure of the complex has been determined by single crystal X-ray diffraction analyses. The

lead(II) centre in the complex is hemidirectionally coordinated and participates in non-covalent tetrel bonding interactions. Also an interesting hydrogen bonding is observed with the non-coordinated thiocyanate. Finally, the supramolecular interactions have been studied using DFT calculations focusing Pb...Cl tetrel bonds observed in the solid state of the complex.



Scheme. III.B. 1: Schematic representation of the holodirected (left) and hemidirected (right) coordination modes of lead(II), with indication of the location of the inert lone pair.

III.B .2. Experimental section

Nickel(II) thiocyanate tetrahydrate was prepared in our laboratory following the literature method.³³ All other materials were commercially available, reagent grade, and used as purchased from Sigma-Aldrich without further purification.

III.B.2.1: *Synthesis*

III.B.2.1.1: *Synthesis of Schiff base ligands*

III.B.2.1.1.1: *Preparation of the ligand, 2,2'-[(2,2-dimethyl-1,3-propanediyl)bis(iminomethylene)]bis[6-ethoxy-Phenol] (H_2L^1)*

H_2L^1 ligand preparation has been given in II.2.1 (See Chapter 2).

III.B.2.1.1.2: *Preparation of $[(H_2O)(DMSO)NiLPbCl](SCN)$ (6)*

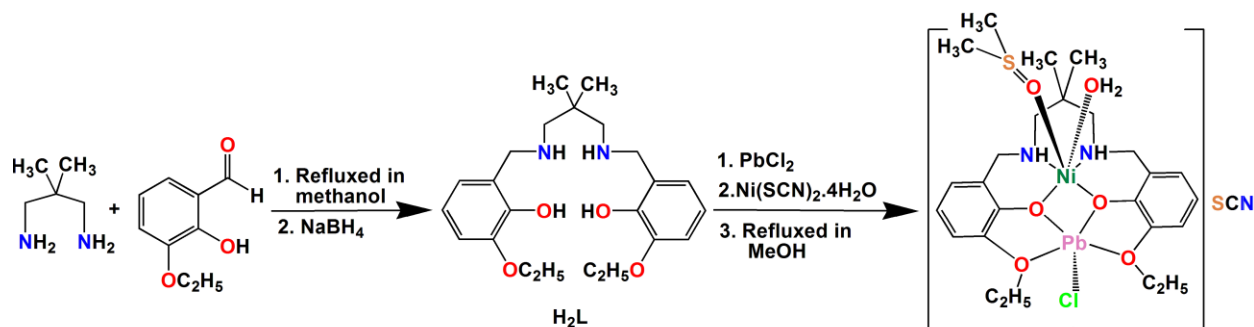
To a solution of the ligand, H_2L in methanol (10 mL) was added a methanol solution (5 mL) of nickel(II) thiocyanate tetrahydrate (250 mg, 1 mmol) with constant stirring. A water (5 mL) solution of lead(II) chloride (278 mg, 1 mol) was then added to it and the stirring was continued for about 30 min. The solution was then refluxed for ca. 1h. A few drops of DMSO were then added to the solution. The resulting reaction mixture was left unperturbed for slow evaporation at room temperature. After few days, blue crystals, suitable for X-Ray diffraction were collected by filtration.

Yield: 839 mg (~49%) based on nickel(II). Anal. Calc. for $C_{52}H_{80}Cl_2N_6Ni_2O_{12}Pb_2S_4$ (FW: 1712.14): C, 36.48; H, 4.71; N, 4.91; Found: C, 36.3; H, 4.6; N, 5.1%. FT-IR (KBr, cm^{-1}): 3369 (O-H); 3289-3278 (N-H); 2998-2867 (C-H); 2052 (SCN). λ_{max} (nm) [ϵ_{max} (lit $mol^{-1} cm^{-1}$)] (MeOH): 242(1.07×10^2); 284 (0.59×10^2); 348 (0.76×10^2); 601 (2.62)); 848 (2.12). Magnetic moment = 3.13 BM.

III.B .3. Results and discussion

III.B .3. 1: Synthesis

2,2-dimethyl-1,3-diaminopropane was refluxed with 3-ethoxysalicylaldehyde in 1:2 ratio followed by the addition of NaBH_4 to form $\text{N}_2\text{O}_2\text{O}'_2$ donor compartmental reduced Schiff base (H_2L^1) following the literature methods.¹² The ligand (H_2L^1) on reaction with nickel(II) thiocyanate and lead(II) chloride produced the complex. Formation of the complex has been shown in Scheme. III.B. 2.



Scheme. III.B. 2: Preparation of ligand and the complex.

III.B .3. 2: Description of $[(\text{H}_2\text{O})(\text{DMSO})\text{NiLPbCl}](\text{SCN})$ (6)

The molecular structure of the complex was established by X-ray single crystal diffraction measurement. It reveals that the complex crystallizes in the monoclinic space group, $P2_1/n$, with $Z = 2$. The complex consists of a cationic dinuclear cation $[(\text{H}_2\text{O})(\text{DMSO})\text{NiLPbCl}]$ (6) along with an uncoordinated thiocyanate anion. The molecular structure with selected atom

numbering scheme has been shown in Figure III.B.1. Crystal data and refinement details have been given in Table III.B.1. Important bond angles have been gathered in Table III.B.3.

The $\text{N}_2\text{O}_2\text{O}_2'$ donor compartmental reduced Schiff base ligand (H_2L) is used to prepare the complex in which nickel(II) centre, Ni(1), is placed in the inner N_2O_2 cavity and lead(II) centre, Pb(1), is placed in the outer $\text{O}_2\text{O}_2'$ cavity with a Ni(1)···Pb(1) distance of 3.488(2) Å. The nickel(II) centre [Ni(1)] is hexacoordinated having pseudo octahedral geometry, where two amine nitrogen atoms, N(1) and N(2), and two phenoxo oxygen atoms, O(1) and O(2), of the deprotonated reduced Schiff base (L)²⁻ constituting the equatorial plane. Fifth and sixth coordination sites are occupied by two oxygen atoms; O(5), from a DMSO molecule and O(6) from a water molecule. All nickel(II)–nitrogen and nickel(II)–oxygen bond lengths are comparable to those observed in other complexes with similar structures.¹³

Lead(II) centre in the complex is pentacoordinated where two phenoxo oxygen atoms, O(1) and O(2), also coordinate to lead(II) centre. The potential donor ethoxy oxygen atoms, O(3) and O(4), of deprotonated reduced Schiff base also coordinate to lead(II) centre, but at much longer distances to form equatorial planes. All lead(II)–oxygen bond lengths are comparable to those observed in other complexes with similar structures.¹⁴ The fifth coordination site is occupied by one chlorido ligand, Cl(1) in axial position with a Pb(1)–Cl(1) distance of 2.729(4) Å in the complex. The geometry of any penta-coordinated metal centre may conveniently be measured by the Addison parameter (τ)¹⁵ [$\tau = (\Theta - \Phi) / 60$, where Θ and Φ are the two largest ligand-metal-ligand angles of the coordination sphere]. In the complex, the geometry around the lead(II) center assume square pyramidal geometry with $\tau = 0.45$. The angle between Ni(1)O(1)O(2) and O(1)O(2)Pb(1) plane is 4.12° and also the dihedral angle of the

O(1)Ni(1) O(2)Pb(1) is $3.5(3)^\circ$, make the NiO₂Pb core almost planar. The bridging angles, Ni(1)–O(1)–Pb(1) and Ni(1)–O(2)–Pb(1), are $104.0(3)^\circ$ and $104.4(3)^\circ$ respectively. The angle of Cl(1)–Pb(1)–Ni(1) is $83.62(7)^\circ$. The saturated six membered chelate ring [Ni(1)–N(1)–C(10)–C(11)–C(14)–N(2)] has envelope conformation with puckering parameters $q=0.596(11)$ Å; $\theta=15.6(10)^\circ$; $\phi=184(4)^\circ$.

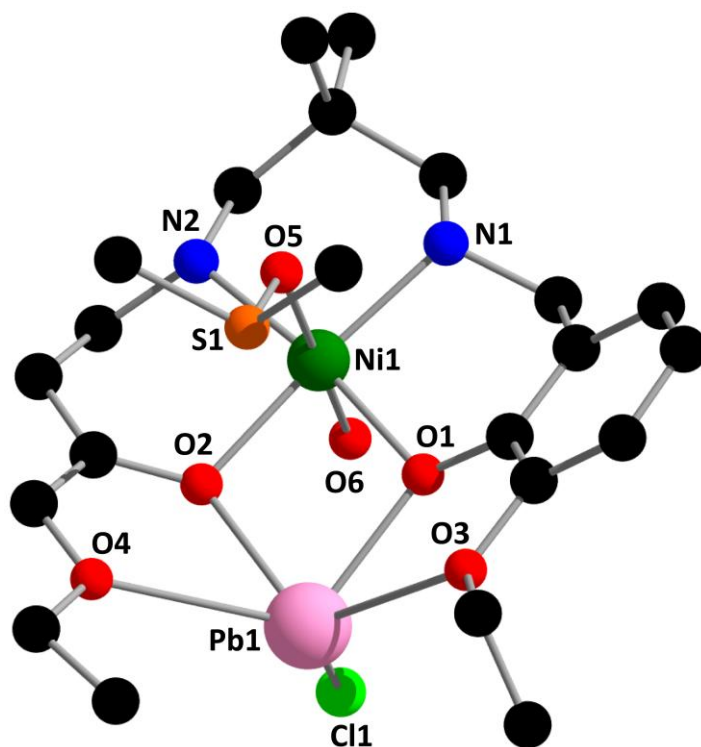


Fig. III.B.1: Perspective view of the complex with a selective atom numbering scheme.

Hydrogen atoms and uncoordinated thiocyanate ion have been omitted for clarity.

III.B .3. 3: Supramolecular interactions

The water molecule bonded to nickel(II) forms a strong donor hydrogen bonds. The hydrogen atom, H(6B), attached to oxygen atom, O(6), of the coordinated water molecule forms an intramolecular hydrogen bond with a nitrogen atom, N(3), of the uncoordinated thiocyanate. Hydrogen bonded structure of the complex has been given in Figure III.B.2.

A significant C-H $\cdots\pi$ interaction is observed. The hydrogen atom, H(24C), attached to carbon atom, C(24), is involved in an intra-molecular C-H $\cdots\pi$ interaction with a phenyl ring [C(3)–C(4)–C(5)–C(6)–C(7)–C(8)] (Figure III.B.3).

An additional interesting aspect is that there is another interaction from Pb(1) to the chloride Cl(1)^a from an adjacent molecule (^a = -x, 1-y, 1-z) at 3.339(3) Å in the complex which leads to the formation of a tetranuclear molecule, as shown in Figure III.B.4. It worth noting that this bond is on the same side of the equatorial plane as O(1) leading to a very irregular geometry. It may be that the presence of the two ethoxy groups close to the vacant site in the equatorial plane has precluded further bonding in that plane. The distance between the Pb(1)^a (^a = -x, 1-y, 1-z) and Pb(1) is 4.841(2) Å. The bridging angle of Pb(1)–Cl(1) \cdots Pb(1)^a is 105.39(11)°.

Although literature shows reports on experimental and theoretical investigations devoted to tetrel bonding²⁴⁻²⁸, only two are containing chlorides with hemidirected lead(II) centres (Table III.B.4). Both complexes were not found to form supramolecular dimer containing Pb₂Cl₂ cores.

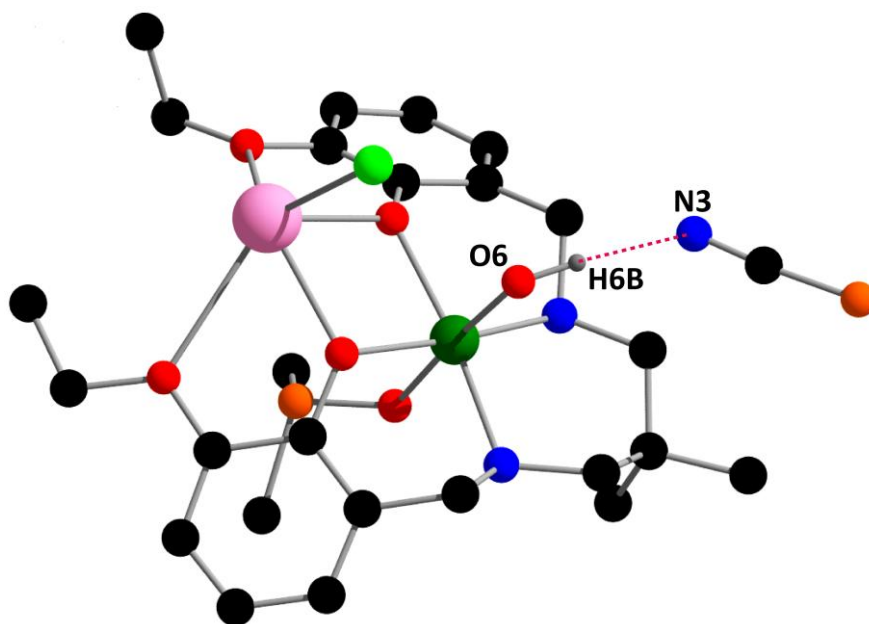


Fig. III.B.2: Hydrogen bonded structure of the complex. Only the relevant hydrogen atoms have been shown for clarity. Where, $N(3)-H(6B) = 0.93(8) \text{ \AA}$, $H(6B)\cdots O(6) = 1.87(2) \text{ \AA}$, $N(3)\cdots O(6) = 2.77(2) \text{ \AA}$, $\angle N(3)-H(6B)\cdots O(6) = 160(8)^\circ$.

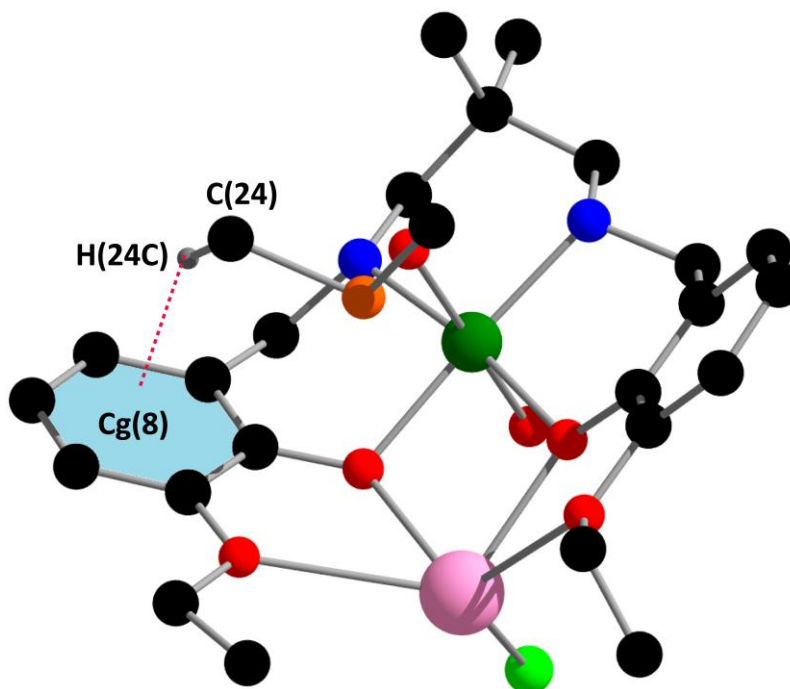


Fig. III.B.3: C–H $\cdots\pi$ interactions observed in the complex. Only the relevant atoms have been shown for clarity. Where, H(24C) \cdots Cg(8) = 0.93(8) Å, C(24)–H(24C) \cdots Cg(8) = 145°, C(24) \cdots Cg(8) = 3.662(19) Å.

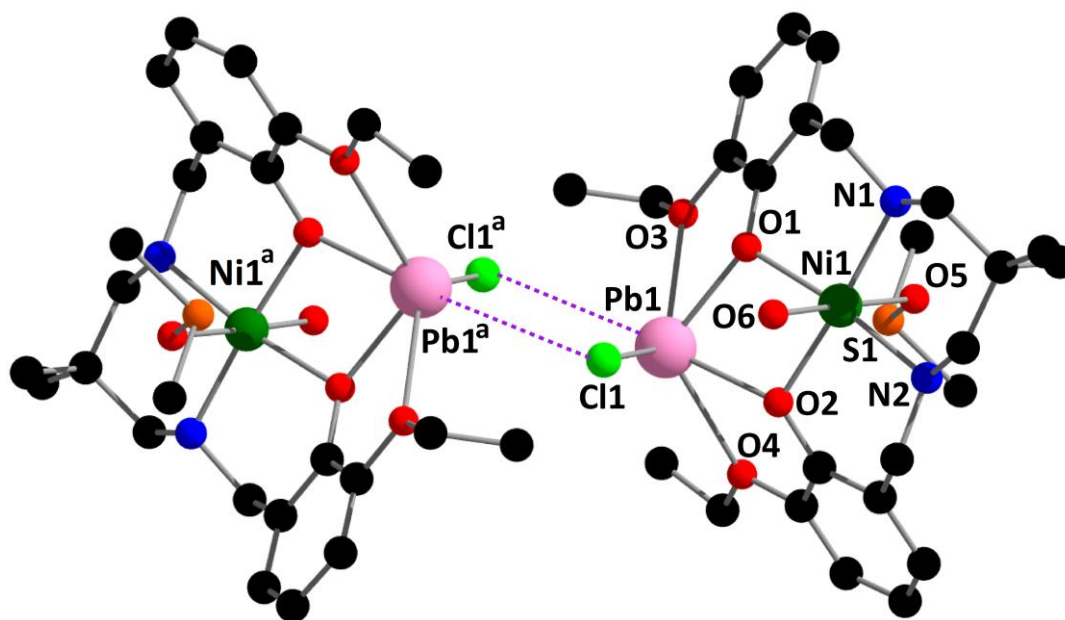


Fig. III.B.4: Non-covalent Pb \cdots Cl interactions. Symmetry elements (^a = -x, 1-y, 1-z).

Table. III.B.1: Crystal data and refinement details of the complex.

Formula	$\text{C}_{52}\text{H}_{80}\text{Cl}_2\text{N}_6\text{Ni}_2\text{O}_{12}\text{Pb}_2\text{S}_4$ (6)
Formula Weight	1712.14
Temperature (K)	273
Crystal system	Monoclinic
Space group	$P2_1/n$
a(Å)	9.874(5)
b(Å)	17.314(7)
c(Å)	19.651(14)
Γ	79.476(2)
Z	2
d_{calc} (g cm ⁻³)	1.705 g cm ⁻³
μ (mm ⁻¹)	5.852
$F(000)$	1696
Total Reflections	40265
Unique Reflections	4895
Observed data [$I > 2 \sigma(I)$]	7365
No. of parameters	324
R(int)	0.068
R1,wR2(all data)	0.1159, 0.2836
R1,wR2 [$I > 2 \sigma(I)$]	0.08240, 0.2367
CCDC	1946110

Table. III.B.2: Selected bond lengths (Å) of the complex.

Pb(1)–O(1)	2.338(7)	Ni(1)–O(1)	2.083(7)
Pb(1)–O(2)	2.320(7)	Ni(1)–O(2)	2.091(7)
Pb(1)–O(3)	2.855(8)	Ni(1)–N(1)	2.084(7)
Pb(1)–O(4)	2.831(12)	Ni(1)–N(2)	2.087(9)
Pb(1)–Cl(1)	2.729(4)	Ni(1)–O(5)	2.125(9)
Ni(1)–O(6)	2.086(10)		

Table III.B.3: Selected bond angles (°) of the complex.

Cl(1)–Pb(1)–O(1)	84.10(19)	O(1)–Ni(1)–O(2)	80.6(3)
Cl(1)–Pb(1)–O(2)	88.6(2)	O(1)–Ni(1)–O(5)	93.1(3)
Cl(1)–Pb(1)–O(3)	123.5(2)	O(1)–Ni(1)–O(6)	88.1(3)
Cl(1)–Pb(1)–O(4)	130.1(2)	O(1)–Ni(1)–N(1)	173.8(3)
Cl(1)–Pb(1)–Cl(1) ^a	74.61(9)	O(1)–Ni(1)–N(2)	91.6(3)
O(1)–Pb(1)–O(2)	70.8(2)	O(2)–Ni(1)–O(5)	93.6(3)
O(1)–Pb(1)–O(3)	61.9(2)	O(2)–Ni(1)–O(6)	89.8(3)
O(1)–Pb(1)–O(4)	118.8(3)	O(2)–Ni(1)–N(1)	93.7(3)
Cl(1) ^a –Pb(1)–O(1)	158.70(19)	O(2)–Ni(1)–N(2)	172.1(3)
O(2)–Pb(1)–O(3)	116.6(2)	O(5)–Ni(1)–O(6)	176.5(3)
O(2)–Pb(1)–O(4)	63.1(3)	O(5)–Ni(1)–N(1)	85.0(3)
Cl(1) ^a –Pb(1)–O(2)	107.34(16)	O(5)–Ni(1)–N(2)	86.2(3)
O(3)–Pb(1)–O(4)	106.2(3)	O(6)–Ni(1)–N(1)	94.2(3)
Cl(1) ^a –Pb(1)–O(3)	131.79(18)	O(6)–Ni(1)–N(2)	90.5(3)
Cl(1) ^a –Pb(1)–O(4)	76.2(2)	N(1)–Ni(1)–N(2)	94.1(3)

[^a represents symmetry element -x, 1-y,1-z].

Table III.B. 4: Reported X-ray characterized nickel(II)/lead(II) and lead(II) complexes comprising tetrel bonding interaction.

Complex (CCDC)	Formula	Coordination mode of lead	Bonding	Pb-X (Å)	Ref
YISROI	$[\{L^a Ni\}Pb(NC_5H_5)Cl]_2$	Hemidirected	Tetrel	3.272(1)	24
TAGMOG	$[(Cl)PbL^b] \cdot CH_3OH$	Hemidirected	Tetrel	3.155(2)	25
-	$[(H_2O)(DMSO)NiLPbCl](SCN)$	Hemidirected	Tetrel	3.339(3)	This Work

L^a = tris-((2-hydroxybenzylidene)-aminoethyl)-amine; H_2L^b = N'-(phenyl(pyridin-2-yl)methylene)isonicotinohydrazide.

III.C .3. 4: IR and electronic spectra

A band near the range of 3289-3278 cm^{-1} indicates the presence of amine N-H stretching in the complex.¹⁶ Broad bands in the range of 2998-2867 cm^{-1} due to alkyl C-H stretching vibrations are routinely noticed in IR spectrum of the complex.¹⁷ A broad band at 3369 cm^{-1} indicates the presence of the O-H stretching frequency of the water molecule.¹⁸ An intense band at 2052 cm^{-1} indicates the presence of uncoordinated thiocyanate.¹⁹ IR spectrum of the complex has been given in Figure III.B.5.

The electronic spectrum of the complex (Figure III.B.6) shows five bands at 242 nm, 284 nm, 348 nm, 601 nm and 848 nm. The absorption band at 601 nm may be assigned as ${}^3T_{1g}(F) \leftarrow {}^3A_{2g}(F)$, whereas band at 848 nm may be assigned as ${}^3T_{2g}(F) \leftarrow {}^3A_{2g}(F)$.²⁰ A higher energy d-d band, ${}^3T_{1g}(P) \leftarrow {}^3A_{2g}(F)$, cannot be observed as it is obscured by a strong charge transfer

transition (348 nm) in this case.²¹ The UV absorption band at 284 nm may be assigned to intra ligand n- π^* transition.²² A band at 242 nm may be attributed to π - π^* transitions.²³

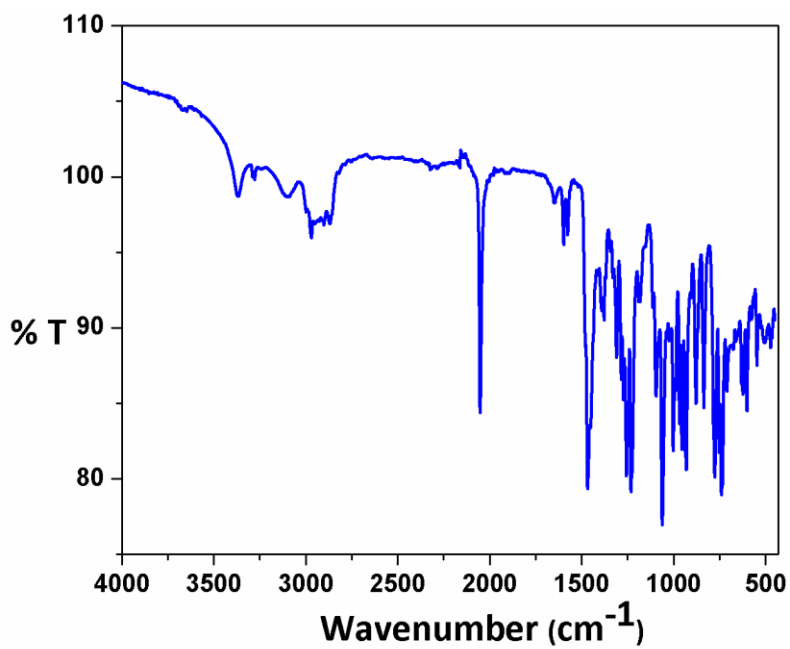


Fig. III.B.5: IR spectrum of the complex.

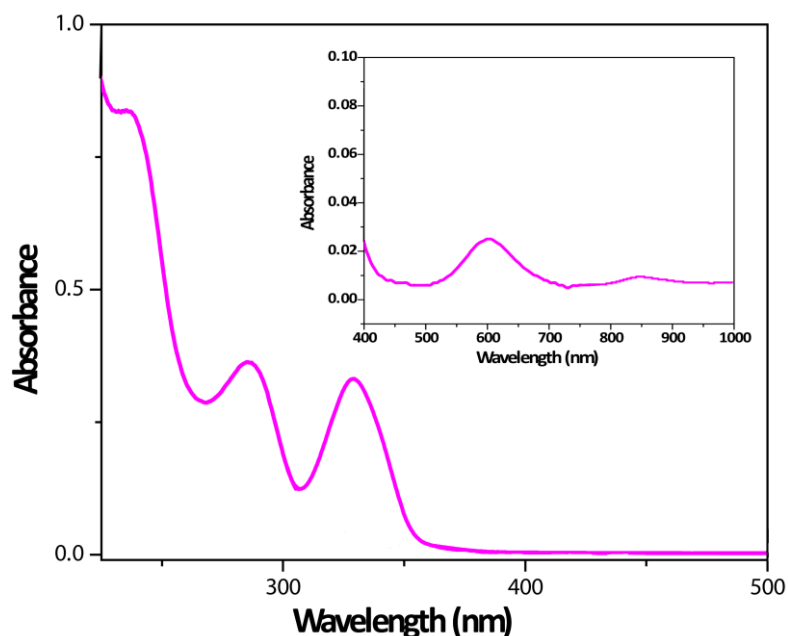


Fig. III.B.6: UV-Vis spectrum of the complex. Inset shows spectrum in 400-1000 nm range.

III.B .3.5: Hirshfeld surfaces

The Hirshfeld surface emerged from an attempt to define the space occupied by a molecule in a crystal for the purpose of subdividing the crystal electron density into molecular fragments.²⁹ d_{norm} is a normalised contact distance.³⁰ Intermolecular contacts are highlighted in the d_{norm} surface (when atoms make intermolecular contacts closer than the sum of their van der Waals radii, these contacts will be highlighted in red whereas longer contacts are blue, and contacts around the sum of van der Waals radii are white). Hirshfeld surfaces of the complex have been mapped over d_{norm} (range of -0.1 to 1.5 Å), shape index and curvedness [Figure III.B.7]. Red spots on these surfaces denote the dominant interactions [S \cdots H/H \cdots S, N \cdots H/H \cdots N, O \cdots H/H \cdots O and Cl \cdots H/H \cdots Cl]. As the Hirshfeld surface defines the shape of the molecule in terms of its surrounding crystalline environment, the local shape of the surface may provide some chemical insight whereas shape index is a qualitative measure of shape and can be

sensitive to very subtle changes in surface shape, particularly in regions where the total curvature (or the curvedness) is very low.³¹ We are particularly interested to investigate if the Pb...Cl non covalant bond can also be evidenced by means of Hirshfeld surface analysis. Gratifyingly, the non covalant bond was characterized by the spikes of the breakdown fingerprint plot.

The complex exhibits Pb...Cl/Cl...Pb non covalant bond that contribute 1.2% of the total Hirshfeld surface area and is evident in the (d_i , d_e) region of (2.742 Å, 2.661 Å). A close inspection of the fingerprint plot revealed that the sharp spikes with the shortest ($d_e + d_i$) = 3.098 Å in the complex correspond to Pb...Cl/Cl...Pb interaction.

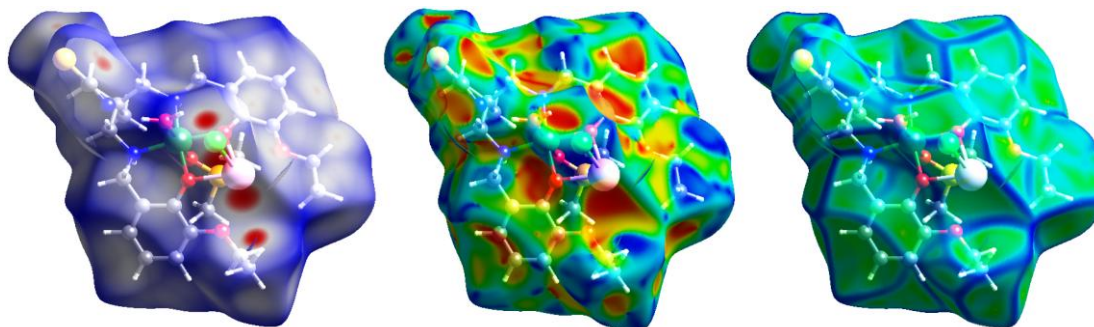


Fig. III.B.7: Hirshfeld surfaces of the complex mapped over d_{norm} (left), shape index (middle), curvedness (right).

The 2D fingerprint plots,³² which are used to analyze the intermolecular contacts at the same time, revealed that the main intermolecular interactions in the complex are S...H/H...S, Cl...H/H...Cl, O...H/H...O and N...H/H...N. Figure III.B.8 represents the 2D plots of the complex.

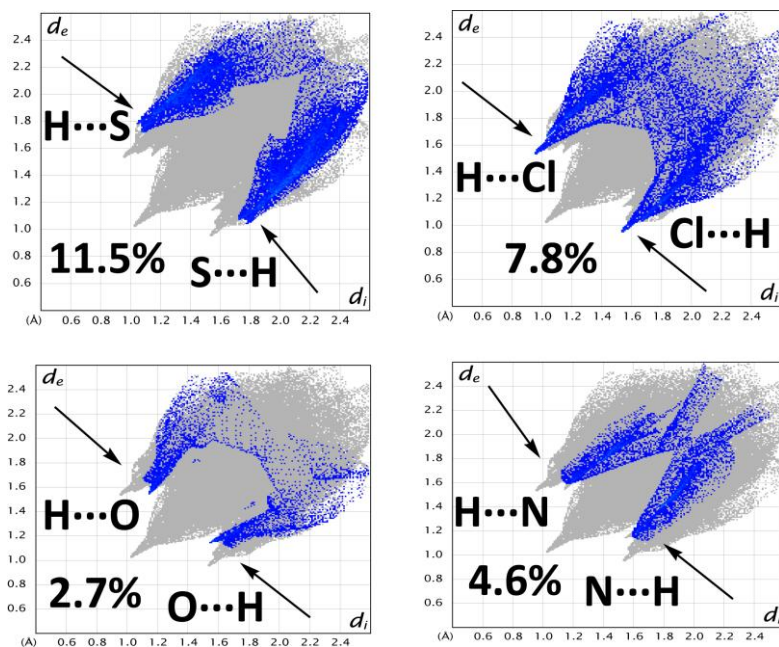


Fig. III.B.8: Fingerprint plots of the complex.

Interesting Pb...Cl contact (Fig. 7) is observed in the complex. The contact may lead to the formation of different unconventional supramolecular interactions which is quite captivating. Also small amount of Cl...Cl contact is observed (Figure III.B.9).

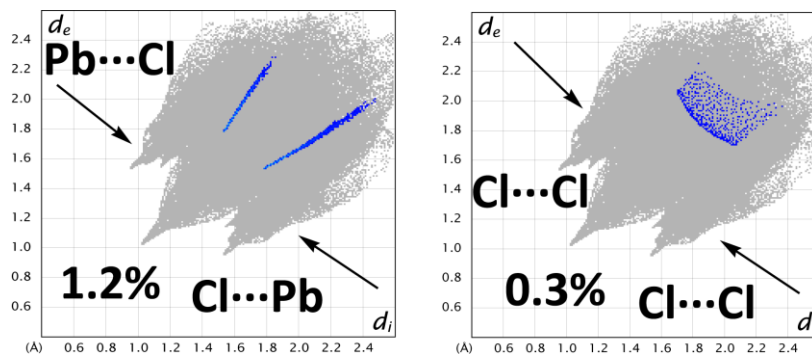


Fig. III.B. 9: Fingerprint plot resolved into Pb...Cl/Cl...Pb contact and Cl...Cl/Cl...Cl contact contributed to the total Hirshfeld Surface area of the complex.

III.B.3.6: Theoretical study

The theoretical study is focused on the tetrel bonding interaction described above in Figure III.B.4 and further characterized by the Hirshfeld analysis (Figure III.B.9). Since the

coordination of the Pb(II) is hemidirected, the σ -hole at the tetrel atom is accessible as shown in Figure III.B.10. It can be observed that the molecular electrostatic potential (MEP) is positive at the Pb atom (+25 kcal/mol) that is located between both OEt groups. The most negative region is located at the SCN counter-ion, as expected. The MEP value is also negative at the chlorido ligand. This analysis indicates that the tetrel bond between the Pb atom and the chlorido ligand is favored from an electrostatic point of view.

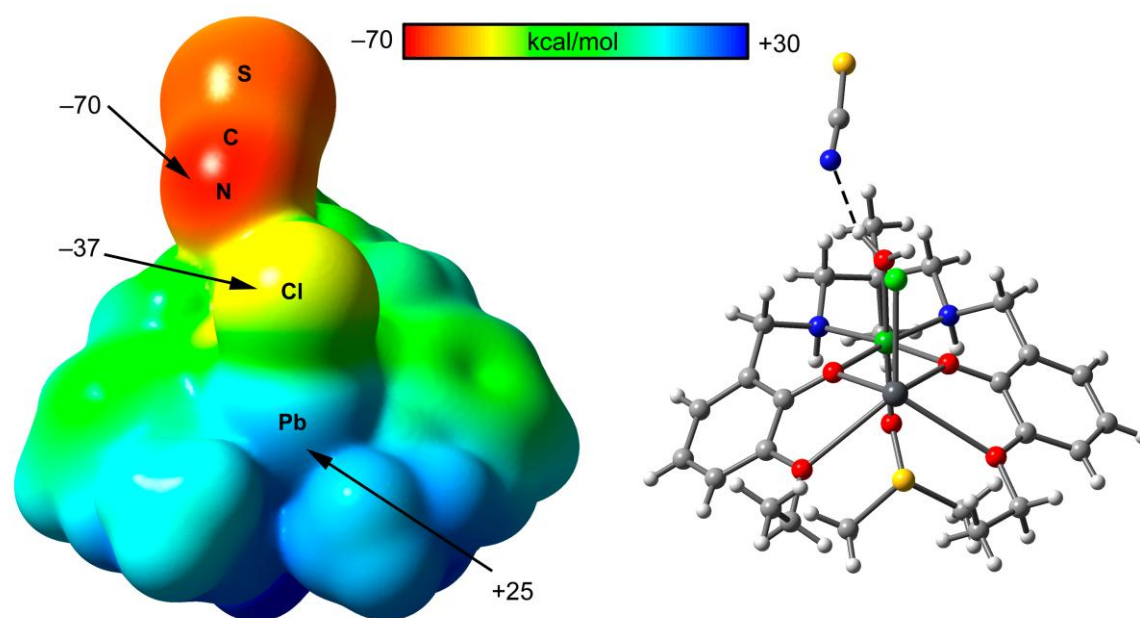


Fig. III.B.10: MEP surface (left) of the complex (isosurface 0.001 a.u.) at the B3LYP-D/def2-SVP level of theory. The values at selected points of the surface are indicated in kcal/mol. The complex represented in the same orientation used for building the MEP surface is also shown on the right.

Figure III.B.11a shows the self-assembled dimer retrieved from the X-ray of structure of the complex (H-atoms omitted), where two symmetrically equivalent Pb \cdots Cl tetrel bonding interactions are formed. We have evaluated the interaction energy of this dimer, which is very strong $\Delta E_1 = -34.9$ kcal/mol thus confirming the relevance of this interaction as predicted by

MEP surface. A close examination of the dimer reveals that each Cl ligand also establishes a H-bonding interaction with one H-atom of the ethyl group of the Schiff base ligand (2.54 Å, see Fig 11a). To evaluate the contribution of this ancillary interaction we have computed a theoretical model where the ethyl groups have been changed by methyl groups. (see Figure III.B.11b) As a result the H-bonds are not formed and the interaction energy in the mutated complex is slightly reduced to $\Delta E_2 = -33.7$ kcal/mol, thus suggesting that these H-bonds are very weak and that the dimer formation is totally dominated by the tetrel bonding. A likely explanation for the small contribution of the H-bonds is that the Cl atom is already participating in other interactions like the tetrel bond and an intramolecular H-bonding with the water molecule (see blue dashed lines in Figure III.B.11). Therefore, the electron-donor ability of the Cl atom is significantly reduced.

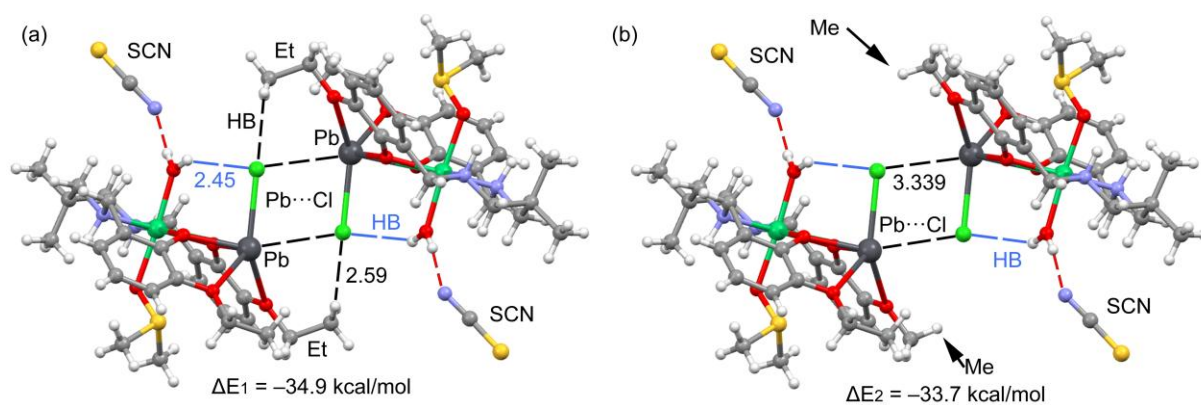


Fig. III.B.11 (a,b): Theoretical models used to evaluate the noncovalent interactions in the dimer of the complex. Distances in Å.

To further characterize the interactions described above, we have used the Bader's theory of atoms-in-molecules since it allows an easy characterization of the noncovalent interactions. Figure III.B.12 shows the distribution of critical points and bond paths of the self-

assembled dimer. Each tetrel bond is characterized by the presence of a bond CP (green sphere) and bond path connecting the Pb atom to the Cl atom, thus confirming the existence of the tetrel bonds. Moreover, a ring CP (yellow sphere) also appears upon complexation due to the formation of a supramolecular ring (Pb_2Cl_2). The QTAIM analysis also confirms the existence of the H-bonds between the Cl ligands and the H-atoms of the ethyl groups. Moreover, each intramolecular $\text{O}-\text{H}\cdots\text{Cl}$ H-bond is characterized by a bond CP and bond path interconnecting the Cl and H atoms. The values of the electron charge density (ρ) at the bond CPs that characterize the noncovalent interactions are also indicated in Figure III.B.12. The values of $\rho(r)$ are smaller for the $\text{C}-\text{H}\cdots\text{Cl}$ bonds (0.0132 a.u.) in agreement with the energetic results commented above.

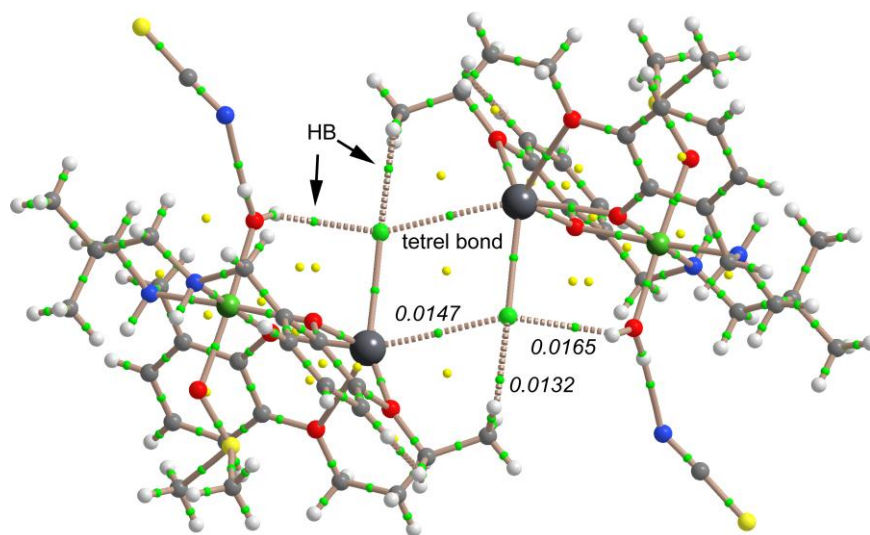


Fig. III.B.12: QTAIM distribution of bond and ring CPs (green and yellow spheres, respectively) and bond paths for the dimer of the complex. The values of $\rho(r)$ at selected bond CPs are indicated in italics (a.u.)

III.B. 4: Concluding remarks

In conclusion, we report the synthesis and structural characterization of a new heteronuclear nickel(II)/lead(II) complex with compartmental reduced Schiff base ligand. The complex forms a tetranuclear supramolecule via non-covalent Pb \cdots Cl tetrel bonding interaction, which are strong as evidenced by DFT calculations and MEP surface analysis. The QTAIM and the Hirshfeld analyses have been used to characterize the tetrel bonding interactions and stress the importance of tetrel bonds involving hemicoordinated Pb(II) in crystal engineering. Our results might be important to understand the X-ray structure of organic-inorganic material systems containing organic aromatic molecules and hemidirectionally coordinated lead(II) centres.

References

1. (a) P. Bhowmik, S. Jana, P. P. Jana, K. Harms and S. Chattopadhyay, *Inorg. Chem. Commun.*, 2012, **18**, 50–56; (b) M. Das, S. Chatterjee and S. Chattopadhyay, *Inorg. Chem. Commun.*, 2011, **14**, 1337–1340; (c) S. Roy, A. Bhattacharyya, S. Purkait, A. Bauza, A. Frontera and S. Chattopadhyay, *Dalton Trans.*, 2016, **45**, 15048–15059; (d) A. Bhattacharyya, S. Roy, J. Chakraborty and S. Chattopadhyay, *Polyhedron*, 2016, **112**, 109–117; (e) P. Bhowmik, S. Jana, P. P. Jana, K. Harms and S. Chattopadhyay, *Inorg. Chim. Acta*, 2012, **390**, 53–60.
2. (a) W. L. Ping, J. S. Bo, Z. W. Feng, L. Y. Qi and Y. Gui, *Chin. Sci. Bull.*, 2013, **58**, 2733–2740; (b) D. Sadhukhan, A. Ray, G. Pilet, C. Rizzoli, G. M. Rosair, C. J. Gomez-García, S. Signorella, S. Bell and S. Mitra, *Inorg. Chem.*, 2011, **50**, 8326–8339; (c) C.-L. Hu and J.-G. Mao, *Coord. Chem. Rev.*, 2015, **288**, 1–17; (d) G. N. D. Francesco, A. Gaillard, I. Ghiviriga, K. A. Abboud and L. J. Murray, *Inorg. Chem.*, 2014, **53**, 4647–4654; (e) S. Chattopadhyay, M. G. B. Drew, C. Diaz and A. Ghosh, *Dalton Trans.*, 2007, 2492–2494; (f) K. Ghosh, S. Roy, A. Ghosh, A. Banerjee, A. Bauzá, A. Frontera and S. Chattopadhyay, *Polyhedron*, 2016, **112**, 6–17.
- 3 (a) Y. Shen, N. Ma, L. Wu and H.-H. Song, *Inorg. Chim. Acta*, 2015, **429**, 51–60; (b) Y.-S. Yang, Y.-P. Yang, M. Liu, Q.-M. Qiu, Q.-H. Jin, J.-J. Sun, H. Chen, Y.-C. Dai and Q.-X. Meng, *Polyhedron*, 2015, **85**, 912–917; (c) S. Carboni, C. Gennari, L. Pignataro and U. Piarulli, *Dalton Trans.*, 2011, **40**, 4355–4373; (d) A. Bhattacharyya, P. K. Bhaumik, P. P. Jana and S. Chattopadhyay, *Polyhedron*, 2014, **78**, 40–45.
- 4 (a) G. Mahmoudi, A. Bauzá and A. Frontera, *Dalton Trans.*, 2016, **45**, 4965–4969. (b) C. A. Hunter and J. K. M. Sanders, *J. Am. Chem. Soc.*, 1990, **112**, 5525–5534; (c) S. K. Burley and G. A.

Petsko, *Science*, 1985, **229**, 23–28; (d) K. S. Kim, P. Tarakeshwar and J. Y. Lee, *Chem. Rev.*, 2000, **100**, 4145–4185; (e) J. C. Ma and D. A. Dougherty, *Chem. Rev.*, 1997, **97**, 1303–1324; (f) K. S. Kim, J. Y. Lee, S. J. Lee, T.-K. Ha and D. H. Kim, *J. Am. Chem. Soc.*, 1994, **116**, 7399–7400; (g) M. Nishio, M. Hirota and Y. Umezawa, in *The C–H/p Interaction: Evidence, Nature, Consequences*, Wiley-VCH, New York, 1998; (h) D. Quiñonero, C. Garau, C. Rotger, A. Frontera, P. Ballester, A. Costa and P. M. Deyà, *Angew. Chem., Int. Ed.*, 2002, **41**, 3389–3392; (i) M. Egli and S. Sarkhel, *Acc. Chem. Res.*, 2007, **40**, 197–205; (j) T. J. Mooibroek, P. Gamez and J. Reedijk, *CrystEngComm*, 2008, **10**, 1501–1515; (k) J. Ran and P. Hobza, *J. Chem. Theory Comput.*, 2009, **5**, 1180–1185; (l) M. Barceló-Oliver, C. Estarellas, A. García-Raso, A. Terrón, A. Frontera, D. Quiñonero, E. Molins and P. M. Deyà, *CrystEngComm*, 2010, **12**, 362–365; (m) M. Nishio, *CrystEngComm*, 2004, **6**, 130–156.

5 (a) J. Xiao, P. Broz, A. W. Puri, E. Deu, M. Morell, D. M. Monack and M. Boggyo, *J. Am. Chem. Soc.*, 2013, **135**, 9130–9138; (b) S. Naskar, D. Mishra, R. J. Butcher and S. K. Chattopadhyay, *Polyhedron*, 2007, **26**, 3703–3714; (c) A. Bauzá, D. Quiñonero, P. M. Deyà and A. Frontera, *Chem.–Asian J.*, 2013, **8**, 2708–2713. (d) L. M. Salonen, M. Ellermann and F. Diederich, *Angew. Chem., Int. Ed.*, 2011, **50**, 4808.

6 (a) D. Paolantoni, J. Rubio-Magnieto, S. Cantel, J. Martinez, P. Dumy, M. Surin and S. Ulrich, *Chem. Commun.*, 2014, **50**, 14257; (b) C. Estarellas, A. Frontera, D. Quiñonero and P. M. Deyà, *Angew. Chem., Int. Ed.*, 2011, **50**, 415; (c) S. Jana, K. Harms and S. Chattopadhyay, *J. Coord. Chem.*, 2014, **67**, 2954–2966.

- 7 (a) G. Mahmoudi, A. Bauzá, M. Amini, E. Molins, J. T. Maged and A. Frontera, *Dalton Trans.*, 2016, **45**, 10708–10716 (b) A. Bauzá, T. J. Mooibroek and A. Frontera, *Angew. Chem., Int. Ed.*, 2013, **52**, 12317–12321; (c) A. Bauzá, T. J. Mooibroek and A. Frontera, *Chem. – Eur. J.*, 2014, **20**, 10245–10248; (d) R. S. Ruoff, T. Emilsson, A. I. Jaman, T. C. Germann and H. S. Gutowsky, *J. Chem. Phys.*, 1992, **96**, 3441–3446; (e) S. J. Grabowski, *Phys. Chem. Chem. Phys.*, 2014, **16**, 1824–1834; (f) I. Alkorta, I. Rozas and J. Elguero, *J. Phys. Chem. A*, 2001, **105**, 743–749; (g) E. C. Escudero-Ada'n, A. Bauzá, A. Frontera and P. Ballester, *ChemPhysChem.*, 2015, **16**, 2530–2533; (h) A. Bauzá, T. J. Mooibroek and A. Frontera, *Phys. Chem. Chem. Phys.*, 2014, **16**, 19192–19197; (i) A. Bauzá, T. J. Mooibroek and A. Frontera, *Chem. Commun.*, 2014, **50**, 12626–12629; (j) A. Bundhun, P. Ramasami, J. S. Murray and P. Politzer, *J. Mol. Model.*, 2013, **19**, 2739–2746; (k) A. Bauzá, T. J. Mooibroek and A. Frontera, *Chem. Rec.*, 2016, **16**, 473–487.
8. (a) G. Mahmoudi, A. Bauzá and A. Frontera, *Dalton Trans.*, 2016, **45**, 4965–4969; (b) M. S. Gargari, V. Stilinovic', A. Bauzá, A. Frontera, P. McArdle, D. V. Derveer, S. W. Ng, and G. Mahmoudi, *Chem. Eur. J.*, 2015, **21**, 17951–17958.
9. (a) C. Gourlaouen, O. Parisel and H. G'érard, *Dalton Trans.*, 2011, **40**, 11282–11288; (b) L. Shimon-Livny, J. P. Glusker, and C. W. Bock, *Inorg. Chem.* 1998, **37**, 1853-1867
10. (a) S. Mirdya, S. Roy, S. Chatterjee, A. Bauza, A. Frontera and S. Chattopadhyay, *Cryst. Growth Des.*, DOI: 10.1021/acs.cgd.9b00881. (b) G. Mahmoudi, A. Bauzá, M. Amini, E. Molins, J. T. Maged and A. Frontera, *Dalton Trans.*, 2016, **45**, 10708–10716

- 11 (a) C. Gourlaouen, O. Parisel and H. Gerard, *Dalton Trans.*, 2011, **40**, 11282–11288; (b) L. Shimoni-Livny, J. P. Glusker and C. W. Bock, *Inorg. Chem.*, 1998, **37**, 1853–1867; (c) R. L. Davidovich, V. Stavila, D. V. Marinin, E. I. Voit and K. H. Whitmire, *Coord. Chem. Rev.*, 2009, **253**, 1316–1352.
12. (a) A. Hazari, L. K. Das, R. M. Kadam, A. Bauzá, A. Frontera and A. Ghosh, *Dalton Trans.*, 2015, **44**, 3862–3876; (b) A. Hazari, T. K. Ghosh, C. J. G.-García, A. Ghosh, *Inorg. Chim. Acta*, 2018, **471**, 168–175.
13. (a) S. Roy, A. Bhattacharyya, S. Purkait, A. Bauza, A. Frontera and S. Chattopadhyay, *Dalton Trans.*, 2016, **45**, 15048–15059; (b) S. Roy, M. G. B. Drew, A. Bauza, A. Frontera and S. Chattopadhyay, *ChemistrySelect*, 2017, **2**, 10586–10594; (c) S. Roy, M. G. B. Drew, A. Bauza, A. Frontera and S. Chattopadhyay, *ChemistrySelect*, 2017, **2**, 7880–7887.
14. (a) S. Mondal, S. Hazra, S. Sarkar, S. Sasmal and S. Mohanta, *J. Mol. Struct.*, 2011, **1004**, 204–214; (b) R. Kurtaran, L. T. Yildirim, A. D. Azaz, H. Namli and O. Atakol, *J. Inorg. Biochem.*, 2005, **99**, 1937–1944; (c) Edwin C. Constable, G. Zhang, C. E. Housecroft, M. Neuburger and J. A. Zampese, *Inorg. Chim. Acta*, 2010, **363**, 4207–4213; (d) S. Hazra, S. Sasmal, M. Nayak, H. A. Sparkes, J. A. K. Howard and S. Mohanta, *CrystEngComm.*, 2010, **12**, 470–477.
15. A. W. Addison, T. N. Rao, J. Reedijk, J. V. Rijn, G. C. Verschoor, *J. Chem. Soc., Dalton Trans.*, 1984, 1349–1356.
16. (a) M. Das, S. Chatterjee, K. Harms, T. K. Mondal and S. Chattopadhyay, *Dalton Trans.*, 2014, **43**, 2936–2947; (b) S. Chattopadhyay, M. S. Ray, S. Chaudhuri, G. Mukhopadhyay, G. Bocelli, *Inorg. Chim. Acta*, 2006, **359**, 1367–1375.

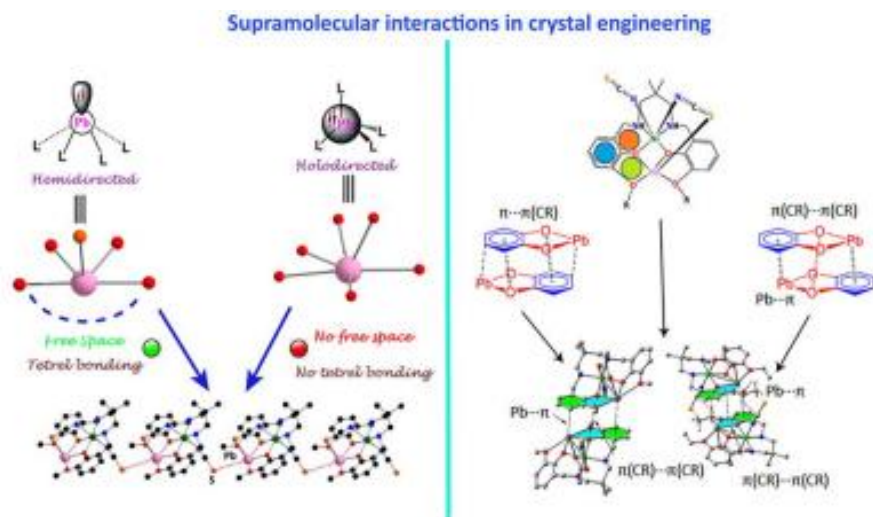
17. (a) M. A. Khan, A. A. Alqadami, M. Otero, M. R. Siddiqui, Z. A. Allothman, I. Alsohaimi, M. Rafatullah, A. E. Hamedelniel, *Chemosphere* 2019, **218**, 1089–1099; (b) S. Roy, T. Basak, S. Khan, M. G. B. Drew, A. Bauza', A. Frontera and S. Chattopadhyay, *ChemistrySelect*, 2017, **2**, 9336–9343.
18. (a) K. Nakamoto, *Infrared and Raman Spectra of Organic and Coordination Compounds*, John Wiley and Sons, New York, 3rd edn, 1978, p. 227; (b) P. Chakraborty, I. Majumder, H. Kara, S. K. Chattopadhyay, E. Zangrando, D. Das, *Inorg. Chim. Acta*, 2015, **436**, 139–145; (c) P. Bhowmik, K. Harms and S. Chattopadhyay, *Polyhedron*, 2013, **49**, 113–120.
19. T. Basak, K. Ghosh and Shouvik Chattopadhyay, *Polyhedron*, 2018, **146**, 81–92.
20. (a) A. Bhattacharyya, P. K. Bhaumik, M. Das, A. Bauza', P. P. Jana, K. Harms, A. Frontera and S. Chattopadhyay, *Polyhedron*, 2015, **101**, 257–269; (b) S. Chattopadhyay, M. G. B. Drew and A. Ghosh, *Polyhedron*, 2007, **26**, 3513–3522.
21. (a) M. Nazarov and D. Y. Noh, *New Generation of Europium and Terbium-Activated Phosphors: From Syntheses to Applications*, Pan Stanford Publishing, 6000 Broken Sound Pkwy NW, 2011, p. 211; (b) S. Roy, M. G. B. Drew, A. Bauza', A. Frontera and S. Chattopadhyay, *Dalton Trans.*, 2017, **46**, 5384–5397.
22. J. Costamagna, J. Vargas, R. Latorre, A. Alvarado and G. Mena, *Coord. Chem. Rev.*, 1992, **119**, 67–88.
23. A. Bhattacharyya, P. K. Bhaumik, P. P. Jana and S. Chattopadhyay, *Polyhedron*, 2014, **78**, 40–45.
24. A. Mustapha, K. Busch, M. Patykiewicz, A. Apedaile, J. Reglinski, A. R. Kennedy and T. J. Prior, *Polyhedron*, 2008, **27**, 868–878.

25. G. Mahmoudi, D. A. Safin, M. P. Mitoraj, M. Amini, M. Kubicki, T. Doert, F. Locherere and M. Fleck, *Inorg. Chem. Front.*, 2017, **4**, 171–182.
26. A. Bauzá, S. K. Seth and A. Frontera, *Coord. Chem. Rev.*, 2019, **384**, 107–125.
27. G. Mahmoudi, A. Bauzá and A. Frontera, *Dalton Trans.*, 2016, **45**, 4965–4969.
28. S. Roy, M. G. B. Drew, A. Bauzá, A. Frontera and S. Chattopadhyay, *New J. Chem.*, 2018, **42**, 6062–6076.
29. F. L. Hirshfeld, *Theor. Chim. Acta.*, 1977, **44**, 129–138.
30. J. J. McKinnon, D. Jayatilaka, M. A. Spackman, *ChemCommun.*, 2007, 3814–3816.
31. J. J. McKinnon, M. A. Spackman and A. S. Mitchell, *ActaCryst. B.*, 2004, **60**, 627–668.
32. M. A. Spackman and J. J. McKinnon, *CrystEngComm*, 2002, **4**, 378–392.
33. K. P. Sharma and R. K. Poddar, *Transition Met. Chem.*, 1984, **9**, 135–138.
34. G.M. Sheldrick, *Acta Crystallogr., Sect.*, 2015, **C 71**, 3–8.
35. G. M. Sheldrick, SADABS, V2014/5, Software for Empirical Absorption Correction, University of Göttingen, Institute für Anorganische Chemie der Universität, Göttingen, Germany, 1999–2003.
36. (a) M. A. Spackman and D. Jayatilaka, *CrystEngComm*, 2009, **11**, 19–32; (b) H. F. Clausen, M. S. Chevallier, M. A. Spackman and B. B. Iversen, *New J. Chem.*, 2010, **34**, 193–199.

37. S. K. Wolff, D. J. Grimwood, J. J. McKinnon, D. Jayatilaka and M. A. Spackman, Crystal Explorer 2.0, University of Western Australia, Perth, Australia, 2007, <http://hirshfeldsurfacenet.blogspot.com>.
38. M. J. Frisch, G. W. Trucks, H. B. Schlegel, G. E. Scuseria, M. A. Robb, J. R. Cheeseman, G. Scalmani, V. Barone, B. Mennucci, G. A. Petersson, H. Nakatsuji, M. Caricato, X. Li, H. P. Hratchian, A. F. Izmaylov, J. Bloino, G. Zheng, J. L. Sonnenberg, M. Hada, M. Ehara, K. Toyota, R. Fukuda, J. Hasegawa, M. Ishida, T. Nakajima, Y. Honda, O. Kitao, H. Nakai, T. Vreven, J. A. Montgomery, Jr., J. E. Peralta, F. Ogliaro, M. Bearpark, J. J. Heyd, E. Brothers, K. N. Kudin, V. N. Staroverov, R. Kobayashi, J. Normand, K. Raghavachari, A. Rendell, J. C. Burant, S. S. Iyengar, J. Tomasi, M. Cossi, N. Rega, J. M. Millam, M. Klene, J. E. Knox, J. B. Cross, V. Bakken, C. Adamo, J. Jaramillo, R. Gomperts, R. E. Stratmann, O. Yazyev, A. J. Austin, R. Cammi, C. Pomelli, J. W. Ochterski, R. L. Martin, K. Morokuma, V. G. Zakrzewski, G. A. Voth, P. Salvador, J. J. Dannenberg, S. Dapprich, A. D. Daniels, Ö. Farkas, J. B. Foresman, J. V. Ortiz, J. Cioslowski and D. J. Fox, Gaussian 09 (Gaussian, Inc., Wallingford CT, 2009).
39. S. Grimme, J. Antony, S. Ehrlich and H. Krieg, *J. Chem. Phys.*, 2010, **132**, 154104.
40. S. F. Boys and F. Bernardi, *Mol. Phys.*, 1970, **19**, 553-566.
41. T. A. Keith, *AIMAll (Version 13.05.06)*, TK Gristmill Software, Overland Park, KS, 2013.

Section IIIC

Importance of π -Interactions Involving Chelate Rings in Addition to the Tetrel Bonds in a Series of Hemi-directed Nickel(II)/Lead(II) Complexes



III.C .1. Introduction

Lead is a heavy metal with an ability to adopt different coordination numbers and valences. The coordination chemistry of lead has attracted synthetic inorganic chemists to prepare new lead(II) complexes with different molecular and crystalline architecture.¹⁻⁴ Although lead(II) is associated with serious pollution, materials possessing lead(II) are increasingly used in batteries, ferroelectric materials, semiconductors and non-linear optical materials.⁵⁻¹¹ On the other hand, salen-type ligands are well known in the literature for their easy synthetic approach and the ability to ligate several transition metal ions in tetradentate N_2O_2 cores.¹²⁻¹⁹ Many of them may then be used as metallo-ligands to form lead (II) complexes.²⁰⁻²² In the present work, two $N_2O_2O'_2$ donor compartmental Schiff base ligands have been reduced to form 'reduced Schiff bases', which were then used to arrest nickel(II) in their inner N_2O_2 cores. These metallo-ligands have, in turn, been used to encapsulate lead(II) in their outer $O_2O'_2$ cores. The valence shell electronic configuration of lead being $[Xe]4f^{14}5d^{10}6s^26p^2$, the presence of poorly screening f^{14} and d^{10} electrons makes the $6s^2$ electron pair inert, mostly due to increasing effective nuclear charge. In addition, the high penetrating property of the $6s$ orbital and relativistic stabilization of $6s^2$ electrons are also responsible.²³⁻²⁶ The magnitude to which the lone pair is stereochemically active^{27,28} is currently arousing interest in theoretical chemists to explore this area further.²⁹⁻³² Heavy atoms of groups IV to VII are gaining special interest nowadays in the field of supramolecular chemistry. This is because of their participation in strong σ -hole interaction in complexes where these atoms are covalently bonded to electronegative ones.³³⁻⁴⁰ These interactions have been widely designated for

chalcogen, pnictogen and halogen atoms. Nonetheless, those of group IV comprising tetrel bonding interactions (specially for lead complexes) are relatively less explored.⁴¹⁻⁴⁴ Solid state crystal structures are stabilized due to various non-covalent interactions like hydrogen bonding, π - π stacking, cation- π , anion- π , C-H $\cdots\pi$ interactions.⁴⁵⁻⁵² The influence of these interactions in crystal packing has been widely studied. However the attention has now shifted towards more unconventional interactions like C-H $\cdots\pi$ (chelate), π (arene)- π (chelate) etc.⁵³⁻⁵⁹ In recent years, “non-classical” interactions have become an interesting topic for research as they have been proven to be equal or even dominating contributors to metal-organic crystal structure formation.

In the present work, two $\text{N}_2\text{O}_2\text{O}'_2$ donor compartmental reduced Schiff bases, 2,2'-[(2,2-dimethyl-1,3-propanediyl)bis(iminomethylene)]bis[6-methoxy-phenol] (H_2L^1) and 2,2'-[(2,2-dimethyl-1,3-propanediyl)bis(iminomethylene)]bis[6-ethoxy-phenol] (H_2L^2) were used to prepare five hetero-nuclear nickel(II)/lead(II) complexes, [(SCN)NiL¹($\mu_{1,3}$ -NCS)Pb] (**7**), [(SCN)NiL¹(μ -OAc)Pb] (**8**), [(SCN)NiL²(μ -OAc)Pb] (**9**). Their structures have been determined by single crystal X-ray diffraction analyses. The lead centres in complexes **7-9** are hemidirectionally coordinated and participates in non-covalent tetrel bonding interactions. Moreover, supramolecular interactions were studied by means of DFT calculations focusing our attention on Pb \cdots S and Pb $\cdots\pi$ tetrel bonds observed in the solid state architecture of complexes **7-9**. Furthermore, π -stacking assemblies between aromatic rings and five-membered Pb-chelate rings were detected and studied both with regard to their energies and by using the non-covalent (NCI) plot index.

III.C .2. EXPERIMENTAL SECTION

III.C.2.1: *Synthesis*

III.C.2.1.1: *Synthesis of Schiff base ligands*

III.C.2.1.1.1: Preparation of the ligand, 2,2'-[(2,2-dimethyl-1,3-propanediyl)bis(iminomethylene)]bis[6-methoxy-phenol] (H_2L^1) and 2,2'-[(2,2-dimethyl-1,3-propanediyl)bis(iminomethylene)]bis[6-ethoxy-phenol] (H_2L^2)

H_2L^1 and H_2L^2 ligand preparation has been given in II.2.1 (See Chapter 2).

III.C.2.1.3. *Synthesis of complexes*

III.C.2.1.3.1: *Preparation of [(SCN)NiL¹($\mu_{1,3}$ -NCS)Pb] (7)*

A methanol solution (5 mL) of nickel(II) thiocyanate tetrahydrate (250 mg, 1 mmol) was added to the methanol solution (10 mL) of the reduced Schiff base ligand H_2L^1 , with constant stirring. A methanol (5 mL) solution of lead(II) nitrate (331 mg, 1 mol) was then added to it and the stirring was continued for about 1h. The resulting mixture was then refluxed for ca. 2h. Single crystals, suitable for X-ray diffraction, were obtained after 4-5 days upon slow evaporation of the solution in an open atmosphere.

Yield: 527 mg (~70%) based on nickel(II). Anal. Calc. for $C_{23}H_{28}N_4NiO_4PbS_2$ (FW: 754.50): C, 36.71; H, 3.48; N, 7.45; Found: C, 36.6; H, 3.3; N, 7.5%. FT-IR (KBr, cm^{-1}): 3264 (ν_{N-H}); 2963-

2839 ($\nu_{\text{C-H}}$); 2074 (ν_{NCS}). λ_{max} (nm) [ϵ_{max} (lit mol⁻¹ cm⁻¹)] (acetonitrile): 251(1.11 X 10³); 286 (5.9 X 10²); 603(25.2)

III.C.2.1.3.2: Preparation of [(SCN)NiL¹(μ -OAc)Pb] (8)

Complex **8** was prepared in a similar method to that of complex **7**, except that the lead(II) acetate trihydrate (379 mg, 1 mmol) was added instead of lead(II) nitrate. Single crystals, suitable for X-ray diffraction, were obtained after 4-5 days upon slow evaporation of the solution in an open atmosphere.

Yield: 512 mg (~68%) based on nickel(II). Anal. Calc. for C₂₄H₃₁N₃NiO₆PbS (FW: 755.47): C, 38.26; H, 3.88; N, 5.58. Found: C, 38.1; H, 3.7; N, 5.7 %, FT-IR (KBr, cm⁻¹): 3286 ($\nu_{\text{N-H}}$); 2970-2818 ($\nu_{\text{C-H}}$); 2087 (ν_{NCS}), 1250, 1226 (ν_{COO^-}). λ_{max} (nm) [ϵ_{max} (lit mol⁻¹ cm⁻¹)] (acetonitrile): 237 (1.93 X 10³); 286 (1.59 X 10²); 608 (33.9).

III.C.2.1.3.3: Preparation of [(SCN)NiL²(μ -OAc)Pb] (9)

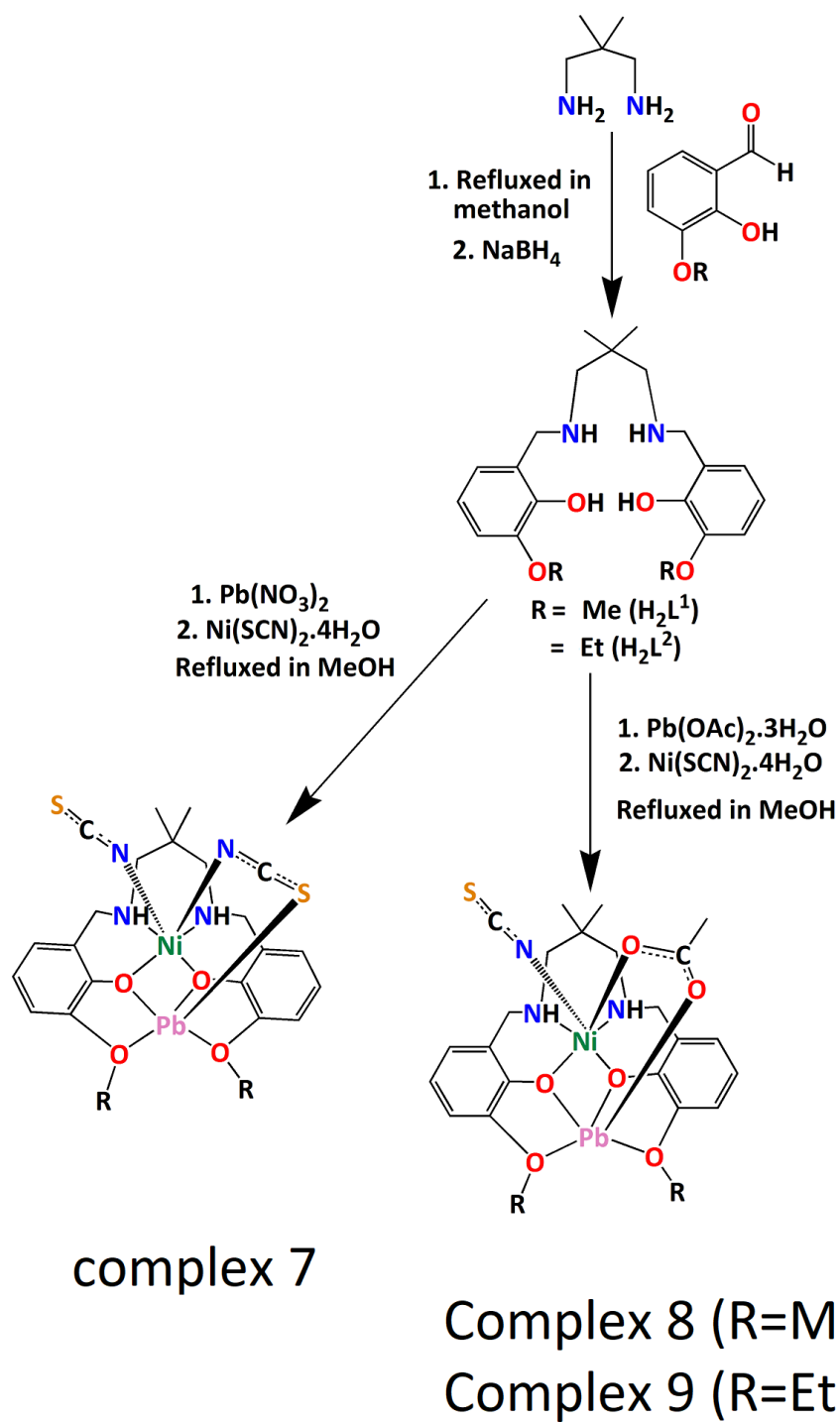
Complex **9** was prepared in a similar method to that of complex **8**, except that H₂L² was used instead of H₂L¹. Single crystals, suitable for X-ray diffraction, were obtained after 4-5 days upon slow evaporation of the solution in an open atmosphere.

Yield: 540 mg (~69%) based on nickel(II). Anal. Calc. for C₂₆H₃₅N₃NiO₆PbS (FW: 783.52): C, 39.96; H, 4.26; N, 5.38; Found: C, 39.8; H, 4.2; N, 5.5%. FT-IR (KBr, cm⁻¹): 3211 ($\nu_{\text{N-H}}$); 2922-2842 ($\nu_{\text{C-H}}$); 2088 (ν_{NCS}), 1250, 1229 (ν_{COO^-}). λ_{max} (nm) [ϵ_{max} (lit mol⁻¹ cm⁻¹)] (acetonitrile): 243 (2.32x10³); 286 (1.59 X 10²); 602(31.20).

III.C .3. Results and discussion

III.C .3. 1: Synthesis

2, 2-dimethyl-1, 3-diaminopropane was refluxed with 3-methoxysalicylaldehyde and 3-ethoxysalicylaldehyde in 1:2 ratio respectively, followed by the addition of NaBH_4 to form two $\text{N}_2\text{O}_2\text{O}'_2$ donor compartmental reduced Schiff bases (H_2L^1 and H_2L^2) following standard literature methods.⁶⁰⁻⁶² These ligands (H_2L^1 and H_2L^2) on reaction with different ratios of nickel(II) and lead(II) salts in different solvents produced the complexes. Formation of complexes **7-9** has been shown in Scheme. III. C.1.



Scheme. III. C.1: Synthetic route to complexes **7-9**. Lattice solvent molecules have been omitted for clarity.

III.C.3.2. Structure description

III.C.3.2.1. Description of $[(SCN)NiL^1(\mu_{1,3}-NCS)Pb]$ (**7**), $[(SCN)NiL^1(\mu-OAc)Pb]$ (**8**) and $[(SCN)NiL^2(\mu-OAc)Pb]$ (**9**)

Single crystal X-ray diffraction measurements reveal that complexes **7**, **8** and **9** are built from isolated hetero-dinuclear molecules of $[(SCN)NiL^1(\mu_{1,3}-NCS)Pb]$, $[(SCN)NiL^1(\mu-OAc)Pb]$ and $[(SCN)NiL^2(\mu-OAc)Pb]$ respectively (Figure. III. C. 1). Crystallographic data and refinement details are provided in Table III. C. 1. Important bond lengths and bond angles are summarized in Tables III. C. 2 and Tables III. C. 3 (Supporting Information, SI), respectively.

Two $N_2O_2O'_2$ donor compartmental reduced Schiff bases (H_2L^1 and H_2L^2) were used to prepare complexes **7**, **8** and **9** in which nickel(II) centres are placed in inner N_2O_2 cavities and lead(II) centres in outer $O_2O'_2$ cavities. The nickel(II) centre [Ni(1)] has a distorted octahedral geometry, where two amine nitrogen atoms, N(1) and N(2) and two phenoxo oxygen atoms, O(1) and O(2) of the deprotonated reduced Schiff base constitute the equatorial plane. Deviations of coordinating atoms from the mean equatorial planes passing through them and those of the nickel(II) centre of the same plane in both complexes are listed in Table.III.C.4. One nitrogen atom, N(3) from a terminal thiocyanate coordinates with a nickel(II) centre to fulfill the fifth coordination. The sixth coordination site is occupied by a nitrogen atom, N(4) from a bridging thiocyanate in case of complex **7** whereas in complexes **8** and **9** it is occupied by an oxygen atom, O(5) from an acetate molecule.

The lead(II) centre in each complex is penta-coordinated. Phenoxo oxygen atoms, O(1) and O(2) along with alkoxy oxygen atoms, O(3) and O(4) [methoxy for complexes **7** and **8** and ethoxy for complex **9**] of deprotonated reduced Schiff bases also coordinate to a lead(II) centre but at much longer distances to form equatorial planes. The fifth coordination site is occupied by a sulphur atom S(2) from a bridging thiocyanate in case of complex **7** whereas in complexes **8** and **9** it is occupied by an oxygen atom, O(6) from a bridging acetate molecule. The geometry of any penta-coordinated metal centre may conveniently be measured by the Addison parameter (τ)⁶³ [$\tau = (\Theta - \Phi)/60$, where Θ and Φ are the two largest ligand-metal-ligand angles of the coordination sphere]. In complexes **7**, **8** and **9**, the geometries around the lead(II) center assume square pyramidal geometries with $\tau = 0.43$, 0.07 and 0.24 for complexes **7**, **8** and **9** respectively. Ni(1)O(1)Pb(1)O(2) dihedral angles are 7.7(2)°, 13.7(2)° and -16.29(9)° in complexes **7**, **8** and **9** respectively. The distance between Ni(1) and Pb(1) is 3.491(1) Å (complex **7**), 3.362(1) Å (complex **8**) and 3.346(8) Å (complex **9**). The bridging angles Ni(1)–O(1)–Pb(1) and Ni(1)–O(2)–Pb(1) are 105.1(2)° and 104.8(2)° respectively for complex **7**, 97.8(3)° and 101.1(3)° for complex **8** and 99.2(1)° and 99.93(9)° for complex **9** respectively.

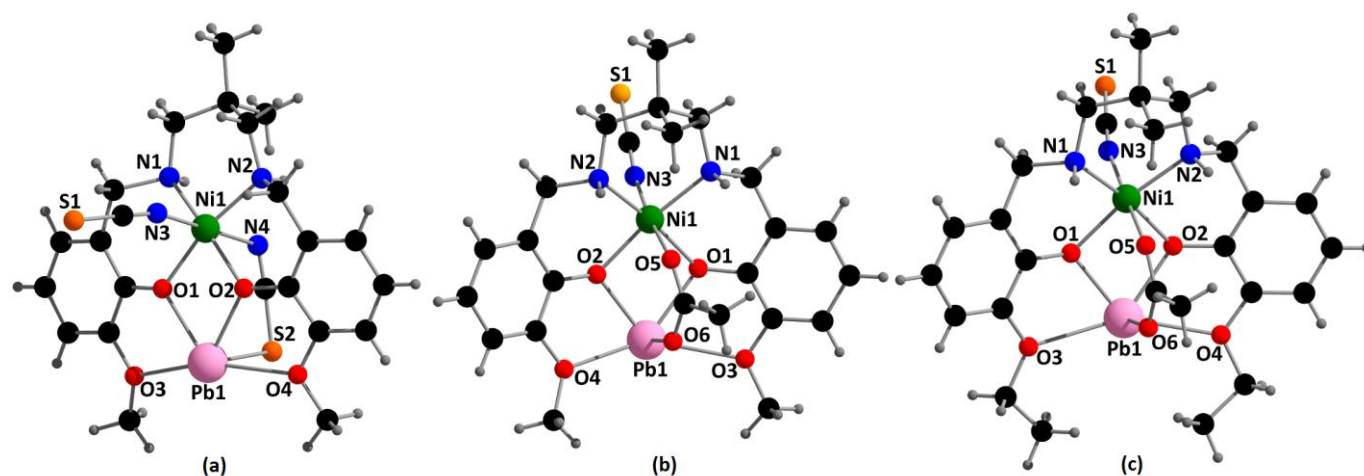


Fig.III.C.1: Perspective view of complexes (a) **7**, (b) **8** and (c) **9** with selective atom numbering scheme.

Table III. C. 1: Crystal data and refinement details of complexes **7**, **8** and **9**.

Complex	7	8	9
Formula	C ₂₃ H ₂₈ PbNiN ₄ O ₄ S ₂	C ₂₄ H ₃₁ PbNiN ₃ O ₆ S	C ₂₆ H ₃₅ N ₃ NiO ₆ PbS
Formula Weight	754.50	755.47	783.52
Temperature (K)	273	273	273
Crystal system	Triclinic	Monoclinic	Monoclinic
Space group	$P\bar{1}$	$P2_1/n$	$P2_1/c$
a(Å)	9.3341(8)	10.5402(9)	8.2144(6)
b(Å)	9.4091(8)	15.1178(13)	27.361(2)
c(Å)	15.2174(13)	17.8145(18)	13.1439(10)
α	83.558(3)	-	-
β	75.284(3)	99.613(3)	101.617(3)
γ	79.946(3)	-	-
Z	2	4	4
d_{calc} (g cm ⁻³)	1.974	1.793	1.799
μ (mm ⁻¹)	7.566	6.796	6.577
$F(000)$	736	1480	1544

Total Reflections	26594	30361	80213
Unique Reflections	4481	4971	5095
Observed data [$I > 2 \sigma(I)$]	4296	4066	4622
No. of parameters	324	296	343
R(int)	0.055	0.076	0.061
R1,wR2(all data)	0.0467, 0.1283	0.0999, 0.2395	0.0280, 0.0535
R1,wR2 [$I > 2 \sigma(I)$]	0.0449, 0.1263	0.0897, 0.2270	0.0230, 0.0511
CCDC	1938676	1938677	1938678

Table. III.C. 2: Selected bond lengths (Å) of complexes **7**, **8** and **9**.

Complex	7	8	9	Complex	7	8	9
Pb(1)–O(1)	2.353(6)	2.327(7)	2.295(3)	Ni(1)–N(2)	2.064(7)	2.085(9)	2.081(3)
Pb(1)–O(2)	2.338(6)	2.285(7)	2.284(2)	Ni(1)–N(3)	2.028(8)	2.037(11)	2.053(4)
Pb(1)–O(3)	2.650(7)	2.643(10)	2.685(3)	Pb(1)–S(2)	2.827(3)	—	—
Pb(1)–O(4)	2.611(7)	2.576(9)	2.597(3)	Ni(1)–N(4)	2.432(10)	—	—
Ni(1)–O(1)	2.038(6)	2.130(8)	2.096(2)	Ni(1)–O(5)	—	2.070(9)	2.097(3)
Ni(1)–O(2)	2.061(6)	2.067(7)	2.084(2)	Pb(1)–O(6)	—	2.308(8)	2.321(3)
Ni(1)–N(1)	2.069(7)	2.093(10)	2.075(3)				

Table.III.C. 3: Selected bond angles (°) of complexes **7-9**.

Complex	1	2	3
O(1)–Pb(1)–O(2)	68.7(2)	74.3(3)	73.73(8)
O(1)–Pb(1)–O(3)	63.3(2)	65.0(3)	64.63(8)
O(1)–Pb(1)–O(4)	131.72(19)	138.1(3)	138.66(8)
O(1)–Pb(1)–O(6)	—	81.3(3)	87.24(9)

O(2)–Pb(1)–O(3)	131.6(2)	136.5(3)	138.09(8)
O(2)–Pb(1)–O(4)	64.44(19)	66.7(3)	65.91(8)
O(2)–Pb(1)–O(6)	—	84.3(3)	84.46(9)
O(3)–Pb(1)–O(4)	157.15(19)	142.6(3)	152.96(9)
O(3)–Pb(1)–O(6)	—	75.3(3)	88.94(9)
O(4)–Pb(1)–O(6)	—	80.2(3)	80.52(9)
S(2)–Pb(1)–O(1)	88.91(15)	—	—
S(2)–Pb(1)–O(2)	89.17(16)	—	—
S(2)–Pb(1)–O(3)	83.99(17)	—	—
S(2)–Pb(1)–O(4)	79.75(15)	—	—
O(1)–Ni(1)–O(2)	80.4(2)	83.2(3)	82.19(9)
O(1)–Ni(1)–O(5)	—	87.8(3)	88.54(10)
O(1)–Ni(1)–N(1)	92.4(3)	91.8(3)	90.88(10)
O(1)–Ni(1)–N(2)	167.9(3)	173.3(3)	170.90(11)
O(1)–Ni(1)–N(3)	93.4(3)	92.2(3)	93.27(12)
O(2)–Ni(1)–O(5)	—	89.2(3)	87.80(10)
O(2)–Ni(1)–N(1)	168.1(3)	172.4(3)	171.51(10)
O(2)–Ni(1)–N(2)	89.6(3)	91.1(3)	89.66(10)
O(2)–Ni(1)–N(3)	96.6(3)	95.6(4)	93.58(12)
O(2)–Ni(1)–N(4)	87.3(3)	—	—
N(1)–Ni(1)–N(2)	96.3(3)	93.5(4)	96.88(11)
N(1)–Ni(1)–N(3)	93.2(3)	90.3(4)	91.68(13)
N(2)–Ni(1)–N(3)	94.5(3)	92.0(4)	91.24(13)
O(1)–Ni(1)–N(4)	84.4(3)	—	—
N(1)–Ni(1)–N(4)	82.6(3)	—	—
N(2)–Ni(1)–N(4)	88.3(3)	—	—
N(3)–Ni(1)–N(4)	175.2(3)	—	—

O(5)–Ni(1)–N(1)	—	84.9(4)	87.14(11)
O(5)–Ni(1)–N(2)	—	88.6(4)	87.12(11)
O(5)–Ni(1)–N(3)	—	175.2(5)	177.85(12)

III.C .3. 3: Supramolecular interactions

The solid state structures of the complexes are stabilized through various non-covalent interactions (e.g. hydrogen bonding, C-H $\cdots\pi$, $\pi\cdots\pi$, cation $\cdots\pi$ interactions etc). The complexes were prepared while changing the ligand moieties along with bridging ligands which result in five different nickel(II)/lead(II) complexes. These trivial changes in ligand moieties along with bridging ligands play significant roles in the formation of diverse molecular architectures. Different supramolecular interactions are discussed below in the light of hirshfeld surface analyses. Complexes **7**, **8** and **9** are isostructural and show similar types of interactions. These complexes form supramolecular dimeric structure via cation $\cdots\pi$ interactions. The lead(II) centre, Pb(1), is involved in cation $\cdots\pi$ interactions with symmetry related [(1-x,1-y,-z) for complex **7**; (1-x,1-y,1-z) for complex **8** and **9**] phenyl rings, {[C(15)–C(16)–C(17)–C(18)–C(19)–C(20)] for complexes **7** and **8**; [C(16)–C(17)–C(18)–C(19)–C(20)–C(21)] for complex **9** shown in Figure. III.C.2. Details of the geometric features of cation $\cdots\pi$ interactions were given in Table.III.C.5. It should be mentioned that these interactions can (be)x also be defined as tetrel bonds where the electron donor is the π -system of the aromatic ring. This aspect is further analyzed in the theoretical part.

In complex **9**, the hydrogen atom, H(2), attached to nitrogen atom, N(2), is engaged in an intermolecular hydrogen bonding interaction with a symmetry related (1+x, y, z) sulfur atom,

S(1) of a coordinated terminal thiocyanate to form a chain structure (Figure.III.C.3). The dimensions are $H\cdots S = 2.58(3) \text{ \AA}$, $N\cdots S = 3.371(3) \text{ \AA}$, $\angle N-H\cdots S = 138(6)^\circ$.

In complex **7**, the phenyl ring, $[C(2)-C(3)-C(4)-C(5)-C(6)-C(7)]$ forms a $\pi\cdots\pi$ stacking interaction [dimensions, $Cg(9)\cdots Cg(10) = 3.759(5) \text{ \AA}$, $Cg(9)\cdots Prep = 3.487(4) \text{ \AA}$, $Cg(10)\cdots Prep = 3.521(3) \text{ \AA}$, $\alpha = 14.4(4)^\circ$; where $Cg(9) = C(2)-C(3)-C(4)-C(5)-C(6)-C(7)$, $Cg(10) = C(15)-C(16)-C(17)-C(18)-C(19)-C(20)$, $Cg(9)\cdots Prep$ = Perpendicular distance of $Cg(9)$ on ring $Cg(10)$, $Cg(10)\cdots Prep$ = Perpendicular distance of $Cg(10)$ on ring $Cg(9)$, α = Dihedral Angle between planes 9 and 10] with a symmetry-related $(1+x,y,z)$ phenyl ring, $[C(15)-C(16)-C(17)-C(18)-C(19)-C(20)]$, which leads to the formation of a chain structure (Figure.III.C.4a). The fascinating tetrel bonding interaction is observed between the lead(II) atom, Pb(1), with symmetry $(x,-1+y,z)$ related sulfur atom, S(1), of a thiocyanate from an adjacent molecule at $3.688(3) \text{ \AA}$ which leads to the formation of a chain. This is shown in Figure.III.C.4b.

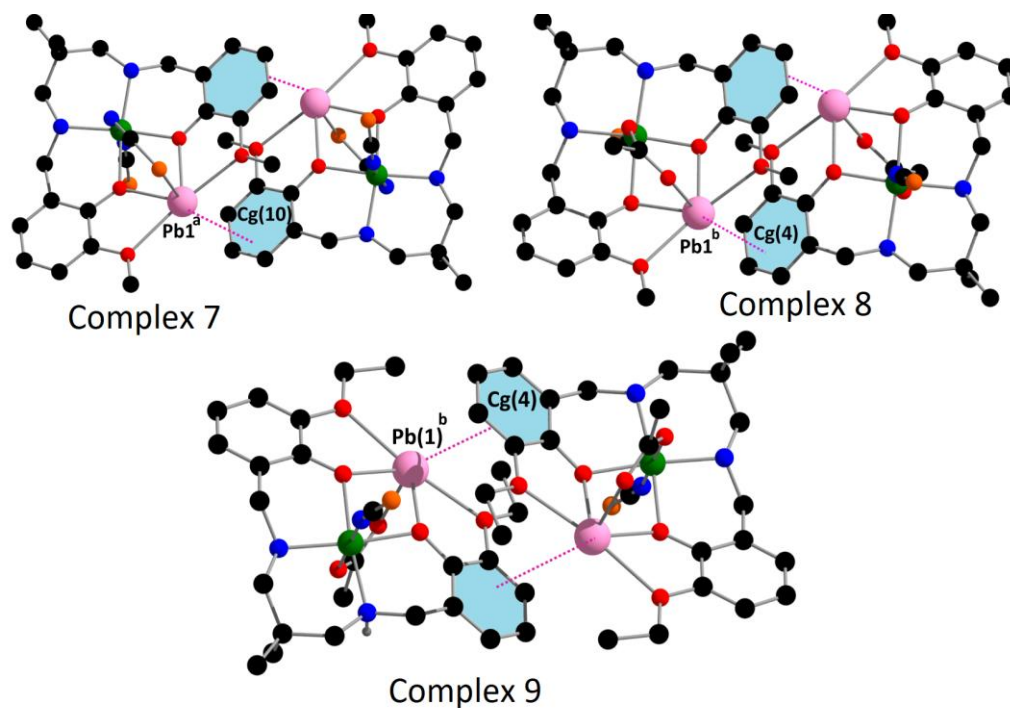


Fig. III.C.2: Cation... π interactions in complexes **7**, **8** and **9**. Only the relevant atoms have been shown for clarity. (Symmetry transformation ^a = 1-x,1-y,-z; ^b = 1-x,1-y,1-z).

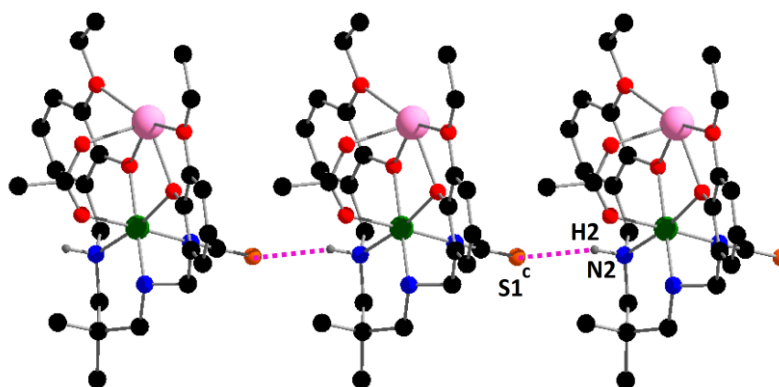


Fig.III.C.3: Supramolecular chain structure of complex **9** via hydrogen bonding interaction. Only the relevant atoms are shown for clarity. (Symmetry transformation ^c = 1+x, y, z).

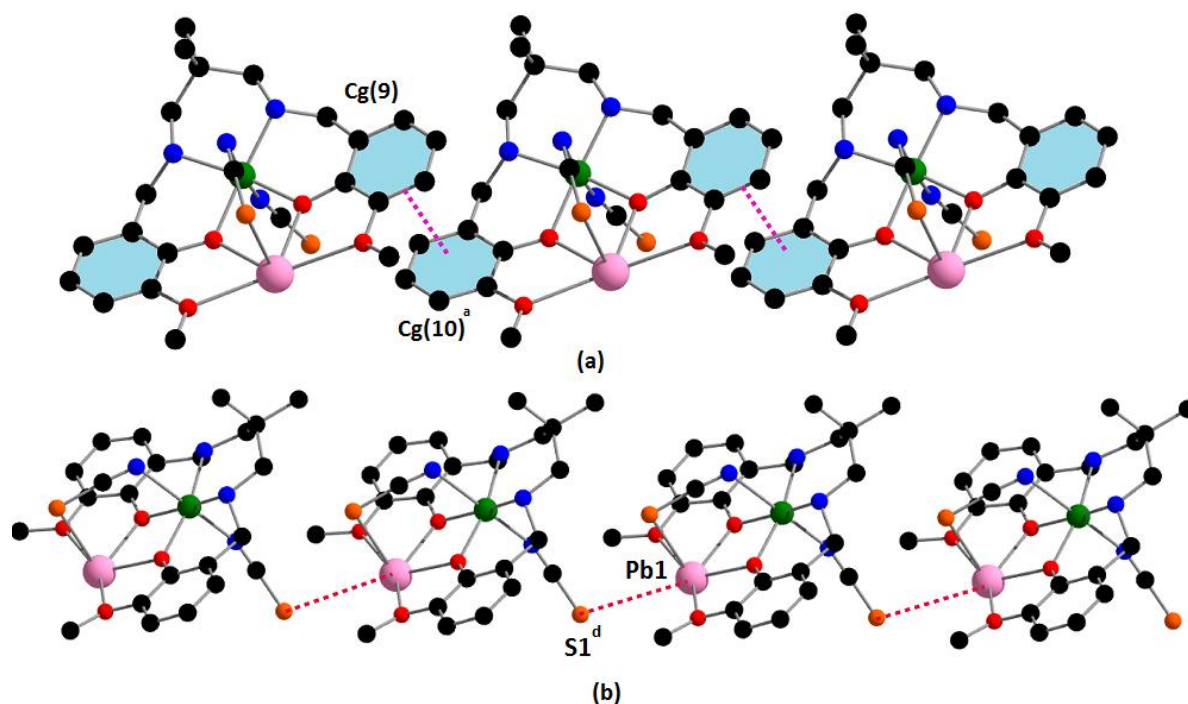


Fig.III.C.4: $\pi \cdots \pi$ (a) and $\text{Pb} \cdots \text{S}$ (b) interactions observed in complex **7**. Only the relevant atoms have been shown for clarity. Symmetry transformations ^a = 1+x,y,z and ^d = x,-1+y,z.

III.C .3. 4: IR and electronic spectra and PXRD

The strong bands around 2080 cm^{-1} indicate the presence of thiocyanate in complexes **7**, **8** and **9**.⁶⁴ The bands around $3008\text{-}3286 \text{ cm}^{-1}$ indicate the presence of amine N-H stretching in all complexes.⁶⁵ The broad bands in the range of $2970\text{-}2818 \text{ cm}^{-1}$ due to alkyl C-H stretching vibrations were routinely noticed in IR spectra of the complexes.⁶⁶ In complexes **8** and **9**, the bands around 1250 and 1229 cm^{-1} indicate the presence of an acetate group.⁶⁷

The electronic spectrum of each complex in acetonitrile displays three bands around 242 nm , 285 nm and 600 nm . The absorption around $\sim 242 \text{ nm}$ and $\sim 285 \text{ nm}$ may be assigned to

charge transfer transitions^{68,69} whereas the band around ~600 nm could be assigned to d-d transition.⁷⁰

Experimental PXRD patterns of the bulk products are in good agreement with simulated XRD patterns from single crystal X-ray diffraction results, indicating consistency in bulk samples. The simulated patterns of the complexes are calculated from the single crystal structural datas (CIF) using the CCDC Mercury software. Experimental and simulated PXRD patterns of complex **7** are shown in Figure.III.C.5. The experimental and simulated PXRD patterns of complexes **8** and **9** are given in Figure.III.C.6 and Figure.III.C.7, respectively.

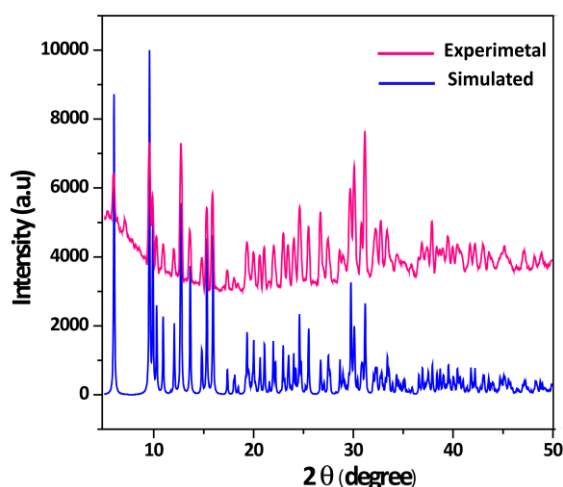


Fig.III.C.5: Experimental and simulated PXRD patterns of complex **7** confirming purity of the bulk material

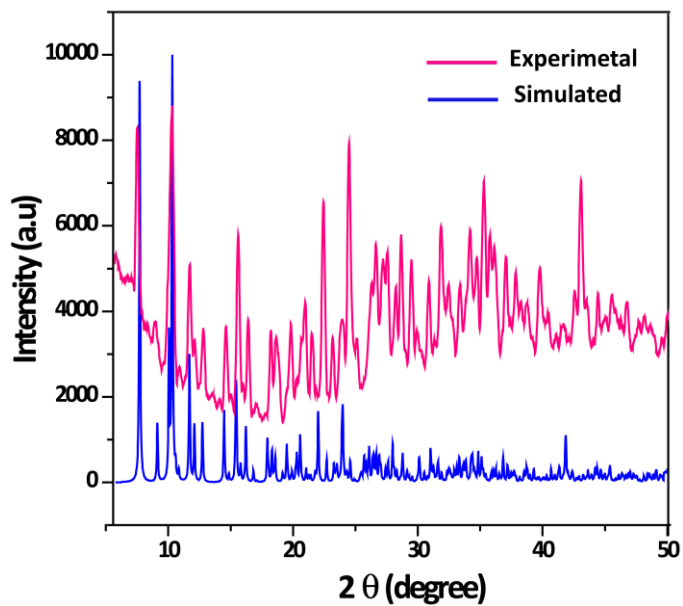


Fig.III.C.6: Experimental and simulated PXRD patterns of complex **8** confirming purity of the bulk material.

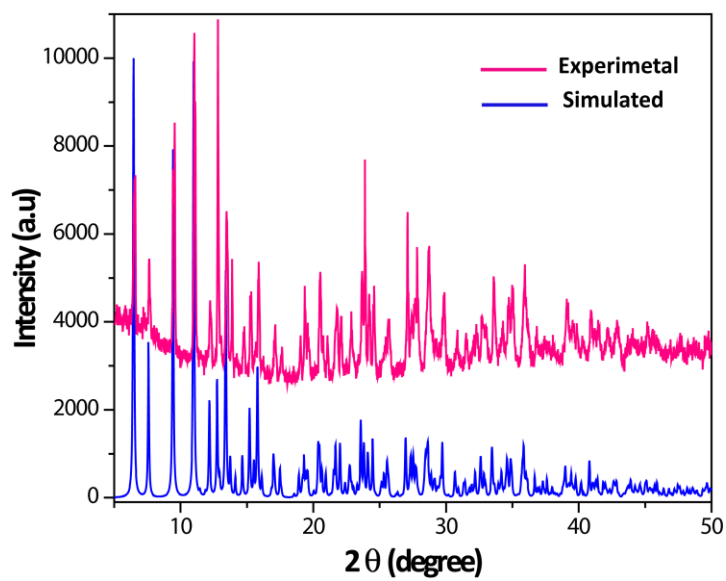


Fig.III.C.7: Experimental and simulated PXRD patterns of complex **9** confirming purity of the bulk material.

III.B.3.5: Theoretical study

The theoretical study is devoted to the analysis of interesting tetrel bonding interactions observed in the solid state of complexes **7-9**, where coordination of the lead(II) atom is hemidirected and consequently the σ -hole at the lead(II) atom is accessible to interact with electron donors (π -system or thiocyanate ligand). Using complex **7** as exemplifying molecule, the molecular electrostatic potential (MEP) was computed and plotted onto the van der Waals surface (isosurface 0.001 a.u.) in order to investigate the electron rich and electron deficient regions of the complex. The MEP surface is represented in Figure.III.C.8. It can be observed that the most positive region is located on the lead(II) atom, approximately in the PbO_4 mean plane (+37 kcal/mol) between both methoxy(-OMe) groups. The most negative region as expected is located at the anionic thiocyanate (-SCN) ligand. The MEP value is negative over the aromatic ring and slightly positive over the lead(II)-chelate ring. This analysis indicates that the most favoured interaction from an electrostatic point of view should be a tetrel bond between the lead(II) atom and the pseudohalide. Moreover, the MEP surface also reveals that π -stacking interactions between aromatic rings and chelate rings are also electrostatically favoured. Finally, it is worthy to comment on the unexpected positive MEP value observed at the sulphur atom of the bridged thiocyanate ligand at the extension of the thiocyanate bond revealing the existence of a σ -hole at the chalcogen atom suitable to establish weak σ -hole interactions.

Figure.III.C.9 shows two dimers retrieved from the X-ray of structures of complex **7** (hydrogen-atoms omitted for clarity), where relevant and unconventional interactions are observed. The first dimer corresponds to the cation- π (or tetrel- π) complex highlighted in Figure.III.C.2 and the second one has been extracted from the infinite 1D supramolecular chain

described in Figure.III.C.4b (bottom). A close examination of the self-assembled dimer represented in Figure.III.C.9a reveals that the five-membered Pb-chelate ring (CR, represented in blue) is stacked above the aromatic ring (represented in green). This type of interaction is described in hemidirected lead(II) complexes with hydrazide-based ligands.⁷¹ In fact, the lead atom basically interacts with one carbon atom of the aromatic. The interaction energy of this dimer was evaluated and found to be very large ($\Delta E_1 = -29.9$ kcal/mol) thus confirming the relevance of $\pi-\pi$ (CR) interactions. The Pb \cdots S dimer is represented in Figure.III.C.9b and it can be observed that the negative sulphur-atom of the mono coordinated thiocyanate ligand is situated exactly at a position predicted by the MEP surface (maximum value of shown in Figure.III.C.8). In addition, the σ -hole at the sulphur-atom of the bridged thiocyanate interacts with the electron rich carbon-atom of the thiocyanate ligand, also in agreement with the MEP analysis. Both interactions contribute to the binding energy that are moderately strong ($\Delta E_2 = -19.6$ kcal/mol). To further characterize the interactions described above, the NCI plot index was used since it allows an easy assessment of host-guest complementarity and the extent to which weak interactions stabilize a complex. Figure.III.C.9c shows the NCI plot of the stacked dimer. The presence of an extended green (energetically favorable) isosurface between aromatic and chelate rings observed confirm the existence of the interaction. Moreover, a smaller green isosurface is located between the lead atom and one carbon-atom of the ring characterizing the Pb \cdots C tetrel bond. The NCI plot also reveals the existence of several C-H \cdots SCN interactions involving the methoxy (-OCH₃) and C-H groups characterized by two isosurfaces. For the Pb \cdots S dimer, the tetrel bond is characterized by a green isosurface located between the sulphur and lead(II) atoms (see Figure.III.C.9d). This interaction is complemented by two C-H \cdots S hydrogen-

bonding interactions involving methyl groups. Finally, the S \cdots C(SCN) interaction is characterized by a small isosurface located between both atoms.

As previously shown in Figure.III.C.2, complexes **8** and **9** also form Pb \cdots π (or cation \cdots π) dimers in solid state. Both dimers are shown in Fig. 11 from where it can be observed that they are slightly different compared to complex **7**. In fact, for complex **8** the lead(II) atom is located approximately over the center of the aromatic ring instead of being connected to a single carbon-atom. This provokes a displacement of the π -systems and the π - π (CR) interaction is not formed; instead a π (CR)- π (CR) stacking is established in combination with two Pb \cdots π interactions (see Scheme.III.C.2). Therefore, differences between both these arrangements were analyzed with regard to energy. In Figure.III.C.10a the Pb \cdots π dimer of complex **8** has been represented and it was found that the interaction energy is almost identical ($\Delta E_3 = -29.0$ kcal/mol) to the dimer of complex **7** (see Figure.III.C.9a) suggesting both combinations are basically isoenergetic. The dimer of complex **9** is not strictly comparable because of the presence of an ethyl group instead of a methyl group. This provokes a displacement of the π -systems (parallel displaced arrangement) that provokes an enlargement of both π (CR)- π (CR) stacking and Pb \cdots π distances and the formation of C-H \cdots SCN interactions (marked in red in Fig. Figure.III.C.10b). As a consequence, the interaction energy of this dimer is the most favorable ($\Delta E_4 = -35.9$ kcal/mol) due to additional interactions.

There are examples in the literature of experimental and theoretical investigations devoted to tetrel bonding. Table.III.C.6 shows examples of such X-ray characterized heteronuclear nickel(II)/lead(II) complexes along with lead(II) complexes where the lead(II) centre is hemidirected and subjected to a tetrel bonding interaction. Now it has to be mentioned that no

such report has been found where tetrel bonding was explored in heteronuclear nickel(II)/lead(II) complexes with reduced Schiff bases. Thus the present work is the first systematic study that explores tetrel bonding interactions in hemidirected heteronuclear nickel(II)/lead(II) complexes.

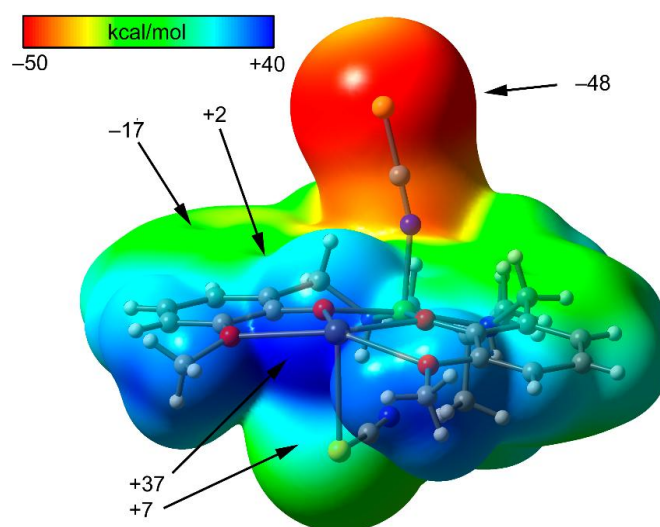


Fig.III.C.8: MEP surface of complex **7** (isosurface 0.001 a.u.) at the PBE0/def2-TZVP level of theory. The values at selected points of the surface are indicated in kcal/mol.

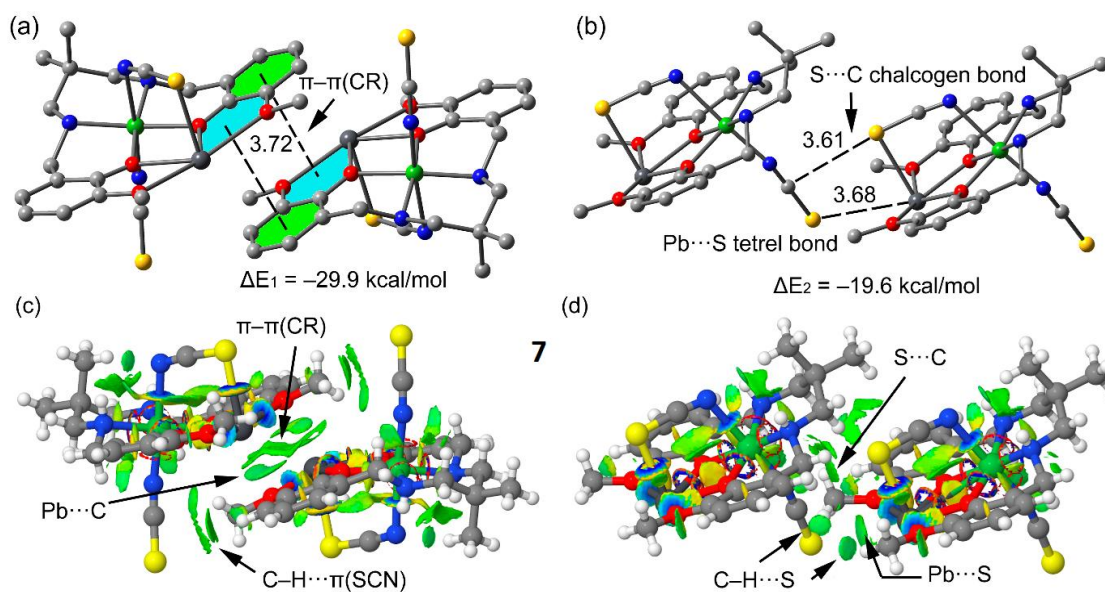
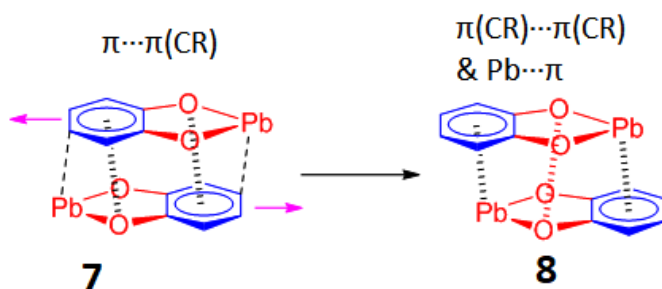


Fig.III.C.9 (a,b): Theoretical models used to evaluate the non-covalent interactions. **(c,d)** NCI plots of the dimers in complex **7**. The gradient cut-off is $s = 0.35$ au, and the color scale is $-0.04 < \rho < 0.04$ au.



Scheme.III.C.2: Schematic representation of the π -stacking assemblies in complexes **7** and **8**.

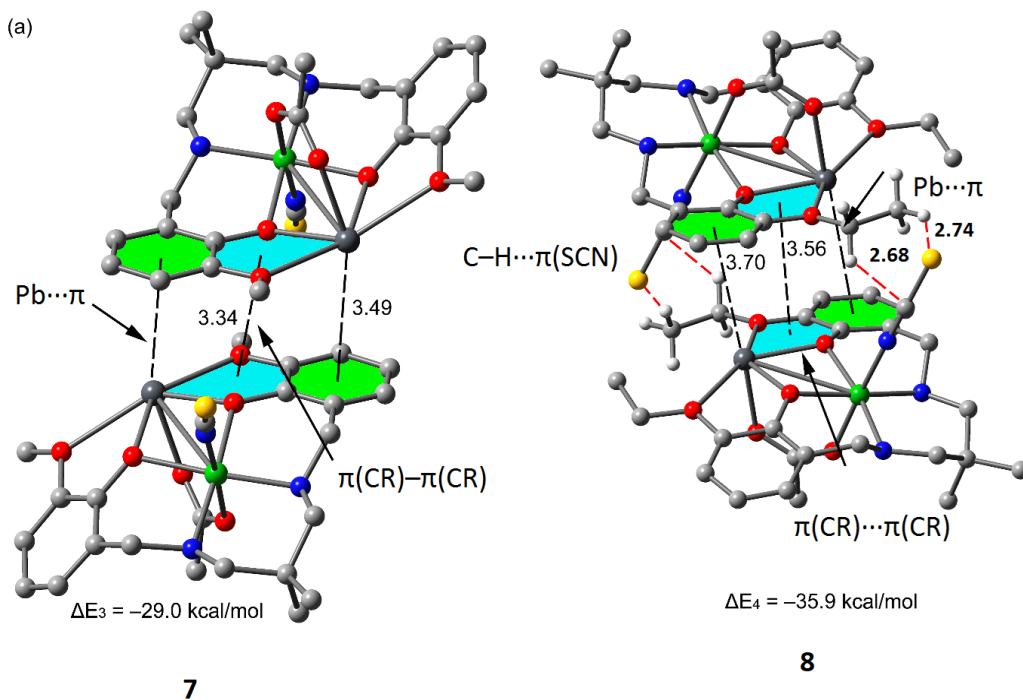


Fig. 11 (a,b). Theoretical models used to evaluate the non-covalent interactions in complexes **8** and **9**. Distances in Å.

Table.III.C.4: Deviation of coordinating atoms from the least square mean plane passing through them and that of nickel(II) from the same plane in complexes **7-9**.

Complex	Deviations of atoms in Å				
	O(1)	O(2)	N(1)	N(2)	Ni(1)
1	-0.008(6)	-0.051(6)	-0.052(7)	-0.014(7)	0.125(10)
2	0.001(7)	-0.036(7)	-0.035(10)	-0.002(9)	0.071(13)
3	0.009(2)	0.023(2)	0.025(3)	0.012(3)	-0.0692(4)

Table.III.C.5: Geometric features (distances in Å and angles in°) of the cation... π interactions obtained for complexes **7, 8** and **9**.

Complex	Cg...M(Cation)	Cg...M (Å)	M...Prep (Å)
1	Cg(10)...Pb(1) ^a	3.595(8)	-3.324(5)
2	Cg(4)...Pb(1) ^b	3.494(1)	3.443(6)
3	Cg(4)...Pb(1) ^b	3.700(5)	-3.390(3)

Symmetry transformations: ^a = 1-x, 1-y, -z and ^b = 1-x, 1-y, 1-z.

Table.III.C.6: Reported X-ray characterized nickel(II)/lead(II) and lead(II) complexes comprising tetrel bonding interaction.

Complex (CCDC)	Formula	Coordination mode of lead	Bonding	Pb-X (Å)	Ref
YISROI	[{L ^a Ni}Pb(NC ₅ H ₅)Cl] ₂	Hemidirected	Tetrel	3.272(1)	72

YISRUO	$[(L^bNi)_2Pb] \cdot Py \cdot H_2O$	Hemidirected	Tetrel	3.221(2)	72
QUQBIP	$[(SCN)PbL^c[(\mu_{1,1}-SCN)]_2] \cdot CH_3OH$	Hemidirected	Tetrel	3.042(1)	73
QUQBOV	$[(SCN)_2PbL^c]$	Hemidirected	Tetrel	3.403(2)	73
TAGMUM	$[(I)PbL^d] \cdot CH_3OH$	Hemidirected	Tetrel	3.241(1)	74
TAGMOG	$[(Cl)PbL^d] \cdot CH_3OH$	Hemidirected	Tetrel	3.155(2)	74
TAGNET	$[(SCN)PbL^d]$	Hemidirected	Tetrel	3.224(8)	74
TAGNEX	$[(NO_3)PbL^d] \cdot CH_3OH$	Hemidirected	Tetrel	3.408(1)	74
IPAHEO	$[Pb_2(HL^c)_2(NO_3)_4]$	Hemidirected	Tetrel	2.923(3)	73
IPAHAK	$[(OAc)PbL^c]$	Hemidirected	Tetrel	3.424(7)	73
JERPAA	$[Pb_2(H_2L^c)(NO_3)_4]_2$	Hemidirected	Tetrel	3.060(1) 3.350(1)	73
HAFVAO	$[Pb(L^cN_3)]_n$	Hemidirected	Tetrel	3.436(4)	75
HAFVES	$[(NO_3)(SCN)Pb(HL^c)]_2$	Hemidirected	Tetrel	3.225(1)	75
HAFVIW	$[(OAc)PbL^c]$	Hemidirected	Tetrel	3.488(3) 3.409(4)	75
HAFVUI	$[PbL^c(NO_2)]_n$	Hemidirected	Tetrel	3.299(5)	75
REZFIO	$[(SCN)NiL^ePb(NO_3)]$	Hemidirected	Tetrel	3.064(2)	54
ZETLES	$[(H_2O)Ni(SCN)L^fPb(OAc)] \cdot DMSO$	Hemidirected	Tetrel	3.379(4)	54
-	$[(SCN)NiL^1(\mu_{1,3}-NCS)Pb]$	Hemidirected	Tetrel	3.688(3)	This Work
-	$[(SCN)NiL^1(\mu-OAc)Pb]$	Hemidirected	-	-	This Work

-	[(SCN)NiL ² (μ-OAc)Pb]	Hemidirected	-	-	This Work
---	-----------------------------------	--------------	---	---	-----------

L^a = tris-((2-hydroxybenzylidene)-aminoethyl)-amine; L^b = tris-((-2-hydroxybenzylidene)-aminomethyl)propane; H₂L^c = N'-(1-(2-pyridyl)ethylidene)nicotinohydrazide; H₂L^d = N'-(phenyl(pyridin-2-yl) methylene)isonicotinohydrazide; H₂L^e = N,N'-bis(3-ethoxysalicylidene)propane-1,3-diamine; H₂L^f = [N,N'-bis(3-methoxysalicylidene)-2,2-dimethylpropane-1,3-diamine].

III.C .3.6: Hirshfeld surfaces

The Hirshfeld surface emerged from an attempt to define the space occupied by a molecule in a crystal for the purpose of subdividing the crystal electron density into molecular fragments.¹² d_{norm} is a normalised contact distance.¹³ Intermolecular contacts are highlighted in the d_{norm} surface (when atoms make intermolecular contacts closer than the sum of their van der Waals radii, these contacts will be highlighted in red whereas longer contacts are blue, and contacts around the sum of van der Waals radii are white). Hirshfeld surfaces of complexes **7-9** have been mapped over d_{norm} (range of -0.1 to 1.5 Å) [Figure.III.C.12]. Red spots on these surfaces denote the dominant interactions [N⋯H/H⋯N, S⋯H/H⋯S and O⋯H/H⋯O]. As the Hirshfeld surface defines the shape of the molecule in terms of its surrounding crystalline environment, the local shape of the surface may provide some chemical insight whereas shape index is a qualitative measure of shape and can be sensitive to very subtle changes in surface shape, particularly in regions where the total curvature (or the curvedness) is very low.¹⁴

The 2D fingerprint plots,¹⁵ which are used to analyze the intermolecular contacts at the same time, revealed that the main intermolecular interactions in the complexes are S \cdots H/H \cdots S, N \cdots H/H \cdots N and O \cdots H/H \cdots O. Figure.III.C.13 represents the 2D plots of complexes **7**, **8** and **9**. The O \cdots H interactions are higher in complexes **8** and **9** compared to complex **7** due to the presence of acetate group which is absent in complex **7**. Complex **7** contains an extra thiocyanate which results in more S \cdots H (16.7%) interaction compared to the other ones.

Interesting Pb \cdots S and S \cdots S contacts (Figure.III.C.14) are observed in complexes **7** and **8**. These contacts are not present in isostructural complex **9**. It is due to the steric crowding of ethoxy group [compared to methoxy group (for complexes **7** and **8**)] which averts the sulphur atom of a thiocyanate to come in closer contact with the lead(II) center prevent such contacts. These contacts may lead to the formation of different unconventional supramolecular interactions which is quite fascinating. To investigate these, theoretical calculations have been done and the interaction energies have been calculated.

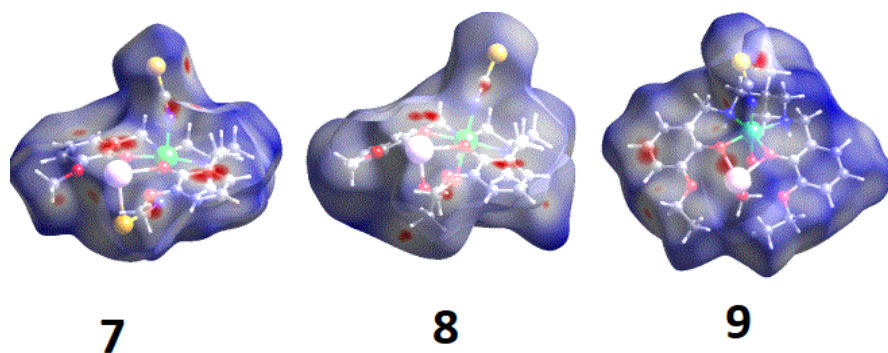


Fig.III.C. 12: Hirshfeld surfaces (d_{norm}) of complexes **7-9**.

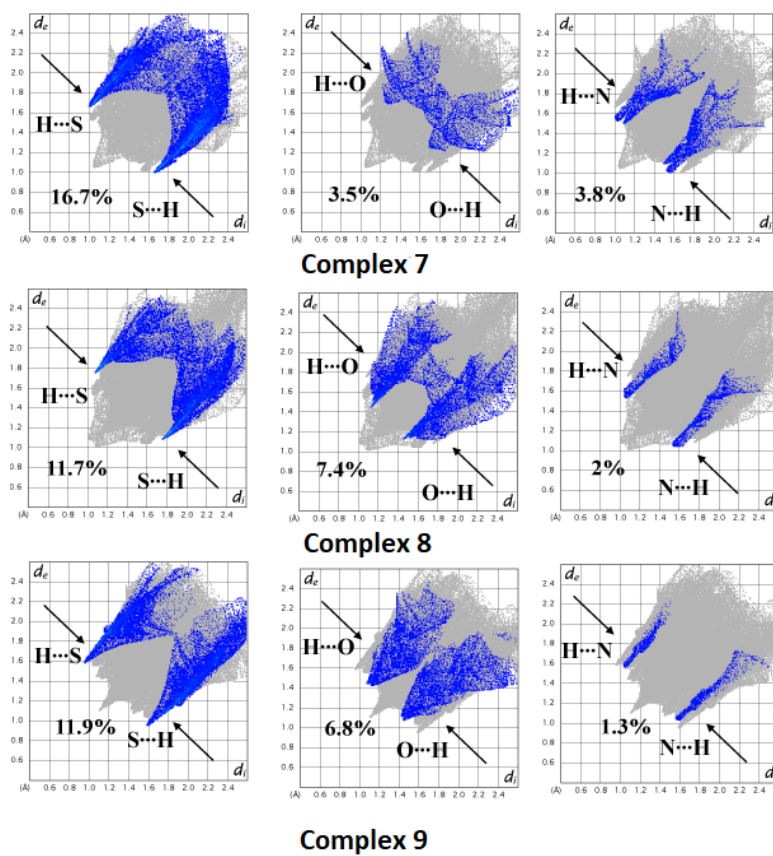


Fig. III.C.13: Fingerprint plots of complexes 7, 8 and 9.

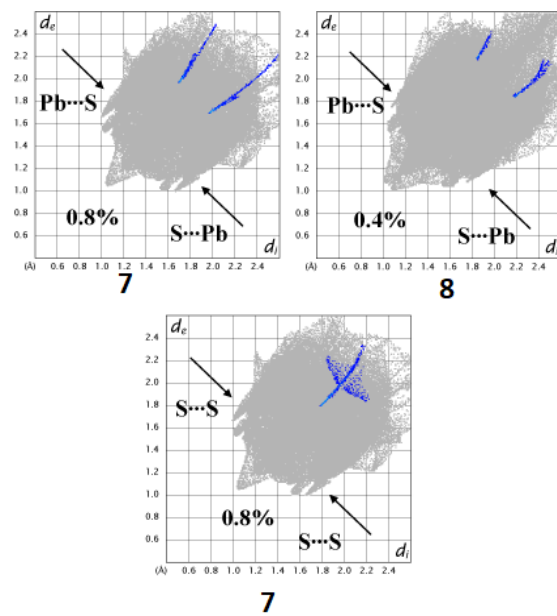


Fig.III.C.14: Fingerprint plot resolved into Pb...S/S...Pb and S...S/S...S contacts contributed to the total Hirshfeld Surface area of complexes **7** and **8**.

III.C. 4: Concluding remarks

In conclusion, syntheses and structural characterizations of three hetero-nuclear nickel(II)/lead(II) complexes with compartmental reduced Schiff base ligands have been reported where five membered Pb-chelate rings in the hemicoordinated complexes **7–9** play a relevant role. Moreover, supramolecular tetrel bonding interactions of these complexes have been investigated and the interaction energies calculated and characterized using NCI plot index. Remarkably, the combination of interactions observed in the π -stacking assembly in complex **7**, a pair of π - π (CR) interactions, is energetically equivalent to the formation of one π (CR)- π (CR) interaction and two cation- π interactions (or Pb... π tetrel bonds) observed in complex **8**.

References

- (1) Hancock, R. D.; Reibenspies, J. H.; Maumela, H. Structural Effects of the Lone Pair on Lead(II), and Parallels with the Coordination Geometry of Mercury(II). Does the Lone Pair on Lead(II) Form H-Bonds? Structures of the Lead(II) and Mercury(II) Complexes of the Pendant-Donor Macrocycle DOTAM(1,4,7,10-Tetrakis(carbamoylmethyl)-1,4,7,10-tetraazacyclododecane). *Inorg. Chem.* **2004**, *43*, 2981–2987.
- (2) Platas-Iglesias, C.; Esteban-Gomez, D.; Enriquez-Perez, T.; Avecilla, F.; de Blas A.; Rodriguez-Blas, T. Lead(II) Thiocyanate Complexes with Bibrachial Lariat Ethers: An X-ray and DFT Study. *Inorg. Chem.* **2005**, *44*, 2224–2233.
- (3) Reger, D. L.; Wright, T. D.; Little, C. A.; Lamba, J. J. S.; Smith, M. D. Control of the stereochemical Impact of the Lone Pair in Lead(II) Tris(pyrazolyl)methane Complexes. Improved Preparation of Na{B[3,5-(CF₃)₂C₆H₃]₄}. *Inorg. Chem.* **2001**, *40*, 3810–3814.
- (4) Fleischer, H.; Schollmeyer, D. Synthesis of and Structural Studies on Lead(II) Cysteamine Complexes. *Inorg. Chem.* **2004**, *43*, 5529–5536.
- (5) Zhang, L.; Qin, Y.-Y.; Li, Z.-J.; Lin, Q.-P.; Cheng, J.-K.; Zhang, J.; Yao, Y.-G. Topology Analysis and Nonlinear Optical-Active Properties of Luminescent Metal-Organic Framework Materials Based on Zinc/Lead Isophthalates. *Inorg. Chem.* **2008**, *47*, 8286–8293.
- (6) Olvera, A.; Shi, G.; Djieutedjeu, H.; Page, A.; Uher, C.; Kioupakis, E.; Poudeu, P. F. P. Pb₇Bi₄Se₁₃: A Lillianite Homologue with Promising Thermoelectric Properties. *Inorg. Chem.* **2015**, *54*, 746–755.
- (7) Cheng, F.; Liang, J.; Tao, Z.; Chen, J. Functional Materials for Rechargeable Batteries. *Adv. Mater.*, **2011**, *23*, 1695–1715.

- (8) Cheng, Y.; Emge, T. J.; Brennan, J. G. Pyridineselenolate Complexes of Tin and Lead: $\text{Sn}(2\text{-SeNC}_5\text{H}_4)_2$, $\text{Sn}(2\text{-SeNC}_5\text{H}_4)_4$, $\text{Pb}(2\text{-SeNC}_5\text{H}_4)_2$, and $\text{Pb}(3\text{-Me}_3\text{Si-2-SeNC}_5\text{H}_3)_2$. Volatile CVD Precursors to Group IV-Group VI Semiconductors. *Inorg. Chem.* **1996**, *35*, 342-346.
- (9) Randall, C. A.; Bhalla, A. S.; Shrout, T. R.; Cross, L. E. Classification and consequences of complex lead perovskite ferroelectrics with regard to B-site cation order. *J. Mater. Res.* **1990**, *5*, 829-834.
- (10) Masek, J. Electronic states in mixed (Cd, Pb)S semiconductors. *J. Phys. C: Solid State Phys.* **1988**, *21*, 2821-2827.
- (11) Guo, M.; Law, W.-C.; Liu, X.; Cai, H.; Liu, L.; Swihart, M. T.; Zhang, X.; Prasad, P. N. *Plasmonics* **2014**, *9*, 893-898.
- (12) Liu, T.-T.; Liang, J.; Huang, Y.-B.; Cao, R. A bifunctional cationic porous organic polymer based on a Salen-(Al) metalloligand for the cycloaddition of carbon dioxide to produce cyclic Carbonates. *Chem. Commun.* **2016**, *52*, 13288-13291.
- (13) Lyons, C. T.; Daniel, T.; Stack, P. Recent advances in phenoxyl radical complexes of salen-type ligands as mixed-valent galactose oxidase models. *Coord. Chem. Rev.*, **2013**, *257*, 528-540.
- (14) Cozzi, P. G. Metal-Salen Schiff base complexes in catalysis: practical aspects. *Chem. Soc. Rev.* **2004**, *33*, 410-421.
- (15) Baleizao, C.; Garcia, H. Chiral Salen Complexes: An Overview to Recoverable and Reusable Homogeneous and Heterogeneous Catalysts. *Chem. Rev.* **2006**, *106*, 3987-4043.
- (16) Constable, E. C.; Zhang, G.; Housecroft, C. E.; Zampese, J. A. Amalgamating metalloligands with coordination networks. *Dalton Trans.* **2010**, *39*, 1941-1947.

- (17) Abdel-Rahman, L. H.; Abu-Dief, A. M.; Abdel-Mawgoud, A. A. H. Development, structural investigation, DNA binding, antimicrobial screening and anticancer activities of two novel quaridentate VO(II) and Mn (II) mononuclear complexes. *JKSUS*. **2019**, 31, 52-60.
- (18) Abdel-Rahman, L. H.; Abu-Dief, A. M.; Aboelezb, M. O.; Abdel-Mawgoud, A. A. H. DNA interaction, antimicrobial, anticancer activities and molecular docking study of some new VO(II), Cr(III), Mn(II) and Ni(II) mononuclear chelates encompassing quaridentate imine ligand. *J. Photochem. Photobiol. B*. **2017**, 170, 271-285.
- (19) Abu-Dief, A. M.; Diaz-Torres, R.; Sanudo, E. C.; Abdel-Rahman, L. H.; Aliaga-Alcalde, N. Novel sandwich triple-decker dinuclear Nd^{III}-(bis-N,N'-p-bromo-salicylideneamine-1,2-diaminobenzene)complex. *Polyhedron* **2013**, 64, 203-208.
- (20) Roy, S.; Halder, S.; Drew, M. G. B.; Ray, P. P.; Chattopadhyay, S. Fabrication of an Active Electronic Device Using a Hetero-bimetallic Coordination Polymer. *ACS Omega* **2018**, 3, 12788–12796.
- (21) Thurston, J. H.; Tang, C. G.-Z.; Trahan, D. W.; Whitmire, K. H. Toward Rational Control of Metal Stoichiometry in Heterobimetallic Coordination Complexes: Synthesis and Characterization of Pb(Hsal)₂(Cu(salen*))₂, [Pb(NO₃)(Cu(salen*))₂](NO₃), Pb(OAc)₂(Cu(salen*)), and [Pb(OAc)(Ni(salen*))₂](OAc). *Inorg. Chem.* **2004**, 43, 2708-2713.
- (22) Bhattacharya, S.; Mohanta, S. Heterometallic copper(II)–lead(II), nickel(II)–lead(II) and copper(II)–indium(III) compounds derived from an acyclic double-compartment Schiff base ligand. *Inorg. Chim. Acta* **2015**, 432, 169-175.
- (23) Pitzer, K. S. Relativistic Effects on Chemical Properties. *Acc. Chem. Res.* **1979**, 12, 271–276.

- (24) Pyykkö, P.; Desclaux, J.-P. Relativity and the periodic system of elements. *Acc. Chem. Res.* **1979**, *12*, 276–281.
- (25) Pyykkö, P. Relativistic Effects in Structural Chemistry. *Chem. Rev.* **1988**, *88*, 563–594.
- (26) Sidgwick, N. V.; Powell, H. M. Bakerian Lecture: Stereochemical types and valency groups. *Proc. R. Soc. (London)*, **1940**, A176, 153.
- (27) Reger, D. L.; Huff, M. F.; Rheingold, A. L.; Haggert, B. S. Control of Structure in Lead(II) Complexes Using Poly(pyrazolyl)borate Ligands. Stereochemically Inactive Lone Pair in Octahedral $[\text{HB}(3,5\text{-Me}_2\text{pz})_3]_2\text{Pb}$ (pz = Pyrazolyl Ring). *J. Am. Chem. Soc.* **1992**, *114*, 579–584.
- (28) Gillespie, R. J.; Nyholm, R. S. Inorganic Stereochemistry. *Q. Rev. (London)*, **1957**, *11*, 339–380.
- (29) Luckay, R.; Cukrowski, I.; Mashishi, J.; Reibenspies, J. H.; Bond, A. H.; Rogers, R. D.; Hancock, R. D. Synthesis, stability and structure of the complex of bismuth(III) with the nitrogen-donor macrocycle 1,4,7,10-tetraazacyclododecane. The role of the lone pair on bismuth(III) and lead(II) in determining co-ordination geometry. *J. Chem. Soc. Dalton Trans.* **1997**, 901–908.
- (30) Walsh, A.; Watson, G. W. The origin of the stereochemically active Pb(II) lone pair: DFT calculations on PbO and PbS. *J. Solid State Chem.* **2005**, *178*, 1422–1428.
- (31) Hancock, R. D.; Shaikjee, M. S.; Dobson, S. M.; Boeyens, J. C. The Stereochemical Activity or Non-activity of the ‘Inert’ Pair of Electrons on Lead(II) in Relation to its Complex Stability and Structural Properties. Some Considerations in Ligand Design. *Inorg. Chim. Acta.* **1988**, *154*, 229–238.

- (32) Esteban-Gómez, D.; Platas-Iglesias, C.; Enriquez-Pérez, T.; Avecilla, F.; Blas, A.; Rodríguez-Blas, T. Lone-Pair Activity in Lead(II) Complexes with Unsymmetrical Lariat Ethers. *Inorg. Chem.* **2006**, *45*, 5407–5416.
- (33) Bauzá, A.; Mooibroek, T. J.; Frontera, A. Tetrel-Bonding Interaction: Rediscovered Supramolecular Force? *Angew. Chem. Int. Ed.* **2013**, *52*, 12317-12321.
- (34) Grabowski, S. J. Tetrel bond– σ -hole bond as a preliminary stage of the S_N^2 reaction. *Phys. Chem. Chem. Phys.* **2014**, *16*, 1824-1834.
- (35) Bauzá, A.; Mooibroek, T. J.; Frontera, A. Small Cycloalkane $(CN)_2C-C(CN)_2$ Structures Are Highly Directional Non-covalent Carbon-Bond Donors. *Chem. -Eur. J.* **2014**, *20*, 10245-10248.
- (36) Escudero-Adán, E. C.; Bauzá, A.; Frontera, A.; Ballester, P. Nature of Noncovalent Carbon-Bonding Interactions Derived from Experimental Charge-Density Analysis. *ChemPhysChem.* **2015**, *16*, 2530-2533.
- (37) Bauzá, A.; Mooibroek, T. J.; Frontera, A. Influence of ring size on the strength of carbon bonding complexes between anions and perfluorocycloalkanes. *Phys. Chem. Chem. Phys.* **2014**, *16*, 19192-19197.
- (38) Bauzá, A.; Mooibroek, T. J.; Frontera, A. Non-covalent sp^3 carbon bonding with $ArCF_3$ is analogous to $C-H\cdots\pi$ interactions. *Chem. Commun.* **2014**, *50*, 12626-12629.
- (39) Murray, J. S.; Lane, P.; Politzer, P. Expansion of the σ -hole concept. *J. Mol. Model.* **2009**, *15*, 723-729.

- (40) Bundhun, A.; Ramasami, P.; Murray, J. S.; Politzer, P. Trends in σ -hole strengths and interactions of F_3MX molecules ($M = C, Si, Ge$ and $X = F, Cl, Br, I$). *J. Mol. Model.* **2013**, *19*, 2739-2746.
- (41) Bauzá, A.; Mooibroek, T. J.; Frontera, A. Tetrel Bonding Interactions. *Chem. Rec.* **2016**, *16*, 473-487.
- (42) Gargari, M. S.; Stilinović, V.; Bauzá, A.; Frontera, A.; McArdle, P.; Derveer, D. V.; Ng, S. W.; Mahmoudi, G. Design of Lead(II) Metal–Organic Frameworks Based on Covalent and Tetrel Bonding, *Chem. Eur. J.* **2015**, *21*, 17951–17958.
- (43) Mahmoudi, G.; Zangrando, E.; Mitoraj, M. P.; Gurbanov, A. V.; Zubkov, F. I.; Moosavifar, M.; Konyaeva, I. A.; Kirillov, A. M.; Safin, D. A. Extended lead(II) architectures engineered *via* tetrel bonding interactions, *New J. Chem.*, 2018, *42*, 4959-4971.
- (44) Grabowski, S. J. Tetrel bonds, penta- and hexa-coordinated tin and lead centres, *Appl Organometal Chem.* 2017, *31*, e3727-e3737.
- (45) Hunter, C. A.; Sanders, J. K. M. The nature of pi-pi Interactions. *J. Am. Chem. Soc.* **1990**, *112*, 5525–5534.
- (46) Burley, S. K.; Petsko, G. A. Aromatic-aromatic interaction: a mechanism of protein structure stabilization. *Science*. **1985**, *229*, 23–28.
- (47) Kim, K. S.; Tarakeshwar, P.; Lee, J. Y. Molecular Clusters of π -Systems: Theoretical Studies of Structures, Spectra, and Origin of Interaction Energies. *Chem. Rev.* **2000**, *100*, 4145–4185.

- (48) Ma, J. C.; Dougherty, D. A. The Cation- π Interaction. *Chem. Rev.* **1997**, *97*, 1303–1324.
- (49) Kim, K. S.; Lee, J. Y.; Lee, S. J.; Ha, T.-K.; Kim, D. H. On Binding Forces between Aromatic Ring and Quaternary Ammonium Compound. *J. Am. Chem. Soc.* **1994**, *116*, 7399–7400.
- (50) Nishio, M.; Hirota, M.; Umezawa, Y. In the C-H/ π Interaction: Evidence, Nature, Consequences, *Wiley-VCH*, New York, **1998**.
- (51) Egli, M.; Sarkhel, S. Lone Pair-Aromatic Interactions: To Stabilize or Not to Stabilize. *Acc. Chem. Res.* **2007**, *40*, 197–205.
- (52) Mooibroek, T. J.; Gamez, P.; Reedijk, J. Lone pair- π interactions: a new supramolecular bond? *CrystEngComm.* **2008**, *10*, 1501–1515.
- (53) Sathiyaraj, E.; Thirumaran, S.; Selvanayagam, S.; Sridhar, B.; Ciattin, S. C-H \cdots Ni and C-H $\cdots\pi$ (chelate) interactions in nickel(II) complexes involving functionalized dithiocarbamates and triphenylphosphine. *J. Mol. Struct.* **2018**, *1159*, 156-166.
- (54) Roy, S.; Drew, M. G. B.; Bauzá, A.; Frontera, A.; Chattopadhyay, S. Non-covalent tetrel bonding interactions in hemidirectional lead(II) complexes with nickel(II)-salen type metalloligands, *New J. Chem.* **2018**, *42*, 6062-6076.
- (55) Roy, S.; Drew, M. G. B.; Bauzá, A.; Frontera, A.; Chattopadhyay, S. A Combined Experimental and Theoretical Study to Explore the Importance of σ -Hole Carbon Bonding Interactions in Stabilizing Molecular Assemblies. *ChemistrySelect.* **2017**, *2*, 10586–10594.

- (56) Mahmoudi, G.; Zaręba, J. K.; Bauzá, A.; Kubicki, M.; Bartyzel, A.; Keramidas, A. D.; Butusov, L.; Mirosław, B.; Frontera, A. Recurrent supramolecular motifs in discrete complexes and coordination polymers based on mercury halides: prevalence of chelate ring stacking and substituent effects. *CrystEngComm*. **2018**, *20*, 1065–1076.
- (57) Mahmoudi, G.; Khandar, A. A.; Afkhami, F. A.; Mirosław, B.; Gurbanov, A. V.; Zubkov, F. I.; Kennedy, A.; Franconetti, A.; Frontera, A. Modulation of coordination in pincer-type isonicotinohydrazone Schiff base ligands by proton transfer. *CrystEngComm*. **2019**, *21*, 108–117.
- (58) Tan, Y. S.; Halim, S. N. A.; Molloy, K. C.; Sudlow, A. L.; Otero-de-la-Roza, A.; Tiekink, E. R. T. Persistence of C–H \cdots π (chelate ring) interactions in the crystal structures of Pd(S₂COR)₂. The utility of Pd(S₂COR)₂ as precursors for palladium sulphide materials. *CrystEngComm*. **2016**, *18*, 1105–1117.
- (59) Mahmoudi, G.; Bauzá, A.; Gurbanov, A. V.; Zubkov, F. I.; Maniukiewicz, W.; Rodríguez-Diéguez, A.; López-Torres, E.; Frontera, A. The role of unconventional stacking interactions in the supramolecular assemblies of Hg(II) coordination compounds. *CrystEngComm*. **2016**, *18*, 9056–9066.
- (60) Karmakar, M.; Basak, T.; Chattopadhyay, S. Phosphatase-mimicking activity of a unique penta-nuclear zinc(II) complex with a reduced Schiff base ligand: assessment of its ability to sense nitroaromatics. *New J. Chem.* **2019**, *43*, 4432–4443.

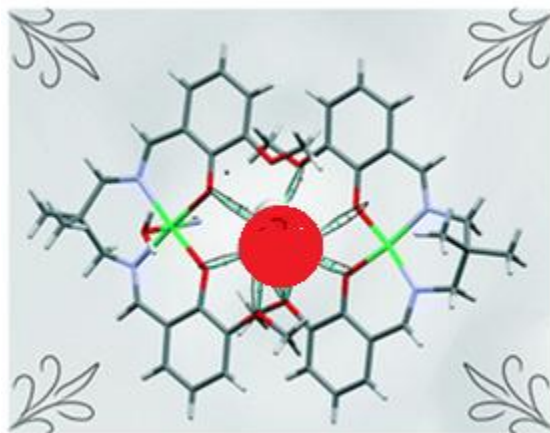
- (61) Karmakar, M.; Roy, S.; Chattopadhyay, S. A series of trinuclear zinc(II) complexes with reduced Schiff base ligands: turn-off fluorescent chemosensors with high selectivity for nitroaromatics. *New J. Chem.* **2019**, *43*, 10093–10102.
- (62) Mirdya, S.; Basak T.; Chattopadhyay, S. Photocatalytic ability of two hetero-tetranuclear complexes with CuO₂Cd cores to degrade methylene blue: Influence of their structures on activity. *Polyhedron*. **2019**, *170*, 253–263.
- (63) Addison, A. W.; Rao, T. N.; Reedijk, J.; Rijn, J. V.; Verschoor, G. C. Synthesis, Structure, and Spectroscopic Properties of Copper(II) Compounds containing Nitrogen-Sulphur Donor Ligands; the Crystal and Molecular Structure of Aqua[I,7-bis(N-methylbenzimidazol-2'-yl)-2,6-dithiaheptane]copper(ii) Perchlorate. *J. Chem. Soc., Dalton Trans.* **1984**, 1349-1356.
- (64) Mautner, F.; Scherzer, M.; Berger, C.; Fischer, R. C.; Vicente, R.; Massoud, S. S. Synthesis and characterization of five new thiocyanate- and cyanato-metal(II) complexes with 4-azidopyridine as co-ligand. *Polyhedron*. **2015**, *85*, 20–26.
- (65) Das, M.; Chatterjee, S.; Harms, K.; Mondal, T. K.; Chattopadhyay, S. Formation of bis(μ -tetrazolato)dinickel(II) complexes with N,N,O-donor Schiff bases via in situ 1,3-dipolar cyclo-additions: isolation of a novel bi-cyclic trinuclear nickel(II)–sodium(I)–nickel(II) complex. *Dalton Trans.* **2014**, *43*, 2936–2947.
- (66) Roy, S.; Basak, T.; Khan, S.; Drew, M. G. B.; Bauzá, A.; Frontera, A.; Chattopadhyay, S. A Combined Experimental and Theoretical Study on the Formation of a Cyclic Tetrameric Water Cluster and a Similar Type of Cyclic Cluster in Copper(II) Schiff Base Complexes. *ChemistrySelect*, **2017**, *2*, 9336–9343.

- (67) Chattopadhyay, S.; Drew, M. G. B.; Ghosh, A. Methylene Spacer-Regulated Structural Variation in Cobalt(II/III) Complexes with Bridging Acetate and Salen- or Salpn-Type Schiff-Base Ligands. *Eur. J. Inorg. Chem.* **2008**, 1693–1701.
- (68) Nakamoto, K. *Infrared and Raman Spectra of Organic and Coordination Compounds*. John Wiley and Sons, New York, 3rd edn, **1978**, p. 227.
- (69) Bhowmik, P.; Harms, K.; Chattopadhyay, S. Formation of polynuclear copper(II)–sodium(I) heterometallic complexes derived from salen-type Schiff bases. *Polyhedron*. **2013**, *49*, 113–120.
- (70) Agarwal, R. K.; Kumar, A. Synthesis, Physico-chemical and Biological Properties of Some Mixed Ligand Complexes of Trivalent Lanthanides with 4[N-4'-Dimethylamino-Benzalidene)Amino] antipyrine Thiosemicarbazone and Pyridine. *J. Appl. Chem. Res.* **2011**, *16*, 40-58.
- (71) Nazarov, M.; Noh, D. Y. *New Generation of Europium and Terbium-Activated Phosphors: From Syntheses to Applications*. Pan Stanford Publishing, 6000 Broken Sound Pkwy NW. **2011**, p. 211.
- (72) Roy, S.; Drew, M. G. B.; Bauzá, A.; Frontera, A.; Chattopadhyay, S. Estimation of conventional C–H \cdots π (arene), unconventional C–H \cdots π (chelate) and C–H \cdots π (thiocyanate) interactions in hetero-nuclear nickel(II)–cadmium(II) complexes with a compartmental Schiff base. *Dalton Trans.* **2017**, *46*, 5384–5397.
- (73) Bhattacharyya, A.; Bhaumik, P. K.; Jana, P. P.; Chattopadhyay, S. Anion mediated diversity in the nuclearity of nickel(II) complexes with a N₂O donor Schiff base: Formation of a supra-molecular chain via Br \cdots Br interactions. *Polyhedron*. **2014**, *78*, 40–45.

- (74) Mahmoudi, G.; Bauzá, A.; Frontera, A. Concurrent agostic and tetrel bonding interactions in lead(II) complexes with an isonicotinohydrazide based ligand and several anions. *Dalton Trans.* **2016**, *45*, 4965–4969.
- (75) Mustapha, A.; Busch, K.; Patykiewicz, M.; Apedaile, A.; Reglinski, J.; Kennedy, A. R.; Prior, T. J. Multidentate ligands for the synthesis of multi-metallic complexes. *Polyhedron* **2008**, *27*, 868–878.
- (76) Bauzá, A.; Seth, S. K.; Frontera, A. Tetrel bonding interactions at work: Impact on tin and lead coordination compounds. *Coord. Chem. Rev.* **2019**, *384*, 107–125.
- (77) Mahmoudi, G.; Safin, D. A.; Mitoraj, M. P.; Amini, M.; Kubicki, M.; Doert, T.; Locherere, F.; Fleck, M. Anion-driven tetrel bond-induced engineering of lead(II) architectures with N'-(1-(2-pyridyl)ethylidene)nicotinohydrazide: experimental and theoretical findings. *Inorg. Chem. Front.* **2017**, *4*, 171–182.
- (78) Mahmoudi, G.; Bauzá, A.; Frontera, A. Concurrent agostic and tetrel bonding interactions in lead(II) complexes with an isonicotinohydrazide based ligand and several anions. *Dalton Trans.* **2016**, *45*, 4965–4969.

Chapter IV

Two trinuclear complexes with $\text{Pb}(\text{O}_2\text{Ni})_2$ cores



IV.1. Introduction

Several transition and non-transition metal complexes were synthesized by different synthetic inorganic chemists using varieties of chelating ligands [1–19]. Among them, ‘salen type’ N,O-donor salicylaldimine Schiff bases are very popular probably for their easy synthetic routes and wide-ranging stability [20–29]. We have written a series of reviews on the synthetic strategy, structures and applications of transition and non-transition metal complexes with these ‘salen type’ Schiff bases [30–34]. On the other hand, the symmetrical Schiff bases derived from 2-pyridyl carbonyl compounds are also stable in wide range of oxidizing and reducing conditions; and they have also been used since long for the synthesis of complexes of different transition and non-transition metals [35–63]. In this review we would like to discuss only the synthesis, structure and properties of lead(II) and mercury(II) complexes. Both lead and mercury are very toxic and their application in material science is limited. Metallic lead is extensively used in car batteries, grenades, cable covering, lead crystal glass, radiation protection etc. It is sometimes used to store corrosive liquids. Mercury is widely used in thermometers, barometers, etc. Although many other liquids could also be used in these devices, mercury is used because its high density requires less space. Mercury is also a good conductor of electricity, and hence is used in electrical switches. Lead(II) and mercury(II) complexes are synthesized mainly for academic interest as they may show interesting non-covalent interactions in their solid state structures (*vide infra*). Lead(II) is an element of group 14 (and therefore is a congener of C), but the most stable oxidation state of lead is +2 because of the inert pair effect, which stabilizes 6s² electrons of lead. The geometric and electronic structures of lead(II) compounds are greatly influenced by the presence of this inert pair of

electrons [64–70,38,71–80]. Two types of geometries are possible for lead(II) complexes, e.g. (i) holo-directed {in which the bonds of lead(II) centre to donor atoms are symmetrically distributed throughout the surface of an surrounding sphere} and (ii) homo-directed {in which the bonds of lead(II) centre to ligand atoms are distributed only throughout a hemisphere producing a clear void around lead (II)} [81]. Hemi-directed geometry has been observed for relatively lower coordination number (i.e. 2-5) of lead(II). On the other hand, holo-directed geometries are found for higher coordination numbers (viz. nine and ten). For the intermediate coordination numbers, six to eight, any one of the two geometries are possible. In the solid state structure of these complexes, σ -hole interactions (a non-covalent interaction between the σ -hole, created on lead(II), and the electron rich atoms of the species) are frequently present. This is sometimes referred to as tetrel bonding interactions [82–85]. Similar σ -hole interaction involving mercury(II) (or any other group 12 element) is called spodium bond [86,87]. This type of σ -hole interaction is however not specific for lead and mercury, as similar interactions are also found in the solid state structures for the complexes of group 6 (called wolfium bond) [88], Group 7 (called matere bond) [89], group 8 (called osme bonds) [90], Group 15 (called pnictogen bond) [91], group 11 elements (called coinage bonds) also [92]. The increase in polarizability of the metal center increases the size and electron deficiency of σ -holes, thereby enhancing their importance in crystal engineering.

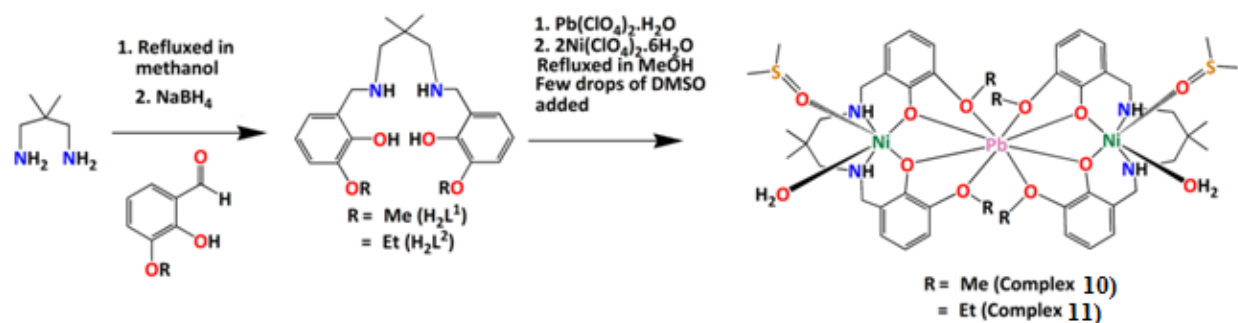
In the present work, two $N_2O_2O'_2$ donor compartmental reduced Schiff bases, 2,2'-[(2,2-dimethyl-1,3-propanediyl)bis(iminomethylene)]bis[6-methoxy-phenol] (H_2L^1) and 2,2'-[(2,2-dimethyl-1,3-propanediyl)bis(iminomethylene)]bis[6-ethoxy-phenol] (H_2L^2) were used to prepare two hetero-nuclear nickel(II)/lead(II) complexes, $\{[(DMSO)(H_2O)NiL^1]_2Pb\}(ClO_4)_2$ (**10**)

$[(\text{DMSO})(\text{H}_2\text{O})\text{NiL}^2]_2\text{Pb}](\text{ClO}_4)_2 \cdot 4\text{DMSO}$ (**11**). Their structures have been determined by single crystal X-ray diffraction analyses. The lead centres in complexes **10-11** are hemidirectionally coordinated and participates in non-covalent tetrel bonding interactions. Moreover, supramolecular interactions were studied by means of DFT calculations focusing our attention on $\text{Pb}\cdots\text{S}$ and $\text{Pb}\cdots\pi$ tetrel bonds observed in the solid state architecture of complexes **10-11**. Furthermore, π -stacking assemblies between aromatic rings and five-membered Pb-chelate rings were detected and studied both with regard to their energies and by using the non-covalent (NCI) plot index. In complexes **10** and **11** the lead centres are holodirected resulting in different trinuclear structures where interesting hydrogen bonding has been observed with non-coordinated perchlorates.

IV.2. Results and discussion

IV.2.1. Synthesis

2, 2-dimethyl-1, 3-diaminopropane was refluxed with 3-methoxysalicylaldehyde and 3-ethoxysalicylaldehyde in 1:2 ratio respectively, followed by the addition of NaBH_4 to form two $\text{N}_2\text{O}_2\text{O}'_2$ donor compartmental reduced Schiff bases (H_2L^1 and H_2L^2) following standard literature methods.⁹³⁻⁹⁵ These ligands (H_2L^1 and H_2L^2) on reaction with different ratios of nickel(II) and lead(II) salts in different solvents produced the complexes. Formation of complexes **10-11** has been shown in Scheme IV.1.



Scheme IV.1: Synthetic route to complexes **10-11**. Lattice solvent molecules have been omitted for clarity.

IV.2.2. Description of $[\{(\text{DMSO})(\text{H}_2\text{O})\text{NiL}^1\}_2\text{Pb}](\text{ClO}_4)_2$ (**10**) and $[\{(\text{DMSO})(\text{H}_2\text{O})\text{NiL}^2\}_2\text{Pb}](\text{ClO}_4)_2 \cdot 4\text{DMSO}$ (**11**)

The asymmetric unit of complex **10** contains hetero-trinuclear $[\{(\text{DMSO})(\text{H}_2\text{O})\text{NiL}^1\}_2\text{Pb}]$ dication with two non-coordinating perchlorate anions (Fig. IV.1a). The oxygen atoms, O(13), O(15) and O(17), O(19) of two non-coordinated perchlorates are disordered in complex **10**. Two sets of positions; (O13A, O13B), (O15A, O15B) and (O17, O17A), (O19, O19A) were refined with occupancies of x and $1-x$, respectively with $x = 0.712$. Complex **11** is centrosymmetric and contains hetero-trinuclear $[\{(\text{DMSO})(\text{H}_2\text{O})\text{NiL}^1\}_2\text{Pb}]$ dication with two non-coordinating perchlorate anions along with four lattice DMSO molecules (Fig. IV.1b). Crystallographic data and refinement details of both complexes are provided in Table IV.1. Important bond lengths are summarized in Tables IV.2.

Table IV.1: Crystal data and refinement details of complexes **10** and **11**.

Complex	4	5
---------	---	---

Formula	C ₄₆ H ₇₂ PbNi ₂ N ₄ O ₂₀ S ₂ Cl ₂	C ₅₈ H ₁₀₄ PbNi ₂ N ₄ O ₂₄ S ₆ Cl ₂
Formula Weight	1460.68	1829.29
Temperature (K)	150	150
Crystal system	Monoclinic	Monoclinic
Space group	<i>P2₁/c</i>	<i>I2/a</i>
a(Å)	13.3953(11)	17.9651(16)
b(Å)	24.316(2)	17.7582(14)
c(Å)	18.4399(16)	26.3234(17)
β	91.537(3)	105.848(5)
Z	4	4
<i>d</i> _{calc} (g cm ⁻³)	1.616	1.504
μ(mm ⁻¹)	3.648	2.831
<i>F</i> (000)	2960	3760
Total Reflections	73608	47959
Unique Reflections	10905	7149
Observed data [<i>I</i> > 2 σ (<i>I</i>)]	8275	6210
No. of parameters	741	454
R(int)	0.068	0.079
R1,wR2(all data)	0.0590, 0.0937	0.0566, 0.1378
R1,wR2 [<i>I</i> > 2 σ(<i>I</i>)]	0.0369, 0.0820	0.0471, 0.1301
CCDC	1938679	1938680

Table IV.2: Selected bond lengths (Å) of complexes **10** and **11**.

Complex	10	11	Complex	10	11
Pb(1)–O(1)	2.434(3)	2.430(4)	Pb(1)–O(7)	2.460(3)	-
Pb(1)–O(2)	2.418(3)	2.444(4)	Pb(1)–O(8)	2.445(3)	-
Pb(1)–O(3)	2.696(4)	2.869(5)	Pb(1)–O(9)	2.921(5)	-

Pb(1)–O(4)	2.873(4)	2.954(5)	Pb(1)–O(10)	2.742(4)	-
Ni(1)–O(1)	2.100(3)	2.135(4)	Ni(2)–O(7)	2.030(3)	-
Ni(1)–O(2)	2.001(3)	2.016(4)	Ni(2)–O(8)	2.082(3)	-
Ni(1)–N(1)	2.062(4)	2.060(5)	Ni(2)–O(11)	2.128(4)	-
Ni(1)–N(2)	2.073(5)	2.075(6)	Ni(2)–O(12)	2.099(3)	-
Ni(1)–O(5)	2.108(4)	2.095(4)	Ni(2)–N(3)	2.073(4)	-
Ni(1)–O(6)	2.106(3)	2.130(4)	Ni(2)–N(4)	2.078(4)	-

$\text{N}_2\text{O}_2\text{O}'_2$ donor compartmental reduced Schiff bases (H_2L^1 and H_2L^2) were used to prepare complexes **10** and **11** respectively in which nickel(II) centres are placed in the inner N_2O_2 cavities. The nickel(II) centres [Ni(1) and Ni(2) for complex **10** and Ni(1) and Ni(1)^m for complex **11**, where ^m=½-x, y, 1-z] are coordinated with two amine nitrogen atoms [N(1), N(2) for Ni(1); N(3), N(4) for Ni(2) in complex **10** and N(1), N(2) for Ni(1); N(1)^m, N(2)^m for Ni(1)^m in complex **11**] and two phenoxo oxygen atoms [O(1), O(2) for Ni(1); O(7), O(8) for Ni(2) in complex **10** and O(1), O(2) for Ni(1); O(1)^m, O(2)^m for Ni(1)^m in complex **11**] of the deprotonated reduced Schiff base ligands. The fifth site is coordinated by an oxygen atom [being O(5) for Ni(1); O(11) for Ni(2) in complex **10** and O(5) for Ni(1); O(5)^m for Ni(1)^m of complex **11**] from water molecules. Another oxygen atom [O(6) for Ni(1); O(12) for Ni(2) of complex **10** and O(6) for Ni(1); O(6)^m for Ni(1)^m of complex **11**] from DMSO molecules coordinated with the nickel(II) centers to fulfil their distorted octahedral geometries. Deviations of the coordinating atoms from the mean equatorial planes passing through them and those of the nickel(II) centres from the same planes in complexes **10** are listed in Table IV.3.

Table IV.3: Deviation of coordinating atoms along with nickel(II) from the least square mean plane passing through them in complex **10**.

Deviations of atoms in Å					
Complex	O(1)	O(2)	N(1)	N(2)	Ni(1)
10	0.088(3)	-0.093(3)	-0.080(5)	0.079(5)	0.0065(5)
Deviations of atoms in Å					
Complex	O(7)	O(8)	N(3)	N(4)	Ni(2)
10	0.069(3)	-0.061(3)	-0.055(4)	0.062(4)	-0.0138(5)

The central lead(II) is octa-coordinated by four phenoxy oxygen atoms, [O(1), O(2), O(7), O(8) in case of complex **10** and O(1), O(2), O(1)^m, O(2)^m for complex **11**] and four alkoxy [methoxy in case of complex **10** and ethoxy for complex **11**] oxygen atoms, [O(3), O(4), O(9), O(10) for complex **10** and O(3), O(4), O(3)^m, O(4)^m for complex **11**] of two deprotonated reduced Schiff base ligands assuming bicapped trigonal prismatic geometry (Fig. IV.2). In each complex, the lead(II) centre is crammed between two {(DMSO)(H₂O)NiL^{*}} [where L^{*} = L¹ (for complex **10**) and L² (for complex **11**)] moieties forming a sandwich-type configuration.⁹⁶ The Pb-O(phenoxy) distances [2.460(4)–2.418(4) Å] are smaller compared to the Pb-O(methoxy) distances [2.954(5)–2.696(5) Å]. Distances between the metal centres are ~3.564 Å for Pb(1)-Ni(1) and ~3.575 Å for Pb(1)-Ni(2). The angles, Ni(1)-O(1)-Pb(1), Ni(1)-O(2)-Pb(1), Ni(2)-O(7)-Pb(1) and Ni(2)-O(8)-Pb(1) are with the range of 102-107°. In complex **10**, Ni(1)O(1)Pb(1)O(2) and Ni(2)O(7)Pb(1)O(8) dihedral angles are 4.05(12)° and -2.30(10)° respectively. The angle between Ni(1)O(1)O(2)Pb(1) and Ni(2)O(7)O(8)Pb(1) cores is 79.77(11)°. In complex **11**,

Ni(1)O(1)Pb(1)O(2) dihedral angle is $-7.63(13)^\circ$. The angle between Ni(1)O(1)O(2)Pb(1) and Ni(1)^mO(1)^mO(2)^mPb(1) [where ^m= $\frac{1}{2}$ -x, y, 1-z] cores is measured to be $72.75(13)^\circ$.

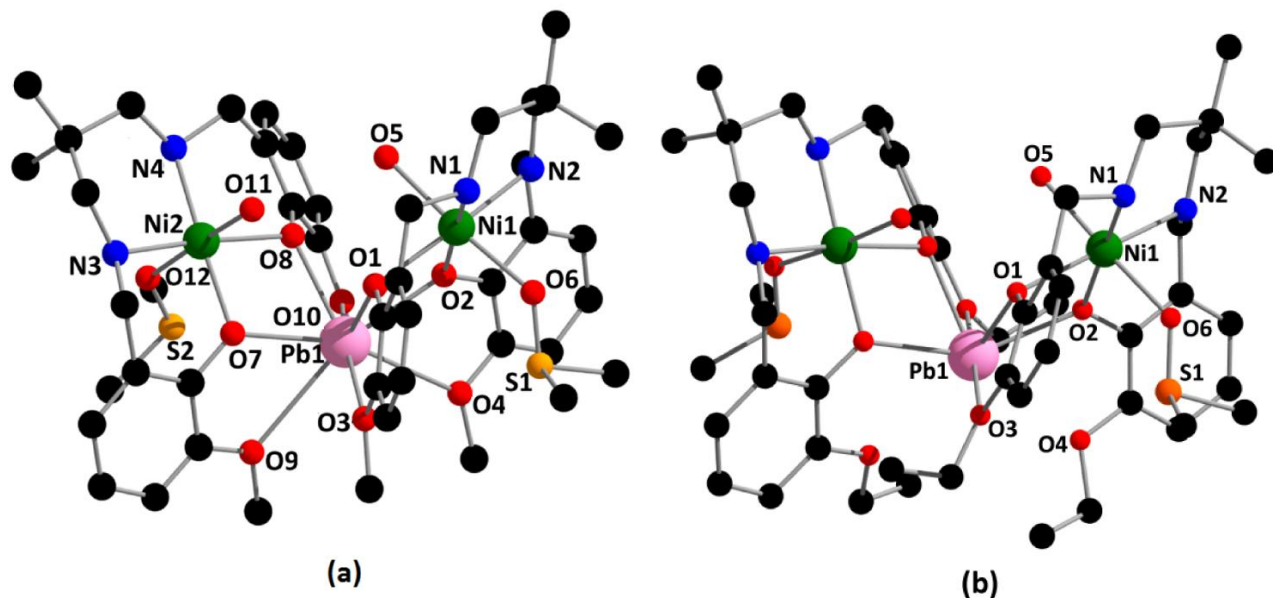


Fig. IV.1. Perspective view of complexes (a) **10** and (b) **11** with selective atom numbering scheme. Hydrogen atoms, perchlorate ion and the non-coordinating solvent molecules have been omitted for clarity.

The saturated six membered chelate rings, Ni(1)–N(1)–C(9)–C(10)–C(13)–N(2) and Ni(2)–N(3)–C(32)–C(33)–C(36)–N(4) in complex **10** has envelope conformations with puckering parameters⁹⁸⁻⁹⁹ $q=0.566(6)$ Å; $\theta=167.5(6)^\circ$; $\phi=14(3)^\circ$ and $q=0.552(5)$ Å; $\theta=19.5(4)^\circ$; $\phi=169(15)^\circ$, respectively. Similarly, the saturated six membered chelate ring, Ni(1)–N(1)–C(10)–C(11)–C(14)–N(2) also has envelope conformation with puckering parameters⁹⁸⁻⁹⁹ $q=0.573(7)$ Å; $\theta=8.6(6)^\circ$; $\phi=175(5)^\circ$ in complex **11**.

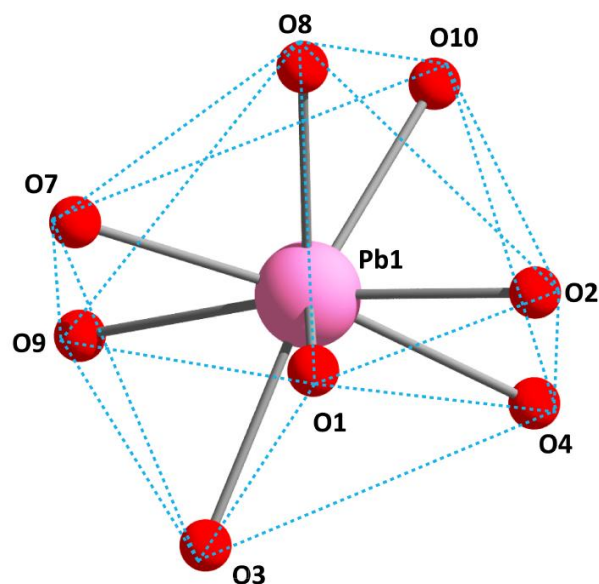


Fig. IV.2. Perspective view of the bicapped trigonal prismatic geometry around lead(II) in complex **10**.

IV.2.3. IR, electronic spectra and PXRD

A broad band around 3400 cm^{-1} indicates the presence of coordinated water in complex **10**.¹⁰⁰⁻¹⁰¹ A strong band in the range of $1085\text{-}1011\text{ cm}^{-1}$ indicates the presence of perchlorate ions in complex **11**.¹⁰²

The electronic spectrum of each complex in acetonitrile displays three bands around 242 nm, 285 nm and 600 nm. The absorption around $\sim 242\text{ nm}$ and $\sim 285\text{ nm}$ may be assigned to charge transfer transitions¹⁰³⁻¹⁰⁴ whereas the band around $\sim 600\text{ nm}$ could be assigned to d-d transition.¹⁰⁵

Experimental PXRD patterns of the bulk products are in good agreement with simulated XRD patterns from single crystal X-ray diffraction results, indicating consistency in bulk samples.

The simulated patterns of the complexes are calculated from the single crystal structural datas (CIF) using the CCDC Mercury software.

IV.2.4. Supramolecular interactions

The solid state structures of the complexes are stabilized through various non-covalent interactions (e.g. hydrogen bonding, C-H \cdots π , $\pi\cdots\pi$, cation $\cdots\pi$ interactions etc). The complexes were prepared while changing the ligand moieties along with bridging ligands which result in five different nickel(II)/lead(II) complexes. These trivial changes in ligand moieties along with bridging ligands play significant roles in the formation of diverse molecular architectures. Different supramolecular interactions are discussed below in the light of hirshfeld surface analyses.

In complex **10**, the hydrogen atoms, H(5A), attached to oxygen atom, O(5), and H(11O), attached to oxygen atom, O(11), are hydrogen bonded with oxygen atoms, O(14) and O(13B) respectively of a perchlorate anion. Similarly, the hydrogen atoms, H(5B), attached to oxygen atom, O(5) and H(11), attached to oxygen atom, O(11), are involved in hydrogen bonding interactions with phenoxo oxygen atoms, O(8) and O(1), respectively of the reduced Schiff base ligand as shown in Fig. IV.3. Additionally, the hydrogen atom, H(4N), attached to nitrogen atom, N(4), is engaged in symmetry related $[2-x, 1/2+y, 1/2-z]$ hydrogen bonding interaction with the oxygen atom, O(17), of a perchlorate anion (Fig. IV.3). A weak hydrogen bonding interaction is also observed between the hydrogen atom, H(1N), attached to nitrogen atom, N(1), with a symmetry $(-1+x, y, z)$ related oxygen atom, O(18), of a perchlorate anion. Details of the geometric features of the hydrogen bonding interactions are summarized in Table IV.4.

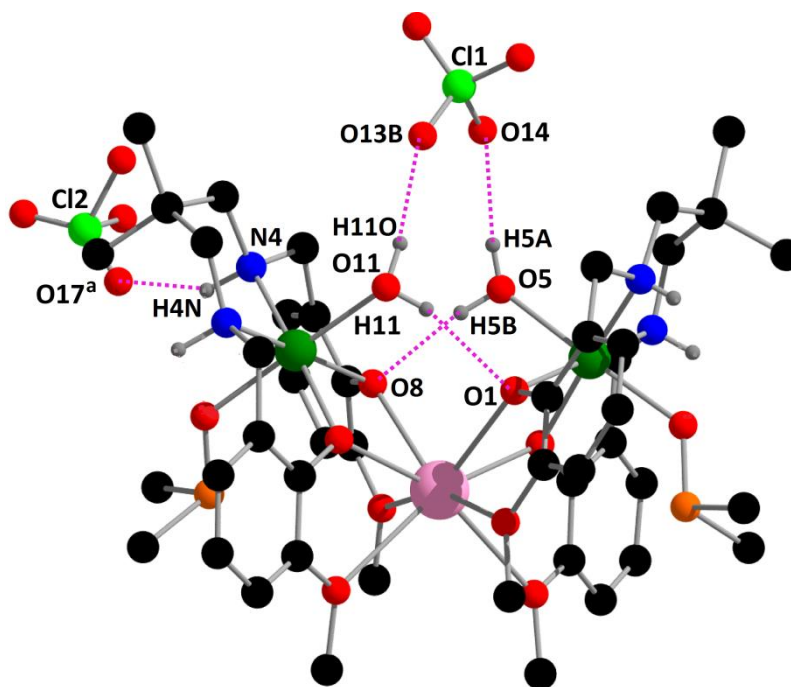


Fig. IV.3. Hydrogen bonding interactions in complex **10**. Only the relevant atoms have been shown for clarity. Symmetry transformations ^a = 2-x, 1/2+y, 1/2-z.

Table IV.4: Geometric features (distances in Å and angles in°) of the hydrogen bonding interactions obtained for complex **10**.

Complex	D–H···A	D–H	H···A	D···A	∠D–H···A
4	O(5)–H(5A)···O(14)	0.81(7)	2.04(7)	2.836(7)	168(5)
	O(5)–H(5B)···O(8)	0.84(4)	1.99(3)	2.815(5)	167(3)
	O(11)–H(H11O)···O(13B)	0.73(5)	2.13(5)	2.840(14)	163(6)
	O(11)–H(H11)···O(1)	0.84(4)	2.09(3)	2.917(6)	170(3)
	N(4)–H(4N)···O(17) ^a	1(4)	2.24(8)	3.119(9)	146(3)

	N(1)–H(1N)···O(18) ^b	0.82(5)	2.86(5)	3.526(1)	140(4)
--	---------------------------------	---------	---------	----------	--------

Symmetry transformations ^a=2-x, 1/2+y, 1/2-z; ^b = -1+x, y, z.

Five C–H··· π interactions are also observed in complex **10**. The hydrogen atom, H(23A), attached to the carbon atom C(23), is involved in an inter-molecular C–H··· π interaction with a symmetry related (x,1/2-y,1/2+z) phenyl ring [C(25)–C(26)–C(27)–C(28)–C(29)–C(30)] to form a supramolecular zigzag structure (Fig. S6, SI). Hydrogen atoms, H(22C), H(23B), H(45B) and H(46C), attached to carbon atoms, C(22), C(23), C(45) and C(46) respectively are involved in intra-molecular C–H··· π interactions with the phenyl ring [C(2)–C(3)–C(4)–C(5)–C(6)–C(7)], [C(15)–C(16)–C(17)–C(18)–C(19)–C(20)], [C(25)–C(26)–C(27)–C(28)–C(29)–C(30)] and [C(38)–C(39)–C(40)–C(41)–C(42)–C(43)], respectively. The details of the geometric features of the C–H··· π interactions have been gathered in Table IV.5.

Complex **11** also shows three C–H··· π interactions. The hydrogen atom, H(1A), attached to carbon atom, C(1), is involved in a C–H··· π interaction with symmetry related (1/2-x,y,1-z) phenyl ring [C(16)–C(17)–C(18)–C(19)–C(20)–C(21)]. The hydrogen atom, H(24C) and H(25A), attached to carbon atom, C(24) and C(25), respectively, are involved in intra-molecular C–H··· π interactions with phenyl rings [C(16)–C(17)–C(18)–C(19)–C(20)–C(21)] and [C(3)–C(4)–C(5)–C(6)–C(7)–C(8)] respectively. Details of the geometric features of the C–H··· π interactions have been gathered in Table IV.5.

Table IV.5: Geometric features (distances in Å and angles in °) of the C–H··· π interactions for complexes **10** and **11**.

Complex	C–H...Cg (Ring)	H...Cg (Å)	C–H...Cg (°)	C...Cg (Å)
10	C(22)-H(22C)...Cg(7)	2.88	145	3.726(8)
	C(23)-H(23A)...Cg(9) ^a	2.89	172	3.864(8)
	C(23)-H(23B)...Cg(8)	2.94	152	3.837(8)
	C(45)-H(45B)...Cg(9)	2.98	156	3.897(7)
	C(46)-H(46C)...Cg(10)	2.85	143	3.685(6)
11	C(1)-H(1A)...Cg(5) ^b	2.94	127	3.612(11)
	C(24)-H(24C)...Cg(5)	2.61	148	3.482(9)
	C(25)-H(25A)...Cg(4)	2.86	148	3.729(10)

Symmetry transformations; ^a = x, 1/2-y, 1/2+z and ^b = 1/2-x, y, 1-z .

IV.3. Concluding remarks

In conclusion, syntheses and structural characterizations of five hetero-nuclear nickel(II)/lead(II) complexes with compartmental reduced Schiff base ligands have been reported where C-H... π interactions are commonly observed in complexes **10** and **11**. Finally, the results reported herein stress on the importance of π -interactions involving chelate ring in crystal engineering in addition to the tetrel bonds involving hemicoordinated lead(II).

Reference

- [1] P. Ghorai, A. Chakraborty, A. Panja, T.K. Mondal, A. Saha, *RSC adv.* 6 (2016) 36020–36030.
- [2] T.K. Ghosh, S. Jana, S. Jana, A. Ghosh, *New J. Chem.* 44 (2020) 14733–14743.
- [3] R. Ghosh, S.H. Rahaman, G.M. Rosair, B.K. Ghosh, *Inorg. Chem. Commun.* 10 (2007) 61–65.
- [4] P.K. Dhara, S. Pramanik, T.H. Lu, M.G.B. Drew, P. Chattopadhyay, *Polyhedron* 23 (2004) 2457–2464.
- [5] S. Goswami, G. Leitus, B.K. Tripuramallu, I. Goldberg, *Cryst. Growth Des.* 17 (2017) 4393–4404.
- [6] S. Chattopadhyay, G. Bocelli, A. Musatti, A. Ghosh, *Inorg. Chim. Acta* 9 (2006) 1053–1057.
- [7] S. Biswas, A. Adhikary, S. Goswami, S. Konar, *Dalton Trans.* 42 (2013) 13331–13334.
- [8] A. Bhunia, E. Zangrando, S. Khatua, S.C. Manna, *J. Mol. Struct.* 1267 (2022) 133562.
- [9] S. Kulovi, L. Nandi, H. Puschmann, E. Zangrando, S. Dalai, *ChemistrySelect* 6 (2021) 8950–8958.
- [10] T. Basak, K. Ghosh, S. Chattopadhyay, *Polyhedron* 146 (2018) 81–92.
- [11] F. Haque, A. Halder, S. Ghosh, D. Ghoshal, *Polyhedron* 161 (2019) 289–297.
- [12] S. Roy, S. Pramanik, T. Ghorui, S. Dinda, S.C. Patra, K. Pramanik, *New J. Chem.* 42 (2018) 5548–5555.
- [13] S. Chattopadhyay, M.G.B. Drew, C. Diaz, A. Ghosh, *Dalton Trans.* (2007) 2492–2494.

- [14] R. Naskar, S. Sinhababu, A. Majumder, R. Maity, *ChemistrySelect* 7 (2022) e202201615.
- [15] R. Modak, Y. Sikdar, S. Mandal, C.J. Gómez-García, S. Benmansour, S. Chatterjee, S. Goswami, *Polyhedron* 70 (2014) 155–163.
- [16] M. Yadav, A. Bhunia, S.K. Jana, P.W. Roesky, *Inorg. Chem.* 55 (2016) 2701–2708.
- [17] M. Das, S. Chatterjee, K. Harms, T.K. Mondal, S. Chattopadhyay, *Dalton Trans.* 43 (2014) 2936–2947.
- [18] P. Mahata, G. Sankar, G. Madras, S. Natarajan, *Chem. Commun.* (2005) 5787–5789.
- [19] S. Chattopadhyay, M.S. Ray, S. Chaudhuri, G. Mukhopadhyay, G. Bocelli, A. Cantoni, A. Ghosh, *Inorg. Chim. Acta* 359 (2006) 1367–1375.
- [20] P. Bhowmik, S. Chatterjee, S. Chattopadhyay, *Polyhedron* 63 (2013) 214–221.
- [21] P. Mahapatra, S. Ghosh, S. Giri, V. Rane, R. Kadam, M.G.B. Drew, A. Ghosh, *Inorg. Chem.* 56 (2017) 5105–5121.
- [22] P. Bhowmik, S. Jana, P.P. Jana, K. Harms, S. Chattopadhyay, *Inorg. Chem. Commun.* 18 (2012) 50–56.
- [23] S. Ghosh, S. Biswas, A. Bauza, M. Barceló-Oliver, A. Frontera, A. Ghosh, *Inorg. Chem.* 52 (2013) 7508–7523.
- [24] S. Chattopadhyay, G. Bocelli, A. Cantoni, A. Ghosh, *Inorg. Chim. Acta* 359 (2006) 4441–4446.

- [25] L.K. Das, S.W. Park, S.J. Cho, A. Ghosh, Dalton Trans. 41 (2012) 11009–11017.
- [26] S. Roy, A. Bhattacharyya, S. Purkait, A. Bauzá, A. Frontera, S. Chattopadhyay, Dalton Trans. 45 (2016) 15048–15059.
- [27] A. Panja, N. Shaikh, P. Vojtišek, S. Gao, P. Banerjee, New J. Chem. 26 (2002) 1025–1028.
- [28] S. Chattopadhyay, M.G.B. Drew, A. Ghosh, Eur. J. Inorg. Chem. 2008 (2008) 1693–1701.
- [29] A. Panja, N. Shaikh, M. Ali, P. Vojtišek, P. Banerjee, Polyhedron 22 (2003) 1191–1198.
- [30] A. Banerjee, P. Ghosh, N. Chowdhury, S. Chattopadhyay, Polyhedron 218 (2022) 115756.
- [31] K. Shaikh, A. Santra, S. Chattopadhyay, Polyhedron 224 (2022) 115977.
- [32] M. Karmakar, S. Roy, S. Chattopadhyay, Polyhedron 215 (2022) 115652.
- [33] T.G. Dastidar, S. Chattopadhyay, Polyhedron 211 (2022) 115511.
- [34] S. Bera, S. Chattopadhyay, Polyhedron 223 (2022) 115935.
- [35] L. Hashemi, A. Morsali, J. Coord. Chem. 64 (2011) 4088–4097.
- [36] S. Roy, S. Choubey, K. Bhar, S. Khan, P. Mitra, B.K. Ghosh, J. Mol. Struct. 1051 (2013) 328–335.
- [37] L. Hashemi, A. Morsali, Inorg. Chim. Acta 386 (2012) 56–59.
- [38] S. Chattopadhyay, K. Bhar, S. Choubey, S. Khan, P. Mitra, B.K. Ghosh, Inorg. Chem. Commun. 16 (2012) 21–24.

- [39] G. Mahmoudi, V. Stilinovič, A. Bauž, A. Frontera, A. Bartyzel, C. R. -Pereze, A. M. Kirillov, *RSC Adv.* 6 (2016) 60385-60393.
- [40] J. de O. Cabral, M. F. Cabral, W. J. Cummins, M. G. B. Drew, A. Rodgers, S. M. Nelson, *Inorg. Chim. Acta.* 30 (1978) 313-316.
- [41] S. Ulrich, J.-M. Lehn, *J. Am. Chem. Soc.* 131 (2009) 5546–5559.
- [42] A. A. Khandar, V. T. Yilmaz, F. Costantino, S. Gumus, S. A. H. -Yazdi, G. Mahmoudi, *Inorg. Chim. Acta* 394 (2013) 36-44.
- [43] S. Satapathi, S. Chattopadhyay, S. Roy, K. Bhar, P. Mitra, B.K. Ghosh, *J. Mol. Struct.* 1030 (2012) 138–144.
- [44] S. Chattopadhyay, K. Bhar, S. Das, S. Satapathi, H.-K. Fun, P. Mitra, B.K. Ghosh, *Polyhedron* 29 (2010) 1667–1675.
- [45] M. Abedi, A.A. Khandar, M.S. Gargari, A.V. Gurbanov, S.A. Hosseini, G. Mahmoudi, *Z. Anorg. Allg. Chem* 640 (2014) 2193–2197.
- [46] S.A. Hosseini, G. Mahmoudi, P. Garczarek, P. Hazendonk, M. Abedi, M.S. Gargari, *J. Mol. Struct.* 1105 (2016) 159–168.
- [47] G. Mahmoudi, M.S. Gargari, F.A. Afkhami, C. Lampropoulos, M. Abedi, S. A. Corrales, A.A. Khandar, J. Mague, D.V. Derveer, B.K. Ghosh, A. Masummi, *Polyhedron* 93 (2015) 46–54.
- [48] X.-M. Wang, S. Chen, R.-Q. Fan, F.-Q. Zhangb, Y.-L. Yang, *Dalton Trans.* 44 (2015) 8107–8125.

- [49] J.N. Melville, P.V. Bernhardt, *Inorg. Chem.* 60 (2021) 9709–9719.
- [50] J. Huang, L.-H. Huo, Z.-P. Deng, S. Gao, *Polyhedron* 122 (2017) 46–54.
- [51] C.J. Cooper, M.D. Jones, S.K. Brayshaw, B. Sonnex, M.L. Russell, M.F. Mahoon, D. R. Allan, *Dalton Trans.* 40 (2011) 3677–3682.
- [52] A. Jozwiuk, Z. Wang, D.R. Powell, R.P. Houser, *Inorg. Chim. Acta* 394 (2013) 415–422.
- [53] J. Fielden, D.-L. Long, M. Speldrich, P. Kögerler, L. Cronin, *Dalton Trans.* 41 (2012) 4927–4934.
- [54] V. Amendola, L. Fabbrizzi, L. Gianelli, C. Maggi, C. Mangano, P. Pallavicini, M. Zema, *Inorg. Chem.* 40 (2001) 3579–3587.
- [55] V. Amendola, L. Fabbrizzi, L. Linati, C. Mangano, P. Pallavicini, V. Pedrazzini, M. Zema, *Chem. Eur. J.* 5 (1999) 3679–3688.
- [56] S.J. Coles, A. Sengul, O. Kurt, S. Altin, *Acta Crystallogr. E* 64 (2008) m1435.
- [57] S. Gournbatsis, N. Hadjiliadis, *Trans. Met. Chem.* 23 (1998) 599–604.
- [58] E. Guney, V.T. Yilmaz, A. Sengul, O. Büyükgüngör, *Z. Anorg. Allg. Chem.* 637 (2011) 246–250.
- [59] S. Chattopadhyay, M.G.B. Drew, A. Ghosh, *Inorg. Chim. Acta* 359 (2006) 4519–4525.
- [60] S. Chattopadhyay, M. G. B. Drew, A. Ghosh, *Polyhedron* 26 (2007) 3513–3522.
- [61] S. Chattopadhyay, P. Chakraborty, M.G.B. Drew, A. Ghosh, *Inorg. Chim. Acta* 362

(2009) 502–508.

[62] S. Khan, A.A. Masum, M.M. Islam, M.G.B. Drew, A. Bauzá, A. Frontera, S. Chattopadhyay, *Polyhedron* 103 (2017) 334–343.

[63] M. Das, S. Chattopadhyay, *Polyhedron* 50 (2013) 443–451.

[64] S.-R. Fan, L.-G. Zhu, *Inorg. Chem.* 46 (2007) 6785–6793.

[65] Y.-H. Zhao, H.-B. Xu, Y.-M. Fu, K.-Z. Shao, S.-Y. Yang, Z.-M. Su, X.-R. Hao, D.-X. Zhu, E.-B. Wang, *Cryst. Growth Des.* 8 (2008) 3566–3576.

[66] J. Yang, G.-D. Li, J.-J. Cao, Q. Yue, G.-H. Li, J.-S. Chen, *Chem. Eur. J.* 13 (2007) 3248–3261.

[67] B. Ding, Y.Y. Liu, X.X. Wu, X.-J. Zhao, G.X. Du, E.-C. Yang, X.G. Wang, *Cryst. Growth Des.* 9 (2009) 4176–4180.

[68] X.-L. Wang, Y.-Q. Chen, J.-X. Zhang, G.-C. Liu, H.-Y. Lin, A.-X. Tian, *Z. Anorg. Allg. Chem.* 636 (2010) 830–834.

[69] M.-L. Hu, A. Morsali, L. Aboutorabi, *Coord. Chem. Rev.* 255 (2011) 2821–2859.

[70] S. Chattopadhyay, K. Bhar, S. Khan, P. Mitra, R.J. Butcher, B.K. Ghosh, *J. Mol. Struct.* 966 (2010) 102–106.

[71] A.C. Wibowo, S.A. Vaughn, M.D. Smith, H.-C.-Z. Loye, *Inorg. Chem.* 49 (2010) 11001–11008.

[72] J. Yang, J.-F. Ma, Y.-Y. Liu, J.-C. Ma, S.R. Batten, *Inorg. Chem.* 46 (2007) 6542–6555.

- [73] L. Zhang, Z.-J. Li, Q.-P. Lin, Y.-Y. Qin, J. Zhang, P.-X. Yin, J.-K. Cheng, Y.-G. Yao, *Inorg. Chem.* 48 (2009) 6517–6525.
- [74] Y.-X. Tan, F.-Y. Meng, M.-C. Wu, M.-H. Zeng, *J. Mol. Struct.* 928 (2009) 176–181.
- [75] J. Yang, J.-F. Ma, Y.-Y. Liu, J.-C. Ma, S.R. Batten, *Cryst. Growth Des.* 9 (2009) 1894–1911.
- [76] L. S. -Livny, J. P. Glusker, C. W. Bock, *Inorg. Chem.* 37 (1998) 1853–1867.
- [77] J.S. Magyar, T.C. Weng, C.M. Stern, D.F. Dye, B.W. Rous, J.C. Payne, B. M. Bridgewater, A. Mijovilovich, G. Parkin, J.M. Zaleski, J.E. Penner-Hahn, H. A. Godwin, *J. Am. Chem. Soc.* 127 (2005) 9495–9505.
- [78] R.D. Hancock, J.H. Reibenspies, H. Maumela, *Inorg. Chem.* 43 (2004) 2981–2987.
- [79] Q.-Y. Liu, L. Xu, *Eur. J. Inorg. Chem.* 2006 (2006) 1620–1628.
- [80] R.J. Andersen, R.C. Targiani, R.D. Hancock, C.L. Stern, D.P. Goldberg, H. A. Godwin, *Inorg. Chem.* 45 (2006) 6574–6576.
- [81] A. Banerjee, D. Chowdhury, R. Gomila, S. Chattopadhyay, *Polyhedron* 216 (2022) 115670.
- [82] S. Mirdya, S. Roy, S. Chatterjee, A. Frontera, S. Chattopadhyay, *Cryst. Growth Des.* 19 (2019) 5869–5881.
- [83] S. Roy, M.G.B. Drew, A. Bauza, A. Frontera, S. Chattopadhyay, *New J. Chem.* 42 (2018) 6062–6076.
- [84] S. Mirdya, A. Frontera, S. Chattopadhyay, *CrystEngComm* 21 (2019) 6859–6868.

- [85] S. Mirdya, S. Banerjee, S. Chattopadhyay, *CrystEngComm* 22 (2020) 237–247.
- [86] M. Karmakar, A. Frontera, S. Chattopadhyay, T.J. Mooibroek, A. Bauza, *Int. J. Mol. Sci.* 21 (2020) 7091.
- [87] T. Basak, A. Frontera, S. Chattopadhyay, *CrystEngComm* 23 (2021) 2703–2710.
- [88] A. Frontera, A. Bauza, *Chem. Eur. J.* 28 (2022) e202201660.
- [89] A. Daolio, A. Pizzi, G. Terraneo, A. Frontera, G. Resnati, *Chem. Phys. Chem.* 22 (2021) 2281–2285.
- [90] A. Daolio, A. Pizzi, M. Calabrese, G. Terraneo, S. Bordinon, A. Frontera, G. Resnati, *Angew. Chem. Int. Ed.* 60 (2021) 20723–20727.
- [91] L. d. A. Santos, T. A. Hamlin, T. C. Ramalho, F. M. Bickelhaupt, *Phys. Chem. Chem. Phys.* 23 (2001) 13842–13852.
- [92] A. Daolio, A. Pizzi, G. Terraneo, M. Ursini, A. Frontera, G. Resnati, *Angew. Chem. Int. Ed.* 60 (2021) 14385–14389.
- [93] Karmakar, M.; Basak, T.; Chattopadhyay, S. Phosphatase-mimicking activity of a unique penta-nuclear zinc(II) complex with a reduced Schiff base ligand: assessment of its ability to sense nitroaromatics. *New J. Chem.* **2019**, 43, 4432–4443.
- [94] Karmakar, M.; Roy, S.; Chattopadhyay, S. A series of trinuclear zinc(II) complexes with reduced Schiff base ligands: turn-off fluorescent chemosensors with high selectivity for nitroaromatics. *New J. Chem.* **2019**, 43, 10093–10102.

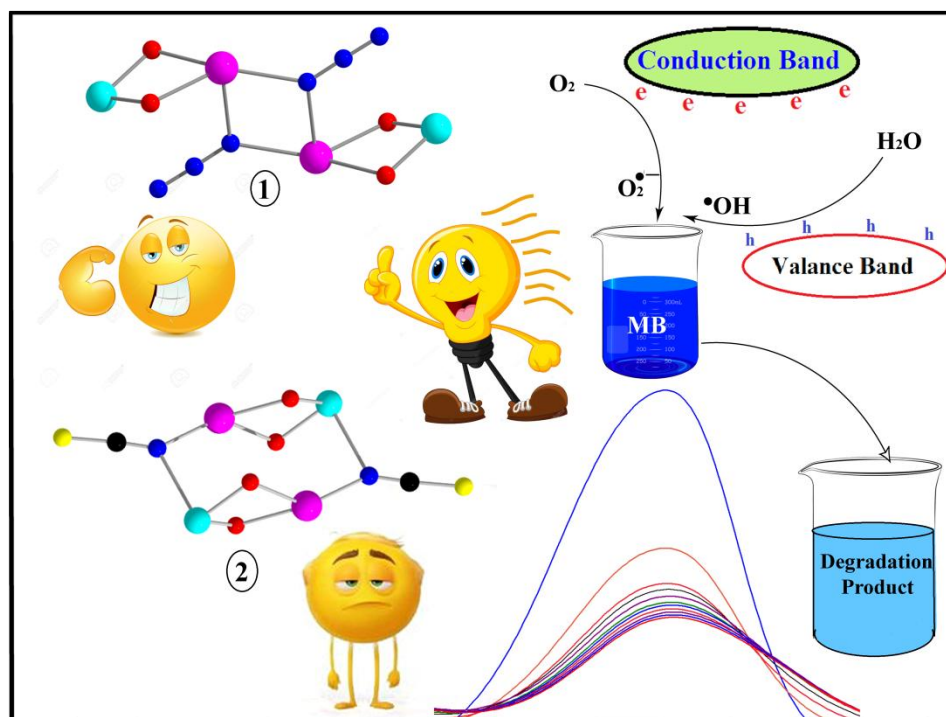
- [95] Mirdya, S.; Basak T.; Chattopadhyay, S. Photocatalytic ability of two hetero-tetranuclear complexes with CuO₂Cd cores to degrade methylene blue: Influence of their structures on activity. *Polyhedron*. **2019**, *170*, 253–263.
- [96] Addison, A. W.; Rao, T. N.; Reedijk, J.; Rijn, J. V.; Verschoor, G. C. Synthesis, Structure, and Spectroscopic Properties of Copper(II) Compounds containing Nitrogen-Sulphur Donor Ligands; the Crystal and Molecular Structure of Aqua[1,7-bis(N-methylbenzimidazol-2'-yl)-2,6-dithiaheptane]copper(ii) Perchlorate. *J. Chem. Soc., Dalton Trans.* **1984**, 1349-1356.
- [97] Wang, H.; Zhang, D.; Ni, Z.-H.; Li, X.; Tian, L.; Jiang, J. Synthesis, Crystal Structures, and Luminescent Properties of Phenoxo-Bridged Heterometallic Trinuclear Propeller- and Sandwich-Like Schiff-Base Complexes. *Inorg. Chem.* **2009**, *48*, 5946-5956.
- [98] Cremer, D.; Pople, J. A. A General Definition of Ring Puckering Coordinates. *J. Am. Chem. Soc.* **1975**, *97*, 1354-1358.
- [99] D. Cremer, On the correct usage of the Cremer-Pople puckering parameters as quantitative descriptors of ring shapes - a reply to recent criticism by Petit, Dillen and Geise. *Acta Crystallogr., Sect. B: Struct. Sci.* **1984**, *40*, 498–500.
- [100] Chattopadhyay, S.; Drew, M. G. B.; Ghosh, A. Methylene Spacer-Regulated Structural Variation in Cobalt(II/III) Complexes with Bridging Acetate and Salen- or Salpn-Type Schiff-Base Ligands. *Eur. J. Inorg. Chem.* **2008**, 1693–1701.
- [101] Nakamoto, K. *Infrared and Raman Spectra of Organic and Coordination Compounds*. John Wiley and Sons, New York, 3rd edn, **1978**, p. 227.

- [102] Bhowmik, P.; Harms, K.; Chattopadhyay, S. Formation of polynuclear copper(II)–sodium(I) heterometallic complexes derived from salen-type Schiff bases. *Polyhedron*. **2013**, *49*, 113–120.
- [103] Agarwal, R. K.; Kumar, A. Synthesis, Physico-chemical and Biological Properties of Some Mixed Ligand Complexes of Trivalent Lanthanides with 4[N-4'-Dimethylamino-Benzalidene)Amino] antipyrine Thiosemicarbazone and Pyridine. *J. Appl. Chem. Res.* **2011**, *16*, 40-58.
- [104] Nazarov, M.; Noh, D. Y. *New Generation of Europium and Terbium-Activated Phosphors: From Syntheses to Applications*. Pan Stanford Publishing, 6000 Broken Sound Pkwy NW. **2011**, p. 211.
- [105] Roy, S.; Drew, M. G. B.; Bauzá, A.; Frontera, A.; Chattopadhyay, S. Estimation of conventional C–H... π (arene), unconventional C–H... π (chelate) and C–H... π (thiocyanate) interactions in hetero-nuclear nickel(II)–cadmium(II) complexes with a compartmental Schiff base. *Dalton Trans.* **2017**, *46*, 5384–5397.

Chapter V

Tetranuclear complexes with CuO_2Cd cores:

Exploration of their photocatalytic ability to degrade methylene blue



V.1. Introduction

Different groups of coordination chemists were synthesizing varieties of homo and hetero polynuclear complexes of transition and non-transition metals with salen type di-Schiff base ligands (prepared by the condensation of several diamines with salicylaldehyde) for long [1-5]. In this method, the ability of phenoxo oxygen atoms of salicylaldimine Schiff bases was utilized to bridge different metal centres [6-11]. Our group was also engaged in the synthesis and characterization of such complexes [12-14]. Several 'half salen' type mono-condensed Schiff bases have also been used to prepare such complexes [15-18]. Ability of many of these complexes in mimicking several enzymes, e.g. phosphatase, phenoxazinone synthase, catechol oxidase etc was investigated [19-25]. Opto-electronic properties of few such complexes were explored [26, 27]. Few complexes were found effective to degrade methylene blue under visible light irradiation [28-30]. The denticity of these 'salen' type Schiff bases may be increased by using 3-alkoxysalicylaldehyde instead of salicylaldehyde [31-33]. In this method, 'salen' type hexadentate N_2O_4 donor compartmental Schiff bases were produced affording a facile synthetic route to multimetallic complexes with greater ease. N,N' -bis(3-methoxysalicylidene)-2,2-dimethylpropane-1,3-diamine is a well known compartmental Schiff base, containing inner N_2O_2 and outer O_4 compartments. We have prepared many heterometallic complexes with this ligand [34, 35]. Many other groups were also used this ligand to prepare hetero-metallic complexes [36-38]. Usually, transition metals are placed in the inner N_2O_2 compartment as their radii matches well with the radius of this compartment. On the other hand, non-transition metals of larger size usually fit well in the outer O_4 compartment [39-43].

In this work, we have reduced the Schiff base ligand with borohydride to get a more flexible reduced Schiff base ligand which was then used to prepare tetranuclear heterometallic copper(II)/cadmium(II) complexes, $(\mu_{1,1}-N_3)_2[(H_2O)Cu(L^R)Cd(N_3)]_2 \cdot 2CH_3OH$ (**12**) and $(\mu_{1,1}-NCS)_2[CuL^R Cd(SCN)]_2 \cdot 2CH_3OH$ (**13**), where $H_2L^R = 2,2'-[(2,2\text{-dimethyl-1,3-propanediyl})bis(iminomethylene)][bis[6\text{-methoxy-phenol}]]$. Both complexes were characterized with single crystal X-ray diffraction analysis. Both complexes could be used as photo-catalyst to degrade methylene blue under visible light irradiation, although complex **12** was found to be better catalyst than complex **13**. Methylene blue is an organic dye pollutant released by textile industries and it is necessary to destroy methylene blue from industrial waste to minimize environmental pollution [44-46]. A probable mechanistic pathway for the photocatalytic degradation of the organic dye by these complexes has been proposed. The difference in their photocatalytic performance has also been correlated with their structures.

V.2. Experimental Section

V.2.1. Synthesis

V.2.1.1. Synthesis of Schiff base ligands

V.2.1.1.1: Preparation of the ligand, $2,2'-[(2,2\text{-dimethyl-1,3-propanediyl})bis(iminomethylene)][bis[6\text{-methoxy-phenol}]] (H_2L^1)$

H_2L^1 ligand preparation has been given in II.2.1 (See Chapter 2).

V.2.1.3. Synthesis of complexes

V.2.1.3.1. Synthesis of $(\mu_{-1,1}\text{-N}_3)_2[(\text{H}_2\text{O})\text{Cu}(\text{L}^R)\text{Cd}(\text{N}_3)]_2 \cdot 2\text{CH}_3\text{OH}$ (**12**)

A methanol solution (5 mL) of copper(II) acetate monohydrate (~400 mg, 2 mmol) was added to the methanol solution (10 mL) of the reduced Schiff base ligand H_2L^R , with constant stirring. A methanol (10 mL) solution of cadmium(II) acetate dihydrate (~540 mg, 2 mmol) was then added to it and the stirring was continued for about 2h. A methanol–water (2:1) solution (10 mL) of sodium azide (260 mg, 4 mmol) was added and the resulting mixture was refluxed for ca. 2h. Crystalline product was obtained after few days on very slow evaporation. Single crystals, suitable for X-ray diffraction, were isolated from the crystalline product.

Yield: 914 mg (~67%) based on copper(II). Anal. Calc. for $\text{C}_{44}\text{H}_{68}\text{Cd}_2\text{Cu}_2\text{N}_{16}\text{O}_{12}$ (FW: 1365.06): C, 39.88; H, 4.46; N, 17.72. Found: C, 39.7; H, 4.3; N, 17.9 %, FT-IR (KBr, cm^{-1}): 3412 ($\nu_{\text{O-H}}$), 3246-3166 ($\nu_{\text{N-H}}$), 2972-2835 ($\nu_{\text{C-H}}$), 2060 ($\nu_{\mu_{-1,1}\text{-N}_3}$), 2035 (ν_{N_3}). UV–Vis, λ_{max} (nm), [ϵ_{max} (L $\text{mol}^{-1} \text{cm}^{-1}$)] (DMF): 242 (1.5×10^4), 280 (7.9×10^3), 336 (8.9×10^2), 414 (1.0×10^3), 591 (2.2×10^2).

V.2.1.3.2. Synthesis of $(\mu_{-1,1}\text{-NCS})_2[\text{CuL}^R\text{Cd}(\text{SCN})]_2 \cdot 2\text{CH}_3\text{OH}$ (**13**)

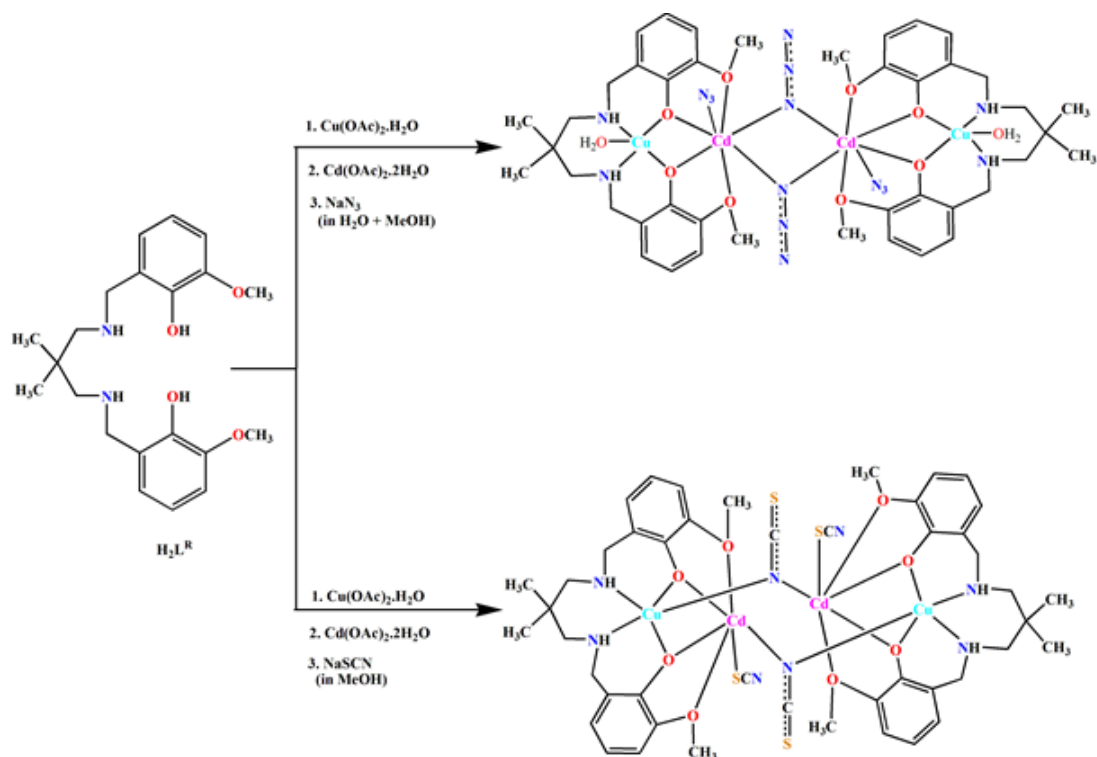
Complex **13** was prepared in a similar method to that of complex **12**, except that sodium thiocyanate (~330 mg, 4 mmol) was added instead of sodium azide. Crystalline product was obtained after few days on very slow evaporation. Single crystals, suitable for X-ray diffraction, were isolated from the crystalline product.

Yield: 905 mg (~65%) based on copper(II). Anal. Calc. for $C_{48}H_{64}Cd_2Cu_2N_8O_{10}S_4$ (FW: 1393.23): C, 41.57; H, 4.25; N, 8.43. Found: C, 41.3; H, 4.1; N, 8.6%, FT-IR (KBr, cm^{-1}): 3220-3145 (ν_{N-H}), 2972-2835 (ν_{C-H}), 2081 ($\nu_{\mu-1,1-NCS}$), 2017 (ν_{SCN}). UV-Vis, λ_{max} (nm), [ϵ_{max} ($L\ mol^{-1}\ cm^{-1}$)] (DMF): 240 (1.8×10^4), 280 (1.0×10^4), 336 (1.1×10^3), 410 (1.3×10^3), 595 (2.7×10^2).

V.3. Results and discussion

V.3.1. Synthesis

2,2-dimethyl-1,3-diaminopropane was refluxed with 3-methoxysalicylaldehyde in a 1:2 ratio to form a N_2O_4 donor compartmental Schiff base ligand, H_2L , following a literature method and $NaBH_4$ was used as a reducing agent to prepare reduced Schiff base ligand (H_2L^R) [50, 51]. This reduced Schiff base (H_2L^R) on reaction with copper(II) acetate monohydrate followed by the addition of cadmium(II) acetate dihydrate and sodium azide in methanol gave rise to complex **12**. The complex **13** was synthesized in similar method to that of complex **12**, except that sodium thiocyanate is used instead of sodium azide. Synthetic route to the formation of both complexes **12** and **13** have been shown in Scheme 12.



Scheme V.1: Synthetic route to complexes **12** and **13**

V.3.2. Structure description

V.3.2.1. Description of structures $(\mu_{1,1}-N_3)_2[(H_2O)Cu(L^R)Cd(N_3)]_2 \cdot 2CH_3OH$ (**12**) and $(\mu_{1,1}-NCS)_2[CuL^RCd(SCN)]_2 \cdot 2CH_3OH$ (**13**)

Structure determination reveals that complex **12** crystallizes in the monoclinic space group $P2_1/c$. The complex is a centrosymmetric zigzag tetramer and is built up of two dinuclear units, $[(H_2O)Cu(L^R)Cd(N_3)]$, connected through two end-on azide bridges. A perspective view of the complex with selective atom numbering scheme has been shown in Fig.V.1. In the asymmetric unit, the copper(II) centre, Cu(1), and cadmium(II) centre, Cd(1), respectively

occupy the inner N_2O_2 and outer O_4 sites of a potential compartmental reduced Schiff base H_2L^R , with a $Cu(1) \cdots Cd(1)$ distance of 3.378(6) Å.

Copper(II) centre is penta-coordinated being bonded to two amine nitrogen atoms, N(1) and N(2), and two phenoxo oxygen atoms, O(1) and O(2), of the deprotonated reduced Schiff base ligand, $(L^R)^{2-}$ and one oxygen atom, O(5), from a coordinated water molecule. The geometry of any penta-coordinated metal centre may conveniently be measured by the Addison parameter (τ) [52]. The geometry of copper(II) centre is slightly distorted square pyramidal with $\tau = 0.06$ ($\tau = 0$ indicates perfect square pyramid). On the other hand, cadmium(II) centre, Cd(1), is hepta-coordinated and its geometry is distorted pentagonal bipyramidal. Cd(1) is coordinated by two phenoxo oxygen atoms, O(1) and O(2), two methoxy oxygen atoms, O(3) and O(4), and one nitrogen atom, N(3), of an end-on bridging azide, which constitute the pentagonal plane. The sixth site is occupied by a nitrogen atom, N(6), from a terminal azide. The seventh coordination site is occupied by another nitrogen atom, N(3), from an end-on bridging azide, which bridges Cd(1) and its symmetry $\{ '= 1-x, 1-y, 1-z \}$ related counterpart, Cd(1'). The saturated six-membered chelate ring [Cu(1)–N(1)–C(9)–C(10)–C(13)–N(2)] has envelope conformation with puckering parameters, $q = 0.523(6)$ Å; $\theta = 23.0(5)^\circ$; $\varphi = 177.6(14)^\circ$ [53, 54].

Complex **13** crystallizes in triclinic space group, $P\bar{1}$. It is basically a centrosymmetric cyclic tetramer with $[-Cd-(\mu_{1,1}-NCS)CuO_2Cd(\mu_{1,1}-NCS)-Cu-]$ core, in which two hetero-dinuclear $[CuL^RCd(SCN)]$ units are linked through two end-on thiocyanate bridges. A perspective

view with selective atom numbering scheme has been shown in Fig.V.2. Cu(1)···Cd(1') {symmetry transformation $' = 1-x, 1-y, 1-z$ } distance in the tetrameric unit is 3.617(9) Å.

Copper(II) centre, Cu(1), is square pyramidal being coordinated equatorially by two amine nitrogen atoms, N(1) and N(2), and two phenoxo oxygen atoms, O(1) and O(2), of the deprotonated reduced Schiff base, $(L^R)^{2-}$. The fifth position is occupied by a nitrogen atom, N(3'), of the bridging thiocyanate. The square pyramidal geometry of copper(II) centre is confirmed by τ , here $\tau = 0.01$ [52]. On the other hand, the coordination geometry of cadmium(II) centre, Cd(1), is distorted octahedral, where two phenoxo oxygen atoms, O(1) and O(2), and two methoxy oxygen atoms, O(3) and O(4), of the reduced Schiff base constitute the equatorial plane. One axial site is occupied by a sulfur atom, S(1), from terminal thiocyanate and another axial site is occupied by nitrogen atom, N(3), from thiocyanate which is act as a bridge between the cadmium(II) centre, Cd(1) and the symmetry related copper(II) centre, Cu(1'). The saturated six-membered chelate ring [Cu(1)–N(1)–C(9)–C(10)–C(13)–N(2)] has envelope conformation with the puckering parameters, $q = 0.524(6)$ Å; $\theta = 148.2(5)^\circ$; $\varphi = 2.6(11)^\circ$ [53, 54].

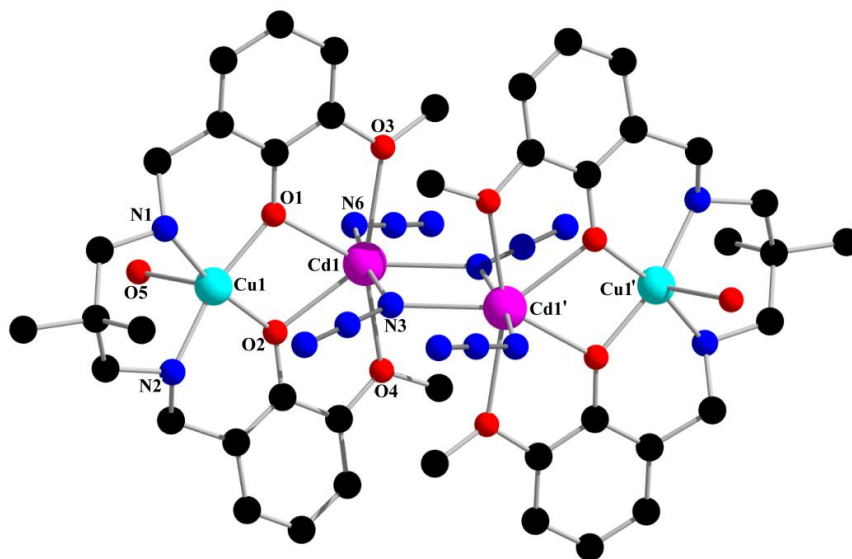


Fig.V.1: Perspective view of complex **12** with selective atom numbering. Hydrogen atoms and the lattice methanol molecule have been omitted for clarity.

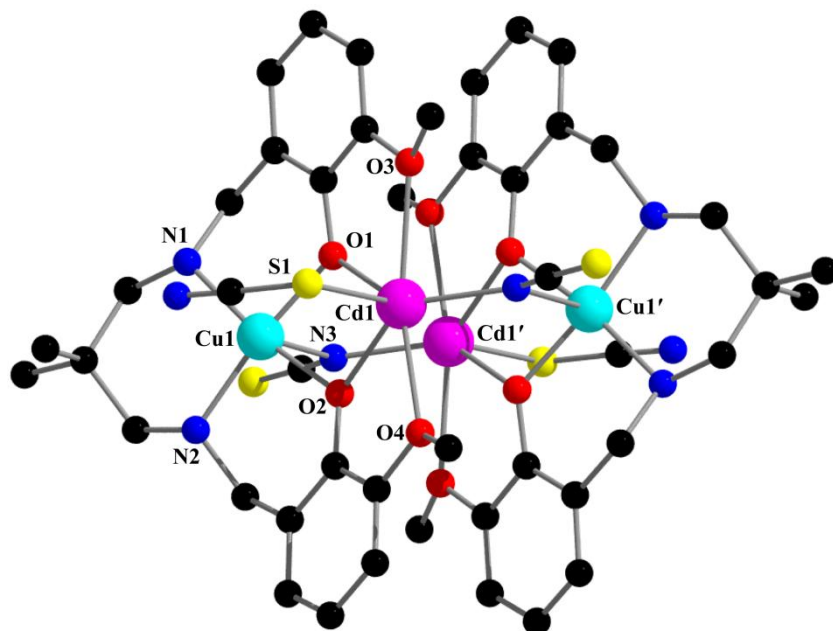


Fig.V.2: Perspective view of complex **13** with selective atom numbering. Hydrogen atoms and the lattice methanol molecule have been omitted for clarity.

V.3.3. Comparison of structures of **12** and **13**

It is interesting to note here that in complex **12**, cadmium(II) centre of one asymmetric unit is connected with a cadmium(II) centre of a symmetry related counterpart via end-on azide bridges. This makes the copper(II) centres free to be used in any catalytic reaction. On the other hand, cadmium(II) centre of one asymmetric unit in complex **13** is connected with a copper(II) centre of a symmetry related dinuclear unit via end-on thiocyanate bridges. Thus both copper(II) and cadmium(II) are confined in a cyclic tetrameric unit, making copper(II) less available to take part any catalytic reaction.

V.3.4. Supramolecular interactions in solid state of complexes **12** and **13**

Solid state structures of both complexes are stabilized through significant non-covalent interactions such as hydrogen bonding and C–H \cdots π . Complex **12** shows five significant hydrogen bonding interactions. The hydrogen atom, H(1), attached to amine nitrogen atom, N(1), involve in hydrogen bonding interaction with the symmetry related ($x, 1.5-y, -0.5+z$) oxygen atom, O(6ⁱ), of the lattice methanol molecule. Another hydrogen atom, H(5C), attached to oxygen atom, O(5), of coordinated water molecule participate in hydrogen bonding interaction with the symmetry related ($1-x, 1/2+y, 3/2-z$) azide nitrogen atom N(8^j). These two intermolecular hydrogen bonding interactions form a two dimensional layer structure. On the other hand, the oxygen atom, O(6), of the lattice methanol molecule forms hydrogen bond with the hydrogen atom, H(5D), attached with the oxygen atom, O(5), of the coordinated water molecule. Again,

hydrogen atom, H(6), of the same lattice methanol molecule, forms an additional hydrogen bond with azide nitrogen atom, N(6). Another hydrogen atom, H(2), attached to amine nitrogen atom N(2), participates in hydrogen bond formation with the azide nitrogen atom, N(5). Two dimensional layer structure of the complex has been shown in Fig.V.3 and selected small part of the two dimensional structure of hydrogen bonding has been shown in Fig.V.4. Details of the hydrogen bonding interactions have been given in Table.V.4.

The hydrogen atom, H(22A), attached to the carbon atom, C(22), of the lattice methanol molecule, is involved in a C–H \cdots π interaction with the symmetry related (x,1.5-y,0.5+z) phenyl ring [C(2)–C(3)–C(4)–C(5)–C(6)–C(7)]. Twodimensional layer structure of C–H \cdots π interaction has been shown in Fig.V.5 and selected small part of C–H \cdots π interaction with specific atom numbering has been shown in Fig.V.6. Details of the geometric feature of the C–H \cdots π interaction have been given in Table.V.5.

Three types of supramolecular interactions have been observed in complex **13** (H-bonding, C–H \cdots π and $\pi\cdots\pi$ interactions). The hydrogen atom, H(2N), attached to amine nitrogen atom, N(2), of the reduced Schiff base is engaged in intramolecular hydrogen bonding interaction with the same symmetry related oxygen atom, O(5), of lattice methanol molecule, as shown in Fig.V.7. Details of the hydrogen bonding interaction have been gathered in Table V.4.

The hydrogen atom, H(24B), attached to the carbon atom, C(24), of lattice methanol molecule is involved in the C–H \cdots π interaction with a phenyl ring [C(15)–C(16)–C(17)–C(18)–C(19)–C(20)]. The C–H \cdots π interaction of the complex has been shown

in Fig.V.8. Detail of the C–H \cdots π interaction has been given in Table V.5. Complex **13** shows a significant $\pi\cdots\pi$ stacking interaction (Fig.V.9) between an aromatic ring [C(2)–C(3)–C(4)–C(5)–C(6)–C(7)] with a symmetry-related (1–x,1–y,1–z) aromatic ring [C(15)–C(16)–C(17)–C(18)–C(19)–C(20)]. Details of the $\pi\cdots\pi$ interaction have been given in TableV.6.

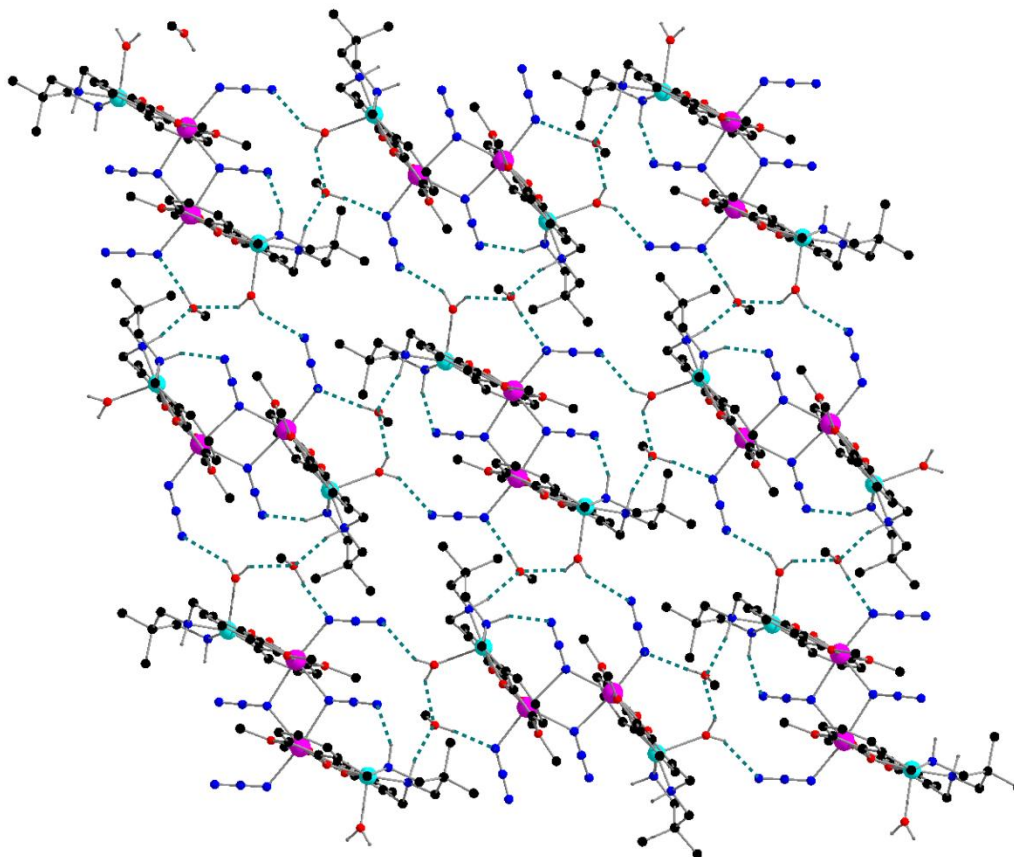


Fig.V.3: Hydrogen bonded layer structure of complex **12**. Only the relevant hydrogen atoms have been shown.

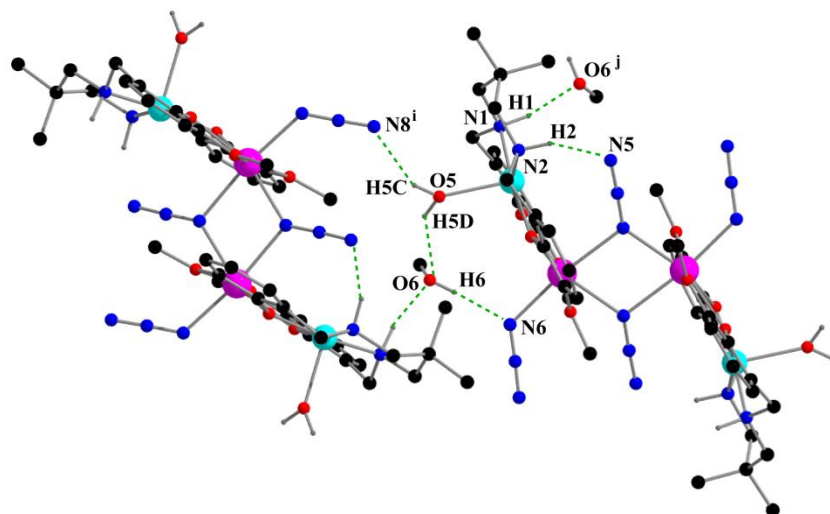


Fig.V.4: Selected small part of hydrogen bonded structure of complex **12**. Only the relevant hydrogen atoms have been shown. Symmetry transformation $^i = x, 1.5-y, 0.5+z$, $^j = 1-x, 0.5+y, 1.5-z$

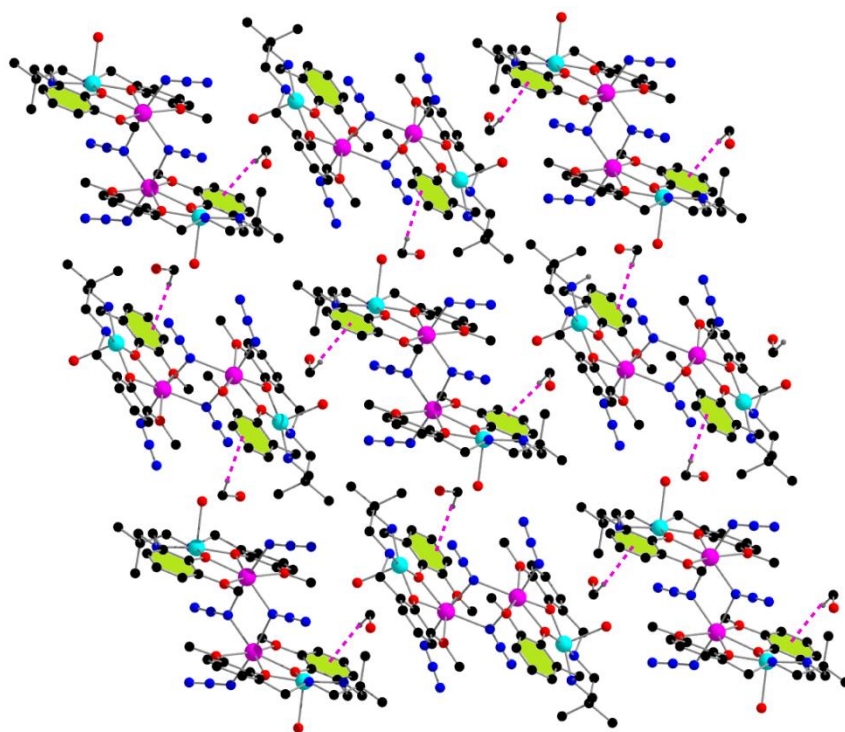


Fig.V.5: Two dimensional supramolecular C-H... π interactions in complex **12**. Only the relevant hydrogen atoms have been shown for clarity. Symmetry transformation: $^{\#} = x, 1.5-y, 0.5+z$.

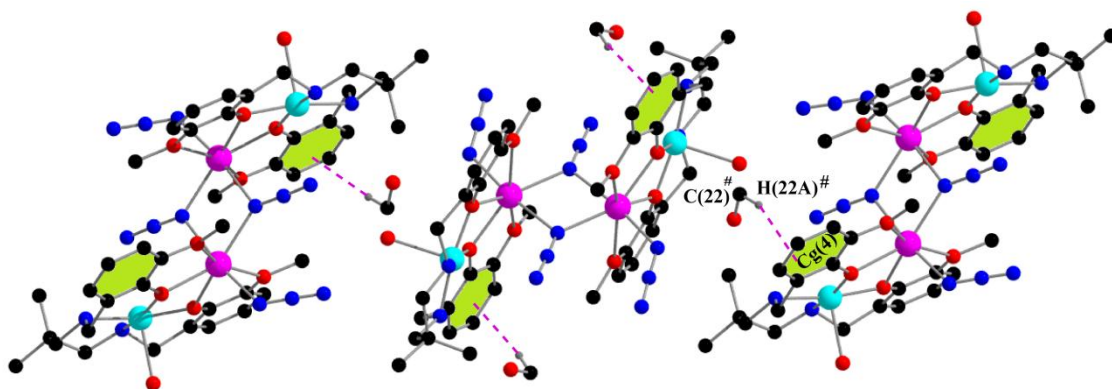


Fig.V.6: Selected small part of C–H \cdots π interactions of complex **12**. Only the relevant hydrogen atoms have been shown. Symmetry transformation $\# = x, 1.5 - y, 0.5 + z$.

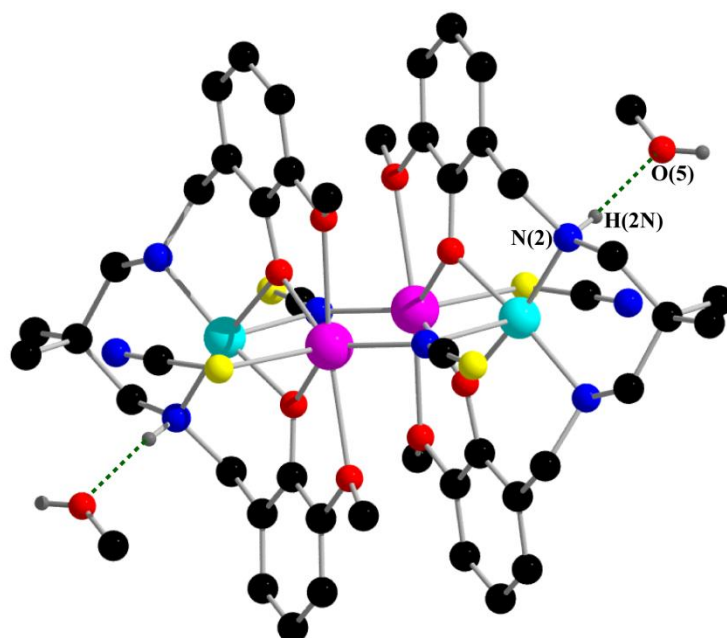


Fig.V.7: Hydrogen bonding structure of complex **13** with lattice methanol molecule. Only the relevant hydrogen atoms have been shown.

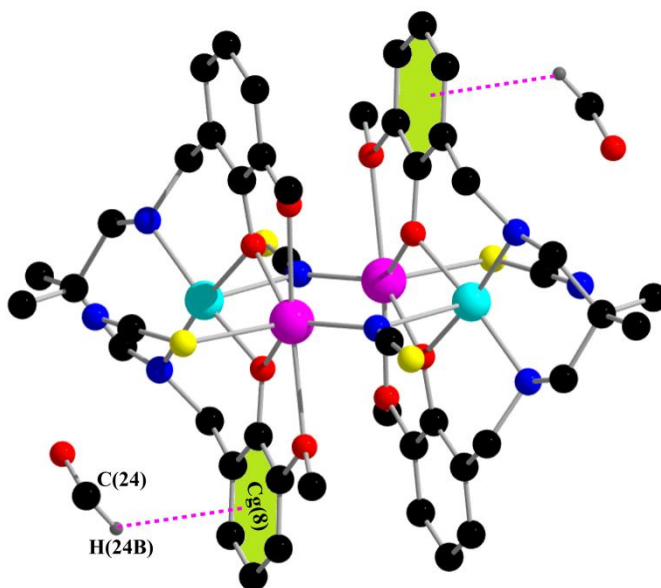


Fig.V.8: C–H \cdots π interaction of complex **13** with lattice methanol molecule. Only the relevant hydrogen atoms have been shown.

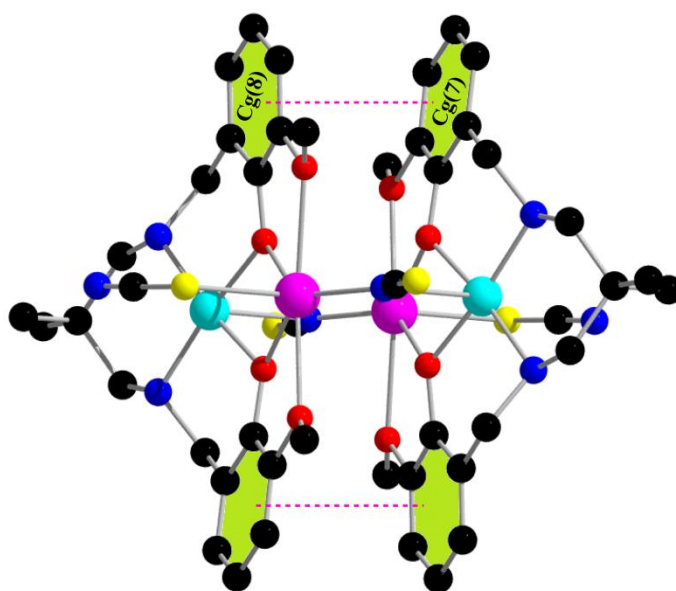


Fig.V.9: Intramolecular $\pi\cdots\pi$ stacking interactions in complex **13**. Hydrogen atoms and lattice methanol molecules have been omitted for clarity.

TableV.1: Crystal data and refinement details of complexes **12** and **13**.

Complex	12	13
Formula	C ₄₄ H ₆₈ Cd ₂ Cu ₂ N ₁₆ O ₁₂	C ₄₈ H ₆₄ Cd ₂ Cu ₂ N ₈ O ₁₀ S ₄
Formula Weight	1365.06	1393.23
Temperature (K)	273	273
Crystal system	Monoclinic	Triclinic
Space group	<i>P</i> 2 ₁ / <i>c</i>	<i>P</i> $\bar{1}$
<i>a</i> (Å)	10.5544(9)	11.6584(13)
<i>b</i> (Å)	18.0146(14)	11.6797(12)
<i>c</i> (Å)	15.1340(11)	12.7556(14)
α	90	108.983(3)
β	103.804(2)	99.804(3)
γ	90	116.542(3)
<i>Z</i>	2	1
<i>d</i> _{calc} (g cm ⁻³)	1.622	1.697
μ (mm ⁻¹)	1.573	1.755
<i>F</i> (000)	1388	706
Total Reflections	31902	15213
Unique Reflections	5032	4851
Observed data [<i>I</i> > 2 σ (<i>I</i>)]	4343	4271
No. of parameters	353	347
R(int)	0.030	0.044
R1,wR2 (all data)	0.0437, 0.1294	0.0499, 0.1360
CCDC NO	1891988	1891989

Table V.2: Selected bond lengths (Å) of complexes **12** and **13**.

Complex	12	13
Cd(1)–O(1)	2.287(3)	2.256(3)
Cd(1)–O(2)	2.307(3)	2.262(2)
Cd(1)–O(3)	2.471(4)	2.511(3)
Cd(1)–O(4)	2.472(4)	2.496(4)
Cd(1)–N(3)	2.354(5)	2.201(5)
Cu(1)–O(1)	1.956(3)	1.964(3)
Cu(1)–O(2)	1.953(3)	1.968(4)
Cu(1)–N(1)	2.028(4)	2.022(4)
Cu(1)–N(2)	2.032(4)	2.017(4)
Cd(1)–N(6)	2.259(5)	—
Cd(1)–N(3')	2.341(4)	—
Cu(1)–O(5)	2.317(4)	—
Cd(1)–S(1)	—	2.636(2)
Cu(1)–N(3')	—	2.626(5)

Symmetry transformation: ' = 1-x, 1-y, 1-z.

TableV.3: Selected bond angles (°) of complexes **12** and **13**.

Complex	12	13
O(1)–Cd(1)–O(2)	66.46(10)	66.97(10)
O(1)–Cd(1)–O(3)	67.19(15)	68.20(9)
O(1)–Cd(1)–O(4)	132.15(11)	134.87(10)
O(1)–Cd(1)–N(3)	90.02(12)	136.20(14)
O(2)–Cd(1)–O(3)	133.63(14)	135.15(11)
O(2)–Cd(1)–O(4)	66.41(11)	67.98(12)
O(2)–Cd(1)–N(3)	85.43(13)	136.67(15)
O(3)–Cd(1)–O(4)	158.23(15)	156.56(11)
O(3)–Cd(1)–N(3)	95.93(16)	80.21(13)
O(4)–Cd(1)–N(3)	94.09(16)	81.70(14)
O(1)–Cu(1)–O(5)	99.67(18)	78.70(13)
O(1)–Cu(1)–N(1)	90.59(15)	91.68(14)
O(1)–Cu(1)–N(2)	165.34(13)	170.44(16)
O(2)–Cu(1)–N(1)	168.94(13)	169.80(12)
O(2)–Cu(1)–N(2)	92.04(14)	92.07(14)
O(1)–Cd(1)–N(6)	96.86(12)	—
O(1)–Cd(1)–N(3')	143.99(14)	—
O(2)–Cd(1)–N(6)	100.24(15)	—
O(2)–Cd(1)–N(3')	141.12(15)	—
O(3)–Cd(1)–N(6)	83.85(18)	—
O(3)–Cd(1)–N(3')	82.14(18)	—
O(4)–Cd(1)–N(6)	83.69(17)	—
O(4)–Cd(1)–N(3')	82.05(14)	—
N(3)–Cd(1)–N(6)	172.41(13)	—
N(3)–Cd(1)–N(3')	74.31(15)	—

N(3')–Cd(1)–N(6)	98.17(15)	—
O(1)–Cu(1)–O(2)	80.15(13)	—
O(2)–Cu(1)–O(5)	92.80(15)	—
O(5)–Cu(1)–N(1)	94.72(16)	—
O(2)–Cu(1)–N(2)	92.04(14)	—
N(1)–Cu(1)–N(2)	95.65(15)	97.37(16)
S(1)–Cd(1)–O(1)	—	101.08(11)
S(1)–Cd(1)–O(2)	—	101.46(10)
S(1)–Cd(1)–O(3)	—	85.74(9)
S(1)–Cd(1)–O(4)	—	85.09(10)
S(1)–Cd(1)–N(3)	—	106.13(13)
O(1)–Cu(1)–N(3')	—	88.88(13)
O(2)–Cu(1)–N(3')		89.83(15)
N(1)–Cu(1)–N(3')		93.41(16)
N(2)–Cu(1)–N(3')		93.63(14)
O(5)–Cu(1)–N(2)	93.04(18)	—

Symmetry transformation: ' = 1-x, 1-y, 1-z.

Table V.4: Hydrogen bond distances (Å) and angles (°) of complexes **12** and **13**.

Complex	D–H···A	D–H	H···A	D···A	∠D–H···A
12	N(1)–H(1)–O(6')	0.9800	2.0800	3.039(5)	167.00
	N(2)–H(2)–N(5)	0.9800	2.4800	3.182(6)	129.00
	O(6)–H(6)–N(6)	0.8200	2.0200	2.831(5)	169.00

	O(5)–H(5C)–N(8)	0.88(9)	2.20(9)	2.926(8)	140(7)
	O(5)–H(5D)–O(6)	0.82(8)	2.22(10)	2.915(7)	143(10)
13	N(2)–H(2N)–O(5)	0.87(6)	2.16(6)	3.027(9)	171(5)

Symmetry transformation: $i = x, 1.5-y, 0.5+z$.

Table V.5: Geometric features (distances in Å and angles in °) of the C–H⋯Cg interactions for complex **12** and **13**.

Complex	C–H⋯Cg (Ring)	H⋯Cg (Å)	C–H⋯Cg (°)	C⋯Cg (Å)	Symmetry
12	C(22)–H(22A)⋯Cg(4) [#]	2.89	164	3.825(9)	$x, 3/2-y, 1/2+z$
13	C(24)–H(24B)⋯Cg(8)	2.85	125	3.499(11)	x, y, z

Symmetry transformation: [#] = $x, 1.5-y, 0.5+z$. Cg(4) = centre of gravity of the ring [C(2)–C(3)–C(4)–C(5)–C(6)–C(7)] and Cg(8) = centre of gravity of the ring [C(15)–C(16)–C(17)–C(18)–C(19)–C(20)].

Table V.6: Geometric parameters (Å) for the π – π interactions for the complex **13**.

Cg(I)⋯Cg(J)	Cg⋯Cg (Å)	α	Cg(I)⋯Perp (Å)	Cg(J)⋯Perp (Å)
Cg(8)⋯Cg(7) ⁱ	3.735(3)	11.1(3)	3.467(2)	3.468(2)

Symmetry transformations: ⁱ = $1-x, 1-y, 1-z$; α = dihedral angle between ring I and ring J, Cg(I)⋯Perp. = perpendicular distance of Cg(I) on ring J, Cg(J)⋯Perp. = perpendicular distance of

Cg(J) on ring I. Cg(7) = centre of gravity of the ring [C(2)–C(3)–C(4)–C(5)–C(6)–C(7)] and Cg(8) = centre of gravity of the ring [C(15)–C(16)–C(17)–C(18)–C(19)–C(20)] for the complex **13**.

V.3.5. Hirshfeld surfaces analysis

The Hirshfeld surfaces of both complexes mapped over d_{norm} (range -0.1 Å to 1.5 Å), shape index and curvedness have been shown in Fig.V.10. Red spots on these surfaces denote the dominant interactions. Analysis of Hirshfeld surfaces indicates that there are interactions mainly between nitrogen and hydrogen atoms in complex **12**, whereas, there are significant interactions between sulphur and hydrogen atoms in complex **13**. Other visible spots in Hirshfeld surfaces correspond to C⋯H and H⋯H contacts. The intermolecular interactions appear as distinct spikes in the 2D fingerprint plot (Fig.V.11).

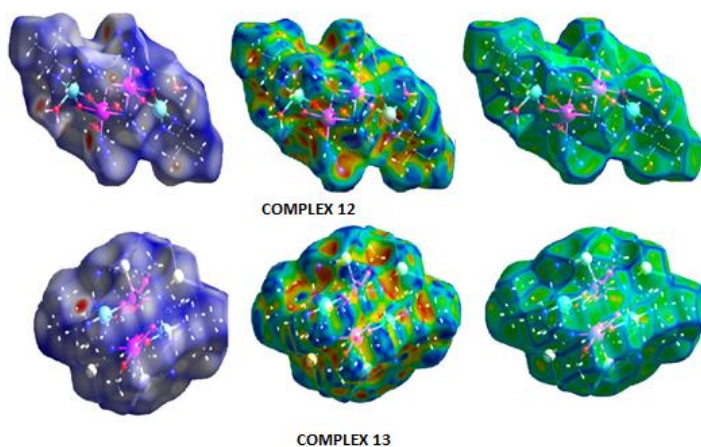


Fig.V.10:Hirshfeld surfaces of both complexes **12** and **13** mapped over d_{norm} (left), shape index (middle), curvedness (right).

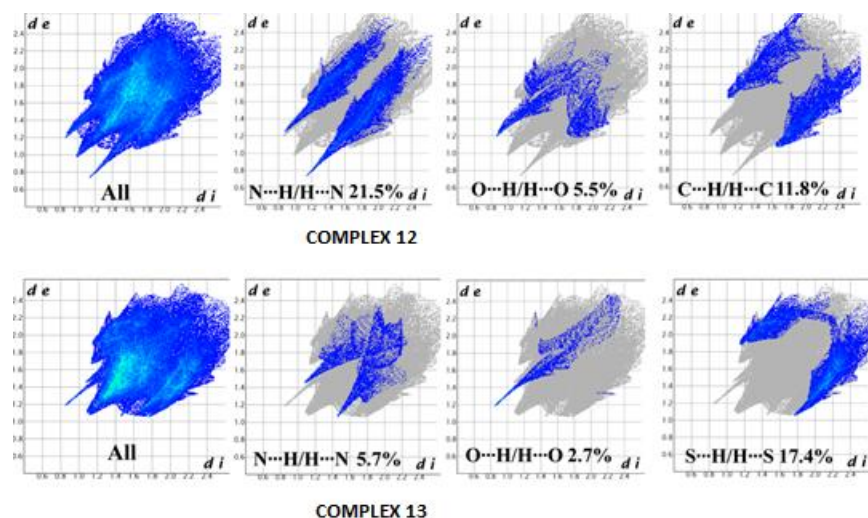


Fig.V.11:Fingerprint plot: different contacts contributed to the total Hirshfeld surface area of complexes **12**and **13**.

V.3.6. IR and electronic spectra

In the IR spectrum of complex **12**, a sharp peak at 2060 cm^{-1} and an associated small peak at 2036 cm^{-1} indicate the presence of bridging and terminal azides [55-57]. In IR spectrum of complex **13**, there are two successive strong peaks observed at 2081 and 2017 cm^{-1} , indicating the presence of terminal (S-bonded) and end-on bridged thiocyanates (N-bonded), respectively [58]. A moderately strong band due to stretching vibration of N–H bond appears around $3213\text{--}3166\text{ cm}^{-1}$ for both complexes [59]. A broad peak around 3412 cm^{-1} indicates the presence of coordinating water molecule in complex **12** [60]. Bands near the range of $2972\text{--}2835\text{ cm}^{-1}$ are due to alkyl C–H bond stretching vibrations, which are customarily noticed in the IR spectra of both complexes [61]. The IR spectra of both complexes have been shown in Fig.V.12

Electronic spectrum of each complex in DMF displays one absorption band in the visible region around 590 nm which may be considered as ${}^2T_{2g}(D) \leftarrow {}^2E_g(D)$ transition for copper(II) [35,60]. Bands around 410 nm (407 nm for complex **12** and 414 nm for complex **13**) may be attributed to LMCT transition from the N donor centres of Schiff base to copper(II) [62, 63]. Another bands around 335 nm (for both **12** and **13**) may be attributed to LMCT transition from the O donor centres of Schiff base to cadmium(II) [64]. The high intensity band occur at 242 (for **12**) and 240 (for **13**) nm is attributed to $\pi \rightarrow \pi^*$ transition of the ligand. Another intense band observe in the region of 275-285 is correspond to $n \rightarrow \pi^*$ transition for both complexes [62, 65]. The UV-vis spectra of both complexes have been shown in Fig.V.13and Fig.V.14, respectively..

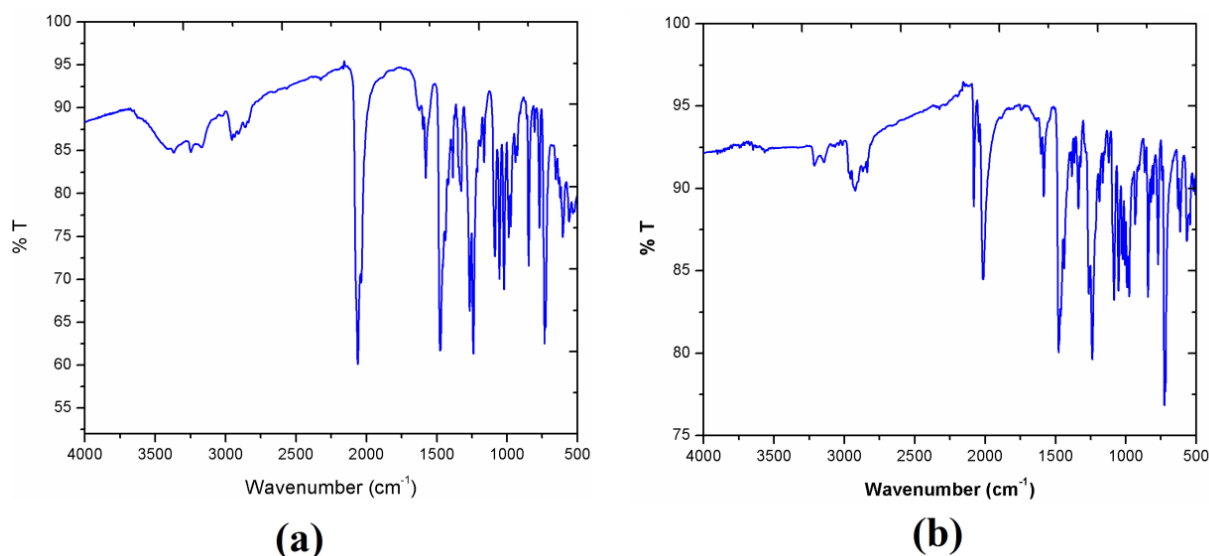


Fig.V.12: IR spectra of (a) complex **12** and (b) complex **13**.

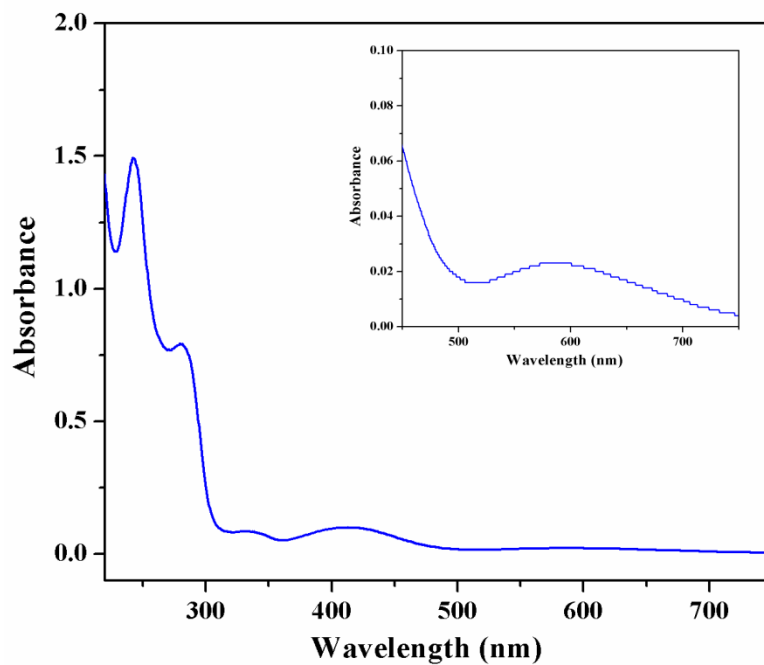


Fig. 13. UV-vis spectra of complex **12**. Inset shows the visible range spectrum.

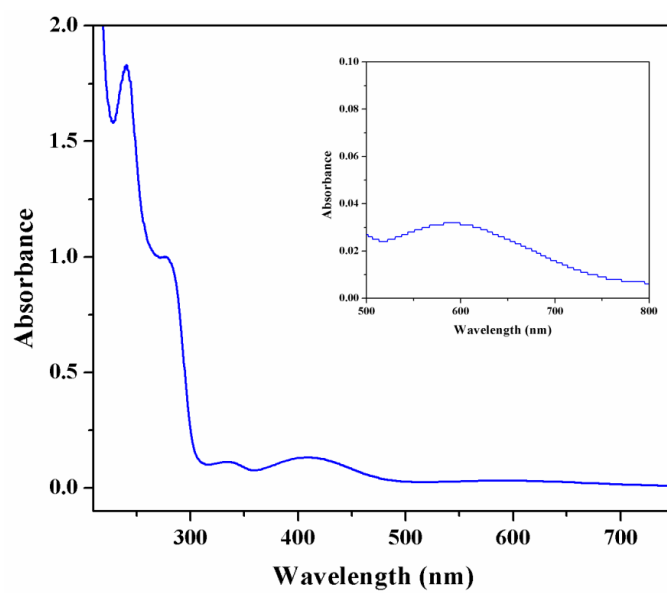


Fig. 14. UV-vis spectra of complex **13**. Inset shows the visible range spectrum.

V.4. APPLICATION

V.4.1. Photocatalytic activity

The ability of both complexes (**12** and **13**) to be used as photo-catalyst for the degradation of organic dye, viz. methylene blue (MB), has been investigated under visible light irradiation. The degradation efficiencies are defined as C/C_0 , where C and C_0 represent the residual and initial concentration of organic dyes, respectively. The degradation efficiencies (C/C_0) is calculated by the following equation:-

$$\text{Degradation efficiencies (\%)} = (C_0 - C)/C_0 \times 100.$$

As shown in Fig.V.15 the residual concentration of the dye in an aqueous solution gradually decreased as a function of the increasing reaction time, indicating that both complexes degrade organic dyes. Both complexes are efficient for the degradation of MB and the ratio of the degradation reaches around 62% (for complex **12**) and 30% (for complex **13**) using 10 mg of complexes.

To prove the photocatalytic efficiency of both complexes to MB, comparative experiments without catalyst under visible light irradiation have been performed, which showed only very little decomposition. The photocatalytic activity of cadmium(II) acetate and copper(II) acetate have also been studied to MB under similar conditions (mentioned in the Fig.V.16), which showed that the rate of degradation was still very slow using 10 mg of bare cadmium(II) as well as bare copper(II). It is revealed that the intensity of the characteristic

absorption peak of MB decreased with the increase of irradiation time in the degradation process. Kinetic plots of both complexes have been shown in Fig.V.16.

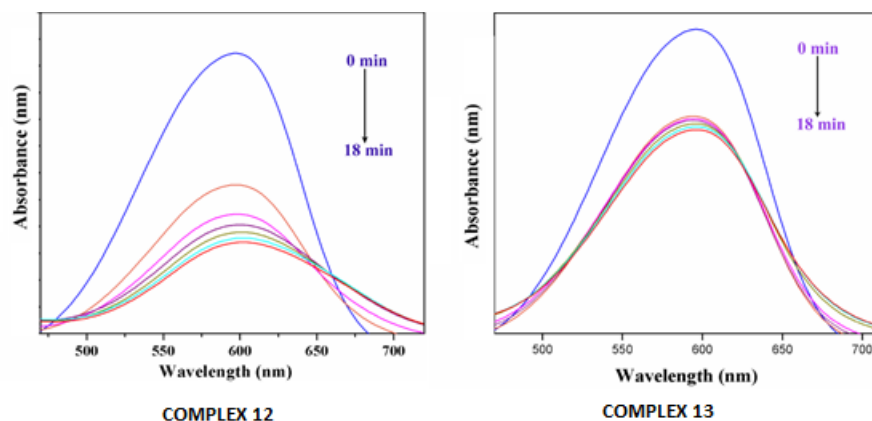


Fig.V. 15: UV–Vis absorption spectra of MB solution with both complexes (sample taken = 10 mg), used as a catalyst.

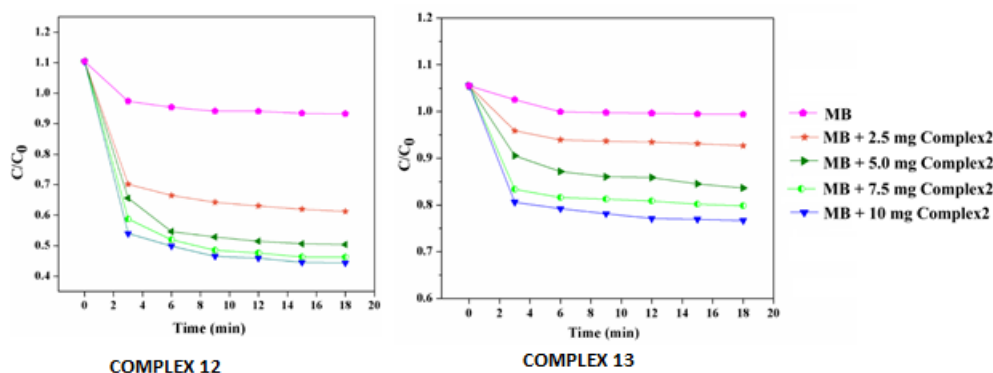


Fig.V.16: Degradation efficiency of MB in presence of complex **12** and complex **13**.

Experimental condition [MB]= 20 mg/L.

In order to verify whether both complexes are capable of maintaining its structural integrity during photocatalytic decomposition of MB, IR experiments for both complexes were performed during the course of photocatalytic reactions. The IR experiments indicated that the

patterns are nearly identical when compared with the pure complex. Hence the IR experiments imply that both complexes maintain their structural integrity even after getting involved in the photocatalytic reactions. IR spectra of both complexes **12** and **13** (before and after degradation) have been shown in Fig.V.17 and in Fig.V.18, respectively.

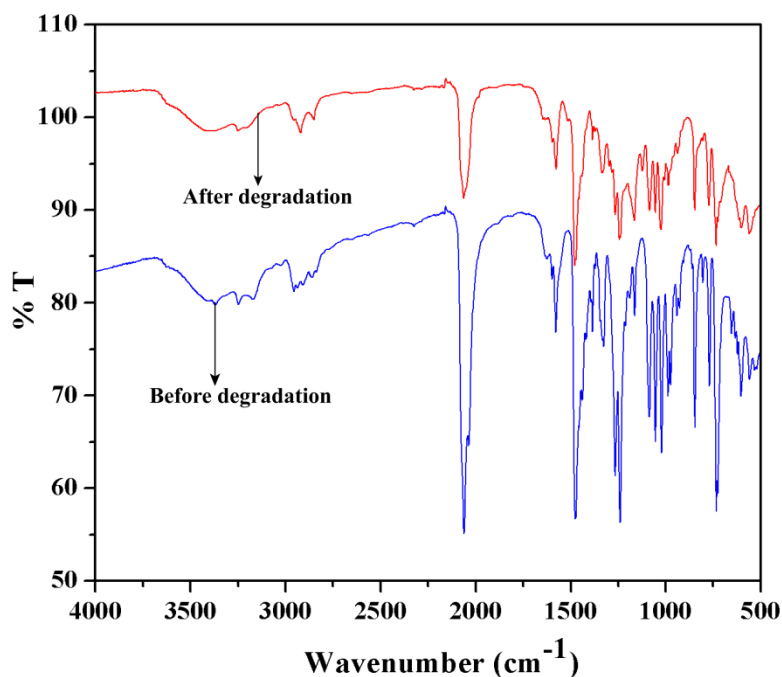


Fig.V.17: IR spectra of complex **12** before (blue) and after (red) photodegradation process.

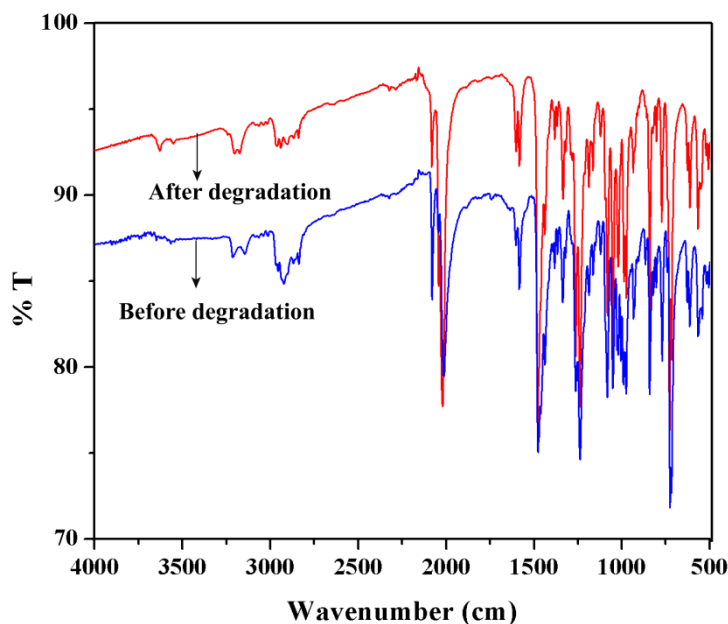


Fig.V.18:IR spectra of complex**13** before (blue) and after (red)photodegradation process.

The first step of the process is excitation of electrons from the valence band to the conduction band which creates equal amounts of positives vacancies or holes in valence band. It is well-established that holes act as powerful oxidants and electrons as powerful reductants. The second step is adsorption of oxygen or water on the surfaces of catalyst. Electrons in the conduction band is scavenged by oxygen molecule to produce $O_2^{\bullet-}$ anion radical, which provides peroxide radical ($^{\bullet}OOH$) and then decomposed to active hydroxyl radical ($^{\bullet}OH$). On the other hand, the holes in the valence band interact with H_2O or $^{\bullet}OH$ to produce highly active hydroxyl radical ($^{\bullet}OH$). Finally, the effective degradation of methylene blue is occurred by these generated hydroxyl radicals ($^{\bullet}OH$).

V.4.2. *Structure-activity relationship*

The photocatalytic degradation study has been carried out with visible light irradiation. So the degradation process must be initiated with visible light absorption. Absorption spectra of both complexes contain peaks around 590 nm in the visible region, originating from copper(II)-based ${}^2T_{2g}(D) \leftarrow {}^2E_g(D)$ transition. Thus copper(II) centres may be considered as the initiator of the degradation process. As already mentioned, copper(II) centre in complex **12** is relatively more free to take part in any reaction for its open zigzag structure. High efficiency of complex **12** to degrade the dye (MB) is therefore justified from its structure. On the other hand, copper(II) is rigidly imprisoned in a cyclic tetranuclear skeleton in complex **13** and is less free to take part in reaction. This explains the less catalytic efficiency of complex **13** compared to complex **12**.

A comparative study has also been done to compare the degradation efficiency of these complexes with all reported complexes, which has been characterized structurally. The comparative study has been shown in Table V.7. This indicates our complexes are good enough to be explored in industrial chemistry, although better complexes are also known in literature. However, it should be noted that many of the previously reported catalysts have been prepared using Schiff bases as ligands and therefore their application in aqueous medium is limited (Schiff bases are susceptible to hydrolysis). Our complexes are containing reduced Schiff bases as ligands and may, therefore, be used in aqueous medium without any problem related to destruction of the ligands via hydrolysis.

Table V.7: Kinetic studies for the degradation of methylene blue by some previously reported compounds and the present complexes.

Complex	Degradation time (min)	Degradation percentage	Refs.
$[\text{Zn}(\mu_{1,1}\text{-N}_3)_2\{\text{Zn}(\text{L}^a)(\text{N}_3)\}_2]$	18	90%	[30]
$[\text{Zn}(\mu_{1,1}\text{-N}_3)_2\{\text{Zn}(\text{L}^a)(\text{N}_3)\}_2] \cdot 0.5\text{CH}_3\text{OH}$	60	90%	[49]
$\{[\text{CdL}^a(\mu_{1,1}\text{-N}_3)]_2\text{Cd}(\mu_{1,1}\text{-N}_3)_2 \cdot 1.76\text{CH}_3\text{OH}\}_n$	40	99%	[66]
$[\text{Zn}(\text{DCTP})(\text{L}^b)]_n$	120	96.9%	[67]
$[\text{Zn}(\text{L}^c)(\text{DCTP})]_n$	120	81.4%	[67]
$[\text{Cd}_2(\text{L}^d)_2(\text{hfpd})]_n$	180	94.1%	[68]
$[\text{Zn}(\text{L}^d)(\text{tbta})]_n$	180	93.9%	[68]
$[\text{Cd}_2(\text{L}^e)_2(\mu_{1,3}\text{-SCN})_2(\text{CH}_3\text{OH})_2]$	40	85%	[69]
$[\text{Co}(\text{L}^f)(\text{tbta})] \cdot \text{H}_2\text{O}]_n$	135	82.8%	[70]
$[\text{Co}(\text{L}^d)(\text{nip})]_n$	135	84.7%	[70]
$[\text{Fe}(\text{L}^g)]$	75	96.5%	[71]
$\{[\text{Cd}_3\text{L}^h_2(\text{H}_2\text{O})_5] \cdot \text{H}_2\text{O}\}_n$	180	88.7%	[72]

$\{[\text{Cd}_3\text{L}^{\text{h}}_2(\text{hbmb})(\text{H}_2\text{O})_2]\cdot 2.5\text{H}_2\text{O}\}_n$	180	65.9%	[72]
$\{[\text{Cd}_3\text{L}^{\text{h}}_2(\text{btbb})(\text{H}_2\text{O})_2]\cdot 2\text{EtOH}\cdot 1.5\text{H}_2\text{O}\}_n$	180	85.8%	[72]
$\{[\text{Cd}_6\text{L}^{\text{h}}_4(\text{bipy})_2(\text{H}_2\text{O})_6]\cdot 3\text{H}_2\text{O}\}_n$	180	63.8%	[72]
$[(\text{N}_3)\text{L}^{\text{i}}\text{Co}^{\text{III}}\text{L}^{\text{j}}\text{Co}^{\text{III}}\text{L}^{\text{i}}]$	90	55%	[73]
$(\mu_{-1,1}\text{-N}_3)_2[(\text{H}_2\text{O})\text{Cu}(\text{L}^{\text{R}})\text{Cd}(\text{N}_3)]_2\cdot 2\text{CH}_3\text{OH}$	18	62%	Complex 12
$(\mu_{-1,1}\text{-NCS})_2[\text{CuL}^{\text{R}}\text{Cd}(\text{SCN})]_2\cdot 2\text{CH}_3\text{OH}$	18	32%	Complex 13

$\text{L}^{\text{a}} = [2 - ((3 - (\text{dimethylamino})\text{propylimino})\text{methyl}) - 6\text{-ethoxyphenol}]$; $\text{L}^{\text{b}} = 1,3\text{-bis}(5,6\text{-dimethylbenzimidazol-1-ylmethyl})\text{benzene}$; $\text{L}^{\text{c}} = 1,4\text{-bis}(\text{benzimidazol-1-ylmethyl})\text{benzene}$;
 $\text{L}^{\text{d}} = 1,5\text{-bis}(2\text{-methylbenzimidazol-1-yl})\text{pentane}$; $\text{L}^{\text{e}} = 2 - (3 - (\text{methylamino})\text{propyliminomethyl}) - 4,6\text{-dichlorophenol}$; $\text{L}^{\text{f}} = 1,5\text{-bis}(\text{benzimidazolyl})\text{pentane}$; $\text{L}^{\text{g}} = \text{porphyrin } 5 - (2 - (\text{N-benzoyl-5-carboxyl}) - 1\text{-amino}) - 10,15,20\text{-triphenyl porphyrin}$; $\text{L}^{\text{h}} = 3,4\text{-bi}(4\text{-carboxyphenyl})\text{-benzoic acid}$; $\text{L}^{\text{i}} = 2 - ((1\text{-hydroxybutan-2-ylimino})\text{methyl}) - 4\text{-bromophenol}$; $\text{L}^{\text{j}} = 2\text{-amino-1-butanol}$

$\text{H}_2\text{DCTP} = 2,5\text{-ichloroterephthalic acid}$; $\text{H}_4\text{hfpd} = 4,40\text{-(hexafluoroisopropylidene)diphthalic acid}$,
 $\text{H}_2\text{tbta} = \text{tetrabromoterephthalic acid}$. $\text{H}_2\text{tbta} = \text{tetrabromoterephthalic acid}$; $\text{H}_2\text{nip} = 5\text{-nitroisophthalic acid}$; $\text{hbmb} = 1,1' - (1,6\text{-hexane})\text{bis}(2\text{-methylbenzimidazole})$, $\text{btbb} = 1,4\text{-bis}(2 - (4\text{-thiazolyl})\text{benzimidazole-1-ylmethyl})\text{benzene}$, $4,4'\text{-bipy} = 4,4'\text{-bipyridine}$.

V.5. Concluding remarks

Synthesis and X-ray characterization of two new hetero-tetranuclear copper(II)–cadmium(II) complexes with same reduced Schiff base ligand have been described in this paper. In both complexes **12** and **13**, copper(II) and cadmium(II) resides on N_2O_2 and O_4 donor sites, respectively. The bridging mode in complex **13** is quite different than that of complex **12**. In complex **12**, two cadmium(II) centres are bridged by end-on bridging azide whereas in complex **13**, the copper(II) and cadmium(II) is bridged by end-on bridging thiocyanate instead of two cadmium(II) centres. Both complexes show significant supramolecular interactions in their solid state structures. Photocatalytic degradation study of both complexes gives a reliable result as it is the first report of the degradation study for heterometallic complexes with reduced Schiff base ligands. Both complexes have catalytic ability for the degradation of organic pollutant, MB, under visible light irradiation. Complex **12** shows a good catalytic degradation property than complex **13**. The structural variation upon the degradation process has also been rationalized. Finally, efficient catalytic ability of both complexes for the photo-degradation of organic pollutant under visible light irradiation indicates the potential application of the complex in industrial chemistry.

References

- [1] T. K. Ghosh, S. Jana, A. Ghosh, *Inorg. Chem.* 57 (2018) 15216–15228.
- [2] S. Dutta, S. Jana, P. Mahapatra, A. Bauzá, A. Frontera, A. Ghosh, *CrystEngComm* 20 (2018) 6490–6501
- [3] P. Mahapatra, S. Giri, M. G. B. Drew, A. Ghosh, *Dalton Trans.* 47 (2018) 3568–3579
- [4] P. Mahapatra, M. G. B. Drew, A. Ghosh, *Inorg. Chem.* 57 (2018) 8338–8353
- [5] S. Maity, S. Ghosh, P. Mahapatra, A. Ghosh, *Inorg. Chim. Acta* 482 (2018) 807–812.
- [6] M. Mousavi, V. Bereau, J.-P. Costes, C. Duhayon, J.-P. Sutter, *CrystEngComm* 13 (2011) 5908–5914.
- [7] A. Hazari, L. Kanta Das, A. Bauzá, A. Frontera, A. Ghosh, *Dalton Trans.* 45 (2016) 5730–5740.
- [8] P. Seth, A. Figuerola, J. Jover, E. Ruiz, A. Ghosh, *Inorg. Chem.* 53 (2014) 9296–9305.
- [9] V. Bereau, S. Dhers, J.-P. Costes, C. Duhayon, J.-P. Sutter, *Eur. J. Inorg. Chem.* (2018) 66–73.
- [10] C. Biswas, M. G. B. Drew, E. Ruiz, M. Estrader, C. Diaz, A. Ghosh, *Dalton Trans.* 39 (2010) 7474–7484.
- [11] J. Mukherjee, R. Mukherjee, *Inorg. Chim. Acta* 337 (2002) 429–438.
- [12] S. Chattopadhyay, G. Bocelli, A. Musatti, A. Ghosh, *Inorg. Chem. Commun.* 9 (2006) 1053–1057.

- [13] S. Chattopadhyay, M. G. B. Drew, A. Ghosh, *Eur. J. Inorg. Chem.* 2008, 1693-1701.
- [14] A. Bhattacharyya, S. Sen, K. Harms, S. Chattopadhyay, *Polyhedron* 88 (2015) 156-163.
- [15] X. Pang, R. Duan, X. Li, Z. Sun, H. Zhang, X. Wang, X. Chen, *Polym. Chem.* 5(2014) 6857–6864.
- [16] R. Duan, B. Gao, X. Li, X. Pang, X. Wang, H. Shao, X. Chen, *Polymer* 71 (2015) 1-7
- [17] D. J. Darensbourg, O. Karroonnirun, S. J. Wilson, *Inorg. Chem.* 50 (2011) 6775–6787.
- [18] M. Mandal, U. Monkowius, D. Chakraborty, *New J. Chem.* 40 (2016) 9824--9839.
- [19] S. K. Barman, T. Mondal, D. Koley, F. Lloret, R Mukherjee, *Dalton Trans.* 46 (2017) 4038–4054.
- [20] C. Belle, I. G.-Luneau, L. Karmazin, J.-L. Pierre, S. Albedyhl, B. Krebs, M. Bonin, *Eur. J. Inorg. Chem.* (2002) 3087–3090.
- [21] O. V. Amirkhanov, O. V. Moroz, K. O. Znovjyak, T. Yu. Sliva, L. V. Penkova, T. Yushchenko, L. Szyrwił, I. S. Konovalova, V. V. Dyakonenko, O. V. Shishkin, V. M. Amirkhanov, *Eur. J. Inorg. Chem.*(2014) 3720–3730.
- [22] S. Albedyhl, D. Schnieders, A. Jancso, T. Gajda, B. Krebs, *Eur. J. Inorg. Chem.* (2002) 1400–1409.
- [23] S. K. Dey, A. Mukherjee, *Coord. Chem. Rev.* 310 (2016) 80–115.
- [24] M. Mahato, D. Mondal, H. P. Nayek, *ChemistrySelect* 1 (2016) 6777 – 6782.

- [25] P Kar, MGB Drew, A Ghosh, *Inorg. Chim. Acta* 405 (2013) 349-355.
- [26] V. Stavila, A. A. Talin, M. D. Allendorf, *Chem. Soc. Rev.* 43 (2014) 5994–6010.
- [27] N. Hoshino, F. Iijima, G. N. Newton, N. Yoshida, T. Shiga, H. Nojiri, A. Nakao, R. Kumai, Y. Murakami, H. Oshio, *Nat. Chem.* 4 (2012) 921-926.
- [28] H.-H. Wang, J. Yang, Y.-Y. Liu, S. Song, J.-F. Ma, *Cryst. Growth Des.* 15 (2015) 4986–4992.
- [29] S. Farhadi, M. M. Amini, M. Dusek, M. Kucerakova, F. Mahmoudi, *J. Mol. Struct.* 1130 (2017) 592-602.
- [30] T. Basak, M. G. B. Drew, S. Chattopadhyay, *Inorg. Chem. Commun.* 98 (2018) 92–98.
- [31] M. Andruh, *Chem. Commun.* 47 (2011) 3025–3042.
- [32] A. Aguiari, E. Bullita, U. Casellato, P. Guerriero, S. Tamburini, P. A. Vigato, *Inorg. Chim. Acta*, 202 (1992) 157-171.
- [33] U. Casellato, P. Guerriero, S. Tamburini, P. A. Vigato, C. Benelli, *Inorg. Chim. Acta*, 207 (1993) 39-58
- [34] P. Seth, A. Figuerola, J. Jover, E. Ruiz, A. Ghosh, *Inorg. Chem.* 53 (2014) 9296–9305
- [35] A. Hazari, L. Kanta Das, A. Bauzá, A. Fronter, A. Ghosh, *Dalton Trans.* 43 (2014) 8007–8015
- [36] T. Kajiwarra, M. Nakano, K. Takahashi, S. Takaishi, M. Yamashita, *Chem. Eur. J.* 17 (2011) 196–205.

- [37] T. Kajiwarara, K. Takahashi, T. Hiraizumi, S. Takaishi, M. Yamashita, *Polyhedron* 28 (2009) 1860–1863.
- [38] Z.-X. Wang, L.-F. Wu, X.-K. Hou, M. Shao, H.-P. Xiao, M.-X. Li, *Z.Anorg.Allg.Chemie.* 640 (2014) 229-235.
- [39] T. Ishida, R. Watanabe, K. Fujiwara, A. Okazawa, N. Kojima, G. Tanaka, S. Yoshii and H. Nojiri, *Dalton Trans.* 41 (2012) 13609–13619.
- [40] X.-C. Huang, X.-H. Zhao, D. Shao, X.-Y. Wang, *Dalton Trans.*, 46 (2017) 7232–7241.
- [41] J.-P. Costes, F. Dahan, A. Dupuis, *Inorg. Chem.* 39(2000)165-168.
- [42] J.-P. Costes, F. Dahan, A. Dupuis, J.-P. Laurent, *New J. Chem.* (1998) 1525-1529.
- [43] V. Bereau, H. Bolvin, C. Duhayon, J.-P. Sutter, *Eur. J. Inorg. Chem.* (2016) 4988–4995.
- [44] V.K. Garg, M. Amita, R. Kumar, R. Gupta, *Dyes Pigm.* 63 (2004) 243-250.
- [45] V. K. Gupta, Suhas, I. Ali, V. K. Saini, *Ind. Eng. Chem. Res.* 43 (2004) 1740-1747.
- [46] P. M. K. Reddy, B. R. Raju, J. Karuppiyah, E. L. Reddy, C. Subrahmanyam, *Chem. Eng. J.* 217 (2013) 41–47.
- [47] G.M. Sheldrick, *Acta Crystallogr., Sect. C* 71 (2015) 3–8.
- [48] G. M. Sheldrick, *SADABS*, V2014/5, Software for Empirical Absorption Correction, University of Göttingen, Institute für Anorganische Chemie der Universität, Göttingen, Germany, 1999–2003.

- [49] T. Basak, A. Bhattacharyya, K. Harms, S. Chattopadhyay, *Polyhedron* 157 (2019) 449–457.
- [50] A. Hazari, T. K. Ghosh, C. J. G.-García, A. Ghosh, *Inorg. Chim. Acta* 471 (2018) 168–175. [51] A. Hazari, L. K. Das, R. M. Kadam, A. Bauzá, A. Frontera, A. Ghosh, *Dalton Trans.* 44 (2015) 3862–3876.
- [52] A. W. Addison, T. N. Rao, J. Reedijk, J. V. Rijn, G. C. Verschoor, *J. Chem. Soc., Dalton Trans.* (1984) 1349–1356.
- [53] D. Cremer, J. A. Pople, *J. Am. Chem. Soc.* 97 (1975) 1354–1358.
- [54] D. Cremer, *Acta Crystallogr., Sect. B: Struct. Sci.* 40 (1984) 498–500.
- [55] M. A. S. Goher, N. A. Al-Salem, F. A. Mautner, K. O. Klepp, *Polyhedron* 16 (1997) 825–831.
- [56] F. A. Mautner, M. Scherzer, C. Berger, R. C. Fischer, R. Vicente, S. S. Massoud, *Polyhedron* 85 (2015) 329–336.
- [57] F. A. Mautner, M. Traber, R. C. Fischer, K. Reichmann, R. Vicente, *Polyhedron* 144 (2018) 30–35.
- [58] F. A. Mautner, M. Scherzer, C. Berger, R. C. Fischer, R. Vicente, S. S. Massoud, *Polyhedron* 85 (2015) 20–26.
- [59] S. Chattopadhyay, M. S. Ray, S. Chaudhuri, G. Mukhopadhyay, G. Bocelli, *Inorg. Chimica Acta* 359 (2006) 1367–1375.
- [60] P. Chakraborty, I. Majumder, H. Kara, S. K. Chattopadhyay, E. Zangrando, D. Das, *Inorg. Chim. Acta* 436 (2015) 139–145.

- [61] M. A. Khan, A. A. Alqadami, M. Otero, M. R. Siddiqui, Z. A. Alothman, I. Alsohaimi, M. Rafatullah, A. E. Hamedelniei, *Chemosphere* 218 (2019) 1089–1099.
- [62] S. Ghorai, A. Sarmah, R. K. Roy, A. Tiwari, C. Mukherjee, *Inorg. Chem.* 55 (2016) 1370–1380.
- [63] A. Biswas, L. K. Das, M. G. B. Drew, C. Diaz, A. Ghosh, *Inorg. Chem.* 51 (2012) 10111–10121.
- [64] A. Golcu, M. Tumer, H. Demirelli, R. A. Wheatley, *Inorg. Chim. Acta* 358 (2005) 1785–1797.
- [65] S. Roy, A. Bauzá, A. Frontera, S. Chattopadhyay, *Inorg. Chim. Acta* 453 (2016) 51–61.
- [66] S. Roy, K. Harms, A. Bauzá, A. Frontera, S. Chattopadhyay, *Polyhedron*, 121 (2017) 199–205.
- [67] X. Wei, Y. Li, Z. Qin, G. Cui, *J. Mol. Struct.* 1175 (2019) 253–260.
- [68] X. Zhao, Z. Qin, Y. Li, G. Cui, *Polyhedron*, 153 (2018) 197–204.
- [69] S. Roy, K. Harms, S. Chattopadhyay, *Polyhedron* 127 (2017) 471–477.
- [70] X. Zhao, Z. Qin, Y. Li, G. Cui, *Polyhedron*, 146 (2018) 65–72.
- [71] T. Liu, T. Hu, C. Hu, J. Lang, *Inorg. Chem. Commun.* 90 (2018) 26–28.
- [72] L. Liu, J. Ding, C. Huang, M. Li, H. Hou, Y. Fan, *Cryst. Growth. Des.* 14 (2014) 3035–3043.
- [73] K. Ghosh, K. Harms, A. Franconetti, A. Frontera, S. Chattopadhyay, *J. Organomet. Chem.* 883 (2019) 52–64.

Chapter VI

Highlights of the thesis

The entire research work contained within this dissertation mainly focuses on synthesis and characterization of multi-metallic complexes with reduced Schiff base ligands. The studies of different weak interactions in the solid state are esteemed and might be useful to understand the stability of new supramolecular assemblies or synthetic host-guest systems. In terms of application, few complexes have shown good result towards catalysis. The exciting observations are gathered below.

Synthesis and characterization of four (hydrogen bonded) dimeric nickel(II) complexes with reduced Schiff base blocking ligands have been described in Chapter II. The energy of these hydrogen bonds has been estimated by DFT calculation. The energy associated to the low barrier hydrogen bond is found to be very large due to the strong covalent character of the interaction.

A hemi-directed copper(II)/lead(II) complex has been synthesized and characterized in Section A of Chapter III. The energy of chalcogen–chalcogen and tetrel bonding interactions in this complex was analyzed by DFT calculations. On the other hand, a hetero-nuclear nickel(II)/lead(II) complex has been synthesized and characterized in Section B of Chapter III. The tetrel bonding interactions established between the σ -hole at the hemi-coordinated lead(II) and the electron rich chlorido ligand has been analyzed by DFT study.

Synthesis and characterization of a series of hemi- and holodirected nickel(II)/lead(II) complexes were reported in Section C of Chapter III and also in Chapter IV. A density functional theory study is devoted to analyze the tetrel bonding interactions that are established between the σ -hole at the hemicoordinated lead(II) and either the electron-rich thiocyanate or the π -system of the aromatic ligand.

Two new tetra-nuclear copper(II)/cadmium(II) complexes with CuO₂Cd cores have been synthesized and characterized in Chapter V. Their ability to act as photo-catalyst in degrading methylene blue has been explored. The difference in their photocatalytic performance may be correlated with their structures.

Appendix

List of publications

1. Importance of π -Interactions Involving Chelate Rings in Addition to the Tetrel Bonds in a Series of Hemi-directed Nickel(II)/Lead(II) Complexes.

S. Mirdya, S. Roy, S. Chatterjee, A. Bauza, A. Frontera and S. Chattopadhyay, *Cryst.GrowthDes.* 2019, 19, 10, 5869–5881

2. Formation of a tetranuclear supramolecule via non-covalent Pb \cdots Cl tetrel bonding interaction in a hemidirectedlead(II) complex with a nickel(II) containing metaloligand.

S. Mirdya, A. Frontera and S. Chattopadhyay, *CrystEngComm*, 2019,21, 6859-6868.

3. An insight into the non-covalent Pb \cdots S and S \cdots S interactions in the solid-state structure of a hemidirectedlead(II) complex.

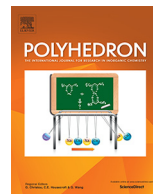
S. Mirdya, S. Banerjee and S. Chattopadhyay, *CrystEngComm*, 2020, 22, 237-247

4. Tetranuclear complexes with CuO₂Cd cores: Exploratrion of their photocatalytic ability to degrade methylene blue.

S. Mirdya, T.; Basak, S. Chattopadhyay, *Polyhedron*. 2019, 170, 253–263.

5. A series of hydrogen bond mediated dinuclearnickel(II) complexes with reduced Schiff base ligands: An insight into the nature of hydrogen bonds in them

S. Mirdya, M. G. B. Drew, A. K. Chandra, A. Banerjee, A. Frontera, and S. Chattopadhyay, *Polyhedron* 2020, 179, 114374.



A series of hydrogen bond mediated dinuclear nickel(II) complexes with reduced Schiff base ligands: An insight into the nature of their short intermolecular hydrogen bonds

Saikat Mirdya^a, Michael G.B. Drew^b, Akash Kumar Chandra^a, Abhisek Banerjee^{a,*}, Antonio Frontera^{c,*}, Shouvik Chattopadhyay^{a,*}

^a Department of Chemistry, Inorganic Section, Jadavpur University, Kolkata 700032, India

^b School of Chemistry, The University of Reading, P. O. Box 224, Whiteknights, Reading RG6 6AD, UK

^c Departament de Química, Universitat de les Illes Balears, Crta de Valldemossa km 7.5, 07122 Palma de Mallorca (Balears), Spain

ARTICLE INFO

Article history:

Received 20 November 2019

Accepted 15 January 2020

Available online 17 January 2020

Keywords:

Dinuclear

Nickel

Reduced Schiff base

Hydrogen bond

DFT

ABSTRACT

A series of isostructural centrosymmetric hydrogen bonded dimeric nickel(II) complexes of general formula, $[\text{Ni}_2(\text{HL})_2(\text{DMSO})_2(\text{H}_2\text{O})_2]\text{X}$ {where $\text{H}_2\text{L} = \text{N}_2\text{O}_4$ donor reduced Schiff base ligand, $[\text{H}_2\text{L}^1 = (2,2\text{-dimethyl-1,3-propanediyl})\text{bis}(\text{iminomethylene})\text{bis}(6\text{-methoxyphenol})$ and $\text{H}_2\text{L}^2 = (2,2\text{-dimethyl-1,3-propanediyl})\text{bis}(\text{iminomethylene})\text{bis}(6\text{-ethoxyphenol})$] and $\text{X} = \text{counter anion}$ }, are synthesized and characterized by elemental analysis, infrared and electronic spectra. The structures of all complexes have been confirmed by single crystal X-ray diffraction analysis. Each complex forms $\text{O} \cdots \text{H} \cdots \text{O}$ hydrogen bonded dimer in the solid state, where the $\text{O} \cdots \text{O}$ distance is very short, ranging from 2.424(3) to 2.437(3) Å. The hydrogen bonds are very strong as can be seen from the DFT estimated energy of these hydrogen bonds. Non-covalent interaction plot (NCI plot) index has been used to characterize them.

© 2020 Elsevier Ltd. All rights reserved.

1. Introduction

The interaction energy of conventional hydrogen bonds basically depends on their geometric features like length and linearity. However, the difference in the pK_a values (where pK_a is the negative logarithm of K_a) of the heavy atoms sharing the proton is also important [1]. The ΔH of formation of the water dimer is ~ 5 kcal/mol¹ in the gas phase. However, the $\text{HO}-\text{H} \cdots \text{OH}_2$ hydrogen bond in water is weaker due to the large difference between the pK_a values of the donor group and the conjugate acid of the acceptor group (15.7 for H_2O and -1.7 for H_3O^+) [2]. In the gas and solid state phases, hydrogen bonds between hetero atoms with similar pK_a values can be very short and strong (up to 30 kcal mol⁻¹) [3–6]. When groups of equal pK_a establish an hydrogen bond, three different situations different situations may occur (see Fig. 1). The classical hydrogen bond where the hydrogen atom is covalently bonded to one of both oxygen atoms (dipole \cdots dipole interaction, see Fig. 1a). As the $\text{O} \cdots \text{O}$ distance is progressively shortened, the energy barrier lowers until it reaches the lower vibrational energy levels, thus leading to a low barrier hydrogen bond (LBHB, see

Fig. 1b). In this case, the hydrogen atom can move freely between the two oxygen atoms with its average position is the center (high covalent character) [7]. Further shortening leads to a single-well hydrogen bond with the highest covalent character and interaction energy of the three situations.

In this manuscript, we report the synthesis and X-ray characterization of a series of mononuclear nickel(II) complexes that form $\text{O} \cdots \text{H} \cdots \text{O}$ hydrogen bonded dimers in the solid state where the $\text{O} \cdots \text{O}$ distance is very short, ranging from 2.424(3) to 2.437(3) Å. We have analyzed the hydrogen bonds using DFT calculations

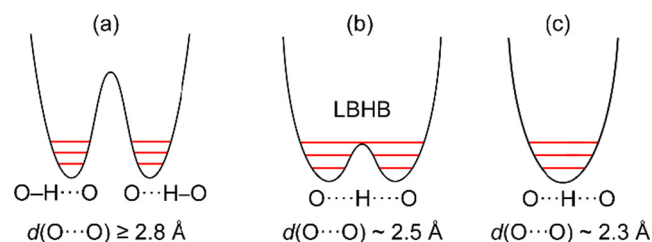


Fig. 1. Energy diagrams for $\text{OH} \cdots \text{H}$ hydrogen bonds between groups of identical pK_a . (a) Standard hydrogen bond with $\text{O} \cdots \text{O}$ distance $d(\text{O} \cdots \text{O}) \geq 2.8$ Å. (b) Low barrier hydrogen bond of $d(\text{O} \cdots \text{O}) \sim 2.55$ Å (average position in the center). (c) Single-well hydrogen bond with $d(\text{O} \cdots \text{O}) \sim 2.3$ Å.

* Corresponding authors at: Tel.: +033-24572941 (S. Chattopadhyay).

E-mail addresses: abhiseksrk@gmail.com (A. Banerjee), toni.frontera@uib.es (A. Frontera), shouvik.chem@gmail.com (S. Chattopadhyay).

and the non-covalent interaction plot (NCI plot) index to distinguish between the three possible situations represented in Fig. 1.

2. Experimental section

2.1. Materials

Nickel(II) thiocyanate tetrahydrate was prepared in our laboratory following the literature method [8]. All other materials are commercially available, reagent grade and used as purchased from Sigma-Aldrich without further purification.

Caution!!! Although no problems were encountered in this work, perchlorate salts in presence of organic ligands are potentially explosive. Only a small amount of the materials should be prepared and they must be handled with care.

2.2. Synthesis

2.2.1. Synthesis of Schiff base ligands

2.2.1.1. Synthesis of H_2L^a [N,N' -bis(3-methoxysalicylidene)-2,2-dimethyl-1,3-propanediamine], H_2L^b [N,N' -bis(3-ethoxysalicylidene)-2,2-dimethyl-1,3-propanediamine], H_2L^c [N,N' -bis(3-methoxysalicylidene)-1,3-propanediamine] and H_2L^d [N,N' -bis(3-ethoxysalicylidene)-1,3-propanediamine]. A methanol solution (10 mL) of 2,2-dimethyl-1,3-propanediamine (1 mmol, 0.12 mL) was mixed separately with of 3-methoxysalicylaldehyde (2 mmol, 304 mg) and 3-ethoxysalicylaldehyde, (2 mmol, 332 mg) and the resulting solutions were allowed to reflux for ca. 2 h to synthesize two hexadentate N_2O_4 donor Schiff base ligands, H_2L^a [N,N' -bis(3-ethoxysalicylidene)-2,2-dimethyl-1,3-propanediamine] and H_2L^b [N,N' -bis(3-ethoxysalicylidene)-2,2-dimethyl-1,3-propanediamine] respectively. Other two hexadentate Schiff bases, H_2L^c [N,N' -bis(3-methoxysalicylidene)-1,3-propanediamine] and H_2L^d [N,N' -bis(3-ethoxysalicylidene)-1,3-propanediamine] were synthesized following the similar procedure as mentioned above except 1,3-propanediamine (1 mmol, 0.11 mL) was used as the diamine instead of 2,2-dimethyl-1,3-propanediamine.

2.2.2. Synthesis of the reduced Schiff base ligands

2.2.2.1. Synthesis of H_2L^1 [(2,2-dimethyl-1,3-propanediyl)bis(iminomethylene)bis(6-methoxyphenol)]. The prepared Schiff base solution, H_2L^a was cooled to 0 °C, and solid sodium borohydride (4 mmol, 150 mg) was then added gently to this solution with constant stirring. The solution was further acidified with glacial acetic acid (10 mL) and placed under reduced pressure in a rotary evaporator (~60 °C). The residue was dissolved in water (15 mL) and extracted with dichloromethane (15 mL) using a separating funnel. Finally the dichloromethane part was dried using anhydrous sodium acetate to get the desired hexadentate N_2O_4 donor reduced Schiff base ligand, H_2L^1 . The ligand was not purified and used directly for the synthesis of complex 1.

2.2.2.2. Synthesis of H_2L^2 [(2,2-dimethyl-1,3-propanediyl)bis(iminomethylene)bis(6-ethoxyphenol)]. A potential hexadentate N_2O_4 donor reduced Schiff base was synthesized following the similar procedure as used for Schiff base, H_2L^1 , except H_2L^b was used as the Schiff base derivative. It was not purified and was used directly for the synthesis of complex 2.

2.2.2.3. Synthesis of H_2L^3 [(1,3-propanediyl)bis(iminomethylene)bis(6-methoxyphenol)]. A potential hexadentate N_2O_4 donor reduced Schiff base was synthesized following the same procedure as described above, except H_2L^c was used as the Schiff base derivative. It was not purified and was used directly for the synthesis of complex 3.

2.2.2.4. Synthesis of H_2L^4 [(1,3-propanediyl)bis(iminomethylene)bis(6-ethoxyphenol)]. A potential hexadentate N_2O_4 donor reduced Schiff base was synthesized following the same procedure as described above, except H_2L^d was used as the Schiff base derivative. It was not purified and was used directly for the synthesis of complex 4.

2.2.3. Synthesis of complexes

2.2.3.1. Synthesis of $[Ni_2(HL^1)_2(DMSO)_2(H_2O)_2](ClO_4)_2 \cdot 2H_2O$ (**1**). A methanol solution of nickel(II) perchlorate hexahydrate, (0.99 mmol, 257 mg), was added into the methanol solution of a reduced Schiff base ligand, H_2L^1 , with constant stirring and colour of the solution turned into dark green. Few drops of DMSO were added and the resulting solution was kept for crystallization. Dark green single crystals, suitable for X-ray diffraction, were obtained after 3–4 days on slow evaporation of the solution in open atmosphere.

Yield: 350 mg, (~54%, based on Ni). Anal. Calc. for $C_{23}H_{38}N_2NiO_{10.5}Cl$ (FW = 636.77): C, 42.87; H, 5.74; N, 4.35%. Found: C, 42.8; H, 5.8; N, 4.3%. FT-IR (KBr, cm^{-1}): 3400 (ν_{O-H}), 3270 (ν_{N-H}), 2990–2850 (ν_{C-H}). UV-Vis, λ_{max} (nm), [ϵ_{max} ($dm^3 mol^{-1} cm^{-1}$)] (DMSO), 730 (1.01×10^2), 625 (2.00×10^2), 355 (2.65×10^3), 280 (5.6×10^3).

2.2.3.2. Synthesis of $[Ni_2(HL^2)_2(DMSO)_2(H_2O)_2](ClO_4)_2$ (**2**). Complex **2** was synthesized following the similar procedure as that for complex **1** except that the reduced Schiff base ligand, H_2L^2 , was used instead of H_2L^1 . Dark green coloured crystalline complex suitable for X-ray diffraction, started to separate from the solution after 3–4 days on standing at room temperature and was collected by filtration.

Yield: 343 mg, (~53%, based on Ni). Anal. Calc. for $C_{25}H_{41}ClN_2NiO_{10}S$ (FW = 655.82): C, 53.5; H, 5.8; N, 4.2%. Found: C, 53.4; H, 5.7; N, 4.3%. FT-IR (KBr, cm^{-1}): 3395 (ν_{O-H}), 3280 (ν_{N-H}), 2990–2865 (ν_{C-H}). UV-Vis, λ_{max} (nm), [ϵ_{max} ($dm^3 mol^{-1} cm^{-1}$)] (DMSO), 720 (0.89×10^2), 620 (1.80×10^2), 355 (4.84×10^3), 274 (9.38×10^4).

2.2.3.3. Synthesis of $[Ni_2(HL^3)_2(DMSO)_2(H_2O)_2](NCS)_2 \cdot 2CH_3OH$ (**3**). **Yield:** 392 mg, (~60%, based on Ni). Anal. Calc. for $C_{24}H_{41}N_3NiO_8S_3$ (FW = 654.48): C, 44.0; H, 6.2; N, 6.4%. Found: C, 43.7; H, 6.2; N, 6.6%. FT-IR (KBr, cm^{-1}): 3390 (ν_{O-H}), 3260 (ν_{N-H}), 3012–2840 (ν_{C-H}), 2045 (ν_{NCS}). UV-Vis, λ_{max} (nm), [ϵ_{max} ($dm^3 mol^{-1} cm^{-1}$)] (DMSO), 718 (1.40×10^2), 622 (2.78×10^3), 355 (4.34×10^2), 280 (9.49×10^4).

A methanol solution of nickel(II) thiocyanate tetrahydrate (1.01 mmol, 250 mg) was added into the methanol solution of a reduced Schiff base ligand, H_2L^3 , with constant stirring and colour of the solution turned into dark green. Few drops of DMSO were added and the resulting solution was kept for crystallization. Dark green single crystals, suitable for X-ray diffraction, were obtained after 2–3 days on slow evaporation of the solution in open atmosphere.

2.2.3.4. Synthesis of $[Ni_2(HL^4)_2(DMSO)_2(H_2O)_2](ClO_4)_2$ (**4**). Complex **4** was synthesized following the similar procedure as that for complex **3** except that the reduced Schiff base ligand, H_2L^4 , was used instead of H_2L^3 . Dark green coloured crystalline complex suitable for X-ray diffraction, started to separate from the solution after 2–3 days on standing at room temperature and was collected by filtration.

Yield: 344 mg, (~54%, based on Ni). Anal. Calc. for $C_{23}H_{37}N_2NiO_{10}Cl$ (FW = 627.75): C, 43.9; H, 5.9; N, 4.4%. Found: C, 43.8; H, 5.8; N, 4.5%. FT-IR (KBr, cm^{-1}): 3420 (ν_{O-H}), 3265 (ν_{N-H}), 2995–2870 (ν_{C-H}). UV-Vis, λ_{max} (nm), [ϵ_{max} ($dm^3 mol^{-1} cm^{-1}$)] (DMSO), 755 (0.58×10^2), 635 (0.93×10^2), 360 (3.8×10^3), 271 (8.86×10^3).

2.3. Physical measurements

Elemental analyses (carbon, hydrogen and nitrogen) were carried out using a Perkin Elmer 240C elemental analyzer. IR spectra in KBr (4500–500 cm^{-1}) were recorded with a Perkin Elmer Spectrum Two spectrophotometer. Electronic spectra in acetonitrile (200–800 nm) were recorded on a Perkin Elmer Lambda 35 UV-visible spectrophotometer.

2.4. X-ray crystallography

Suitable single crystals of all the complexes were used for data collection using a 'Bruker D8 QUEST area detector' diffractometer equipped with graphite-monochromated Mo K_{α} radiation ($\lambda = 0.71073$ Å). The molecular structures were solved by direct methods and refined by full-matrix least squares on F^2 using the SHELXL-16/6 package [9]. Non-hydrogen atoms were refined with anisotropic thermal parameters. Hydrogen atoms attached to nitrogen and oxygen atoms were located by difference Fourier maps and refined with distance constraints. There were two molecules in the asymmetric unit in complexes **1** and **2**. In complex **3**, it proved impossible to locate the thiocyanate anion due to excessive disorder and the SQUEEZE option was applied via the PLATON program [10] to account for the electron density. The calculation showed 174 electrons in the voids which would allow for one thiocyanate anion together with methanol solvent molecules in the asymmetric unit. This program was also used for the cavity in complex **2**. All four structures contained very short intramolecular OH...O distances in the range 2.424(3)–2.437(3) Å. It was assumed that it was most likely that on average the hydrogen atom occupied a central position between the oxygen atoms in these structures and distance constraints were applied accordingly such that the hydrogen was so placed. Other hydrogen atoms bonded to oxygen and nitrogen atoms were refined with distance constraints but those bonded to carbon were placed in their geometrically idealized positions and constrained to ride on their parent atoms. Disorder was also modelled in the perchlorate anions and the attached ethanol molecules in **2** and **4**. Multi-scan empirical absorption corrections were applied to the data using the program SADABS [11]. A summary of the crystallographic data has been given in Table 1.

Table 2

Selected bond lengths (Å) of complexes **1–2** (around Ni(1), Ni(2) in dimers A and B respectively) and complexes **3–4**.

Complex	1	2	3	4
Ni(1)–O(1)	2.079(3)	2.085(4)	2.076(2)	2.096(3)
Ni(1)–O(2)	2.071(3)	2.086(5)	2.090(2)	2.101(3)
Ni(1)–O(3)	2.101(3)	2.087(5)	2.089(2)	2.092(3)
Ni(1)–O(4)	2.080(3)	2.074(5)	2.085(3)	2.087(3)
Ni(1)–N(1)	2.096(3)	2.100(7)	2.097(3)	2.096(3)
Ni(1)–N(2)	2.102(4)	2.092(6)	2.090(3)	2.103(3)
Ni(2)–O(8)	2.081(3)	2.076(4)	–	–
Ni(2)–O(9)	2.077(3)	2.089(5)	–	–
Ni(2)–O(10)	2.103(4)	2.077(4)	–	–
Ni(2)–N(3)	2.095(3)	2.084(5)	–	–
Ni(2)–N(4)	2.095(3)	2.094(4)	–	–
Ni(2)–O(7)	2.078(3)	2.080(4)	–	–

Programs used: SHELX-2016/6 [9], PLATON [10], WINGX [12], ORTEP [13] and MERCURY [14]. Selected bond lengths for all four complexes are given in Tables 2. Selected bond angles of all complexes are given in Table S2 (see supporting information, SI).

2.5. Theoretical methods

The energies of the complexes reported in this study were computed at the B3LYP-D/def2-SVP level of theory using the crystallographic coordinates by means of the Gaussian-09 program [15]. The Grimme's dispersion [16] correction has also been used since it is adequate for the evaluation of non-covalent interactions. The basis set superposition error for the calculation of interaction energies has been corrected using the counterpoise method [17]. The NCI index and NCI plot [18] isosurfaces have been used to characterize the non-covalent interactions. They correspond to both favorable and unfavorable interactions, as differentiated by the sign of the second density Hessian eigen value and defined by the isosurface color. The color scheme is a red-yellow-green-blue scale with red for ρ_{cut}^+ (repulsive) and blue for ρ_{cut}^- (attractive), whereas yellow and green isosurfaces correspond to weak repulsive and weak attractive interactions, respectively [19].

Table 1

Crystal data and refinement details of complexes **1–4**.

Complex	1	2	3	4
Formula	$\text{C}_{23}\text{H}_{38}\text{N}_2\text{NiO}_{10.5}\text{SCl}$	$\text{C}_{25}\text{H}_{41}\text{ClN}_2\text{NiO}_{20}\text{S}$	$\text{C}_{21}\text{H}_{33}\text{N}_2\text{NiO}_6\text{S} + \text{NCS anion} + \text{methanol solvent molecules}$	$\text{C}_{23}\text{H}_{37}\text{N}_2\text{NiO}_{10}\text{SCl}$
Formula Weight	636.77	655.82	500.24	627.75
Crystal System	Triclinic	Triclinic	Monoclinic	Monoclinic
Space group	$P\bar{1}$	$P\bar{1}$	$P2_1/n$	$C2/c$
a(Å)	13.044(11)	12.344(3)	13.422(1)	22.317(2)
b(Å)	14.575(13)	14.130(3)	15.229(4)	15.316(11)
c(Å)	17.002(15)	20.995(4)	13.651(2)	16.547(13)
$\alpha(^{\circ})$	83.19(2)	80.25(5)	(90)	(90)
$\beta(^{\circ})$	68.10(4)	78.99(5)	106.16(3)	91.15(3)
$\gamma(^{\circ})$	88.22(15)	65.07(5)	(90)	(90)
$V(\text{\AA}^3)$	2978.0(5)	3243.6(12)	2680.4(6)	5655.0(7)
Z	2	2	2	4
$d(\text{calc}) [\text{g cm}^{-3}]$	1.418	1.343	1.240	1.475
$\mu [\text{mm}^{-1}]$	0.866	0.796	0.835	0.910
$F(0\ 0\ 0)$	1336	1384	1060	2640
Total Reflections	81,257	75,605	28,688	34,336
Unique Reflections	9526	11,546	4778	5009
Observed data $I > 2\sigma(I)$	8266	7735	3638	4135
R(int)	0.032	0.070	0.090	0.042
*R1, wR2 (all data)	0.0546, 0.1517	0.1170, 0.2655	0.0676, 0.1439	0.0706, 0.1861
R1, wR2 ($I > 2\sigma(I)$)	0.0470, 0.1429	0.0772, 0.2120	0.0469, 0.1222	0.0594, 0.1747
Residual Electron Density ($\text{e}\text{\AA}^{-3}$)	1.423, −0.815	1.047, −0.958	0.512, −0.614	1.520, −0.950

*R1 = $\sum ||F_o| - |F_c|| / \sum |F_o|$ and wR2 = $\sum w(|F_o|^2 - |F_c|^2)^2 / \sum w|F_o|^4$.

3. Results and discussion

3.1. Synthesis

Two moles of 3-alkoxysalicylaldehydes (3-methoxy and 3-ethoxy) have been used to condense separately with 2,2-dimethyldiaminopropane and 1,3-diaminopropane in methanol medium to prepare four Schiff bases, H_2L^a , H_2L^b , H_2L^c and H_2L^d . These Schiff bases were then reduced with $NaBH_4$ in methanol under constant stirring at 0 °C to prepare four respective reduced Schiff bases, H_2L^1 , H_2L^2 , H_2L^3 and H_2L^4 respectively following the literature method [20] (Scheme 1).

These reduced Schiff bases on then reaction with nickel(II) perchlorate hexahydrate or nickel(II) thiocyanate in methanol and on adding few drops of DMSO to the individual reaction mixture gave rise to complexes **1–4** (Scheme 2).

Use of reduced Schiff base ligands seems to be crucial in forming these types of hydrogen bonded dimeric complexes, as the non-reduced Schiff bases were unable to produce such complexes. Many synthetic inorganic chemistry groups have prepared many homo and heteronuclear complexes with the corresponding non-reduced Schiff base ligands, but did not obtain complexes similar to complexes **1–4**. This is probably due to the greater flexibility of the reduced Schiff bases compared to their non-reduced precursors.

3.2. Description of structures

3.2.1. $[Ni_2(HL^1)_2(DMSO)_2(H_2O)_2](ClO_4)_2 \cdot H_2O$ (**1**), and $[Ni_2(HL^2)_2(DMSO)_2(H_2O)_2](ClO_4)_2$ (**2**)

X-ray crystal structure determinations reveal that complexes **1** and **2** crystallize in triclinic space group, $P\bar{1}$ with two molecules in the asymmetric unit. Potential N_2O_4 donor hexadentate reduced

Schiff bases, H_2L^1 and H_2L^2 , have been used to prepare these complexes respectively. Each complex actually possesses a dinuclear moiety formed via strong hydrogen bonds. Each structure consists of two independent centrosymmetric dimers (A and B) with equivalent geometry. Views of the A dimers of complexes **1** and **2** are given in Figs. 2 and 3 respectively. The structure of dimer B of each complex is very similar to the structure of dimer A (Figs. S1 and S2 in SI).

In each dimeric unit, nickel(II) centers are hexa-coordinated and adopt distorted octahedral geometry. Each nickel(II) center, {Ni(1)}

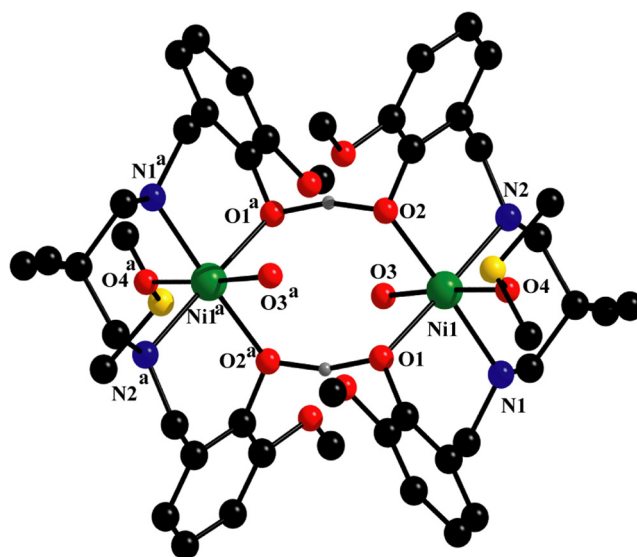
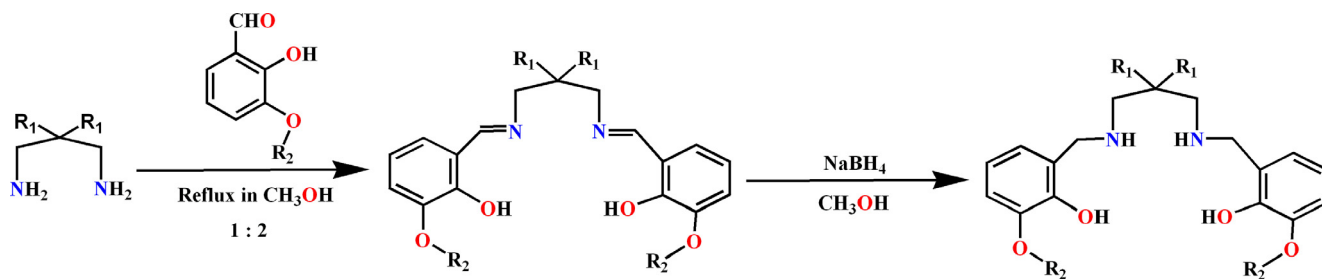
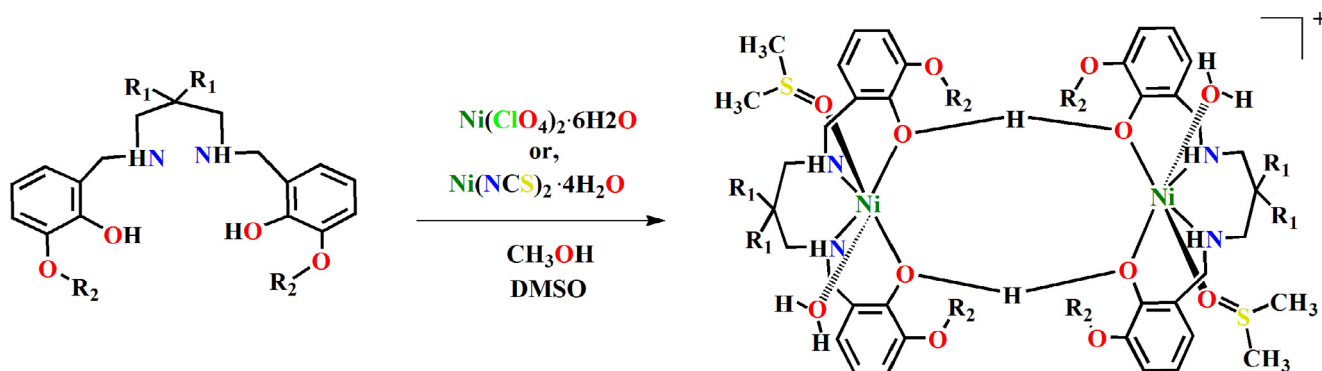


Fig. 2. Perspective view of dimer A of complex **1** with selective atom-numbering scheme. Non co-ordinated perchlorate ions have been omitted for clarity. Only the hydrogen atoms between the phenolic oxygen atoms are shown.



Scheme 1. Synthetic route to 'reduced Schiff base' ligands.



Scheme 2. Synthetic route to complexes **1** ($R_1 = Me$, $R_2 = Me$), **2** ($R_1 = Me$, $R_2 = Et$), **3** ($R_1 = H$, $R_2 = Me$) and **4** ($R_1 = H$, $R_2 = Et$). Non coordinated counter anions have not been shown here.

of A and Ni(2) of B) is equatorially coordinated by two amine nitrogen atoms, {N(1) and N(2) for Ni(1) and N(3) and N(4) for Ni(2)}, two phenoxo oxygen atoms, {O(1) and O(2) for Ni(1) and O(7) and O(8) for Ni(2)}, of the reduced Schiff base units. The axial sites are coordinated by two oxygen atoms, {O(3) and O(4) for Ni(1) and O(9) and O(10) for Ni(2)} of coordinated water and DMSO molecule. Each of the reduced Schiff bases are dibasic in character, but loses only one proton to form mononegative anion, which, in turn, connects with another such moiety via strong hydrogen bonding to form the symmetric dimeric structure. The deprotonations of the hydroxyl group are well reflected in the nickel(II)-oxygen bond lengths (Table 2). The deprotonated hydroxyl groups are bound strongly (shorter bond length) with nickel(II) centers compared with the non-deprotonated hydroxyl groups [21]. The saturated six membered chelate rings, Ni(1)-N(1)-C(9)-C(10)-C(13)-N(2) and Ni(1)-N(1)-C(10)-C(11)-C(14)-N(2), in dimer A of complexes **1** and **2** respectively represent individual chair conformations with puckering parameters [22], $q(2) = 0.583(4) \text{ \AA}$, $\varphi = 168(2)^\circ$, and $q(2) = 0.589(8) \text{ \AA}$, $\varphi = 199(7)^\circ$ respectively. Similarly the saturated six membered chelate rings, Ni(2)-N(3)-C(32)-C(33)-C(36)-N(4) and Ni(2)-N(3)-C(35)-C(36)-C(39)-N(4), in dimer B of complexes **1** and **2** respectively also represent individual chair

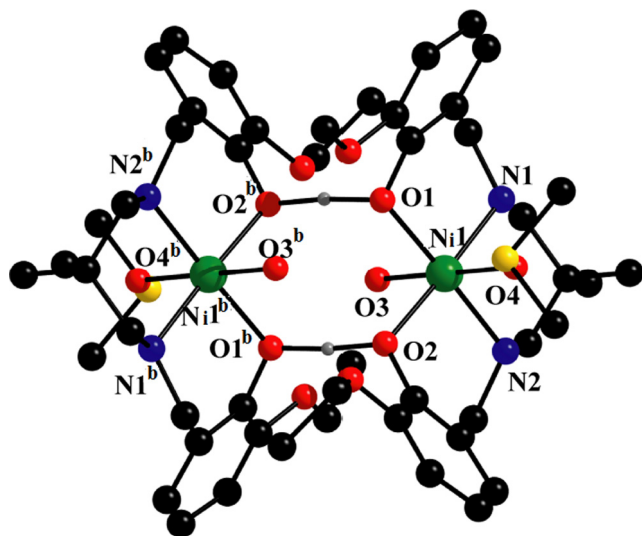


Fig. 3. Perspective view of dimer A of complex **2** with selective atom-numbering scheme. Non co-ordinated counter anions are not shown. Hydrogen atoms are omitted for clarity apart from those between the phenolic oxygen atoms.

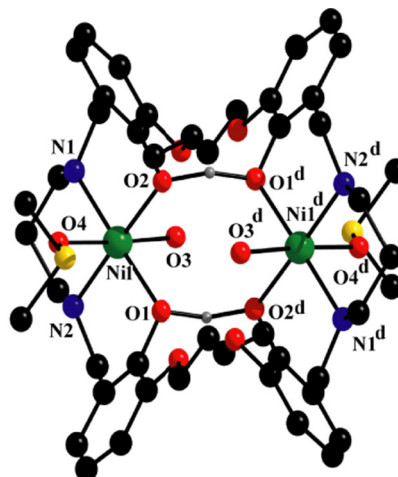
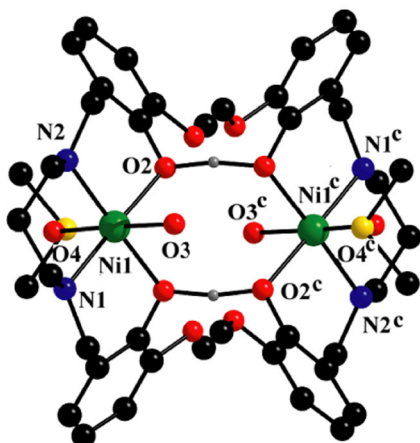


Fig. 4. Perspective view of complexes **3** (left) and **4** (right) with selective atom-numbering scheme. Non co-ordinated perchlorate ions are not shown. Hydrogen atoms are omitted for clarity apart from those between the phenolic oxygen atoms.

conformations with puckering parameters, $q(2) = 0.563(7) \text{ \AA}$, $\varphi = 180(3)^\circ$ and $q(2) = 0.563(7) \text{ \AA}$, $\varphi = 180(3)^\circ$ respectively.

3.2.2. $[\text{Ni}_2(\text{HL}^3)_2(\text{DMSO})_2(\text{H}_2\text{O})_2](\text{NCS})_2 \cdot 2\text{CH}_3\text{OH}$ (**3**) and $[\text{Ni}_2(\text{HL}^4)_2(\text{DMSO})_2(\text{H}_2\text{O})_2](\text{ClO}_4)_2$ (**4**)

X-ray crystal structure determination reveals that complexes **3** and **4** crystallize in monoclinic space groups $P2_1/n$ and $C2/c$ respectively. Potential N_2O_4 donor hexadentate reduced Schiff bases, H_2L^3 and H_2L^4 , have been used to prepare complexes **3** and **4** respectively. Each complex contains one centrosymmetric dinuclear moiety formed via strong hydrogen bonds. The structures of complexes **3** and **4** are jointly shown in Fig. 4. The geometry around each nickel(II) centers is quite similar to that described for complexes **1–2**. Both the nickel(II) centers are hexa-coordinated and adopt distorted octahedral geometry. Each nickel(II) center is equatorially coordinated by two amine nitrogen atoms, {N(1) and N(2)} and two phenoxo oxygen atoms, {O(1) and O(2)}, of the reduced Schiff base unit. The axial sites are coordinated by two oxygen atoms, {O(3) and O(4)}, of coordinated water and DMSO molecule respectively. The saturated six membered chelate rings, Ni(1)-N(1)-C(9)-C(10)-C(11)-N(2) and Ni(1)-N(1)-C(10)-C(11)-C(12)-N(2), of complexes **3** and **4** respectively represent individual chair conformations with puckering parameters, $q(2) = 0.610(6) \text{ \AA}$, $\varphi = 3(9)^\circ$ and $q(2) = 0.589(5) \text{ \AA}$, $\varphi = 182(2)^\circ$ respectively.

3.3. Supramolecular interactions in solid state

The details of hydrogen bonding interactions in complexes **1–4** are given in Table 3. Complexes **1** and **2** show similar kinds of hydrogen bonding interactions. Three hydrogen atoms, H(10), H(3A) and H(3B), available in the ligand part in each complex are involved in effective hydrogen bonding. A hydrogen atom, H(10), attached to a phenoxo oxygen atom, O(1), forms a strong intermolecular hydrogen bonding interaction with symmetry related phenoxo oxygen atom, O(2), which leads to the formation of a dimeric unit, $[\text{Ni}]_2$. Two remaining hydrogen atoms, H(3A) and H(3B), attached to an oxygen atom, O(3), are involved in intermolecular hydrogen bonding interactions with symmetry related alkoxy oxygen atoms, O(6) and O(5), respectively. Similar kinds of hydrogen bonding interactions are also observed in dimer B unit in each complex (Table 3). Pictorial representation of hydrogen bond interactions in dimer A of complexes **1** and **2** are shown in Figs. 5 and 6.

However in complexes **3** and **4**, a hydrogen atom, H(10) attached to a phenoxo oxygen atom, O(1), is hydrogen bonded with its adjacent symmetry related phenoxo oxygen atom, O(2) to form

Table 3
Hydrogen bond distances (Å) and angles (°) for the complex **1–4**.

Complex	D–H...A	D–H	H...A	D...A	∠D–H...A
1	O(1)–H(10)...O(2) ^a	1.23(3)	1.22(3)	2.426(4)	165(6)
	O(3)–H(3A)...O(6) ^a	0.85(5)	1.99(4)	2.804(5)	163(4)
	O(3)–H(3B)...O(5) ^a	0.86(4)	1.95(4)	2.777(5)	162(4)
	O(8)–H(8O)...O(7) ^e	1.20(3)	1.23(3)	2.424(4)	172(3)
	O(10)–H(10A)...O(12) ^e	0.85(4)	1.95(4)	2.767(4)	161(4)
	O(10)–H(10B)...O(11) ^e	0.84(3)	1.96(2)	2.762(4)	160(4)
2	O(1)–H(10)...O(2) ^b	1.22(6)	1.21(6)	2.424(6)	174(9)
	O(3)–H(3A)...O(6) ^b	0.86(4)	2.05(6)	2.821(8)	150(8)
	O(3)–H(3B)...O(5) ^b	0.85(6)	2.00(6)	2.825(8)	163(5)
	O(8)–H(8O)...O(7) ^f	1.21(6)	1.23(6)	2.427(6)	168(5)
	O(9)–H(9A)...O(12) ^f	0.85(4)	2.02(4)	2.831(6)	162(8)
	O(9)–H(9B)...O(11) ^f	0.84(6)	1.97(7)	2.793(6)	167(6)
3	O(1)–H(10)...O(2) ^c	1.23(4)	1.21(3)	2.433(3)	169(3)
	O(3)–H(3A)...O(5) ^c	0.84(3)	1.94(3)	2.759(4)	165(4)
	O(3)–H(3B)...O(6) ^c	0.84(4)	1.93(4)	2.766(4)	175(5)
4	O(1)–H(10)...O(2) ^d	1.23(7)	1.25(7)	2.437(4)	159(5)
	O(3)–H(31)...O(5) ^d	0.83(3)	2.06(4)	2.838(5)	154(6)

D = donor; H = hydrogen; A = acceptor; Symmetry transformations: ^a = 1 – x, 1 – y, 1 – z, ^b = 1 – x, –y, 1 – z, ^c = 2 – x, 1 – y, 1 – z, ^d = 3/2 – x, 3/2 – y, 1 – z, ^e = 1 – x, 2 – y, 2 – z, ^f = –x, 1 – y, 2 – z.

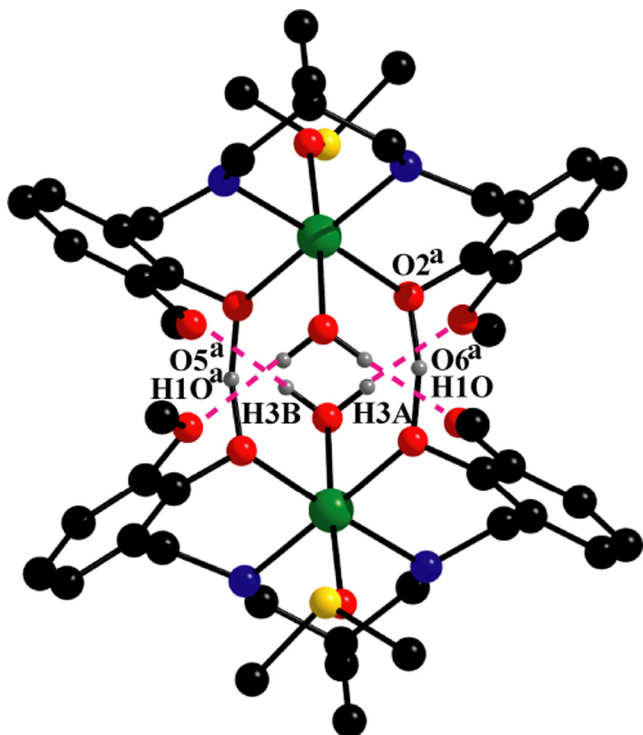


Fig. 5. Perspective view of intermolecular hydrogen bonding interactions in dimer A of complex **1**. Only the relevant hydrogen atoms have been shown for clarity. Symmetry transformation: ^a = 1 – x, 1 – y, 1 – z.

a dimeric unit. Additionally in complex **3**, two other hydrogen atoms, H(3A) and H(3B), attached to oxygen atom, O(3), are involved in intermolecular hydrogen bonding interactions with symmetry related alkoxy oxygen atoms, O(5) and O(6), respectively. The hydrogen bonding interactions in complexes **3** and **4** are shown in Figs. S4 and S5 (supporting information) respectively.

These hydrogen bonded dimeric units are further stabilized by strong C–H... π interactions. The details of C–H... π interactions are listed in Table 4. However no significant π ... π interactions are found in any of the complexes. Complex **1** shows significant C–H... π interactions involving the hydrogen atom, H(1B), attached to a carbon atom, C(1), with suitable symmetry related

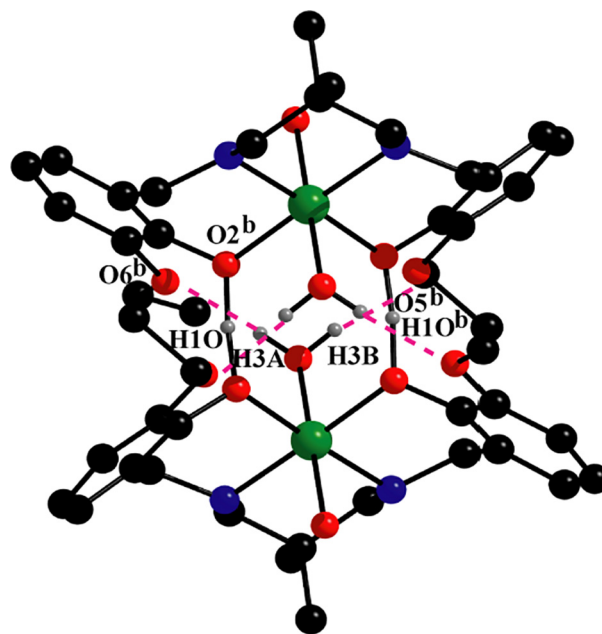


Fig. 6. Perspective view of intermolecular hydrogen bonding interaction in dimer A of complex **2**. Coordinated dmsol molecules have been omitted for clarity. Only the relevant hydrogen atoms are shown here. Symmetry transformation: ^b = 1 – x, –y, 1 – z.

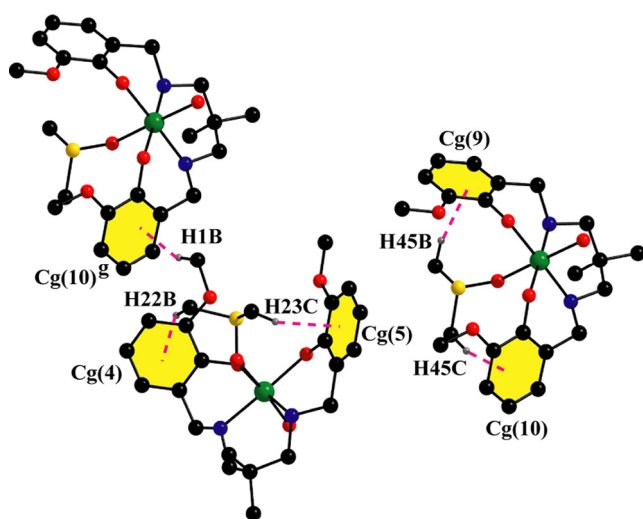
phenyl ring, C(38)–C(39)–C(40)–C(41)–C(42)–C(43). Again two hydrogen atoms, H(22B) and H(23C) attached to two different methyl carbon atoms, C(22) and C(23), respectively are involved in intramolecular C–H... π interactions with two separate phenyl rings, C(2)–C(3)–C(4)–C(5)–C(6)–C(7) and C(15)–C(16)–C(17)–C(18)–C(19)–C(20), respectively.

Moreover two similar hydrogen atoms, H(45B) and H(46B), attached to two different methyl carbon atoms, C(45) and C(46), respectively of another subunit show similar type of intramolecular C–H... π interactions with two separate phenyl rings, C(25)–C(26)–C(27)–C(28)–C(29)–C(30) and C(38)–C(39)–C(40)–C(41)–C(42)–C(43), respectively. The hydrogen bonding interactions in complex **1** are shown in Fig. 7.

Complexes **2** and **3** exhibit similar types of intermolecular C–H... π interactions with phenyl rings. Two hydrogen atoms,

Table 4Geometric features (distances in Å and angles in °) of the C—H... π interactions obtained for complexes **1–4**.

Complexes	C—H...Cg(ring)	H...Cg(Å)	C—H...Cg	C...Cg (Å)
1	C(1)–H(1B)...Cg(1) ^g	2.65	165	3.585(6)
	C(22)–H(22B)...Cg(2)	2.92	155	3.814(8)
	C(23)–H(23C)...Cg(3)	2.88	140	3.667(9)
	C(45)–H(45B)...Cg(4)	2.80	144	3.626(7)
	C(46)–H(46C)...Cg(1)	2.75	157	3.649(6)
2	C(24)–H(24B)...Cg(4)	2.79	156	3.683(12)
	C(25)–H(25C)...Cg(5)	2.81	145	3.648(14)
3	C(20)–H(20A)...Cg(4)	2.74	151	3.608(6)
	C(21)–H(21C)...Cg(5)	2.62	152	3.500(6)
4	C(11)–H(11A)...Cg(4) ^h	2.62	146	3.463(6)
	C(22)–H(22C)...Cg(5)	2.68	146	3.523(7)
	C(23)–H(23B)...Cg(4)	2.91	152	3.787(8)

Symmetry transformation: ^g = x, y, –1 + z, ^h = 3/2 – x, –1/2 – y, 1/2 – z.For complex **1**: Cg(1) = Centre of gravity of the ring [C(38)–C(39)–C(40)–C(41)–C(42)–C(43)]; Cg(2) = Centre of gravity of the ring [C(2)–C(3)–C(4)–C(5)–C(6)–C(7)]; Cg(3) = Centre of gravity of the ring [C(15)–C(16)–C(17)–C(18)–C(19)–C(20)]; Cg(4) = Centre of gravity of the ring [C(25)–C(26)–C(27)–C(28)–C(29)–C(30)].For complex **2**: Cg(4) = Centre of gravity of the ring [C(3)–C(4)–C(5)–C(6)–C(7)–C(8)]; Cg(5) = Centre of gravity of the ring [C(16)–C(17)–C(18)–C(19)–C(20)–C(21)].For complex **3**: Cg(4) = Centre of gravity of the ring [C(2)–C(3)–C(4)–C(5)–C(6)–C(7)]; Cg(5) = Centre of gravity of the ring [C(13)–C(14)–C(15)–C(16)–C(17)–C(18)].For complex **4**: Cg(4) = Centre of gravity of the ring [C(3)–C(4)–C(5)–C(6)–C(7)–C(8)]; Cg(5) = Centre of gravity of the ring [C(14)–C(15)–C(16)–C(17)–C(18)–C(19)].**Fig. 7.** Perspective view of significant C—H... π interactions in complex **1** with selective atom numbering scheme. Only relevant atoms are shown in the figure for clarity. Symmetry transformation: ^g = x, y, –1 + z.

H(24B) and H(25C), in complex **2** and H(20A) and H(21C) in complex **3**, attached to the respective carbon atoms, C(24), C(25) and C(20) and C(21) respectively, participate in intermolecular C—H... π interactions with the phenyl rings, C(3)–C(4)–C(5)–C(6)–C(7)–C(8), C(16)–C(17)–C(18)–C(19)–C(20)–C(21), C(2)–C(3)–C(4)–C(5)–C(6)–C(7) and C(13)–C(14)–C(15)–C(16)–C(17)–C(18), respectively. The hydrogen bonding interactions in complexes **2** and **3** are shown in Fig. 8.

In complex **4**, H(22C) and H(23B), attached to the methyl carbon atom, C(22) and C(23), respectively, participate in intramolecular C—H... π interactions with two separate phenyl rings, C(14)–C(15)–C(16)–C(17)–C(18)–C(19) and C(3)–C(4)–C(5)–C(6)–C(7)–C(8), respectively while another hydrogen atom, H(11A), attached to a carbon atom, C(11), is involved in intermolecular C—H... π interaction with proper symmetry related phenyl ring, C(3)–C(4)–C(5)–C(6)–C(7)–C(8) to form a supramolecular chain (Fig. 9).

3.4. Hirshfeld surfaces analysis

The Hirshfeld surface emerged from an attempt to delineate the space covered by a molecule in a crystal for the purpose of dividing

the crystal electron density into molecular fragments [23]. The Hirshfeld surfaces of four complexes are mapped over d_{norm} (range –0.1 Å to 1.5 Å), shape index and curvedness (Fig. 10). Red spots appear on the Hirshfeld surfaces mapped with d_{norm} represent the dominant interactions within the complex in solid state. Various intermolecular interactions are summed up effectively in the spots with the large circular depressions (deep red) noticeable on the d_{norm} surfaces indicates the dominance of hydrogen bonding interactions and other weak interactions. The 2D fingerprint plot of Hirshfeld surfaces for all complexes and the comparative contributions of different interactions overlapping in full fingerprint plots are provided in Fig. S5. In the 2D fingerprint plot intermolecular interactions appear as distinct spikes. Complementary regions are observable in the 2D fingerprint plots where one molecule act as donor ($d_e > d_i$) and the other as an acceptor ($d_e < d_i$). The relative percentages of intermolecular interactions of four complexes are shown in Fig. S5 (see SI).

3.5. DFT results

The X-ray structures of complexes **1–4** reveal that they crystallize forming dicationic dimers where two strong hydrogen bonds are formed between the phenoxy oxygen atoms of the ligands (Figs. 2–4). The O...O distance is shorter than 2.44 Å and both O atoms are of identical pK_a . Therefore, these hydrogen bonds have strong covalent character and could therefore be examples of LBHBs or single-well hydrogen bonds. The nature of these hydrogen bonds has therefore been analyzed using B3LYP-D/def2-SVP calculations. The energy profile of complex **1** has been computed as a representative model. The plot of the energy profile is shown in Fig. 11 and shows that the hydrogen bonds correspond to LBHBs with a barrier of 2.36 kcal/mol for the synchronous movement of both hydrogen atoms in opposite directions.

Therefore the barrier for each hydrogen bond is only 1.18 kcal/mol, in agreement with the short O...O distance (2.426(4) Å in the model used for the calculations). These results suggest that in complexes **1–4** the hydrogen atoms can move freely between the two oxygen atoms and on average are positioned at the centre of the O...O vector which is consistent with their placement in the structure refinement.

The other additional hydrogen bonds between the coordinated water molecules O(3) and the methoxy groups of the ligand, O(5) and O(6) (see blue dashed lines in Fig. 12) have also been analyzed. The dimerization energy is very large ($\Delta E_1 = -107.7$ kcal/mol) due

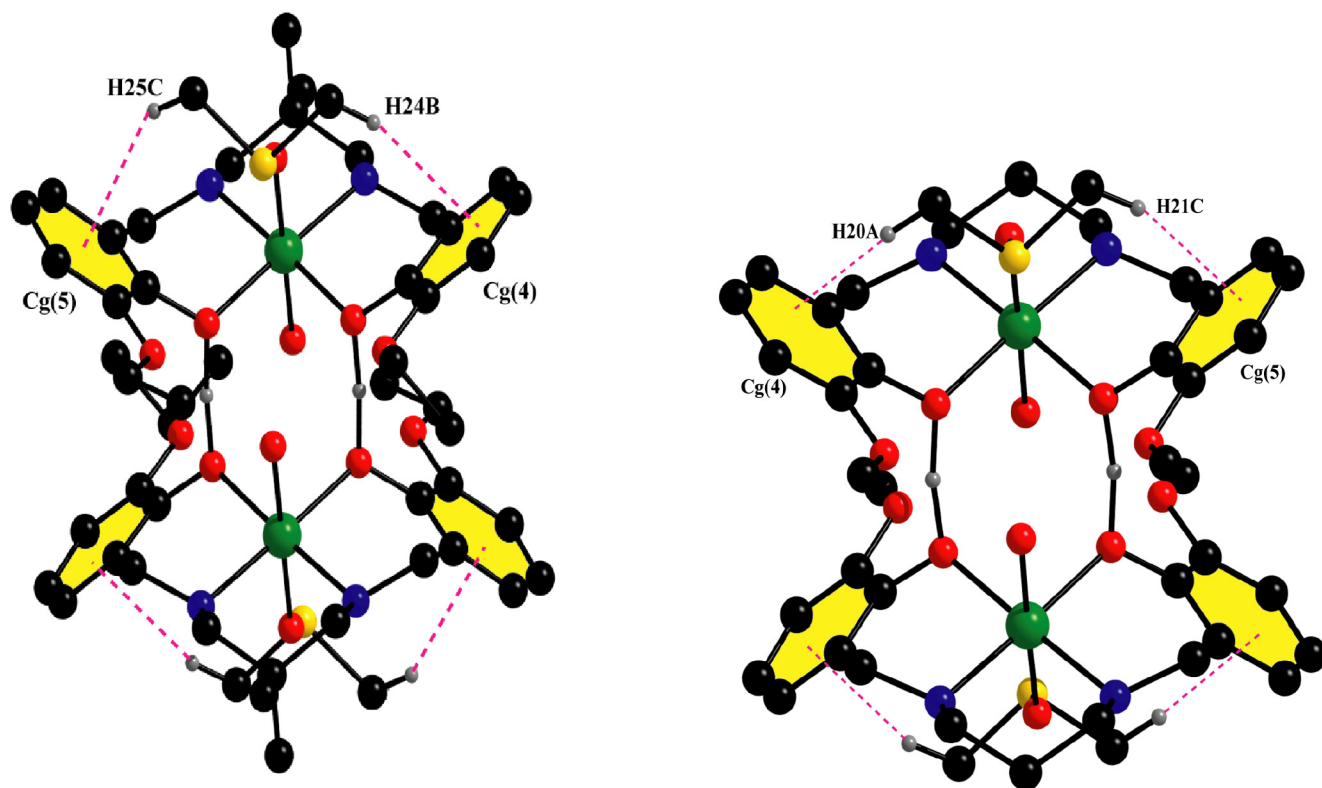


Fig. 8. Perspective view of intramolecular C—H... π stacking interactions in complexes **2** (left) and **3** (right). Only relevant hydrogen atoms are shown in the figure for clarity.

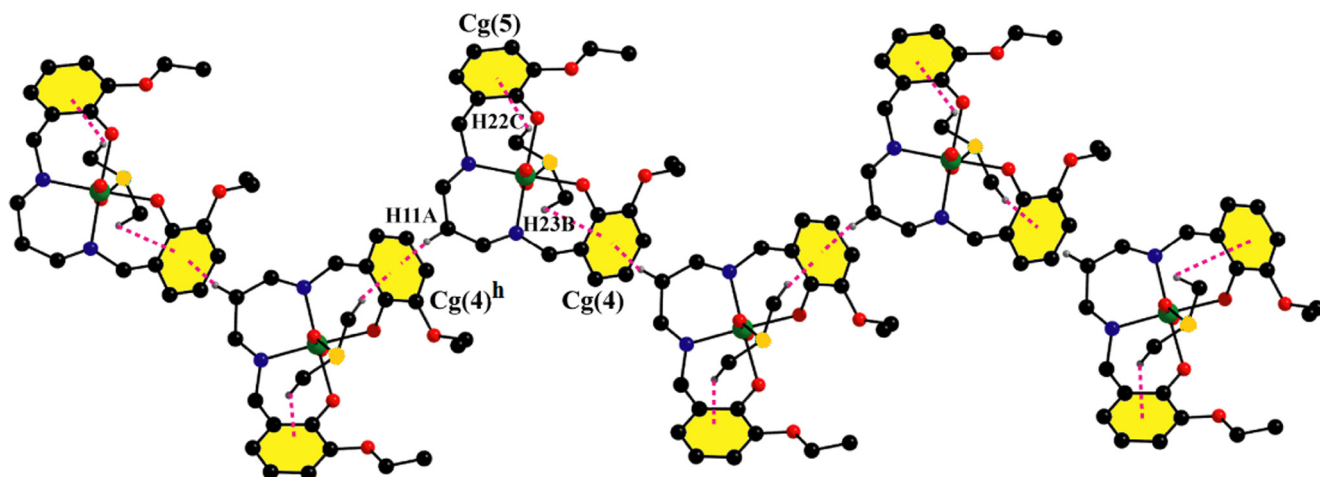


Fig. 9. Perspective view of a supramolecular chain through intermolecular C—H... π stacking interactions in complex **4**. Only relevant atoms are shown in the figure for clarity. Symmetry transformation: ^h = $3/2 - x, -1/2 - y, 1/2 - z$.

to the contribution of the strong LBHBs and the conventional O—H...O bonds that are expected to be also strong due to the enhanced acidity of these protons due to the coordination of the water molecule to the nickel(II) metal center. In an effort to estimate the contribution of the LBHBs, a theoretical model has been used in which the water molecules are eliminated (Fig. 12b). As a result, the conventional hydrogen bonds are not established and the interaction energy drops to $\Delta E_2 = -73.3$ kcal/mol, that corresponds to the contribution of both LBHBs and also some additional van der Waals interactions established between the bulk of both molecules. This large interaction energy confirms the strong covalent nature of these hydrogen bonds. This result is agreement with

previous investigations in hydrogen bonds between hetero atoms with identical pK_a values where the ΔH of formation can approach 30 kcal/mol [4]. Furthermore, the difference between ΔE_1 and ΔE_2 provides a rough estimation of the four O—H...O bonds established by the coordinated water molecules and methoxy groups (-8.6 kcal/mol per hydrogen bond).

Finally, non-covalent interaction plot (NCI plot) index has been made to further characterize the hydrogen bonds. It allows a direct assessment of host-guest complementarity and the extent to which non-covalent interactions stabilize a complex. Fig. 13 shows the NCI plot obtained for the self-assembled dimer extracted from the solid state of complex **1**. The NCI index indicates that the LBHBs

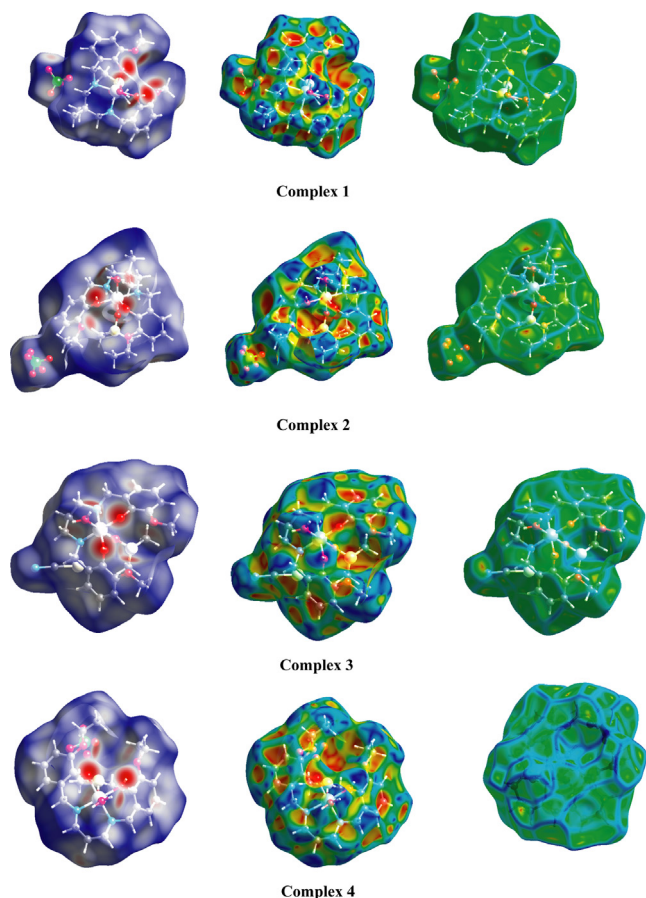


Fig. 10. Hirshfeld surfaces mapped with d_{norm} (left column), shape index (middle) and curvedness (right column) of complexes **1–4**.

are covalent bonds, since no isosurface is found between the H and O atoms. The O—H...O hydrogen bonds involving the coordinated water molecules are characterized by small and intense blue

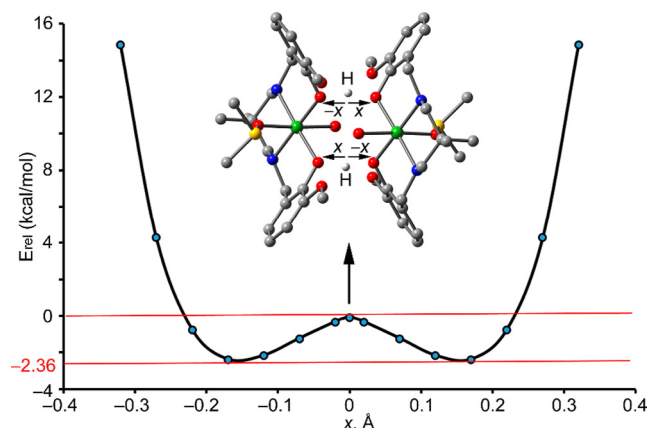


Fig. 11. Energy diagram obtained for complex **1** at the B3LYP-D/def2-SVP level of theory. The energies are relative to the maximum. In the calculation the two hydrogen atoms were moved in opposite directions to maintain the inversion center of symmetry.

isosurfaces, thus supporting the strong nature of the interactions. Several green isosurfaces are also present between both monomeric units, thus revealing the existence of additional weak interactions that also stabilize the assembly.

3.6. IR and electronic spectra

A moderately sharp band in the range of 3280–3225 cm^{-1} has been noticed in the IR spectrum of each complex which may be assigned as the N—H stretching vibration of the reduced Schiff base ligand [24,25]. Broad bands in the range of 3010–2865 cm^{-1} due to alkyl C—H stretching vibrations are routinely noticed in IR spectra of all complexes [26,27]. Appearance of a broad band in each complex around 3400 cm^{-1} indicates the presence of O—H stretching vibrations of water molecules. A very strong band is obtained around 2045 cm^{-1} only in complex **3** due to the presence of non-coordinated thiocyanate ions [28,29]. IR spectra of all complexes are given in Figs. S6–S9 (SI).

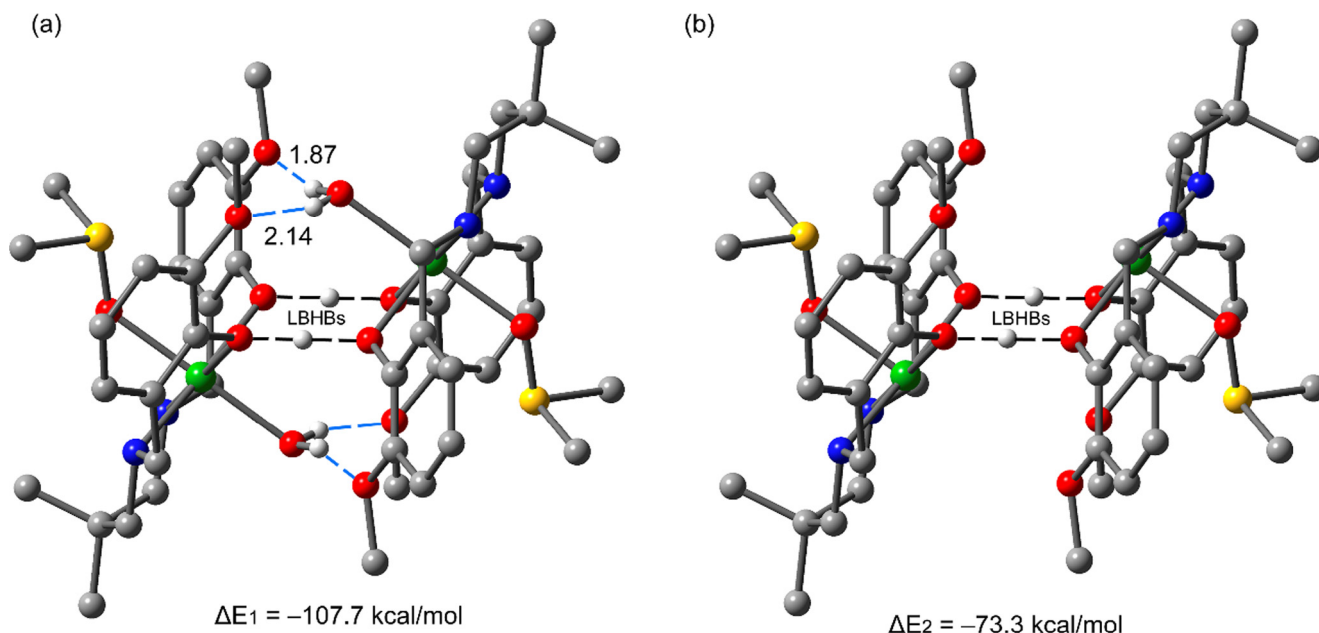


Fig. 12. Theoretical models used to evaluate the LBHBs in complex **1** (a) and a model complex where the two coordinated water molecules have been eliminated (b). Distances in Å.

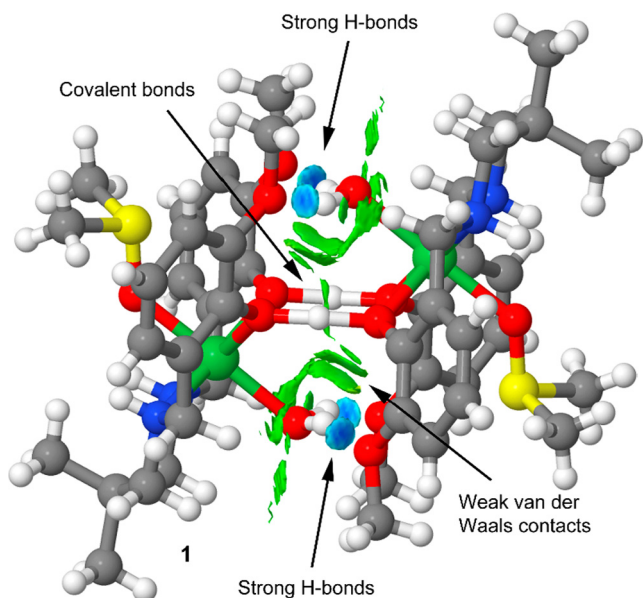


Fig. 13. NCI plot of the self-assembled dimer of complex **1**. The gradient cut-off is $s = 0.35$ au, and the color scale is $-0.04 < \rho < 0.04$ au.

Electronic spectra of all four complexes in DMSO show two distinguished bands in the visible range around 625 nm and 735 nm. These bands may be assigned as ${}^3T_{1g}(F) \leftarrow {}^3A_{2g}(F)$ and ${}^3T_{2g}(F) \leftarrow {}^3A_{2g}(F)$, respectively [30]. The intense absorption bands at ~ 355 nm may be assigned as ligand to metal charge transfer (LMCT) bands, which obscure the 3rd d–d band, ${}^3T_{1g}(P) \leftarrow {}^3A_{2g}(F)$, expected for any octahedral nickel(II) [31]. In addition, high energy absorption bands around 275 nm are assigned to intra-ligand $\pi \rightarrow \pi^*$ transitions [32,33]. Electronic spectra of all complexes are given in Figs. S10–S13 (SI).

4. Conclusion

In summary, we have synthesized and characterized four nickel (II) complexes (**1–4**) that form self-assembled dimers in the solid state where low barrier hydrogen bonds appear to play a prominent role. Structures of all complexes were confirmed by single crystal X-ray diffraction study. Each complex may be represented by a general formula $[Ni_2(HL)_2(DMSO)_2(H_2O)_2]X$ [$H_2L = N_2O_4$ donor reduced Schiff base ligand, $X =$ counter anion]; X is perchlorate in **1**, **2** and **4** and $X =$ thiocyanate in **3**. Use of reduced Schiff bases seems to be essential to form this type of hydrogen bonded dimeric species, as the non-reduced analogues of these Schiff bases fails to prepare such complexes. More flexibility of the reduced Schiff bases compared to their Schiff base precursor may be the driving force in forming these complexes. The hydrogen bonds are evaluated energetically and using the non-covalent interaction plot. We conclude that the barrier is very low and, consequently, the hydrogen atoms can move freely with their average position between both oxygen atoms. The energy associated to the low barrier hydrogen bonds is very large due to the strong covalent character of the interaction.

Author contribution section

Saikat Mirdya: Synthesized two complexes; Michael G. B. Drew: Crystallographer; Akash Kumar Chandra: Synthesized two complexes; Abhisek Banerjee: Characterized the complexes by spectral and elemental analysis and performed all necessary works related to publication.

Antonio Frontera: Performed theoretical calculations; Shouvik Chattopadhyay: The Ph.D. supervisor of S. Mirdya. He is also the corresponding author.

Acknowledgments

S.M. thanks CSIR, India, for awarding a Junior Research Fellowship [Sanction No. 09/096(0990)2019-EMR-1]. A.B thanks the UGC, India, for awarding a Junior Research Fellowship. A.F thanks the MINECO/AEI of Spain (project CTQ2017-85821-R FEDER funds) for financial support.

Appendix A. Supplementary data

Hirshfeld surface analysis, Tables from S1–S2 and Figures from S1–S14. CCDC 1948661–1948664 contain the supplementary crystallographic data for complexes **1–4**. This data can be obtained free of charge via <http://www.ccdc.cam.ac.uk/conts/retrieving.html>, or from the Cambridge Crystallographic Data Centre, 12 Union Road, Cambridge CB2 1EZ, UK; fax: (+44) 1223-336-033; or e-mail: deposit@ccdc.cam.ac.uk. Supplementary data to this article can be found online at <https://doi.org/10.1016/j.poly.2020.114374>.

References

- [1] W.W. Cleland, P.A. Frey, J.A. Gerlt, *J. Biol. Chem.* **273** (1998) 25529–25532.
- [2] G.A. Jeffrey, *Introduction to Hydrogen Bonding*, Oxford University Press, New York, 1997.
- [3] M. Garcia-Viloca, A. Gonzalez-Lafont, J.M. Lluch, *J. Am. Chem. Soc.* **119** (1997) 1081–1086.
- [4] M.A. McAllister, *Can. J. Chem.* **75** (1997) 1195–1202.
- [5] K. Abu-Dari, K.N. Raymond, D.P. Freyberg, *J. Am. Chem. Soc.* **101** (1979) 3688–3689.
- [6] K. Abu-Dari, D.P. Freyberg, K.N. Raymond, *Inorg. Chem.* **18** (1979) 2427–2433.
- [7] P. Gilli, V. Bertolase, V. Ferretti, G. Gilli, *J. Am. Chem. Soc.* **116** (1994) 909–915.
- [8] K.P. Sarma, R.K. Poddar, *Transition Met. Chem.* **9** (1984) 135–138.
- [9] G.M. Sheldrick, *Acta Crystallogr., Sect. C* **71** (2015) 3–8.
- [10] A.L. Spek, *Acta Crystallogr. D* **65** (2009) 148–155.
- [11] G.M. Sheldrick, *SADABS*, V2014/5, Software for Empirical Absorption Correction, University of Göttingen, Institute für Anorganische Chemie der Universität, Göttingen, Germany, 1999–2003.
- [12] J.L. Farrugia, *J. Appl. Crystallogr.* **45** (2012) 849–854.
- [13] M.N. Burnett, C.K. Johnson, *ORTEP-3: Oak Ridge Thermal Ellipsoid Plot Program for Crystal Structure Illustrations*, Report ORNL-6895, Oak Ridge National Laboratory, Oak Ridge, TN, USA, 1996.
- [14] C.F. Macrae, I.J. Bruno, J.A. Chisholm, P.R. Edgington, P. McCabe, E. Pidcock, L.R. Monge, R. Taylor, J.V.D. Streek, P.A. Wood, *J. Appl. Crystallogr.* **41** (2008) 466–470.
- [15] M.J. Frisch, G.W. Trucks, H.B. Schlegel, G.E. Scuseria, M.A. Robb, J.R. Cheeseman, G. Scalmani, V. Barone, B. Mennucci, G.A. Petersson, H. Nakatsuji, M. Caricato, X. Li, H.P. Hratchian, A.F. Izmaylov, J. Bloino, G. Zheng, J.L. Sonnenberg, M. Hada, M. Ehara, K. Toyota, R. Fukuda, J. Hasegawa, M. Ishida, T. Nakajima, Y. Honda, O. Kitao, H. Nakai, T. Vreven, J.A. Montgomery Jr., J.E. Peralta, F. Ogliaro, M. Bearpark, J.J. Heyd, E. Brothers, K.N. Kudin, V.N. Staroverov, R. Kobayashi, J. Normand, K. Raghavachari, A. Rendell, J.C. Burant, S.S. Iyengar, J. Tomasi, M. Cossi, N. Rega, J.M. Millam, M. Klene, J.E. Knox, J.B. Cross, V. Bakken, C. Adamo, J. Jaramillo, R. Gomperts, R.E. Stratmann, O. Yazyev, A.J. Austin, R. Cammi, C. Pomelli, J.W. Ochterski, R.L. Martin, K. Morokuma, V.G. Zakrzewski, G.A. Voth, P. Salvador, J.J. Dannenberg, S. Dapprich, A.D. Daniels, Ö. Farkas, J.B. Foresman, J.V. Ortiz, J. Cioslowski, D.J. Fox, *Gaussian 09*, Gaussian Inc, Wallingford CT, 2009.
- [16] S. Grimme, J. Antony, S. Ehrlich, H. Krieg, *J. Chem. Phys.* **132** (2010) 154104–154117.
- [17] S.F. Boys, F. Bernardi, *Mol. Phys.* **19** (1970) 553–566.
- [18] J. Contreras-García, E.R. Johnson, S. Keinan, R. Chaudret, J.-P. Piquemal, D.N. Beratan, W. Yang, *J. Chem. Theory Comput.* **7** (2011) 625–632.
- [19] E.R. Johnson, S. Keinan, P. Mori-Sánchez, J. Contreras-García, A.J. Cohen, W. Yang, *J. Am. Chem. Soc.* **132** (2010) 6498–6506.
- [20] A. Banerjee, A. Frontera, S. Chattopadhyay, *Dalton Trans.* **48** (2019) 11433–11447.
- [21] D. Matoga, J. Szklarzewicz, K. Stadnicka, M.S. Shongwe, *Inorg. Chem.* **46** (2007) 9042–9044.
- [22] D. Cremer, J.A. Pople, *J. Am. Chem. Soc.* **97** (1975) 1354.
- [23] F.L. Hirshfeld, *Theor. Chim. Acta* **44** (1977) 129–138.
- [24] A. Banerjee, S. Chattopadhyay, A benzoate bridged dinuclear mixed valence cobalt(III/II) complex with CollO4Coll core: Synthesis, structure and investigation of its phenoxazinone synthase mimicking activity, *Polyhedron* **177** (2020), <https://doi.org/10.1016/j.poly.2019.114290>.

- [25] S. Mirdya, A. Frontera, S. Chattopadhyay, *CrystEngComm* (2019), <https://doi.org/10.1039/C9CE01283D>.
- [26] S. Roy, T. Basak, S. Khan, M.G.B. Drew, A. Bauzá, A. Frontera, S. Chattopadhyay, *ChemistrySelect* 2 (2017) 9336–9343.
- [27] S. Mirdya, T. Basak, S. Chattopadhyay, *Polyhedron* 170 (2019) 253–263.
- [28] S. Mirdya, S. Roy, S. Chatterjee, A. Bauzá, A. Frontera, S. Chattopadhyay, *Cryst. Growth Des.* 19 (2019) 5869–5881.
- [29] K. Ghosh, K. Harms, A. Bauzá, A. Frontera, S. Chattopadhyay, *Dalton Trans.* 47 (2018) 331–347.
- [30] A. Bhattacharyya, P.K. Bhaumik, M. Das, A. Bauzá, P.P. Jana, K. Harms, A. Frontera, S. Chattopadhyay, *Polyhedron* 101 (2015) 257–269.
- [31] S. Chattopadhyay, M.G.B. Drew, A. Ghosh, *Polyhedron* 26 (2007) 3513–3522.
- [32] A. Bhattacharyya, P.K. Bhaumik, P.P. Jana, S. Chattopadhyay, *Polyhedron* 78 (2014) 40–45.
- [33] S. Chattopadhyay, M. Sinha Ray, S. Chaudhuri, G. Mukhopadhyay, G. Bocelli, A. Cantoni, A. Ghosh, Nickel (II) and copper (II) complexes of tetradentate unsymmetrical Schiff base ligands: first evidence of positional isomerism in such system, *Inorganica Chimica Acta* 359 (2006) 1367–1375.

PAPER



Cite this: *CrystEngComm*, 2020, 22, 237

An insight into the non-covalent Pb \cdots S and S \cdots S interactions in the solid-state structure of a hemidirected lead(II) complex†

Saikat Mirdya,^a Snehasis Banerjee ^b and Shouvik Chattopadhyay ^{*a}

A heterodinuclear copper(II)/lead(II) complex with a compartmental ‘reduced Schiff base’ ligand (having inner N₂O₂ and outer O₂O₂′ compartments) has been synthesized and characterized. Single-crystal X-ray diffraction analysis confirmed its structure. The X-ray data indicate that the inner N₂O₂ compartment of the compartmental reduced Schiff base is occupied by copper(II) while the outer O₂O₂′ compartment is occupied by lead(II). A thiocyanate anion is coordinated to the copper(II) center *via* its N-end, whereas, another thiocyanate ion is linked to the lead(II) center *via* its S-end and is semi-coordinated to the copper(II) center through its N-end. A hemidirectionally coordinated lead(II) center is well suited for establishing tetrel bonding interactions. We estimated the BSSE (basis set superposition error) corrected energies of non-covalent S \cdots S, Pb \cdots π , and $\pi\cdots\pi$ interactions and N–H hydrogen bonding along with tetrel bonding by DFT calculations. To obtain an insight into the physical nature of these bonds, we extensively used Bader’s quantum theory of atoms-in-molecules (QTAIM). Additionally, the non-covalent interaction reduced density gradient (NCI-RDG) method established nicely the presence of such non-covalent intermolecular interactions. Here, we also used natural bond orbital (NBO) analysis to find out the origin of S \cdots S and Pb \cdots S bonding.

Received 1st October 2019,
Accepted 9th November 2019

DOI: 10.1039/c9ce01548e

rsc.li/crystengcomm

Introduction

Lead is a heavy metal with an atomic number of 82. Its large radius, ability to adopt different coordination numbers from 2 to 8 and ability to exist in variable valence states leading to versatile coordination chemistry attracted synthetic inorganic chemists to prepare new complexes of lead.^{1–4} Lead containing materials are extensively used in semiconductors, batteries, ferroelectric materials and non-linear optical materials.^{5–9} On the other hand, lead is very toxic even in a very low concentration and is a dangerous biological poison similar to mercury, if not more dangerous.^{10–16} Disodium calcium EDTA is used in chelation therapy to take away lead(II) from the human body.^{17–21} Many bio-inorganic chemists are working to develop other chelating ligands for the treatment of lead intoxication.^{22–25}

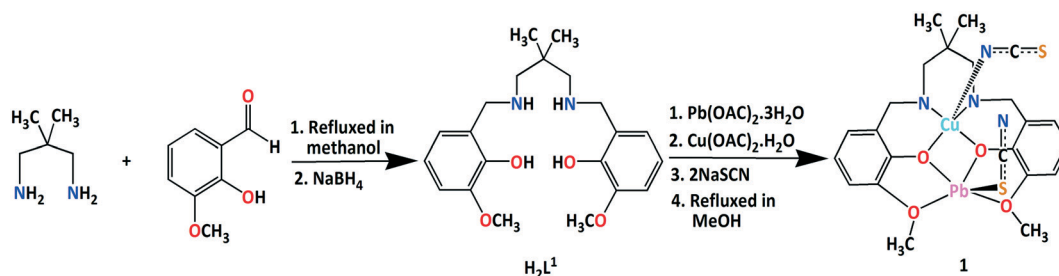
[Xe]4f¹⁴5d¹⁰6s²6p² is the electronic configuration of lead (Pb). Due to their very weak screening efficiency, fourteen electrons in the 4f orbitals and ten electrons in the 3d orbitals increase the effective nuclear charge of lead acting on the outermost 6s² electrons and make the electron pair essentially inert. The penetrating property of the 6s orbital is also very high and has a pronounced effect on lowering the energy of these two electrons. A relativistic increase in the mass of the 6s² electrons also stabilizes the 6s² electrons. Lead, therefore, shows a +2 oxidation state in most of its complexes and contains a lone pair of electrons.^{26–31} In some of these complexes, this lone pair is, however, stereochemically active leading to hemidirectional complexes^{32,33} and in the rest of the complexes, the lone pair is stereochemically inactive leading to holodirected complexes.^{34,35} Theoretical chemists are currently engaged in rationalizing the extent to which the lone pair is stereochemically active in lead(II) complexes.^{36–40}

Supramolecular chemistry deals with various non-covalent interactions,^{41–43} including a large range of attractive and repulsive forces^{42,43} such as ion–ion interactions, hydrogen bonding, $\pi\cdots\pi$ interactions, ion–dipole interactions, van der Waals forces, dipole–dipole interactions, *etc.*^{44–47} These are often jointly working in one supramolecular complex. These non-covalent forces are attributable to the self-assembly of large molecules, crystal packing, and biological pattern

^a Department of Chemistry, Inorganic Section, Jadavpur University, Kolkata-700032, India. E-mail: shouvik.chem@gmail.com

^b Govt. College of Engineering and Leather Technology, Salt Lake Sector-III, Block-LB, Kolkata-700106, India. E-mail: sbanchem@gmail.com

† Electronic supplementary information (ESI) available: Hirshfeld surface analysis, Table S1 and Fig. S1–S4 are given in the ESI. CCDC 1953301 contains the supplementary crystallographic data for the investigated complex. For ESI and crystallographic data in CIF or other electronic format see DOI: 10.1039/c9ce01548e



Scheme 1 Synthetic route to the complex.

identification.^{48–51} Other well-known non-covalent interactions, such as short contacts among halogen/chalcogen atoms,^{52–56} may also promote the formation of interesting supramolecular assemblies.^{57–60} Another important non-covalent interaction is the σ -hole interaction, which is less studied. Strong σ -hole interactions may occur in complexes of group IV elements which usually involve tetrel bonding interactions, especially in the cases of lead.^{61–72}

In one of our previous studies, few ‘nickel(II)–salen’ type metalloligands with a reduced Schiff base was used to prepare a few holodirected and hemidirected lead(II) complexes.^{73,74} In this work, we have reduced a compartmental ‘salen type’ Schiff base into a compartmental ‘reduced Schiff base’ (having N_2O_2 and $O_2O'_2$ pockets), which entraps copper(II) and lead(II) in the inner N_2O_2 and outer $O_2O'_2$ compartments respectively to produce a heterodinuclear copper(II)/lead(II) complex, $[(SCN)CuL^1Pb(SCN)]$. Lead(II) shows a hemi-directed geometry in the complex. Non-covalent interactions in the supramolecular assembly of the complex were studied energetically by means of theoretical DFT calculations. The most interesting observation is the existence of $S\cdots S$ and $Pb\cdots S$ interactions. These interactions have also been analyzed using several computational tools, including Bader's ‘atoms-in-molecules’ (AIM) and MEP analyses.

Results and discussion

Synthesis

2,2-Dimethyl-1,3-diaminopropane was refluxed with 3-methoxysalicylaldehyde in a 1 : 2 ratio, followed by the addition of $NaBH_4$ to form an $N_2O_2O'_2$ donor compartmental reduced Schiff base ligand, H_2L^1 , following the literature method.^{75,76} The ligand (H_2L^1) on reaction with copper(II) acetate monohydrate followed by lead(II) acetate trihydrate and sodium thiocyanate in a 1 : 1 : 2 ratio produced the heterodinuclear complex. The formation of the complex is shown in Scheme 1.

Description of $[(SCN)CuL^1Pb(SCN)]$

X-ray crystal structure determination reveals that the complex crystallizes in the triclinic space group, $P\bar{1}$. The crystal structure of the complex is built from isolated heterodinuclear molecules of $[(SCN)CuL^1Pb(SCN)]$. The molecular structure of

the complex is shown in Fig. 1. The details of crystallographic data and refinements are given in Table 1. Important bond lengths are gathered in Table 2.

The $N_2O_2O'_2$ donor compartmental reduced Schiff base ligand (H_2L^1) is used to prepare the complex in which a copper(II) center, Cu(1), is placed in the inner N_2O_2 cavity and a lead(II) center, Pb(1), is placed in the outer $O_2O'_2$ cavity. Both the copper(II) and lead(II) centers are pentacoordinated. The copper(II) center, Cu(1), has a square pyramidal geometry, where two amine nitrogen atoms, N(1) and N(2), and two phenoxo oxygen atoms, O(1) and O(2), of the deprotonated reduced Schiff base constitute the equatorial plane. The axial position of the copper(II) center is occupied by a nitrogen atom, N(3), from a terminal thiocyanate molecule. The geometry of any pentacoordinated metal centre may conveniently be measured by the Addison parameter (τ)⁷⁷ [$\tau = (\theta - \Phi)/60$, where θ and Φ are the two largest ligand–metal–ligand angles of the coordination sphere]. In the title complex, the geometry around the copper(II) center, Cu(1), is square pyramidal with $\tau = 0.02$. On the other hand, the phenoxo oxygen atoms, O(1) and O(2), of the deprotonated reduced Schiff base also coordinate to the lead(II) center, Pb(1). The potential donor methoxy oxygen atoms, O(3) and O(4), of the compartmental

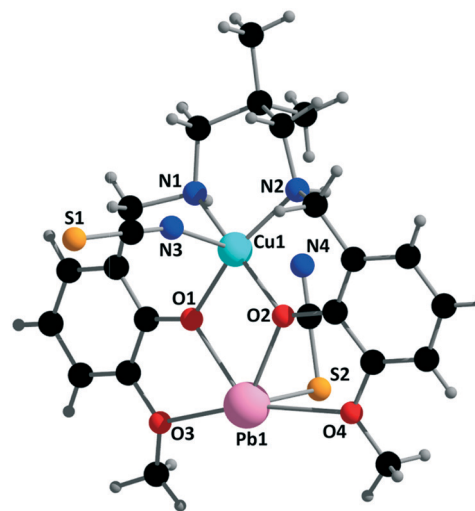


Fig. 1 Perspective view of the complex with a selective atom numbering scheme.

Table 1 Crystal data and refinement details of the complex

Formula	C ₂₃ H ₂₈ PbCuN ₄ O ₄ S ₂
Formula weight	759.36
Temperature (K)	273
Crystal system	Triclinic
Space group	$P\bar{1}$
<i>a</i> (Å)	9.3667(7)
<i>b</i> (Å)	9.5064(7)
<i>c</i> (Å)	15.1076(11)
α	84.047(2)
β	75.365(2)
γ	79.476(2)
<i>Z</i>	2
<i>d</i> _{calc} (g cm ⁻³)	1.974
μ (mm ⁻¹)	7.615
<i>F</i> (000)	738
Total reflections	38 018
Unique reflections	5206
Observed data [<i>I</i> > 2 σ (<i>I</i>)]	4885
No. of parameters	324
<i>R</i> (int)	0.054
<i>R</i> ₁ , <i>wR</i> ₂ (all data)	0.0287, 0.0652
<i>R</i> ₁ , <i>wR</i> ₂ [<i>I</i> > 2 σ (<i>I</i>)]	0.0258, 0.0638
Largest diff. peak/hole (e Å ⁻³)	1.90, -0.87

reduced Schiff base also coordinate to lead(II), but at much longer distances to form equatorial planes. The lead(II) center adopts a geometry intermediate between square pyramidal and trigonal bipyramidal as indicated from the Addison parameter value ($\tau = 0.493$), which is close to 0.5. The sulphur atom, S(2), from the terminal thiocyanate molecule coordinates to the lead(II) center in the axial position with a Pb(1)–S(2)–C(23) angle of 96.8(2)°, where the N-terminal of the same thiocyanate molecule is directed towards the copper(II) center with a Cu(1)⋯N(4)–S(2) angle of 95.7(1)°. The N(4)⋯Cu(1) distance [3.057(4) Å] is larger than the distances of N(1)–Cu(1) [2.019(4)], N(2)–Cu(1) [2.037(3)] and also Pb(1)–S(2) [2.791(1) Å], which indicates partial bridging interaction of thiocyanate between Cu(1) and Pb(1). The deviations of the four coordinating atoms, O(1), O(2), N(1) and N(2), in the basal plane from the mean plane passing through them and those of the copper(II) center from the same planes are -0.008(3), -0.075(3), -0.077(3), -0.016(4) and 0.175 (5) Å respectively for the complex. The saturated six-membered chelate ring [Cu(1)–N(1)–C(9)–C(10)–C(13)–N(2)] has an envelope conformation with puckering parameters^{78,79} $q = 0.531(5)$ Å; $\theta = 25.2(4)^\circ$; $\phi = 185.1(12)^\circ$. The Cu(1)O(1)O(2)Pb(1) core is almost planar as the angle between the Cu(1)O(1)O(2) and O(1)O(2)Pb(1) planes is 7.29(9)°, and the dihedral angle of O(1)Pb(1)O(2)Cu(1) is 5.74(11)°. The distance between Cu(1) and Pb(1) is 3.504(5)

Å. The bridging angles Cu(1)–O(1)–Pb(1) and Cu(1)–O(2)–Pb(1) are 106.5(1)° and 106.0(1)°, respectively.

Supramolecular interactions

The solid-state structure of the complex is well constructed through several non-covalent interactions such as hydrogen bonding, $\pi\cdots\pi$ stacking interaction, and cation $\cdots\pi$ interaction. The hydrogen atom, H(1), attached to the amine nitrogen atom, N(1), forms bifurcated H-bonds with the nitrogen atom, N(4), and a symmetry related nitrogen atom, N(4)* { $*$ = 1 - *x*, 1 - *y*, 1 - *z*}, of a neighboring moiety to form a dimeric structure, as shown in Fig. 2.

The phenyl ring Cg(7) [Cg(7) = center of mass of the ring C(2)–C(7)] exhibits a strong face-to-face $\pi\cdots\pi$ stacking interaction with the neighboring phenyl ring Cg(8) [Cg(8) = center of mass of the ring C(15)–C(20)] of symmetry^a = -1 + *x*, *y*, *z*. A one-dimensional array is formed because of this type of $\pi\cdots\pi$ stacking interaction (Fig. 3).

A cation $\cdots\pi$ interaction is also observed in the complex. The lead(II) center, Pb(1), is involved in a cation $\cdots\pi$ interaction with a symmetry-related (1 - *x*, 1 - *y*, -*z*) phenyl ring Cg(8), which leads to the formation of a dimeric structure (Fig. 4).

Relying on the structural discussion by Shimoni-Livny *et al.*,⁸⁰ the hemidirectionally coordinated lead(II) center has a significant void opposite to the ligand (H₂L¹) and thiocyanate co-ligand, which is similar to other lead(II) complexes.⁸¹ All bonds around the lead(II) atom are basically concentrated within less than one hemisphere of the coordination sphere, leaving a large gap on the lead(II) ion. This also allows a close interaction with the sulfur atom, (S1)^c, of the thiocyanate from an adjacent molecule (^c = *x*, -1 + *y*, *z*) of a 3.517(2) Å distance which leads to the formation of a 1D polymeric chain, as shown in Fig. 5. There is another interesting interaction between S(1) and S(1)^d [^d = 2 - *x*, 2 - *y*, -*z*] of a 3.593(2) Å distance which leads to the formation of another supramolecular dimeric structure, as shown in Fig. 6. Both Pb1⋯S1^a and S1⋯S1^b interactions lead to the formation of a 2D polymeric network, as shown in Fig. S1 [ESI†].

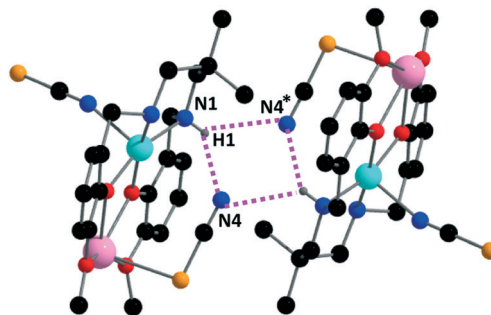


Fig. 2 Perspective view of the hydrogen bonding interactions in the solid state structure of the complex. Only the relevant atoms are shown in the figure. Symmetry transformation: $*$ = 1 - *x*, 1 - *y*, 1 - *z*, where N(1)⋯H(1) = 0.79(4) Å, H(1)⋯N(4) = 2.65(4) Å, H(1)⋯N(4)* = 2.77(5) Å, N(1)⋯N(4)* = 3.367(5) Å, N(1)⋯N(4) = 3.193(6) Å, \angle N(1)–H(1)⋯N(4) = 127(4)° and \angle N(1)–H(1)⋯N(4)* = 134(4)°.

Table 2 Selected bond lengths (Å) of the complex

Pb(1)–O(1)	2.375(3)	Cu(1)–O(1)	1.988(3)
Pb(1)–O(2)	2.358(3)	Cu(1)–O(2)	2.021(3)
Pb(1)–O(3)	2.631(4)	Cu(1)–N(1)	2.019(3)
Pb(1)–O(4)	2.609(4)	Cu(1)–N(2)	2.037(4)
Pb(1)–S(2)	2.7914(15)	Cu(1)–N(3)	2.232(4)

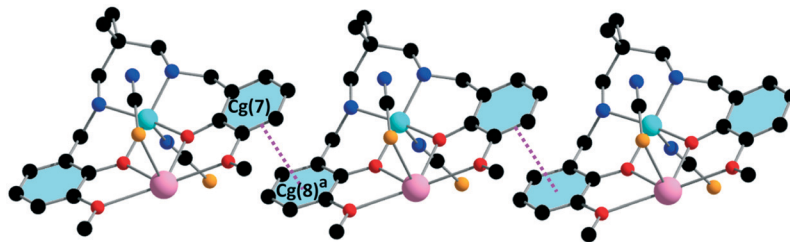


Fig. 3 1D chain of intermolecular $\pi\cdots\pi$ stacking interactions. All hydrogen atoms and uncoordinated perchlorate anions are omitted for clarity. Symmetry elements: $^a = 1 + x, y, z$, where $\text{Cg}(7)\cdots\text{Cg}(8)^a = 3.771(3) \text{ \AA}$, $\text{Cg}(I)\cdots\text{Perp} = 3.5404(19) \text{ \AA}$, $\text{Cg}(J)\cdots\text{Perp} = 3.5648(18)$, and $\alpha = 13.5(2)^\circ$ [α = dihedral angle between ring I and ring J, $\text{Cg}(I)\cdots\text{Perp}$ = perpendicular distance of Cg(I) from ring J, $\text{Cg}(J)\cdots\text{Perp}$ = perpendicular distance of Cg(J) from ring I for the complex].

IR and electronic spectra

The IR spectrum of the complex is in good agreement with the X-ray structural data. In the IR spectrum of the complex, there are two successive strong bands observed at 2091 and 2068 cm^{-1} , indicating the presence of terminal N-bonded and terminal S-bonded thiocyanate, respectively.⁸² A moderately strong band due to stretching vibrations of the N–H bond appears in the range of 3248–3232 cm^{-1} .^{83,84} Bands near the range of 2951–2838 cm^{-1} are due to alkyl C–H bond stretching vibrations, which are customarily noticed in the IR spectrum of the complex.⁸⁵ The IR spectrum of the complex is shown in Fig. 7.

The electronic spectrum of the complex in DMF displays one absorption band in the visible region at 618 nm which may be ascribed to the $^2T_{2g}(\text{D}) \leftarrow ^2E_g(\text{D})$ transition for copper(II).^{86,87} A broad band of low intensity features near 405 nm may be attributed to ligand-to-metal charge transfer (LMCT) transition from the ligand to copper(II).^{88,89} Another very low intensity band at 335 nm may be attributed to the $n \rightarrow \pi^*$ transition of the ligand.⁹⁰ The high intensity band that appeared at 282 nm is attributed to the $\pi \rightarrow \pi^*$ transition of

the ligand.⁹¹ The UV-Vis spectrum of the complex is shown in Fig. 8.

Theoretical work

The focus of the theoretical work is to evaluate the electronic and energetic features of $\text{Pb}\cdots\text{S}$ tetrel bonding and some other weak non-covalent interactions, namely $\text{S}\cdots\text{S}$ bonding and $\text{N}\cdots\text{H}$ hydrogen bonding, which are further characterized by the Hirshfeld analysis (Fig. S1 and S2†), and also $\text{Pb}\cdots\pi$ and $\pi\cdots\pi$, found in the solid-state of the investigated complex. As discussed in the experimental section, we used the dimer of the title complex to explore such interactions.

S···S interactions

As observed in the crystal structure, the short distance between two sulfur atoms (3.59 Å) indicates significant chalcogen–chalcogen interactions (Fig. 6) as we have found in the literature.^{92,93} The literature results suggest that in the chalcogen–chalcogen interactions, $p\text{--}\sigma^*$ plays an important role to stabilize such interactions as shown in Fig. 9. In our case, as shown in Fig. 9, the $\text{S}\cdots\text{S}$ interaction is stabilized by the overlap of a filled $3p_s$ orbital of the sulfur atom of one monomer and an empty σ_{s-c}^* anti-bonding orbital of the sulfur atom of another monomer. Also, Fig. 9 shows the NBO calculated donor and acceptor orbitals. The estimated stabilization energy $E^{(2)}$ associated with the $p_s \rightarrow \sigma_{s-c}^*$ charge transfer (de-localization) is 0.34 kcal mol^{-1} computed at the $B_3\text{LYP/LanL2DZ/6-31G(d)}$ level using NBO analysis.

Moreover, the $\text{S}\cdots\text{S}$ interaction is also supported using Bader's theory of atoms in molecules. As shown in Fig. 11, we found a bond critical point, CP3 ($\rho \approx 0.0633 \text{ a.u.}$), between two sulfur atoms of two different monomers. We also computed the Lagrangian kinetic energy and potential energy densities at the BCP and the corresponding values are 0.1086 and -0.1001 a.u. , respectively.

Furthermore, the reduced density gradient (RDG), s , was calculated to represent the deviation from a homogeneous electron distribution.⁹⁴ As presented in the following equation (eqn (1)), ∇ is the gradient operator and $|\nabla\rho|$ is the electronic density gradient mode. Now, this is a useful approach to explore and visualize different kinds of non-covalent interactions (NCIs) in real space such as both intra-

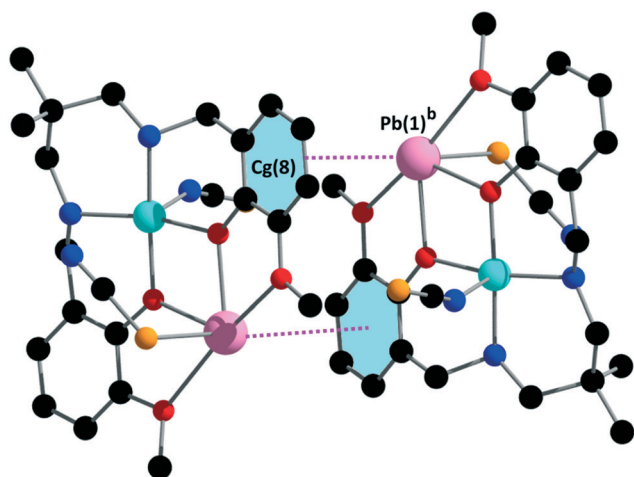


Fig. 4 Supramolecular dimer of the complex generated through cation $\cdots\pi$ interactions. All hydrogen atoms and uncoordinated perchlorate anions are omitted for clarity. Symmetry elements: $^b = 1 - x, 1 - y, -z$, where $\text{Cg}(8)\cdots\text{Pb}(1) = 3.563 \text{ \AA}$, $\text{Pb}(1)\cdots\text{Perp} = 3.359 \text{ \AA}$, and $\beta = 19.43^\circ$.

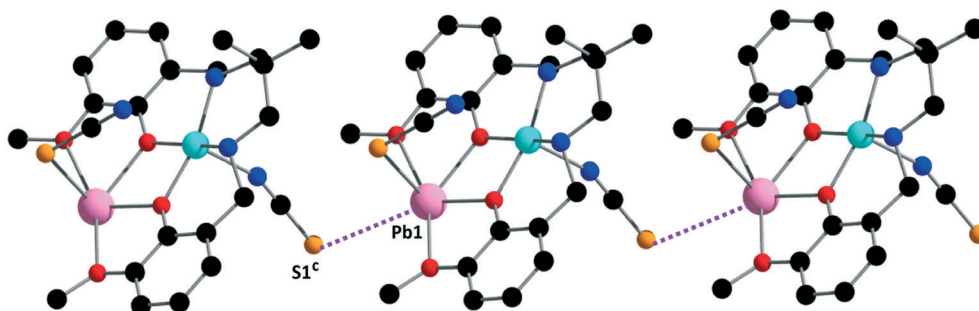


Fig. 5 1D coordination polymer of the complex considering an interaction between Pb(1) and S(1)^a of 3.517(2) Å. Symmetry transformation: ^c = *x*, −1 + *y*, *z*.

and intermolecular weak interactions like hydrogen bonds and van der Waals forces. Therefore, the NCI index is used to investigate NCIs in the investigated complex.

$$s = \frac{1}{2(3\pi^2)^{\frac{1}{3}}} \frac{|\nabla\rho|}{\rho^{\frac{4}{3}}} \quad (1)$$

The color mapped isosurfaces and corresponding scatter diagrams of RDG *versus* $\text{sign}(\lambda_2)\rho$ for the investigated complex in the monomeric and dimeric forms are shown in Fig. 13. As stated, the results are used to characterize the types of multiple weak interactions like S⋯S, Pb⋯S and H-bonds *via* colored isosurfaces according to the values of $\text{sign}(\lambda_2)\rho$. The sign of λ_2 is used to distinguish bonded ($\lambda_2 < 0$) and non-bonded ($\lambda_2 > 0$) interactions, whereas the electron density is an indicator of the bonding strength. Large negative values of $\text{sign}(\lambda_2)\rho$ are indicative of attractive interactions (such as hydrogen bonding), whereas, if $\text{sign}(\lambda_2)\rho$ is large and positive, the interaction is non-bonding (usually steric effect). Values near zero indicate weak vdW interactions. The color of RDG (*s*) *vs.* $\text{sign}(\lambda_2)\rho$ and the isosurfaces have the same meaning; blue color represents hydrogen bonds; green, van der Waals forces; red, steric hindrance. The darker the corresponding color, the stronger the interaction.

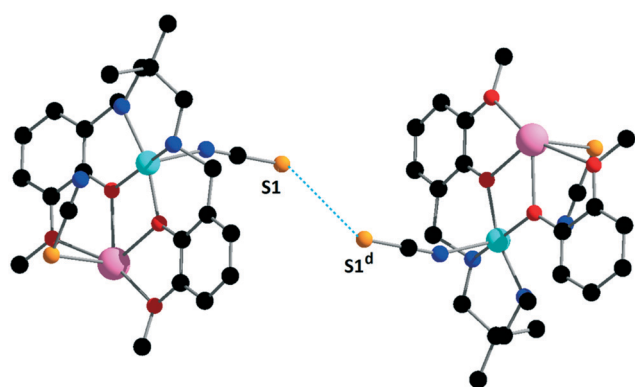


Fig. 6 Dimeric form of the complex considering an interaction between S(1) and S(1)^d of 3.593(2) Å. Symmetry transformation: ^d = 2 − *x*, 2 − *y*, −*z*.

The color mapped isosurfaces and corresponding scatter diagrams of RDG *versus* $\text{sign}(\lambda_2)\rho$ for the complex in dimeric form is shown in Fig. 13. The green region in Fig. 13a clearly characterizes the weak S⋯S interaction between two monomers in the solid-state. The BSSE corrected interaction energy calculated for the S⋯S interactions is −1.6 kcal mol^{−1}.

Pb⋯S tetrel bonding

In the solid state structure of the investigated complex, the existence of intermolecular tetrel bonding interactions is observed (Fig. 5) and characterized by a bond critical point (CP1) and a bond path interconnecting the S and Pb atoms in a dimeric unit ($\rho = 0.06936$ a.u.). The strengths are significantly strong which is evident from the MEP analysis. The MEP surface at the S and Pb atoms shows that a σ -hole of 22 kcal mol^{−1} is observed at the Pb center along with a strong nucleophilic center at the S atom of −20 kcal mol^{−1} (Fig. 12a). As a result, the BSSE corrected interaction energy computed for the tetrel bonding is −13.6 kcal mol^{−1}. The NBO analysis shows that the stabilization energy $E^{(2)}$ associated with the charge transfer (delocalization) from the S to the Pb center is 13.79 kcal mol^{−1} computed at the B₃LYP/LanL2DZ/6-31G(d) level (Fig. 10). Additionally, we have characterized the

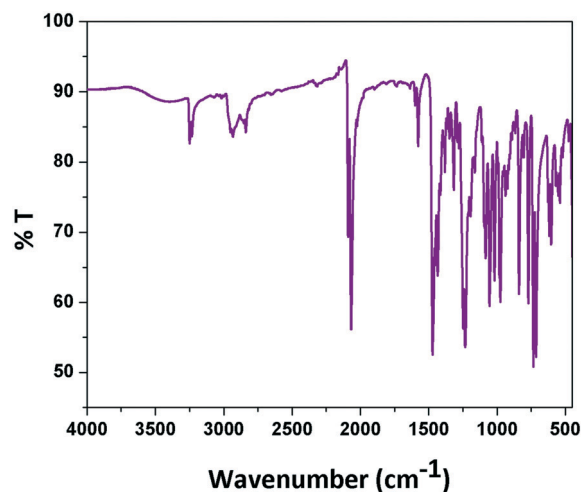


Fig. 7 IR spectrum of the complex.

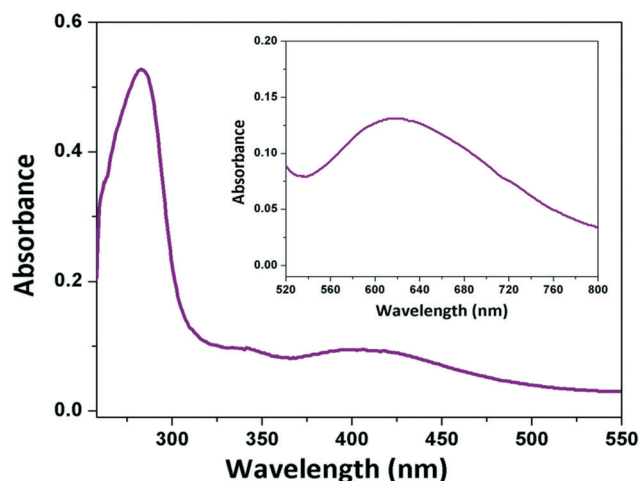


Fig. 8 UV-vis spectrum of the complex. Inset shows the spectrum in the 520–800 nm range.

existence of the $\text{Pb} \cdots \text{S}$ tetrel bond with the RDG plots and NCI surfaces (Fig. 13d).

H-Bonding

We characterized two types of H-bonding in the investigated complex: intramolecular and intermolecular. The intramolecular H-bonding is characterized by AIM analysis, which gives an orange sphere as a BCP (Fig. 11f) between the N of SCN and amine hydrogen of the reduced Schiff base. The existence of such H-bonding is well supported by the RDG plots and NCI surfaces as shown in Fig. 13c. In the H-bonded dimer of the complex (Fig. 2), we have found some additional intermolecular H-bonding as characterized very clearly from the NCI surfaces and by AIM analysis. We identified a BCP ($\rho = 0.0149$ a.u.) between the hydrogen atom, H(1) {attached to

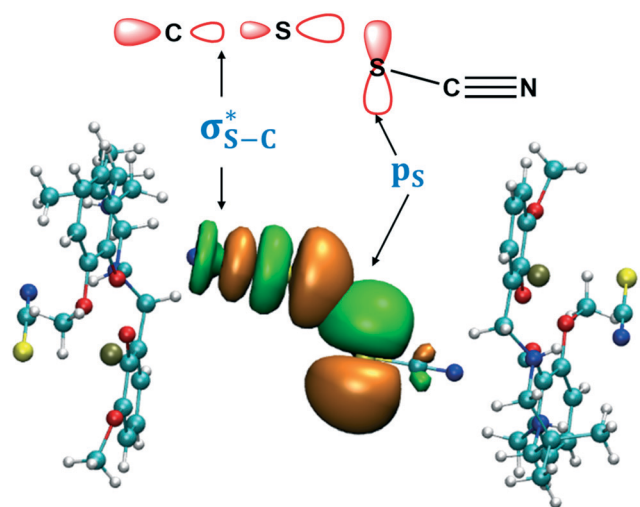


Fig. 9 Isosurfaces for a value of 0.03 a.u. showing the interaction of the filled p orbital of the S center of one monomer and empty σ^* orbital of the S center of another monomer computed using NBO analyses.

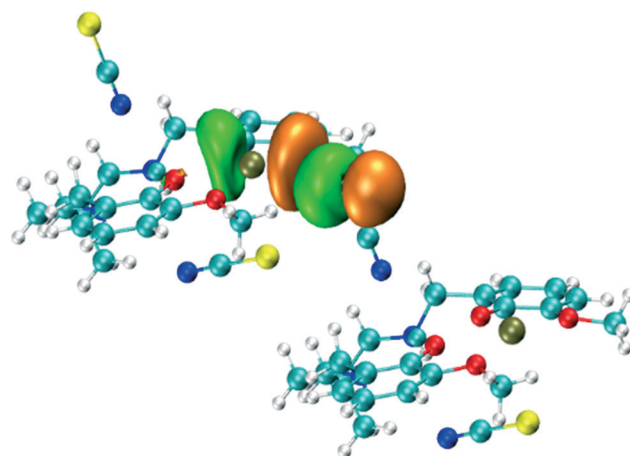


Fig. 10 Isosurfaces for a value of 0.03 a.u. showing the interaction between the orbital of S of one monomer and orbital of Pb of another monomer indicating a tetrel bond computed using NBO analysis.

the amine nitrogen atom, N(1)}, and the thiocyanate nitrogen atom, N(4)*, of a symmetry related $\{^* = 1 - x, 1 - y, 1 - z\}$ neighboring moiety. Additionally, the scatter RDG plot shows some additional blue dots at the left side to identify the intermolecular H-bonding (Fig. 13b and c). As a consequence, the BSSE corrected interaction energy of this complex is -7.1 kcal mol^{-1} .

$\text{Pb} \cdots \pi$ and $\pi \cdots \pi$ interactions

As stated in the experimental section, we have found a $\pi \cdots \pi$ interaction (Fig. 3) between two benzene rings on two monomers. In the investigated complex, we confirmed the existence of the $\pi \cdots \pi$ interactions by using AIM analysis. In the dimer (Fig. 3), the computed results show that two BCPs are found, one of which (CP2) is shown in Fig. 11, between the σ (C–H) framework of one ring and π -electrons on another ring. The attractive interaction is also evident from the MEP surfaces (Fig. 12b). Further, we established the existence of the $\pi \cdots \pi$ stacking by utilizing RDG surfaces as shown in Fig. 13(e). A very clean image of green color between two rings strongly supports this statement. As a result of the $\pi \cdots \pi$ interactions, we computed a BSSE interaction energy of -1.15 kcal mol^{-1} .

Interestingly, from the AIM analysis, we detected another weak interaction between the cation Pb(II) and π -electrons, referred to as $\text{Pb} \cdots \pi$ interaction (Fig. 4). The properties of the BCP (CP4) show that this interaction is stronger ($\rho = 0.02394$ a.u.) than the other CPs discussed previously. The MEP surface of the $\text{Pb} \cdots \pi$ interaction (Fig. 12b) clearly indicates that this is electrostatically very favorable due to the potential difference between the strong σ -hole at the Pb center ($+18$ kcal mol^{-1}) and aromatic ring (-6.9 kcal mol^{-1}). The interaction is further characterized with an NCI-RDG surface showing a green plate between the Pb(II) center and aromatic ring as shown in Fig. 13f. As a consequence, the computed BSSE corrected interaction energy of the $\text{Pb} \cdots \pi$ interaction is -13.6 kcal mol^{-1} .

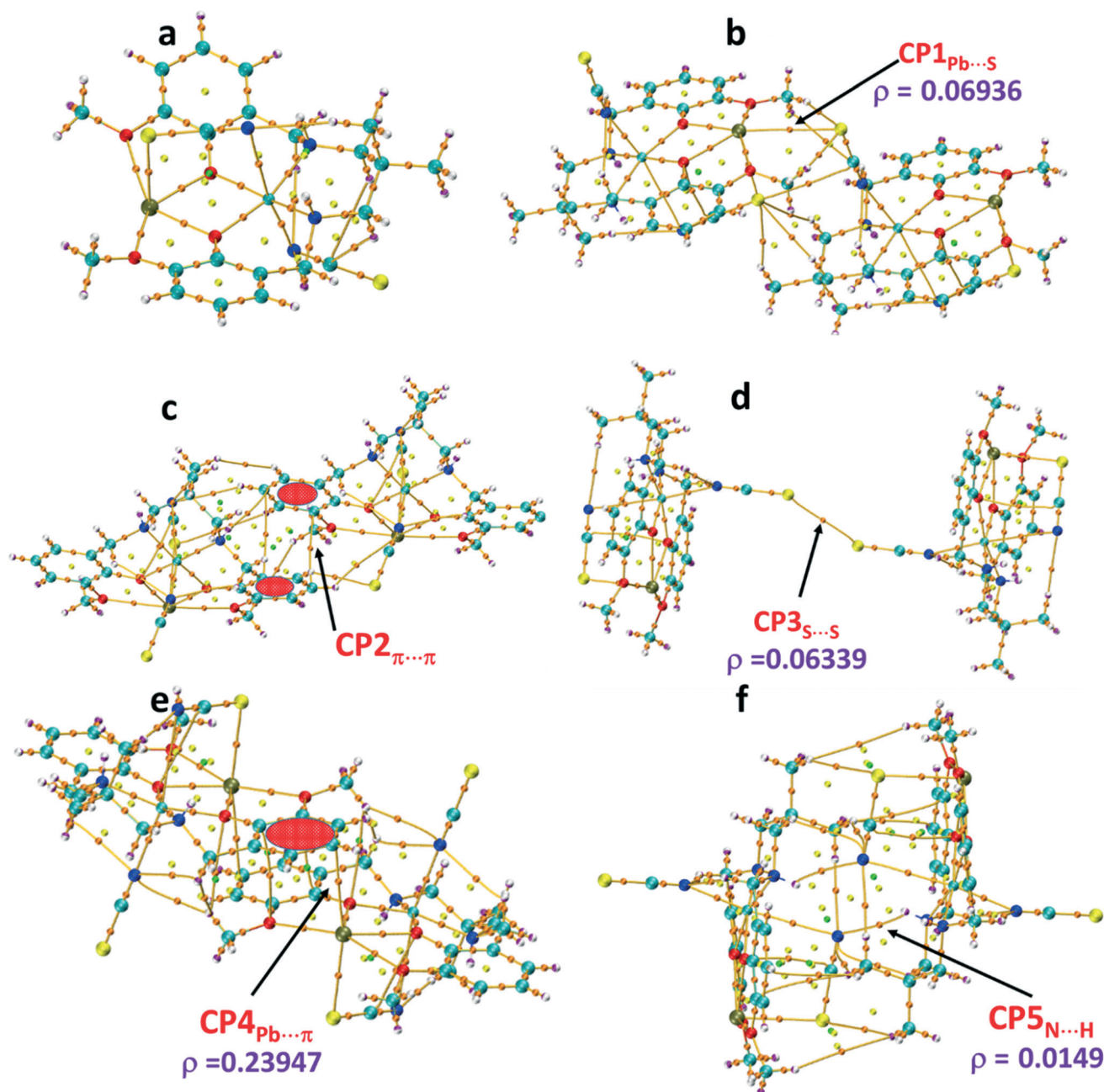


Fig. 11 AIM analyses of the monomer (a) and dimers of the investigated complex showing (b) Pb...S, (c) $\pi\cdots\pi$, (d) S...S, (e) Pb... π and (f) intermolecular hydrogen bonding, N...H-N. Bonds, rings and cage critical points are represented by orange, yellow and green spheres, respectively.

Concluding remarks

In summary, we report the syntheses and structural characterization of a new heterodinuclear copper(II)/lead(II) complex with an N_2O_4 donor compartmental reduced Schiff base ligand. In the solid-state, the complex exhibits relevant tetrel bonding and chalcogen–chalcogen interactions that generate interesting supramolecular assemblies. The complex contains a hemidirectionally coordinated lead(II) center and an organic aromatic molecule which can be important to understand the

X-ray structure of organic–inorganic material systems. In addition to the use of NCI-RDG analysis, which support the existence of tetrel bonding, NBO results show that the tetrel bonding is formed between the donor S atom of SCN and acceptor Pb atom ($\text{lp}_\text{S} \rightarrow \text{lp}_\text{Pb}^*$) with a high second-order stabilization energy of $E^{(2)} \approx 13.8 \text{ kcal mol}^{-1}$. Further, the S...S interaction, like general chalcogen–chalcogen bonds, is a $\text{p}_\text{S} \rightarrow \sigma_{\text{S}-\text{C}}^*$ orbital delocalization with $E^{(2)} \approx 0.34 \text{ kcal mol}^{-1}$. The other three interactions, namely Pb... π , $\pi\cdots\pi$ and both intra- and intermolecular H-bonding, are well supported

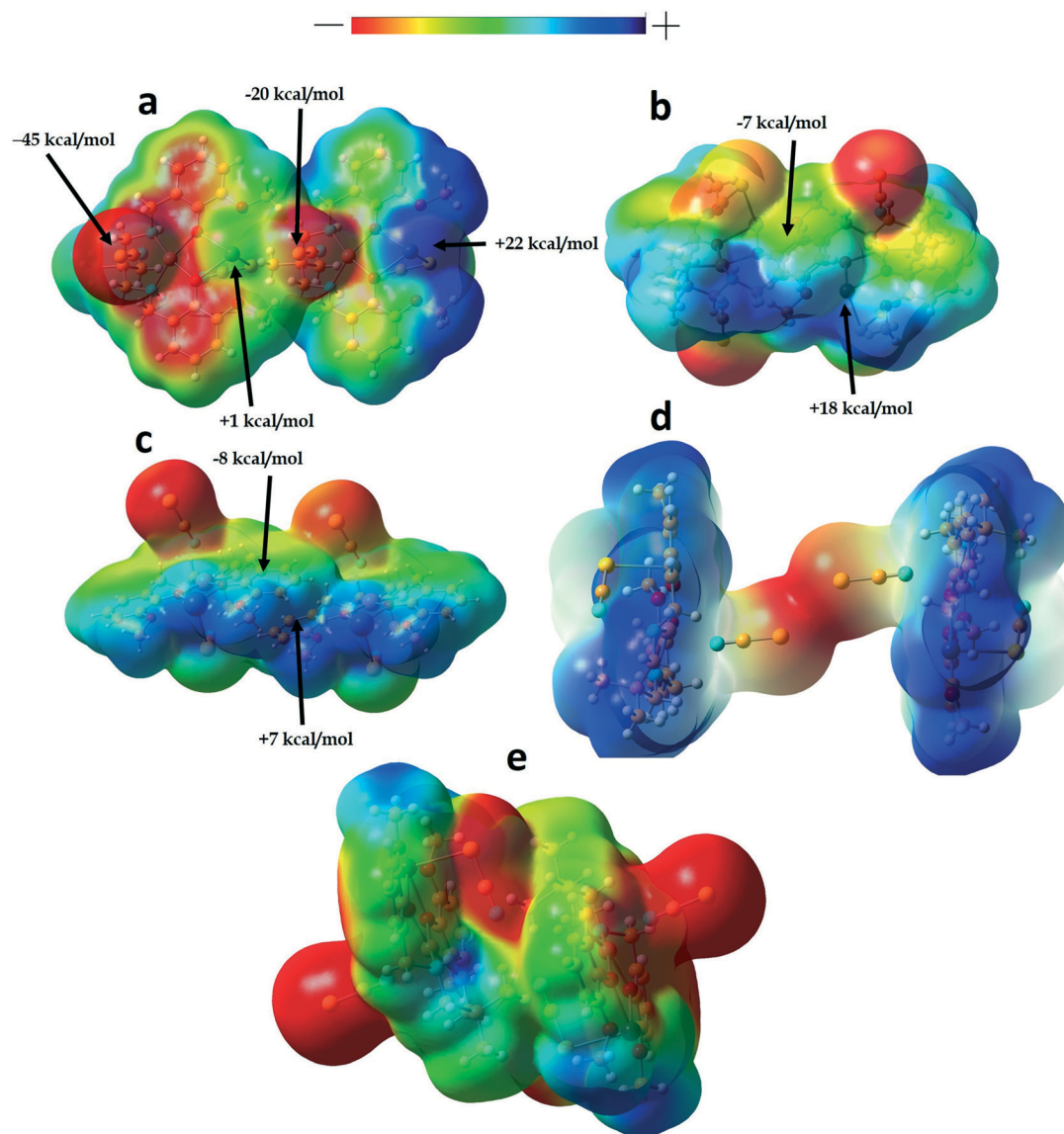


Fig. 12 MEP surface (isosurface = 0.001 a.u.) of the investigated complex. MEP values at selected points of the surface in the complex showing (a) Pb \cdots S, (b) Pb \cdots π , (c) $\pi\cdots\pi$, (d) S \cdots S and (e) H-bonding interactions.

qualitatively and quantitatively with the help of NCI-RDG, QTAIM, MEP surface, and NBO analyses. Among these interactions, we have found that Pb \cdots π has the highest interaction energy of $-13.6 \text{ kcal mol}^{-1}$.

Computational details

A DFT study is carried out to understand the electronic structure of the investigated complex. All geometry optimizations of the complex are carried out using the density functional theory method at the B₃LYP level with the Gaussian 09 program package. The Los Alamos effective core potential lanL₂-DZ basis set was employed for the Pb and Cu atoms. On the other hand, the split-valence 6-31G(d) basis set was applied for the other atoms. The starting structure of the investigated complex was derived from its X-ray crystallographic data. The

geometry optimization is performed without any constraints, and the nature of stationary points was confirmed by normal-mode analysis. The topological features derived from Bader's theory of atoms in molecules (AIM) approach was applied to understand the electron-density features like charge density (ρ) and Laplacian of charge density ($\nabla^2\rho$) using ADF2014.10. The recently developed reduced density gradient (RDG) based NCI (non-covalent interactions) index calculations were applied for real-space visualization of both attractive (van der Waals and hydrogen bonding) and repulsive (steric) interactions based on the properties of the electron density. Herein, the single-point calculations were based on the structure obtained from the X-ray studies and in these structures, the hydrogen atom positions were normalized before computation. This is already discussed in the Theoretical work section. Natural bond orbital (NBO) analysis was applied to

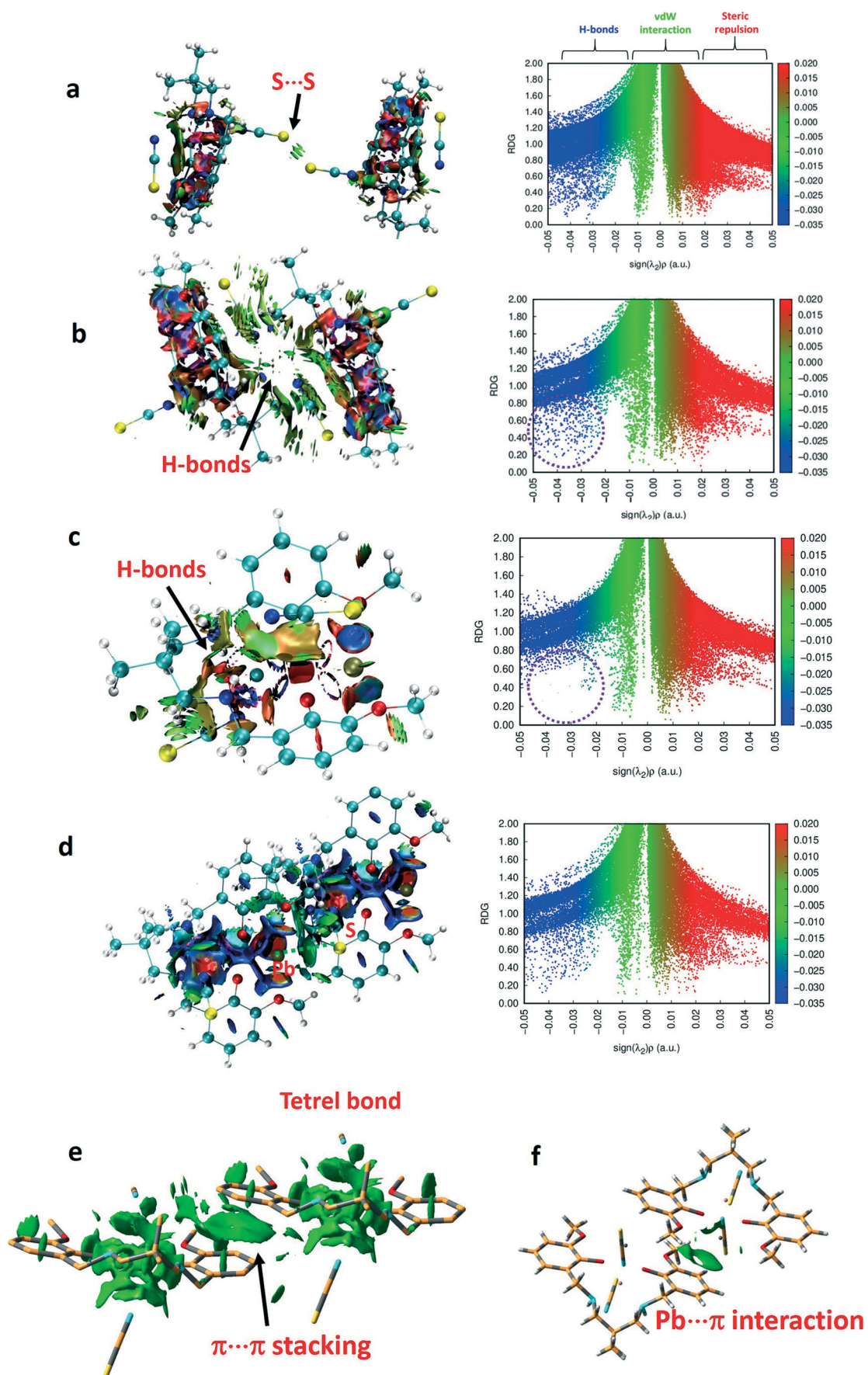


Fig. 13 Non-covalent interaction (NCI) analysis of the investigated complex computed at the B₃LYP/LanL2DZ/6-31G(d) level showing (a) S...S interaction, (b) intermolecular H-bonding, (c) intramolecular H-bonding, (d) Pb...S tetrel bonding, (e) $\pi\cdots\pi$ interaction and (f) Pb... π interaction.

investigate the stability of the molecule arising from charge delocalization. The interaction energies of dimers were calculated using basis set superposition error (BSSE) corrections by the following method:

$$\Delta E(AB) = E(AB) - E(A) - E(B) + (\text{BSSE value of dimer})$$

Conflicts of interest

The authors declare no competing financial interest.

Acknowledgements

S. M. thanks CSIR, India for awarding a Junior Research Fellowship [Sanction No. 09/096(0990)2019-EMR-1].

References

- D. L. Reger, T. D. Wright, C. A. Little, J. J. S. Lamba and M. D. Smith, *Inorg. Chem.*, 2001, **40**, 3810–3814.
- H. Fleischer and D. Schollmeyer, *Inorg. Chem.*, 2004, **43**, 5529–5536.
- A. Morsali and A. R. Mahjoub, *Helv. Chim. Acta*, 2004, **87**, 2717–2722.
- J. Parr, *Polyhedron*, 1997, **16**, 551–566.
- A. Olvera, G. Shi, H. Djieutedjeu, A. Page, C. Uher, E. Kioupakis and P. F. P. Poudeu, *Inorg. Chem.*, 2015, **54**, 746–755.
- C. A. Randall, A. S. Bhalla, T. R. Shrout and L. E. Cross, *J. Mater. Res.*, 1990, **5**, 829–834.
- F. Cheng, J. Liang, Z. Tao and J. Chen, *Adv. Mater.*, 2011, **23**, 1695–1715.
- L. Zhang, Y.-Y. Qin, Z.-J. Li, Q.-P. Lin, J.-K. Cheng, J. Zhang and Y.-G. Yao, *Inorg. Chem.*, 2008, **47**, 8286–8293.
- Y. Cheng, T. J. Emge and J. G. Brennan, *Inorg. Chem.*, 1996, **35**, 342–346.
- J. J. Chisholm, *Sci. Am.*, 1971, **224**, 15–23.
- B. P. Lanphear, D. A. Burgoon, S. W. Rust, S. Eberly and W. Galke, *Environ. Res.*, 1998, **76**, 120–130.
- T. G. Spiro and W. M. Stigliani, *Chemistry of the Environment*, Prentice Hall, Upper Saddle River, NJ, 1996.
- F. Cuenot, M. Meyer, A. Bucaille and R. A. Guillard, *J. Mol. Liq.*, 2005, **118**, 89–99.
- R. M. Harrison and D. R. H. Laxen, *Lead Pollution*, Chapman & Hall, London, 1981.
- J. M. Christensen and J. Kristiansen, in *Handbook of Metals in Clinical and Analytical Chemistry*, ed. H. Seiler, G. A. Sigel, H. Sigel and M. Dekker, New York, 1994, pp. 425–440.
- R. A. Goyer, in *Handbook on Toxicity of Inorganic Compounds*, ed. H. G. Seiler, H. Sigel, A. Sigel and M. Dekker, New York, 1988.
- D. A. Cory-Slechta, B. Weiss and C. Cox, *J. Pharmacol. Exp. Ther.*, 1987, **243**, 804–813.
- D. E. Glotzer, K. A. Freedberg and H. Baucher, *Med. Decis. Mak.*, 1995, **15**, 13–24.
- D. E. Glotzer and H. Baucher, *J. Pediatr.*, 1992, **89**, 614–618.
- CDC (Centers for Disease Control), *Preventing Lead Poisoning in Young Children, A statement by The Centers for Disease Control*, U.S. Department of Health and Human Services/Public Health Service/Centers for Disease Control, 1991.
- M. E. Markowitz and J. F. Rosen, *J. Pediatr.*, 1991, **119**, 305–310.
- R. Ferreirs-Martínez, D. Esteban-Gomez, E. Toth, A. de Blas, C. Platas-Iglesias and T. Rodríguez-Blas, *Inorg. Chem.*, 2011, **50**, 3772–3784.
- J. M. Ratcliffe, *Lead in Man and Environment*, John Wiley & Sons, New York, 1981.
- M. D. J. J. Chisolm Jr, *J. Pediatr.*, 1968, **73**, 1–38.
- S.-R. Fan and L.-G. Zhu, *Inorg. Chem.*, 2007, **46**, 6785–6793.
- P. Pykkö and J.-P. Desclaux, *Acc. Chem. Res.*, 1979, **12**, 276–281.
- N. V. Sidgwick and H. M. Powell, Bakerian Lecture: Stereochemical types and valency groups, *Proc. R. Soc. London, Ser. A*, 1940, **176**, 153.
- M. S. Banna, *J. Chem. Educ.*, 1985, **62**, 197–198.
- K. S. Pitzer, *Acc. Chem. Res.*, 1979, **12**, 271–276.
- P. Pykkö, *Chem. Rev.*, 1988, **88**, 563–594.
- D. R. McKeney, *J. Chem. Educ.*, 1983, **60**, 112–116.
- J. R. Thompson, D. Snider, J. E. C. Wren, S. Kroeker, V. E. Williams and D. B. Lenzoff, *Eur. J. Inorg. Chem.*, 2017, 88–98.
- R. L. Davidovich, V. Stavila, D. V. Marinin, E. I. Voit and K. H. Whitmire, *Coord. Chem. Rev.*, 2009, **253**, 1316–1352.
- R. J. Gillespie and R. S. Nyholm, *Inorganic Stereochemistry, Q. Rev., Chem. Soc.*, 1957, **11**, 339–380.
- D. L. Reger, M. F. Huff, A. L. Rheingold and B. S. Haggert, *J. Am. Chem. Soc.*, 1992, **114**, 579–584.
- R. Luckay, I. Cukrowski, J. Mashishi, J. H. Reibenspies, A. H. Bond, R. D. Rogers and R. D. Hancock, *J. Chem. Soc., Dalton Trans.*, 1997, 901–908.
- C. Platas-Iglesias, D. Esteban-Gomez, T. Enriquez-Perez, F. Avecilla, A. de Blas and T. Rodríguez-Blas, *Inorg. Chem.*, 2005, **44**, 2224–2233.
- D. Esteban-Gómez, C. Platas-Iglesias, T. Enriquez-Pérez, F. Avecilla, A. Blas and T. Rodríguez-Blas, *Inorg. Chem.*, 2006, **45**, 5407–5416.
- A. Walsh and G. W. Watson, *J. Solid State Chem.*, 2005, **178**, 1422–1428.
- R. D. Hancock, M. S. Shaikjee, S. M. Dobson and J. C. Boeyens, *Inorg. Chim. Acta*, 1988, **154**, 229–238.
- J.-M. Lehn, *Supramolecular Chemistry: Concepts and Perspectives*, VCH, Weinheim, 1995.
- J. W. Steed and J. L. Atwood, *Supramolecular Chemistry*, John Wiley & Sons, Chichester, 2000.
- H. J. Schneider and A. Yatsimirsky, *Principles and Methods in Supramolecular Chemistry*, John Wiley & Sons, Chichester, 2000.
- Y. Shen, N. Ma, L. Wu and H.-H. Song, *Inorg. Chim. Acta*, 2015, **429**, 51–60.
- Y.-S. Yang, Y.-P. Yang, M. Liu, Q.-M. Qiu, Q.-H. Jin, J.-J. Sun, H. Chen, Y.-C. Dai and Q.-X. Meng, *Polyhedron*, 2015, **85**, 912–917.
- S. Carboni, C. Gennari, L. Pignataro and U. Piarulli, *Dalton Trans.*, 2011, **40**, 4355–4373.

- 47 A. Bhattacharyya, P. K. Bhaumik, P. P. Jana and S. Chattopadhyay, *Polyhedron*, 2014, **78**, 40–45.
- 48 J. Xiao, P. Broz, A. W. Puri, E. Deu, M. Morell, D. M. Monack and M. A. Bogoy, *J. Am. Chem. Soc.*, 2013, **135**, 9130–9138.
- 49 S. Naskar, D. Mishra, R. J. Butcher and S. K. Chattopadhyay, *Polyhedron*, 2007, **26**, 3703–3714.
- 50 A. Bauzá, D. Quiñonero, P. M. Deyà and A. Frontera, *Chem. - Asian J.*, 2013, **8**, 2708–2713.
- 51 L. M. Salonen, M. Ellermann and F. Diederich, *Angew. Chem., Int. Ed.*, 2011, **50**, 4808–4842.
- 52 V. R. Pedireddi, D. S. Reddy, B. S. Goud, D. C. Craig, A. D. Rae and G. R. Desiraju, *J. Chem. Soc., Perkin Trans. 2*, 1994, 2353–2360.
- 53 R. E. Rosenfield, R. Parthasarathy and J. D. Dunitz, *J. Am. Chem. Soc.*, 1977, **99**, 4860–4862.
- 54 J. P. Glusker, *Top. Curr. Chem.*, 1998, **198**, 1–56.
- 55 T. N. Guru Row and R. Parthasarathy, *J. Am. Chem. Soc.*, 1981, **103**, 477–479.
- 56 N. Ramasubbu and R. Parthasarathy, *Phosphorus Sulfur Relat. Elem.*, 1987, **31**, 221–229.
- 57 J. M. Williams, J. R. Ferraro, R. J. Thorn, K. D. Carlson, U. Geiser, H. H. Wang, A. M. Kini and M.-H. Whangbo, *Organic Superconductors*, Prentice Hall, Englewood Cliffs, NJ, 1992.
- 58 D. Paolantoni, J. Rubio-Magnieto, S. Cantel, J. Martinez, P. Dumy, M. Surin and S. Ulrich, *Chem. Commun.*, 2014, **50**, 14257–14260.
- 59 C. Estarellas, A. Frontera, D. Quiñonero and P. M. Deyà, *Angew. Chem., Int. Ed.*, 2011, **50**, 415–418.
- 60 S. Jana, K. Harms and S. Chattopadhyay, *J. Coord. Chem.*, 2014, **67**, 2954–2966.
- 61 G. Mahmoudi, A. Bauzá, M. Amini, E. Molins, J. T. Magued and A. Frontera, *Dalton Trans.*, 2016, **45**, 10708–10716.
- 62 A. Bauzá, T. J. Mooibroek and A. Frontera, *Angew. Chem., Int. Ed.*, 2013, **52**, 12317–12321.
- 63 A. Bauzá, T. J. Mooibroek and A. Frontera, *Chem. - Eur. J.*, 2014, **20**, 10245–10248.
- 64 R. S. Ruoff, T. Emilsson, A. I. Jaman, T. C. Germann and H. S. Gutowsky, *J. Chem. Phys.*, 1992, **96**, 3441–3446.
- 65 S. J. Grabowski, *Phys. Chem. Chem. Phys.*, 2014, **16**, 1824–1834.
- 66 I. Alkorta, I. Rozas and J. Elguero, *J. Phys. Chem. A*, 2001, **105**, 743–749.
- 67 E. C. Escudero-Adán, A. Bauzá, A. Frontera and P. Ballester, *ChemPhysChem*, 2015, **16**, 2530–2533.
- 68 A. Bauzá, T. J. Mooibroek and A. Frontera, *Phys. Chem. Chem. Phys.*, 2014, **16**, 19192–19197.
- 69 A. Bauzá, T. J. Mooibroek and A. Frontera, *Chem. Commun.*, 2014, **50**, 12626–12629.
- 70 A. Bundhun, P. Ramasami, J. S. Murray and P. Politzer, *J. Mol. Model.*, 2013, **19**, 2739–2746.
- 71 A. Bauzá, T. J. Mooibroek and A. Frontera, *Chem. Rec.*, 2016, **16**, 473–487.
- 72 C. Goulaouen, O. Parisel and H. Gerard, *Dalton Trans.*, 2011, **40**, 11282–11288.
- 73 S. Mirdya, S. Roy, S. Chatterjee, A. Bauza, A. Frontera and S. Chattopadhyay, *Cryst. Growth Des.*, 2019, **19**, 5869–5881.
- 74 S. Mirdya, A. Frontera and S. Chattopadhyay, *CrystEngComm*, 2019, **21**, 6859–6868.
- 75 A. Hazari, L. K. Das, R. M. Kadam, A. Bauzá, A. Frontera and A. Ghosh, *Dalton Trans.*, 2015, **44**, 3862–3876.
- 76 S. Mirdya, T. Basak and S. Chattopadhyay, *Polyhedron*, 2019, **170**, 253–263.
- 77 A. W. Addison, T. N. Rao, J. Reedijk, J. V. Rijn and G. C. Verschoor, *J. Chem. Soc., Dalton Trans.*, 1984, 1349–1356.
- 78 D. Cremer and J. A. Pople, *J. Am. Chem. Soc.*, 1975, **97**, 1354–1358.
- 79 D. Cremer, *Acta Crystallogr., Sect. B: Struct. Sci.*, 1984, **40**, 498–500.
- 80 L. Shimoni-Livny, J. P. Glusker and C. W. Bock, *Inorg. Chem.*, 1998, **37**, 1853–1867.
- 81 M.-L. Hu, A. Morsali and L. Aboutorabi, *Coord. Chem. Rev.*, 2011, **255**, 2821–2859.
- 82 F. Mautner, M. Scherzer, C. Berger, R. C. Fischer, R. Vicente and S. S. Massoud, *Polyhedron*, 2015, **85**, 20–26.
- 83 M. Das, S. Chatterjee, K. Harms, T. K. Mondal and S. Chattopadhyay, *Dalton Trans.*, 2014, **43**, 2936–2947.
- 84 M. Karmakar, S. Roy and S. Chattopadhyay, *New J. Chem.*, 2019, **43**, 10093–10102.
- 85 M. Andruh, *Chem. Commun.*, 2011, **47**, 3025–3042.
- 86 S. Roy, A. Bhattacharyya, S. Herrero, R. González-Prieto, A. Frontera and S. Chattopadhyay, *ChemistrySelect*, 2017, **2**, 6535–6543.
- 87 M. A. Khan, A. A. Alqadami, M. Otero, M. R. Siddiqui, Z. A. Alothman, I. Alsohaimi, M. Rafatullah and A. E. Hamedelnie, *Chemosphere*, 2019, **218**, 1089–1099.
- 88 A. Biswas, L. K. Das, M. G. B. Drew, C. Diaz and A. Ghosh, *Inorg. Chem.*, 2012, **51**, 10111–10121.
- 89 A. Golcu, M. Tumer, H. Demirelli and R. A. Wheatley, *Inorg. Chim. Acta*, 2005, **358**, 1785–1797.
- 90 S. Roy, T. Basak, S. Khan, M. G. B. Drew, A. Bauzá, A. Frontera and S. Chattopadhyay, *ChemistrySelect*, 2017, **2**, 9336–9343.
- 91 S. Roy, K. Harms, A. Bauzá, A. Frontera and S. Chattopadhyay, *Polyhedron*, 2017, **121**, 199–205.
- 92 C. Bleiholder, D. B. Werz, H. Köppel and R. Gleiter, Theoretical Investigations on Chalcogen–Chalcogen Interactions: What Makes These Nonbonded Interactions Bonding?, *J. Am. Chem. Soc.*, 2006, **128**, 2666–2674.
- 93 R. Gleiter, G. Haberhauer, D. B. Werz, F. Rominger and C. Bleiholder, *Chem. Rev.*, 2018, **118**, 2010–2041.
- 94 J. Contreras-García, W. Yang and E. R. Johnson, *J. Phys. Chem. A*, 2011, **115**, 12983–12990.



Cite this: *CrystEngComm*, 2019, 21, 6859

Formation of a tetranuclear supramolecule *via* non-covalent Pb⋯Cl tetrel bonding interaction in a hemidirected lead(II) complex with a nickel(II) containing metaloligand†

Saikat Mirdya,^a Antonio Frontera ^{*b} and Shouvik Chattopadhyay ^{*a}

A hetero-dinuclear nickel(II)/lead(II) complex with a compartmental ‘reduced Schiff base’ ligand (having inner N₂O₂ and outer O₂O₂′ compartments) has been prepared and characterized by elemental and spectral analysis. Single crystal X-ray diffraction analysis confirms its structure. Nickel(II) is placed in the inner N₂O₂ compartment and lead(II) is placed in the outer O₂O₂′ compartment of the compartmental reduced Schiff base. The complex forms a tetranuclear supramolecule *via* non-covalent Pb⋯Cl tetrel bonding interactions. The DFT study is devoted to analyze these tetrel bonding interactions that involve the σ-hole at the hemicoordinated Pb(II) atom. The tetrel bonding interactions have been characterized using Bader’s theory of atoms in molecules (AIM).

Received 14th August 2019,
Accepted 15th September 2019

DOI: 10.1039/c9ce01283d

rsc.li/crystengcomm

Introduction

A significant number of supramolecular coordination compounds have been synthesized in recent years¹ and shown to have the potential to be used as probes, sensors and photonic devices.² The most commonly used approach for engineering the crystal structure of such complexes employs non-covalent intermolecular forces, *e.g.* hydrogen bonding, π–π stacking, cation–π, C–H⋯π interactions, *etc.*³ Other well recognized non-covalent interactions, such as halogen bonding and ion pairing, have also been used to direct the formation of many supramolecular assemblies.⁴ They play a vital role in drug–receptor interactions, crystal engineering, enzyme inhibition, protein folding, *etc.*⁵ Structures of bio-molecules could also be controlled by these interactions.⁶ On the other hand, σ-hole interactions have been studied less. Strong σ-hole interactions may occur in complexes of group IV elements and usually involves tetrel bonding interactions, especially in the case of lead.⁷ Tetrel bonds⁸ are generally characterized by two distinct classes of structural organizations, *viz.* holodirected⁹ and hemidirected¹⁰ geometries (Scheme 1). In the case of the former, the bonds of lead to donor atoms are directed throughout the surface of an encompassing sphere, while in

the case of the latter, the bonds of lead to ligand atoms are directed throughout a hemisphere, thereby exhibiting a clear void in the distribution of bonds to the ligands.¹¹

In the present work, one N₂O₂O₂′ donor compartmental reduced Schiff base, 2,2′-[(2,2-dimethyl-1,3-propanediyl)bis(iminomethylene)]bis[6-ethoxy-phenol] (H₂L), has been used to prepare a hetero-dinuclear nickel(II)/lead(II) complex, [(H₂O)(DMSO)NiLPbCl]SCN. The structure of the complex has been determined by single crystal X-ray diffraction analyses. The lead(II) centre in the complex is hemidirectionally coordinated and participates in non-covalent tetrel bonding interactions. Also an interesting hydrogen bonding is observed with non-coordinated thiocyanate. Finally, the supramolecular interactions have been studied using DFT calculations focusing on Pb⋯Cl tetrel bonds observed in the solid state of the complex.

Results and discussion

Synthesis

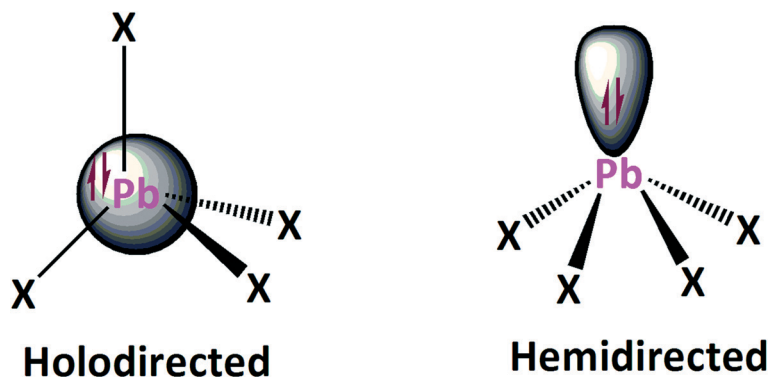
2,2-Dimethyl-1,3-diaminopropane was refluxed with 3-ethoxysalicylaldehyde in a 1:2 ratio followed by the addition of NaBH₄ to form the N₂O₂O₂′ donor compartmental reduced Schiff base (H₂L) following literature methods.¹² The ligand (H₂L) on the reaction with nickel(II) thiocyanate and lead(II) chloride produced the complex. The formation of the complex is shown in Scheme 2.

Description of [(H₂O)(DMSO)NiLPbCl](SCN). The molecular structure of the complex was established by X-ray single crystal diffraction measurement. It reveals that the complex crystallizes in the monoclinic space group, *P*2₁/*n*,

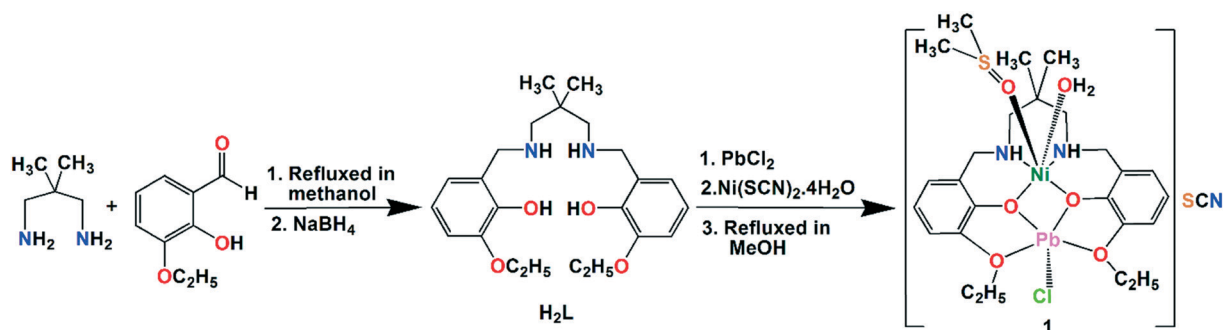
^a Department of Chemistry, Inorganic Section, Jadavpur University, Kolkata-700032, India. E-mail: shouvik.chem@gmail.com; Tel: +033 24572941

^b Departament de Química, Universitat de les Illes Balears, Crta de Valldemossa km 7.5, 07122 Palma de Mallorca, Balears, Spain. E-mail: toni.frontera@uib.es

† Electronic supplementary information (ESI) available. CCDC 1946110. For ESI and crystallographic data in CIF or other electronic format see DOI: 10.1039/c9ce01283d



Scheme 1 Schematic representation of the holodirected (left) and hemidirected (right) coordination modes of lead(II), with indication of the location of the inert lone pair.



Scheme 2 Preparation of the ligand and the complex.

with $Z = 2$. The complex consists of a cationic dinuclear cation $[(\text{H}_2\text{O})(\text{DMSO})\text{NiLPbCl}]$ along with an uncoordinated thiocyanate anion. The molecular structure with a selected atom numbering scheme is shown in Fig. 1. Important bond angles are listed in Table S1 (ESI[†]).

The $\text{N}_2\text{O}_2\text{O}_2'$ donor compartmental reduced Schiff base ligand (H_2L) is used to prepare the complex in which the nickel(II) centre, Ni(1), is placed in the inner N_2O_2 cavity and the lead(II) centre, Pb(1), is placed in the outer $\text{O}_2\text{O}_2'$ cavity with a $\text{Ni}(1)\cdots\text{Pb}(1)$ distance of 3.488(2) Å. The nickel(II) centre [Ni(1)] is hexacoordinated having a pseudo octahedral geometry, where two amine nitrogen atoms, N(1) and N(2), and two phenoxo oxygen atoms, O(1) and O(2), of the deprotonated reduced Schiff base (L)²⁻ constitute the equatorial plane. The fifth and sixth coordination sites are occupied by two oxygen atoms, O(5), from a DMSO molecule and O(6) from a water molecule. All nickel(II)–nitrogen and nickel(II)–oxygen bond lengths are comparable to those observed in other complexes with similar structures.¹³

The lead(II) centre in the complex is pentacoordinated where two phenoxo oxygen atoms, O(1) and O(2), also coordinate to the lead(II) centre. The potential donor ethoxy oxygen atoms, O(3) and O(4), of the deprotonated reduced Schiff base also coordinate to the lead(II) centre, but at much longer distances to form equatorial planes. All lead(II)–oxygen bond lengths are comparable to those observed in other complexes with similar structures.¹⁴ The fifth coordination site is occupied by one chlorido ligand, Cl(1) in the axial

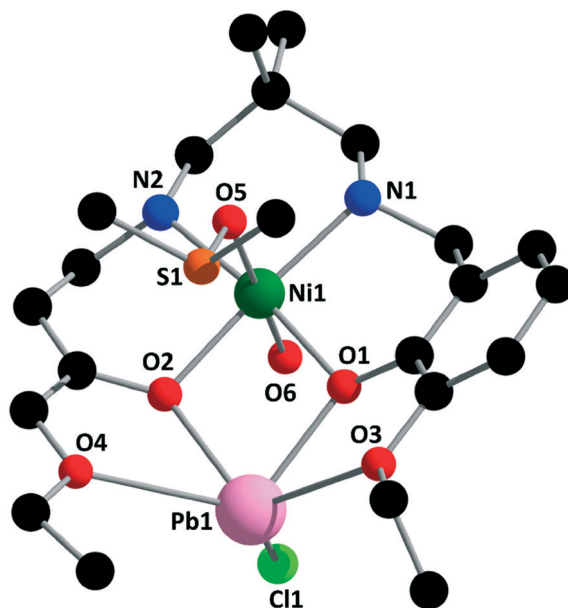


Fig. 1 Perspective view of the complex with a selective atom numbering scheme. Hydrogen atoms and the uncoordinated thiocyanate ion have been omitted for clarity. Selected bond lengths (Å): Pb(1)–Cl(1) 2.729(4), Pb(1)–O(1) 2.338(7), Pb(1)–O(2) 2.320(7), Pb(1)–O(3) 2.855(8), Pb(1)–O(4) 2.831(12), Ni(1)–O(1) 2.083(7), Ni(1)–O(2) 2.091(7), Ni(1)–O(5) 2.125(9), Ni(1)–O(6) 2.086(10), Ni(1)–N(1) 2.084(7), and Ni(1)–N(2) 2.087(9).

position with a Pb(1)–Cl(1) distance of 2.729(4) Å in the complex. The geometry of any penta-coordinated metal centre may conveniently be measured by the Addison parameter (τ)¹⁵ [$\tau = (\theta - \Phi)/60$, where θ and Φ are the two largest ligand–metal–ligand angles of the coordination sphere]. In the complex, the geometry around the lead(II) centre assumes a square pyramidal geometry with $\tau = 0.45$. The angle between the Ni(1)O(1)O(2) and O(1)O(2)Pb(1) planes is 4.12° and also the dihedral angle of the O(1)Ni(1) and O(2)Pb(1) planes is 3.5(3)°, making the NiO₂Pb core almost planar. The bridging angles, Ni(1)–O(1)–Pb(1) and Ni(1)–O(2)–Pb(1), are 104.0(3)° and 104.4(3)°, respectively. The angle of Cl(1)–Pb(1)–Ni(1) is 83.62(7)°. The saturated six membered chelate ring [Ni(1)–N(1)–C(10)–C(11)–C(14)–N(2)] has an envelope conformation with puckering parameters, $q = 0.596(11)$ Å; $\theta = 15.6(10)^\circ$; $\phi = 184(4)^\circ$.

IR and electronic spectra

A band near the range of 3289–3278 cm^{−1} indicates the presence of amine N–H stretching in the complex.¹⁶ Broad bands in the range of 2998–2867 cm^{−1} due to alkyl C–H stretching vibrations are routinely noticed in the IR spectrum of the complex.¹⁷ A broad band at 3369 cm^{−1} indicates the presence of the O–H stretching frequency of the water molecule.¹⁸ An intense band at 2052 cm^{−1} indicates the presence of uncoordinated thiocyanate.¹⁹ The IR spectrum of the complex is given in Fig. 2.

The electronic spectrum of the complex (Fig. 3) shows five bands at 242 nm, 284 nm, 348 nm, 601 nm and 848 nm. The absorption band at 601 nm may be assigned to $^3T_{1g}(F) \leftarrow ^3A_{2g}(F)$, whereas the band at 848 nm may be assigned to $^3T_{2g}(F) \leftarrow ^3A_{2g}(F)$.²⁰ A higher energy d–d band, $^3T_{1g}(P) \leftarrow ^3A_{2g}(F)$, cannot be observed as it is obscured by a strong charge transfer transition (348 nm) in this case.²¹ The UV absorption band at 284 nm may be assigned to the

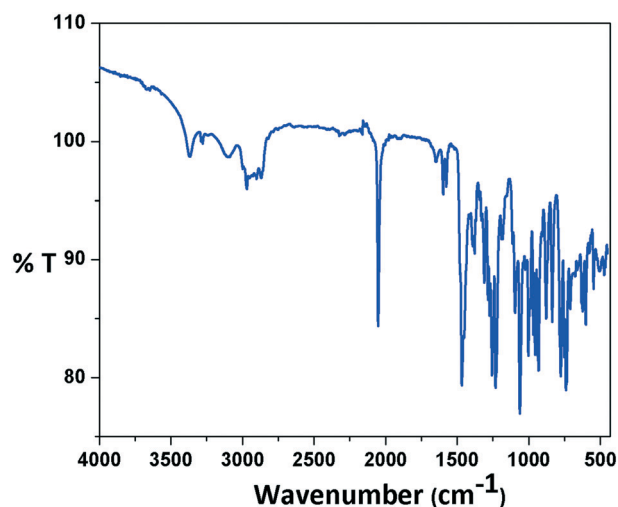


Fig. 2 IR spectrum of the complex.

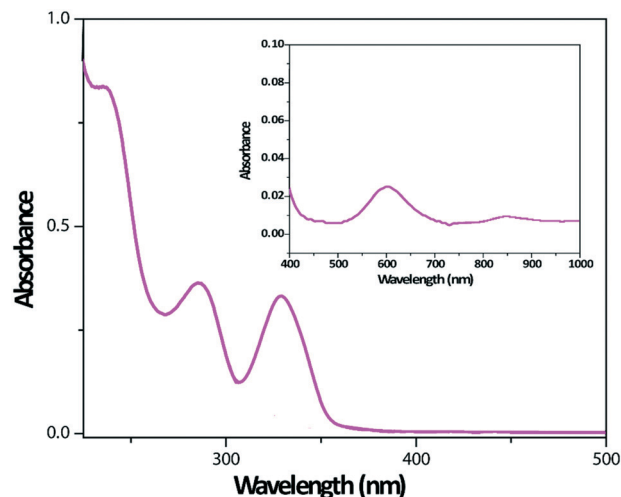


Fig. 3 UV-vis spectrum of the complex. Inset shows the spectrum in the 400–1000 nm range.

intraligand n– π^* transition.²² A band at 242 nm may be attributed to π – π^* transition.²³

Supramolecular interactions and Hirshfeld surface analyses

The water molecule bonded to nickel(II) forms a strong donor hydrogen bond. The hydrogen atom, H(6B), attached to the oxygen atom, O(6), of the coordinated water molecule forms an intramolecular hydrogen bond with a nitrogen atom, N(3), of the uncoordinated thiocyanate. The hydrogen bonded structure of the complex is given in Fig. 4.

A significant C–H $\cdots\pi$ interaction is observed. The hydrogen atom, H(24C), attached to the carbon atom, C(24), is involved in an intra-molecular C–H $\cdots\pi$ interaction with a phenyl ring [C(3)–C(4)–C(5)–C(6)–C(7)–C(8)] (Fig. 5).

An additional interesting aspect is that there is another interaction from Pb(1) to the chloride Cl(1)^a from an adjacent molecule (^a = $-x, 1 - y, 1 - z$) at 3.339(3) Å in the complex which

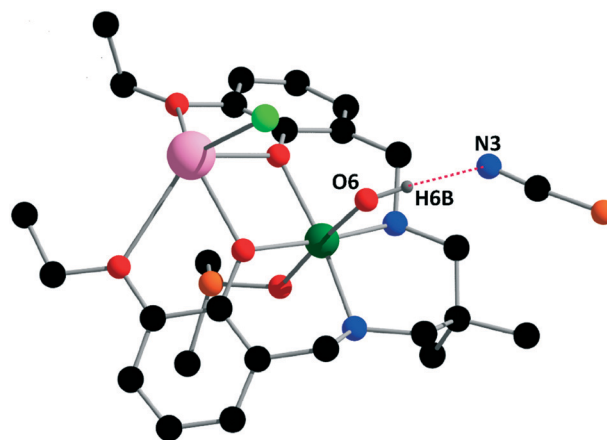


Fig. 4 Hydrogen bonded structure of the complex. Only the relevant hydrogen atoms are shown for clarity, where N(3)–H(6B) = 0.93(8) Å, H(6B) \cdots O(6) = 1.87(2) Å, N(3) \cdots O(6) = 2.77(2) Å, and \angle N(3)–H(6B) \cdots O(6) = 160(8)°.

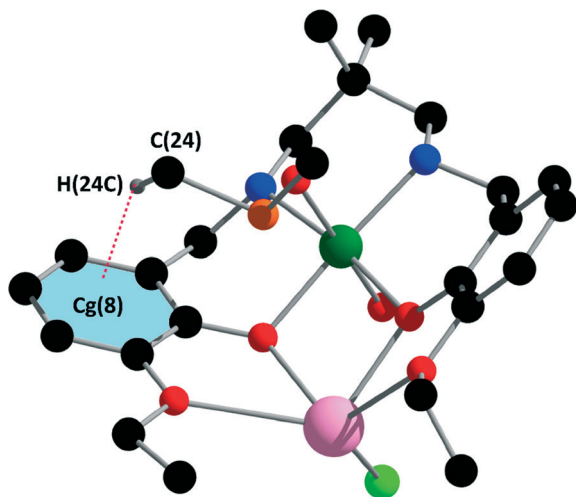


Fig. 5 C–H... π interactions observed in the complex. Only the relevant atoms are shown for clarity, where $\text{H}(24\text{C})\cdots\text{Cg}(8) = 0.93(8) \text{ \AA}$, $\text{C}(24)\cdots\text{H}(24\text{C})\cdots\text{Cg}(8) = 145^\circ$, and $\text{C}(24)\cdots\text{Cg}(8) = 3.662(19) \text{ \AA}$.

leads to the formation of a tetranuclear molecule, as shown in Fig. 6. It is worth noting that this bond is on the same side of the equatorial plane as O(1) leading to a very irregular geometry. This may be because the presence of the two ethoxy groups close to the vacant site in the equatorial plane has precluded further bonding in that plane. The distance between the $\text{Pb}(1)^a$ ($^a = -x, 1 - y, 1 - z$) and $\text{Pb}(1)$ is $4.841(2) \text{ \AA}$. The bridging angle of $\text{Pb}(1)\text{--Cl}(1)\cdots\text{Pb}(1)^a$ is $105.39(11)^\circ$.

Although the literature shows reports on experimental and theoretical investigations devoted to tetrel bonding,^{24–28} only two contain chlorides with hemidirected lead(II) centres (Table 1). Both complexes were not found to form a supramolecular dimer containing Pb_2Cl_2 cores.

Hirshfeld surfaces

The Hirshfeld surface emerged from an attempt to define the space occupied by a molecule in a crystal for the purpose of

subdividing the crystal electron density into molecular fragments.²⁹ d_{norm} is a normalised contact distance.³⁰ Intermolecular contacts are highlighted in the d_{norm} surface (when atoms make intermolecular contacts closer than the sum of their van der Waals radii, these contacts will be highlighted in red whereas longer contacts are in blue, and contacts around the sum of van der Waals radii are in white). The Hirshfeld surfaces of the complex have been mapped over d_{norm} (range of -0.1 to 1.5 \AA), the shape index and curvedness [Fig. 7]. The red spots on these surfaces denote the dominant interactions [$\text{S}\cdots\text{H}/\text{H}\cdots\text{S}$, $\text{N}\cdots\text{H}/\text{H}\cdots\text{N}$, $\text{O}\cdots\text{H}/\text{H}\cdots\text{O}$ and $\text{Cl}\cdots\text{H}/\text{H}\cdots\text{Cl}$]. As the Hirshfeld surface defines the shape of the molecule in terms of its surrounding crystalline environment, the local shape of the surface may provide some chemical insight whereas the shape index is a qualitative measure of shape and can be sensitive to very subtle changes in surface shape, particularly in regions where the total curvature (or the curvedness) is very low.³¹ We are particularly interested in investigating if the $\text{Pb}\cdots\text{Cl}$ non-covalent bond can also be evidenced by means of Hirshfeld surface analysis. Gratifyingly, the non-covalent bond was characterized by the spikes of the breakdown fingerprint plot.

The complex exhibits the $\text{Pb}\cdots\text{Cl}/\text{Cl}\cdots\text{Pb}$ non-covalent bond that contributes 1.2% of the total Hirshfeld surface area and is evident in the (d_i , d_e) region of (2.742 \AA , 2.661 \AA). A close inspection of the fingerprint plot revealed that the sharp spikes with the shortest ($d_e + d_i$) = 3.098 \AA in the complex correspond to the $\text{Pb}\cdots\text{Cl}/\text{Cl}\cdots\text{Pb}$ interaction.

The 2D fingerprint plots,³² which are used to analyze the intermolecular contacts at the same time, revealed that the main intermolecular interactions in the complex are $\text{S}\cdots\text{H}/\text{H}\cdots\text{S}$, $\text{Cl}\cdots\text{H}/\text{H}\cdots\text{Cl}$, $\text{O}\cdots\text{H}/\text{H}\cdots\text{O}$ and $\text{N}\cdots\text{H}/\text{H}\cdots\text{N}$. Fig. 8 presents the 2D plots of the complex.

An interesting $\text{Pb}\cdots\text{Cl}$ contact (Fig. 7) is observed in the complex. The contact may lead to the formation of different unconventional supramolecular interactions which is quite captivating. Also a small amount of $\text{Cl}\cdots\text{zCl}$ contact is observed (Fig. 9).

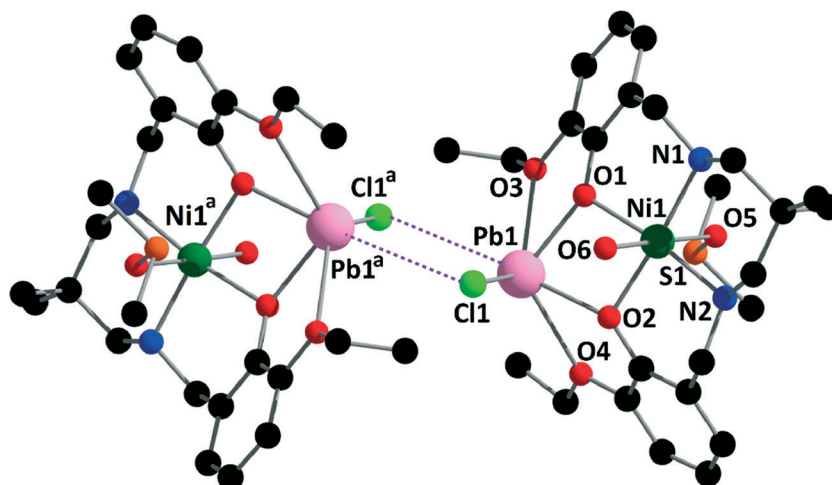
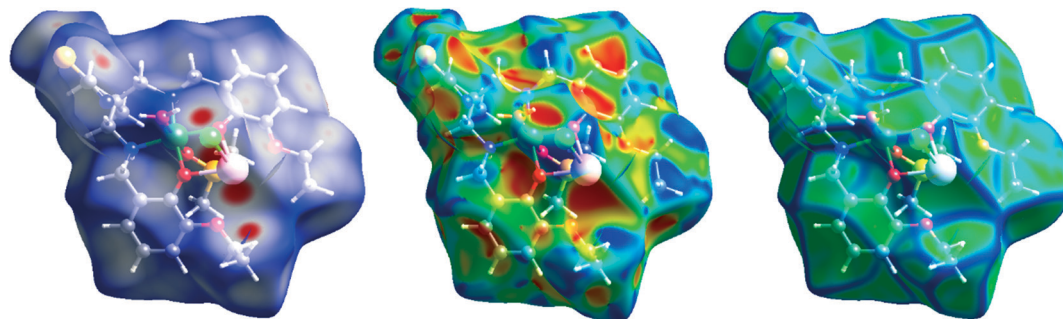
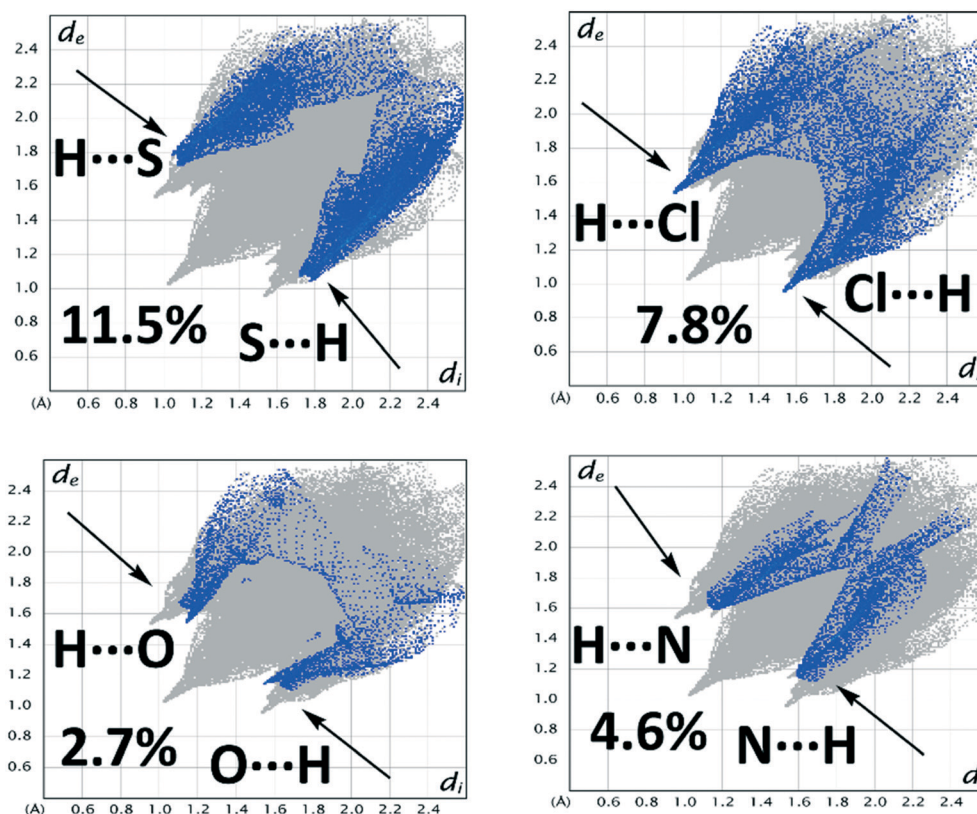


Fig. 6 Non-covalent $\text{Pb}\cdots\text{Cl}$ interactions. Symmetry elements ($^a = -x, 1 - y, 1 - z$).

Table 1 Reported X-ray characterized nickel(II)/lead(II) and lead(II) complexes comprising tetrel bonding interaction

Complex (CCDC)	Formula	Coordination mode of lead	Bonding	Pb–X (Å)	Ref.
YISROI	$[\{L^aNi\}Pb(NC_5H_5)Cl]_2$	Hemidirected	Tetrel	3.272(1)	24
TAGMOG	$[(Cl)PbL^b] \cdot CH_3OH$	Hemidirected	Tetrel	3.155(2)	25
—	$[(H_2O)(DMSO)NiLPbCl](SCN)$	Hemidirected	Tetrel	3.339(3)	This Work

L^a = tris-((2-hydroxybenzylidene)-aminoethyl)-amine; H_2L^b = N'-(phenyl(pyridin-2-yl) methylene)isonicotinohydrazide.

**Fig. 7** Hirshfeld surfaces of the complex mapped over d_{norm} (left), the shape index (middle), and curvedness (right).**Fig. 8** Fingerprint plots of the complex.

Theoretical studies

The theoretical study is focused on the tetrel bonding interaction described above in Fig. 6 and further characterized by the Hirshfeld analysis (Fig. 9). Since the coordination of the Pb(II) is hemidirected, the σ -hole at the tetrel atom is accessible as shown in Fig. 10. It can be

observed that the molecular electrostatic potential (MEP) is positive at the Pb atom ($+25 \text{ kcal mol}^{-1}$) that is located between both OEt groups. The most negative region is located at the SCN counter-ion, as expected. The MEP value is also negative at the chlorido ligand. This analysis indicates that the tetrel bond between the Pb atom and the chlorido ligand is favored from an electrostatic point of view.

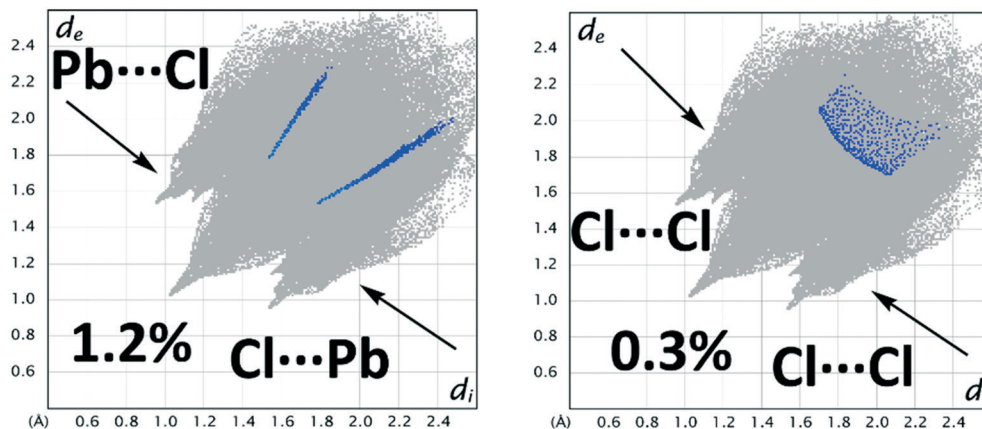


Fig. 9 Fingerprint plot resolved into the Pb...Cl/Cl...Pb contact and Cl...Cl/Cl...Cl contact contributing to the total Hirshfeld surface area of the complex.

Fig. 11a shows the self-assembled dimer retrieved from the X-ray of structure of the complex (H-atoms omitted), where two symmetrically equivalent Pb...Cl tetrel bonding interactions are formed. We have evaluated the interaction energy of this dimer, which is very strong $\Delta E_1 = -34.9 \text{ kcal mol}^{-1}$ thus confirming the relevance of this interaction as predicted by the MEP surface. A close examination of the dimer reveals that each Cl ligand also establishes a H-bonding interaction with one H-atom of the ethyl group of the Schiff base ligand (2.54 \AA , see Fig. 11a). To evaluate the contribution of this ancillary interaction we have computed a theoretical model where the ethyl groups have been changed by methyl groups (see Fig. 11b). As a result, the H-bonds are not formed and the interaction energy in the mutated complex is slightly reduced to $\Delta E_2 = -33.7 \text{ kcal mol}^{-1}$, thus suggesting that these H-bonds are very weak and that the dimer formation is totally dominated by the tetrel bonding. A likely explanation for the small contribution of the H-bonds is that the Cl atom is already participating in other interactions like the tetrel bond and an intramolecular H-bonding with the water molecule (see blue dashed lines in

Fig. 11). Therefore, the electron-donor ability of the Cl atom is significantly reduced.

To further characterize the interactions described above, we have used Bader's theory of atoms-in-molecules since it allows easy characterization of the noncovalent interactions. Fig. 12 shows the distribution of critical points and bond paths of the self-assembled dimer. Each tetrel bond is characterized by the presence of a bond CP (green sphere) and a bond path connecting the Pb atom to the Cl atom, thus confirming the existence of the tetrel bonds. Moreover, a ring CP (yellow sphere) also appears upon complexation due to the formation of a supramolecular ring (Pb_2Cl_2). The QTAIM analysis also confirms the existence of the H-bonds between the Cl ligands and the H-atoms of the ethyl groups. Moreover, each intramolecular O-H...Cl H-bond is characterized by a bond CP and a bond path interconnecting the Cl and H atoms. The values of the electron charge density (ρ) at the bond CPs that characterize the noncovalent interactions are also indicated in Fig. 12. The values of $\rho(r)$ are smaller for the C-H...Cl bonds (0.0132 a.u.) in agreement with the energetic results discussed above.

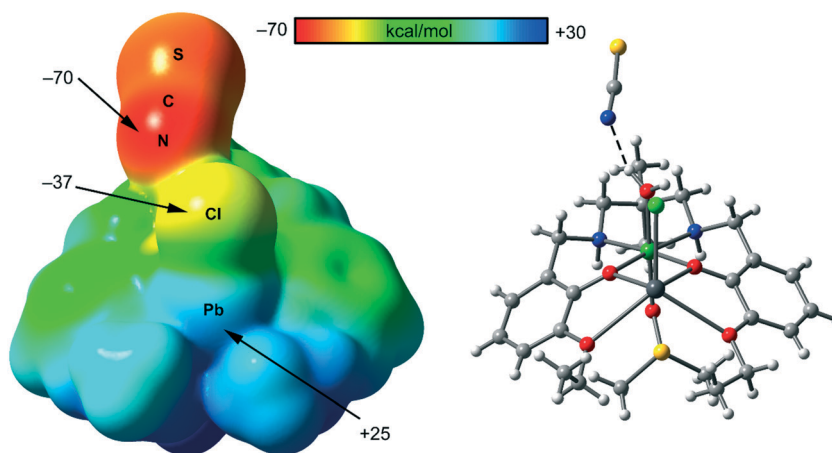


Fig. 10 MEP surface (left) of the complex (isosurface 0.001 a.u.) at the B3LYP-D/def2-SVP level of theory. The values at selected points of the surface are indicated in kcal mol^{-1} . The complex represented in the same orientation used for building the MEP surface is also shown in the right.

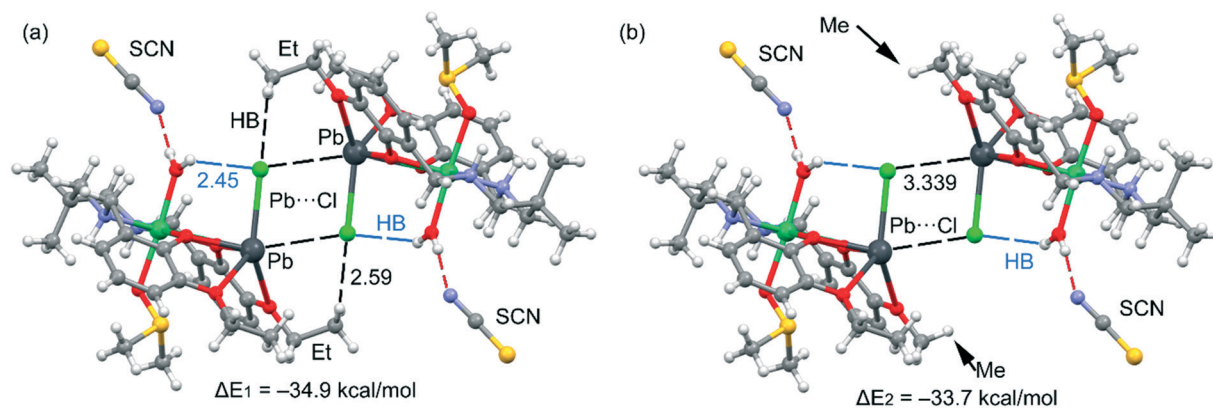


Fig. 11 (a and b) Theoretical models used to evaluate the noncovalent interactions in the dimer of the complex. Distances in Å.

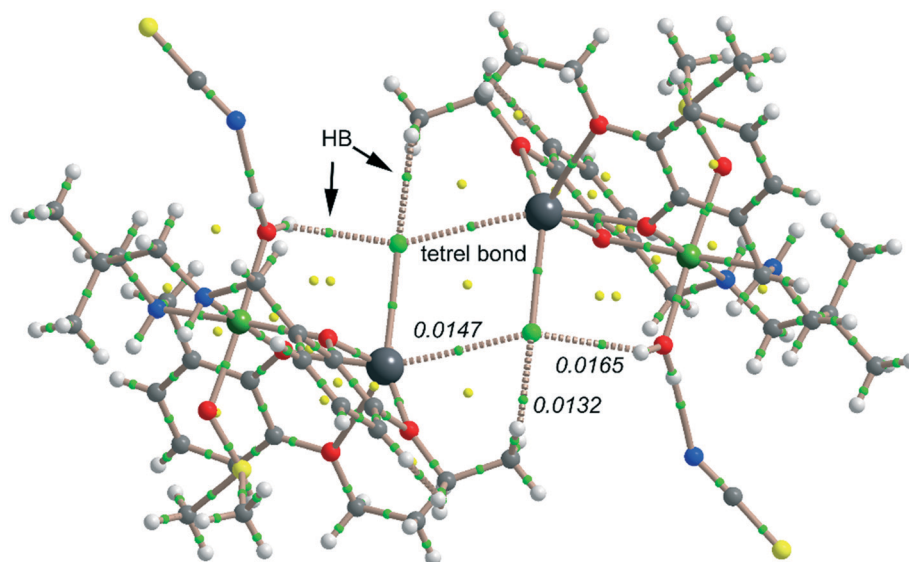


Fig. 12 QTAIM distribution of bond and ring CPs (green and yellow spheres, respectively) and bond paths for the dimer of the complex. The values of $\rho(r)$ at selected bond CPs are indicated in italics (a.u.)

Concluding remarks

In conclusion, we report the synthesis and structural characterization of a new heteronuclear nickel(II)/lead(II) complex with a compartmental reduced Schiff base ligand. The complex forms a tetranuclear supramolecule *via* non-covalent Pb...Cl tetrel bonding interaction, which is strong as evidenced by DFT calculations and MEP surface analysis. The QTAIM and the Hirshfeld analyses have been used to characterize the tetrel bonding interactions and stress the importance of tetrel bonds involving hemicoordinated Pb(II) in crystal engineering. Our results might be important to understand the X-ray structure of organic-inorganic material systems containing organic aromatic molecules and hemidirectionally coordinated lead(II) centres.

Experimental section

Nickel(II) thiocyanate tetrahydrate was prepared in our laboratory following a literature method.³³ All other materials

were commercially available, of reagent grade, and used as purchased from Sigma-Aldrich without further purification.

Preparation of the ligand, 2,2'-[(2,2-dimethyl-1,3-propanediyl)bis(iminomethylene)]bis[6-ethoxy-phenol] (H₂L)

A methanol solution (10 mL) of 2,2-dimethyl-1,3-propanediamine (0.1 mL, 1 mmol) and 3-ethoxysalicylaldehyde (305 mg, 2 mmol) (10 mL) was heated under reflux for *ca.* 1 h to prepare a Schiff base ligand. It was not purified but used directly for the preparation of the reduced Schiff base ligand (H₂L). After cooling to room temperature, solid sodium borohydride (4 mmol, 151.32 mg) and glacial acetic acid (2 mL) were added sequentially. Then the resulting solution was stirred for 10 minutes. After that, the solution was evaporated to dryness under reduced pressure in a rotary evaporator ($\sim 60^\circ\text{C}$). The residue was then dissolved in water (15 mL) and extracted with dichloromethane (15 mL). The organic part was dried over

anhydrous sodium acetate and the solvent (*i.e.* dichloromethane) was evaporated under reduced pressure using a rotary evaporator to obtain the reduced Schiff base ligand (H₂L).

Preparation of [(H₂O)(DMSO)NiLPbCl](SCN)

A methanol solution (5 mL) of nickel(II) thiocyanate tetrahydrate (250 mg, 1 mmol) was added to a solution of the ligand, H₂L, in methanol (10 mL) with constant stirring. A water (5 mL) solution of lead(II) chloride (278 mg, 1 mol) was then added to it and the stirring was continued for about 30 min. The solution was then refluxed for *ca.* 1 h. A few drops of DMSO were then added to the solution. The resulting reaction mixture was left unperturbed for slow evaporation at room temperature. After a few days, blue crystals, suitable for X-ray diffraction, were collected by filtration.

Yield: 839 mg (~49%) based on nickel(II). Anal. calc. for C₅₂H₈₀Cl₂N₆Ni₂O₁₂Pb₂S₄ (FW: 1712.14): C, 36.48; H, 4.71; N, 4.91; found: C, 36.3; H, 4.6; N, 5.1%. FT-IR (KBr, cm⁻¹): 3369 (O–H); 3289–3278 (N–H); 2998–2867 (C–H); 2052 (SCN). λ_{max} (nm) [ϵ_{max} (l mol⁻¹ cm⁻¹)] (MeOH): 242 (1.07 × 10²); 284 (0.59 × 10²); 348 (0.76 × 10²); 601 (2.62); 848 (2.12). Crystal data for the complex: C₅₂H₈₀Cl₂N₆Ni₂O₁₂Pb₂S₄, M.W. = 1712.14 g, monoclinic, space group *P*2₁/*n*, *a* = 9.874(5), *b* = 17.314(7), *c* = 19.651(14) Å, *V* = 3335(3), *Z* = 2, *d*_{calc} = 1.705 g cm⁻³, μ = 5.852 mm⁻¹, *F*(000) = 1696, 40 265 total reflections, 4895 unique reflections [*R*(int) = 0.068], observed data [*I* > 2σ(*I*)] = 7365, *R*₁ = 0.1159, *wR*₂ = 0.2836 (all data), *R*₁ = 0.08240, *wR*₂ = 0.2367 [*I* > 2σ(*I*)], temperature = 273 K. Magnetic moment = 3.13 BM.

Physical measurements

Elemental analyses (carbon, hydrogen and nitrogen) were performed using a Perkin-Elmer 240C elemental analyzer. IR spectra in KBr (4000–500 cm⁻¹) were recorded with a Perkin-Elmer Spectrum Two spectrophotometer. An electronic spectrum in acetonitrile was recorded on a JASCO J-630 spectrophotometer.

X-ray crystallography

A suitable single crystal of the complex was used for data collection using a 'Bruker D8 QUEST area detector' diffractometer with graphite-monochromated Mo K α radiation (λ = 0.71073 Å). The molecular structure was solved by direct methods and refined by full-matrix least squares on *F*² using the SHELX-18 package.³⁴ Non-hydrogen atoms were refined with anisotropic thermal parameters. The hydrogen atoms attached to nitrogen atoms were located by difference Fourier maps and were kept at fixed positions. All other hydrogen atoms were placed in their geometrically idealized positions and constrained to ride on their parent atoms. Multi-scan empirical absorption corrections were applied to the data using the program SADABS.³⁵

Hirshfeld surfaces

Hirshfeld surfaces³⁶ of the complex were determined using Crystal Explorer.³⁷ 2D fingerprint plots of the Hirshfeld surfaces were also shown as plots of *d*_i against *d*_e.

Theoretical methods

The energetic features of the complexes and models included in this study were calculated at the B3LYP-D/def2-SVP level of theory using the crystallographic coordinates. For the calculations, the GAUSSIAN-09 program has been used.³⁸ Grimme's dispersion correction³⁹ has also been used as implemented in the GAUSSIAN-09 program since it is adequate for the evaluation of non-covalent interactions where dispersion effects are relevant. The basis set superposition error for the calculation of interaction energies has been corrected using the counterpoise method.⁴⁰ Molecular electrostatic potential (MEP) surfaces have been computed at the same level of theory and represented using the 0.001 a.u. isosurface. Bader's quantum theory of "atoms in molecules" (QTAIM) has been used to characterize the noncovalent interactions using the AIMall program.⁴¹

Conflicts of interest

There are no conflicts of interest to declare.

Acknowledgements

S. M. thanks the CSIR, India, for awarding a Junior Research Fellowship [Sanction No. 09/096(0990)/2019-EMR-I]. S. C. gratefully acknowledges the UGC-CAS II program, Department of Chemistry, Jadavpur University, for financial support under the head [Chemicals/Consumables/Glassware]. A. F. thanks MINECO/AEI from Spain, project number CTQ2017-85821-R FEDER funds for financial support.

References

- (a) P. Bhowmik, S. Jana, P. P. Jana, K. Harms and S. Chattopadhyay, *Inorg. Chem. Commun.*, 2012, **18**, 50–56; (b) M. Das, S. Chatterjee and S. Chattopadhyay, *Inorg. Chem. Commun.*, 2011, **14**, 1337–1340; (c) S. Roy, A. Bhattacharyya, S. Purkait, A. Bauza, A. Frontera and S. Chattopadhyay, *Dalton Trans.*, 2016, **45**, 15048–15059; (d) A. Bhattacharyya, S. Roy, J. Chakraborty and S. Chattopadhyay, *Polyhedron*, 2016, **112**, 109–117; (e) P. Bhowmik, S. Jana, P. P. Jana, K. Harms and S. Chattopadhyay, *Inorg. Chim. Acta*, 2012, **390**, 53–60.
- (a) W. L. Ping, J. S. Bo, Z. W. Feng, L. Y. Qi and Y. Gui, *Chin. Sci. Bull.*, 2013, **58**, 2733–2740; (b) D. Sadhukhan, A. Ray, G. Pilet, C. Rizzoli, G. M. Rosair, C. J. Gomez-García, S. Signorella, S. Bell and S. Mitra, *Inorg. Chem.*, 2011, **50**, 8326–8339; (c) C.-L. Hu and J.-G. Mao, *Coord. Chem. Rev.*, 2015, **288**, 1–17; (d) G. N. D. Francesco, A. Gaillard, I. Ghiviriga, K. A. Abboud and L. J. Murray, *Inorg. Chem.*, 2014, **53**, 4647–4654; (e) S. Chattopadhyay, M. G. B. Drew, C.

- Diaz and A. Ghosh, *Dalton Trans.*, 2007, 2492–2494; (f) K. Ghosh, S. Roy, A. Ghosh, A. Banerjee, A. Bauzá, A. Frontera and S. Chattopadhyay, *Polyhedron*, 2016, 112, 6–17.
- 3 (a) Y. Shen, N. Ma, L. Wu and H.-H. Song, *Inorg. Chim. Acta*, 2015, 429, 51–60; (b) Y.-S. Yang, Y.-P. Yang, M. Liu, Q.-M. Qiu, Q.-H. Jin, J.-J. Sun, H. Chen, Y.-C. Dai and Q.-X. Meng, *Polyhedron*, 2015, 85, 912–917; (c) S. Carboni, C. Gennari, L. Pignataro and U. Piarulli, *Dalton Trans.*, 2011, 40, 4355–4373; (d) A. Bhattacharyya, P. K. Bhaumik, P. P. Jana and S. Chattopadhyay, *Polyhedron*, 2014, 78, 40–45.
 - 4 (a) G. Mahmoudi, A. Bauzá and A. Frontera, *Dalton Trans.*, 2016, 45, 4965–4969; (b) C. A. Hunter and J. K. M. Sanders, *J. Am. Chem. Soc.*, 1990, 112, 5525–5534; (c) S. K. Burley and G. A. Petsko, *Science*, 1985, 229, 23–28; (d) K. S. Kim, P. Tarakeshwar and J. Y. Lee, *Chem. Rev.*, 2000, 100, 4145–4185; (e) J. C. Ma and D. A. Dougherty, *Chem. Rev.*, 1997, 97, 1303–1324; (f) K. S. Kim, J. Y. Lee, S. J. Lee, T.-K. Ha and D. H. Kim, *J. Am. Chem. Soc.*, 1994, 116, 7399–7400; (g) M. Nishio, M. Hirota and Y. Umezawa, in *The C–H/p Interaction: Evidence, Nature, Consequences*, Wiley-VCH, New York, 1998; (h) D. Quiñonero, C. Garau, C. Rotger, A. Frontera, P. Ballester, A. Costa and P. M. Deyà, *Angew. Chem., Int. Ed.*, 2002, 41, 3389–3392; (i) M. Egli and S. Sarkhel, *Acc. Chem. Res.*, 2007, 40, 197–205; (j) T. J. Mooibroek, P. Gamez and J. Reedijk, *CrystEngComm*, 2008, 10, 1501–1515; (k) J. Ran and P. Hobza, *J. Chem. Theory Comput.*, 2009, 5, 1180–1185; (l) M. Barceló-Oliver, C. Estarellas, A. García-Raso, A. Terrón, A. Frontera, D. Quiñonero, E. Molins and P. M. Deyà, *CrystEngComm*, 2010, 12, 362–365; (m) M. Nishio, *CrystEngComm*, 2004, 6, 130–156.
 - 5 (a) J. Xiao, P. Broz, A. W. Puri, E. Deu, M. Morell, D. M. Monack and M. Bogyo, *J. Am. Chem. Soc.*, 2013, 135, 9130–9138; (b) S. Naskar, D. Mishra, R. J. Butcher and S. K. Chattopadhyay, *Polyhedron*, 2007, 26, 3703–3714; (c) A. Bauzá, D. Quiñonero, P. M. Deyà and A. Frontera, *Chem. – Asian J.*, 2013, 8, 2708–2713; (d) L. M. Salonen, M. Ellermann and F. Diederich, *Angew. Chem., Int. Ed.*, 2011, 50, 4808.
 - 6 (a) D. Paolantoni, J. Rubio-Magnieto, S. Cantel, J. Martinez, P. Dumy, M. Surin and S. Ulrich, *Chem. Commun.*, 2014, 50, 14257; (b) C. Estarellas, A. Frontera, D. Quiñonero and P. M. Deyà, *Angew. Chem., Int. Ed.*, 2011, 50, 415; (c) S. Jana, K. Harms and S. Chattopadhyay, *J. Coord. Chem.*, 2014, 67, 2954–2966.
 - 7 (a) G. Mahmoudi, A. Bauzá, M. Amini, E. Molins, J. T. Magued and A. Frontera, *Dalton Trans.*, 2016, 45, 10708–10716; (b) A. Bauzá, T. J. Mooibroek and A. Frontera, *Angew. Chem., Int. Ed.*, 2013, 52, 12317–12321; (c) A. Bauzá, T. J. Mooibroek and A. Frontera, *Chem. – Eur. J.*, 2014, 20, 10245–10248; (d) R. S. Ruoff, T. Emilsson, A. I. Jaman, T. C. Germann and H. S. Gutowsky, *J. Chem. Phys.*, 1992, 96, 3441–3446; (e) S. J. Grabowski, *Phys. Chem. Chem. Phys.*, 2014, 16, 1824–1834; (f) I. Alkorta, I. Rozas and J. Elguero, *J. Phys. Chem. A*, 2001, 105, 743–749; (g) E. C. Escudero-Adán, A. Bauzá, A. Frontera and P. Ballester, *ChemPhysChem*, 2015, 16, 2530–2533; (h) A. Bauzá, T. J. Mooibroek and A. Frontera, *Phys. Chem. Chem. Phys.*, 2014, 16, 19192–19197; (i) A. Bauzá, T. J. Mooibroek and A. Frontera, *Chem. Commun.*, 2014, 50, 12626–12629; (j) A. Bundhun, P. Ramasami, J. S. Murray and P. Politzer, *J. Mol. Model.*, 2013, 19, 2739–2746; (k) A. Bauzá, T. J. Mooibroek and A. Frontera, *Chem. Rec.*, 2016, 16, 473–487.
 - 8 (a) G. Mahmoudi, A. Bauzá and A. Frontera, *Dalton Trans.*, 2016, 45, 4965–4969; (b) M. S. Gargari, V. Stilinović, A. Bauzá, A. Frontera, P. McArdle, D. V. Derveer, S. W. Ng and G. Mahmoudi, *Chem. – Eur. J.*, 2015, 21, 17951–17958.
 - 9 C. Gourlaouen, O. Parisel and H. Gérard, *Dalton Trans.*, 2011, 40, 11282–11288.
 - 10 (a) S. Mirdya, S. Roy, S. Chatterjee, A. Bauza, A. Frontera and S. Chattopadhyay, *Cryst. Growth Des.*, DOI: 10.1021/acs.cgd.9b00881; (b) G. Mahmoudi, A. Bauzá, M. Amini, E. Molins, J. T. Magued and A. Frontera, *Dalton Trans.*, 2016, 45, 10708–10716.
 - 11 (a) C. Gourlaouen, O. Parisel and H. Gerard, *Dalton Trans.*, 2011, 40, 11282–11288; (b) L. Shimon-Livny, J. P. Glusker and C. W. Bock, *Inorg. Chem.*, 1998, 37, 1853–1867; (c) R. L. Davidovich, V. Stavila, D. V. Marinin, E. I. Voit and K. H. Whitmire, *Coord. Chem. Rev.*, 2009, 253, 1316–1352.
 - 12 (a) A. Hazari, L. K. Das, R. M. Kadam, A. Bauzá, A. Frontera and A. Ghosh, *Dalton Trans.*, 2015, 44, 3862–3876; (b) A. Hazari, T. K. Ghosh, C. J. G. García and A. Ghosh, *Inorg. Chim. Acta*, 2018, 471, 168–175.
 - 13 (a) S. Roy, A. Bhattacharyya, S. Purkait, A. Bauza, A. Frontera and S. Chattopadhyay, *Dalton Trans.*, 2016, 45, 15048–15059; (b) S. Roy, M. G. B. Drew, A. Bauza, A. Frontera and S. Chattopadhyay, *ChemistrySelect*, 2017, 2, 10586–10594; (c) S. Roy, M. G. B. Drew, A. Bauza, A. Frontera and S. Chattopadhyay, *ChemistrySelect*, 2017, 2, 7880–7887.
 - 14 (a) S. Mondal, S. Hazra, S. Sarkar, S. Sasmal and S. Mohanta, *J. Mol. Struct.*, 2011, 1004, 204–214; (b) R. Kurtaran, L. T. Yildirim, A. D. Azaz, H. Namli and O. Atakol, *J. Inorg. Biochem.*, 2005, 99, 1937–1944; (c) E. C. Constable, G. Zhang, C. E. Housecroft, M. Neuburger and J. A. Zampese, *Inorg. Chim. Acta*, 2010, 363, 4207–4213; (d) S. Hazra, S. Sasmal, M. Nayak, H. A. Sparkes, J. A. K. Howard and S. Mohanta, *CrystEngComm*, 2010, 12, 470–477.
 - 15 A. W. Addison, T. N. Rao, J. Reedijk, J. V. Rijn and G. C. Verschoor, *J. Chem. Soc., Dalton Trans.*, 1984, 1349–1356.
 - 16 (a) M. Das, S. Chatterjee, K. Harms, T. K. Mondal and S. Chattopadhyay, *Dalton Trans.*, 2014, 43, 2936–2947; (b) S. Chattopadhyay, M. S. Ray, S. Chaudhuri, G. Mukhopadhyay and G. Bocelli, *Inorg. Chim. Acta*, 2006, 359, 1367–1375; (c) S. Jana, B. K. Shaw, P. Bhowmik, K. Harms, M. G. B. Drew, S. Chattopadhyay and S. K. Saha, *Inorg. Chem.*, 2014, 53, 8723–8734.
 - 17 (a) M. A. Khan, A. A. Alqadami, M. Otero, M. R. Siddiqui, Z. A. Allothman, I. Alsohaimi, M. Rafatullah and A. E. Hamedelnie, *Chemosphere*, 2019, 218, 1089–1099; (b) S. Roy, T. Basak, S. Khan, M. G. B. Drew, A. Bauzá, A. Frontera and S. Chattopadhyay, *ChemistrySelect*, 2017, 2, 9336–9343.
 - 18 (a) K. Nakamoto, *Infrared and Raman Spectra of Organic and Coordination Compounds*, John Wiley and Sons, New

- York, 3rd edn, 1978, p. 227; (b) P. Chakraborty, I. Majumder, H. Kara, S. K. Chattopadhyay, E. Zangrando and D. Das, *Inorg. Chim. Acta*, 2015, **436**, 139–145; (c) P. Bhowmik, K. Harms and S. Chattopadhyay, *Polyhedron*, 2013, **49**, 113–120; (d) P. K. Bhaumik, K. Harms and S. Chattopadhyay, *Polyhedron*, 2013, **62**, 179–187.
- 19 T. Basak, K. Ghosh and S. Chattopadhyay, *Polyhedron*, 2018, **146**, 81–92.
- 20 (a) A. Bhattacharyya, P. K. Bhaumik, M. Das, A. Bauzá, P. P. Jana, K. Harms, A. Frontera and S. Chattopadhyay, *Polyhedron*, 2015, **101**, 257–269; (b) S. Chattopadhyay, M. G. B. Drew and A. Ghosh, *Polyhedron*, 2007, **26**, 3513–3522.
- 21 (a) M. Nazarov and D. Y. Noh, *New Generation of Europium and Terbium-Activated Phosphors: From Syntheses to Applications*, Pan Stanford Publishing, 6000 Broken Sound Pkwy NW, 2011, p. 211; (b) S. Roy, M. G. B. Drew, A. Bauzá, A. Frontera and S. Chattopadhyay, *Dalton Trans.*, 2017, **46**, 5384–5397.
- 22 J. Costamagna, J. Vargas, R. Latorre, A. Alvarado and G. Mena, *Coord. Chem. Rev.*, 1992, **119**, 67–88.
- 23 A. Bhattacharyya, P. K. Bhaumik, P. P. Jana and S. Chattopadhyay, *Polyhedron*, 2014, **78**, 40–45.
- 24 A. Mustapha, K. Busch, M. Patykiewicz, A. Apedaile, J. Reglinski, A. R. Kennedy and T. J. Prior, *Polyhedron*, 2008, **27**, 868–878.
- 25 G. Mahmoudi, D. A. Safin, M. P. Mitoraj, M. Amini, M. Kubicki, T. Doert, F. Locherere and M. Fleck, *Inorg. Chem. Front.*, 2017, **4**, 171–182.
- 26 A. Bauzá, S. K. Seth and A. Frontera, *Coord. Chem. Rev.*, 2019, **384**, 107–125.
- 27 G. Mahmoudi, A. Bauzá and A. Frontera, *Dalton Trans.*, 2016, **45**, 4965–4969.
- 28 S. Roy, M. G. B. Drew, A. Bauzá, A. Frontera and S. Chattopadhyay, *New J. Chem.*, 2018, **42**, 6062–6076.
- 29 F. L. Hirshfeld, *Theor. Chim. Acta*, 1977, **44**, 129–138.
- 30 J. J. McKinnon, D. Jayatilaka and M. A. Spackman, *Chem. Commun.*, 2007, 3814–3816.
- 31 J. J. McKinnon, M. A. Spackman and A. S. Mitchell, *Acta Crystallogr., Sect. B: Struct. Sci.*, 2004, **60**, 627–668.
- 32 M. A. Spackman and J. J. McKinnon, *CrystEngComm*, 2002, **4**, 378–392.
- 33 K. P. Sharma and R. K. Poddar, *Transition Met. Chem.*, 1984, **9**, 135–138.
- 34 G. M. Sheldrick, *Acta Crystallogr., Sect. C: Struct. Chem.*, 2015, **71**, 3–8.
- 35 G. M. Sheldrick, SADABS, V2014/5, Software for Empirical Absorption Correction, University of Göttingen, Institute für Anorganische Chemie der Universität, Göttingen, Germany, 1999–2003.
- 36 (a) M. A. Spackman and D. Jayatilaka, *CrystEngComm*, 2009, **11**, 19–32; (b) H. F. Clausen, M. S. Chevallier, M. A. Spackman and B. B. Iversen, *New J. Chem.*, 2010, **34**, 193–199.
- 37 S. K. Wolff, D. J. Grimwood, J. J. McKinnon, D. Jayatilaka and M. A. Spackman, Crystal Explorer 2.0, University of Western Australia, Perth, Australia, 2007, <http://hirshfeldsurfacenet.blogspot.com>.
- 38 M. J. Frisch, G. W. Trucks, H. B. Schlegel, G. E. Scuseria, M. A. Robb, J. R. Cheeseman, G. Scalmani, V. Barone, B. Mennucci, G. A. Petersson, H. Nakatsuji, M. Caricato, X. Li, H. P. Hratchian, A. F. Izmaylov, J. Bloino, G. Zheng, J. L. Sonnenberg, M. Hada, M. Ehara, K. Toyota, R. Fukuda, J. Hasegawa, M. Ishida, T. Nakajima, Y. Honda, O. Kitao, H. Nakai, T. Vreven, J. A. Montgomery, Jr., J. E. Peralta, F. Ogliaro, M. Bearpark, J. J. Heyd, E. Brothers, K. N. Kudin, V. N. Staroverov, R. Kobayashi, J. Normand, K. Raghavachari, A. Rendell, J. C. Burant, S. S. Iyengar, J. Tomasi, M. Cossi, N. Rega, J. M. Millam, M. Klene, J. E. Knox, J. B. Cross, V. Bakken, C. Adamo, J. Jaramillo, R. Gomperts, R. E. Stratmann, O. Yazyev, A. J. Austin, R. Cammi, C. Pomelli, J. W. Ochterski, R. L. Martin, K. Morokuma, V. G. Zakrzewski, G. A. Voth, P. Salvador, J. J. Dannenberg, S. Dapprich, A. D. Daniels, Ö. Farkas, J. B. Foresman, J. V. Ortiz, J. Cioslowski and D. J. Fox, *Gaussian 09*, Gaussian, Inc., Wallingford CT, 2009.
- 39 S. Grimme, J. Antony, S. Ehrlich and H. Krieg, *J. Chem. Phys.*, 2010, **132**, 154104.
- 40 S. F. Boys and F. Bernardi, *Mol. Phys.*, 1970, **19**, 553–566.
- 41 T. A. Keith, AIMAll (Version 13.05.06), TK Gristmill Software, Overland Park, KS, 2013.

Importance of π -Interactions Involving Chelate Rings in Addition to the Tetrel Bonds in Crystal Engineering: A Combined Experimental and Theoretical Study on a Series of Hemi- and Holodirected Nickel(II)/Lead(II) Complexes

Saikat Mirdaya,[†] Sourav Roy,[†] Sudipta Chatterjee,^{‡,§} Antonio Bauzá,[§] Antonio Frontera,^{§,*} and Shouvik Chattopadhyay^{*,†,§}

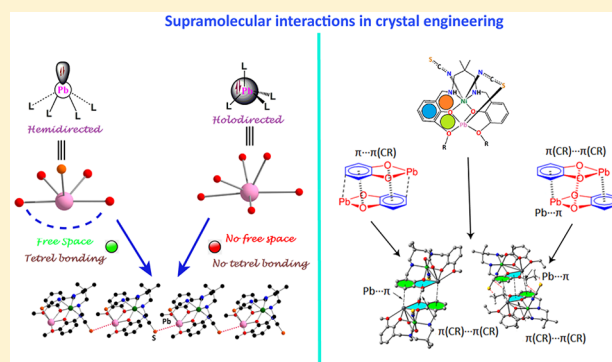
[†]Department of Chemistry, Inorganic Section, Jadavpur University, Kolkata 700032, India

[‡]Department of Chemistry, Serampore College, Serampore, Hooghly 712201, India

[§]Department of Chemistry, Universitat de les Illes Balears, Crta de Valldemossa km 7.5, 07122 Palma de Mallorca (Balears), Spain

S Supporting Information

ABSTRACT: Five heteronuclear nickel(II)/lead(II) complexes with two compartmental reduced Schiff base ligands were prepared and characterized. Their structures were confirmed by single crystal X-ray diffraction analyses. In each complex, nickel(II) is placed in the inner N_2O_2 compartment and lead(II) in the outer O_2O_2' compartment of reduced Schiff base ligands. Interesting molecular architectures were formed via supramolecular interactions in the solid state of the complexes. A density functional theory study is devoted to analyze unconventional tetrel bonding interactions established between the σ -hole at the hemicoordinated lead(II) and either the electron-rich thiocyanate or the π -system of the aromatic ligand. In addition, π -stacking assemblies between both the aromatic rings and five-membered Pb-chelate rings were described and studied both with regard to their energies and by using the noncovalent plot index.



INTRODUCTION

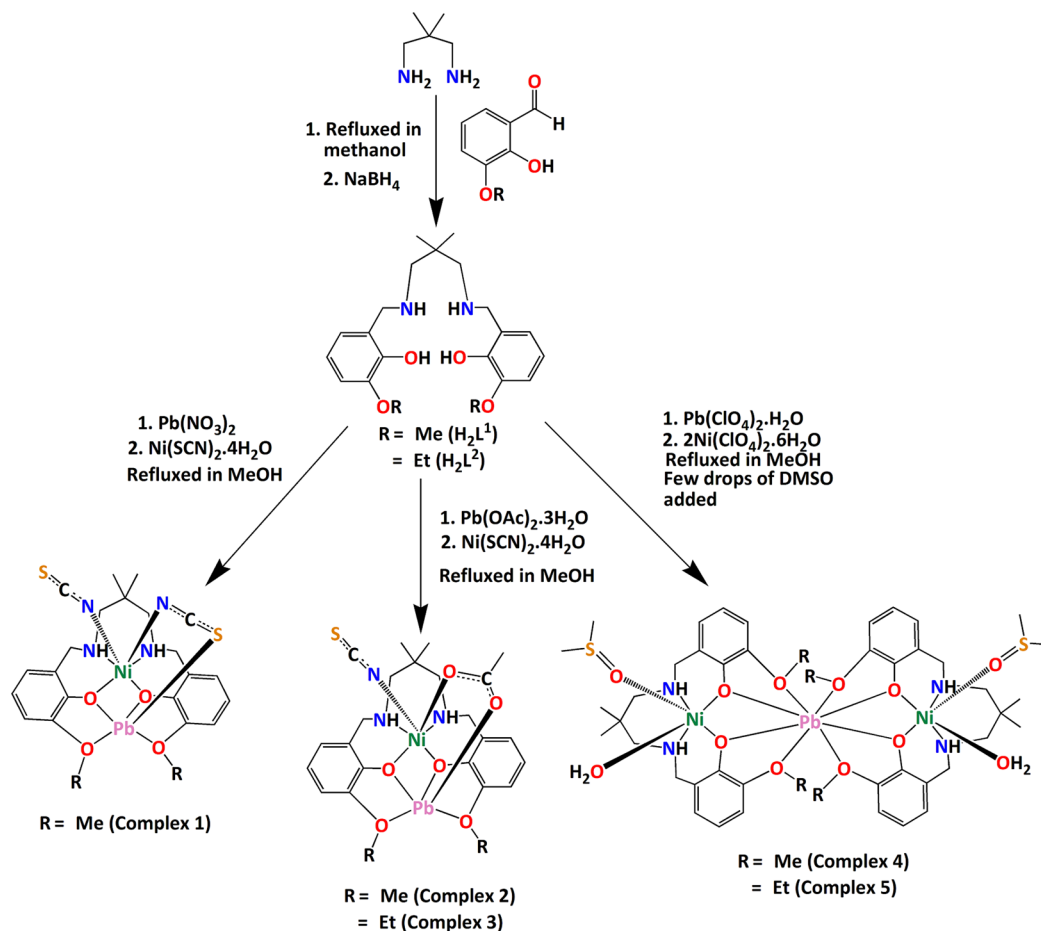
Lead is a heavy metal with an ability to adopt different coordination numbers and valences. The coordination chemistry of lead has attracted synthetic inorganic chemists to prepare new lead(II) complexes with different molecular and crystalline architectures.^{1–4} Although lead(II) is associated with serious pollution, materials possessing lead(II) are increasingly used in batteries, ferroelectric materials, semiconductors, and nonlinear optical materials.^{5–11} On the other hand, salen-type ligands are well-known in the literature for their easy synthetic approach and the ability to ligate several transition metal ions in tetradentate N_2O_2 cores.^{12–19} Many of them may then be used as metallo-ligands to form lead(II) complexes.^{20–22} In the present work, two $N_2O_2O_2'$ donor compartmental Schiff base ligands have been reduced to form “reduced Schiff bases”, which were then used to arrest nickel(II) in their inner N_2O_2 cores. These metallo-ligands have, in turn, been used to encapsulate lead(II) in their outer O_2O_2' cores. The valence shell electronic configuration of lead being $[Xe]4f^{14}5d^{10}6s^26p^2$, the presence of poorly screening f^{14} and d^{10} electrons makes the $6s^2$ electron pair inert, mostly due to the increasing effective nuclear charge. In addition, the high penetrating property of the $6s$ orbital and relativistic

stabilization of $6s^2$ electrons are also responsible.^{23–26} The magnitude to which the lone pair is stereochemically active^{27,28} is currently arousing interest in theoretical chemists to explore this area further.^{29–32} Heavy atoms of groups IV to VII are gaining special interest nowadays in the field of supramolecular chemistry. This is because of their participation in strong σ -hole interaction in complexes where these atoms are covalently bonded to electronegative ones.^{33–40} These interactions have been widely designated for chalcogen, pnictogen, and halogen atoms. Nonetheless, those of group IV comprising tetrel bonding interactions (specially for lead complexes) are relatively less explored.^{41–44} Solid state crystal structures are stabilized due to various noncovalent interactions such as hydrogen bonding, π - π stacking, cation- π , anion- π , and C-H $\cdots\pi$ interactions.^{45–52} The influence of these interactions in crystal packing has been widely studied. However, the attention has now shifted toward more unconventional interactions such as C-H $\cdots\pi$ (chelate), π (arene)- π (chelate), etc.^{53–59} In recent years, “non-classical” interactions have

Received: July 5, 2019

Revised: August 24, 2019

Published: September 3, 2019

Scheme 1. Synthetic Route to Complexes 1–5^a

^aLattice solvent molecules have been omitted for clarity.

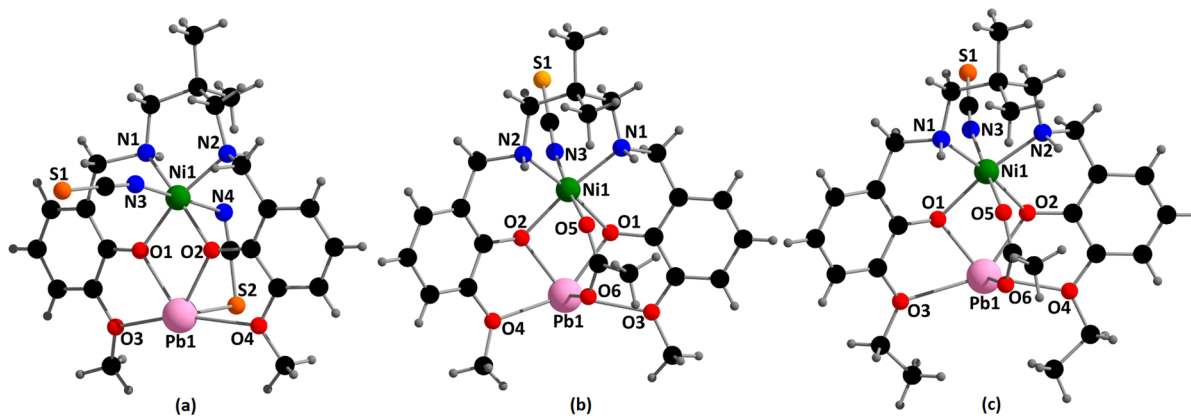


Figure 1. Perspective view of complexes (a) 1, (b) 2, and (c) 3 with selective atom numbering scheme.

become an interesting topic for research as they have been proven to be equal or even dominating contributors to metal–organic crystal structure formation.

In the present work, two N₂O₂O'₂ donor compartmental reduced Schiff bases, 2,2'-[(2,2-dimethyl-1,3-propanediyl)bis(iminomethylene)]bis[6-methoxy-phenol] (H₂L¹) and 2,2'-[(2,2-dimethyl-1,3-propanediyl)bis(iminomethylene)]bis[6-ethoxy-phenol] (H₂L²), were used to prepare five heteronuclear nickel(II)/lead(II) complexes, [(SCN)NiL¹(μ_{1,3}-NCS)Pb] (1), [(SCN)NiL¹(μ-OAc)Pb] (2), [(SCN)NiL²(μ-

OAc)Pb] (3), [{(DMSO)(H₂O)NiL¹}₂Pb](ClO₄)₂ (4), and [{(DMSO)(H₂O)NiL²}₂Pb](ClO₄)₂·4DMSO (5). Their structures were determined by single crystal X-ray diffraction analyses. The lead centers in complexes 1–3 are hemidirectionally coordinated and participate in noncovalent tetrel bonding interactions. Moreover, supramolecular interactions were studied by means of density functional theory (DFT) calculations focusing our attention on Pb⋯S and Pb⋯π tetrel bonds observed in the solid state architecture of complexes 1–3. Furthermore, π-stacking assemblies between aromatic rings

Table 1. Crystal Data and Refinement Details of Complexes 1, 2, and 3

complex	1	2	3
formula	C ₂₃ H ₂₈ PbNiN ₄ O ₄ S ₂	C ₂₄ H ₃₁ PbNiN ₃ O ₆ S	C ₂₆ H ₃₅ N ₃ NiO ₆ PbS
formula weight	754.50	755.47	783.52
temperature (K)	273	273	273
crystal system	triclinic	monoclinic	monoclinic
space group	$P\bar{1}$	$P2_1/n$	$P2_1/c$
<i>a</i> (Å)	9.3341(8)	10.5402(9)	8.2144(6)
<i>b</i> (Å)	9.4091(8)	15.1178(13)	27.361(2)
<i>c</i> (Å)	15.2174(13)	17.8145(18)	13.1439(10)
α	83.558(3)		
β	75.284(3)	99.613(3)	101.617(3)
γ	79.946(3)		
<i>Z</i>	2	4	4
<i>d</i> _{calc} (g cm ⁻³)	1.974	1.793	1.799
μ (mm ⁻¹)	7.566	6.796	6.577
<i>F</i> (000)	736	1480	1544
total reflections	26594	30361	80213
unique reflections	4481	4971	5095
observed data [<i>I</i> > 2 σ (<i>I</i>)]	4296	4066	4622
no. of parameters	324	296	343
<i>R</i> (int)	0.055	0.076	0.061
<i>R</i> ₁ , <i>wR</i> ₂ (all data)	0.0467, 0.1283	0.0999, 0.2395	0.0280, 0.0535
<i>R</i> ₁ , <i>wR</i> ₂ [<i>I</i> > 2 σ (<i>I</i>)]	0.0449, 0.1263	0.0897, 0.2270	0.0230, 0.0511

Table 2. Selected Bond Lengths (Å) of Complexes 1, 2, and 3

complex	1	2	3	complex	1	2	3
Pb(1)–O(1)	2.353(6)	2.327(7)	2.295(3)	Ni(1)–N(2)	2.064(7)	2.085(9)	2.081(3)
Pb(1)–O(2)	2.338(6)	2.285(7)	2.284(2)	Ni(1)–N(3)	2.028(8)	2.037(11)	2.053(4)
Pb(1)–O(3)	2.650(7)	2.643(10)	2.685(3)	Pb(1)–S(2)	2.827(3)		
Pb(1)–O(4)	2.611(7)	2.576(9)	2.597(3)	Ni(1)–N(4)	2.432(10)		
Ni(1)–O(1)	2.038(6)	2.130(8)	2.096(2)	Ni(1)–O(5)		2.070(9)	2.097(3)
Ni(1)–O(2)	2.061(6)	2.067(7)	2.084(2)	Pb(1)–O(6)		2.308(8)	2.321(3)
Ni(1)–N(1)	2.069(7)	2.093(10)	2.075(3)				

Table 3. Deviation of Coordinating Atoms from the Least Square Mean Plane Passing through Them and That of Nickel(II) from the Same Plane in Complexes 1–3

complex	deviations of atoms in Å				
	O(1)	O(2)	N(1)	N(2)	Ni(1)
1	−0.008(6)	−0.051(6)	−0.052(7)	−0.014(7)	0.125(10)
2	0.001(7)	−0.036(7)	−0.035(10)	−0.002(9)	0.071(13)
3	0.009(2)	0.023(2)	0.025(3)	0.012(3)	−0.0692(4)

and five-membered Pb-chelate rings were detected and studied both with regard to their energies and by using the noncovalent (NCI) plot index. In complexes 4 and 5, the lead centers are holodirected, resulting in different trinuclear structures where interesting hydrogen bonding has been observed with noncoordinated perchlorates.

RESULTS AND DISCUSSION

Synthesis. 2,2-Dimethyl-1,3-diaminopropane was refluxed with 3-methoxysalicylaldehyde and 3-ethoxysalicylaldehyde in a 1:2 ratio respectively, followed by the addition of NaBH₄ to form two N₂O₂O'₂ donor compartmental reduced Schiff bases (H₂L¹ and H₂L²) following standard literature methods.^{60–62} These ligands (H₂L¹ and H₂L²) on reaction with different ratios of nickel(II) and lead(II) salts in different solvents produced the complexes. Formation of complexes 1–5 is shown in Scheme 1.

Description of [(SCN)NiL¹(μ_{1,3}-NCS)Pb] (1), [(SCN)NiL¹(μ-OAc)Pb] (2), and [(SCN)NiL²(μ-OAc)Pb] (3). Single crystal X-ray diffraction measurements reveal that complexes 1, 2, and 3 are built from isolated heterodinuclear molecules of [(SCN)-NiL¹(μ_{1,3}-NCS)Pb], [(SCN)NiL¹(μ-OAc)Pb], and [(SCN)-NiL²(μ-OAc)Pb] respectively (Figure 1). Crystallographic data and refinement details are provided in Table 1. Important bond lengths and bond angles are summarized in Tables 2 and S1 (Supporting Information), respectively.

Two N₂O₂O'₂ donor compartmental reduced Schiff bases (H₂L¹ and H₂L²) were used to prepare complexes 1, 2, and 3 in which nickel(II) centers are placed in inner N₂O₂ cavities and lead(II) centers in outer O₂O'₂ cavities. The nickel(II) center [Ni(1)] has a distorted octahedral geometry, where two amine nitrogen atoms, N(1) and N(2), and two phenoxo oxygen atoms, O(1) and O(2), of the deprotonated reduced Schiff base constitute the equatorial plane. Deviations of

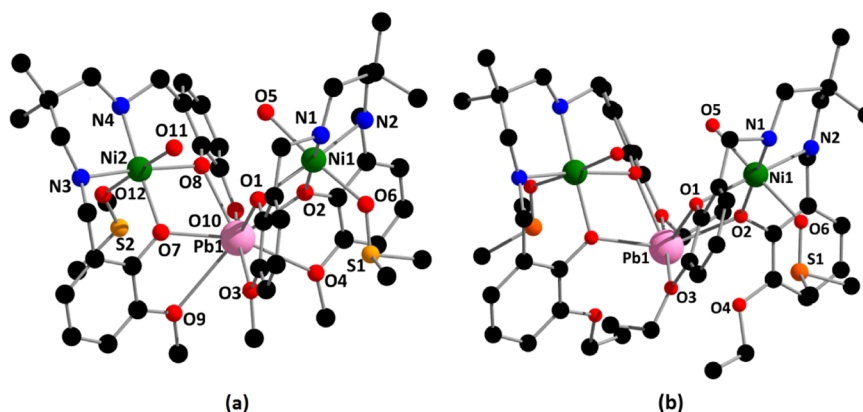


Figure 2. Perspective view of complexes (a) 4 and (b) 5 with selective atom numbering scheme. Hydrogen atoms, perchlorate ion, and the noncoordinating solvent molecules have been omitted for clarity.

coordinating atoms from the mean equatorial planes passing through them and those of the nickel(II) center of the same plane in both complexes are listed in Table 3. One nitrogen atom, N(3), from a terminal thiocyanate coordinates with a nickel(II) center to fulfill the fifth coordination. The sixth coordination site is occupied by a nitrogen atom, N(4), from a bridging thiocyanate in the case of complex 1, whereas in complexes 2 and 3 it is occupied by an oxygen atom, O(5), from an acetate molecule.

The lead(II) center in each complex is pentacoordinated. Phenoxo oxygen atoms, O(1) and O(2), along with alkoxy oxygen atoms, O(3) and O(4), [methoxy for complexes 1 and 2 and ethoxy for complex 3] of deprotonated reduced Schiff bases also coordinate to a lead(II) center but at much longer distances to form equatorial planes. The fifth coordination site is occupied by a sulfur atom S(2) from a bridging thiocyanate in case of complex 1, whereas in complexes 2 and 3 it is occupied by an oxygen atom, O(6), from a bridging acetate molecule. The geometry of any pentacoordinated metal center may conveniently be measured by the Addison parameter (τ)⁶³ [$\tau = (\theta - \Phi)/60$, where θ and Φ are the two largest ligand–metal–ligand angles of the coordination sphere]. In complexes 1, 2, and 3, the geometries around the lead(II) center assume square pyramidal geometries with $\tau = 0.43$, 0.07, and 0.24 for complexes 1, 2, and 3 respectively. Ni(1)O(1)Pb(1)O(2) dihedral angles are 7.7(2)°, 13.7(2)° and –16.29(9)° in complexes 1, 2, and 3 respectively. The distance between Ni(1) and Pb(1) is 3.491(1) Å (complex 1), 3.362(1) Å (complex 2) and 3.346(8) Å (complex 3). The bridging angles Ni(1)–O(1)–Pb(1) and Ni(1)–O(2)–Pb(1) are 105.1(2)° and 104.8(2)° respectively for complex 1, 97.8(3)° and 101.1(3)° for complex 2, and 99.2(1)° and 99.93(9)° for complex 3 respectively.

Description of [(DMSO)(H₂O)NiL¹]₂Pb](ClO₄)₂ (4) and [(DMSO)(H₂O)NiL²]₂Pb](ClO₄)₂·4DMSO (5). The asymmetric unit of complex 4 contains a heterotrimeric [(DMSO)(H₂O)NiL¹]₂Pb dication with two noncoordinating perchlorate anions (Figure 2a). The oxygen atoms, O(13), O(15) and O(17), O(19) of two noncoordinated perchlorates are disordered in complex 4. Two sets of positions (O13A, O13B), (O15A, O15B) and (O17, O17A), (O19, O19A) were refined with occupancies of x and $1 - x$, respectively with $x = 0.712$. Complex 5 is centrosymmetric and contains heterotrimeric [(DMSO)(H₂O)NiL²]₂Pb dication with two noncoordinating perchlorate anions along with four lattice DMSO

molecules (Figure 2b). Crystallographic data and refinement details of both complexes are provided in Table 4. Important bond lengths and bond angles are summarized in Tables 5 and S1, respectively.

Table 4. Crystal Data and Refinement Details of Complexes 4 and 5

complex	4	5
formula	C ₄₆ H ₇₂ PbNi ₂ N ₄ O ₂₀ S ₂ Cl ₂	C ₅₈ H ₁₀₄ PbNi ₂ N ₄ O ₂₄ S ₆ Cl ₂
formula weight	1460.68	1829.29
temperature (K)	150	150
crystal system	monoclinic	monoclinic
space group	P2 ₁ /c	I2/a
<i>a</i> (Å)	13.3953(11)	17.9651(16)
<i>b</i> (Å)	24.316(2)	17.7582(14)
<i>c</i> (Å)	18.4399(16)	26.3234(17)
β	91.537(3)	105.848(5)
<i>Z</i>	4	4
<i>d</i> _{calc} (g cm ^{−3})	1.616	1.504
μ (mm ^{−1})	3.648	2.831
<i>F</i> (000)	2960	3760
total reflections	73608	47959
unique reflections	10905	7149
observed data [<i>I</i> > 2 σ (<i>I</i>)]	8275	6210
no. of parameters	741	454
<i>R</i> (int)	0.068	0.079
<i>R</i> ₁ , <i>wR</i> ₂ (all data)	0.0590, 0.0937	0.0566, 0.1378
<i>R</i> ₁ , <i>wR</i> ₂ [<i>I</i> > 2 σ (<i>I</i>)]	0.0369, 0.0820	0.0471, 0.1301

N₂O₂O'₂ donor compartmental reduced Schiff bases (H₂L¹ and H₂L²) were used to prepare complexes 4 and 5 respectively in which nickel(II) centers are placed in the inner N₂O₂ cavities. The nickel(II) centers [Ni(1) and Ni(2) for complex 4 and Ni(1) and Ni(1)^m for complex 5, where $m = 1/2 - x, y, 1 - z$] are coordinated with two amine nitrogen atoms [N(1), N(2) for Ni(1); N(3), N(4) for Ni(2) in complex 4 and N(1), N(2) for Ni(1); N(1)^m, N(2)^m for Ni(1)^m in complex 5] and two phenoxo oxygen atoms [O(1), O(2) for Ni(1); O(7), O(8) for Ni(2) in complex 4 and O(1), O(2) for Ni(1); O(1)^m, O(2)^m for Ni(1)^m in complex 5] of the deprotonated reduced Schiff base ligands. The fifth site is coordinated by an oxygen atom [being O(5) for Ni(1); O(11) for Ni(2) in complex 4 and O(5) for Ni(1); O(5)^m for Ni(1)^m

Table 5. Selected Bond Lengths (Å) of Complexes 4 and 5

Ccomplex	4	5	complex	4	5
Pb(1)–O(1)	2.434(3)	2.430(4)	Pb(1)–O(7)	2.460(3)	
Pb(1)–O(2)	2.418(3)	2.444(4)	Pb(1)–O(8)	2.445(3)	
Pb(1)–O(3)	2.696(4)	2.869(5)	Pb(1)–O(9)	2.921(5)	
Pb(1)–O(4)	2.873(4)	2.954(5)	Pb(1)–O(10)	2.742(4)	
Ni(1)–O(1)	2.100(3)	2.135(4)	Ni(2)–O(7)	2.030(3)	
Ni(1)–O(2)	2.001(3)	2.016(4)	Ni(2)–O(8)	2.082(3)	
Ni(1)–N(1)	2.062(4)	2.060(5)	Ni(2)–O(11)	2.128(4)	
Ni(1)–N(2)	2.073(5)	2.075(6)	Ni(2)–O(12)	2.099(3)	
Ni(1)–O(5)	2.108(4)	2.095(4)	Ni(2)–N(3)	2.073(4)	
Ni(1)–O(6)	2.106(3)	2.130(4)	Ni(2)–N(4)	2.078(4)	

Table 6. Deviation of Coordinating Atoms along with Nickel(II) from the Least Square Mean Plane Passing through Them in Complex 4

deviations of atoms in Å					
complex	O(1)	O(2)	N(1)	N(2)	Ni(1)
4	0.088(3)	−0.093(3)	−0.080(5)	0.079(5)	0.0065(5)
deviations of atoms in Å					
complex	O(7)	O(8)	N(3)	N(4)	Ni(2)
4	0.069(3)	−0.061(3)	−0.055(4)	0.062(4)	−0.0138(5)

of complex 5] from water molecules. Another oxygen atom [O(6) for Ni(1); O(12) for Ni(2) of complex 4 and O(6) for Ni(1); O(6)^m for Ni(1)^m of complex 5] from DMSO molecules coordinated with the nickel(II) centers to fulfill their distorted octahedral geometries. Deviations of the coordinating atoms from the mean equatorial planes passing through them and those of the nickel(II) centers from the same planes in complex 4 are listed in Table 6.

The central lead(II) is octacoordinated by four phenoxy oxygen atoms, [O(1), O(2), O(7), O(8) in the case of complex 4 and O(1), O(2), O(1)^m, O(2)^m for complex 5] and four alkoxy [methoxy in case of complex 4 and ethoxy for complex 5] oxygen atoms, [O(3), O(4), O(9), O(10) for complex 4 and O(3), O(4), O(3)^m, O(4)^m for complex 5] of two deprotonated reduced Schiff base ligands (Figure 3). In each complex, the lead(II) center is crammed between two {(DMSO)(H₂O)NiL*} [where L* = L¹ (for complex 4) and L² (for complex 5)] moieties forming a sandwich-type configuration.⁶⁴ The Pb–O(phenoxy) distances [2.460(4)–2.418(4) Å] are smaller compared to the Pb–O(methoxy) distances

[2.954(5)–2.696(5) Å]. Distances between the metal centers are ~3.564 Å for Pb(1)–Ni(1) and ~3.575 Å for Pb(1)–Ni(2). The angles, Ni(1)–O(1)–Pb(1), Ni(1)–O(2)–Pb(1), Ni(2)–O(7)–Pb(1), and Ni(2)–O(8)–Pb(1) are with the range of 102–107°. In complex 4, Ni(1)O(1)Pb(1)O(2) and Ni(2)O(7)Pb(1)O(8) dihedral angles are 4.05(12)° and −2.30(10)° respectively. The angle between Ni(1)O(1)O(2)–Pb(1) and Ni(2)O(7)O(8)Pb(1) cores is 79.77(11)°. In complex 5, Ni(1)O(1)Pb(1)O(2) dihedral angle is −7.63(13). The angle between Ni(1)O(1)O(2)Pb(1) and Ni(1)^mO(1)^mO(2)^mPb(1) [where m = 1/2 − x, y, 1 − z] cores is measured to be 72.75(13)°.

The saturated six-membered chelate rings, Ni(1)–N(1)–C(9)–C(10)–C(13)–N(2) and Ni(2)–N(3)–C(32)–C(33)–C(36)–N(4) in complex 4 have envelope conformations with puckering parameters^{65,66} $q = 0.566(6)$ Å; $\theta = 167.5(6)^\circ$; $\varphi = 14(3)^\circ$ and $q = 0.552(5)$ Å; $\theta = 19.5(4)^\circ$; $\varphi = 169(15)^\circ$, respectively. Similarly, the saturated six-membered chelate ring, Ni(1)–N(1)–C(10)–C(11)–C(14)–N(2) also has an envelope conformation with puckering parameters^{65,66} $q = 0.573(7)$ Å; $\theta = 8.6(6)^\circ$; $\varphi = 175(5)^\circ$ in complex 5.

IR, Electronic Spectra, and PXRD. The strong bands around 2080 cm^{−1} indicate the presence of thiocyanate in complexes 1, 2, and 3.⁶⁷ The bands around 3008–3286 cm^{−1} indicate the presence of amine N–H stretching in all complexes.⁶⁸ The broad bands in the range of 2970–2818 cm^{−1} due to alkyl C–H stretching vibrations were routinely noticed in IR spectra of the complexes.⁶⁹ In complexes 2 and 3, the bands around 1250 and 1229 cm^{−1} indicate the presence of an acetate group.⁷⁰ A broad band around 3400 cm^{−1} indicates the presence of coordinated water in complex 4.^{71,72} A strong band in the range of 1085–1011 cm^{−1} indicates the presence of perchlorate ions in complex 5.⁷³

The electronic spectrum of each complex in acetonitrile displays three bands around 242, 285, and 600 nm. The absorption around ~242 nm and ~285 nm may be assigned to charge transfer transitions,^{74,75} whereas the band around ~600 nm could be assigned to a d–d transition.⁷⁶

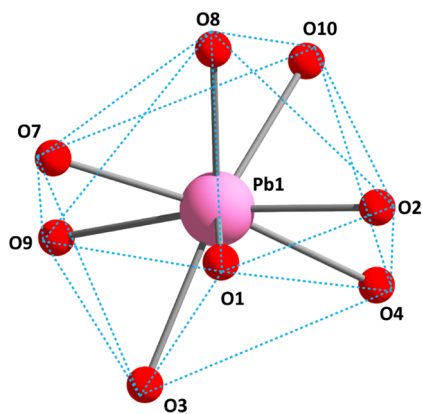


Figure 3. Perspective view of octacoordinated around lead(II) in complex 4.

Experimental PXRD patterns of the bulk products are in good agreement with simulated XRD patterns from single crystal X-ray diffraction results, indicating consistency in bulk samples. The simulated patterns of the complexes are calculated from the single crystal structural data (CIF) using the CCDC Mercury software. Experimental and simulated PXRD patterns of complex 1 are shown in Figure 4. The experimental and simulated PXRD patterns of complexes 2–5 are given in Figures S1–S4, respectively.

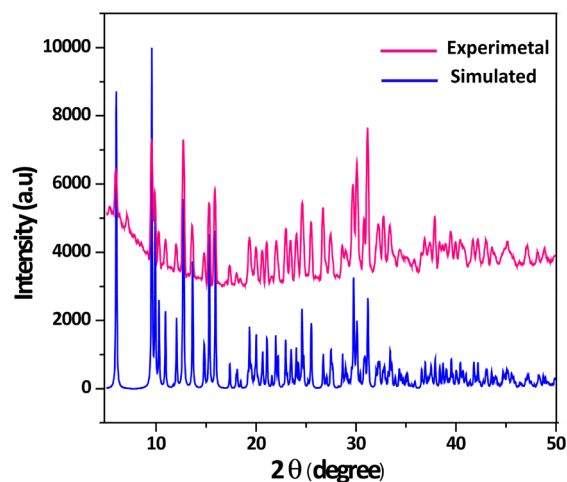


Figure 4. Experimental and simulated PXRD patterns of complex 1 confirming the purity of the bulk material.

Supramolecular Interactions. The solid state structures of the complexes are stabilized through various noncovalent interactions (e.g., hydrogen bonding, C–H $\cdots\pi$, $\pi\cdots\pi$, cation $\cdots\pi$ interactions etc.). The complexes were prepared while changing the ligand moieties along with bridging ligands, which result in five different nickel(II)/lead(II) complexes. These trivial changes in ligand moieties along with bridging

ligands play significant roles in the formation of diverse molecular architectures. Different supramolecular interactions are discussed below in the light of Hirshfeld surface analyses. Complexes 1, 2, and 3 are isostructural and show similar types of interactions. These complexes form supramolecular dimeric structure via cation $\cdots\pi$ interactions. The lead(II) center, Pb(1), is involved in cation $\cdots\pi$ interactions with symmetry-related [(1 – *x*, 1 – *y*, –*z*) for complex 1; (1 – *x*, 1 – *y*, 1 – *z*) for complex 2 and 3] phenyl rings, {[C(15)–C(16)–C(17)–C(18)–C(19)–C(20)] for complexes 1 and 2; [C(16)–C(17)–C(18)–C(19)–C(20)–C(21)] for complex 3 shown in Figure 5. Details of the geometric features of cation $\cdots\pi$ interactions are given in Table 7. It should be mentioned that

Table 7. Geometric Features^a of the Cation $\cdots\pi$ Interactions Obtained for Complexes 1, 2, and 3

complex	Cg \cdots M(cation)	Cg \cdots M (Å)	M \cdots Prep (Å)
1	Cg(10) \cdots Pb(1) ^a	3.595	–3.324
2	Cg(4) \cdots Pb(1) ^b	3.494	3.443
3	Cg(4) \cdots Pb(1) ^b	3.700	–3.390

^aDistances in Å and angles in °. Symmetry transformations. a = 1 – *x*, 1 – *y*, –*z* and b = 1 – *x*, 1 – *y*, 1 – *z*.

these interactions can (be) also defined as tetrel bonds where the electron donor is the π -system of the aromatic ring. This aspect is further analyzed in the theoretical part.

In complex 3, the hydrogen atom, H(2), attached to nitrogen atom, N(2), is engaged in an intermolecular hydrogen bonding interaction with a symmetry-related (1 + *x*, *y*, *z*) sulfur atom, S(1) of a coordinated terminal thiocyanate to form a chain structure (Figure 6). The dimensions are H \cdots S = 2.58(3) Å, N \cdots S = 3.371(3) Å, \angle N–H \cdots S = 138(6)°.

In complex 1, the phenyl ring, [C(2)–C(3)–C(4)–C(5)–C(6)–C(7)] forms a $\pi\cdots\pi$ stacking interaction [dimensions, Cg(9) \cdots Cg(10) = 3.759(5) Å, Cg(9) \cdots Prep = 3.487(4) Å, Cg(10) \cdots Prep = –3.521(3) Å, α = 14.4(4)°; where Cg(9) =

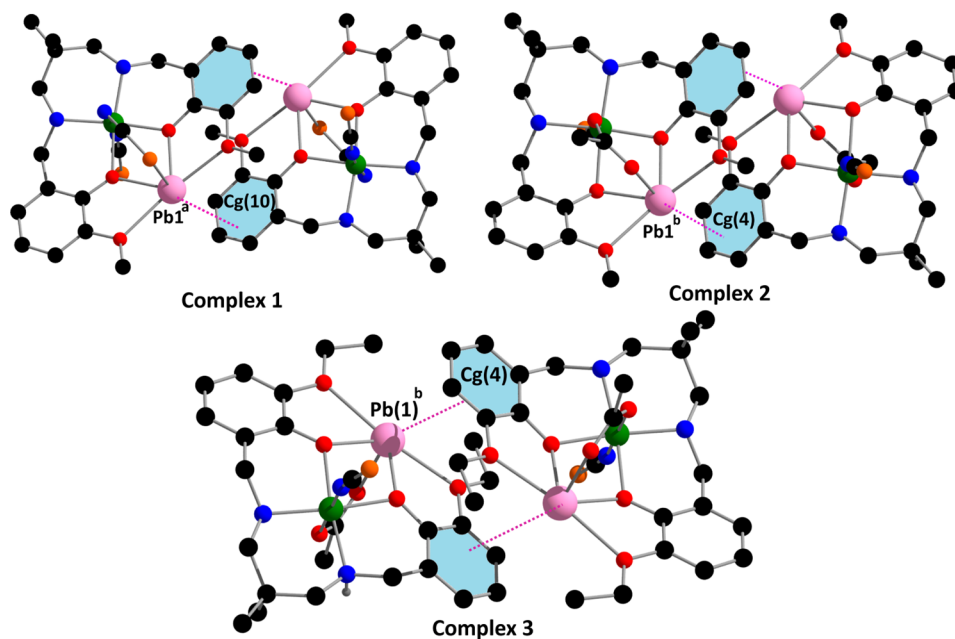


Figure 5. Cation $\cdots\pi$ interactions in complexes 1, 2, and 3. Only the relevant atoms have been shown for clarity. (Symmetry transformation ^a = 1 – *x*, 1 – *y*, –*z*; ^b = 1 – *x*, 1 – *y*, 1 – *z*.)

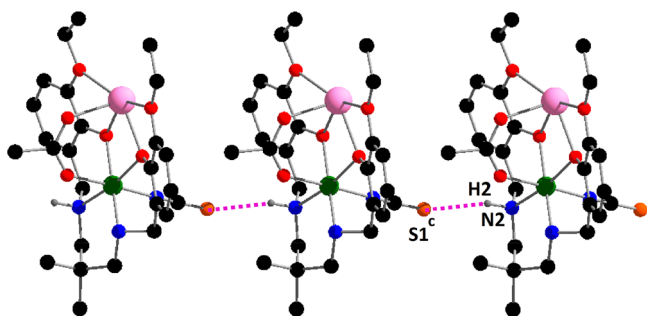


Figure 6. Supramolecular chain structure of complex 3 via hydrogen bonding interaction. Only the relevant atoms are shown for clarity. (Symmetry transformation $c = 1 + x, y, z$).

$C(2)-C(3)-C(4)-C(5)-C(6)-C(7)$, $Cg(10) = C(15)-C(16)-C(17)-C(18)-C(19)-C(20)$, $Cg(9) \cdots Prep$ = Perpendicular distance of $Cg(9)$ on ring $Cg(10)$, $Cg(10) \cdots Prep$ = Perpendicular distance of $Cg(10)$ on ring $Cg(9)$, α = dihedral angle between planes 9 and 10] with a symmetry-related $(1 + x, y, z)$ phenyl ring, $[C(15)-C(16)-C(17)-C(18)-C(19)-C(20)]$, which leads to the formation of a chain structure (Figure 7a). The fascinating tetrel bonding interaction is

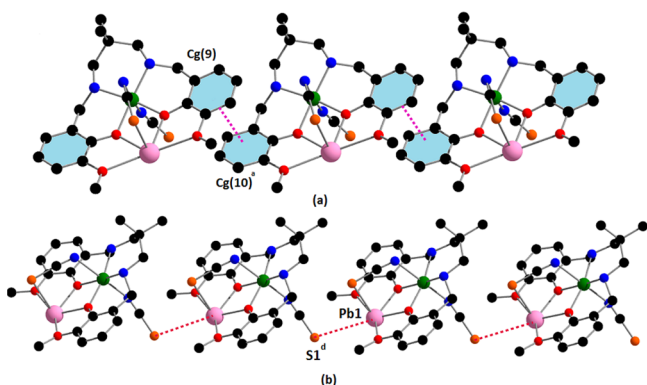


Figure 7. $\pi \cdots \pi$ (a) and $Pb \cdots S$ (b) interactions observed in complex 1. Only the relevant atoms have been shown for clarity. Symmetry transformations $a = 1 + x, y, z$ and $d = x, -1 + y, z$.

observed between the lead(II) atom, $Pb(1)$, with a symmetry-related $(x, -1 + y, z)$ sulfur atom, $S(1)$, of a thiocyanate from an adjacent molecule at $3.688(3)$ Å which leads to the formation of a chain. This is shown in Figure 7b.

In complex 4, the hydrogen atoms, $H(5A)$, attached to oxygen atom, $O(5)$, and $H(11O)$, attached to oxygen atom, $O(11)$, are hydrogen bonded with oxygen atoms, $O(14)$ and $O(13B)$ respectively of a perchlorate anion. Similarly, the hydrogen atoms, $H(5B)$, attached to oxygen atom, $O(5)$ and $H(11)$, attached to oxygen atom, $O(11)$, are involved in hydrogen bonding interactions with phenoxo oxygen atoms, $O(8)$ and $O(1)$, respectively of the reduced Schiff base ligand as shown in Figure 8. Additionally, the hydrogen atom, $H(4N)$, attached to nitrogen atom, $N(4)$, is engaged in symmetry-related $[2 - x, 1/2 + y, 1/2 - z]$ hydrogen bonding interaction with the oxygen atom, $O(17)$, of a perchlorate anion (Figure 8). A weak hydrogen bonding interaction is also observed between the hydrogen atom, $H(1N)$, attached to nitrogen atom, $N(1)$, with a symmetry-related $(-1 + x, y, z)$ oxygen atom, $O(18)$, of a perchlorate anion (Figure S5). Details of the

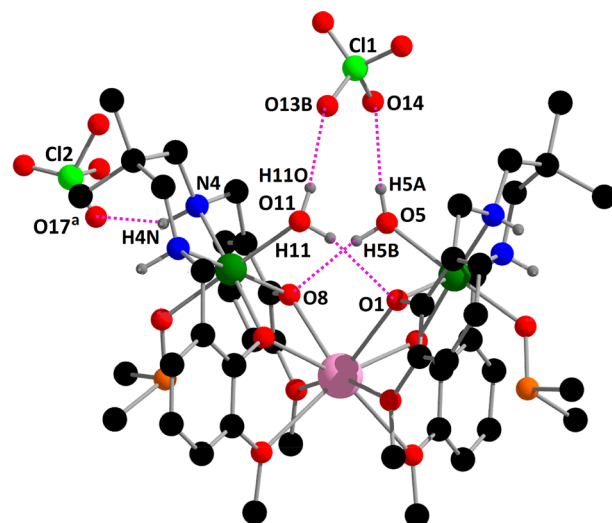


Figure 8. Hydrogen bonding interactions in complex 4. Only the relevant atoms have been shown for clarity. Symmetry transformations $a = 2 - x, 1/2 + y, 1/2 - z$.

geometric features of the hydrogen bonding interactions are summarized in Table 8.

Five $C-H \cdots \pi$ interactions are also observed in complex 4. The hydrogen atom, $H(23A)$, attached to the carbon atom $C(23)$, is involved in an intermolecular $C-H \cdots \pi$ interaction with a symmetry-related $(x, 1/2 - y, 1/2 + z)$ phenyl ring $[C(25)-C(26)-C(27)-C(28)-C(29)-C(30)]$ to form a supramolecular zigzag structure (Figure S6). Hydrogen atoms, $H(22C)$, $H(23B)$, $H(45B)$, and $H(46C)$, attached to carbon atoms, $C(22)$, $C(23)$, $C(45)$, and $C(46)$ respectively are involved in intramolecular $C-H \cdots \pi$ interactions with the phenyl ring $[C(2)-C(3)-C(4)-C(5)-C(6)-C(7)]$, $[C(15)-C(16)-C(17)-C(18)-C(19)-C(20)]$, $[C(25)-C(26)-C(27)-C(28)-C(29)-C(30)]$, and $[C(38)-C(39)-C(40)-C(41)-C(42)-C(43)]$, respectively. These interactions are shown in Figure S7. The details of the geometric features of the $C-H \cdots \pi$ interactions have been gathered in Table 9.

Complex 5 also shows three $C-H \cdots \pi$ interactions. The hydrogen atom, $H(1A)$, attached to carbon atom, $C(1)$, is involved in a $C-H \cdots \pi$ interaction with a symmetry-related $(1/2 - x, y, 1 - z)$ phenyl ring $[C(16)-C(17)-C(18)-C(19)-C(20)-C(21)]$. The hydrogen atoms, $H(24C)$ and $H(25A)$, attached to the carbon atoms, $C(24)$ and $C(25)$, respectively, is involved in intramolecular $C-H \cdots \pi$ interactions with phenyl rings $[C(16)-C(17)-C(18)-C(19)-C(20)-C(21)]$ and $[C(3)-C(4)-C(5)-C(6)-C(7)-C(8)]$ respectively. These interactions are shown in Figure S8. Details of the geometric features of the $C-H \cdots \pi$ interactions have been gathered in Table 9.

Theoretical Study. The theoretical study is devoted to the analysis of interesting tetrel bonding interactions observed in the solid state of complexes 1–3, where coordination of the lead(II) atom is hemidirected, and consequently the σ -hole at the lead(II) atom is accessible to interact with electron donors (π -system or thiocyanate ligand). Using complex 1 as exemplifying molecule, the molecular electrostatic potential (MEP) was computed and plotted onto the van der Waals surface (isosurface 0.001 au) in order to investigate the electron-rich and electron-deficient regions of the complex. The MEP surface is represented in Figure 9. It can be observed

Table 8. Geometric Features^a of the Hydrogen Bonding Interactions Obtained for Complex 4

D–H...A	D–H	H...A	D...A	∠D–H...A
O(5)–H(5A)...O(14)	0.81(7)	2.04(7)	2.836(7)	168(5)
O(5)–H(5B)...O(8)	0.84(4)	1.99(3)	2.815(5)	167(3)
O(11)–H(H11O)...O(13B)	0.73(5)	2.13(5)	2.840(14)	163(6)
O(11)–H(H11)...O(1)	0.84(4)	2.09(3)	2.917(6)	170(3)
N(4)–H(4N)...O(17) ^a	1(4)	2.24(8)	3.119(9)	146(3)
N(1)–H(1N)...O(18) ^b	0.82(5)	2.86(5)	3.526(1)	140(4)

^aDistances in Å and angles in °. Symmetry transformations: a = 2 – x, 1/2 + y, 1/2 – z. b = –1 + x, y, z.

Table 9. Geometric Features^a of the C–H... π Interactions for Complexes 4 and 5

complex	C–H...Cg (ring)	H...Cg (Å)	C–H...Cg (deg)	C...Cg (Å)
4	C(22)–H(22C)...Cg(7)	2.88	145	3.726(8)
	C(23)–H(23A)...Cg(9) ^a	2.89	172	3.864(8)
	C(23)–H(23B)...Cg(8)	2.94	152	3.837(8)
	C(45)–H(45B)...Cg(9)	2.98	156	3.897(7)
	C(46)–H(46C)...Cg(10)	2.85	143	3.685(6)
5	C(1)–H(1A)...Cg(5) ^b	2.94	127	3.612(11)
	C(24)–H(24C)...Cg(5)	2.61	148	3.482(9)
	C(25)–H(25A)...Cg(4)	2.86	148	3.729(10)

^aDistances in Å and angles in °. Symmetry transformations: a = x, 1/2 – y, 1/2 + z and b = 1/2 – x, y, 1 – z.

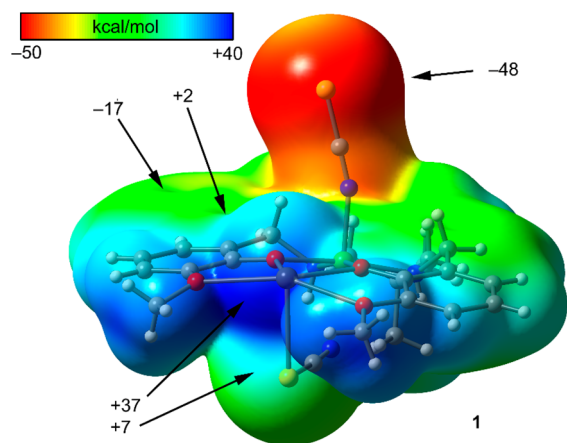


Figure 9. MEP surface of complex 1 (isosurface 0.001 au) at the PBEO/def2-TZVP level of theory. The values at selected points of the surface are indicated in kcal/mol.

that the most positive region is located on the lead(II) atom, approximately in the PbO_4 mean plane (+37 kcal/mol) between both methoxy (–OMe) groups. The most negative region as expected is located at the anionic thiocyanate (–SCN) ligand. The MEP value is negative over the aromatic ring and slightly positive over the lead(II)–chelate ring. This analysis indicates that the most favored interaction from an electrostatic point of view should be a tetrel bond between the lead(II) atom and the pseudohalide. Moreover, the MEP surface also reveals that π -stacking interactions between aromatic rings and chelate rings are also electrostatically favored. Finally, it is worthy to comment on the unexpected positive MEP value observed at the sulfur atom of the bridged thiocyanate ligand at the extension of the thiocyanate bond revealing the existence of a σ -hole at the chalcogen atom suitable to establish weak σ -hole interactions.

Figure 10 shows two dimers retrieved from the X-ray structures of complex 1 (hydrogen atoms omitted for clarity), where relevant and unconventional interactions are observed. The first dimer corresponds to the cation– π (or tetrel– π) complex highlighted in Figure 5, and the second one has been extracted from the infinite 1D supramolecular chain described in Figure 7b (bottom). A close examination of the self-assembled dimer represented in Figure 10a reveals that the five-membered Pb–chelate ring (CR, represented in blue) is stacked above the aromatic ring (represented in green). This type of interaction is described in hemidirected lead(II) complexes with hydrazide-based ligands.⁷⁷ In fact, the lead atom basically interacts with one carbon atom of the aromatic ring. The interaction energy of this dimer was evaluated and found to be very large ($\Delta E_1 = -29.9$ kcal/mol), thus confirming the relevance of π – π (CR) interactions. The Pb...S dimer is represented in Figure 10b, and it can be observed that the negative sulfur-atom of the monocoordinated thiocyanate ligand is situated exactly at a position predicted by the MEP surface (maximum value of shown in Figure 9). In addition, the σ -hole at the sulfur atom of the bridged thiocyanate interacts with the electron-rich carbon atom of the thiocyanate ligand, also in agreement with the MEP analysis. Both interactions contribute to the binding energy that is moderately strong ($\Delta E_2 = -19.6$ kcal/mol). To further characterize the interactions described above, the NCI plot index was used since it allows an easy assessment of host–guest complementarity and the extent to which weak interactions stabilize a complex. Figure 10c shows the NCI plot of the stacked dimer. The presence of an extended green (energetically favorable) isosurface between aromatic and chelate rings observed confirms the existence of the interaction. Moreover, a smaller green isosurface is located between the lead atom and one carbon atom of the ring characterizing the Pb...C tetrel bond. The NCI plot also reveals the existence of several C–H...SCN interactions involving the methoxy (–OCH₃) and C–H groups characterized by two isosurfaces. For the Pb...S dimer, the tetrel bond is characterized by a green isosurface located between the sulfur and lead(II) atoms (see Figure 10d). This interaction is complemented by two C–H...S hydrogen bonding interactions involving methyl groups. Finally, the S...C(SCN) interaction is characterized by a small isosurface located between both atoms.

As previously shown in Figure 5, complexes 2 and 3 also form Pb... π (or cation– π) dimers in the solid state. Both dimers are shown in Figure 11 from where it can be observed that they are slightly different compared to complex 1. In fact, for complex 2, the lead(II) atom is located approximately over the center of the aromatic ring instead of being connected to a single carbon-atom. This provokes a displacement of the π -systems and the π – π (CR) interaction is not formed; instead a

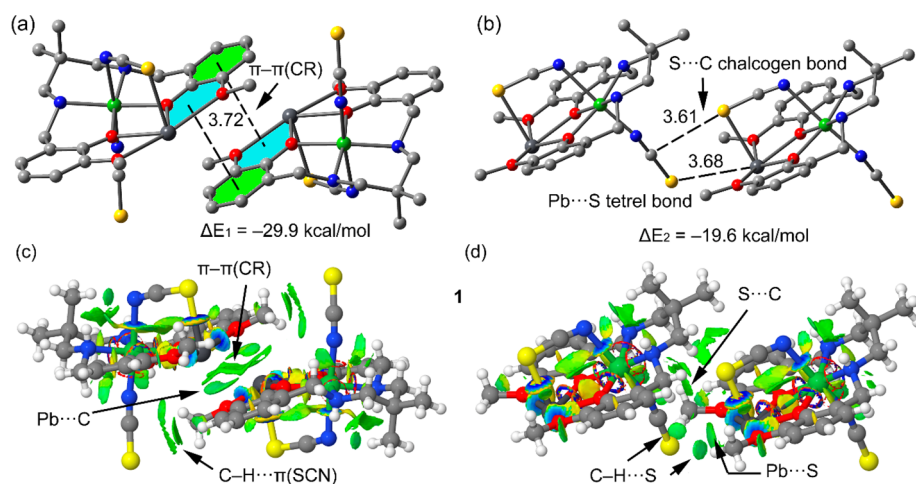


Figure 10. (a, b) Theoretical models used to evaluate the noncovalent interactions. (c, d) NCI plots of the dimers in complex **1**. The gradient cutoff is $s = 0.35$ au, and the color scale is $-0.04 < \rho < 0.04$ au.

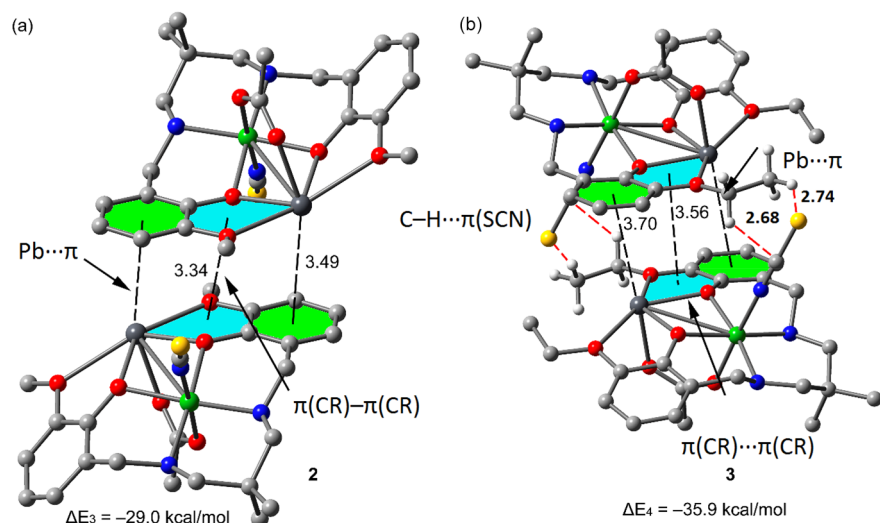
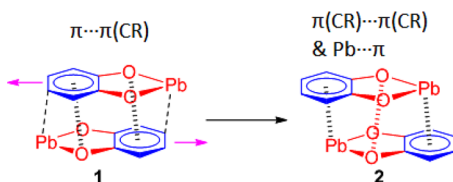


Figure 11. (a, b) Theoretical models used to evaluate the noncovalent interactions in complexes **2** and **3**. Distances in Å.

$\pi(\text{CR})-\pi(\text{CR})$ stacking is established in combination with two $\text{Pb}\cdots\pi$ interactions (see Scheme 2). Therefore, differences

Scheme 2. Schematic Representation of the π -Stacking Assemblies in Complexes **1** and **2**



between both these arrangements were analyzed with regard to energy. In Figure 11a, the $\text{Pb}\cdots\pi$ dimer of complex **2** has been represented, and it was found that the interaction energy is almost identical ($\Delta E_3 = -29.0$ kcal/mol) to the dimer of complex **1** (see Figure 10a), suggesting both combinations are basically isoenergetic. The dimer of complex **3** is not strictly comparable because of the presence of an ethyl group instead of a methyl group. This provokes a displacement of the π -systems (parallel displaced arrangement) that provokes an enlargement of both $\pi(\text{CR})-\pi(\text{CR})$ stacking and $\text{Pb}\cdots\pi$

distances and the formation of $\text{C}-\text{H}\cdots\text{SCN}$ interactions (marked in red in Figure 11b). As a consequence, the interaction energy of this dimer is the most favorable ($\Delta E_4 = -35.9$ kcal/mol) due to additional interactions.

There are examples in the literature of experimental and theoretical investigations devoted to tetrel bonding. Table 10 shows examples of such X-ray characterized heteronuclear nickel(II)/lead(II) complexes along with lead(II) complexes where the lead(II) center is hemidirected and subjected to a tetrel bonding interaction. Now it has to be mentioned that no such report has been found where tetrel bonding was explored in heteronuclear nickel(II)/lead(II) complexes with reduced Schiff bases. Thus, the present work is the first systematic study that explores tetrel bonding interactions in hemidirected heteronuclear nickel(II)/lead(II) complexes.

CONCLUDING REMARKS

In conclusion, syntheses and structural characterizations of five heteronuclear nickel(II)/lead(II) complexes with compartmental reduced Schiff base ligands have been reported where five η -membered Pb -chelate rings in the hemicoordinated complexes **1–3** play a relevant role. Moreover, supramolecular tetrel bonding interactions of these complexes have been

Table 10. Reported X-ray Characterized Nickel(II)/Lead(II) and Lead(II) Complexes Comprising Tetrel Bonding Interaction^a

complex (CCDC)	formula	coordination mode of lead	bonding	Pb–X (Å)	ref
YISROI	[{L ^a Ni}Pb(NC ₅ H ₅)Cl] ₂	hemidirected	tetrel	3.272(1)	78
YISRUO	[{L ^b Ni} ₂ Pb]·Py·H ₂ O	hemidirected	tetrel	3.221(2)	78
QUQBIP	[(SCN)PbL ^c [(μ _{1,1} -SCN)] ₂ ·CH ₃ OH	hemidirected	tetrel	3.042(1)	79
QUQBOV	[(SCN) ₂ PbL ^c]	hemidirected	tetrel	3.403(2)	79
				3.472(3)	79
TAGMUM	[(I)PbL ^d]·CH ₃ OH	hemidirected	tetrel	3.241(1)	80
TAGMOG	[(Cl)PbL ^d]·CH ₃ OH	hemidirected	tetrel	3.155(2)	80
TAGNET	[(SCN)PbL ^d]	hemidirected	tetrel	3.224(8)	80
TAGNEX	[(NO ₃)PbL ^d]·CH ₃ OH	hemidirected	tetrel	3.408(1)	80
IPAHEO	[Pb ₂ (HL ^e) ₂ (NO ₃) ₄]	hemidirected	tetrel	2.923(3)	79
IPAHAK	[(OAc)PbL ^c]	hemidirected	tetrel	3.424(7)	79
JERPAA	[Pb ₂ (H ₂ L ^e)(NO ₃) ₄] ₂	hemidirected	tetrel	3.060(1)	79
				3.350(1)	79
HAFVAO	[Pb(L ^c)N ₃] _n	hemidirected	tetrel	3.436(4)	81
HAFVES	[(NO ₃)(SCN)Pb(HL ^c) ₂]	hemidirected	tetrel	3.225(1)	81
HAFVIW	[(OAc)PbL ^c]	hemidirected	tetrel	3.488(3)	81
				3.409(4)	81
HAFVUI	[PbL ^c (NO ₂) ₂] _n	hemidirected	tetrel	3.299(5)	81
REZFIO	[(SCN)NiL ^e Pb(NO ₃) ₃]	hemidirected	tetrel	3.064(2)	54
ZETLES	[(H ₂ O)Ni(SCN)L ^c Pb(OAc)]·DMSO	hemidirected	tetrel	3.379(4)	54
	[(SCN)NiL ¹ (μ _{1,3} -NCS)Pb]	hemidirected	tetrel	3.688(3)	this work
	[(SCN)NiL ¹ (μ-OAc)Pb]	hemidirected			this work
	[(SCN)NiL ² (μ-OAc)Pb]	hemidirected			this work

^aL^a = tris((2-hydroxybenzylidene)-aminoethyl)-amine; L^b = tris((-2-hydroxybenzylidene)-aminomethyl)propane; H₂L^c = N'-(1-(2-pyridyl)-ethylidene)nicotinohydrazide; H₂L^d = N'-(phenyl(pyridin-2-yl) methylene)isonicotinohydrazide; H₂L^e = N,N'-bis(3-ethoxysalicylidene)propane-1,3-diamine; H₂L^f = [N,N'-bis(3-methoxysalicylidene)-2,2-dimethylpropane-1,3-diamine].

investigated, and the interaction energies were calculated and characterized using NCI plot index. Remarkably, the combination of interactions observed in the π -stacking assembly in complex **1**, a pair of π - π (CR) interactions, is energetically equivalent to the formation of one π (CR)- π (CR) interaction and two cation- π interactions (or Pb... π tetrel bonds) observed in complex **2**. C-H... π interactions are commonly observed in complexes **4** and **5**. Finally, the results reported herein stress the importance of π -interactions involving the chelate ring in crystal engineering in addition to the tetrel bonds involving hemicoordinated lead(II).

■ ASSOCIATED CONTENT

■ Supporting Information

The Supporting Information is available free of charge on the ACS Publications website at DOI: 10.1021/acs.cgd.9b00881.

Experimental details along with Table S1; Figures S1–S12 (PDF)

Accession Codes

CCDC 1938676–1938680 contain the supplementary crystallographic data for this paper. These data can be obtained free of charge via www.ccdc.cam.ac.uk/data_request/cif, or by emailing data_request@ccdc.cam.ac.uk, or by contacting The Cambridge Crystallographic Data Centre, 12 Union Road, Cambridge CB2 1EZ, UK; fax: +44 1223 336033.

■ AUTHOR INFORMATION

Corresponding Authors

*E-mail: shouvik.chem@gmail.com. Tel: +9133-2457-2941 (S.C.).

*E-mail: toni.frontera@uib.es (A.F.).

ORCID

Sudipta Chatterjee: 0000-0002-3273-1751

Antonio Bauzá: 0000-0002-5793-781X

Antonio Frontera: 0000-0001-7840-2139

Shouvik Chattopadhyay: 0000-0001-7772-9009

Notes

The authors declare no competing financial interest.

■ ACKNOWLEDGMENTS

S.M. thanks CSIR, India, for awarding a Junior Research Fellowship [Sanction No. 09/096(0990)2019-EMR-1]. A.B. and A.F. thank the MINECO/AEI of Spain, Project Number CTQ2017-85821-R FEDER funds. S.C. gratefully acknowledges the help of Prof. Saurabh Das, Jadavpur University, in preparing the manuscript.

■ REFERENCES

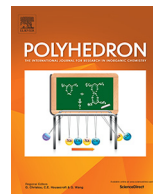
- (1) Hancock, R. D.; Reibenspies, J. H.; Maumela, H. Structural Effects of the Lone Pair on Lead(II), and Parallels with the Coordination Geometry of Mercury(II). Does the Lone Pair on Lead(II) Form H-Bonds? Structures of the Lead(II) and Mercury(II) Complexes of the Pendant-Donor Macrocyclic DOTAM(1,4,7,10-Tetrakis(carbamoylmethyl)-1,4,7,10-tetraazacyclododecane). *Inorg. Chem.* **2004**, *43*, 2981–2987.
- (2) Platas-Iglesias, C.; Esteban-Gomez, D.; Enriquez-Perez, T.; Avecilla, F.; de Blas, A.; Rodriguez-Blas, T. Lead(II) Thiocyanate Complexes with Bibracchial Lariat Ethers: An X-ray and DFT Study. *Inorg. Chem.* **2005**, *44*, 2224–2233.
- (3) Reger, D. L.; Wright, T. D.; Little, C. A.; Lamba, J. J. S.; Smith, M. D. Control of the stereochemical Impact of the Lone Pair in Lead(II) Tris(pyrazolyl)methane Complexes. Improved Preparation of Na{B[3,5-(CF₃)₂C₆H₃]₄}. *Inorg. Chem.* **2001**, *40*, 3810–3814.

- (4) Fleischer, H.; Schollmeyer, D. Synthesis of and Structural Studies on Lead(II) Cysteamine Complexes. *Inorg. Chem.* **2004**, *43*, 5529–5536.
- (5) Zhang, L.; Qin, Y.-Y.; Li, Z.-J.; Lin, Q.-P.; Cheng, J.-K.; Zhang, J.; Yao, Y.-G. Topology Analysis and Nonlinear Optical-Active Properties of Luminescent Metal-Organic Framework Materials Based on Zinc/Lead Isophthalates. *Inorg. Chem.* **2008**, *47*, 8286–8293.
- (6) Olvera, A.; Shi, G.; Djieutedjeu, H.; Page, A.; Uher, C.; Kioupakis, E.; Poudeu, P. F. P. $\text{Pb}_2\text{Bi}_4\text{Se}_{13}$: A Lillianite Homologue with Promising Thermoelectric Properties. *Inorg. Chem.* **2015**, *54*, 746–755.
- (7) Cheng, F.; Liang, J.; Tao, Z.; Chen, J. Functional Materials for Rechargeable Batteries. *Adv. Mater.* **2011**, *23*, 1695–1715.
- (8) Cheng, Y.; Emge, T. J.; Brennan, J. G. Pyridineselenolate Complexes of Tin and Lead: $\text{Sn}(\text{2-SeNC}_5\text{H}_4)_2$, $\text{Sn}(\text{2-SeNC}_5\text{H}_4)_4$, $\text{Pb}(\text{2-SeNC}_5\text{H}_4)_2$, and $\text{Pb}(\text{3-Me}_3\text{Si-2-SeNC}_5\text{H}_3)_2$. Volatile CVD Precursors to Group IV-Group VI Semiconductors. *Inorg. Chem.* **1996**, *35*, 342–346.
- (9) Randall, C. A.; Bhalla, A. S.; Shrout, T. R.; Cross, L. E. Classification and consequences of complex lead perovskite ferroelectrics with regard to B-site cation order. *J. Mater. Res.* **1990**, *5*, 829–834.
- (10) Masek, J. Electronic states in mixed (Cd, Pb)S semiconductors. *J. Phys. C: Solid State Phys.* **1988**, *21*, 2821–2827.
- (11) Guo, M.; Law, W.-C.; Liu, X.; Cai, H.; Liu, L.; Swihart, M. T.; Zhang, X.; Prasad, P. N. *Plasmonics* **2014**, *9*, 893–898.
- (12) Liu, T.-T.; Liang, J.; Huang, Y.-B.; Cao, R. A bifunctional cationic porous organic polymer based on a Salen-(Al) metalloligand for the cycloaddition of carbon dioxide to produce cyclic Carbonates. *Chem. Commun.* **2016**, *52*, 13288–13291.
- (13) Lyons, C. T.; Stack, T. D. P. Recent advances in phenoxyl radical complexes of salen-type ligands as mixed-valent galactose oxidase models. *Coord. Chem. Rev.* **2013**, *257*, 528–540.
- (14) Cozzi, P. G. Metal-Salen Schiff base complexes in catalysis: practical aspects. *Chem. Soc. Rev.* **2004**, *33*, 410–421.
- (15) Baleizao, C.; Garcia, H. Chiral Salen Complexes: An Overview to Recoverable and Reusable Homogeneous and Heterogeneous Catalysts. *Chem. Rev.* **2006**, *106*, 3987–4043.
- (16) Constable, E. C.; Zhang, G.; Housecroft, C. E.; Zampese, J. A. Amalgamating metalloligands with coordination networks. *Dalton Trans* **2010**, *39*, 1941–1947.
- (17) Abdel-Rahman, L. H.; Abu-Dief, A. M.; Abdel-Mawgoud, A. A. H. Development, structural investigation, DNA binding, antimicrobial screening and anticancer activities of two novel quasi-dentate VO(II) and Mn(II) mononuclear complexes. *J. King Saud Univ., Sci.* **2019**, *31*, 52–60.
- (18) Abdel-Rahman, L. H.; Abu-Dief, A. M.; Aboelez, M. O.; Abdel-Mawgoud, A. A. H. DNA interaction, antimicrobial, anticancer activities and molecular docking study of some new VO(II), Cr(III), Mn(II) and Ni(II) mononuclear chelates encompassing quaridentate imine ligand. *J. Photochem. Photobiol., B* **2017**, *170*, 271–285.
- (19) Abu-Dief, A. M.; Diaz-Torres, R.; Sanudo, E. C.; Abdel-Rahman, L. H.; Aliaga-Alcalde, N. Novel sandwich triple-decker dinuclear Nd^{III} -(bis-N,N'-p-bromo-salicylideneamine-1,2-diaminobenzene)complex. *Polyhedron* **2013**, *64*, 203–208.
- (20) Roy, S.; Halder, S.; Drew, M. G. B.; Ray, P. P.; Chattopadhyay, S. Fabrication of an Active Electronic Device Using a Hetero-bimetallic Coordination Polymer. *ACS Omega* **2018**, *3*, 12788–12796.
- (21) Thurston, J. H.; Tang, C. G.-Z.; Trahan, D. W.; Whitmire, K. H. Toward Rational Control of Metal Stoichiometry in Hetero-bimetallic Coordination Complexes: Synthesis and Characterization of $\text{Pb}(\text{Hsal})_2(\text{Cu}(\text{salen}^*))_2$, $[\text{Pb}(\text{NO}_3)(\text{Cu}(\text{salen}^*))_2](\text{NO}_3)$, $\text{Pb}(\text{OAc})_2(\text{Cu}(\text{salen}^*))$, and $[\text{Pb}(\text{OAc})(\text{Ni}(\text{salen}^*))_2](\text{OAc})$. *Inorg. Chem.* **2004**, *43*, 2708–2713.
- (22) Bhattacharya, S.; Mohanta, S. Heterometallic copper(II)-lead(II), nickel(II)-lead(II) and copper(II)-indium(III) compounds derived from an acyclic double-compartment Schiff base ligand. *Inorg. Chim. Acta* **2015**, *432*, 169–175.
- (23) Pitzer, K. S. Relativistic Effects on Chemical Properties. *Acc. Chem. Res.* **1979**, *12*, 271–276.
- (24) Pyykkö, P.; Desclaux, J.-P. Relativity and the periodic system of elements. *Acc. Chem. Res.* **1979**, *12*, 276–281.
- (25) Pyykkö, P. Relativistic Effects in Structural Chemistry. *Chem. Rev.* **1988**, *88*, 563–594.
- (26) Sidgwick, N. V.; Powell, H. M. Bakerian Lecture: Stereochemical types and valency groups. *Proc. R. Soc. (London)* **1940**, *A176*, 153.
- (27) Reger, D. L.; Huff, M. F.; Rheingold, A. L.; Haggerty, B. S. Control of Structure in Lead(II) Complexes Using Poly(pyrazolyl)-borate Ligands. Stereochemically Inactive Lone Pair in Octahedral $[\text{HB}(\text{3,5-Me}_2\text{pz})_3]_2\text{Pb}$ (pz = Pyrazolyl Ring). *J. Am. Chem. Soc.* **1992**, *114*, 579–584.
- (28) Gillespie, R. J.; Nyholm, R. S. Inorganic Stereochemistry. *Q. Rev., Chem. Soc.* **1957**, *11*, 339–380.
- (29) Luckay, R.; Cukrowski, I.; Mashishi, J.; Reibenspies, J. H.; Bond, A. H.; Rogers, R. D.; Hancock, R. D. Synthesis, stability and structure of the complex of bismuth(III) with the nitrogen-donor macrocycle 1,4,7,10-tetraazacyclododecane. The role of the lone pair on bismuth(III) and lead(II) in determining co-ordination geometry. *J. Chem. Soc., Dalton Trans.* **1997**, 901–908.
- (30) Walsh, A.; Watson, G. W. The origin of the stereochemically active Pb(II) lone pair: DFT calculations on PbO and PbS. *J. Solid State Chem.* **2005**, *178*, 1422–1428.
- (31) Hancock, R. D.; Shaikjee, M. S.; Dobson, S. M.; Boeyens, J. C. The Stereochemical Activity or Non-activity of the 'Inert' Pair of Electrons on Lead(II) in Relation to its Complex Stability and Structural Properties. Some Considerations in Ligand Design. *Inorg. Chim. Acta* **1988**, *154*, 229–238.
- (32) Esteban-Gómez, D.; Platas-Iglesias, C.; Enriquez-Pérez, T.; Avecilla, F.; de Blas, A.; Rodríguez-Blas, T. Lone-Pair Activity in Lead(II) Complexes with Unsymmetrical Lariat Ethers. *Inorg. Chem.* **2006**, *45*, 5407–5416.
- (33) Bauzá, A.; Mooibroek, T. J.; Frontera, A. Tetrel-Bonding Interaction: Rediscovered Supramolecular Force? *Angew. Chem., Int. Ed.* **2013**, *52*, 12317–12321.
- (34) Grabowski, S. J. Tetrel bond- σ -hole bond as a preliminary stage of the S_N^2 reaction. *Phys. Chem. Chem. Phys.* **2014**, *16*, 1824–1834.
- (35) Bauzá, A.; Mooibroek, T. J.; Frontera, A. Small Cycloalkane (CN) $_2$ C-C(CN) $_2$ Structures Are Highly Directional Non-covalent Carbon-Bond Donors. *Chem. - Eur. J.* **2014**, *20*, 10245–10248.
- (36) Escudero-Adán, E. C.; Bauzá, A.; Frontera, A.; Ballester, P. Nature of Noncovalent Carbon-Bonding Interactions Derived from Experimental Charge-Density Analysis. *ChemPhysChem* **2015**, *16*, 2530–2533.
- (37) Bauzá, A.; Mooibroek, T. J.; Frontera, A. Influence of ring size on the strength of carbon bonding complexes between anions and perfluorocycloalkanes. *Phys. Chem. Chem. Phys.* **2014**, *16*, 19192–19197.
- (38) Bauzá, A.; Mooibroek, T. J.; Frontera, A. Non-covalent sp^3 carbon bonding with ArCF_3 is analogous to $\text{C-H}\cdots\pi$ interactions. *Chem. Commun.* **2014**, *50*, 12626–12629.
- (39) Murray, J. S.; Lane, P.; Politzer, P. Expansion of the σ -hole concept. *J. Mol. Model.* **2009**, *15*, 723–729.
- (40) Bundhun, A.; Ramasami, P.; Murray, J. S.; Politzer, P. Trends in σ -hole strengths and interactions of F_3MX molecules ($\text{M} = \text{C}, \text{Si}, \text{Ge}$ and $\text{X} = \text{F}, \text{Cl}, \text{Br}, \text{I}$). *J. Mol. Model.* **2013**, *19*, 2739–2746.
- (41) Bauzá, A.; Mooibroek, T. J.; Frontera, A. Tetrel Bonding Interactions. *Chem. Rec.* **2016**, *16*, 473–487.
- (42) Gargari, M. S.; Stilinović, V.; Bauzá, A.; Frontera, A.; McArdle, P.; Van Derveer, D. V.; Ng, S. W.; Mahmoudi, G. Design of Lead(II) Metal-Organic Frameworks Based on Covalent and Tetrel Bonding. *Chem. - Eur. J.* **2015**, *21*, 17951–17958.
- (43) Mahmoudi, G.; Zangrando, E.; Mitoraj, M. P.; Gurbanov, A. V.; Zubkov, F. I.; Moosavifar, M.; Konyaeva, I. A.; Kirillov, A. M.; Safin, D. A. Extended lead(II) architectures engineered via tetrel bonding interactions. *New J. Chem.* **2018**, *42*, 4959–4971.

- (44) Grabowski, S. J. Tetrel bonds, penta and hexa coordinated tin and lead centres. *Appl. Organomet. Chem.* **2017**, *31*, No. e3727.
- (45) Hunter, C. A.; Sanders, J. K. M. The nature of pi-pi Interactions. *J. Am. Chem. Soc.* **1990**, *112*, 5525–5534.
- (46) Burley, S. K.; Petsko, G. A. Aromatic-aromatic interaction: a mechanism of protein structure stabilization. *Science* **1985**, *229*, 23–28.
- (47) Kim, K. S.; Tarakeshwar, P.; Lee, J. Y. Molecular Clusters of π -Systems: Theoretical Studies of Structures, Spectra, and Origin of Interaction Energies. *Chem. Rev.* **2000**, *100*, 4145–4185.
- (48) Ma, J. C.; Dougherty, D. A. The Cation- π Interaction. *Chem. Rev.* **1997**, *97*, 1303–1324.
- (49) Kim, K. S.; Lee, J. Y.; Lee, S. J.; Ha, T.-K.; Kim, D. H. On Binding Forces between Aromatic Ring and Quaternary Ammonium Compound. *J. Am. Chem. Soc.* **1994**, *116*, 7399–7400.
- (50) Nishio, M.; Hirota, M.; Umezawa, Y. *In the C-H/ π Interaction: Evidence, Nature, Consequences*; Wiley-VCH: New York, 1998.
- (51) Egli, M.; Sarkhel, S. Lone Pair-Aromatic Interactions: To Stabilize or Not to Stabilize. *Acc. Chem. Res.* **2007**, *40*, 197–205.
- (52) Mooibroek, T. J.; Gamez, P.; Reedijk, J. Lone pair- π interactions: a new supramolecular bond? *CrystEngComm* **2008**, *10*, 1501–1515.
- (53) Sathiyaraj, E.; Thirumaran, S.; Selvanayagam, S.; Sridhar, B.; Ciattini, S. C-H \cdots Ni and C-H $\cdots\pi$ (chelate) interactions in nickel(II) complexes involving functionalized dithiocarbamates and triphenylphosphine. *J. Mol. Struct.* **2018**, *1159*, 156–166.
- (54) Roy, S.; Drew, M. G. B.; Bauzá, A.; Frontera, A.; Chattopadhyay, S. Non-covalent tetrel bonding interactions in hemidirectional lead(II) complexes with nickel(II)-salen type metal-ligands. *New J. Chem.* **2018**, *42*, 6062–6076.
- (55) Roy, S.; Drew, M. G. B.; Bauzá, A.; Frontera, A.; Chattopadhyay, S. A Combined Experimental and Theoretical Study to Explore the Importance of σ -Hole Carbon Bonding Interactions in Stabilizing Molecular Assemblies. *Chem. Select* **2017**, *2*, 10586–10594.
- (56) Mahmoudi, G.; Zargha, J. K.; Bauzá, A.; Kubicki, M.; Bartyzel, A.; Keramidis, A. D.; Butusov, L.; Mirosław, B.; Frontera, A. Recurrent supramolecular motifs in discrete complexes and coordination polymers based on mercury halides: prevalence of chelate ring stacking and substituent effects. *CrystEngComm* **2018**, *20*, 1065–1076.
- (57) Mahmoudi, G.; Khandar, A. A.; Afkhami, F. A.; Mirosław, B.; Gurbanov, A. V.; Zubkov, F. I.; Kennedy, A.; Franconetti, A.; Frontera, A. Modulation of coordination in pincer-type isonicotinohydrazone Schiff base ligands by proton transfer. *CrystEngComm* **2019**, *21*, 108–117.
- (58) Tan, Y. S.; Halim, S. N. A.; Molloy, K. C.; Sudlow, A. L.; Otero-De-La-Roza, A.; Tiekink, E. R. T. Persistence of C-H $\cdots\pi$ (chelate ring) interactions in the crystal structures of Pd(S₂COR)₂. The utility of Pd(S₂COR)₂ as precursors for palladium sulphide materials. *CrystEngComm* **2016**, *18*, 1105–1117.
- (59) Mahmoudi, G.; Bauzá, A.; Gurbanov, A. V.; Zubkov, F. I.; Maniukiewicz, W.; Rodríguez-Diéguez, A.; López-Torres, E.; Frontera, A. The role of unconventional stacking interactions in the supramolecular assemblies of Hg(II) coordination compounds. *CrystEngComm* **2016**, *18*, 9056–9066.
- (60) Karmakar, M.; Basak, T.; Chattopadhyay, S. Phosphatase-mimicking activity of a unique penta-nuclear zinc(II) complex with a reduced Schiff base ligand: assessment of its ability to sense nitroaromatics. *New J. Chem.* **2019**, *43*, 4432–4443.
- (61) Karmakar, M.; Roy, S.; Chattopadhyay, S. A series of trinuclear zinc(II) complexes with reduced Schiff base ligands: turn-off fluorescent chemosensors with high selectivity for nitroaromatics. *New J. Chem.* **2019**, *43*, 10093–10102.
- (62) Mirdya, S.; Basak, T.; Chattopadhyay, S. Photocatalytic ability of two hetero-tetranuclear complexes with CuO₂Cd cores to degrade methylene blue: Influence of their structures on activity. *Polyhedron* **2019**, *170*, 253–263.
- (63) Addison, A. W.; Rao, T. N.; Reedijk, J.; van Rijn, J.; Verschoor, G. C. Synthesis, Structure, and Spectroscopic Properties of Copper(II) Compounds containing Nitrogen-Sulphur Donor Ligands; the Crystal and Molecular Structure of Aqua[1,7-bis(N-methylbenzimidazol-2'-yl)-2,6-dithiaheptane]copper(II) Perchlorate. *J. Chem. Soc., Dalton Trans.* **1984**, 1349–1356.
- (64) Wang, H.; Zhang, D.; Ni, Z.-H.; Li, X.; Tian, L.; Jiang, J. Synthesis, Crystal Structures, and Luminescent Properties of Phenoxo-Bridged Heterometallic Trinuclear Propeller- and Sandwich-Like Schiff-Base Complexes. *Inorg. Chem.* **2009**, *48*, 5946–5956.
- (65) Cremer, D.; Pople, J. A. A General Definition of Ring Puckering Coordinates. *J. Am. Chem. Soc.* **1975**, *97*, 1354–1358.
- (66) Cremer, D. On the correct usage of the Cremer-Pople puckering parameters as quantitative descriptors of ring shapes - a reply to recent criticism by Petit, Dillen and Geise. *Acta Crystallogr., Sect. B: Struct. Sci.* **1984**, *40*, 498–500.
- (67) Mautner, F.; Scherzer, M.; Berger, C.; Fischer, R. C.; Vicente, R.; Massoud, S. S. Synthesis and characterization of five new thiocyanate- and cyanato-metal(II) complexes with 4-azidopyridine as co-ligand. *Polyhedron* **2015**, *85*, 20–26.
- (68) Das, M.; Chatterjee, S.; Harms, K.; Mondal, T. K.; Chattopadhyay, S. Formation of bis(μ -tetrazolato)dinickel(II) complexes with N,N,O-donor Schiff bases via in situ 1,3-dipolar cyclo-additions: isolation of a novel bi-cyclic trinuclear nickel(II)-sodium(I)-nickel(II) complex. *Dalton Trans* **2014**, *43*, 2936–2947.
- (69) Roy, S.; Basak, T.; Khan, S.; Drew, M. G. B.; Bauzá, A.; Frontera, A.; Chattopadhyay, S. A Combined Experimental and Theoretical Study on the Formation of a Cyclic Tetrameric Water Cluster and a Similar Type of Cyclic Cluster in Copper(II) Schiff Base Complexes. *Chemistry Select* **2017**, *2*, 9336–9343.
- (70) Chattopadhyay, S.; Drew, M. G. B.; Ghosh, A. Methylene Spacer-Regulated Structural Variation in Cobalt(II/III) Complexes with Bridging Acetate and Salen- or Salpn-Type Schiff-Base Ligands. *Eur. J. Inorg. Chem.* **2008**, *2008*, 1693–1701.
- (71) Nakamoto, K. *Infrared and Raman Spectra of Organic and Coordination Compounds*, 3rd ed.; John Wiley and Sons: New York, 1978; p 227.
- (72) Bhowmik, P.; Harms, K.; Chattopadhyay, S. Formation of polynuclear copper(II)-sodium(I) heterometallic complexes derived from salen-type Schiff bases. *Polyhedron* **2013**, *49*, 113–120.
- (73) Agarwal, R. K.; Kumar, A. Synthesis, Physico-chemical and Biological Properties of Some Mixed Ligand Complexes of Trivalent Lanthanides with 4[N-4'-Dimethylamino-Benzalidene]Amino] anti-pyrene Thiosemicarbazone and Pyridine. *J. Appl. Chem. Res.* **2011**, *16*, 40–58.
- (74) Nazarov, M.; Noh, D. Y. *New Generation of Europium and Terbium-Activated Phosphors: From Syntheses to Applications*; Pan Stanford Publishing: Boca Raton, FL, 2011; p 211.
- (75) Roy, S.; Drew, M. G. B.; Bauzá, A.; Frontera, A.; Chattopadhyay, S. Estimation of conventional C-H $\cdots\pi$ (arene), unconventional C-H $\cdots\pi$ (chelate) and C-H $\cdots\pi$ (thiocyanate) interactions in hetero-nuclear nickel(II)-cadmium(II) complexes with a compartmental Schiff base. *Dalton Trans* **2017**, *46*, 5384–5397.
- (76) Bhattacharyya, A.; Bhaumik, P. K.; Jana, P. P.; Chattopadhyay, S. Anion mediated diversity in the nuclearity of nickel(II) complexes with a N₂O donor Schiff base: Formation of a supra-molecular chain via Br \cdots Br interactions. *Polyhedron* **2014**, *78*, 40–45.
- (77) Mahmoudi, G.; Bauzá, A.; Frontera, A. Concurrent agostic and tetrel bonding interactions in lead(II) complexes with an isonicotinohydrazide based ligand and several anions. *Dalton Trans* **2016**, *45*, 4965–4969.
- (78) Mustapha, A.; Busch, K.; Patykiewicz, M.; Apedaile, A.; Reglinski, J.; Kennedy, A. R.; Prior, T. J. Multidentate ligands for the synthesis of multi-metallic complexes. *Polyhedron* **2008**, *27*, 868–878.
- (79) Bauzá, A.; Seth, S. K.; Frontera, A. Tetrel bonding interactions at work: Impact on tin and lead coordination compounds. *Coord. Chem. Rev.* **2019**, *384*, 107–125.
- (80) Mahmoudi, G.; Safin, D. A.; Mitoraj, M. P.; Amini, M.; Kubicki, M.; Doert, T.; Locherer, F.; Fleck, M. Anion-driven tetrel bond-

induced engineering of lead(II) architectures with N'-(1-(2-pyridyl)-ethylidene)nicotinohydrazide: experimental and theoretical findings. *Inorg. Chem. Front.* **2017**, *4*, 171–182.

(81) Mahmoudi, G.; Bauzá, A.; Frontera, A. Concurrent agostic and tetrel bonding interactions in lead(II) complexes with an isonicotinohydrazide based ligand and several anions. *Dalton Trans* **2016**, *45*, 4965–4969.



Photocatalytic ability of two hetero-tetranuclear complexes with CuO₂Cd cores to degrade methylene blue: Influence of their structures on activity

Saikat Mirdya, Tanmoy Basak, Shouvik Chattopadhyay*

Department of Chemistry, Inorganic Section, Jadavpur University, Kolkata 700032, India

ARTICLE INFO

Article history:

Received 4 February 2019

Accepted 21 May 2019

Available online 31 May 2019

Keywords:

Compartmental reduced Schiff base

Hetero-tetranuclear complexes

Copper(II)

Cadmium(II)

Photocatalytic degradation

ABSTRACT

Two centrosymmetric hetero-tetranuclear copper(II)/cadmium(II) complexes, $(\mu_{1,1}-N_3)_2[(H_2O)Cu(L^R)Cd(N_3)]_2 \cdot 2CH_3OH$ (**1**) and $(\mu_{1,1}-NCS)_2[CuL^R Cd(SCN)]_2 \cdot 2CH_3OH$ (**2**), have been prepared with a compartmental reduced Schiff base ligand, $H_2L^R = 2,2'-[(2,2\text{-dimethyl-1,3-propanediyl})bis(iminomethylene)]bis[6\text{-methoxyphenol}]$. Both complexes have been characterized elemental and spectral analyses. Structures of both complexes have been confirmed by single crystal X-ray diffraction technique. Both complexes contain CuO₂Cd cores. Here the bridging mode of azide and thiocyanate is quite different. Complex **1** contains $\mu_{1,1}$ -azide bridges between two cadmium(II) centres whereas in complex **2**, $\mu_{1,1}$ -thiocyanate bridges occur between copper(II) and cadmium(II) centres. The ability of both complexes to be used as photocatalyst in degrading methylene blue (MB) has been explored. The difference in photocatalytic performance may be correlated with their structures. Complex **1** shows better catalytic activity compared to complex **2**, and can degrade almost 62% MB in 18 min. Comparative IR studies (before and after the photocatalytic degradation process) confirmed the stability of both catalysts.

© 2019 Elsevier Ltd. All rights reserved.

1. Introduction

Different groups of coordination chemists were synthesizing varieties of homo and hetero polynuclear complexes of transition and non-transition metals with salen type di-Schiff base ligands (prepared by the condensation of several diamines with salicylaldehyde) for long [1–5]. In this method, the ability of phenoxo oxygen atoms of salicylaldehyde Schiff bases was utilized to bridge different metal centres [6–11]. Our group was also engaged in the synthesis and characterization of such complexes [12–14]. Several ‘half salen’ type mono-condensed Schiff bases have also been used to prepare such complexes [15–18]. Ability of many of these complexes in mimicking several enzymes, e.g. phosphatase, phenoxazinone synthase, catechol oxidase etc was investigated [19–25]. Opto-electronic properties of few such complexes were explored [26,27]. Few complexes were found effective to degrade methylene blue under visible light irradiation [28–30]. The denticity of these ‘salen’ type Schiff bases may be increased by using 3-alkoxysalicylaldehyde instead of salicylaldehyde [31–33]. In this method, ‘salen’ type hexadentate N₂O₄ donor compartmental Schiff bases were produced affording a facile synthetic route to multimetallic

complexes with greater ease. N,N'-bis(3-methoxysalicylidene)-2,2-dimethylpropane-1,3-diamine is a well known compartmental Schiff base, containing inner N₂O₂ and outer O₄ compartments. Synthetic inorganic chemist used this ligand to prepare heterometallic complexes [34–37]. Usually, transition metals are placed in the inner N₂O₂ compartment as their radii matches well with the radius of this compartment. On the other hand, non-transition metals of larger size usually fit well in the outer O₄ compartment [38–42].

In this work, we have reduced the Schiff base ligand with borohydride to get a more flexible reduced Schiff base ligand which was then used to prepare tetranuclear heterometallic copper(II)/cadmium(II) complexes, $(\mu_{1,1}-N_3)_2[(H_2O)Cu(L^R)Cd(N_3)]_2 \cdot 2CH_3OH$ (**1**) and $(\mu_{1,1}-NCS)_2[CuL^R Cd(SCN)]_2 \cdot 2CH_3OH$, where $H_2L^R = 2,2'-[(2,2\text{-dimethyl-1,3-propanediyl})bis(iminomethylene)]bis[6\text{-methoxyphenol}]$. Both complexes were characterized with single crystal X-ray diffraction analysis. Both complexes could be used as photo-catalyst to degrade methylene blue under visible light irradiation, although complex **1** was found to be better catalyst than complex **2**. Methylene blue is an organic dye pollutant released by textile industries and it is necessary to destroy methylene blue from industrial waste to minimize environmental pollution [43–45]. A probable mechanistic pathway for the photocatalytic degradation of the organic dye by these complexes has been

* Corresponding author.

E-mail address: shouvik.chem@gmail.com (S. Chattopadhyay).

proposed. The difference in their photocatalytic performance has also been correlated with their structures.

2. Experimental

All starting materials and solvents were commercially available, reagent grade, and used as purchased from Sigma-Aldrich without further purification.

Caution!!! Although no problem was encountered in this work, azide complexes are potentially explosive. Only a small amount of the materials should be prepared and they must be handled with care.

2.1. Preparation

2.1.1. Preparation of the ligand, 2,2'-[(2,2-dimethyl-1,3-propanediyl)bis(iminomethylene)]bis[6-methoxy-Phenol] (H_2L^R)

A hexadentate Schiff base ligand, H_2L^R [N,N'-Bis(3-hydroxysalicylidene)-2,2-dimethyl-1,3-propanediamine], was synthesized by refluxing of 2,2-dimethyl-1,3-propanediamine (0.2 mL, 2 mmol) with 3-methoxysalicylaldehyde (~610 mg, 4 mmol) in methanol solution (10 mL) for ca. 2 h. The Schiff base was not purified but used directly for the preparation of the reduced Schiff base ligand, H_2L^R . The methanol solution (10 mL) was then cooled to 0 °C and solid sodium borohydride (8 mmol, 310 mg) was added to it slowly with constant stirring. Then the resulting solution was acidified with glacial acetic acid (2 mL) and stirred for 10 minutes. The solution was evaporated to dryness under reduced pressure in a rotary evaporator (~60 °C). The residue was dissolved in water (15 mL) and extracted with dichloromethane (15 mL). The organic phase was dried over anhydrous sodium acetate and the solvent i.e. dichloromethane was evaporated under reduced pressure using a rotary evaporator to give the reduced Schiff base ligand, H_2L^R .

2.1.2. Preparation of the complex $(\mu_{-1,1-N_3})_2[(H_2O)Cu(L^R)Cd(N_3)]_2 \cdot 2CH_3OH$ (**1**)

A methanol solution (5 mL) of copper(II) acetate monohydrate (~400 mg, 2 mmol) was added to the methanol solution (10 mL) of the reduced Schiff base ligand H_2L^R , with constant stirring. A methanol (10 mL) solution of cadmium(II) acetate dihydrate (~540 mg, 2 mmol) was then added to it and the stirring was continued for about 2 h. A methanol–water (2:1) solution (10 mL) of sodium azide (260 mg, 4 mmol) was added and the resulting mixture was refluxed for ca. 2 h. Crystalline product was obtained after few days on very slow evaporation. Single crystals, suitable for X-ray diffraction, were isolated from the crystalline product.

Yield. 914 mg (~67%) based on copper(II). **Anal.** Calc. for $C_{44}H_{68}Cd_2Cu_2N_{16}O_{12}$ (FW: 1365.06): C, 39.88; H, 4.46; N, 17.72. Found: C, 39.7; H, 4.3; N, 17.9%. FT-IR (KBr, cm^{-1}): 3412 (ν_{O-H}), 3246–3166 (ν_{N-H}), 2972–2835 (ν_{C-H}), 2060 ($\nu_{\mu-1,1-N_3}$), 2035 (ν_{N_3}). UV–Vis, λ_{max} (nm), [ϵ_{max} (L mol $^{-1}$ cm $^{-1}$)] (DMF): 242 (1.5×10^4), 280 (7.9×10^3), 336 (8.9×10^2), 414 (1.0×10^3), 591 (2.2×10^2).

2.1.3. Preparation of the complex $(\mu_{-1,1-NCS})_2[CuL^RCd(SCN)]_2 \cdot 2CH_3OH$ (**2**)

Complex **2** was prepared in a similar method to that of complex **1**, except that sodium thiocyanate (~330 mg, 4 mmol) was added instead of sodium azide. Crystalline product was obtained after few days on very slow evaporation. Single crystals, suitable for X-ray diffraction, were isolated from the crystalline product.

Yield. 905 mg (~65%) based on copper(II). **Anal.** Calc. for $C_{48}H_{64}Cd_2Cu_2N_8O_{10}S_4$ (FW: 1393.23): C, 41.57; H, 4.25; N, 8.43. Found: C, 41.3; H, 4.1; N, 8.6%. FT-IR (KBr, cm^{-1}): 3220–3145 (ν_{N-H}),

2972–2835 (ν_{C-H}), 2081 ($\nu_{\mu-1,1-NCS}$), 2017 (ν_{SCN}). UV–Vis, λ_{max} (nm), [ϵ_{max} (L mol $^{-1}$ cm $^{-1}$)] (DMF): 240 (1.8×10^4), 280 (1.0×10^4), 336 (1.1×10^3), 410 (1.3×10^3), 595 (2.7×10^2).

2.2. Physical measurement

Elemental analysis (carbon, hydrogen and nitrogen) was performed using a Perkin-Elmer 240C elemental analyzer. IR spectra in KBr (4500–500 cm^{-1}) were recorded with a Perkin-Elmer Spectrum Two spectrophotometer. Electronic spectra were recorded on a JASCO J-630 spectrophotometer.

2.3. X-ray crystallography

Suitable crystals of both complexes were used for data collection using a 'Bruker D8 QUEST area detector' diffractometer equipped with graphite-monochromated Mo K_{α} radiation ($\lambda = 0.71073$ Å). The molecular structures were solved by direct method and refined by full-matrix least squares on F^2 using the SHELXL-18/1 package [46]. Non-hydrogen atoms were refined with anisotropic thermal parameters. The hydrogen atoms attached to nitrogen and oxygen atoms were located by difference Fourier maps and were kept at fixed positions. All other hydrogen atoms were placed in their geometrically idealized positions and constrained to ride on their parent atoms. Multi-scan empirical absorption corrections were applied to the data using the program SADABS [47]. The details of crystallographic data and refinements have been given in Table 1. Important bond lengths and angles have been listed in Tables 2 and 3, respectively.

2.4. Photocatalytic measurement

The photocatalytic experiment in aqueous solution has been carried out in usual process [48]. The catalytic degradation has been carried out separately with 100 mL of Methylene Blue (MB) solution (20 mg L $^{-1}$) with the complex using as catalyst. The mixture has been stirred for 10 min in a dark environment to get a balance between adsorption and desorption. The solution has been then stirred constantly. A 3 mL sample has been taken from the reaction system in an interval of 3 min and the supernatant liquid obtained by centrifugation has been used for collecting the UV–Vis spectrum. The characteristic peak for methylene blue (~600 nm) has been employed to monitor the photocatalytic degradation.

Table 1
Crystal data and refinement details of complexes **1** and **2**.

Complex	1	2
Formula	$C_{44}H_{68}Cd_2Cu_2N_{16}O_{12}$	$C_{48}H_{64}Cd_2Cu_2N_8O_{10}S_4$
Formula weight	1365.06	1393.23
<i>T</i> (K)	273	273
Crystal system	monoclinic	triclinic
Space group	$P2_1/c$	$P\bar{1}$
<i>a</i> (Å)	10.5544(9)	11.6584(13)
<i>b</i> (Å)	18.0146(14)	11.6797(12)
<i>c</i> (Å)	15.1340(11)	12.7556(14)
α	90	108.983(3)
β	103.804(2)	99.804(3)
γ	90	116.542(3)
<i>Z</i>	2	1
<i>D</i> _{calc} (g cm $^{-3}$)	1.622	1.697
μ (mm $^{-1}$)	1.573	1.755
<i>F</i> (0 0 0)	1388	706
Total reflections	31 902	15 213
Unique reflections	5032	4851
Observed data [<i>I</i> > 2 σ (<i>I</i>)]	4343	4271
No. of parameters	353	347
<i>R</i> _{int}	0.030	0.044
<i>R</i> ₁ , <i>wR</i> ₂ (all data)	0.0437, 0.1294	0.0499, 0.1360

Table 2
Selected bond lengths (Å) of complexes **1** and **2**.

Complex	1	2
Cd(1)–O(1)	2.287(3)	2.256(3)
Cd(1)–O(2)	2.307(3)	2.262(2)
Cd(1)–O(3)	2.471(4)	2.511(3)
Cd(1)–O(4)	2.472(4)	2.496(4)
Cd(1)–N(3)	2.354(5)	2.201(5)
Cu(1)–O(1)	1.956(3)	1.964(3)
Cu(1)–O(2)	1.953(3)	1.968(4)
Cu(1)–N(1)	2.028(4)	2.022(4)
Cu(1)–N(2)	2.032(4)	2.017(4)
Cd(1)–N(6)	2.259(5)	—
Cd(1)–N(3')	2.341(4)	—
Cu(1)–O(5)	2.317(4)	—
Cd(1)–S(1)	—	2.636(2)
Cu(1)–N(3')	—	2.626(5)

Symmetry transformation: $'=1-x, 1-y, 1-z$.**Table 3**
Selected bond angles (°) of complexes **1** and **2**.

Complex	1	2
O(1)–Cd(1)–O(2)	66.46(10)	66.97(10)
O(1)–Cd(1)–O(3)	67.19(15)	68.20(9)
O(1)–Cd(1)–O(4)	132.15(11)	134.87(10)
O(1)–Cd(1)–N(3)	90.02(12)	136.20(14)
O(2)–Cd(1)–O(3)	133.63(14)	135.15(11)
O(2)–Cd(1)–O(4)	66.41(11)	67.98(12)
O(2)–Cd(1)–N(3)	85.43(13)	136.67(15)
O(3)–Cd(1)–O(4)	158.23(15)	156.56(11)
O(3)–Cd(1)–N(3)	95.93(16)	80.21(13)
O(4)–Cd(1)–N(3)	94.09(16)	81.70(14)
O(1)–Cu(1)–O(5)	99.67(18)	78.70(13)
O(1)–Cu(1)–N(1)	90.59(15)	91.68(14)
O(1)–Cu(1)–N(2)	165.34(13)	170.44(16)
O(2)–Cu(1)–N(1)	168.94(13)	169.80(12)
O(2)–Cu(1)–N(2)	92.04(14)	92.07(14)
O(1)–Cd(1)–N(6)	96.86(12)	—
O(1)–Cd(1)–N(3')	143.99(14)	—
O(2)–Cd(1)–N(6)	100.24(15)	—
O(2)–Cd(1)–N(3')	141.12(15)	—
O(3)–Cd(1)–N(6)	83.85(18)	—
O(3)–Cd(1)–N(3')	82.14(18)	—
O(4)–Cd(1)–N(6)	83.69(17)	—
O(4)–Cd(1)–N(3')	82.05(14)	—
N(3)–Cd(1)–N(6)	172.41(13)	—
N(3)–Cd(1)–N(3')	74.31(15)	—
N(3')–Cd(1)–N(6)	98.17(15)	—
O(1)–Cu(1)–O(2)	80.15(13)	—
O(2)–Cu(1)–O(5)	92.80(15)	—
O(5)–Cu(1)–N(1)	94.72(16)	—
O(2)–Cu(1)–N(2)	92.04(14)	—
N(1)–Cu(1)–N(2)	95.65(15)	97.37(16)
S(1)–Cd(1)–O(1)	—	101.08(11)
S(1)–Cd(1)–O(2)	—	101.46(10)
S(1)–Cd(1)–O(3)	—	85.74(9)
S(1)–Cd(1)–O(4)	—	85.09(10)
S(1)–Cd(1)–N(3)	—	106.13(13)
O(1)–Cu(1)–N(3')	—	88.88(13)
O(2)–Cu(1)–N(3')	—	89.83(15)
N(1)–Cu(1)–N(3')	—	93.41(16)
N(2)–Cu(1)–N(3')	—	93.63(14)
O(5)–Cu(1)–N(2)	93.04(18)	—

Symmetry transformation: $'=1-x, 1-y, 1-z$.

3. Results and discussion

3.1. Synthesis

2,2-Dimethyl-1,3-diaminopropane was refluxed with 3-methoxysalicylaldehyde in a 1:2 ratio to form a N_2O_4 donor compartmental Schiff base ligand, H_2L , following a literature method and $NaBH_4$ was used as a reducing agent to prepare reduced Schiff

base ligand (H_2L^R) [49,50]. This reduced Schiff base (H_2L^R) on reaction with copper(II) acetate monohydrate followed by the addition of cadmium(II) acetate dihydrate and sodium azide in methanol gave rise to complex **1**. The complex **2** was synthesized in similar method to that of complex **1**, except that sodium thiocyanate is used instead of sodium azide. Synthetic route to the formation of both complexes **1** and **2** have been shown in Scheme 1.

3.2. Description of structures

3.2.1. $(\mu_{1,1}-N_3)_2[(H_2O)Cu(L^R)Cd(N_3)]_2 \cdot 2CH_3OH$ (**1**)

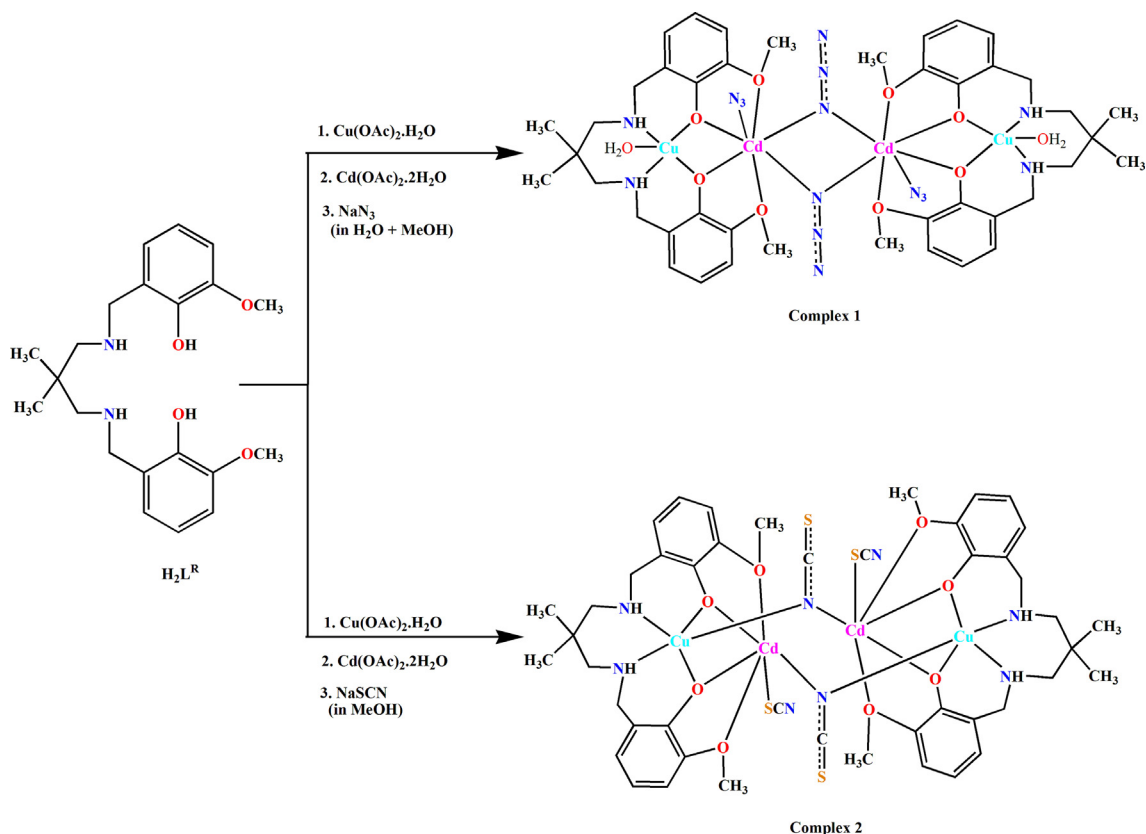
Structure determination reveals that complex **1** crystallizes in the monoclinic space group $P2_1/c$. The complex is a centrosymmetric zigzag tetramer and is build up of two dinuclear units, $[(H_2O)Cu(L^R)Cd(N_3)]$, connected through two end-on azide bridges. A perspective view of the complex with selective atom numbering scheme has been shown in Fig. 1. In the asymmetric unit, the copper(II) centre, Cu(1), and cadmium(II) centre, Cd(1), respectively occupy the inner N_2O_2 and outer O_4 sites of a potential compartmental reduced Schiff base H_2L^R , with a Cu(1)···Cd(1) distance of 3.378(6) Å.

Copper(II) centre is penta-coordinated being bonded to two amine nitrogen atoms, N(1) and N(2), and two phenoxo oxygen atoms, O(1) and O(2), of the deprotonated reduced Schiff base ligand, $(L^R)^{2-}$ and one oxygen atom, O(5), from a coordinated water molecule. The geometry of any penta-coordinated metal centre may conveniently be measured by the Addison parameter (τ) [51]. The geometry of copper(II) centre is slightly distorted square pyramidal with $\tau = 0.06$ ($\tau = 0$ indicates perfect square pyramid). On the other hand, cadmium(II) centre, Cd(1), is hepta-coordinated and its geometry is distorted pentagonal bipyramidal. Cd(1) is coordinated by two phenoxo oxygen atoms, O(1) and O(2), two methoxy oxygen atoms, O(3) and O(4), and one nitrogen atom, N(3), of an end-on bridging azide, which constitute the pentagonal plane. The sixth site is occupied by a nitrogen atom, N(6), from a terminal azide. The seventh coordination site is occupied by another nitrogen atom, N(3), from an end-on bridging azide, which bridges Cd(1) and its symmetry $\{'=1-x, 1-y, 1-z\}$ related counterpart, Cd(1'). The saturated six-membered chelate ring $[Cu(1)-N(1)-C(9)-C(10)-C(13)-N(2)]$ has envelope conformation with puckering parameters, $q = 0.523(6)$ Å; $\theta = 23.0(5)^\circ$; $\phi = 177.6(14)^\circ$ [52,53].

3.2.2. $(\mu_{1,1}-NCS)_2[Cu(L^R)Cd(SCN)]_2 \cdot 2CH_3OH$ (**2**)

Complex **2** crystallizes in triclinic space group, $P\bar{1}$. It is basically a centrosymmetric cyclic tetramer with $[-Cd-(\mu_{1,1}-NCS)CuO_2Cd(\mu_{1,1}-NCS)-Cu-]$ core, in which two hetero-dinuclear $[CuL^RCd(SCN)]$ units are linked through two end-on thiocyanate bridges. A perspective view with selective atom numbering scheme has been shown in Fig. 2. Cu(1)···Cd(1') {symmetry transformation $'=1-x, 1-y, 1-z$ } distance in the tetrameric unit is 3.617(9) Å.

Copper(II) centre, Cu(1), is square pyramidal being coordinated equatorially by two amine nitrogen atoms, N(1) and N(2), and two phenoxo oxygen atoms, O(1) and O(2), of the deprotonated reduced Schiff base, $(L^R)^{2-}$. The fifth position is occupied by a nitrogen atom, N(3'), of the bridging thiocyanate. The square pyramidal geometry of copper(II) centre is confirmed by τ , here $\tau = 0.01$ [51]. On the other hand, the coordination geometry of cadmium(II) centre, Cd(1), is distorted octahedral, where two phenoxo oxygen atoms, O(1) and O(2), and two methoxy oxygen atoms, O(3) and O(4), of the reduced Schiff base ligand constitute the equatorial plane. One axial site is occupied by a sulfur atom, S(1), from terminal thiocyanate and another axial site is occupied by nitrogen atom, N(3), from thiocyanate which acts as a bridge between the cadmium(II) centre, Cd(1) and the symmetry related copper(II)



Scheme 1. Synthetic route to complexes **1** and **2**.

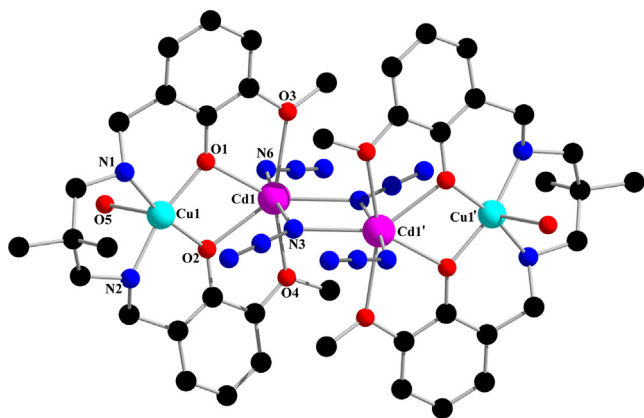


Fig. 1. Perspective view of complex **1** with selective atom numbering. Hydrogen atoms and the lattice methanol molecule have been omitted for clarity.

centre, $Cu(1')$. The saturated six-membered chelate ring [$Cu(1)-N(1)-C(9)-C(10)-C(13)-N(2)$] has envelope conformation with the puckering parameters, $q = 0.524(6)$ Å; $\theta = 148.2(5)^\circ$; $\phi = 2.6(11)^\circ$ [52,53].

3.3. Comparison of structures of **1** and **2**

It is interesting to note here that in complex **1**, cadmium(II) centre of one asymmetric unit is connected with a cadmium(II) centre of a symmetry related counterpart via end-on azide bridges. This makes the copper(II) centres free to be used in any catalytic reaction. On the other hand, cadmium(II) centre of one asymmetric unit in complex **2** is connected with a copper(II) centre of a sym-

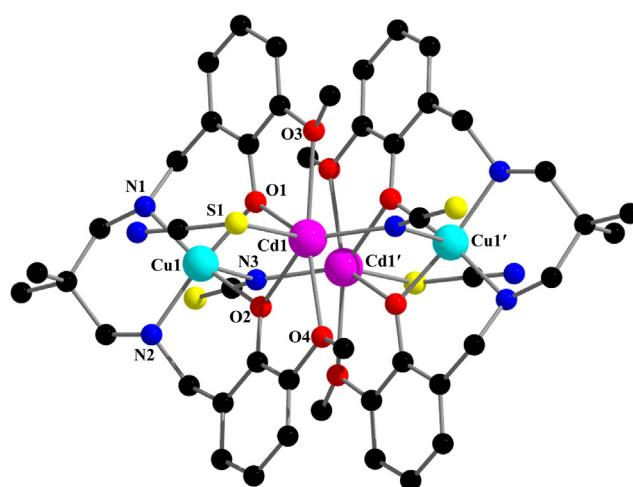


Fig. 2. Perspective view of complex **2** with selective atom numbering. Hydrogen atoms and the lattice methanol molecule have been omitted for clarity.

metry related dinuclear unit via end-on thiocyanate bridges. Thus both copper(II) and cadmium(II) are confined in a cyclic tetrameric unit, making copper(II) less available to take part any catalytic reaction.

3.4. Supramolecular interactions

Solid state structures of both complexes are stabilized through significant non-covalent interactions such as hydrogen bonding and $C-H \cdots \pi$. Complex **1** shows five significant hydrogen bonding interactions. The hydrogen atom, $H(1)$, attached to amine nitrogen

atom, N(1), involve in hydrogen bonding interaction with the symmetry related ($x, 1.5 - y, -0.5 + z$) oxygen atom, O(6ⁱ), of the lattice methanol molecule. Another hydrogen atom, H(5C), attached to oxygen atom, O(5), of coordinated water molecule participate in hydrogen bonding interaction with the symmetry related ($1 - x,$

$1/2 + y, 3/2 - z$) azide nitrogen atom N(8ⁱ). These two intermolecular hydrogen bonding interactions form a two dimensional layer structure. On the other hand, the oxygen atom, O(6), of the lattice methanol molecule forms hydrogen bond with the hydrogen atom, H(5D), attached with the oxygen atom, O(5), of the coordinated

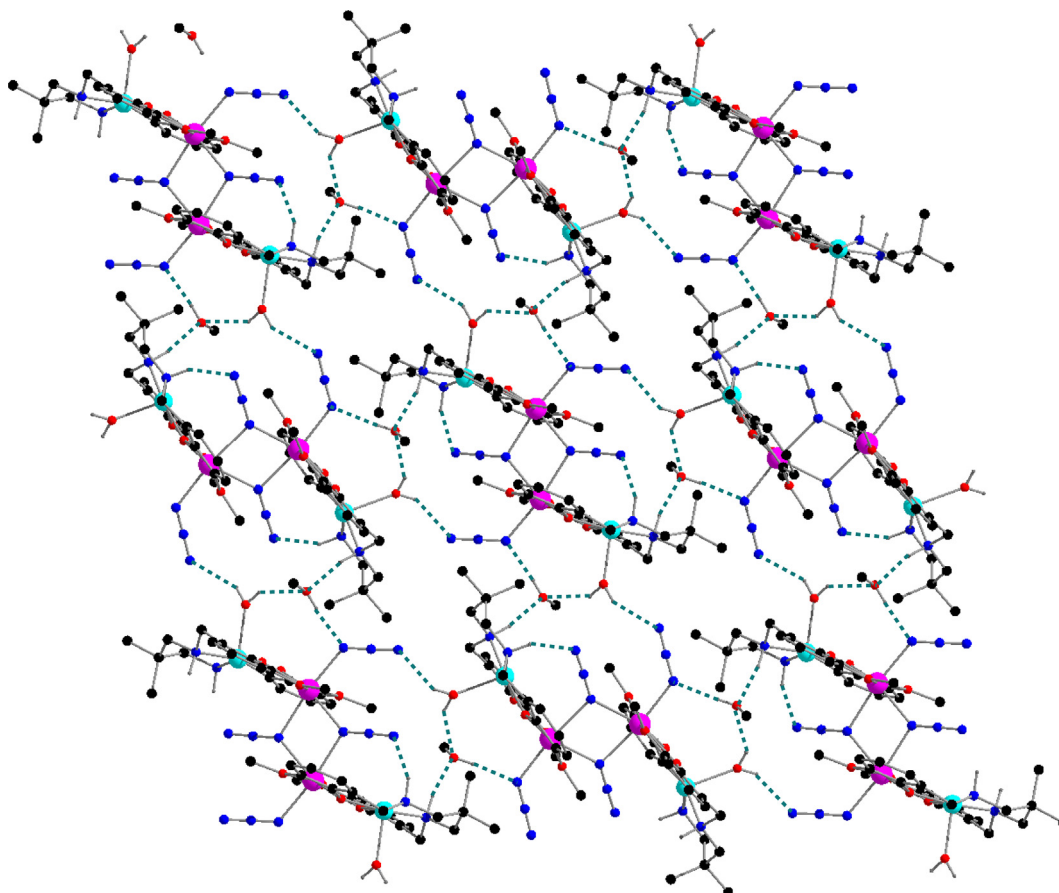


Fig. 3. Hydrogen bonded layer structure of complex 1. Only the relevant hydrogen atoms have been shown.

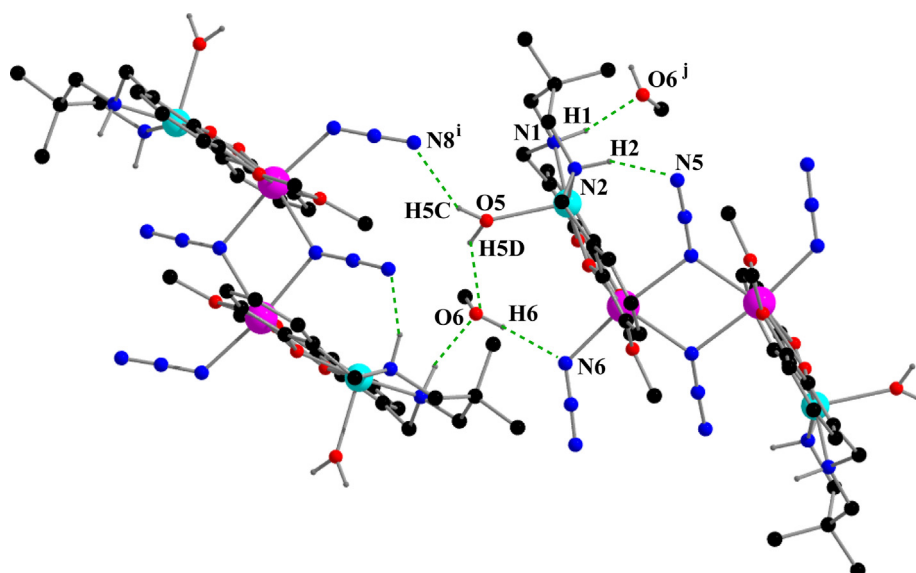


Fig. 4. Selected small part of hydrogen bonded structure of complex 1. Only the relevant hydrogen atoms have been shown. Symmetry transformation ⁱ = $x, 1.5 - y, 0.5 + z$, ^j = $1 - x, 0.5 + y, 1.5 - z$.

water molecule. Again, hydrogen atom, H(6), of the same lattice methanol molecule, forms an additional hydrogen bond with azide nitrogen atom, N(6). Another hydrogen atom, H(2), attached to amine nitrogen atom N(2), participates in hydrogen bond formation with the azide nitrogen atom, N(5). Two dimensional layer structure of the complex has been shown in Fig. 3 and selected small part of the two dimensional structure of hydrogen bonding has been shown in Fig. 4. Details of the hydrogen bonding interactions have been given in Table 4.

The hydrogen atom, H(22A), attached to the carbon atom, C(22), of the lattice methanol molecule, is involved in a C–H... π interaction with the symmetry related ($x, 1.5 - y, 0.5 + z$) phenyl ring [C(2)–C(3)–C(4)–C(5)–C(6)–C(7)]. Two dimensional layer structure of C–H... π interaction has been shown in Fig. 5 and selected small part of C–H... π interaction with specific atom numbering has been shown in Fig. 6. Details of the geometric feature of the C–H... π interaction have been given in Table 5.

Table 4
Hydrogen bond distances (Å) and angles (°) of complexes **1** and **2**.

Complex	D–H...A	D–H	H...A	D...A	\angle D–H...A
1	N(1)–H(1)–O(6 ⁱ)	0.9800	2.0800	3.039(5)	167.00
	N(2)–H(2)–N(5)	0.9800	2.4800	3.182(6)	129.00
	O(6)–H(6)–N(6)	0.8200	2.0200	2.831(5)	169.00
	O(5)–H(5C)–N(8)	0.88(9)	2.20(9)	2.926(8)	140(7)
	O(5)–H(5D)–O(6)	0.82(8)	2.22(10)	2.915(7)	143(10)
2	N(2)–H(2N)–O(5)	0.87(6)	2.16(6)	3.027(9)	171(5)

Symmetry transformation: ⁱ = $x, 1.5 - y, 0.5 + z$.

Three types of supramolecular interactions have been observed in complex **2** (H-bonding, C–H... π and π ... π interactions). The hydrogen atom, H(2N), attached to amine nitrogen atom, N(2), of the reduced Schiff base is engaged in intramolecular hydrogen bonding interaction with the same symmetry related oxygen atom, O(5), of lattice methanol molecule, as shown in Fig. 7. Details of the hydrogen bonding interaction have been gathered in Table 4.

The hydrogen atom, H(24B), attached to the carbon atom, C(24), of lattice methanol molecule is involved in the C–H... π interaction with a phenyl ring [C(15)–C(16)–C(17)–C(18)–C(19)–C(20)]. The C–H... π interaction of the complex has been shown in Fig. 8. Detail of the C–H... π interaction has been given in Table 5. Complex **2** shows a significant π ... π stacking interaction (Fig. 9) between an aromatic ring [C(2)–C(3)–C(4)–C(5)–C(6)–C(7)] with a symmetry-related ($1 - x, 1 - y, 1 - z$) aromatic ring [C(15)–C(16)–C(17)–C(18)–C(19)–C(20)]. Details of the π ... π interaction have been given in Table 6.

3.5. Hirshfeld surfaces analysis

The Hirshfeld surfaces of both complexes mapped over d_{norm} (range -0.1 Å to 1.5 Å), shape index and curvedness have been shown in Fig. 10. Red spots on these surfaces denote the dominant interactions. Analysis of Hirshfeld surfaces indicates that there are interactions mainly between nitrogen and hydrogen atoms in complex **1**, whereas, there are significant interactions between sulphur and hydrogen atoms in complex **2**. Other visible spots in Hirshfeld surfaces correspond to C...H and H...H contacts.

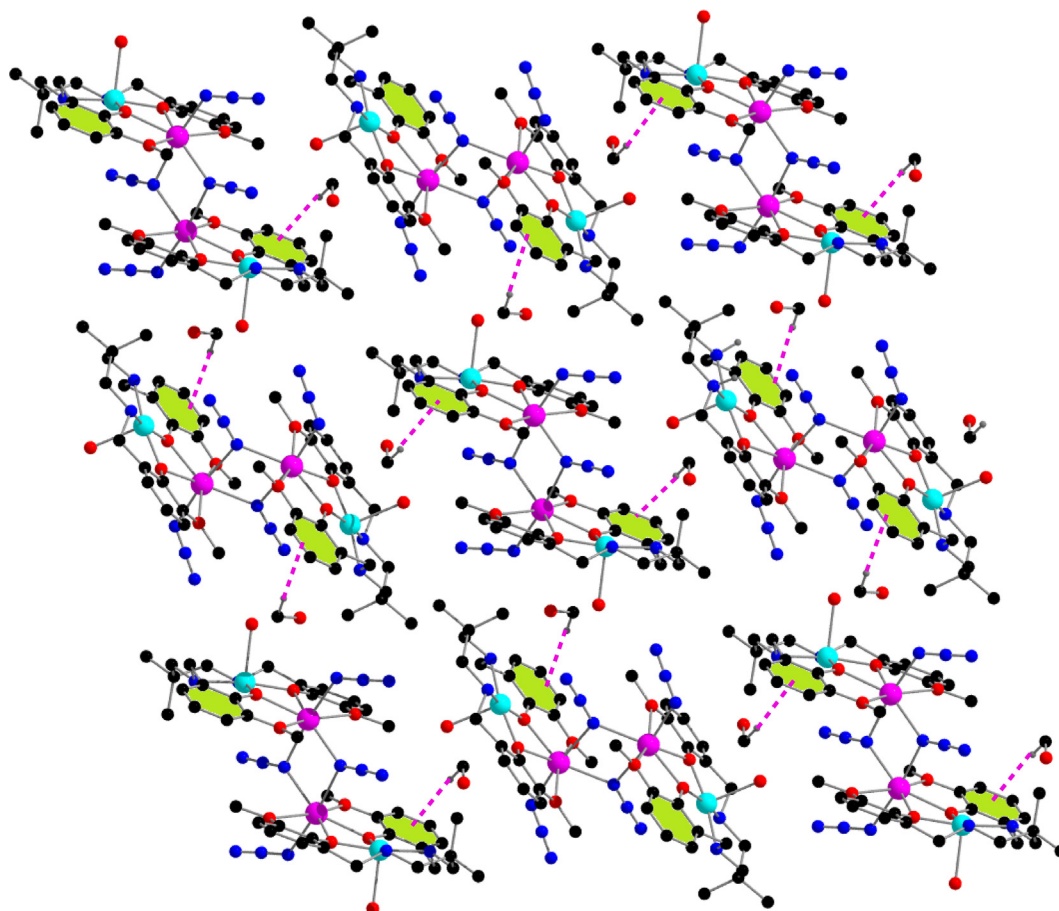


Fig. 5. Two dimensional supramolecular C–H... π interactions in complex **1**. Only the relevant hydrogen atoms have been shown for clarity. Symmetry transformation: [#] = $x, 1.5 - y, 0.5 + z$.

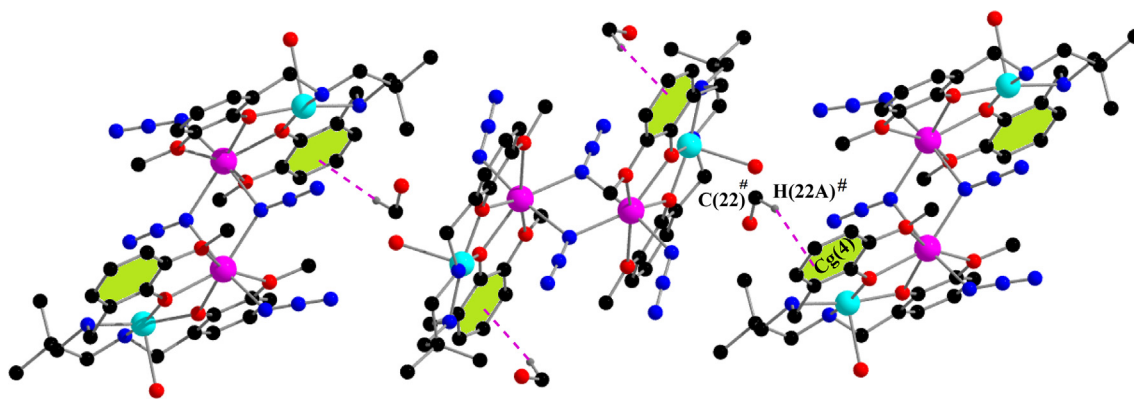


Fig. 6. Selected small part of C—H... π interactions of complex **1**. Only the relevant hydrogen atoms have been shown. Symmetry transformation $\# = x, 1.5 - y, 0.5 + z$.

Table 5

Geometric features (distances in Å and angles in °) of the C—H...Cg interactions for complex **1** and **2**.

Complex	C—H...Cg (Ring)	H...Cg (Å)	C—H...Cg (°)	C...Cg (Å)	Symmetry
1	C(22)–H(22A)...Cg(4) $\#$	2.89	164	3.825(9)	$x, 3/2 - y, 1/2 + z$
2	C(24)–H(24B)...Cg(8)	2.85	125	3.499(11)	x, y, z

Symmetry transformation: $\# = x, 1.5 - y, 0.5 + z$. Cg(4) = centre of gravity of the ring [C(2)–C(3)–C(4)–C(5)–C(6)–C(7)] and Cg(8) = centre of gravity of the ring [C(15)–C(16)–C(17)–C(18)–C(19)–C(20)].

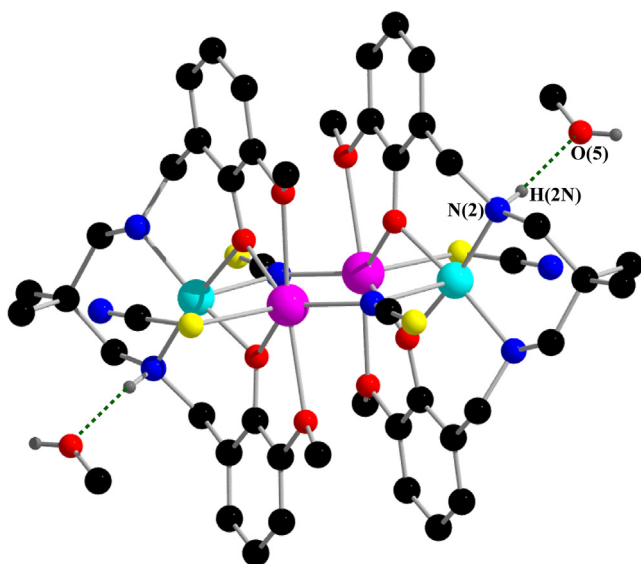


Fig. 7. Hydrogen bonding structure of complex **2** with lattice methanol molecule. Only the relevant hydrogen atoms have been shown.

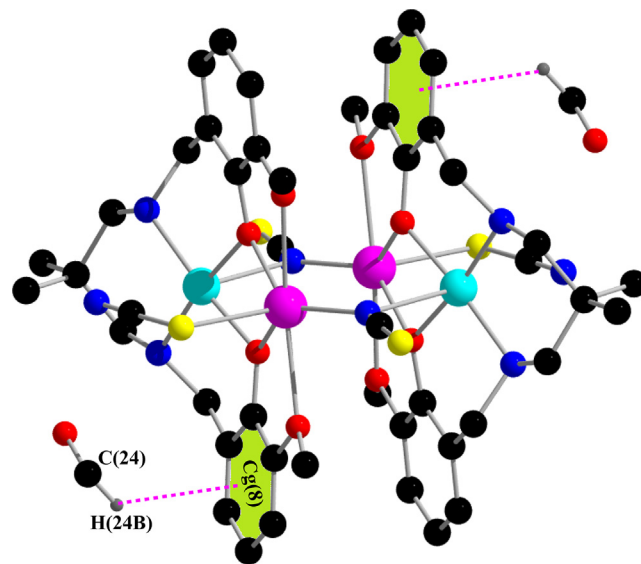


Fig. 8. C—H... π interaction of complex **2** with lattice methanol molecule. Only the relevant hydrogen atoms have been shown.

The intermolecular interactions appear as distinct spikes in the 2D fingerprint plot (Fig. S1).

3.6. IR and electronic spectra

In the IR spectrum of complex **1**, a sharp peak at 2060 cm^{-1} and an associated small peak at 2036 cm^{-1} indicate the presence of bridging and terminal azides [54–56]. In IR spectrum of complex **2**, there are two successive strong peaks observed at 2081 and 2017 cm^{-1} , indicating the presence of terminal (S-bonded) and end-on bridged thiocyanates (N-bonded), respectively [57]. A moderately strong band due to stretching vibration of N—H bond appears around $3213\text{--}3166\text{ cm}^{-1}$ for both complexes [58]. A broad peak around 3412 cm^{-1} indicates the presence of coordinating

water molecule in complex **1** [59]. Bands near the range of $2972\text{--}2835\text{ cm}^{-1}$ are due to alkyl C—H bond stretching vibrations, which are customarily noticed in the IR spectra of both complexes [60]. The IR spectra of both complexes have been shown in Fig. S2 (Electronic Supplementary Information, ESI).

Electronic spectrum of each complex in DMF displays one absorption band in the visible region around 590 nm which may be considered as ${}^2T_{2g}(\text{D}) \leftarrow {}^2E_g(\text{D})$ transition for copper(II) [34,59]. Bands around 410 nm (407 nm for complex **1** and 414 nm for complex **2**) may be attributed to LMCT transition from the N donor centres of Schiff base to copper(II) [61,62]. Another bands around 335 nm (for both **1** and **2**) may be attributed to LMCT transition from the O donor centres of Schiff base to cadmium(II) [63]. The high intensity band occur at 242 (for **1**) and 240 (for **2**)

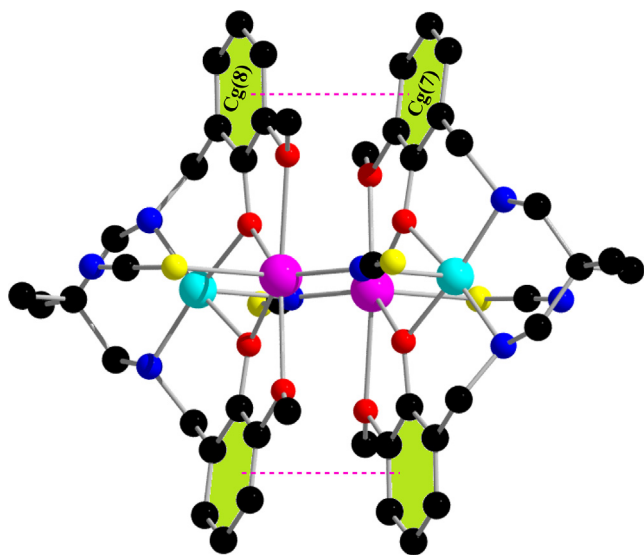


Fig. 9. Intramolecular $\pi \cdots \pi$ stacking interactions in complex 2. Hydrogen atoms and lattice methanol molecules have been omitted for clarity.

nm is attributed to $\pi \rightarrow \pi^*$ transition of the ligand. Another intense band observe in the region of 275–285 is correspond to $n \rightarrow \pi^*$ transition for both complexes [61,64]. The UV–Vis spectra of both complexes have been shown in Fig. 11 and Fig. S3 (ESI), respectively.

Table 6
Geometric parameters (Å) for the $\pi \cdots \pi$ interactions for the complex 2.

Cg(I)···Cg(J)	Cg···Cg (Å)	α	Cg(I)···Perp (Å)	Cg(J)···Perp (Å)
Cg(8)···Cg(7) ⁱ	3.735(3)	11.1(3)	3.467(2)	3.468(2)

Symmetry transformations: ⁱ = 1–x, 1–y, 1–z; α = dihedral angle between ring I and ring J, Cg(I)···Perp. = perpendicular distance of Cg(I) on ring J, Cg(J)···Perp. = perpendicular distance of Cg(J) on ring I, Cg(7) = centre of gravity of the ring [C(2)–C(3)–C(4)–C(5)–C(6)–C(7)] and Cg(8) = centre of gravity of the ring [C(15)–C(16)–C(17)–C(18)–C(19)–C(20)] for the complex 2.

3.7. Photocatalytic activity

The ability of both complexes (**1** and **2**) to be used as photo-catalyst for the degradation of organic dye, viz. methylene blue (MB), has been investigated under visible light irradiation. The degradation efficiencies are defined as C/C_0 , where C and C_0 represent the residual and initial concentration of organic dyes, respectively. The degradation efficiencies (C/C_0) is calculated by the following equation:-

$$\text{Degradation efficiencies (\%)} = (C_0 - C)/C_0 \times 100.$$

As shown in Fig. 12, the residual concentration of the dye in an aqueous solution gradually decreased as a function of the increasing reaction time, indicating that both complexes degrade organic dyes. Both complexes are efficient for the degradation of MB and the ratio of the degradation reaches around 62% (for complex **1**) and 30% (for complex **2**) using 10 mg of complexes.

To prove the photocatalytic efficiency of both complexes to MB, comparative experiments without catalyst under visible light irradiation have been performed, which showed only very little decomposition. The photocatalytic activity of cadmium(II) acetate and copper(II) acetate have also been studied to MB under similar conditions (mentioned in the Fig. 13), which showed that the rate of degradation was still very slow using 10 mg of bare cadmium(II) as well as bare copper(II). It is revealed that the intensity of the characteristic absorption peak of MB decreased with the increase of irradiation time in the degradation process. Kinetic plots of both complexes have been shown in Fig. 13.

In order to verify whether both complexes are capable of maintaining its structural integrity during photocatalytic decomposition of MB, IR experiments for both complexes were performed during the course of photocatalytic reactions. The IR experiments indicated that the patterns are nearly identical when compared with the pure complex. Hence the IR experiments imply that both complexes maintain their structural integrity even after getting involved in the photocatalytic reactions. IR spectra of both complexes **1** and **2** (before and after degradation) have been shown in Fig. 14 and S4, respectively.

The first step of the process is excitation of electrons from the valence band to the conduction band which creates equal amounts of positives vacancies or holes in valence band. It is well-established that holes act as powerful oxidants and electrons as

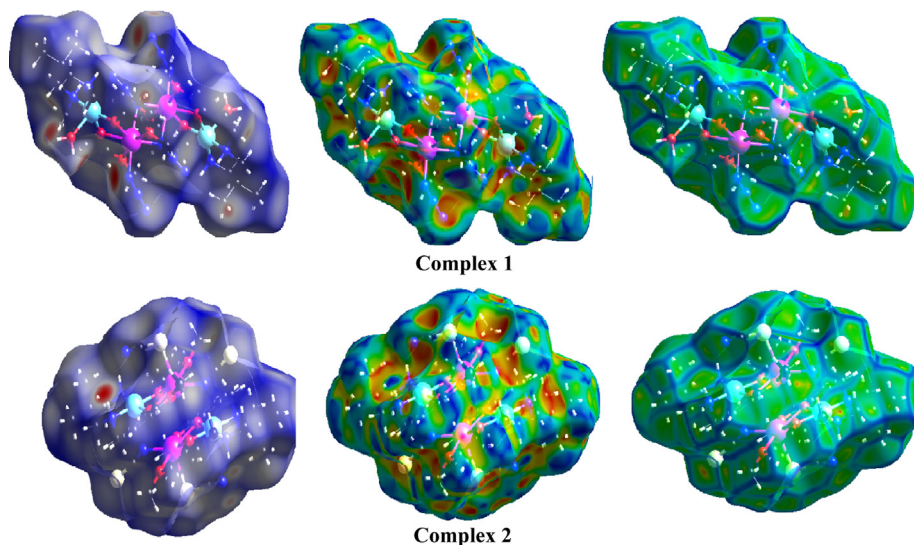


Fig. 10. Hirshfeld surfaces of both complexes **1** and **2** mapped over d_{norm} (left), shape index (middle), curvedness (right).

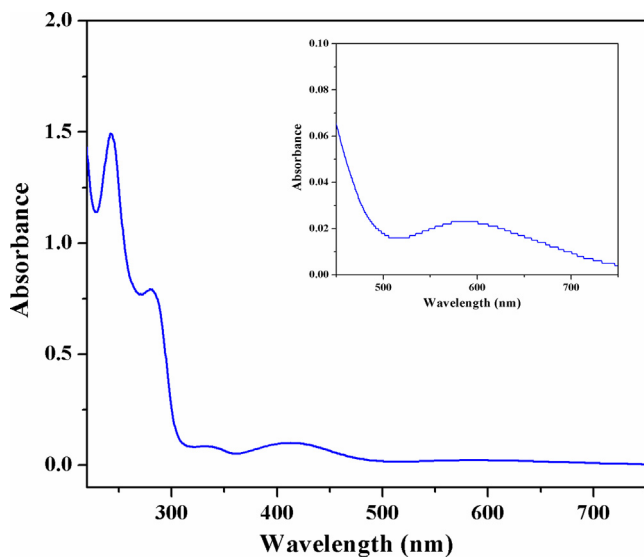


Fig. 11. UV-Vis spectra of complex 1. Inset shows the visible range spectrum.

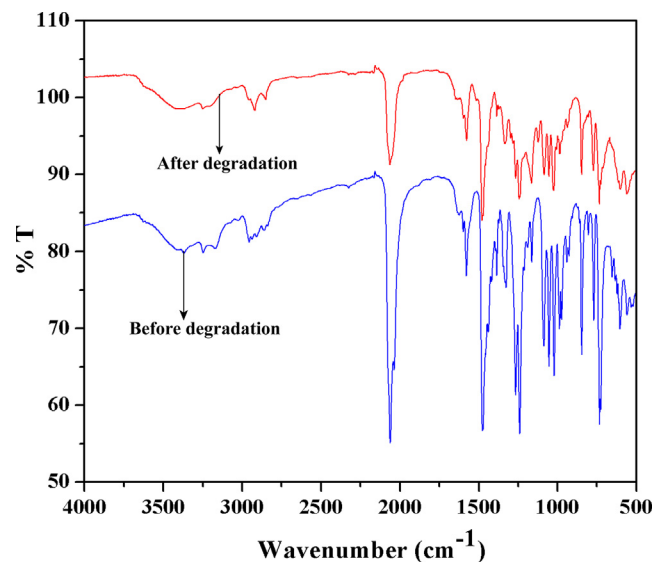


Fig. 14. IR spectra of complex 1 before (blue) and after (red) photodegradation process. (Color online.)

powerful reductants. The second step is adsorption of oxygen or water on the surfaces of catalyst. Electrons in the conduction band is scavenged by oxygen molecule to produce O_2^- anion radical,

which provides peroxide radical ($\cdot OOH$) and then decomposed to active hydroxyl radical ($\cdot OH$). On the other hand, the holes in the valence band interact with H_2O or $\cdot OH$ to produce highly active

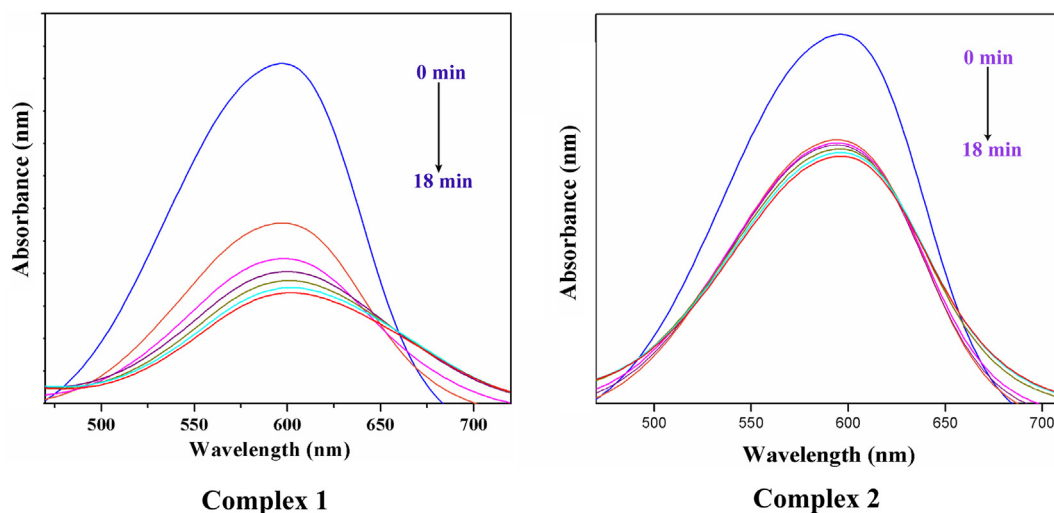


Fig. 12. Absorption spectra of MB solution with complexes (sample taken = 10 mg), used as a catalyst.

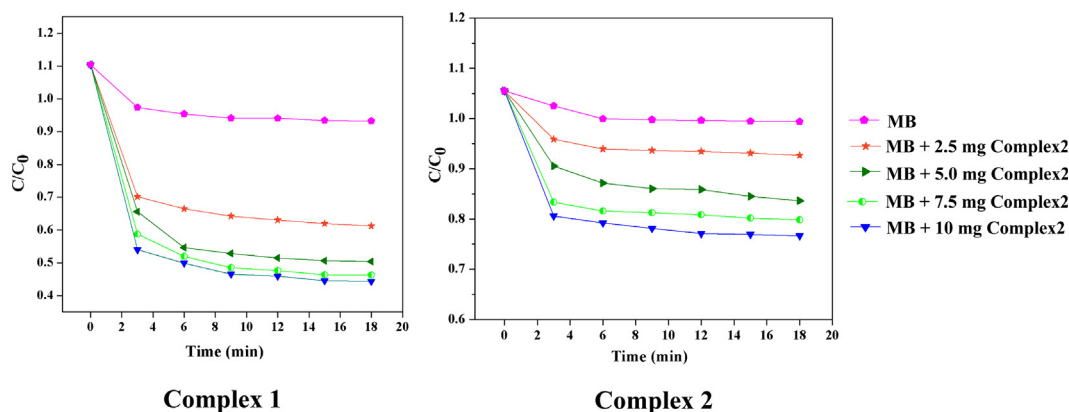


Fig. 13. Degradation efficiency of MB in presence of complex 1 and complex 2. Experimental condition [MB] = 20 mg/L.

Table 7

Kinetic studies for the degradation of methylene blue by some previously reported compounds and the present complexes.

Complex	Degradation time (min)	Degradation percentage (%)	Refs.
$[\text{Zn}(\mu_{1,1}\text{-N}_3)_2\{\text{Zn}(\text{L}^a)(\text{N}_3)_2\}]$	18	90	[30]
$[\text{Zn}(\mu_{1,1}\text{-N}_3)_2\{\text{Zn}(\text{L}^a)(\text{N}_3)_2\} \cdot 0.5\text{CH}_3\text{OH}]$	60	90	[48]
$[\{\text{Cd}(\text{L}^c)(\mu_{1,1}\text{-N}_3)_2\}_2\text{Cd}(\mu_{1,1}\text{-N}_3)_2 \cdot 1.76\text{CH}_3\text{OH}]_n$	40	99	[65]
$[\text{Zn}(\text{DCTP})(\text{L}^b)]_n$	120	96.9	[66]
$[\text{Zn}(\text{L}^f)(\text{DCTP})]_n$	120	81.4	[66]
$[\text{Cd}_2(\text{L}^d)_2(\text{hfpd})]_n$	180	94.1	[67]
$[\text{Zn}(\text{L}^d)(\text{tbta})]_n$	180	93.9	[67]
$[\text{Cd}_2(\text{L}^e)_2(\mu_{1,3}\text{-SCN})(\text{CH}_3\text{OH})_2]$	40	85	[68]
$[\text{Co}(\text{L}^f)(\text{tbta}) \cdot \text{H}_2\text{O}]_n$	135	82.8	[69]
$[\text{Co}(\text{L}^d)(\text{nip})]_n$	135	84.7	[69]
$[\text{Fe}(\text{L}^g)]$	75	96.5	[70]
$[\{\text{Cd}_3\text{L}_2^h(\text{H}_2\text{O})_5\} \cdot \text{H}_2\text{O}]_n$	180	88.7	[71]
$[\{\text{Cd}_3\text{L}_2^h(\text{hbmb})(\text{H}_2\text{O})_2\} \cdot 2.5\text{H}_2\text{O}]_n$	180	65.9	[71]
$[\{\text{Cd}_3\text{L}_2^h(\text{btbb})(\text{H}_2\text{O})_2\} \cdot 2\text{EtOH} \cdot 1.5\text{H}_2\text{O}]_n$	180	85.8	[71]
$[\{\text{Cd}_6\text{L}_4^i(\text{bipy})_2(\text{H}_2\text{O})_6\} \cdot 3\text{H}_2\text{O}]_n$	180	63.8	[71]
$[(\text{N}_3)\text{L}^i\text{Co}^{\text{III}}\text{L}^j\text{Co}^{\text{III}}\text{L}^i]$	90	55	[72]
$(\mu_{1,1}\text{-N}_3)_2\{(\text{H}_2\text{O})\text{Cu}(\text{L}^k)\text{Cd}(\text{N}_3)_2\}_2 \cdot 2\text{CH}_3\text{OH}$	18	62	Complex 1
$(\mu_{1,1}\text{-NCS})_2\{\text{CuL}^k\text{Cd}(\text{SCN})\}_2 \cdot 2\text{CH}_3\text{OH}$	18	32	Complex 2

$\text{L}^a = [2\text{-}((3\text{-}((\text{dimethylamino})\text{propylimino})\text{methyl})\text{-}6\text{-ethoxyphenol})]$; $\text{L}^b = 1,3\text{-bis}(5,6\text{-dimethylbenzimidazol-}1\text{-ylmethyl})\text{benzene}$; $\text{L}^c = 1,4\text{-bis}(\text{benzimidazol-}1\text{-ylmethyl})\text{benzene}$; $\text{L}^d = 1,5\text{-bis}(2\text{-methylbenzimidazol-}1\text{-yl})\text{pentane}$; $\text{L}^e = 2\text{-}(3\text{-}((\text{methylamino})\text{propylimino})\text{methyl})\text{-}4,6\text{-dichlorophenol}$; $\text{L}^f = 1,5\text{-bis}(\text{benzimidazolyl})\text{pentane}$; $\text{L}^g = \text{porphyrin } 5\text{-}(2\text{-}(\text{N-benzoyl-}5\text{-carboxyl})\text{-}1\text{-amino})\text{-}10,15,20\text{-triphenyl porphyrin}$; $\text{L}^h = 3,4\text{-bi}(4\text{-carboxyphenyl})\text{-benzoic acid}$; $\text{L}^i = 2\text{-}((1\text{-hydroxybutan-}2\text{-ylimino})\text{methyl})\text{-}4\text{-bromophenol}$; $\text{L}^j = 2\text{-amino-}1\text{-butanol}$

$\text{H}_2\text{DCTP} = 2,5\text{-ichloroterephthalic acid}$; $\text{H}_4\text{hfpd} = 4,40\text{-}(\text{hexafluoroisopropylidene})\text{diphthalic acid}$; $\text{H}_2\text{tbta} = \text{tetrabromoterephthalic acid}$; $\text{H}_2\text{tbta} = \text{tetrabromoterephthalic acid}$; $\text{H}_2\text{nip} = 5\text{-nitroisophthalic acid}$; $\text{hbmb} = 1,1'\text{-}(1,6\text{-hexane})\text{bis}(2\text{-methylbenzimidazole})$, $\text{btbb} = 1,4\text{-bis}(2\text{-}(4\text{-thiazolyl})\text{benzimidazole-}1\text{-ylmethyl})\text{benzene}$, $4,4'\text{-bipy} = 4,4'\text{-bipyridine}$.

hydroxyl radical ($\cdot\text{OH}$). Finally, the effective degradation of methylene blue is occurred by these generated hydroxyl radicals ($\cdot\text{OH}$).

3.8. Structure-activity relationship

The photocatalytic degradation study has been carried out with visible light irradiation. So the degradation process must be initiated with visible light absorption. Absorption spectra of both complexes contain peaks around 590 nm in the visible region, originating from copper(II)-based ${}^2\text{T}_{2g}(\text{D}) \leftarrow {}^2\text{E}_g(\text{D})$ transition. Thus copper(II) centres may be considered as the initiator of the degradation process. As already mentioned, copper(II) centre in complex **1** is relatively more free to take part in any reaction for its open zigzag structure. High efficiency of complex **1** to degrade the dye (MB) is therefore justified from its structure. On the other hand, copper(II) is rigidly imprisoned in a cyclic tetranuclear skeleton in complex **2** and is less free to take part in reaction. This explains the less catalytic efficiency of complex **2** compared to complex **1**.

A comparative study has also been done to compare the degradation efficiency of these complexes with all reported complexes, which has been characterized structurally. The comparative study has been shown in Table 7. This indicates our complexes are good enough to be explored in industrial chemistry, although better complexes are also known in literature. However, it should be noted that many of the previously reported catalysts have been prepared using Schiff bases as ligands and therefore their application in aqueous medium is limited (Schiff bases are susceptible to hydrolysis). Our complexes are containing reduced Schiff bases as ligands and may, therefore, be used in aqueous medium without any problem related to destruction of the ligands via hydrolysis.

4. Concluding remarks

Synthesis and X-ray characterization of two new heterotetranuclear copper(II)–cadmium(II) complexes with same reduced Schiff base ligand have been described in this paper. In both complexes copper(II) and cadmium(II) reside on N_2O_2 and

O_4 donor sites, respectively. The bridging mode in complex **2** is quite different than that of complex **1**. In complex **1**, two cadmium(II) centres are bridged by end-on bridging azide whereas in complex **2**, the copper(II) and cadmium(II) are bridged by end-on bridging thiocyanate. Both complexes show significant supramolecular interactions in their solid state structures. Both complexes have catalytic ability for the degradation of organic pollutant, MB, under visible light irradiation. Complex **1** shows better catalytic degradation ability than complex **2**. The structural variation upon the degradation process has also been rationalized. Finally, efficient catalytic ability of both complexes for the photodegradation of organic pollutant under visible light irradiation indicates the potential application of the complex in industrial chemistry.

Acknowledgements

S.M. thanks the CSIR, India, for awarding a Junior Research Fellowship. T.B. thanks the CSIR, India, for awarding a Senior Research Fellowship [Sanction No. 09/096(0861)/2016-EMR-I]. S.C. gratefully acknowledges UGC-CAS II program, Department of Chemistry, Jadavpur University, for financial support under the head [Chemicals/Consumables/Glassware].

Appendix A. Supplementary data

CCDC 1891988–1891989 contains the supplementary crystallographic data for complexes **1** and **2**. These data can be obtained free of charge via <http://www.ccdc.cam.ac.uk/conts/retrieving.html>, or from the Cambridge Crystallographic Data Centre, 12 Union Road, Cambridge CB2 1EZ, UK; fax: (+44) 1223-336-033; or e-mail: deposit@ccdc.cam.ac.uk. Supplementary data to this article can be found online at <https://doi.org/10.1016/j.poly.2019.05.043>.

References

- [1] T.K. Ghosh, S. Jana, A. Ghosh, *Inorg. Chem.* 57 (2018) 15216.
- [2] S. Dutta, S. Jana, P. Mahapatra, A. Bauzá, A. Frontera, A. Ghosh, *CrystEngComm* 20 (2018) 6490.

- [3] P. Mahapatra, S. Giri, M.G.B. Drew, A. Ghosh, *Dalton Trans.* 47 (2018) 3568.
- [4] P. Mahapatra, M.G.B. Drew, A. Ghosh, *Inorg. Chem.* 57 (2018) 8338.
- [5] S. Maity, S. Ghosh, P. Mahapatra, A. Ghosh, *Inorg. Chim. Acta* 482 (2018) 807.
- [6] M. Mousavi, V. Bereau, J.-P. Costes, C. Duhayon, J.-P. Sutter, *CrystEngComm* 13 (2011) 5908.
- [7] A. Hazari, L. Kanta Das, A. Bauzá, A. Frontera, A. Ghosh, *Dalton Trans.* 45 (2016) 5730.
- [8] P. Seth, A. Figuerola, J. Jover, E. Ruiz, A. Ghosh, *Inorg. Chem.* 53 (2014) 9296.
- [9] V. Bereau, S. Dhers, J.-P. Costes, C. Duhayon, J.-P. Sutter, *Eur. J. Inorg. Chem.* (2018) 66.
- [10] C. Biswas, M.G.B. Drew, E. Ruiz, M. Estrader, C. Diaz, A. Ghosh, *Dalton Trans.* 39 (2010) 7474.
- [11] J. Mukherjee, R. Mukherjee, *Inorg. Chim. Acta* 337 (2002) 429.
- [12] S. Chattopadhyay, G. Bocelli, A. Musatti, A. Ghosh, *Inorg. Chem. Commun.* 9 (2006) 1053.
- [13] S. Chattopadhyay, M.G.B. Drew, A. Ghosh, *Eur. J. Inorg. Chem.* (2008) 1693.
- [14] A. Bhattacharyya, S. Sen, K. Harms, S. Chattopadhyay, *Polyhedron* 88 (2015) 156.
- [15] X. Pang, R. Duan, X. Li, Z. Sun, H. Zhang, X. Wang, X. Chen, *Polym. Chem.* 5 (2014) 6857.
- [16] R. Duan, B. Gao, X. Li, X. Pang, X. Wang, H. Shao, X. Chen, *Polymer* 71 (2015) 1.
- [17] D.J. Darensbourg, O. Karroonnirun, S.J. Wilson, *Inorg. Chem.* 50 (2011) 6775.
- [18] M. Mandal, U. Monkowius, D. Chakraborty, *New J. Chem.* 40 (2016) 9824.
- [19] S.K. Barman, T. Mondal, D. Koley, F. Lloret, R. Mukherjee, *Dalton Trans.* 46 (2017) 4038.
- [20] C. Belle, I.G. Luneau, L. Karmazin, J.-L. Pierre, S. Albedyhl, B. Krebs, M. Bonin, *Eur. J. Inorg. Chem.* (2002) 3087.
- [21] O.V. Amirkhanov, O.V. Moroz, K.O. Znoviyak, T.Yu. Sliva, L.V. Penkova, T. Yushchenko, L. Szyrwiel, I.S. Kononova, V.V. Dyakonenko, O.V. Shishkin, V.M. Amirkhanov, *Eur. J. Inorg. Chem.* (2014) 3720.
- [22] S. Albedyhl, D. Schnieders, A. Jancso, T. Gajda, B. Krebs, *Eur. J. Inorg. Chem.* (2002) 1400.
- [23] S.K. Dey, A. Mukherjee, *Coord. Chem. Rev.* 310 (2016) 80.
- [24] M. Mahato, D. Mondal, H.P. Nayek, *Chemistry Select* 1 (2016) 6777.
- [25] P. Kar, M.G.B. Drew, A. Ghosh, *Inorg. Chim. Acta* 405 (2013) 349.
- [26] V. Stavila, A.A. Talin, M.D. Allendorf, *Chem. Soc. Rev.* 43 (2014) 5994.
- [27] N. Hoshino, F. Iijima, G.N. Newton, N. Yoshida, T. Shiga, H. Nojiri, A. Nakao, R. Kumai, Y. Murakami, H. Oshio, *Nat. Chem.* 4 (2012) 921.
- [28] H.-H. Wang, J. Yang, Y.-Y. Liu, S. Song, J.-F. Ma, *Cryst. Growth Des.* 15 (2015) 4986.
- [29] S. Farhadi, M.M. Amini, M. Dusek, M. Kucerakova, F. Mahmoudi, *J. Mol. Struct.* 1130 (2017) 592.
- [30] T. Basak, M.G.B. Drew, S. Chattopadhyay, *Inorg. Chem. Commun.* 98 (2018) 92.
- [31] M. Andruh, *Chem. Commun.* 47 (2011) 3025.
- [32] A. Aguiari, E. Bullita, U. Casellato, P. Guerriero, S. Tamburini, P.A. Vigato, *Inorg. Chim. Acta* 202 (1992) 157.
- [33] U. Casellato, P. Guerriero, S. Tamburini, P.A. Vigato, C. Benelli, *Inorg. Chim. Acta* 207 (1993) 39.
- [34] A. Hazari, L. Kanta Das, A. Bauzá, A. Frontera, A. Ghosh, *Dalton Trans.* 43 (2014) 8007.
- [35] T. Kajiwar, M. Nakano, K. Takahashi, S. Takaishi, M. Yamashita, *Chem. Eur. J.* 17 (2011) 196.
- [36] T. Kajiwar, K. Takahashi, T. Hiraizumi, S. Takaishi, M. Yamashita, *Polyhedron* 28 (2009) 1860.
- [37] Z.-X. Wang, L.-F. Wu, X.-K. Hou, M. Shao, H.-P. Xiao, M.-X. Li, Z. Anorg, *Allg. Chem.* 640 (2014) 229.
- [38] T. Ishida, R. Watanabe, K. Fujiwara, A. Okazawa, N. Kojima, G. Tanaka, S. Yoshii, H. Nojiri, *Dalton Trans.* 41 (2012) 13609.
- [39] X.-C. Huang, X.-H. Zhao, D. Shao, X.-Y. Wang, *Dalton Trans.* 46 (2017) 7232.
- [40] J.-P. Costes, F. Dahan, A. Dupuis, *Inorg. Chem.* 39 (2000) 165.
- [41] J.-P. Costes, F. Dahan, A. Dupuis, J.-P. Laurent, *New J. Chem.* (1998) 1525.
- [42] V. Bereau, H. Bolvin, C. Duhayon, J.-P. Sutter, *Eur. J. Inorg. Chem.* (2016) 4988.
- [43] V.K. Garg, M. Amita, R. Kumar, R. Gupta, *Dyes Pigm.* 63 (2004) 243.
- [44] V.K. Gupta, Suhas, I. Ali, V.K. Saini, *Ind. Eng. Chem. Res.* 43 (2004) 1740.
- [45] P.M.K. Reddy, B.R. Raju, J. Karupiah, E.L. Reddy, C. Subrahmanyam, *Chem. Eng. J.* 217 (2013) 41.
- [46] G.M. Sheldrick, *Acta Crystallogr. Sect. C* 71 (2015) 3.
- [47] G. M. Sheldrick, SADABS, V2014/5, Software for Empirical Absorption Correction, University of Göttingen, Institute für Anorganische Chemie der Universität, Göttingen, Germany, 1999–2003.
- [48] T. Basak, A. Bhattacharyya, K. Harms, S. Chattopadhyay, *Polyhedron* 157 (2019) 449.
- [49] A. Hazari, T.K. Ghosh, C.J.G. García, A. Ghosh, *Inorg. Chim. Acta* 471 (2018) 168.
- [50] A. Hazari, L.K. Das, R.M. Kadam, A. Bauzá, A. Frontera, A. Ghosh, *Dalton Trans.* 44 (2015) 3862.
- [51] A.W. Addison, T.N. Rao, J. Reedijk, J.V. Rijn, G.C. Verschoor, *J. Chem. Soc., Dalton Trans.* (1984) 1349.
- [52] D. Cremer, J.A. Pople, *J. Am. Chem. Soc.* 97 (1975) 1354.
- [53] D. Cremer, *Acta Crystallogr. Sect. B: Struct. Sci.* 40 (1984) 498.
- [54] M.A.S. Goher, N.A. Al-Salem, F.A. Mautner, K.O. Klepp, *Polyhedron* 16 (1997) 825.
- [55] F.A. Mautner, M. Scherzer, C. Berger, R.C. Fischer, R. Vicente, S.S. Massoud, *Polyhedron* 85 (2015) 329.
- [56] F.A. Mautner, M. Traber, R.C. Fischer, K. Reichmann, R. Vicente, *Polyhedron* 144 (2018) 30.
- [57] F.A. Mautner, M. Scherzer, C. Berger, R.C. Fischer, R. Vicente, S.S. Massoud, *Polyhedron* 85 (2015) 20.
- [58] S. Chattopadhyay, M.S. Ray, S. Chaudhuri, G. Mukhopadhyay, G. Bocelli, *Inorg. Chim. Acta* 359 (2006) 1367.
- [59] P. Chakraborty, I. Majumder, H. Kara, S.K. Chattopadhyay, E. Zangrando, D. Das, *Inorg. Chim. Acta* 436 (2015) 139.
- [60] M.A. Khan, A.A. Alqadami, M. Otero, M.R. Siddiqui, Z.A. Allothman, I. Alsouhaimi, M. Rafatullah, A.E. Hamedelnie, *Chemosphere* 218 (2019) 1089.
- [61] S. Ghorai, A. Sarmah, R.K. Roy, A. Tiwari, C. Mukherjee, *Inorg. Chem.* 55 (2016) 1370.
- [62] A. Biswas, L.K. Das, M.G.B. Drew, C. Diaz, A. Ghosh, *Inorg. Chem.* 51 (2012) 10111.
- [63] A. Golcu, M. Tumer, H. Demirelli, R.A. Wheatley, *Inorg. Chim. Acta* 358 (2005) 1785.
- [64] S. Roy, A. Bauzá, A. Frontera, S. Chattopadhyay, *Inorg. Chim. Acta* 453 (2016) 51.
- [65] S. Roy, K. Harms, A. Bauzá, A. Frontera, S. Chattopadhyay, *Polyhedron* 121 (2017) 199.
- [66] X. Wei, Y. Li, Z. Qin, G. Cui, *J. Mol. Struct.* 1175 (2019) 253.
- [67] X. Zhao, Z. Qin, Y. Li, G. Cui, *Polyhedron* 153 (2018) 197.
- [68] S. Roy, K. Harms, S. Chattopadhyay, *Polyhedron* 127 (2017) 471.
- [69] X. Zhao, Z. Qin, Y. Li, G. Cui, *Polyhedron* 146 (2018) 65.
- [70] T. Liu, T. Hu, C. Hu, J. Lang, *Inorg. Chem. Commun.* 90 (2018) 26.
- [71] L. Liu, J. Ding, C. Huang, M. Li, H. Hou, Y. Fan, *Cryst. Growth. Des.* 14 (2014) 3035.
- [72] K. Ghosh, K. Harms, A. Franconetti, A. Frontera, S. Chattopadhyay, *J. Organomet. Chem.* 883 (2019) 52.